Version 9.0
October, 2004

Wide Field and Planetary Camera 2 Instrument Handbook for Cycle 14

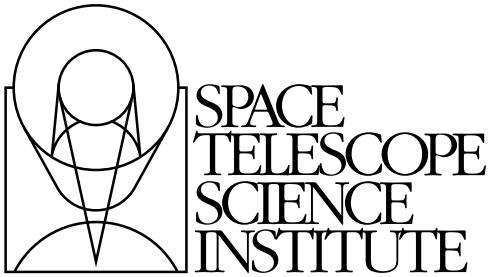

Space Telescope Science Institute
3700 San Martin Drive
Baltimore, Maryland 21218
help@stsci.edu

Operated by the Association of Universities for Research in Astronomy, Inc., for the National Aeronautics and Space Administration

User Support

For prompt answers to any question, please contact the STScI Help Desk.

- **E-mail:** help@stsci.edu
- **Phone:** (410) 338-1082
  (800) 544-8125 (U.S. only, toll free)

World Wide Web

Information, software tools, and other resources are available on the WFPC2 World Wide Web page:

- URL:

  http://www.stsci.edu/instruments/wfpc2/wfpc2_top.html

Revision History

Instrument	Version	Date	Editor
WF/PC-1	1.0; 2.0; 2.1	October 1985; May 1989; May 1990	Richard Griffiths
WF/PC-1	3.0	April 1992	John W. MacKenty
WFPC2	1.0; 2.0; 3.0	March 1993; May 1994; June 1995	Christopher J. Burrows
WFPC2	4.0	June 1996	John A. Biretta
WFPC2	Update	June 1998	Andrew Fruchter, Inge Heyer
WFPC2	Update	June 1999	Stefano Casertano
WFPC2	5.0	June 2000	John A. Biretta, Inge Heyer
WFPC2	6.0	June 2001	John A. Biretta, Inge Heyer
WFPC2	6.1	July 2001	John A. Biretta, Inge Heyer
WFPC2	7.0	October 2002	John A. Biretta, Lori M. Lubin
WFPC2	8.0	October 2003	Anton Koekemoer, Inge Heyer
WFPC2	9.0	October 2004	Inge Heyer, John A. Biretta

Send comments or corrections to:
Space Telescope Science Institute
3700 San Martin Drive
Baltimore, Maryland 21218
E-mail:help@stsci.edu

Acknowledgments

Handbook Authors and Contributors

Sylvia Baggett, John Biretta, Gabriel Brammer, Chris Burrows, Stefano Casertano, Mark Clampin, Harry Ferguson, Andrew Fruchter, Ron Gilliland, Shireen Gonzaga, Richard Griffiths, Inge Heyer, Jon Holtzman, Steve Hulbert, Anton Koekemoer, Vera Kozhurina-Platais, John Krist, Lori Lubin, Jennifer Mack, John MacKenty, Matt McMaster, Keith Noll, Christopher O'Dea, James Rhoads, Adam Riess, Susan Rose, Al Schultz, Mark Stevens, Massimo Stiavelli, Anatoly Suchkov, Jean Surdej, Michael Wiggs, Brad Whitmore.

Attribution

In publications please refer to this document as:

"Heyer, Biretta, et al. 2004, WFPC2 Instrument Handbook, Version 9.0 (Baltimore: STScI)."

Table of Contents

CHAPTER 1:

Introduction

In this chapter . . .

1.1 Instrument Overview

Wide Field and Planetary Camera 2 (WFPC2) is a two-dimensional imaging photometer which is located at the center of the Hubble Space Telescope (HST) focal plane and covers the spectral range between approximately 1150Å to 10500Å. It simultaneously images a 150″ x 150″ "L"-shaped region with a spatial sampling of 0.1″ per pixel, and a smaller 34″ x 34″ square field with 0.046″ per pixel. The total system quantum efficiency (WFPC2+HST) ranges from 4% to 14% at visual wavelengths, and drops to ~0.1% in the far UV. Detection of faint targets is limited by either the sky background (for broad filters) or by noise in the read-out electronics (for narrow and UV filters) with an RMS equivalent to 5 detected photons. Bright targets can cause saturation (>53000 detected photons per pixel), but there are no related safety issues. The sections below give a more detailed overview.

1.1.1 Field-of-View

The WFPC2 field-of-view is divided into four cameras by a four-faceted pyramid mirror near the HST focal plane. Each of the four cameras contains an 800x800 pixel Loral CCD detector. Three cameras operate at an image scale of 0.1″ per pixel (F/12.9) and comprise the Wide Field Camera (WFC) with an "L" shaped field-of-view. The fourth camera operates at 0.046″ per pixel (F/28.3) and is referred to as the Planetary Camera (PC). There are thus four sets of relay optics and CCD sensors in WFPC2. The four cameras are called PC1, WF2, WF3, and WF4, and their fields-of-view are illustrated in Figure 1.1 on page 2 (see also Section 7.8). Each image is a mosaic of three F/12.9 images and one F/28.3 image.

Figure 1.1: WFPC2 Field-of-View Projected on the Sky. The readout direction is marked with arrows near the start of the first row in each CCD. The X-Y coordinate directions are for POS-TARG commands. The position angle of V3 varies with pointing direction and observation epoch, and is given in the calibrated science header by keyword PA_V3.

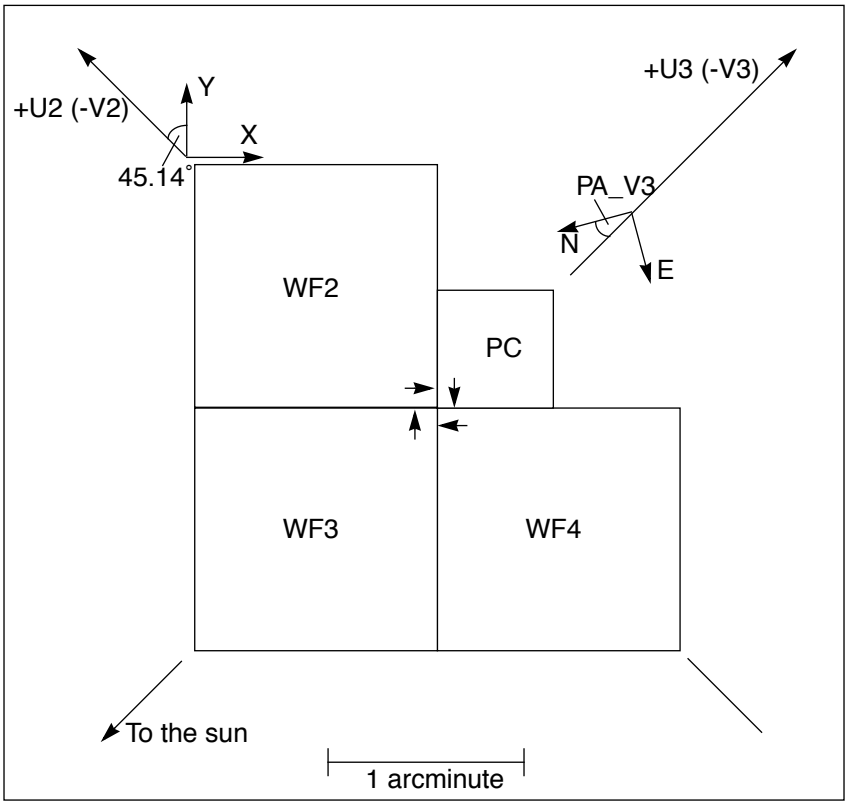

1.1.2 Spectral Filters

The WFPC2 contains 48 filters mounted in 12 wheels of the Selectable Optical Filter Assembly (SOFA). These include a set of broad band filters

approximating Johnson-Cousins UBVRI, as well as a set of wide U, B, V, and R filters, and a set of medium bandwidth Strömgren *u, v*, *b*, and *y* filters.

Narrow band filters include those for emission lines of Ne V (3426Å), CN (~3900Å), [OIII] (4363Å and 5007Å), He II (4686Å), Hβ (4861Å), He I (5876Å), [OI] (6300Å), Hα (6563Å), [NII] (6583Å), [SII] (6716Å and 6731Å), and [SIII] (9531Å). The narrow-band filters are designed to have the same dimensionless bandpass profile. Central wavelengths and profiles are uniformly accurate over the filter apertures, and laboratory calibrations include profiles, blocking, and temperature shift coefficients.

There are also two narrow band "quad" filters, each containing four separate filters which image a limited field-of-view: the UV quad contains filters for observing redshifted [OII] emission and are centered at 3767Å, 3831Å, 3915Å, and 3993Å. The Methane quad contains filters at 5433Å, 6193Å, 7274Å, and 8929Å. Finally, there is a set of narrow band "linear ramp filters" (LRFs) which are continuously tunable from 3710Å to 9762Å; these provide a limited field-of-view with diameter ~10″.

At ultraviolet wavelengths there is a solar-blind Wood's UV filter (1200-1900Å). The UV capability is also enhanced by control of UV absorbing molecular contamination, the capability to remove UV absorbing accumulations on cold CCD windows without disrupting the CCD quantum efficiencies and flat field calibrations, and an internal source of UV reference flat field images.

Finally, there is a set of four polarizers set at four different angles, which can be used in conjunction with other filters for polarimetric measurements. However, due to the relatively high instrumental polarization of WFPC2, they are best used on strongly polarized sources (>3% polarized). Sources with weaker polarization will require very careful calibration of the instrumental polarization.

1.1.3 Quantum Efficiency and Exposure Limits

The quantum efficiency (QE) of WFPC2+HST peaks at 14% in the red, and remains above 4% over the visible spectrum. The UV response extends to Lyman α wavelengths (QE~0.1%). Internal optics provide a spherical aberration correction.

Exposures of bright targets are limited by saturation effects, which appear above ~53000 detected photons per pixel (for setting ATD-GAIN=15), and by the shortest exposure time which is 0.11 seconds. There are no instrument safety issues associated with bright targets. Detection of faint targets is limited by the sky background for broad band filters at visual wavelengths. For narrow band and ultraviolet filters, detections are limited by noise in the read-out amplifier ("read noise"), which contributes an RMS noise equivalent to ~5 detected photons per pixel.

1.1.4 CCD Detector Technology

The WFPC2 CCDs are thick, front-side illuminated devices made by Loral Aerospace. They support multi-pinned phase (MPP) operation which eliminates quantum efficiency hysteresis. They have a Lumogen phosphor coating to give UV sensitivity. Details may be summarized as follows:

- **Read noise:** WFPC2 CCDs have ~5e^- RMS read noise which provides good faint object and UV imaging capabilities.
- **Dark noise:** Inverted phase operation yields low dark noise for WFPC2 CCDs. They are being operated at -88˚C and the median dark current is about 0.0045 e^- $pixel^{-1}$ s^{-1}.
- **Flat field:** WFPC2 CCDs have a uniform pixel-to-pixel response (<2% pixel-to-pixel non-uniformity) which facilitates accurate photometric calibration.
- **CTE:** Low level charge traps are present in the WFPC2 devices at the present operating temperature of -88˚C. For bright stellar images, there is a ~4% signal loss when a star image is clocked down through all rows of the CCD. Fainter images show a larger effect which also appears to increase with time. The effect can be as large as tens of percent for faint stars (few hundred electrons) seen against a low background (<0.1 DN) in data taken during later Cycles. For most typical applications, CTE is either negligible or can be calibrated, and pre-flash exposures are not required. This avoids the increase in background noise, and the decrease in operational efficiency that results from a preflash.
- **Gain switch:** Two CCD gains are available with WFPC2, a 7 e^- DN^{-1} channel which saturates at about 27000 e^- (4096 DN with a bias of about 300 DN) and a 14 e^- DN^{-1} channel which saturates at about 53000 e^-. The Loral devices have a full well capacity of ~90,000 e^- and are linear up to 4096 DN in both channels.
- **DQE:** The peak CCD DQE in the optical is 40% at 7000Å. In the UV (1100-4000Å) the DQE is determined by the phosphorescent Lumogen coating, and is 10 - 15%.
- **Image Purge:** The residual image resulting from a 100x (or more) full-well over-exposure is well below the read noise within 30 minutes. No CCD image purge is needed after observations of very bright objects. The Loral devices bleed almost exclusively along the columns.
- **Quantization:** The systematic Analog-to-Digital converter errors have been largely eliminated, contributing to a lower effective read noise.

- **QEH:** Quantum Efficiency Hysteresis (QEH) is not a significant problem in the Loral CCDs because they are front side illuminated and use MPP operation. The absence of any significant QEH means that the devices do not need to be UV-flooded and the chips can be warmed monthly for decontamination purposes without needing to maintain a UV-flood.
- **Detector MTF:** The Loral devices do suffer from low level detector MTF (Modulation Transfer Function) perhaps caused by scattering in the front side electrode structure. The effect is to blur images and decrease the limiting magnitude by about 0.5 magnitudes.

1.1.5 UV Imaging

WFPC2 had a design goal of 1% photometric stability at 1470Å over a month. This requires a contamination collection rate of less than 47 ng cm^{-2} $month^{-1}$ on the cold CCD window. Hence, the following features were designed into WFPC2 in an effort to reduce contaminants:

1. Venting and baffling, particularly of the electronics, were redesigned to isolate the optical cavity.
2. There was an extensive component selection and bake-out program, and specialized cleaning procedures.
3. Molecular absorbers (Zeolite) were incorporated.

The CCDs were initially operated at -77˚C after launch, which was a compromise between being as warm as possible for contamination reasons, while being sufficiently cold for an adequate dark rate. However, at this temperature significant photometric errors were introduced by low-level traps in the CCDs. This problem with the charge transfer efficiency of the CCDs has been reduced since 23 April 1994 by operating the CCDs at -88˚C, but this leads to significantly higher contamination rates than hoped for. On-orbit measurements indicate that there is now a decrease in throughput at a repeatable rate of ~30% per month at 1700Å. Monthly decontamination procedures are able to remove the contaminants completely and recover this loss. As of Cycle 12, the interval between decontaminations has been increased from 30 days to approximately 49 days.

1.1.6 Aberration Correction and Optical Alignment

WFPC2 contains internal corrections for the spherical aberration of the HST primary mirror. These corrections are made by highly aspheric surfaces figured onto the Cassegrain relay secondary mirror inside each of

the four cameras. Complete correction of the aberration depends on a precise alignment between the OTA pupil and these relay mirrors.

Mechanisms inside WFPC2 allow optical alignment on-orbit. The 47˚ pick-off mirror has two-axis tilt capabilities provided by stepper motors and flexure linkages, to compensate for uncertainties in our knowledge of HST's latch positions (i.e., instrument tilt with respect to the HST optical axis). These latch uncertainties would be insignificant in an unaberrated telescope, but must be compensated for in a corrective optical system. In addition, three of the four fold mirrors, internal to the WFPC2 optical bench, have limited two-axis tilt motions provided by electrostrictive ceramic actuators and invar flexure mountings. Fold mirrors for the PC1, WF3, and WF4 cameras are articulated, while the WF2 fold mirror has a fixed invar mounting. A combination of the pick-off mirror and actuated fold mirror (AFMs) has allowed us to correct for pupil image misalignments in all four cameras. Since the initial alignment, stability has been such that mirror adjustments have not been necessary. The mechanisms are not available for GO commanding.

1.2 Which Instrument to Use: WFPC2, ACS, NICMOS, or STIS?

In this section we compare briefly the performance of HST instruments with imaging capability in the UV to near-IR spectral range. These instruments include WFPC2 and STIS, as well as NICMOS, which was revived through the installation of the cryo-cooler, and the Advanced Camera for Surveys (ACS), which was installed during the HST Servicing Mission 3b[1]. Important imaging parameters for all instruments are summarized in Table 1.1 on page 7.

1. The FOC also had UV imaging capability, but it has been physically replaced by ACS.

Table 1.1: Comparison of WFPC2, ACS, NICMOS, and STIS Instrumental Imaging Parameters.

Parameter	WFPC2	ACS	NICMOS	STIS
Wavelength range	1150Å - 11,000Å	WFC: 3700 Å - 11000 Å HRC: 2000 Å - 11000 Å SBC: 1150 Å - 1700 Å	8000Å - 25,000Å	FUV-MAMA: 1150Å - 1700Å NUV-MAMA: 1700Å - 3100Å CCD: 2000Å - 11,000Å
Detector	Si CCDs	CCDs (WFC, HRC) MAMA (SBC)	HgCdTe arrays	CCD, MAMAs
Image Format	4 x 800 x 800	WFC: 2 butted 2048x4096 HRC: 1024x1024 SBC: 1024x1024	3 x 256 x 256	1024 x 1024
Field-of-view and pixel size	150" x 150" @ 0.1" /pix 34"x 34" @ 0.046"/pix [(a)]	WFC: 202"x202" @0.05" /pix HRC: 29"x26" @0.028"x0.025" /pix SBC: 35"x31" @0.033"x0.030" /pix	NIC1: 11"x 11" @ 0.043" /pix NIC2: 19" x 19" @ 0.075″ /pix NIC3: 51″ x 51″ @ 0.2″ /pix	MAMAs: 25" x 25" @ 0.024"/pix CCD: 51" x 51" @ 0.05″ /pix [(b)]
Read noise	5 e^-	WFC: 5 e^- HRC: 4.7 e^- SBC: 0 e^-	30 e^-	MAMAs: 0 e^- CCD: 5.4e^-
Dark current	0.002[WF2] - 0.006[PC] e^- /s/pix	WFC: 0.002 e^-/s/pix HRC: 0.0025 e^-/s/pix SBC: 1.2x10^{-5} e^-/s/pix	<0.1 e^- /s/pix	NUV-MAMA: 0.0001 e^- /s/pix FUV-MAMA: 7x10^{-6} e^- /s/pix CCD: 0.004 e^- /s/pix
Saturation	53,000 e^-	WFC: 80,000 e^- HRC: 140,000 e^- SBC: 100 counts/s/pix	200,000 e^-	MAMAs: 100 counts/s/pix CCD: 140,000 e^-

a. “L”-shaped field-of-view using 3 CCDs with 0.1" pixels, and one CCD with 0.046" pixels.
b. Field-of-view is up to 51" x 51" if no filter is used, and down to 12" x 12" for some neutral density filters.

1.2.1 Comparison of WFPC2 and ACS

Advantages of each instrument may be summarized as follows.
WFPC2 advantages are:

- Wider field of view in the UV - effective area of 134"x134" vs. 35"x31".
- Wider field of view in many narrow band filters - effective area of 134"x134" vs. up to 40"x70" (ACS LRFs).

ACS advantages are:

- Wider field of view in broad band optical filters - effective area of 202"x202" vs. 134"x134".
- Factor of ~2 better sampling of the PSF.

- Higher detective efficiency (factor of 2-10 depending on wavelength). Table 1.2 on page 8 compares the detective efficiency for WFPC2 and ACS filters with similar band passes.
- True solar blind imaging in the UV due to the MAMA detector.
- Coronagraphic capability.

For projects using optical broad band filters, ACS is better suited due to its wider field of view, better sampling of the PSF, and higher throughput.

For projects using UV and narrow band filters the choice may depend on source size. For relatively compact objects, ACS is better due to the better PSF sampling and higher throughput and solar blind performance. For larger objects, e.g., the large planets Jupiter and Saturn, and diffuse galactic nebula such as the Orion and Eagle Nebulae, the larger field of view of WFPC2 makes it competitive.

Table 1.2: Comparison of WFPC2 and ACS Filters.

WFPC2			ACS				ACS / WFPC2 Wide-Field Imaging Effic'y[a]
Filter	FOV (arcsec)[b]	Approx Peak Effic'y[c]	Filter	Camera	FOV (arcsec)[d]	Approx Peak Effic'y[c]	
	Broad Band						
F160W	90" x 90"	0.07%	F150LP	SBC	31" x 35"	3%	5.74
F170W	134" x 134"	0.17%	F165LP	SBC	31" x 35"	0.9%	0.32
F185W	134" x 134"	0.19%	-	-	-	-	-
F218W	134" x 134"	0.28%	F220W	HRC	26" x 29"	5%	0.75
F255W	134" x 134"	0.45%	F250W	HRC	26" x 29"	6.1%	0.56
F300W	134" x 134"	1.9%	-	-	-	-	-
F336W	134" x 134"	3.5%	F330W	HRC	26" x 29"	10.5%	0.13
F380W	134" x 134"	3.7%	-	-	-	-	-
F439W	134" x 134"	3.9%	F435W	WFC HRC	202" x 202" 26" x 29"	33% 22%	19.2 0.24
F450W	134" x 134"	8.5%	F475W	WFC HRC	202" x 202" 26" x 29"	36% 24%	9.62 0.12
F555W	134" x 134"	11%	F555W	WFC HRC	202" x 202" 26" x 29"	37% 23%	7.64 0.09
F569W	134" x 134"	11%	-	-	-	-	-
F606W	134" x 134"	14%	F606W	WFC HRC	202" x 202" 26" x 29"	44% 27%	7.14 0.08
F622W	134" x 134"	14%	F625W	WFC HRC	202" x 202" 26" x 29"	43% 26%	6.98 0.08

Table 1.2: Comparison of WFPC2 and ACS Filters.

WFPC2			ACS				ACS / WFPC2 Wide-Field Imaging Effic'y[a]
Filter	FOV (arcsec)[b]	Approx Peak Effic'y[c]	Filter	Camera	FOV (arcsec)[d]	Approx Peak Effic'y[c]	
F675W	134" x 134"	14%	-	-	-	-	-
F702W	134" x 134"	14%	-	-	-	-	-
F785LP	134" x 134"	5%	-	-	-	-	-
F791W	134" x 134"	9%	F775W	WFC HRC	202" x 202" 26" x 29"	42% 22%	10.6 0.10
F814W	134" x 134"	10%	F814W	WFC HRC	202" x 202" 26" x 29"	42% 22%	9.54 0.09
F850LP	134" x 134"	3.9%	F850LP	WFC HRC	202" x 202" 26" x 29"	25% 13%	14.6 0.14
	Medium Band						
F122M	134" x 134"	0.11%	F122M	SBC	31" x 35"	0.9%	0.49
F410M	134" x 134"	4%	-	-	-	-	-
F467M	134" x 134"	5.5%	B. Ramp (FR459M)	WFC HRC	65" x 100" 26" x 29"	29%	0.44
F547M	134" x 134"	11%	F550M	WFC HRC	202" x 202" 26" x 29"	40% 25%	8.26 0.10
F1042M	134" x 134"	0.5%	B. Ramp (FR914M)	WFC HRC	65" x 100" 26" x 29"	4%	1.0
	Narrow Band						
F343N	134" x 134"	0.39%	F344N	HRC	26" x 29"	10%	1.08
F375N	134" x 134"	0.9%	OII Ramp (FR388N)	WFC HRC	65" x 100" 26" x 29"	4%	0.22
FQUVN 3767Å	60" x 60"	1.3%	OII Ramp (FR388N)	WFC HRC	65" x 100" 26" x 29"	6%	1.2
FQUVN 3831Å	67" x 67"	1.5%	OII Ramp (FR388N)	WFC HRC	65" x 100" 26" x 29"	8%	1.0
FQUVN 3915Å	67" x 67"	1.9%	OII Ramp (FR388N)	WFC HRC	65" x 100" 26" x 29"	10%	0.9
FQUVN 3993Å	67" x 67"	2.3%	OII Ramp (FR388N)	WFC HRC	65" x 100" 26" x 29"	10%	0.8
F390N	134" x 134"	1.9%	OII Ramp (FR388N)	WFC HRC	65" x 100" 26" x 29"	10%	0.23
F437N	134" x 134"	3%	OII Ramp (FR423N)	WFC	45" x 85"	10%	0.16

Table 1.2: Comparison of WFPC2 and ACS Filters.

WFPC2			ACS				ACS / WFPC2 Wide-Field Imaging Effic'y[a]
Filter	FOV (arcsec)[b]	Approx Peak Effic'y[c]	Filter	Camera	FOV (arcsec)[d]	Approx Peak Effic'y[c]	
F469N	134" x 134"	3.7%	OII Ramp (FR462N)	WFC	60" x 85"	13%	0.17
F487N	134" x 134"	4.8%	OIII Ramp (FR505N)	WFC HRC	65" x 100" 26" x 29"	18%	0.20
F502N	134" x 134"	5.8%	F502N	WFC HRC	202" x 202" 26" x 29"	28% 19%	11.0 0.14
FQCH4 5435Å	30" x 30"	9.5%	OIII Ramp (FR551N)	WFC	45" x 85"	28%	2.7
F588N	134" x 134"	13%	OIII Ramp (FR551N)	WFC	45" x 85"	34%	0.12
FQCH4 6199Å	30" x 30"	12%	OIII Ramp (FR601N)	WFC	60" x 85"	29%	2.3
F631N	134" x 134"	13%	OIII Ramp (FR601N)	WFC	60" x 85"	31%	0.11
F656N	134" x 134"	11%	Hα Ramp (FR656N)	WFC HRC	65" x 100" 26" x 29"		
F658N	134" x 134"	11%	F658N	WFC HRC	202" x 202" 26" x 29"	44% 26%	9.09 0.10
F673N	134" x 134"	12%	Hα Ramp (FR656N)	WFC HRC	65" x 100" 26" x 29"	28%	0.11
FQCH4 7278Å	30" x 30"	10%	Hα Ramp (FR716N)	WFC	45" x 85"	31%	3
FQCH4 8930Å	30" x 30"	2.9%	F892N	WFC HRC	202" x 202" 26" x 29"	12%	3.47
F953N	134" x 134"	2.2%	IR Ramp (FR931N)	WFC	60" x 85"	12%	0.31

a. Relative efficiency for ACS vs. WFPC2 for wide-field imaging. Defined as [(ACS FOV area)x(ACS efficiency)] / [(WFPC2 FOV area) x (WFPC2 efficiency)]. For WFPC2 we have reduced FOV for the missing "L" shaped region around PC1.
b. The full WFPC2 FOV is a 150" x 150" L-shaped region, with area equivalent to a 134" x 134" square, which we use for comparisons to ACS.
c. Efficiency near filter pivot wavelength; includes HST+instrument+filters.
d. For ACS the full WFC FOV is 202"x202", the full HRC FOV is 26"x29", and the full SBC FOV is 31" x 35". When using the narrow band ramp filters the larger WFC FOV gets reduced, depending on the FOV location. There are three possible locations: inner region (45"x85"), middle region (65"x100"), and outer region (60"x85").

1.2.2 Comparison of WFPC2 and NICMOS

Both WFPC2 and NICMOS are capable of imaging at wavelengths between ~8000Å and ~11,000Å. At longer wavelengths NICMOS must be used; at shorter wavelengths WFPC2, STIS, or ACS must be used. Table 1.3 on page 12 compares the detective efficiency of WFPC2 and NICMOS in the wavelength region where both instruments overlap in capabilities. Count rates for a V=20 star of spectral class A0 are given for all filters at common wavelengths; the signal-to-noise (S/N) is also given for a 1 hour exposure of this same star. For bright continuum sources WFPC2 and NICMOS offer similar efficiency over the spectral range from 8800Å to 10,500Å; the choice of instrument will likely depend on other factors such as field size and details of the passband shape. However, for very faint sources, the lower read noise of WFPC2 ($5e^-$ for WFPC2 vs. $30e^-$ for NICMOS) should prove advantageous.

Both instruments have polarimetry capability, but the WFPC2 polarizers are not viable above 8000Å; above this wavelength NICMOS must be used for polarimetry. We note that the ACS WFC is optimized for the far red and has polarimetric capability.

Table 1.3: Comparison of WFPC2 and NICMOS Count Rates for a V=20 A0 Star.

Instrument	Filter	Mean Wavelength (Å)	Effective Width (Å)	Count Rate ($e^- s^{-1}$)	SNR in 1 hour[a]
WFPC2	F785LP	9366	2095	14	215
	F791W	8006	1304	30	314
	F814W	8269	1758	33	333
	F850LP	9703	1670	7.1	150
	FQCH4N (Quad D)	8929	64	0.47	34, 29[b]
	F953N	9546	52	0.21	19, 15[b]
	F1042M	10,443	611	0.20	18, 15[b]
	LRF[c]	8000 9000 9762	105 113 126	1.5 0.64 0.23	66 40 20
NICMOS[e]	F090M[d]	8970	1885	17.4	89
	F095N[d]	9536	88	0.883	9.2
	F097N[d]	9715	94	1.19	12
	F108N[d]	10,816	94	1.17	9.9
	F110W (Camera 1)	11,022	5920	73	170
	F110W (Camera 2)	11,035	5915	83.7	290
	F110W (Camera 3)	11,035	5915	75.9	390

a. WFPC2 SNR assuming two 1800s exposures for cosmic ray removal. NICMOS SNR for central pixel of PSF.
b. Values given for WFC (0.10″ pixels) and PC (0.046″ pixels).
c. LRF filter is continuously tunable from 3710Å to 9762Å. LRF field-of-view is 10″x10″.
d. These NICMOS filters are available only on Camera 1 which has 11″x11″ field-of-view.
e. The NICMOS ETC performs S/N calculations for the brightest pixel with the detector temperature at 77.1°K.

1.2.3 Comparison of WFPC2 and STIS

Both WFPC2 and STIS are capable of imaging over the same wavelength ranges between ~1150Å and ~11000Å. At much longer wavelengths NICMOS must be used.

Advantages of each instrument may be summarized as follows.

WFPC2 advantages are:

- Wider field-of-view, effective area of 134″ x 134″ vs. 50″ x 50″ or less.

- Greater selection of filters, including polarizers.
- Bright Targets: WFPC2 has no bright target safety issues, and can give useful data on faint targets near very bright objects. STIS MAMAs can be damaged by bright objects.

STIS advantages are:

- Much higher UV throughput.
- True solar blind imaging in UV due to MAMA detectors. WFPC2 CCDs are very sensitive to filter red-leak.
- PSF sampling: STIS offers 0.024″ pixels vs. 0.046″ on WFPC2.
- High time resolution is possible (τ ~125μs) with the MAMA detectors. Also the STIS CCD may be cycled on ~20s time scale using a sub-array.

In general, WFPC2 has a much greater selection of filters and wider field-of-view than STIS, but STIS has greater detective efficiency in the UV and for its long-pass and unfiltered modes. Table 1.4 on page 14 compares the detective efficiency for WFPC2 and STIS filters with similar bandpasses. For UV imaging STIS is greatly superior due to higher throughput and insensitivity to filter red-leak; only if some detail of a WFPC2 filter bandpass were needed, would it be a viable choice.

For both [OII] 3727Å and [OIII] 5007Å imaging STIS has much higher QE and is preferred, unless the larger WFPC2 field-of-view is an important factor. The WFPC2 [OIII] filter is wider than its STIS counter-part, which may also be useful for redshifted lines. For broad-band imaging the unfiltered and 5500Å long-pass modes of STIS again have higher efficiency than WFPC2, though with reduced field-of-view.

Table 1.4: Comparison of WFPC2 and STIS Detector Efficiencies.

Instrument	Filter	Mean Wavelength (Å)	Bandpass FWHM (Å)[a]	Peak QE[b]
WFPC2	F122M	1420	100	0.11%
STIS	F25LYA	1216	85	0.32%
WFPC2	F160BW	1492	500	0.07%
STIS	25MAMA (FUV)	1370	320	4.5%
WFPC2	F255W	2586	393	0.5%
STIS	25MAMA (NUV)	2220	1200	3.1%
WFPC2	F375N	3738	42	0.9%
STIS	F28X50OII	3740	80	3.7%
WFPC2	F502N	5013	37	5.8%
STIS	F28X50OIII	5007	5	11%
WFPC2	F606W	5935	2200	14%
STIS	F28X50LP	~7300[c]	2720	12%
STIS	50CCD	~5800	4410	15%

a. Note that definition of FWHM is different from "effective width" elsewhere herein.
b. Includes instrument and OTA.
c. 5500Å long pass filter.

1.3 History of WFPC2

The original Wide Field and Planetary Camera (WF/PC-1) served as the prototype for WFPC2. In many respects the two instruments are very similar. Both were designed to operate from 1150Å to 11000Å, both use 800x800 CCD detectors, and both provide spatial samplings of ~0.045″ and ~0.1″ per pixel. The development and construction of WF/PC-1 was led by Prof. J. A. Westphal, Principal Investigator (PI), of the California Institute of Technology. The instrument was built at the Jet Propulsion Laboratory (JPL) and was launched aboard HST in April 1990. It obtained scientific data until it was replaced by WFPC2 during the first servicing mission in December 1993.

Because of its important role in the overall HST mission, NASA decided to build a second Wide Field and Planetary Camera (WFPC2) as a backup clone of WF/PC-1 even before HST was launched. WFPC2 was already in the early stages of construction at JPL when HST was launched. After the discovery of spherical aberration in the HST primary mirror, it was quickly

realized that a modification of the WFPC2 internal optics could correct the aberration and restore most of the originally expected imaging performance. As a result, development of WFPC2 was accelerated. Dr. J. T. Trauger of JPL is the project PI for WFPC2 and led the Investigation Definition Team (IDT[2]).

The WFPC2 completed system level thermal vacuum (SLTV) testing at JPL in April and May 1993. Between June and November there were payload compatibility checks at Goddard Space Flight Center (GSFC), and payload integration at Kennedy Space Center (KSC). WF/PC-1 was replaced by WFPC2 during the first servicing mission in December 1993. WFPC2 was shown to meet most of its engineering and scientific performance requirements by testing conducted during the three month Servicing Mission Observatory Verification (SMOV) period following the servicing mission. The General Observer community has had access to WFPC2 since the start of Cycle 4 in January 1994.

WFPC2 accurately corrects the HST spherical aberration, is a scientifically capable camera configured for reliable operation in space without maintenance, and is an instrument which can be calibrated and maintained without excessive operational overhead. It incorporates evolutionary improvements in photometric imaging capabilities. The CCD sensors, signal chain electronics, filter set, UV performance, internal calibrations, and operational efficiency have all been improved through new technologies and lessons learned from WF/PC-1 operations and the HST experience since launch.

WFPC2 SMOV requirements were developed by the IDT, GSFC, and the STScI to include: verification of the baseline instrument performance; an optical adjustment by focusing and aligning to minimize coma; the estimation of residual wave front errors from the analysis of star images; a photometric calibration with a core set of filters (including both visible and UV wavelengths); and the evaluation of photometric accuracy and stability over the full field with the core filter set. The results of these studies are documented in Holtzman, et al., 1995a and 1995b, and are summarized in this Handbook.

Despite these successes, the first years of scientific operation of WFPC2 have revealed a number of relatively minor instrumental defects that were not expected from the pre-launch testing. These include a low-level charge transfer inefficiency, a higher than expected level of scattered light around bright objects, and variable and lower than expected ultraviolet (UV) efficiency. In addition, we have come to understand the instrument more fully -- particularly in terms of its overall photometric performance, geometric distortion, scale and alignments, hot pixels, and CCD traps. All of this new information is described here.

---

2. The members of the IDT are: John T. Trauger, Christopher J. Burrows, John Clarke, David Crisp, John Gallagher, Richard E. Griffiths, J. Jeff Hester, John Hoessel, Jon Holtzman, Jeremy Mould, and James A. Westphal.

1.4 The Previous vs. Current Generation: WF/PC-1 vs. WFPC2

For historical reasons, it is useful to offer comparisons between the current WFPC2, and its predecessor WF/PC-1, which was returned to Earth in December 1993.

- **Field format:** WF/PC-1 contained 8 cameras and CCDs, each CCD having 800 x 800 pixels. Four were used in the Planetary Camera mode (0.043″ pixels), and four were used in the Wide Field Camera mode (0.10″ pixels). The two pixel formats were selected by rotating the pyramid mirror by 45°. WFPC2 budget and schedule constraints forced a reduction from 8 to 4 camera channels in August 1991. WFPC2 contains only 4 CCDs; the pyramid mirror is fixed and the 4 cameras are physically located in the bays occupied by the WF/PC-1 WFC.
- **Aberration correction:** WF/PC-1 contained no correction for spherical aberration of the OTA primary mirror. Only about 15% of light from a stellar target fell into the core of the PSF (diameter ~0.1″). WFPC2 incorporates corrective figures on the Cassegrain secondary mirrors inside the relay cameras, and as a result places ~60% of the light from a star inside a diameter of 0.1″. Precise alignment of the OTA pupil on these mirrors is required to attain full correction of the spherical aberration. Hence the pick-off mirror (POM) is steerable in WFPC2, and three of the fold mirrors contain tip-tilt actuators.
- **CCD Technology:** Many properties of WF/PC-1 and WFPC2 CCDs are compared in Table 4.1 on page 79. Many differences derive from the fact that the WF/PC-1 CCDs were thinned, backside illuminated devices whereas the WFPC2 CCDs are thick, front side illuminated devices. In the WF/PC-1 CCDs the active silicon layer was a free-standing membrane somewhat less than 10μm thick, with photons impinging directly on the silicon layer, without attenuation in the polysilicon gate structure built on the other ('front') side of the device.
- **Quantum Efficiency Hysteresis (QEH):** The WF/PC-1 CCD's required a UV flood procedure and continuous cold temperatures to avoid QEH and hence non-linearity. A UV flood was performed early in the WF/PC-1 mission, but could not be repeated due to problems with the HST magnetometers. This in turn limited the temperature range allowable during decontaminations, since high temperatures would remove the UV flood, which in turn severely limited UV science capabilities. Some QE instability was also seen, particularly in

the B band, due to changes in the UV flood. WFPC2 CCDs support multi-pinned phase (MPP) operation which eliminates quantum efficiency hysteresis.

- **Charge Transfer Efficiency:** WF/PC-1 devices suffered from significant charge transfer efficiency (CTE) errors at image intensities below ~200 electrons per pixel. This was overcome by preflashing virtually all science images. WFPC2 devices have much less CTE error, and hence no preflash is used. However, low-level charge traps are present in the WFPC2 devices, and are increasing slowly with time. See the discussions in "Photometric Anomalies: CTE and Long vs. Short" on page 99 for details of WFPC2 CTE behavior.
- **Detector MTF:** The WFPC2 Loral devices do suffer from poorer CCD detector MTF than the WF/PC-1 CCDs, perhaps caused by scattering in the front side electrode structure. The effect is to blur images and decrease the limiting magnitude by about 0.5 magnitudes.
- **Flat field quality:** WF/PC-1 CCDs were chemically thinned devices and therefore varied in thickness across the field-of-view causing large features in the flat fields. WFPC2 CCDs are un-thinned and the intrinsic response is uniform to ~3% across the field.
- **DQE:** The WFPC2 CCDs have intrinsically lower QE than WF/PC-1 CCDs above 4800Å, which is due to attenuation by front side electrode structures.
- **Gain switch:** WF/PC-1 had only a single analog-to-digital converter gain setting of 8 e^- DN^{-1} which saturated at about 30,000e^-. Two gains are available with WFPC2: a 7 e^- DN^{-1} channel which gives reasonable sampling of the 5e^- read noise, and which saturates at about 27,000e^-, and a 14 e^- DN^{-1} channel which saturates at about 53,000e^- and extends the useful dynamic range.
- **Quantization:** The systematic analog-to-digital converter errors that were present in the low order bits on WF/PC-1 have been largely eliminated, contributing to a lower effective read noise in WFPC2.
- **Calibration Channel:** WF/PC-1 contained a solar UV flood channel which was physically in the location of the present WFPC2 calibration channel. This transmitted solar UV light into the camera to provide a UV flood capability.
- **Entry Port:** The WF/PC-1 camera was sealed by an afocal MgF_2 window immediately behind the shutter. The WFPC2 entry port is open.

- **Chronographic Capability:** WF/PC-1 contained a low reflectance spot on the pyramid (known as the Baum spot) which could be used to occult bright objects. This has been eliminated from WFPC2, since the spherical aberration severely reduces its utility.
- **Contamination Control:** Since launch, WF/PC-1 suffered from the accumulation of molecular contaminants on the cold (-87˚C) CCD windows. This molecular accumulation resulted in the loss of FUV (1150-2000Å) throughput and attenuation at wavelengths as long as 5000Å. Another feature of the contamination was the "measles" — multiple isolated patches of low volatility contamination on the CCD window. Measles were present even after decontamination cycles, when most of the accumulated molecular contaminants were boiled off by warming the CCDs. In addition to preventing UV imaging, these molecular contamination layers scattered light and seriously impacted the calibration of the instrument. WFPC2 has far less contamination than WF/PC-1 owing to pre-launch cleaning and bake-out procedures, careful design of venting paths to protect the optical bench area, and inclusion of Zeolite molecular absorbers in the design. There is now a decrease in throughput of about 30% per month at 1700Å, but monthly decontamination procedures completely remove this material. This throughput drop is also highly predictable and can be calibrated out during photometric analyses.

1.5 Organization of this Handbook

A description of the instrument is contained in Chapter 2. The filter set is described in Chapter 3. CCD performance is discussed in Chapter 4. A description of the Point Spread Function is given in Chapter 5. The details necessary to estimate exposure times are described in Chapter 6. A summary of observation strategies is given in Chapter 7. Data products, standard calibration methods, and calibration plans are summarized in Chapter 8. A complete list of references is given in Chapter 9.

This document summarizes the performance of the WFPC2 as known in June 2004 after nine years of on-orbit calibration. Observers are encouraged to contact the STScI Help Desk, or to consult the WFPC2 WWW pages (see Section 1.10 below).

HST may transition to use of two instead of three gyroscopes at some point in the future. The present Instrument Handbook describes the state of WFPC2 as used with three gyroscopes. For a discussion of how a decrease to two gyroscopes will affect some characteristics of WFPC2 observing, please refer to the separate Two-Gyro Handbook.

1.6 What's New in Version 6.0 for Cycle 11

Major revisions since Version 5.0 may be summarized as follows:

- Anomalies: Added information on the shutter anomaly, the ORIENT bug, and the FR533N anomaly.
- Dark Current Evolution: New information on the latest results throughout this section.
- Dithering: Updated information on dithering from the new Dithering Handbook throughout this section.
- CTE: Updated CTE monitor figure to reflect the latest results. Added section on mitigating CTE effects.
- Photometry: Updated photometry monitor figure to reflect the latest results.
- Calibration: Added sections on the "On The Fly Reprocessing System" and the "Cycle 10 Calibration Plan".
- Updated references and index.

1.7 What's New in Version 7.0 for Cycle 12

Major revisions since Version 6.0 may be summarized as follows:

- Serial Clocks: Added updated information on the CLOCKS=YES mode.
- Filter Wheel Anomaly: Added updated information on the status of this anomalous rotational offset for many WFPC2 filters.
- CTE and "Long vs. Short": Provided the most up-to-date correction formulae for the CTE effect; Presented the latest conclusions on the cause of the apparent "Long vs. Short" anomaly.
- ETC: Described the new options available in the on-line Exposure Time Calculator.
- Flat Fields: Described the latest flat field reference files and their improved accuracy.
- Calibration Accuracy: Updated the overall accuracies achievable with the WFPC2 calibration.
- Updated references and index.

1.8 What's New in Version 8.0 for Cycle 13

Major revisions since Version 7.0 may be summarized as follows:

- The Phase II proposal preparation tool RPS2 has been replaced with the Astronomer's Proposal Tool (APT). APT is a new suite of powerful tools, including the Visual Target Tuner (see Section 7.8.1), Exposure Time Calculators for all HST instruments, and all Phase II proposal tools that were previously handled by the RPS2 software. Details on APT can be found on our web site at:

http://apt.stsci.edu/

1.9 What's New in Version 9.0 for Cycle 14

Major revisions since Version 8.0 may be summarized as follows:

- Chapter 4.8, *Dark Backgrounds*, on page 87, Chapter 5.11, *Optical Distortion*, on page 143, and Chapter 7.6, *Dithering with WFPC2*, on page 208 have been updated with new information.

1.10 WFPC2 Handbook on the WWW

This Handbook will appear on the WFPC2 WWW pages accessible at:

http://www.stsci.edu/instruments/wfpc2/wfpc2_top.html

and will be updated as new information becomes available.

1.11 The Help Desk at STScI

STScI maintains a Help Desk whose staff quickly provide answers to any HST-related topic, including questions about WFPC2 and the Cycle 13 and 14 proposal process. The Help Desk staff has access to all of the resources available at the Institute. They maintain a database of frequently asked questions and answers, so that many questions can be answered immediately. The Help Desk staff can also provide copies of STScI documentation, in either hardcopy or electronic form, including Instrument Science Reports and Instrument Handbooks.

Questions sent to the Help Desk are usually answered within two business days. Usually, the Help Desk staff will reply with the answer to a

question, but occasionally they will need more time to investigate the answer. In these cases, they will reply with an estimate of the time needed to reply with the full answer.

We ask that you please send *all* initial inquiries to the Help Desk. If your question requires a WFPC2 Instrument Scientist to answer it, the Help Desk staff will put a WFPC2 Instrument Scientist in contact with you. By sending your request to the Help Desk, you are guaranteed that someone will provide a timely response.

To contact the Help Desk at STScI:

- **Send e-mail:** help@stsci.edu
- **Phone:** 1-410-338-1082

The Space Telescope European Coordinating Facility (ST-ECF) also maintains a Help Desk. European users should generally contact the ST-ECF for help; all other users should contact STScI.

To contact the ST-ECF Help Desk in Europe:

- **Send e-mail:** stdesk@eso.org.

1.12 Further Information

The material contained in this Handbook is derived from ground tests and design information obtained by the IDT and the engineering team at JPL, and from on-orbit measurements. Other sources of information are listed below. For a complete reference list please see "References" on page 375.

- *HST Phase II Proposal Instructions*, available only online at:

  `http://www.stsci.edu/public/p2pi.html`[3] and

  `http://www.stsci.edu/hst/programs/`

- *HST Data Handbook*, (Version 4.0, January 2002)

  `http://www.stsci.edu/instruments/wfpc2/Wfpc2_dhb/WFPC2_longdhbcover.html`[3].

- *Calibrating Hubble Space Telescope: Post Service Mission* (1995),

  `http://www.stsci.edu/instruments/wfpc2/Wfpc2_serv/post_serv.html`[3]

- *The 1997 HST Calibration Workshop* (1997), available only online:

  `http://www.stsci.edu/stsci/meetings/cal97/proceedings.html`[3].

- *The 2002 HST Calibration Workshop* (2002), available only online:

3. These documents may be requested by e-mail from `help@stsci.edu`.

http://www.stsci.edu/hst/HST_overview/documents/calworkshop/workshop2002/[3].

- *Proceedings of the CTE Workshop* (2000)

  http://www.stsci.edu/hst/acs/performance/cte_workgroup/cte_papers.html

- *STSDAS Users Guide*, (April 1994, version 1.3).[3]
- *The Reduction of WF/PC Camera Images,* Lauer, T., P.A.S.P. 101, 445 (1989).
- *The Imaging Performance of the Hubble Space Telescope,* Burrows, C. J., et. al., Ap. J. Lett., 369, L21 (1991).
- Interface Control Document (ICD) 19, "PODPS to STSDAS"
- Interface Control Document (ICD) 47, "PODPS to CDBS"
- *The Wide Field/Planetary Camera in The Space Telescope Observatory,* J. Westphal and the WF/PC-1 IDT, IAU 18th General Assembly, Patras, NASA CP-2244 (1982).
- *The WFPC2 Science Calibration Report,* Pre-launch Version 1.2, J. Trauger, editor, (1993). [IDT calibration report]
- *White Paper for WFPC2 Far-Ultraviolet Science,* J. T. Clarke and the WFPC2 IDT (1992)[3].
- *The Performance and Calibration of WFPC2 on the Hubble Space Telescope,* Holtzman, J., et al., P.A.S.P., 107, 156 (1995).
- *The Photometric Performance and Calibration of WFPC2,* Holtzman, J., et al., P.A.S.P., 107, 1065 (1995).
- *Charge-Transfer Efficiency of WFPC2,* B. Whitmore, I. Heyer, S. Casertano, PASP, 111, 1559 (1999).
- The Institute's WFPC2 World Wide Web page at address:

  http://www.stsci.edu/instruments/wfpc2/wfpc2_top.html

- The Institute's WFPC2 Space Telescope Analysis Newsletter (STAN), which is distributed monthly via e-mail, and provides notification of any changes in the instrument or its calibration. To subscribe, send e-mail to help@stsci.edu. Previous issues are at:

  http://www.stsci.edu/instruments/wfpc2/wfpc2_stan.html

CHAPTER 2:

Instrument Description

In this chapter . . .

2.1 Science Objectives

The scientific objective of the WFPC2 is to provide photometrically and geometrically accurate images of astronomical objects over a relatively wide field-of-view (FOV), with high angular resolution across a broad range of wavelengths.

WFPC2 was designed with a goal of l% rms photometric accuracy, which means that the relative response in all 800x800 pixels per CCD must be known to better than 1% through each filter, and that standard calibrations be done at this level. The absolute calibration in the primary broadband photometric filters is accurate at around the 2% level, and there are on-going efforts to further improve the accuracy. Success in this area is dependent on the stability of all elements in the optical train, particularly the CCDs and filters.

The narrow point spread function is essential to all science programs being conducted with the WFPC2, because it allows one to both go deeper than ground based imagery, and to resolve smaller scale structure with higher reliability and dynamic range. Further, many of the scientific goals which originally justified the HST require that these high quality images be obtained across a wide field-of-view. The Cepheid distance scale program, for example, cannot be accomplished without a relatively wide field-of-view.

A unique capability of the WFPC2 is that it provides a sustained, high resolution, wide field imaging capability in the vacuum ultraviolet. Considerable effort has been expended to assure that this capability is maintained. Broad passband far-UV filters, including a Sodium Wood's filter, are included. The Wood's filter has superb red blocking characteristics. Photometry at wavelengths short of 3000Å is improved through the control of internal molecular contamination sources and the ability to put the CCDs through warm-up decontamination cycles without loss of prior calibrations.

2.2 WFPC2 Configuration, Field-of-View, and Resolution

The field-of-view and angular resolution of the wide field and planetary camera is split up as follows (see Chapter 4 for more details on CCDs):

Table 2.1: Summary of Camera Format.

Camera	Pixel and CCD Format	Field-of-View	Pixel Scale	F/ratio
Wide Field	800 × 800 × 3 CCDs	2.5′ × 2.5′ (L-shaped)	~100 milli- arcseconds	12.9
Planetary	800 × 800 × 1 CCD	35″ × 35″	~46 milli- arcseconds	28.3

Figure 2.1: Wide Field Planetary Camera 2 Concept Illustration. The calibration channel, and pick-off mirror mechanisms are not shown.

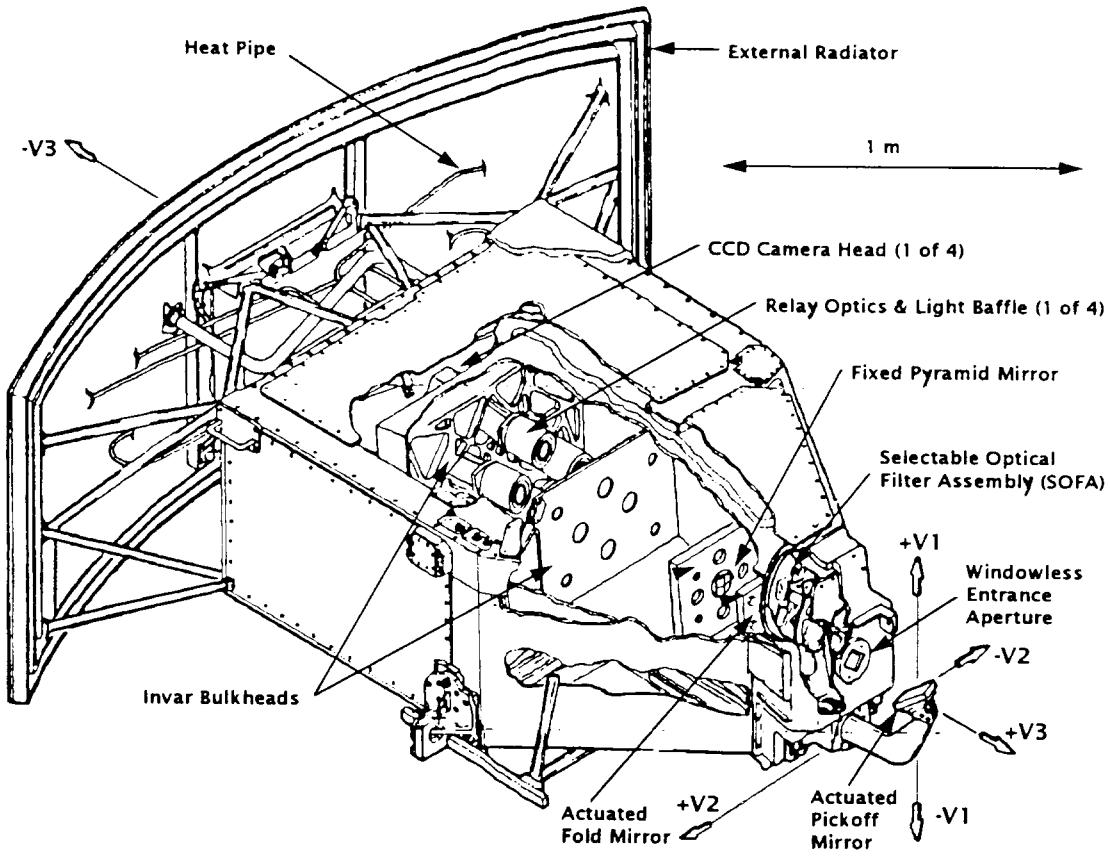

2.3 Overall Instrument Description

The Wide-Field and Planetary Camera 2, illustrated in Figure 2.1 on page 25, occupies the only radial bay allocated to a scientific instrument. Its field-of-view is centered on the optical axis of the telescope and it therefore receives the highest quality images. The three Wide-Field Cameras (WFC) at F/12.9 provide an "L" shaped field-of-view of 2.5x2.5 arcminutes with each 15 μm detector pixel subtending 0.10″ on the sky. In the Planetary Camera (PC) at F/28.3, the field-of-view is 35″ x 35″, and each pixel subtends 0.046″. The three WFCs undersample the point spread function of the Optical Telescope Assembly (OTA) by a factor of 4 at 5800Å in order to provide an adequate field-of-view for studying galaxies, clusters of galaxies, etc. The PC resolution is over two times higher. Its field-of-view is adequate to provide full-disk images of all the planets

except Jupiter (which is 47″ in maximum diameter) and Venus (which is not normally observable with HST). The PC has numerous extra-solar applications, including studies of galactic and extra-galactic objects in which both high angular resolution and excellent sensitivity are needed. In addition to functioning as the prime instrument, the WFPC2 can be used for parallel observations.

Figure 2.2 on page 26 shows the optical arrangement (not to scale) of the WFPC2. The central portion of the OTA F/24 beam is intercepted by a steerable pick-off mirror attached to the WFPC2, and is diverted through an open entry port into the instrument. The beam then passes through a shutter and filters. A total of 48 spectral elements and polarizers are contained in an assembly of 12 filter wheels. Then the light falls onto a shallow-angle, four-faceted pyramid located at the aberrated OTA focus, each face of the pyramid being a concave spherical surface. The pyramid divides the OTA image of the sky into four parts. After leaving the pyramid, each quarter of the full field-of-view is relayed by an optical flat to a Cassegrain relay that forms a second field image on a charge-coupled device (CCD) of 800x800 pixels. Each detector is housed in a cell that is sealed by a MgF_2 window. This window is figured to serve as a field flattener.

The aberrated HST wave front is corrected by introducing an equal but opposite error in each of the four Cassegrain relays. An image of the HST primary mirror is formed on the secondary mirrors in the Cassegrain relays. (The fold mirror in the PC channel has a small curvature to ensure this.) The spherical aberration from the telescope's primary mirror is corrected on these secondary mirrors, which are extremely aspheric.

Figure 2.2: WFPC2 Optical Configuration.

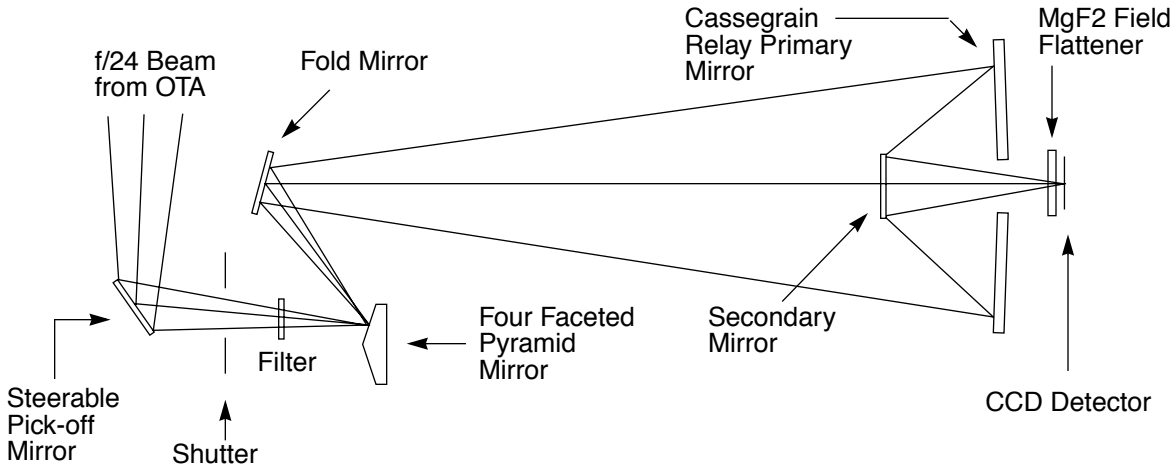

The single most critical and challenging technical aspect of applying a correction is assuring exact alignment of the WFPC2 pupils with the pupil of the HST. If the image of the HST primary does not align exactly with the repeater secondary, the aberrations no longer cancel, leading to a wavefront error and comatic images. An error of only 2% of the pupil diameter would produce a wavefront error of 1/6 wave, leading to degraded spatial resolution and a loss of about 1 magnitude in sensitivity to faint point sources. This error corresponds to mechanical tolerances of only a few microns in the tip/tilt motion of the pick-off mirror, the pyramid, and the fold mirrors.

Mechanisms inside WFPC2 allow optical alignment on-orbit; these are necessary to insure correction of the OTA spherical aberration. The beam alignment is set with a combination of the steerable pick-off mirror and actuated fold mirrors in cameras PC1, WF3 and WF4. The 47° degree pick-off mirror has two-axis tilt capabilities provided by stepper motors and flexure linkages, to compensate for uncertainties in our knowledge of HST's latch positions (i.e., instrument tilt with respect to the HST optical axis). These latch uncertainties would be insignificant in an unaberrated telescope, but must be compensated for in a corrective optical system. In addition, three of the four fold mirrors, internal to the WFPC2 optical bench, have limited two-axis tilt motions provided by electrostrictive ceramic actuators and invar flexure mountings. Fold mirrors for the PC1, WF3, and WF4 cameras are articulated, while the WF2 fold mirror has a fixed invar mounting. A combination of the pick-off mirror and fold mirror actuators has allowed us to correct for pupil image misalignments in all four cameras. Since the initial alignment, stability has been such that mirror adjustments have not been necessary. The mechanisms are not available for GO commanding.

The WFPC2 pyramid cannot be focused or rotated. WFPC2 is focused by moving the OTA secondary mirror, and then other science instruments are adjusted to achieve a common focus for all the HST instruments.

The four CCDs provide a 1600 x 1600 pixel field-format; three of the 800 x 800 CCDs have 0.1″ pixels (WFC), and one has 0.046″ pixels (PC). The CCDs are physically oriented and clocked so that the pixel read-out direction is rotated approximately 90° in succession (see Figure 1.1 on page 2). The (1,1) pixel of each CCD array is thereby located near the apex of the pyramid. As a registration aid in assembling the four frames into a single picture, a light can be turned on at the pyramid to form a series of eleven fixed artificial "stars" (known as Kelsall spots or K-spots) along the boundaries of each of the quadrants. This calibration is normally done in a separate exposure. The K-spot images are aberrated and similar in appearance to the uncorrected HST PSF. The relative alignment of the four channels has been more accurately determined from star fields, and is stable over long periods, but the K-Spot images are useful for verifying the stability.

Figure 2.3: Cooled Sensor Assembly.

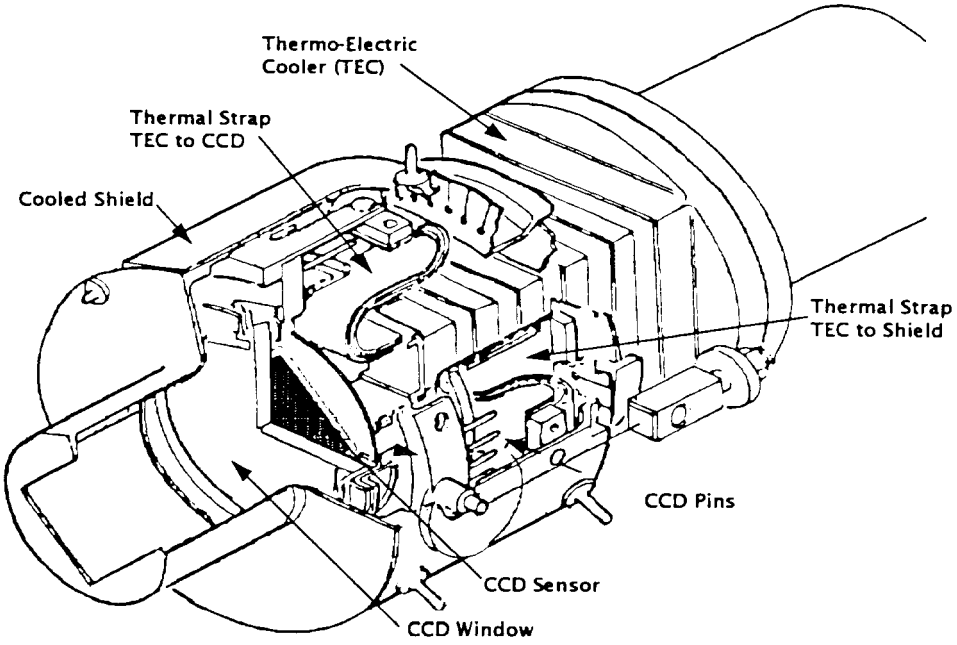

Each CCD is a thick front side-illuminated silicon sensor, fabricated by Loral Aerospace. Each CCD is mounted on a header, is hermetically packaged in a ceramic-tube body that is filled with 1.1 atmosphere of Argon (to prevent degradation of the UV sensitive phosphor), and then is sealed with a MgF_2 field flattener. This complete cell is connected with compliant silver straps to the cold junction of a thermo-electric cooler (TEC). The hot junction of the TEC is connected to the radial bay external radiator by an ammonia heat pipe. This sensor-head assembly is shown in Figure 2.3 on page 28. During operation, each TEC cools its sensor package to suppress dark current in the CCD.

2.4 Quantum Efficiency

The WFPC2 provides useful sensitivity from 1150Å to 11000Å in each detector. The overall spectral response of the system is shown in Figure 2.4 on page 29 (not including filter transmissions). The curves represent the probability that a photon that enters the 2.4m diameter HST aperture at a field position near the center of one of the detectors will pass all the aperture obscurations, reflect from all the mirrors, and eventually be detected as an electron in the CCD. The throughput of the system

combined with each filter is tabulated in Table 6.1 on page 154 and also shown in Appendix A.

Figure 2.4: WFPC2 + OTA System Throughput. This is the current SYNPHOT model (June 2001) as determined by on-orbit measurements.

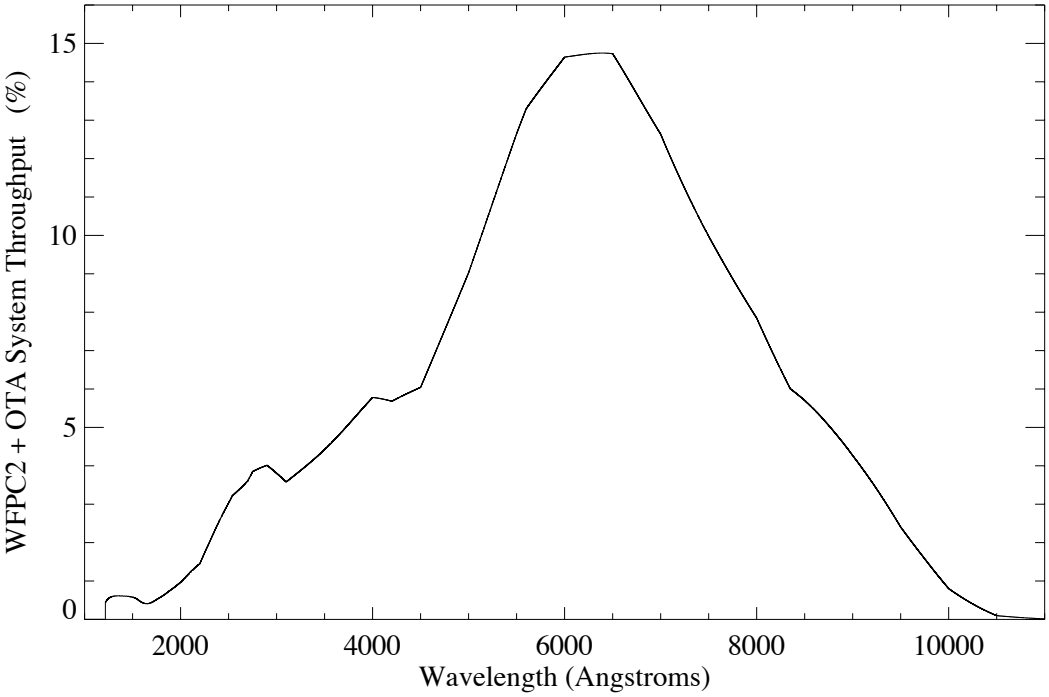

The visible and red sensitivity of the WFPC2 is a property of the silicon from which the CCDs are fabricated. To achieve good ultraviolet response, each CCD is coated with a thin film of Lumogen, a phosphor. Lumogen converts photons with wavelengths less than 4800Å into visible photons with wavelengths between 5100Å and 5800Å, which the CCD detects with good sensitivity. Beyond 4800Å, the Lumogen becomes transparent and acts to some degree as an anti-reflection coating. Thus, the full wavelength response is determined by the MgF_2 field flattener cutoff on the short-wavelength end and the silicon band-gap in the infrared at 1.1 eV (~11000Å).

With the WFPC2 CCD sensors, images may be obtained in any spectral region defined by the chosen filter with high photometric quality, wide dynamic range, and excellent spatial resolution. The bright end of the dynamic range is limited by the 0.11 seconds minimum exposure time, and by the saturation level of the analog-to-digital converter (ADC) at the chosen gain, which is roughly 53000 (gain=14, though called ATD-GAIN=15 when specifying the Phase II) or 27000e^- (gain=7) per pixel. The maximum signal-to-noise ratio corresponding to a fully exposed pixel will be about 230. The faint end of the dynamic range is limited by

photon noise, instrument read noise and, for the wide-band visible and infra-red filters, the sky background.

Table 2.2 on page 30 gives characteristic values of the expected dynamic range in visual magnitudes for point sources. The minimum brightness is given for an integrated S/N ratio of 3, and the maximum corresponds to CCD ADC saturation (selected as 53000e^-). The quoted values assume an effective bandwidth of 1000Å at about 5600Å (filter F569W). The planets and many other resolved sources are observable in this filter with short exposures even if their integrated brightness exceeds the 8.4 magnitude limit.

Table 2.2: WFPC2 Dynamic Range in a Single Exposure.

Configuration	Exposure (seconds)	Min. V Magnitude	Max. V Magnitude
Wide Field	0.11	8.82	17.83
Wide Field	3000.	19.91	28.19
Planetary	0.11	8.40	17.47
Planetary	3000.	19.49	28.25

2.5 Shutter

The shutter is a two-blade mechanism used to control the duration of the exposure. A listing of the possible exposure times is contained in Table 2.3 on page 32. These are the only exposure times which can be commanded. Current policy is to round down non-valid exposure times to the next valid value. However, an exposure time shorter than the minimum allowed (0.11 seconds) is, instead, rounded up to this minimum value.

Some exposures should be split into two (CR-SPLIT) in order to allow cosmic ray events to be removed in post-processing. By default, exposures of more than 10 minutes are CR-SPLIT. If an exposure is CR-SPLIT, the exposure time is divided into two fractions and then rounded down. Normally the fractional split is 50%/50% but, unless constrained by the user with CR-TOLERANCE, the ratio may be up to 70%/30%, as allowed by the default CR-TOLERANCE=0.2. Note that some exposure times in the table do not correspond to commandable values when halved. In preparing a proposal containing an exposure that is to be CR-SPLIT, the simplest procedure to use in order to be sure of a given total exposure time, is to enter double a legal value, and impose CR-TOLERANCE=0.

For the shortest exposure times, it is possible to reconstruct the actual time of flight of the shutter blades. Encoder disks, attached to the shutter blade arms, are timed by means of a photo-transistor. The maximum error

is 5 milliseconds. The necessary information is contained in the WFPC2 engineering data stream, however, this information is not in the processed science header.

Diffraction effects from the edges of the shutter blades affect the point spread function for very short exposures. It is advisable to use exposure times greater than 0.2 seconds when obtaining point spread functions in support of long exposure observations (see the WF/PC-1 IDT OV/SV Report, Chapter 9, for further discussion in the spherically aberrated case).

The control of the initial opening of the WFPC2 shutter during an observation is held by the internal WFPC2 microprocessor in all cases. However, control over closing of the shutter is held by the microprocessor only for exposures less than 180 seconds in duration. For longer exposures, control passes to the Application Processor (AP-17) in the NSSC-1 spacecraft computer. The consequence of this arrangement is that loss of guide star lock will result in the WFPC2 shutter being closed only for those observations with planned durations of 180 seconds or longer. The AP-17 always controls the shutter closing if the serial clocks are enabled during the exposure (CLOCKS=YES), which then has a minimum planned duration of 1 second, and exposures are rounded to the nearest second. If guide star lock is reacquired prior to the end of the planned observation time, the shutter will reopen to obtain a portion of the planned integration. As discussed in the next section, CLOCKS=YES should generally not be used with exposures shorter than 30 sec., if 1% or better photometric accuracy is needed.

Table 2.3: Quantized Exposure Times (Seconds). Exposure times that should not be used for CLOCKS=YES are shaded and flagged with table footnote (a). Exposure times where the PSF is affected by the shutter blade flight time are underlined and flagged with table footnote (b). Exposures normally without loss of lock checking are in italics. Times that are CR-Split by default are in boldface; exposures longer than 5400 seconds must be CR-split. Exposures that take more than one orbit, even when CR-split, are not normally accessible to GOs and are crossed out and flagged with table footnote (c).

0.11 [a,b]	*0.4* [a]	*2.0*	*10.*	*40.*	200.	**900.**	**1900.**	**2900.**	**3900.**	**4900.**	**6200.**	~~**15000**~~[c]
0.12 [a,b]	*0.5* [a]	*2.3* [a]	*12.*	*50.*	230.	**1000.**	**2000.**	**3000.**	**4000.**	**5000.**	**6400.**	~~**20000.**~~[c]
0.14 [a,b]	*0.6* [a]	*2.6* [a]	*14.*	*60.*	260.	**1100.**	**2100.**	**3100.**	**4100.**	**5100.**	**6600.**	~~**25000.**~~[c]
0.16 [a,b]	*0.7* [a]	*3.0*	*16.*	*70.*	300.	**1200.**	**2200.**	**3200.**	**4200.**	**5200.**	**6800.**	~~**30000.**~~[c]
0.18 [a,b]	*0.8* [a]	*3.5* [a]	*18.*	*80.*	350.	**1300.**	**2300.**	**3300.**	**4300.**	**5300.**	**7000.**	~~**40000.**~~[c]
0.20 [a,b]	*1.0*	*4.0*	*20.*	*100.*	400.	**1400.**	**2400.**	**3400.**	**4400.**	**5400.**	**7500.**	~~**50000.**~~[c]
0.23 [a]	*1.2* [a]	*5.0*	*23.*	*120.*	500.	**1500.**	**2500.**	**3500.**	**4500.**	**5500.**	**8000.**	~~**75000.**~~[c]
0.26 [a]	*1.4* [a]	*6.0*	*26.*	*140.*	600.	**1600.**	**2600.**	**3600.**	**4600.**	**5600.**	**8500.**	~~**100000.**~~[c]
0.30 [a]	*1.6* [a]	*7.0*	*30.*	*160.*	**700.**	**1700.**	**2700.**	**3700.**	**4700.**	**5800.**	**9000.**	
0.35 [a]	*1.8* [a]	*8.0*	*35.*	180.	**800.**	**1800.**	**2800.**	**3800.**	**4800.**	**6000.**	**10000.**	

a. Exposure times that should not be used for CLOCKS=YES

b. Exposure times where the PSF is significantly affected by the shutter blade flight time

c. Exposure times that take more than one orbit, even when CR-split; these are not normally accessible to GOs

In August 2000, WFPC2 began experiencing occasional anomalies in the operation of the shutter mechanism. The problem was traced to an encoder wheel and photo transistor assembly that serves to sense the position of the "A" shutter blade. This sensor is polled by the WFPC2 computer prior to each exposure. Later, in October 2000, we began seeing a more serious problem where multiple mis-readings would lead to the "A" shutter blade attempting to close even though the "B" blade was already closed, hence causing a collision of the two shutter blades. Since there was some potential for this to damage the mechanism, we ceased WFPC2 observations for several days until corrective action could be taken. On November 8, 2000, we modified the WFPC2 microprocessor software to activate the position sensor 10 milliseconds earlier, thus giving it more time to respond prior to being read by the microprocessor. An extensive series of tests were run on the shutter after the installation of the software patch, and no unexpected side effects or abnormalities in its operation were seen. No further incidences of the anomaly have been seen as of this writing (June 2004).

The anomaly affected only about 0.3% of the images from August to October 2000. In most cases the shutter failed to open, producing a blank image. A few images were also seen with trailed targets, due to the shutter

being open prior to the nominal exposure start, or due to the shutter remaining open past the nominal exposure end.

As of this writing the exact cause of the anomaly is still not entirely clear. Much evidence points to radiation damage to the photo transistor, causing its response time to slow, while other evidence points to mechanical wear in the encoder wheel linkage, leading to misalignment of the wheel relative to the photo transistor. In most scenarios the software patch should permanently fix the problem, but there is always some small chance it will reappear.

2.6 Serial Clocks

The serial transfer registers of the CCDs can be kept running during an exposure (CLOCKS=YES), or run only during the readout (CLOCKS=NO, the default).

The serial clocks are sometimes used on very bright targets where extensive blooming up and down the CCD columns is expected. CLOCKS=YES causes charge which blooms to the ends of the CCD to be read out and disposed of, thus preventing it from flowing back into the image. They will be useful when any single CCD column contains in excess of $\sim 10^8$ electrons. Note that the serial clocks do not actually suppress the blooming process, instead they merely remove any charge that blooms to the top or bottom of the CCD.

Although only 6% of all WFPC2 observations have been obtained with CLOCKS=YES, this mode has now been calibrated using observations of the standard star GRW+70D5824 (HIC 66578; V=12.77; B-V=-0.09) [proposal ID: 9252]. The comparison between count rates of the standard star for different filters obtained with CLOCKS=YES and CLOCKS=NO indicates that the normal WFPC2 photometric calibration with CLOCKS=NO is sufficient for data obtained with CLOCKS=YES and CLOCKS=NO. The count rates are generally within 2% (0.02 mag) peak to peak of each other with the associated errors being quite small.

Analysis of darks indicate that the count levels for the CLOCKS=YES darks are similar to those for the CLOCKS=NO darks. However, when the 1 minute difference in exposure time between the CLOCKS=YES and CLOCKS=NO dark is taken into account (see below), the CLOCKS=YES dark current is found to be a few percent higher than the CLOCKS=NO dark current. Since the pipeline dark reference files for CLOCKS=YES mode have always been generated from CLOCKS=NO darks (minimizing the number of calibration observations), the difference in dark current may slightly affect the calibration of some CLOCKS=YES observations. In general, it now appears that there are no major artifacts, induced noise, or

cross talk when obtaining data with CLOCKS=YES (Schultz, Baggett & Biretta 2002).

For most circumstances, we recommend CLOCKS=NO. The reasons for this recommendation are:

1. As stated above, CLOCKS=YES is not widely used. Although the consistency of this mode has been examined for a bright star, we cannot guarantee that there are no minor artifacts for very faint targets.
2. The shutter open time when CLOCKS=YES can have significant errors. In this mode, there are delays of up to 0.25 seconds in opening the shutter (which are not present when CLOCKS=NO). This means that for exposures of less than ~30 seconds, there may be photometric errors greater that 1%, unless special precautions are taken in the data reduction. Furthermore, if a non-integral exposure time is specified in the proposal, it will be rounded to the nearest second. See below for details.

On the other hand:

1. We do advise CLOCKS=YES if you expect star images to be so saturated that a significant amount of charge will bleed off the chip during the exposure. This would mean that you expect much more than 10^8 electrons from at least one star in the exposure (more than 1000 pixels would be saturated). Without CLOCKS=YES the bleed-off charge may corrupt other parts of the image.
2. One advantage of CLOCKS=YES is that the overhead time is 1 minute less for exposures longer than 180 seconds. This can be significant if you have a large number of exposure times in the 3 to 10 minute range.
3. Unlike the original WF/PC-1, we do not see a significant variation of WFPC2 dark level with CLOCKS=YES.

In summary:

0-0.8 sec	CLOCKS=NO is required.
1 - 30 sec	Use CLOCKS=NO (or attempt photometric corrections during the analysis of the data).
20 - 180 sec	Use CLOCKS=NO unless more than 10^8 detected electrons from a single star are expected.
180+ sec	Use CLOCKS=NO unless more than 10^8 detected electrons are expected, or if you need to save 1 minute of overhead.

While exposure times are corrupted for CLOCKS=YES, and are not accurately reported in the image headers, correct values can be computed. Details are as follows:

1. Non-integer exposure times <3 minutes are rounded to the nearest integer (e.g., 1.2 sec and 1.4 sec will actually be 1.0 sec long, 3.5 sec exposures take 4.0 sec). This round off is due to the way the spacecraft computer monitors the take-data flag (AP-17 uses its own integer-based timecode). This rounding is reflected properly in the header keywords (keywords UEXPODUR, EXPSTART, EXPEND, EXPTIME, and EXPFLAG in the `.c0h` file headers, or UEXPODUR and CMD_EXP in the `.shh` headers).
2. All CLOCKS=YES exposures are also shortened by either 0.125 or 0.250 seconds. This decrease in exposure time is ***not*** reflected in the file headers; the amount depends upon which shutter blade was in place at the start of the exposure. The decrease in exposure time is due to the manner in which the application processor (AP-17) in the spacecraft computer operates the shutter blades. When CLOCKS=NO (default), the WFPC2 microprocessor opens the shutter, the AP-17 closes the shutter, and the exposure time is as requested. However, with CLOCKS=YES, the AP-17 opens the shutter, first blade A, then blade B. If blade A is closed at the start of the exposure, the actual exposure begins 0.125 seconds after the AP-17 issues the blade command. If blade B is closed at the exposure start, the exposure starts 0.250 seconds later (after the AP-17 sends the open-A command followed by open-B). The shutter in place at exposure start is given in the SHUTTER keyword in the `.c0h` file.

2.7 Overhead Times

Efficient use of the WFPC2 requires an understanding of the overhead times of the instrument. In this section, the various causes of overhead are presented in a manner that should allow the user to make a fairly accurate prediction of the cost in time of a given sequence of exposures. This information is provided for completeness and background. Guidelines given in the Phase I and Phase II Proposal Instructions should be followed to develop Phase I and II proposals, respectively. (See also Section 6.6.)

1. Telescope alignments. A telescope alignment is, in practice, a set of images uninterrupted by target position change or the end of orbit. The start of an alignment requires 1 minute overhead in order to synchronize timing with a major frame (all commands to the instrument take place on major frames which last 1 minute). The end of alignment uses one minute for tape recorder overhead. If images are

requested in real-time, another 2 minutes must be added to the alignment end. There are additional overheads at the start of each target visibility period associated with guide star acquisition (currently 6 minutes), or reacquisition (currently 5 minutes).

2. Filter changes. A filter change requires at least 1 minute, the use of 2 filters requires 2 minutes of overhead. Furthermore, since the filter history is lost across telescope alignments, at least one minute is spent on selecting the filter at an alignment start, regardless of the filter in place before the alignment.

3. CCD clearing. Clearing the CCD is done before every exposure and requires 16 seconds. This time is part of the first major frame of the exposure. Therefore, time taken for a given exposure (excluding all other overheads) is the exposure time plus 16 seconds rounded up to the next integral minute. For example, all legal exposure times up to 40 seconds inclusive cost one minute.

4. CCD readout. The readout time for an exposure is one minute. An additional minute is required for exposures 180 sec. or longer, taken with CLOCKS=NO. This extra minute can be saved by using CLOCKS=YES, but this is not generally recommended (see Section 2.6). If the exposure is CR-SPLIT, the readout overheads (calculated with the split exposure times) are of course doubled. There is normally no overhead time advantage in reading out a subset of the CCDs. The exception is if the WFPC2 readout occurs in parallel with the operation of a second instrument, when at least 2 minutes is required to read all 4 CCDs.

5. Dithering. Dithering is the use of small spatial displacements to allow better removal of chip defects and/or the reconstruction of sub-pixel resolution. During Phase II the user will be given access to “canned” dithering routines which will allow him/her to avoid many of the tricky details involved in planning spatial scans. The spatial offsets will require additional overheads, which must be included. POS-TARG special requirements can also be used to generate offsets.

6. During early proposal Cycles “spatial scans” were used to effect series of offsets, but they are no longer available, and have been replaced with the “dither” commands. The overhead of a spatial scan was similar to that of a sequence of images taken in one alignment; however, at least one minute of overhead was required for each change in pointing. Furthermore, an extra minute of overhead was incurred at the end of the scan, and typically about 1 minute of overhead was used at the beginning of the scan positioning the first image.

In summary, it is not possible to schedule exposures in different filters less than 3 minutes apart: commands to the WFPC2 are processed at

spacecraft “major frame” intervals of one minute. A typical sequence of events is:

- Return filter wheel to “clear” position, select new filter (1 min).
- Expose image (minimum 1 min).
- Readout CCDs (1 or 2 min depending on exposure time and CLOCKS). Hence a simple exposure requires a minimum of 3 minutes.

Table 2.4: Instrument Overheads. The first and last exposures of an alignment contain extra overheads.

Overhead Type	Time (min.)	Overhead
First exposure	1	Major frame uncertainty, clock synchronization
First exposure	1	To put in initial filter
Per image:	1	Per filter change
Per image:	int(t)+1	t=(shutter-open time in seconds +16 seconds)/60
Per image:	1	If CLOCKS=NO (default) and exposure ≥180 sec
Per image:	1	Readout
Per image:	1	If image done in parallel with another instrument
Last exposure	1	Data recorder overhead
Last exposure	2	If data requested down in real-time
Last exposure	1	If a scan was done

2.8 CCD Orientation and Readout

The relation between the rows and columns for the four CCDs is shown in Figure 1.1 on page 2, where the short arrows on each CCD are placed near pixel (1,1) and point in the -Y (readout) direction. Each CCD’s axes are defined by a 90˚ rotation from the adjacent CCD. If a 4-CCD image is taken and then each subimage is displayed with rows in the “X” direction and columns in the “Y” direction, each successive display would appear rotated by 90˚ from its predecessor.

Table 2.5: Inner Field Edges. The CCD X,Y (Column, Row) numbers given vary at the 1-2 pixel level because of bending and tilting of the field edge in detector coordinates due to the camera geometric distortions.

Camera	Start Vignetted Field (Zero Illumination)	50% Illumination	Start Unvignetted Field (100% Illumination)
PC1	X>0 and Y>8	X>44 and Y>52	X>88 and Y>96
WF2	X>26 and Y>6	X>46 and Y>26	X>66 and Y>46
WF3	X>10 and Y>27	X>30 and Y>47	X>50 and Y>67
WF4	X>23 and Y>24	X>43 and Y>44	X>63 and Y>64

Figure 1.1 on page 2 also illustrates the projected orientation of the WFPC2 CCDs onto the sky. The beam is split between the four cameras by a pyramid-shaped mirror in the aberrated HST focal plane. In an effort to insure images from the four CCDs can be reassembled into a single image without gaps, there is a small overlap region on the sky between each CCD and its neighbors (see also Figure 3.12 on page 76). On the CCDs this region appears as a blank "shadow" region along the X~0 and Y~0 edges of each CCD; the exact limits of this region are given in Table 2.5 on page 38 for each CCD. Because the OTA beam is aberrated at the pyramid mirror, the edges of the shadow region are not sharp, but instead there is a gradual transition from zero to full illumination on each CCD. The width of this vignetted region is essentially that of the aberrated OTA beam (~5″). Table 2.5 on page 38 gives approximate limits of this vignetted region on each CCD. Note that astronomical sources in the vignetted region are imaged onto two or more CCDs.

The WFPC2 has two readout formats: full single pixel resolution (FULL Mode), and 2x2 pixel summation (AREA Mode which is obtained by specifying the optional parameter SUM=2x2 as described in the Proposal Instructions). Each line of science data is started with two words of engineering data, followed by 800 (FULL) or 400 (AREA) 16-bit positive numbers as read from the CCDs (with 12 significant bits). In FULL Mode the CCD pixels are followed by 11 "bias" words ("over-clocked" pixels), yielding a total of 813 words per line for 800 lines. In AREA Mode, there are 14 bias words giving a total of 416 words per line for 400 lines. Either pixel format may be used to read out the WFC or PC. These outputs are reformatted into the science image and extracted engineering (over-clocked) data files during processing in the HST ground system prior to delivery to the observer. *Note that calibration support for AREA Mode data has been curtailed since Cycle 10, since this mode is very seldom used.*

The advantage of the AREA Mode (2x2) on-chip pixel summation is that readout noise is maintained at 5 e^- RMS for the summed (i.e., larger) pixels. This pixel summation is useful for some photometric observations

of extended sources particularly in the UV. Note, however, that cosmic ray removal is more difficult in AREA Mode.

The readout direction along the columns of each CCD is indicated by the small arrows near the center of each camera field in Figure 1.1 on page 2 (see also Figure 3.12 on page 76). Columns and rows are parallel and orthogonal to the arrow, respectively. Each CCD is read out from the corner nearest the center of the diagram, with column (pixel) and row (line) numbers increasing from the diagram center. In a saturated exposure, blooming will occur almost exclusively along the columns because of the MPP operating mode of the CCDs. Diffraction spikes caused by the Optical Telescope Assembly and by the internal Cassegrain optics of the WFPC2 are at 45˚ to the edges of the CCDs. Unless specified otherwise in the Phase II proposal, the default pointing position when all 4 CCDs are used is on WF3, approximately 10″ along each axis from the origin (WFALL aperture, see Table 3.14 on page 74).

Observations which require only the field-of-view of a single CCD are best made with the target placed near the center of a single CCD rather than near the center of the 4 CCD mosaic. This results in a marginally better point spread function, and avoids photometric, astrometric, and cosmetic problems in the vicinity of the target caused by the overlap of the cameras. Even so, for such observations the default operational mode is to read out all four CCDs. This policy has resulted in serendipitous discoveries, and sometimes the recovery of useful observations despite pointing or coordinate errors.

On the other hand, any combination of 1, 2 or 3 CCDs may be read out in numerical order (as specified in the Proposal Instructions). This partial readout capability is not generally available to GOs, although it can be used if data volume constraints mandate it, after discussion with the WFPC2 instrument scientists. It does not result in a decrease in the readout overhead time but does conserve space on the HST on-board science data recorders. This was especially useful with the initial science *tape* recorder, which had a capacity slightly over 7 full (4-CCD) WFPC2 observations or 18 single CCD WFPC2 observations on a single tape recorder side (of two sides). Readout of only a subset of the WFPC2 CCDs, or use of AREA mode, was advantageous when many frames needed to be obtained in rapid succession. However, the new Solid State Recorders installed during the 1997 and 1999 servicing missions are capable of holding well over one hundred 4-CCD WFPC2 images. This capability was phased in during Cycle 7, and has lead to relaxation of the above data rate restrictions.

Multiple exposures may be obtained with or without interleaved spacecraft repointings and filter changes without reading the CCDs (READ=NO). These would then be followed by a readout (READ=YES). Note that WFPC2 must be read out at least once per orbit.

2.9 Calibration Channel

An internal flat field system provides reference flat field images over the spectral range of WFPC2. These are provided by a "calibration channel" optical system mounted outside the main shroud of WFPC2. The system consists of a series of lamps and diffusers, and a flip mirror which directs the beam into the WFPC2 entrance aperture. The lamp set contains Tungsten incandescent lamps with spectrum shaping glass filters and a Deuterium UV lamp. The flat field illumination pattern is fairly uniform for wavelengths beyond about 1600Å. Short of 1600Å the flat field is distorted due to refractive MgF_2 optics. In practice, the flat fields used routinely to calibrate WFPC2 data have been generated by combining flats taken with an external stimulus in thermal vacuum testing with Earth "streak" (unpointed) flats to give the low frequency terms in the OTA illumination pattern. The calibration channel is used primarily to check for internal instrumental stability.

CHAPTER 3:

Optical Filters

In this chapter . . .

3.1 Introduction

This chapter describes the overall design of the WPFC2 filter set. Further information on individual filter bandpasses and their characteristic wavelengths may be found in Section 6.1 and Appendix A of this Handbook.

A set of 48 filters are included in WFPC2 with the following features:

1. It approximately replicates the WF/PC-1 "UBVRI" photometry series.
2. The broad-band filter series extends into the far UV.
3. There is a Strömgren series.
4. A Wood's filter is available for far-UV imaging without a red leak.
5. There is a 1% bandpass linear ramp filter series covering 3700-9800Å.
6. The narrow-band series is uniformly specified and well calibrated.

The filters are mounted in the Selectable Optical Filter Assembly (SOFA) between the shutter and the reflecting pyramid. The SOFA contains 12 filter wheels, each of which has 4 filters and a clear "home" position. A listing of all simple optical elements in the SOFA mechanism, and the location of each element (by wheel number 1-12, and position 1-4) is given in Table 3.1 on page 43. Wheel number 1 is located closest to the shutter. The categories are simple filters (F), long-pass (LP), wide (W), medium (M), and narrow (N). Most of these filters are either flat single substrates or sandwiches.

The filter complement includes two solar blind Wood's filters, F160AW, and F160BW. F160BW is used in all science observations because the other filter has some large pinholes that lead to significant red leak.

In addition to the above complement of broad and narrow-band filters, WFPC2 features a set of three specialized quadrant (quad or Q) filters in which each quadrant corresponds to a facet of the pyramid, and therefore to a distinct camera relay. There is one quad containing four narrow-band, redshifted [OII] filters with central wavelengths from 3763Å to 3986Å, one quad with four polarizing elements (POL) with polarization angles, 0°, 45°, 90°, and 135°, and one quad with four methane (CH4) band filters with central wavelengths from 5433Å to 8929Å. The polarizer quad filter can be crossed with any other filter over the wavelength range from 2800Å to 8000Å, with the exception of the Methane Quad and Redshifted [OII] Quad which share the same wheel. The SOFA also contains four linearly variable narrow-band ramp (FR) filters (in the twelfth wheel - closest to the focus). The quad and ramp filters are listed in Table 3.2 on page 44.

In Table 3.1 on page 43 and Table 3.2 on page 44, each of the type "A" filters is equivalent to inserting 5 mm of quartz in terms of optical path length, with compensation for wavelength such that focus is maintained on the CCDs. A configuration with no filters in the beam results in out-of-focus images and generally will not be used. With the exception of the quad polarizer and blocking (Type "B") filters, all filters are designed to be used alone. Type "B" filters introduce no focus shift, so they can be used in combination with any type "A" filter. All combinations where the number of type "A" filters is not unity will result in out-of-focus images. The image blur resulting from two or zero type "A" filters at visible wavelengths is equivalent to 2.3 mm defocus in the F/24 beam, which corresponds to 1/5 wave RMS of defocus at 6328Å, and a geometrical image blur of 0.34″. While this is a large defocus, the images are still of very high quality compared to seeing limited images. Some such combinations may be scientifically attractive. For example, the Wood's filter may be crossed with another UV filter to provide a solar blind passband (although the efficiency will be low).

Table 3.1: WFPC2 Simple Filter Set. The effective wavelength, width, and transmission quoted are defined precisely in Chapter 6, but here are quoted without the system (OTA+WFPC2) response.

Name	Type	Wheel	Slot	Notes	In WF/PC-1?	$\bar{\lambda}$(Å)	$\Delta\bar{\lambda}$(Å)	Peak T (%)	Peak λ (Å)
F122M	A	1	4	H Ly α - Red Leak	Y	1259	224.4	19.3	1240
F130LP	B	2	1	CaF2 Blocker (zero focus)	N	2681	5568.3	94.5	8852
F160AW	A	1	3	Woods A - read leak from pinholes	N	1471	457.2	10.1	1403
F160BW	A	1	2	Woods B	N	1446	457.1	12.1	1400
F165LP	B	2	2	Suprasil Blocker (zero focus)	N	3301	5533.2	95.4	5796
F170W	A	8	1	-	N	1666	434.6	30.7	1655
F185W	A	8	2	-	N	1899	297.4	25.9	1849
F218W	A	8	3	Interstellar feature	N	2117	367.9	21.1	2092
F255W	A	8	4	-	N	2545	408.2	14.8	2489
F300W	A	9	4	Wide U	N	2892	727.6	50.8	2760
F336W	A	3	1	WFPC2 U, Strömgren *u*	Y	3317	370.5	82.6	3447
F343N	A	5	1	Ne V	N	3427	23.5	9.3	3432
F375N	A	5	2	[OII] 3727 RS	Y	3732	24.4	19.5	3736
F380W	A	9	1	-	N	3912	694.8	65.0	3980
F390N	A	5	3	CN	N	3888	45.0	36.5	3886
F410M	A	3	2	Strömgren *v*	N	4086	147.0	70.4	4097
F437N	A	5	4	[OIII]	Y	4369	25.2	52.0	4368
F439W	A	4	4	WFPC2 B	Y	4283	464.4	68.2	4176
F450W	A	10	4	Wide B	N	4410	925.1	91.4	5060
F467M	A	3	3	Strömgren *b*	N	4663	166.4	75.3	4728
F469N	A	6	1	He II	Y	4694	25.0	52.4	4697
F487N	A	6	2	H β	Y	4865	25.9	58.6	4862
F502N	A	6	3	[OIII]	Y	5012	26.9	63.7	5008
F547M	A	3	4	Strömgren y (but wider)	Y	5446	486.6	91.3	5360
F555W	A	9	2	WFPC2 V	Y	5202	1222.6	94.6	5148
F569W	A	4	2	F555W generally preferred[a]	Y	5524	965.7	94.2	5310
F588N	A	6	4	He I & Na I (NaD)	Y	5893	49.0	91.4	5894
F606W	A	10	2	Wide V	Y	5767	1579.0	96.7	6186
F622W	A	9	3	-	Y	6131	935.4	95.6	6034
F631N	A	7	1	[OI]	Y	6306	30.9	85.7	6301
F656N	A	7	2	Hα	Y	6564	21.5	77.8	6562
F658N	A	7	3	[NII]	Y	6591	28.5	79.7	6591
F673N	A	7	4	[SII]	Y	6732	47.2	87.0	6732
F675W	A	4	3	WFPC2 R	Y	6714	889.5	97.3	6780
F702W	A	10	3	Wide R	Y	6940	1480.6	97.1	6538
F785LP	A	2	3	F814W generally preferred[a]	Y	9283	2096.1	91.7	9959
F791W	A	4	1	F814W generally preferred[a]	Y	7969	1304.6	95.9	8082
F814W	A	10	1	WFPC2 I	Y	8203	1758.0	94.8	8387
F850LP	A	2	4	-	Y	9650	1672.4	89.2	10028
F953N	A	1	1	[SIII]	N	9546	52.5	95.6	9528
F1042M	A	11	2	-	Y	10437	611.0	81.6	10139

a. Filters F555W and F814W are generally preferred, as they are part of the "standard" WFPC2 filter set, and will tend to have slightly better photometric calibration. See "Choice of Broad Band Filters" on page 48

The mean wavelength, $\bar{\lambda}$, is similar to that defined in Schneider, Gunn and Hoessel (ApJ 264, 337). The width is the FWHM of a Gaussian filter with the same second moment, and is reasonably close to the FWHM. The values tabulated here do not include the CCD DQE or the transmission of the OTA or WFPC2 optics (as given in Figure 2.4 on page 29). In Chapter 6, the corresponding quantities are given including the effect of the other optical elements and the CCD DQE.

Table 3.2: WFPC2 Quad and Ramp Filters. Segments of the UV and CH4 quads are labeled here by their usual physical designations (A, B, C, and D); see following sections for filter and aperture names which are to be used in writing a Phase II proposal. The quad polarizer is represented for both parallel and perpendicular polarization to its polarization direction, which is different in each quadrant.

Physical Name	Type	Wheel	Slot	Notes	In WF/PC-1?	$\bar{\lambda}$(Å)	$\Delta\bar{\lambda}$(Å)	Peak T (%)	Peak λ (Å)
FQUVN-A	A	11	3	Redshifted [OII] 375	N	3763	73.3	25.9	3769
FQUVN-B	A	11	3	Redshifted [OII] 383	N	3829	57.3	29.5	3828
FQUVN-C	A	11	3	Redshifted [OII] 391	N	3912	59.5	34.3	3909
FQUVN-D	A	11	3	Redshifted [OII] 399	N	3992	63.7	41.0	3989
FQCH4N-A	A	11	4	CH4 543	N	5435	34.4	77.0	5442
FQCH4N-B	A	11	4	CH4 619	N	6199	33.8	82.7	6202
FQCH4N-C	A	11	4	CH4 727	N	7279	38.1	90.9	7278
FQCH4N-D	A	11	4	CH4 892	N	8930	54.8	64.8	8930
POLQ_par	B	11	1	Pol angle 0˚,45˚,90˚,135˚	N	4404	5796.8	90.7	11000
POLQ_per	B	11	1	Pol angle 0˚,45˚,90˚,135˚	N	6682	6654.2	89.7	11000
FR418N	A	12	1	3700-4720	N	W	W/75	~20-50	W
FR533N	A	12	2	4720-6022	N	W	W/75	~40-50	W
FR680N	A	12	3	6022-7683	N	W	W/75	~60-80	W
FR868N	A	12	4	7683-9802	N	W	W/75	~70-85	W

Figure 3.1 on page 46 summarizes the normalized transmission curves for the simple filters and narrow-band quad filters. It does not include curves for the polarizing quad, or the linear ramp filters which are documented in Section 3.5 and Section 3.3, respectively. Figure 3.1 on page 46 divides the filters into the following groups:

1. Long pass filters designed to be used in combination with another filter.
2. Wide bandpass filters with FWHM ~25% of the central wavelength.
3. Approximations to the UBVRI sequence, generally with wider bandpasses, designed for use on faint sources.
4. A photometric set of approximations to UBVRI passbands (see Harris, et al. 1991, AJ 101, 677). Note, however, that the WFPC2 UBVRI series is not the Johnson-Cousins photometric series, neither is it identical with the WF/PC-1 series. See Section 6 for detailed comparisons.
5. Medium bandpass filters with FWHM ~10% of the central wavelength, including an approximation to the Strömgren photometric series.
6. Narrow bandpass filters for isolating individual spectral lines or bands.
7. Redshifted [OII] and CH4 narrow bandpass quad filters.

Note that the UV filters have some degree of "red leak," which is quantified in Chapter 6 where the system response is included. We also note that the F1042M filter suffers an anomalous PSF as described in Section 5.8.

In addition, the flat fields of images taken in most WFPC2 filters reveal an apparently randomly occurring rotational offset of about 0.42 degrees in some images. This quantity closely corresponds to one filter wheel step (0.5 degrees). The pivot point of the rotation implicates the filter wheel as the source of the inconsistency. We expect no impact on observations as any photometric effect is typically only 1%. At this time, the cause of this anomaly, whether it is mechanical or due to a software error, is unknown (Gonzaga, Baggett and Biretta 2001, 2002; Gonzaga and Biretta 2002).

Figure 3.2 on page 47 shows the normalized passbands including the system response. Individual filter transmission curves are shown in Appendix A.

A passband calibration is maintained in the calibration database system (CDBS). It has been updated following on orbit calibrations. The ground based calibration of the narrow-band filters' central wavelengths has not been corrected for temperature effects and is therefore accurate to about 2Å. Because of this, it is not advisable to place narrow emission lines at the half power points of such filters and expect to predict the throughput to high accuracy. The standalone software package XCAL, or SYNPHOT running under IRAF, can be used to access these calibrations which are available on the Institute's WWW page.

Figure 3.1: Summary of Normalized Filter Curves.

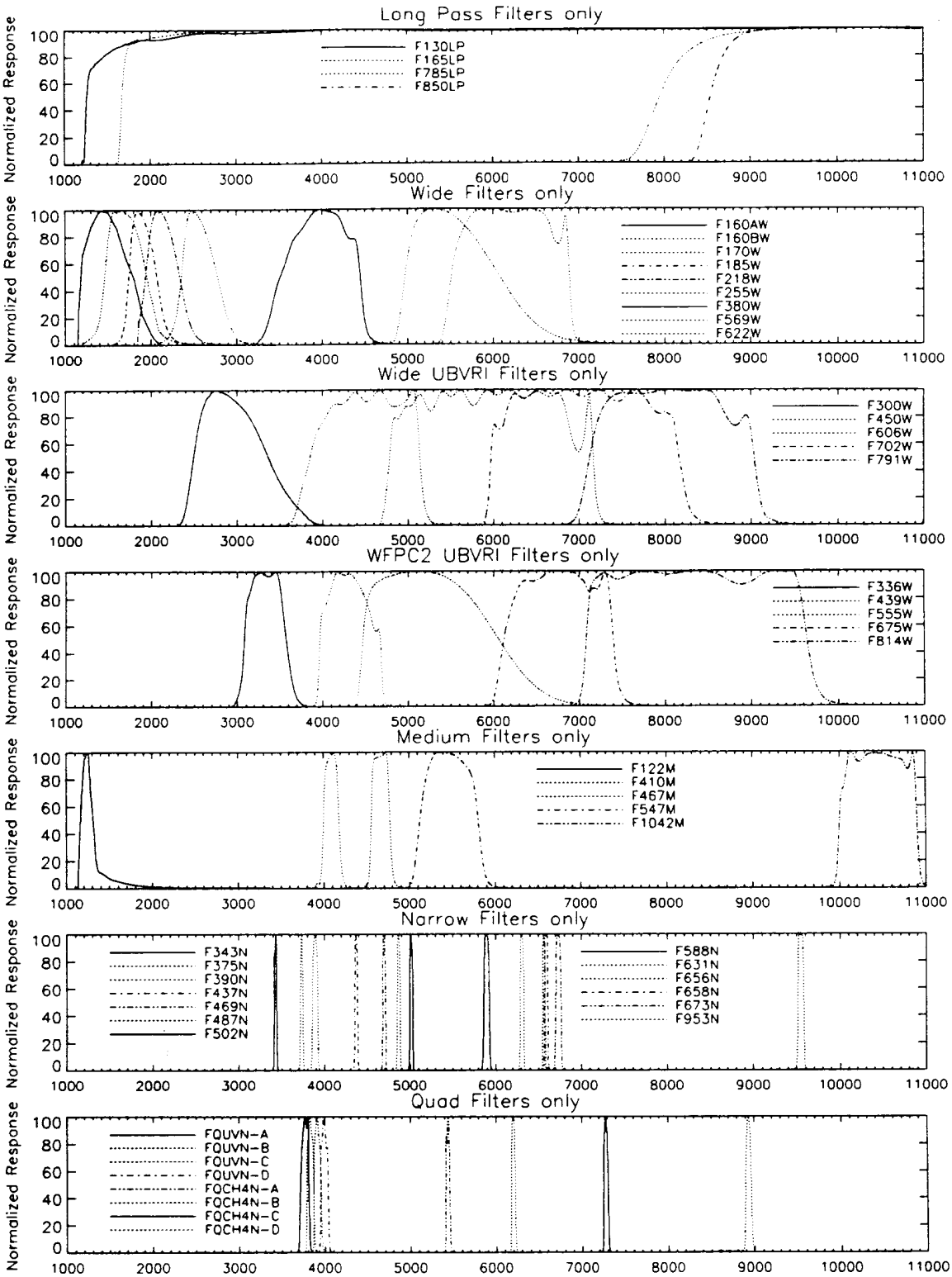

Figure 3.2: Normalized Passbands including System Response.

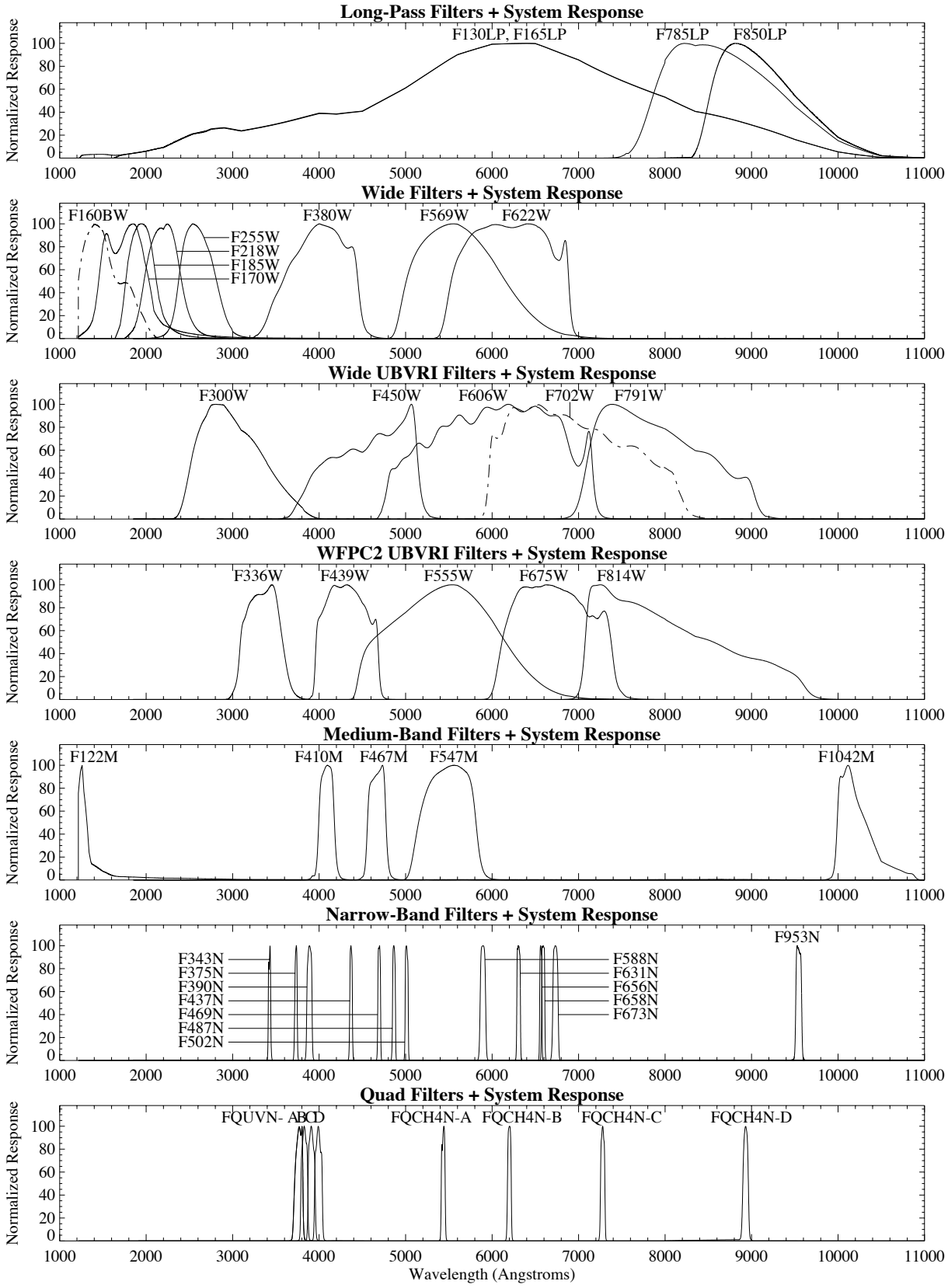

3.2 Choice of Broad Band Filters

A number of different choices are possible on WFPC2 in order to approximate the Johnson-Cousins system often used in ground based observing. These choices differ in throughput, wavelength fidelity, color transformability, and cosmetics. The HST science program as a whole benefits if a standard set can be agreed upon by the community for broad band photometry. This will allow theoretical isochrones and other models to be published in the standard system, and allow ready comparison of the results from different observers. Furthermore, although all filters will be calibrated photometrically and with flat fields, a core set must be chosen for monitoring the instrument both photometrically and in imaging performance. There was a substantial consensus between the accepted Cycle 4 GO programs and the WF/PC-1 and WFPC2 science teams that F336W, F439W, F555W, F675W, and F814W should be the preferred set to approximate the Johnson Cousins U, B, V, R, I passbands. These filters form the basis for the WFPC2 broad band photometric system. As will be seen from the figures in Section 8.9, the preferred set is accurately transformable with the exception of the U bandpass.

On the other hand, there are situations where concerns such as maximum throughput must override the above arguments. For example, filters F300W, F450W, F606W, and F814W were chosen for the Hubble Deep Field (HDF), due to their wider bandpasses.

3.3 Linear Ramp Filters

The linear ramp filters are designed for narrow-band absorption and emission line imaging of moderately extended objects. Each filter is divided into four parallel strips where the central wavelength across each strip varies by approximately 6%. Each CCD pixel is mapped to a unique central wavelength with a FWHM bandwidth of approximately 1.3% of the central wavelength. The maximum size of an object which can be imaged at a given wavelength is approximately 13″ and is determined by the width of the strips and the image size at the filter. The cumulative wavelength range of the four linear ramp filters is 3710Å to 9762Å. Originally intended for a four WFC configuration, the linear ramp filters require partial rotation of the SOFA wheels to +15˚, -18˚ and -33˚ from their nominal positions, to recover wavelength regions which would otherwise fall on the un-imaged region adjacent to the PC CCD. There will be vignetting at some wavelengths for these partial rotations.

3.3.1 Spectral Response

A JPL Memorandum (DFM #2031, 1992) gives the results of a prediction scheme to locate and quantify the passbands of the four WFPC2 ramp filters, FR418N, FR533N, FR680N and FR866N. The results are summarized here.

Laboratory (room temperature) measurements of the passbands of the four ramp filters were made at five equally spaced intervals on each of the four ramp stripes on each filter for a total of 80 passband measurements. The laboratory measurements were made with a narrow beam and were then integrated over an annular area of the filter to simulate the beam profile. The radius of the beam is 3.7 mm, or 13″. The integration was carried out by assuming the nominal linear shift in wavelength with position, and that no significant changes in the passband shape occur across the beam. The integration makes the shape of the passband quite symmetrical.

The resulting spectral response can be fitted to within a few percent with a Munson function:

$$T = T_0 / \{1 + (1-a)x^2 + a(1-b)x^4 + ab(1-c)x^6 + abcx^8\}$$

where a, b and c are shape parameters, and $0 \le (a,b,c) \le 1$; T_0 is the peak transmission of the passband, $T=T_0$ at $x=0$; x is related to wavelength λ by $x=(\lambda-\lambda_0)/H$, $T=T_0/2$ at $x=1$ (so H is the half width at half maximum).

The parameters, (λ_0, T_0, H, a, b, c) were then fitted to polynomial functions of position Y (which starts at 0 inches at the lower wavelength edge of each strip) to predict the filter response for areas of the filters between the tested points. Good quadratic fits are available for all the parameters except for T_0 which requires a cubic. The results are given in Table 3.3 on page 50 through Table 3.6 on page 53, which give the polynomial fit coefficients for the ramp filter parameters. The table entries, except for the first line, are used as parameter=$A_0+A_1Y+A_2Y_2+A_3Y_3$. The short wavelength side of the filter is opposite for alternate ramps. The first line in each table gives the Y position as a function of λ. If the polynomial fit predicts a, b, or $c < 0$ or > 1 then the quantities are set to 0 or 1, respectively.

Use of these fits should be restricted to objects near the center of the ramp, otherwise the beam will combine light from adjacent ramps. The fit should also not be used within 13″ of the end of the ramp. There is enough wavelength overlap between ramps that the extreme ends need not be used, except at the very lowest and highest wavelengths. Figure 3.3 on page 54 shows the fit parameter T_0 as a function of λ_0 for all 16 ramp filter strips. Figure 3.4 on page 54 shows $2H/\lambda_0$.

Table 3.3: Ramp Filter FR418N Parameters.

Quantity	A0	A1	A2	A3
Ramp 1 Position	-26.1083	0.00713888	0.0000	
Wavelength	3657.7	138.7	0.6178	
Peak transmission	-0.01667	0.2188	0.04138	-0.03489
Half width at half max	21.95	-0.8347	2.143	
a	0.2120	0.002857	0.002596	
b	1.181	-0.8138	0.3535	
c	0.3301	-0.3715	0.3825	
Ramp 2 Position	-24.2554	0.00625704	0.0000	
Wavelength	3876.9	158.6	0.5472	
Peak transmission	0.1660	0.2288	-0.1080	0.004005
Half width at half max	21.50	3.315	-0.7079	
a	0.1592	-0.003687	-0.0008497	
b	0.7938	0.2355	-0.09124	
c	0.9306	0.01366	0.007458	
Ramp 3 Position	-24.7145	0.00598254	0.0000	
Wavelength	4130.5	168.8	-0.7389	
Peak transmission	0.1352	0.6200	-0.5226	0.1529
Half width at half max	22.09	1.306	-0.1181	
a	0.2300	0.05586	-0.03044	
b	1.096	-0.3185	0.1396	
c	1.276	-1.279	0.5721	
Ramp 4 Position	-23.4440	0.00536340	0.0000	
Wavelength	4371.3	185.8	0.2913	
Peak transmission	0.3189	0.1287	-0.01160	-0.001712
Half width at half max	25.62	1.015	0.1161	
a	0.3123	-0.2055	0.09535	
b	0.9222	0.1167	-0.04673	
c	1.033	-0.1356	0.05660	

Table 3.4: Ramp Filter FR533N Parameters.

Quantity	A0	A1	A2	A3
Ramp 1 Position	-26.7670	0.00572115	0.0000	
Wavelength	4677.7	177.3	-1.125	
Peak transmission	0.5450	-0.3612	0.3623	-0.1281
Half width at half max	25.67	0.3168	0.8873	
a	-0.009839	0.4644	-0.2039	
b	0.31511	0.9473	-0.4516	
c	-0.3379	2.788	-1.346	
Ramp 2 Position	-24.6600	0.00498393	0.0000	
Wavelength	4948.4	199.2	0.6484	
Peak transmission	0.4546	0.4188	-0.5456	0.1548
Half width at half max	32.10	-1.204	3.171	
a	0.1678	-0.02726	0.09521	
b	0.9345	0.1935	-0.1224	
c	0.9571	0.02919	-0.009393	
Ramp 3 Position	-24.5038	0.00465985	0.0000	
Wavelength	5257.3	217.9	-1.481	
Peak transmission	0.4944	-0.1714	0.1890	-0.0631
Half width at half max	34.03	5.078	-1.347	
a	0.3851	-0.06264	0.003163	
b	0.5605	0.6642	-0.2751	
c	0.9665	0.05543	-0.03654	
Ramp 4 Position	-25.5182	0.00455886	0.0000	
Wavelength	5596.9	220.9	-0.6938	
Peak transmission	0.5058	-0.2715	0.3203	-0.1230
Half width at half max	35.06	-2.856	2.382	
a	0.06553	0.2253	-0.08275	
b	1.043	-0.1190	0.02889	
c	1.162	-0.4910	0.2059	

Table 3.5: Ramp Filter FR680N Parameters.

Quantity	A0	A1	A2	A3
Ramp 1 Position	-21.8962	0.00370137	0.0000	
Wavelength	5916.0	269.4	0.3460	
Peak transmission	0.1198	1.005	-0.4015	-0.00162
Half width at half max	41.50	-5.873	4.038	
a	0.1743	-0.05050	0.06481	
b	0.8320	0.3326	-0.1858	
c	0.9682	-0.09110	0.05122	
Ramp 2 Position	-22.6919	0.00360750	0.0000	
Wavelength	6290.8	275.6	0.7184	
Peak transmission	0.7918	-0.02034	0.1086	-0.05945
Half width at half max	39.48	2.120	0.3703	
a	0.05596	0.3034	-0.1333	
b	1.017	-0.27026	0.04560	
c	0.7244	0.8326	-0.5107	
Ramp 3 Position	-22.0719	0.00330755	0.0000	
Wavelength	6673.5	301.6	0.3321	
Peak transmission	0.9494	-1.008	1.161	-0.3777
Half width at half max	42.81	0.8193	0.4269	
a	0.1038	0.09020	-0.02747	
b	0.8415	0.3045	-0.1930	
c	1.017	-0.1732	0.07463	
Ramp 4 Position	-24.7447	0.00346462	0.0000	
Wavelength	7141.9	289.3	-0.2999	
Peak transmission	0.4823	0.4479	-0.07484	-0.05868
Half width at half max	44.72	0.8952	-0.0756	
a	0.1612	-0.01167	0.01355	
b	0.2708	1.077	-0.4757	
c	0.9941	-0.02694	0.01685	

Table 3.6: Ramp Filter FR868N Parameters.

Quantity	A0	A1	A2	A3
Ramp 1 Position	-23.2685	0.00308029	0.0000	
Wavelength	7555.5	320.4	1.906	
Peak transmission	0.7524	-0.3328	0.4543	-0.1343
Half width at half max	49.32	1.742	0.4914	
a	0.2958	-0.3877	0.2465	
b	1.321	-0.9156	0.3666	
c	0.3762	1.668	-0.9499	
Ramp 2 Position	-22.9766	0.00286673	0.0000	
Wavelength	8014.3	350.5	-0.7500	
Peak transmission	0.8204	-0.3368	0.3815	-0.1057
Half width at half max	54.17	1.579	0.2196	
a	0.05832	0.7525	-0.3625	
b	0.4582	0.8433	-0.4350	
c	0.6422	0.3247	-0.1593	
Ramp 3 Position	-22.6085	0.00265657	0.0000	
Wavelength	8510.7	375.6	0.3706	
Peak transmission	0.5817	-0.1920	0.4517	-0.1627
Half width at half max	55.19	-0.7459	1.433	
a	0.5422	-0.2444	0.03545	
b	1.420	-1.176	0.4814	
c	0.4257	-0.2522	0.1777	
Ramp 4 Position	-23.2142	0.00256976	0.0000	
Wavelength	9034.3	387.2	0.8722	
Peak transmission	0.6241	0.2403	-0.1230	0.02829
Half width at half max	59.69	2.167	-0.1996	
a	0.2376	-0.01879	-0.00864	
b	0.9670	0.02456	-0.00477	
c	0.7829	0.03750	0.02393	

Figure 3.3: Ramp Filter Peak Transmission. The four line types correspond to the four different filters (each containing four ramps).

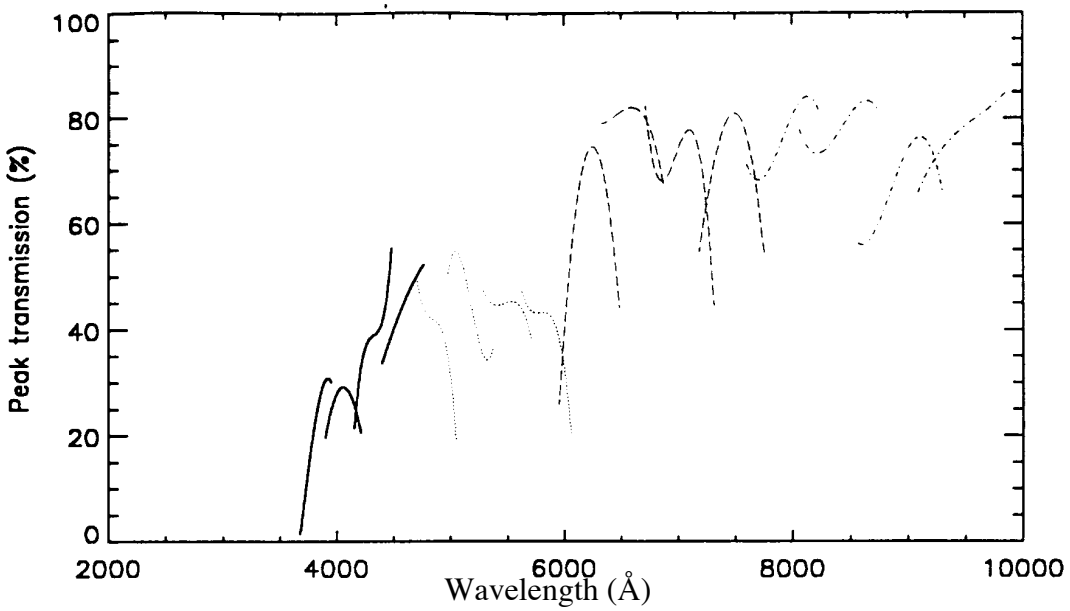

Figure 3.4: Ramp Filter Dimensionless Widths.

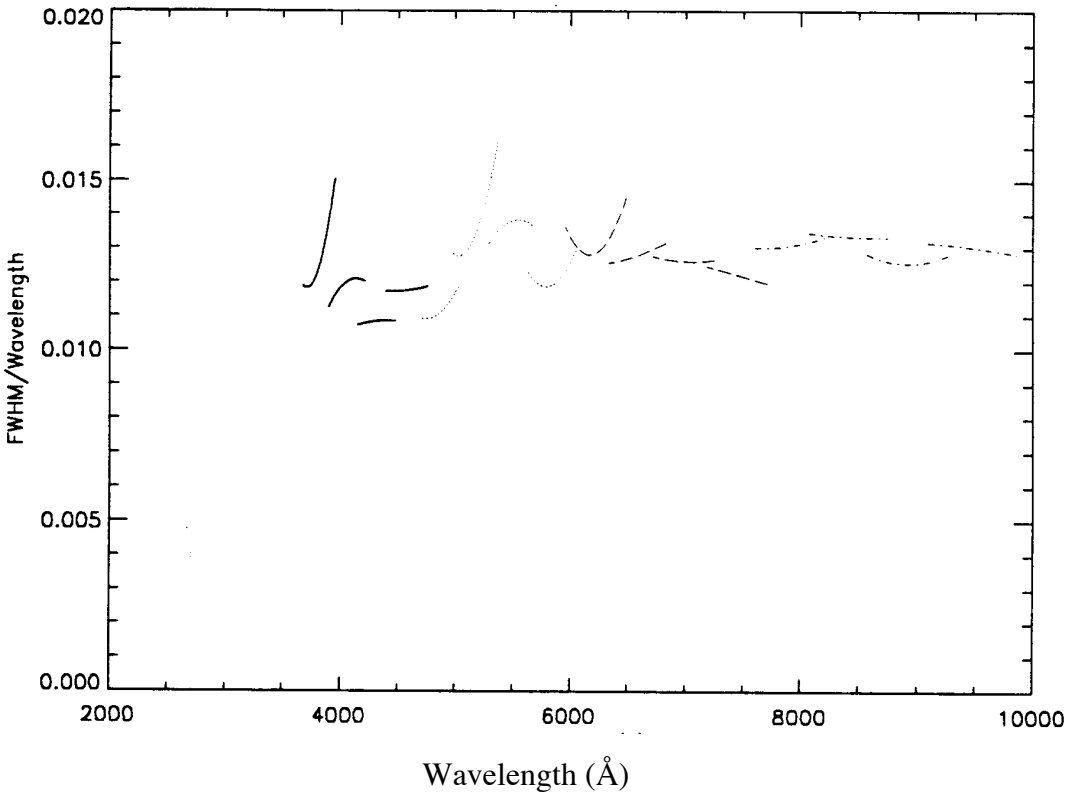

3.3.2 Target Locations

In Figure 3.5 on page 56 and Figure 3.6 on page 57 we show the correspondence between central wavelength and location in the focal plane for the nominal and rotated filter positions. The selection of filter and aperture for the linear ramp filters is transparent to the user who is required only to specify the linear ramp filter name LRF and a central wavelength. Each central wavelength is assigned to a unique filter and CCD location in the Phase II proposal.

Following on-orbit testing of WFPC2, a revised table of linear ramp filter wavelengths was compiled and is shown in Table 3.7 on page 58 (Biretta, et al. 1995, ISR WFPC2 95-05). For each wavelength listed, there is a minimum 10″ diameter unvignetted field-of-view. Some wavelengths can be obtained with several different settings of the ramps, however, for simplicity, the redundant wavelengths have been removed from the table. Note that this table supports observation with the PC and a new +15° rotation of the filter wheel. Table 3.8 on page 60 lists wavelengths which are available, but with some compromise in data quality, so as to avoid gaps in wavelength coverage. Most of these wavelengths are observed slightly off the central wavelength of the passband. This implies a slightly reduced throughput (see estimates of the light reduction in the table), and some additional difficulties in flattening the data to remove variations in the passband across the target. A few other wavelengths are observed slightly off the unvignetted center line of the ramps, and these are indicated by note "FOV" in Table 3.8 on page 60. Again, this vignetting will present some additional complications when calibrating the data. Further details regarding the ramp filter wavelengths and apertures will be made available in a separate instrument science report.

We note that an interactive tool is available on the WFPC2 WWW pages which will compute target locations for LRF observations. The user inputs either the central wavelength or the target location in the field-of-view, and the other quantity is returned.

Figure 3.5: FR418N and FR533N Wavelength Mapping.

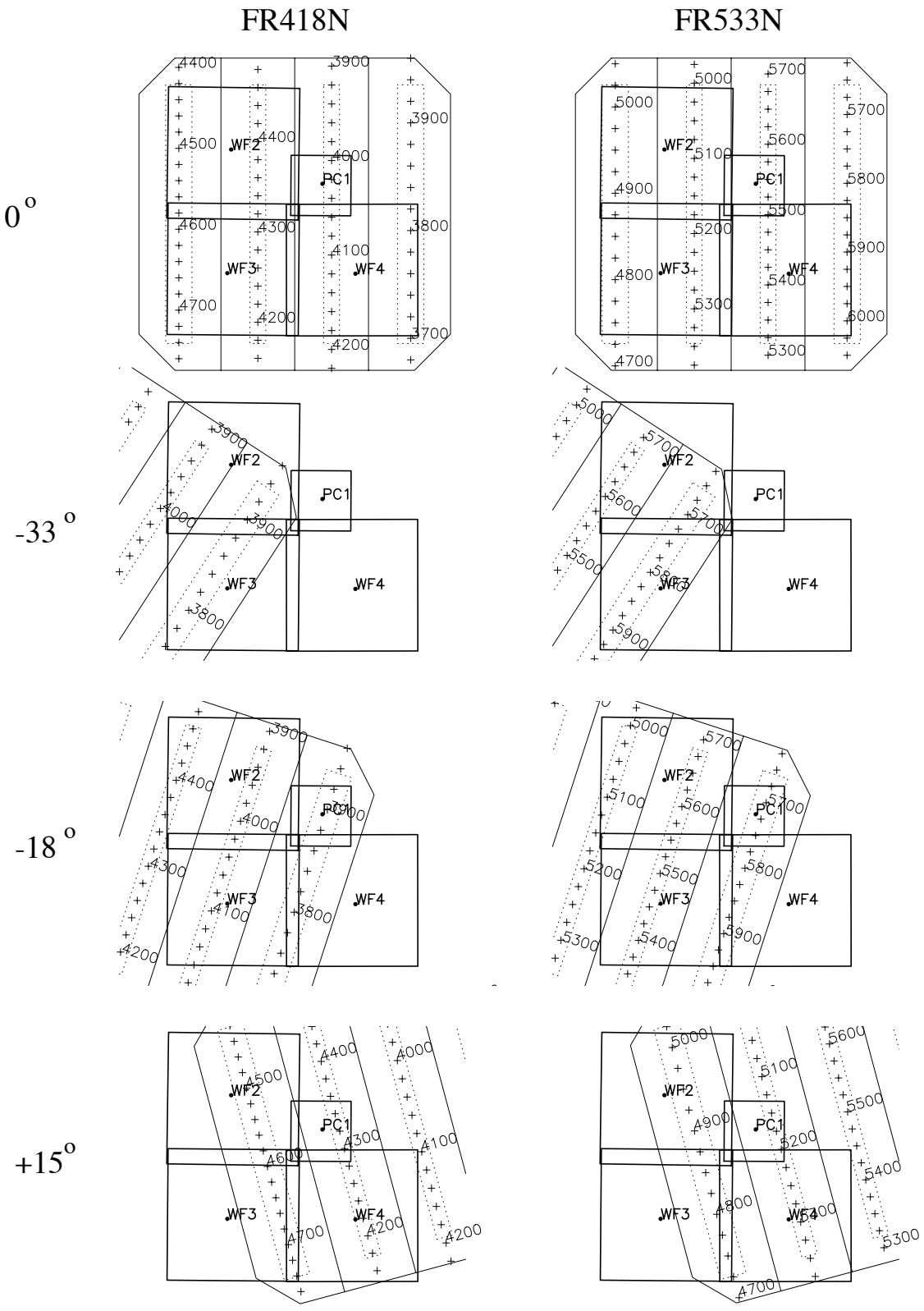

Figure 3.6: FR680N and FR868N Wavelength Mapping.

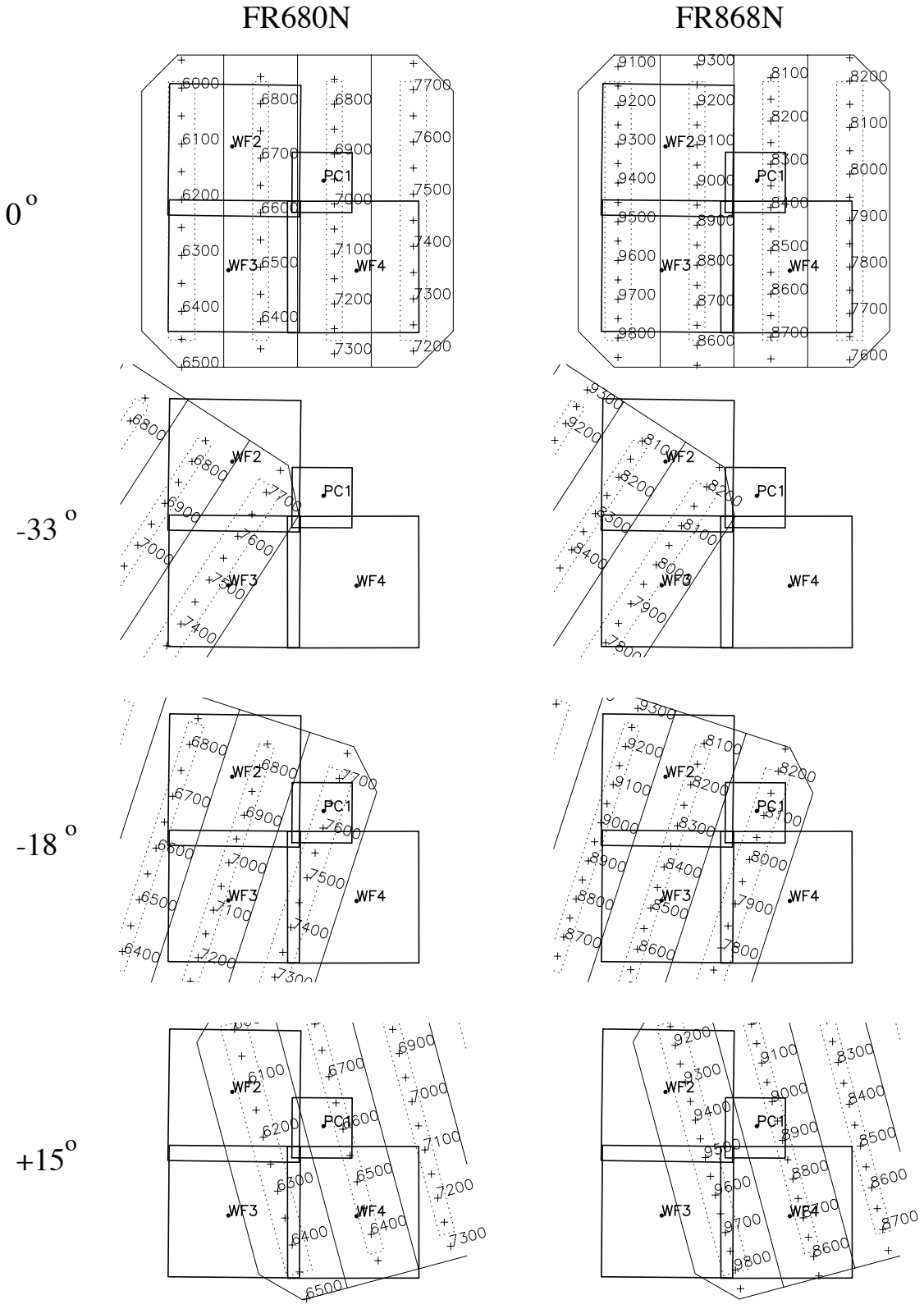

3.3.3 LRF Photometric Calibration

As of this writing, the preferred method of flat fielding LRF data is to use a narrow band flat observed nearby in wavelength. This will remove pixel-to-pixel effects, as well as effects of distortion and vignetting in the cameras, while avoiding the complications of pinholes on the LRFs and spurious variations due to the spectrum of the flat field light source.

Conversion of counts to source flux is best achieved by using the SYNPHOT synthetic photometry package. An LRF filter setting is simply specified by including "LRF#*xxxx*" in the OBSMODE, where *xxxx* is the central wavelength specified on the Phase II proposal (see Biretta, Baggett, and Noll 1996, ISR WFPC2 96-06).

Comparisons between the SYNPHOT predictions and on-orbit observations of standard stars show a small, systematic offset between the two (in the sense that fewer counts are observed than expected), plus scatter about this trend. A linear fit to the photometric offset gives:

$$M_{obs} - M_{calc} = (0.09 \pm 0.01) + (3.11e^{-5} \pm 0.67e^{-5}) * (\lambda - 6500)$$

with an RMS scatter about the trend of 0.12 mag. It may be possible to further reduce the calibration errors for certain wavelength ranges that were well sampled by the calibration programs.

For the FR533N filters, please note that a randomly occurring filter anomaly could affect photometric accuracy for extended targets, please see Section 7.10 for details.

Table 3.7: Aperture Locations and Wavelengths for Ramp Filters.

Start (Å)	End (Å)	Filter	CCD / Aperture	x1 (pix)	y1 (pix)	x2 (pix)	y2 (pix)
3710	3800	FR418N	WF4-FIX	750	736.8	161 .5	737.7
3800	3878	FR418N33	WF3-FIX	669.5	559.2	395.1	128.9
3881	3907	FR418N18	PC1-FIX	402.3	225	515.4	579.5
3907	3929	FR418N33	WF2-FIX	128.4	286.7	250.1	209.9
3929	4008	FR418N18	WF2-FIX	562.7	233	130.1	367.1
4008	4038	FR418N	PC1-FIX	541.3	632.7	543.3	256.5
4038	4100	FR418N18	WF3-FIX	425.3	130.8	532 4	469.9
4100	4177	FR418N	WF4-FIX	309	276.2	750.3	275.5
4186	4210	FR418P15	WF4-FIX	596.5	515.9	469.4	482.1
4210	4308	FR418N	WF3-FIX	248.2	665.9	252.7	128.5
4308	4337	FR418P15	PC1-FIX	690.2	264.6	598.4	599.9
4337	4446	FR418N	WF2-FIX	127.9	247.6	725.4	255.7
4446	4550	FR418N	WF2-FIX	691.7	716.2	180.6	709.2
4550	4571	FR418P15	WF2-FIX	230	253.8	130.7	225.8
4593	4720	FR418N	WF3-FIX	713.7	125.6	708.5	749.9
4746	4863	FR533N	WF3-FIX	689.3	748.9	694.4	135.5
4884	4900	FR533P15	WF2-FIX	128.3	205.1	209	227.9

Table 3.7: Aperture Locations and Wavelengths for Ramp Filters.

Start (Å)	End (Å)	Filter	CCD / Aperture	x1 (pix)	y1 (pix)	x2 (pix)	y2 (pix)
4900	5013	FR533N	WF2-FIX	153.6	689.6	745.9	697.7
5013	5020	FR533N18	WF2-FIX	693.4	642.4	662.9	651.8
5020	5153	FR533N	WF2-FIX	737.3	236.6	130	228.4
5153	5176	FR533P15	PC1-FIX	637.9	614.9	698.6	393.3
5188	5310	FR533N	WF3-FIX	233.5	127.4	228.8	684.7
5310	5335	FR533P15	WF4-FIX	482.8	505.5	593.1	534.9
5339	5450	FR533N	WF4-FIX	750.9	294.7	277.2	295.5
5450	5528	FR533N18	WF3-FIX	504.4	445.3	404.1	127.6
5528	5566	FR533N	PC1-FIX	585.3	277.5	583.4	632.3
5566	5671	FR533N18	WF2-FIX	124.1	348.8	552.3	216.1
5671	5700	FR533N33	WF2-FIX	224.8	203.2	122.3	267.7
5700	5741	FR533N18	PC1-FIX	558.8	577	444.9	220.1
5743	5910	FR533N33	WF3-FIX	370.8	126.5	745.9	714.9
5910	6007	FR533N	WF4-FIX	333.8	747.6	738.8	746.9
6007	6192	FR680N	WF2-FIX	750.3	706.9	122.9	698.4
6192	6208	FR680P15	WF2-FIX	177.1	228.4	124.9	213.6
6238	6409	FR680N	WF3-FIX	703.6	128.1	698.8	708.2
6409	6584	FR680N	WF3-FIX	237.8	705.6	242.6	127
6590	6631	FR680P15	PC1-FIX	699.1	315.3	620.9	601.2
6631	6800	FR680N	WF2-FIX	125.9	237.5	684.5	245.1
6800	6921	FR680N18	WF2-FIX	480.1	248	129.9	356.6
6921	6976	FR680N	PC1-FIX	563.3	639.2	565.3	274.6
6976	7061	FR680N18	WF3-FIX	413.2	126	490.8	371.7
7061	7241	FR680N	WF4-FIX	203	286.4	748.3	285.6
7251	7420	FR680N	WF4-FIX	749.6	743.5	213.3	744.3
7420	7600	FR680N33	WF3-FIX	688.9	608.4	381.6	126.4
7605	7658	FR680N18	PC1-FIX	427	230	538.9	580.6
7658	7690	FR680N33	WF2-FIX	126.2	276.1	212.1	222
7690	7830	FR868N	WF4-FIX	711.5	751.3	316.5	751.9
7830	8072	FR868N33	WF3-FIX	728.2	705.8	360.9	129.7
8077	8140	FR868N18	PC1-FIX	471.5	231	589.7	601.5
8140	8300	FR868N18	WF2-FIX	527.6	213.2	126.2	337.6
8300	8362	FR868N	PC1-FIX	605.4	644.1	607.3	287.9
8362	8460	FR868N18	WF3-FIX	393.1	126.1	470.6	371.7
8460	8661	FR868N	WF4-FIX	196.9	305.7	724.7	304.9
8661	8910	FR868N	WF3-FIX	218.3	731.6	223.4	125.3
8945	8980	FR868P15	PC1-FIX	701.1	467.5	651.9	647.3
8980	9200	FR868N	WF2-FIX	142.7	218.5	678.2	225.8
9200	9415	FR868N	WF2-FIX	668.4	686.5	162.2	679.6

Table 3.7: Aperture Locations and Wavelengths for Ramp Filters.

Start (Å)	End (Å)	Filter	CCD / Aperture	x1 (pix)	y1 (pix)	x2 (pix)	y2 (pix)
9415	9456	FR868P15	WF2-FIX	219.9	220.5	127	194.2
9501	9762	FR868N	WF3-FIX	684.3	135.4	679.2	750.2

Table 3.8: Vignetted Wavelengths for Ramp Filters. The right column gives the maximum throughput reduction (in %) for these settings where the target must be placed away from the optimal location on the filter glass. “FOV” denotes settings where transmission is optimal, but the usable field-of-view is reduced below 10″ to the indicated diameter (in arcseconds).

Start (Å)	End (Å)	Filter	CCD / Aperture	x1 (pix)	y1 (pix)	x2 (pix)	y2 (pix)	Max % Light Loss
3878	3881	FR418N18	PC1-FIX	402.3	225.0	402.3	225.0	2
4177	4182	FR418N	WF4-FIX	750.3	275.5	750.3	275.5	3
4182	4186	FR418P15	WF4-FIX	596.5	515.9	596.5	515.9	2
4571	4582	FR418P15	WF2-FIX	130.7	225.8	130.7	225.8	13
4582	4593	FR418N	WF3-FIX	713.7	125.6	713.7	125.6	13
4720	4733	FR418N	WF3-FIX	708.5	749.9	708.5	749.9	14
4733	4746	FR533N	WF3-FIX	689.3	748.9	689.3	748.9	14
4863	4873	FR533N	WF3-FIX	694.4	135.5	694.4	135.5	8
4873	4884	FR533P15	WF2-FIX	128.3	205.1	128.3	205.1	8
5176	5183	FR533P15	PC1-FIX	698.6	393.3	698.6	325.9	FOV~9”
5183	5188	FR533N	WF3-FIX	233.5	127.4	233.5	127.4	2
5335	5337	FR533P15	WF4-FIX	593.1	534.9	593.1	534.9	1
5337	5339	FR533N	WF4-FIX	750.9	294.7	750.9	294.7	1
5741	5743	FR533N33	WF3-FIX	370.8	126.5	370.8	126.5	1
6208	6221	FR680P15	WF2-FIX	124.9	213.6	124.9	213.6	8
6221	6238	FR680N	WF3-FIX	703.6	128.1	703.6	128.1	11
6584	6587	FR680N	WF3-FIX	242.6	127.0	242.6	127.0	1
6587	6590	FR680P15	PC1-FIX	699.1	294.3	699.1	315.3	FOV~9”
7241	7246	FR680N	WF4-FIX	748.3	285.6	748.3	285.6	2
7246	7251	FR680N	WF4-FIX	749.6	743.5	749.6	743.5	2
7600	7602	FR680N33	WF3-FIX	381.6	126.4	381.6	126.4	1
7602	7605	FR680N18	PC1-FIX	427.0	230.0	427.0	230.0	1
8072	8074	FR868N33	WF3-FIX	360.9	129.7	360.9	129.7	1
8074	8077	FR868N18	PC1-FIX	471.5	231.0	471.5	231.0	1
8910	8920	FR868N	WF3-FIX	223.4	125.3	223.4	125.3	2
8920	8945	FR868P15	PC1-FIX	701.1	339.1	701.1	467.5	FOV~7”
9456	9478	FR868P15	WF2-FIX	127.0	194.2	127.0	194.2	13
9478	9501	FR868N	WF3-FIX	684.3	135.4	684.3	135.4	13

3.4 Redshifted [OII] Quad Filters

The redshifted [OII] quad filter was designed to map onto a four-faceted WFC configuration. A partial SOFA wheel rotation of -33° is required to move filter quadrant 1 (3763Å) into WF2 and WF3, with some vignetting of both camera fields. The projections of the redshifted [OII] filter settings FQUVN and FQUVN33 onto the field-of-view are essentially identical to those of the POLQ and POLQN33 filters, respectively (Figure 3.7 on page 64). The vignetted regions are similar, and the location of aperture FQUVN33 is identical to that of POLQN33.

The nominal and rotated filter wheel positions for the redshifted [OII] quad filter are each associated with different filter names. This allows pipeline calibration and database retrievals to proceed smoothly. The filter names are summarized in Table 3.9 on page 61.

The required central wavelength is selected by filter name and aperture location. Filter element FQUVN (Filter Quad Ultra Violet Narrow) has three possible apertures, each of which is nominally centered in one of the three WF channels and associated with a unique central wavelength. The filter element FQUVN33 corresponds to a single central wavelength. In addition to the filter name and aperture, a central wavelength is also requested in the proposal instructions in order to provide a consistency check. Aperture names are discussed further in Section 3.9.

Table 3.9: Redshifted [OII] Quad Filter Elements.

Filter Name	Aperture Name	FOV Location	Quad	Mean Wavelength (Å)	Effective Width (Å)	Comments
FQUVN	WF2	WF2	D	3992	64	Nominal filter wheel position
FQUVN	WF3	WF3	C	3912	60	Nominal filter wheel position
FQUVN	WF4	WF4	B	3829	57	Nominal filter wheel position
FQUVN33	FQUVN33	WF2	A	3763	73	Filter rotated -33°

3.5 Polarizer Quad Filter

The polarizer quads were also designed to map onto a four-faceted WFC configuration and, consequently, also require a partial filter rotation of -33° to move the filter quadrant 1 (nominal polarization angle 135°) into WFCs 2 and 3, with some vignetting of both camera fields. Several additional partial rotations have been added to allow observations with different polarization angles on the same CCD.

The polarizer quad may be used in several ways: by observing the target with each camera, by observing the target with the same camera using different partial rotations of the polarizer quad, or by observing the target with the same camera using different roll angles of the spacecraft. The first method has the drawback that calibration is complicated by uncertainties in the relative photometric calibration between cameras, while the second method uses the same camera but has non-optimal polarization angles and limited fields of view. The third method may present scheduling difficulties due to constraints on the spacecraft roll angle, and the need to rotate undersampled images. (See Biretta and Sparks 1995, "WFPC2 Polarization Observations: Strategies, Apertures, and Calibration Plans," WFPC2 ISR 95-01.)

The required polarization angle is selected by filter name and aperture location as shown in Table 3.10 on page 62. The transmission of the quad polarizer is shown in Figure 3.8 on page 65. The polarizer is afocal and must therefore usually be used with another filter which will largely define the shape of the passband.

The polarizer is designed for problems where large polarizations are observed, and will need very careful calibration for problems requiring precision of order 3% or better.

Table 3.10: Polarizer Quad Filter. Polarization angle 0˚ lies along +X direction in Figure 3.12 on page 76.

Filter Name	Aperture Name	FOV Location	Polarization Angle	Comments
POLQ	PC1	PC1	135˚	Nominal filter wheel position
POLQ	WF2	WF2	0˚	Nominal filter wheel position
POLQ	WF3	WF3	45˚	Nominal filter wheel position
POLQ	WF4	WF4	90˚	Nominal filter wheel position
POLQN33	POLQN33	WF2	102˚	Filter wheel rotated -33˚
POLQP15	POLQP15P	PC	15˚	Filter wheel rotated +15˚
POLQP15	POLQP15W	WF2	15˚	Filter wheel rotated +15˚
POLQN18	POLQN18	WF2	117˚	Filter wheel rotated -18˚

3.5.1 Polarization Calibration

Substantial improvements in the polarization calibration of WFPC2 were made after Cycle 6. These results are fully described in Biretta and McMaster (1997), and are based on a physical model of the polarization effects in WFPC2, described via Mueller matrices, which includes corrections for the instrumental polarization (diattenuation and phase

retardance) of the pick-off mirror, as well as the high cross-polarization transmission of the polarizer filter. New polarization flat fields were also made available. Comparison of the model against on-orbit observations of polarization calibrators shows that it predicts relative counts in the different polarizer/aperture settings to 1.5% RMS accuracy.

To assist in the analysis of polarization observations, we provide two Web-based utilities, available at

http://www.stsci.edu/instruments/wfpc2/wfpc2_pol_top.html

by which users can simulate and calibrate their data. These tools have been upgraded to include effects related to the MgF_2 coating on the pick-off mirror, as well as the more accurate matrices for the cross-polarization leakage in the polarizer filter. Differences between the previous and current versions of the tools are typically around 1% in fractional polarization.

3.6 Methane Quad Filter

The methane band quad filter, known as the jewel-quad, was designed for a four-faceted WF/PC configuration to permit imaging with both four WFC CCDs and four PC CCDs. The camera was constructed, however, with only one PC CCD and three WF CCDs. WFC imaging is recovered for the first quadrant element of the filter (6193Å) by a partial SOFA wheel rotation of -33˚ which moves quadrant 1 into WF2 and WF3 with some vignetting of both camera fields. PC imaging with all four elements of the methane band jewel-quad cannot be recovered, but partial SOFA wheel rotations of -15˚ and +15˚ are implemented to recover two of the four methane band filters (8929Å and 6193Å). The +15˚ rotation of the filter wheel, however, results in some vignetting of PC1's field-of-view. The filter projections associated with the methane band jewel-quad are shown in Figure 3.9 on page 66. Each of the four filter wheel positions are associated with unique filter names, as summarized in Table 3.11 on page 65.

The required central wavelength is selected by filter name and aperture location. Filter element FQCH4N (Filter Quad Methane Narrow) has three possible apertures, each of which is located in one of the three WF channels and associated with a unique central wavelength, while FQCH4N33 is associated with one possible central wavelength. FQCH4N15 and FQCH4P15 are both associated with one central wavelength for PC1 observations. In addition to the filter name and aperture, a central wavelength is also requested in the proposal instructions in order to provide a consistency check.

Figure 3.7: Polarizer Quads. The schematics show the filter projected onto the field-of-view for all rotated positions. Apertures are marked. Dashed lines indicate the central region of each quad which is free of vignetting and cross-talk. Grey-scale images are VISFLATs of the polarizer with F555W.

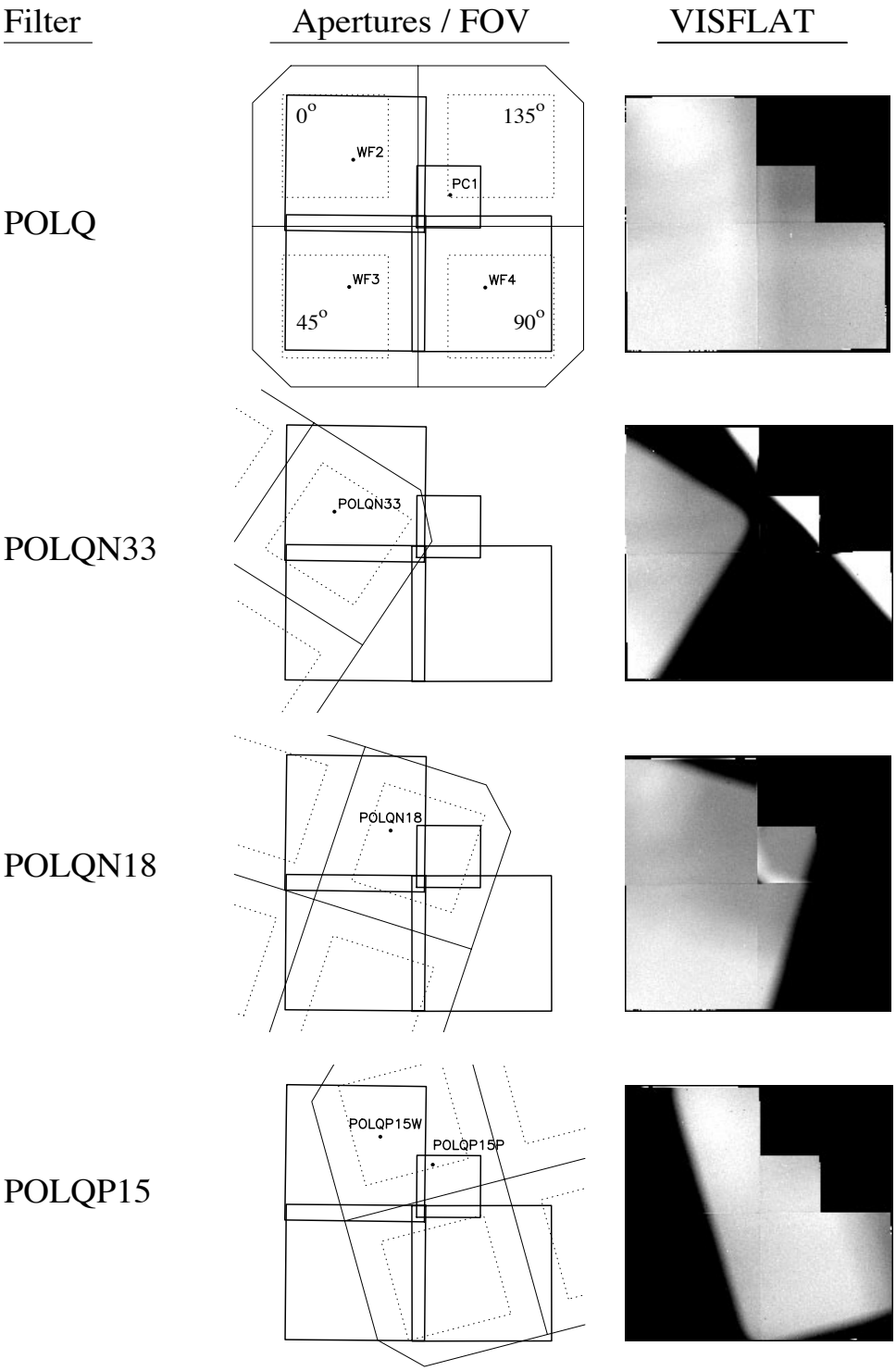

Figure 3.8: Polarizer Transmission for light polarized perpendicular (dotted curve) and parallel (solid curve) to the filter polarization direction.

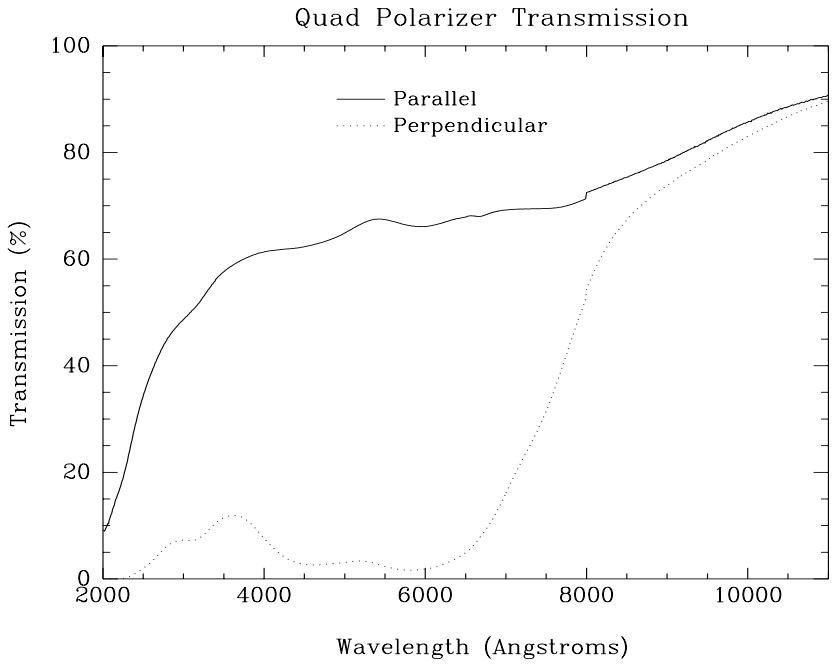

Table 3.11: Methane Band Quad Filter. The filter and aperture names should be specified on the Phase II proposal as shown here.

Filter Name	Aperture Name	FOV Location	Quad	Mean Wavelength (Å)	Effective Width (Å)	Comments
FQCH4N	FQCH4W2	WF2	A	5435	34	Nominal filter position
FQCH4N	FQCH4W3	WF3	D	8930	55	Nominal filter position
FQCH4N	FQCH4W4	WF4	C	7279	38	Nominal filter position
FQCH4N33	FQCH4N33	WF2/WF3	B	6199	34	Filter rotated -33°
FQCH4N15	FQCH4N15	PC1	B	6199	34	Filter rotated -15°
FQCH4P15	FQCH4P15	PC1	D	8930	55	Filter rotated +15°

Figure 3.9: Methane Quad Filter. The mapping to the focal plane for nominal and rotated (-33°, -15°, and +15°) SOFA positions is shown. Dashed lines indicate the limits of the unvignetted field-of-view on each quad.

Filter	Apertures / FOV
FQCH4N	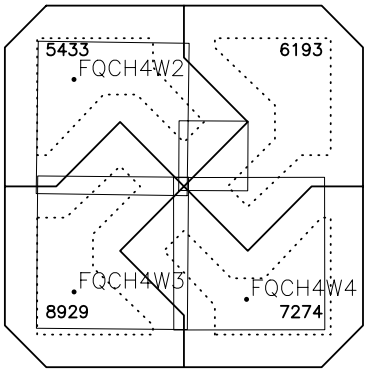
FQCH4N33	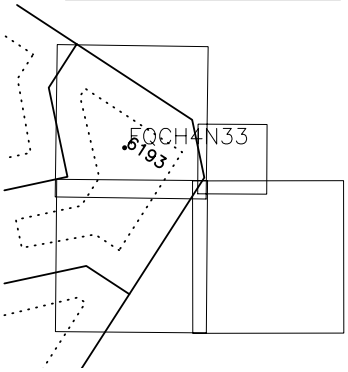
FQCH4N15	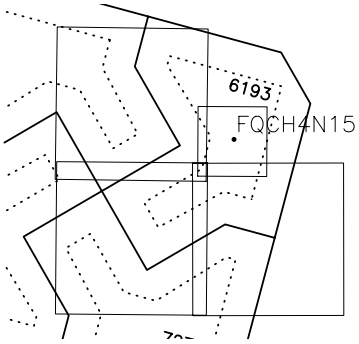
FQCH4P15	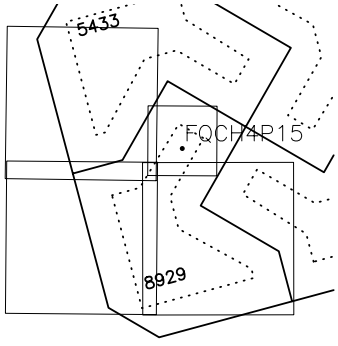

3.7 Wood's Filters

WFPC2 features two solar-blind Wood's filters, for FUV (<2000Å) imaging. It was shown by Wood in the 1930s (Physical Optics, 1934, R. W. Wood) that thin layers of alkali metals transmit FUV wavelengths while providing very efficient long wavelength blocking due to the plasma frequency of the free electrons. Wood's filters have been built for WFPC2 at JPL using thin (5000Å) layers of sodium sandwiched between two MgF_2 substrates. These Wood's filters have a broad bandpass from 1200Å to 2100Å with visible-light transmission lower than 10^{-8}. The best conventional UV filters exhibit visible-light transmission of 10^{-3} to 10^{-4}. Many astronomical objects emit 10^4 to 10^7 visible photons for every FUV photon. In such cases, a Wood's filter (or "solar blind" detector as on STIS) is essential for FUV imaging so that the visible light leak does not dominate the observation. The main problem experienced with Wood's filters is long term instability. Sodium is a very reactive metal, and attempts to passivate the sodium layer have met with limited success. It is possible that, as the Wood's filters age, pinholes will form which transmit visible light. This transmitted light will appear as an increase in the background level at the focal plane. So far no indications of any degradation on-orbit have been observed.

Figure 3.10: Wood's Filters. Greyscale flat field images show the field-of-view available with the two Wood's filter options F160BW and F160BN15.

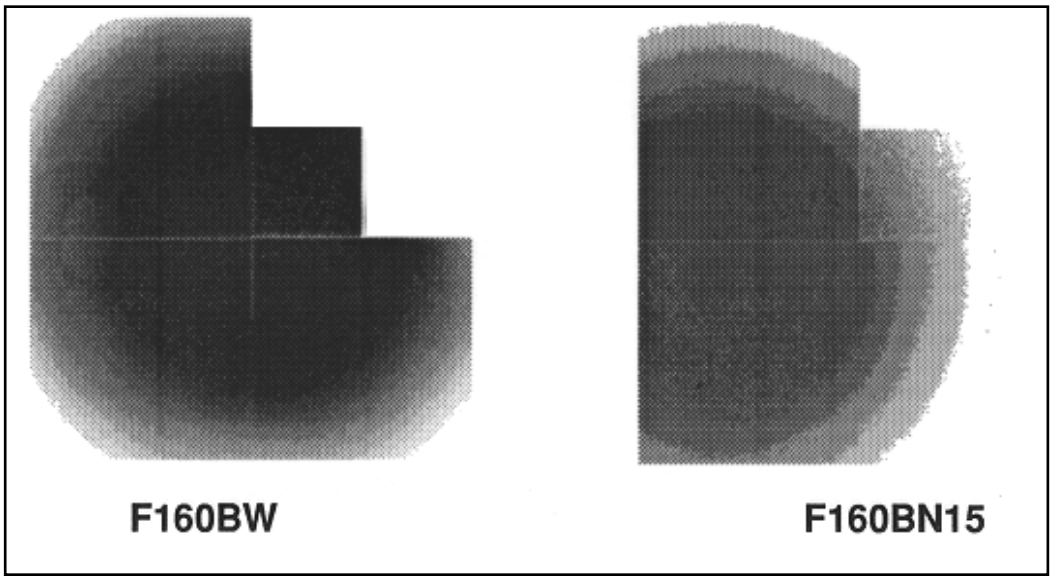

The Wood's filters can be used as a broadband filter, or in combination with the CaF_2 long-pass filter to suppress geocoronal emission, or, crossed with one of the other UV filters, such as the suprasil blocker F165LP, to define a solar-blind UV photometric system. As discussed at the beginning

of this chapter, the image will be out of focus in the last case. WFPC2's Wood's filters are circular with a clear aperture of 41 mm. Two similar Wood's filters (F160AW and F160BW) were mounted in SOFA wheel 1 to provide some redundancy. In Thermal Vacuum testing F160AW showed evidence for pinholes, which cause excessive red leak in some parts of its field. Therefore the preferred filter for far UV imaging with minimal red leak in WFPC2 is F160BW.

In the nominal filter wheel position PC1 has a clear field-of-view, but there is significant vignetting in all three WFCs. A partial filter wheel rotation of -15° produces a larger field-of-view in WF3, although some vignetting remains. The options are illustrated in Figure 3.10 on page 67. The imaging performance of the Wood's filters is continually monitored for signs of aging such as visible light leaks. Additional partial rotations could be implemented in the future, to position an unaffected region of the filter into a WF or PC1, if necessary. The unvignetted filter projections associated with the two planned filter positions are shown schematically in Figure 3.10 on page 67. Each filter position is associated with a unique name as summarized in Table 3.12 on page 68.

The filter name must be selected on the basis of whether a PC or WF3 observation is required.

Table 3.12: Wood's Filters. The filter and aperture names should be specified on the Phase II proposal as shown below.

Filter Name	Aperture Name	FOV Location	Mean Wavelength (Å)	Effective Width (Å)	Comments
F160BW	PC1	PC1	1446	457	Nominal filter position
F160BN15	F160BN15	WF3	1446	457	Filter rotated -15°

3.8 Red Leaks in UV Filters

The "red leaks" in the UV filters are shown in Figure 3.11 on page 69 for F122M, F160BW (the new Wood's filter), F170W, F185W, F218W F255W, F300W, and F336W. The presence of significant red leaks in the UV filters, together with the much greater sensitivity and wavelength coverage in the red part of the spectrum, makes calibration of UV observations difficult. Table 3.13 on page 70 shows red leak estimates as a percentage of the total detected flux from de-reddened stellar sources, ordered by spectral type. In each column, the red leak is defined as the percentage of the detected flux longward of the cutoff wavelength in the third row. In the presence of interstellar reddening, the red leaks will be larger.

Figure 3.11: UV Filter Red Leaks. Includes the on-orbit measurements of system response.

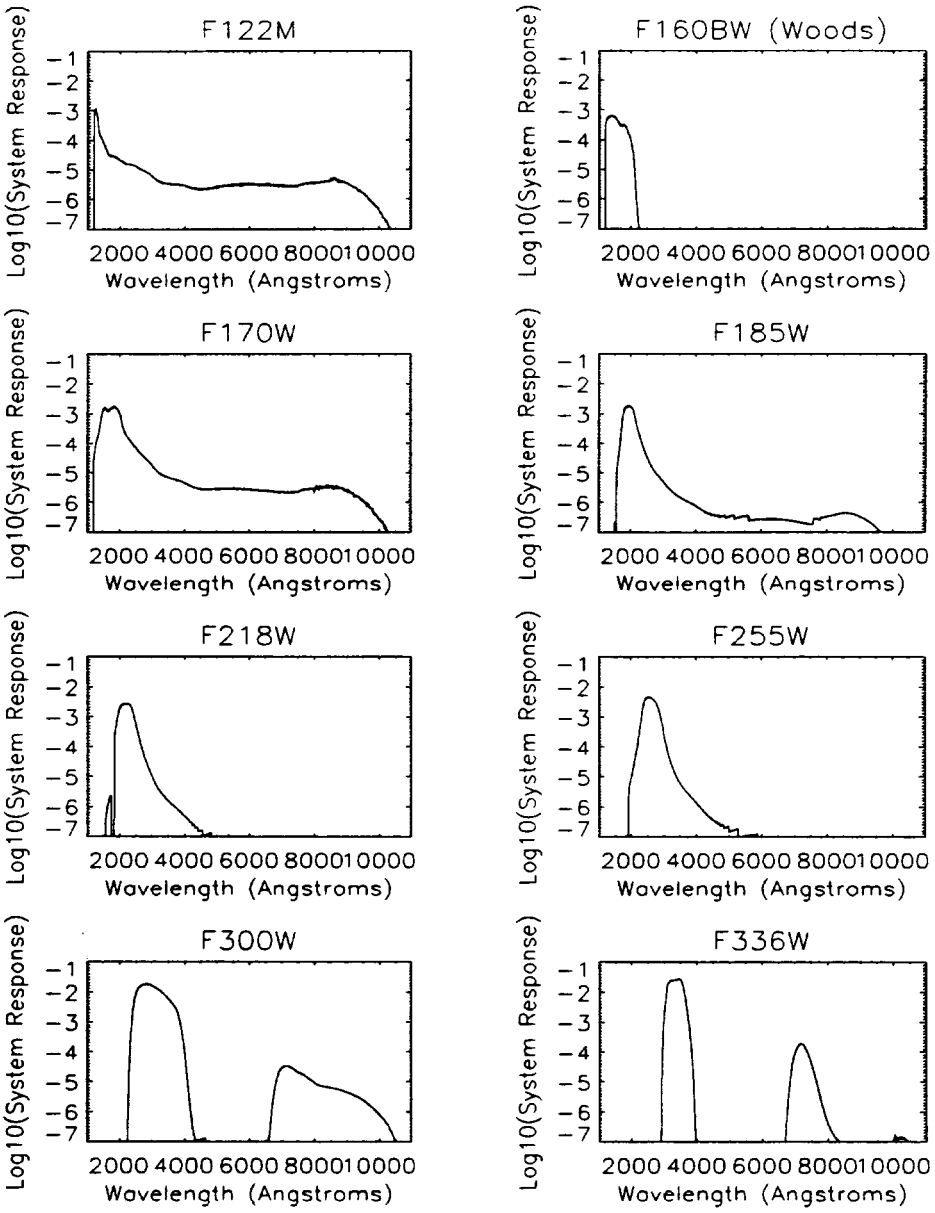

Table 3.13: Red Leak in UV Filters. A synthetic photometry calculation with de-reddened BPGS stellar spectra and system response from on-orbit data.

Filter		F122M	F160BW	F170W	F185W	F218W	F255W	F300W	F336W	F122M	F160BW	F170W	F185W	F218W	F255WI	F300W	F336W
Central λ (nm)		122	160	170	185	218	255	300	336	122	160	170	185	218	255	300	336
Cutoff λ (nm)		140	240	260	260	280	310	400	400	380	380	380	380	380	380	380	380
9 SGR	O5	16.9		0.7	0.4	0.2	0.3		0.1	0.3		0.1				0.5	0.1
9 SGE	O8F	16.9		0.7	0.4	0.2	0.3		0.1	0.3		0.1				0.5	0.1
HR 8D23	O6	21.8		1.0	0.5	0.3	0.4		0.1	0.6		0.1				0.6	0.1
-1935	B1V	20.1		0.8	0.4	0.3	0.4		0.1	0.6		0.1				0.6	0.2
60 CYG	B1V	20.1		0.8	0.4	0.3	0.4		0.1	0.6		0.1				0.6	0.2
102 HER	B2V	22.5		1.2	0.6	0.4	0.4	0.1	0.1	1.1		0.2	0.1			0.8	0.2
ETA HYA	B3V	22.7		1.2	0.6	0.4	0.5	0.1	0.1	1.3		0.3	0.1			0.9	0.2
IOTA HER	B3V	22.7		1.2	0.6	0.4	0.5	0.1	0.2	1.3		0.3	0.1			0.9	0.2
HR 7899	B4V	22.7		1.2	0.6	0.4	0.5	0.1	0.2	1.4		0.3	0.1			0.9	0.2
38 OPH	A1V	30.0		1.6	0.7	0.5	0.5	0.1	0.2	2.9		0.5	0.1			1.1	0.3
HR 7174	B6V	30.7		1.8	0.8	0.5	0.5	0.1	0.3	3.8		0.7	0.2		0.1	1.3	0.4
9 VUL	B7V	30.8		1.8	0.8	0.5	0.5	0.1	0.3	3.9		0.7	0.2		0.1	1.4	0.4
HD 189689	B9V	41.1		2.4	0.9	0.5	0.6	0.2	0.3	7.4		1.0	0.2		0.1	1.6	0.4
THETA VIR	A0V	59.6		4.0	1.2	0.6	0.8	0.3	0.6	20.3		2.2	0.4	0.1	0.1	2.5	0.7
NU CAP	B9V	58.6		3.7	1.2	0.6	0.8	0.3	0.5	18.3		2.0	0.4	0.1	0.1	2.2	0.6
HR 6169	A2V	59.5		4.0	1.2	0.6	0.8	0.3	0.6	20.1		2.2	0.4	0.1	0.1	2.3	0.7
HD 140849A	A1V	73.7		3.8	1.1	0.6	0.7	0.3	0.5	23.7		2.0	0.4	0.1	0.1	2.0	0.6
69 HER	A2V	59.5		3.9	1.2	0.6	0.8	0.3	0.6	20.0		2.2	0.4	0.1	0.1	2.2	0.7
HD 140849B	A3V	89.0		6.5	1.5	0.8	1.0	0.4	0.6	44.0		3.9	0.6	0.1	0.2	2.4	0.7
58 AQL	A0V	75.5		4.3	1.3	0.6	0.8	0.3	0.7	28.6		2.5	0.5	0.1	0.1	2.7	0.8
78 HER	B9V	75.0		4.2	1.2	0.6	0.7	0.3	0.7	27.5		2.4	0.5	0.1	0.1	2.4	0.8
HR 6570	A7V	89.7		7.0	1.6	0.8	1.0	0.4	0.7	47.6		4.4	0.7	0.1	0.2	2.6	0.9
HD 187754	A2V	97.9		11.0	2.1	0.9	1.2	0.5	0.9	64.4		7.4	1.0	0.2	0.2	3.2	1.1
THETA 1 SER	A5V	97.7		9.8	1.9	0.9	1.1	0.4	0.8	60.3		6.2	0.8	0.1	0.2	2.6	0.9
PRAESEPE 276		99.7		12.1	2.2	1.0	1.2	0.5	0.9	67.5		8.1	1.1	0.2	0.2	2.9	1.0
PRAESEPE 114		99.7		11.6	2.2	1.0	1.2	0.5	0.9	66.0		7.6	1.0	0.2	0.2	2.7	1.0
PRAESEPE 154		100.0		17.0	3.0	1.1	1.3	0.5	0.9	71.9		11.4	1.4	0.2	0.2	2.8	1.0
HD 140192	A5V	100.0		17.4	3.0	1.1	1.3	0.6	0.9	72.7		11.7	1.5	0.2	0.2	2.9	1.1
PRAESEPE 226		100.0		17.2	3.0	1.1	1.3	0.6	1.0	72.7		11.6	1.4	0.2	0.2	2.7	1.1
PRAESEPE 37		100.0		38.8	7.7	2.0	1.7	0.6	1.0	80.8		27.0	3.9	0.3	0.3	2.8	1.1

Table 3.13: Red Leak in UV Filters. A synthetic photometry calculation with de-reddened BPGS stellar spectra and system response from on-orbit data.

Filter		F122M	F160BW	F170W	F185W	F218W	F255W	F300W	F336W	F122M	F160BW	F170W	F185W	F218W	F255WI	F300W	F336W
Central λ (nm)		122	160	170	185	218	255	300	336	122	160	170	185	218	255	300	336
Cutoff λ (nm)		140	240	260	260	280	310	400	400	380	380	380	380	380	380	380	380
HD 191177	F4V	100.0		64.9	17.6	3.0	2.3	0.8	1.1	86.1		48.4	10.1	0.6	0.5	3.6	1.3
PRAESEPE 332		100.0		62.4	16.3	2.9	2.2	0.7	1.0	84.6		44.9	8.8	0.5	0.4	2.9	1.1
BD+293891	F6V	100.0		67.4	19.4	3.7	2.5	0.8	1.1	86.4		49.8	11.0	0.7	0.4	3.1	1.2
PRAESEPE 222		100.0		50.7	11.4	2.8	2.2	0.8	1.1	84.7		36.8	6.2	0.5	0.4	2.8	1.2
HD 35246	F8V	100.0		52.1	11.8	2.9	2.2	0.8	1.3	85.8		38.6	6.6	0.5	0.4	2.8	1.4
BD+263780	G0V	100.0		52.4	11.9	2.9	2.2	0.9	1.3	86.0		38.9	6.7	0.5	0.4	2.8	1.4
HD 148816	F9V	100.0		51.1	11.5	2.8	2.2	0.8	1.2	85.0		37.2	6.3	0.5	0.3	2.8	1.3
HD 155675	F8V	100.0		69.0	20.5	4.7	3.4	1.0	1.3	88.7		53.3	12.4	0.9	0.6	3.3	1.4
PRAESEPE 418		100.0		70.2	21.1	4.8	3.5	1.0	1.4	89.4		55.0	13.2	1.0	0.6	3.2	1.5
HYAD 1		100.0		71.4	21.9	4.8	3.5	1.1	1.5	90.0		56.8	14.1	1.0	0.6	3.4	1.6
HD 122693	F8V	100.0		71.6	22.1	4.9	3.5	1.1	1.6	90.1		57.1	14.2	1.1	0.6	3.5	1.7
HD 154417	F8V	100.0		70.6	21.4	4.8	3.5	1.1	1.4	89.5		55.5	13.4	1.0	0.6	3.2	1.5
HYAD 2		100.0		89.2	46.7	7.9	3.4	1.2	1.6	91.2		71.6	30.3	1.7	0.6	3.3	1.7
HD 227547	G5V	100.0		89.5	47.2	8.0	3.4	1.2	1.7	91.4		72.0	30.7	1.7	0.6	3.3	1.8
HD 154760	G2V	100.0		89.3	46.8	7.9	3.4	1.2	1.6	91.3		71.6	30.3	1.7	0.6	3.3	1.7
HD 140605	G2V	100.0		89.9	48.2	8.1	3.5	1.3	1.8	91.8		73.2	32.0	1.8	0.7	3.4	1.9
HYAD 15		100.0		90.1	48.5	8.0	3.5	1.3	1.8	92.1		73.7	32.5	1.8	0.7	3.4	1.9
HD 139777A	K0V	100.0		89.8	47.7	8.0	3.4	1.3	1.8	91.7		72.8	31.5	1.7	0.6	3.5	1.9
HD 136274	G8V	100.0		91.4	51.6	8.3	3.5	1.7	2.3	93.4		77.1	36.6	2.0	0.7	3.6	2.4
HYAD 26		100.0		91.6	52.3	8.3	3.6	1.7	2.3	93.5		77.6	37.3	2.1	0.7	3.6	2.4
HD 150205	G5V	100.0		91.7	52.3	8.4	3.6	1.7	2.4	93.5		77.6	37.4	2.1	0.8	3.8	2.4
HYAD 21		100.0		92.8	55.7	8.6	3.7	2.1	2.8	94.6		80.7	41.8	2.4	0.8	3.9	2.9
+02 3001	G8V	100.0		93.0	56.1	8.6	3.6	2.2	3.1	94.8		81.1	42.3	2.4	0.8	4.3	3.2
HD 190571	G8V	100.0	0.3	99.5	95.2	40.0	11.3	3.4	3.6	96.7	0.1	91.4	80.4	16.0	3.0	6.1	3.7
HYAD 183		100.0	0.3	99.6	96.0	41.6	11.7	4.3	4.6	97.5	0.1	93.1	83.8	18.3	3.4	6.7	4.7
HD 140470	K3V	100.0	0.3	99.6	96.2	42.2	11.9	4.5	4.8	97.5	0.1	93.3	84.4	19.0	3.5	7.0	4.9
HD 154712	K4V	100.0	0.2	99.7	95.7	45.7	15.8	6.6	6.7	98.3	0.1	95.3	87.4	24.6	5.4	9.4	6.8
HYAD 185		100.0	0.2	99.7	96.7	50.0	15.7	8.0	7.9	98.6	0.1	96.0	89.5	28.6	5.5	10.6	8.0
+382457	K8V	100.0	0.2	99.7	96.6	48.6	16.5	8.8	9.1	98.7	0.1	96.4	90.1	28.7	6.3	11.5	9.1

Table 3.13: Red Leak in UV Filters. A synthetic photometry calculation with de-reddened BPGS stellar spectra and system response from on-orbit data.

Filter		F122M	F160BW	F170W	F185W	F218W	F255W	F300W	F336W	F122M	F160BW	F170W	F185W	F218W	F255Wl	F300W	F336W
Central λ (nm)		122	160	170	185	218	255	300	336	122	160	170	185	218	255	300	336
Cutoff λ (nm)		140	240	260	260	280	310	400	400	380	380	380	380	380	380	380	380
HYAD 173		100.0	0.1	99.5	93.8	32.0	8.5	11.8	12.8	99.0		96.9	88.7	19.8	3.8	14.3	12.9
GL 40	M0V	100.0	0.1	99.6	94.9	34.5	8.8	14.5	15.4	99.2		97.5	90.7	22.8	4.2	17.4	15.5
HYAD 189		100.0	0.1	99.6	95.3	35.8	9.1	15.7	16.8	99.3		97.7	91.5	24.3	4.4	18.4	16.9
HD 151288	K7V	100.0	0.1	99.7	95.6	37.0	9.4	16.5	17.4	99.3		97.8	91.9	25.5	4.7	19.3	17.4
HD 157881	K7V	100.0	0.1	99.7	95.6	36.6	9.2	16.7	17.6	99.3		97.8	91.9	25.2	4.5	19.4	17.7
HD 1326d3	M0V	100.0	0.1	99.7	95.8	37.5	9.4	17.7	18.9	99.4		97.9	92.3	26.2	4.7	20.5	18.9
GL 15A	M0V	100.0	0.1	99.8	97.7	48.6	11.5	27.3	26.7	99.6	0.1	98.8	95.6	38.8	6.7	30.4	26.8
GL 49	M2V	100.0	0.1	99.8	97.3	45.8	10.7	25.5	25.0	99.6	0.1	98.7	95.1	35.9	6.0	28.7	25.1
GL 1D9	M4V	100.0	0.1	99.9	98.2	54.5	12.5	34.1	32.2	99.7	0.1	99.1	96.7	46.1	7.9	37.2	32.3
GL 15B	M6V	100.0	0.2	99.9	99.2	69.7	17.7	51.1	46.0	99.9	0.1	99.6	98.4	64.0	13.3	53.5	46.1
GL 83.1	M8V	100.0	0.1	99.7	95.9	38.2	8.9	17.4	15.5	99.4		97.9	92.4	26.8	3.9	20.1	15.5
GL 65	M5V	100.0	0.1	99.8	97.0	43.3	9.2	22.4	17.8	99.6		98.5	94.4	33.0	4.3	25.2	17.9

Note that the SYNPHOT synthetic photometry package can be used to estimate the counts contributed by red leaks for various particular situations, and for filters other than those plotted below.

There is significant time-variation of the UV throughput due to build-up of molecular contaminants on the CCD windows, and monthly decontamination procedures used to remove this contamination are discussed in Section 6.11.

3.9 Apertures

The WFPC2 camera configuration and filter set require a substantial number of apertures for full utilization of its capabilities. All possible aperture and filter combinations are given in Table 3.14 on page 74.

Each camera has an associated 'optimum' aperture close to the geometric center of its field-of-view (FOV). These positions have been adjusted to reflect CCD performance following SMOV and to allow for pyramid vignetting. The aperture designations are WF2, WF3, WF4, and PC1 for the individual cameras and WFALL for the three-WFC combination. WFALL is located close to the pyramid apex in WF3 (see Figure 3.12 on page 76). Observers are expected to place small or unresolved targets on these apertures. Note that normally all four CCDs are read out even if a specific CCD is selected with an aperture. This is discussed in Section 2.8. The positions of these apertures may be updated if bad pixels, etc., appear on the CCDs.

In cases where the observer does not want to use the current 'optimum' centers, a complimentary set of apertures has been implemented specifically for this purpose. These locations remain fixed and correspond roughly to the geometric center of each camera's field-of-view. They are designated WF2-FIX, WF3-FIX, WF4-FIX, PC1-FIX, and WFALL-FIX. Observers are expected to place extended targets on these apertures.

As of July 2004 the 'optimum' apertures have remained identical to their 'FIX' counterparts, with the only exception being WF3 which has moved slightly from WF3-FIX.

An additional set of aperture names have been defined for use with the WFPC2 filters which require partial rotations. The characteristics and uses of these filters are discussed earlier in this chapter. In the nominal filter position, the three WFC segments of the [OII], Methane and Polarizer quad filters can be selected with an aperture for each camera corresponding to the optimum or geometric camera centers. The partially rotated quad filters, which generally fall into more than one camera, have been assigned apertures in the camera which provides the largest clear aperture. The pixel coordinates of these apertures will be reviewed on a regular basis to reflect changes in CCD and filter cosmetics. There are no analogous fixed

apertures for the partially rotated filter configurations. The aperture name is generally the same as the (rotated) filter name. For the Wood's filters, the nominal filter position is used for the PC1 FOV only, while the rotated filter position is used for WFC observations. The linear ramp filters are unique because the ultimate location of the target will be determined from the central wavelength specified, and therefore only the generic aperture name LRF is required.

Occasionally the V2-V3 coordinates of the WFPC2 apertures are updated to correct slow drifts of the HST focal plane relative to the spacecraft (V1, V2, V3) system. Table 3.15 on page 75 shows this history. The V2-V3 coordinates prior to 1996 day 127 for any aperture can be derived by setting ($V2_2$,$V3_2$) to the values in Table 3.14 on page 74, and then computing the earlier coordinates. The V2-V3 coordinates after 1997 day 335 can also be computed in a similar maneuver.

Table 3.14: Aperture Definitions. The pixel coordinate system uses pixel numbers (row, column) for the CCD in use. See Figure 3.12 on page 76 or Figure 1.1 on page 2 for the definition of the V2-V3 coordinate system.

Aperture Name	Filter Name	CCD	Location	CCD Pixel		Coordinates[a]	
				X	Y	V2	V3
PC1		PC	Optimum center PC	420	424.5	2.160	-30.490
WF2		WF2	Optimum center WF2	423.5	414	-51.530	-5.920
WF3		WF3	Optimum center WF3	436[b]	424.5[b]	-0.150	48.470
WF4		WF4	Optimum center WF4	423	421	54.830	-6.320
WFALL		WF3	Optimum near apex	133[c]	149[c]	2.020	7.920
PC1-FIX		PC	Fixed center PC	420	424.5	1.810	-30.900
WF2-FIX		WF2	Fixed center WF2	423.5	414	-51.530	-5.920
WF3-FIX		WF3	Fixed center WF3	416.5	424.5	1.230	47.100
WF4-FIX		WF4	Fixed center WF4	423	421	54.830	-6.320
WFALL-FIX		WF3	Fixed near apex	133[c]	149[c]	2.020	7.920
FQUVN33	FQUVN33	WF2	Optimum for FOV	292	520	-49.924	10.802
POLQN33	POLQN33	WF2	Optimum for FOV	292	520	-49.924	10.802
POLQN18	POLQN18	WF2	Optimum for FOV	380[d]	200[d]	-33.280	-17.717
POLQP15P	POLQP15	PC	Optimum for FOV	200	680	-13.057	-31.643
POLQP15W	POLQP15	WF2	Optimum for FOV	500	260	-45.892	-22.069
FQCH4NW2	FQCH4N	WF2	Optimum for FOV	602	608	-77.669	-5.102
FQCH4NW3	FQCH4N	WF3	Optimum for FOV	602	608	0.928	72.995
FQCH4NW4	FQCH4N	WF4	Optimum for FOV	640	386	67.687	11.323

Table 3.14: Aperture Definitions. The pixel coordinate system uses pixel numbers (row, column) for the CCD in use. See Figure 3.12 on page 76 or Figure 1.1 on page 2 for the definition of the V2-V3 coordinate system.

Aperture Name	Filter Name	CCD	Location	CCD Pixel		Coordinates[a]	
				X	Y	V2	V3
FQCH4N33	FQCH4N33	WF2	Optimum for FOV	264	436	-41.997	6.950
FQCH4N15	FQCH4N15	PC	Optimum for FOV	420	424.5	2.164	-30.494
FQCH4P15	FQCH4P15	PC	Optimum for FOV	400	312	5.129	-26.221
F160BN15	F160BN15	WF3	Optimum for FOV	436	424.5	-0.153	48.470

a. V2-V3 coordinates in effect 1996 day 127 (May 6) to 1997 day 335 (December 1). CCD pixel positions unchanged.
b. CCD pixel position in effect after 1994 day 101 (April 11).
c. WFALL and WFALL-FIX “meta-chip” coordinates are (903,904).
d. CCD pixel position in effect after 1995 day 86 (March 27).

Table 3.15: Updates to (V2,V3) Positions of WFPC2 Apertures.

Date in Effect	V2	V3	Rotation
1994 day 101 - 1996 day 105	$V2_0$	$V3_0$	PA_0
1996 day 105 - 1996 day 127	$V2_1 = V2_0 - 0.12''$	$V3_1 = V3_0 + 0.11''$	$PA_1 = PA_0 + 0.14^\circ$
1996 day 127 - 1997 day 335	$V2_2 = V2_0 + 0.46''$	$V3_2 = V3_0 + 0.39''$	$PA_2 = PA_0 + 0.14^\circ$
> 1997 day 335	$V2_3 = V2_0 + 0.67''$	$V3_3 = V3_0 + 0.61''$	$PA_3 = PA_0 + 0.14^\circ$

Figure 3.12: Precise CCD Alignments and Primary Aperture Locations. “FIX” apertures are in the same locations, unless otherwise indicated. Dashed lines show vignetted region along CCD boundaries. Short lines and “X”s in outer corners indicate directions of CCD bloom and OTA diffraction spikes, respectively. Origin of the (V2, V3) system is at the origin of the plot axes, with V2, V3, and U3 exactly along diagonal lines as marked. (V2,V3) system is post-1996 day 127. CCDs have pixel (1,1) located where the four CCDs overlap.

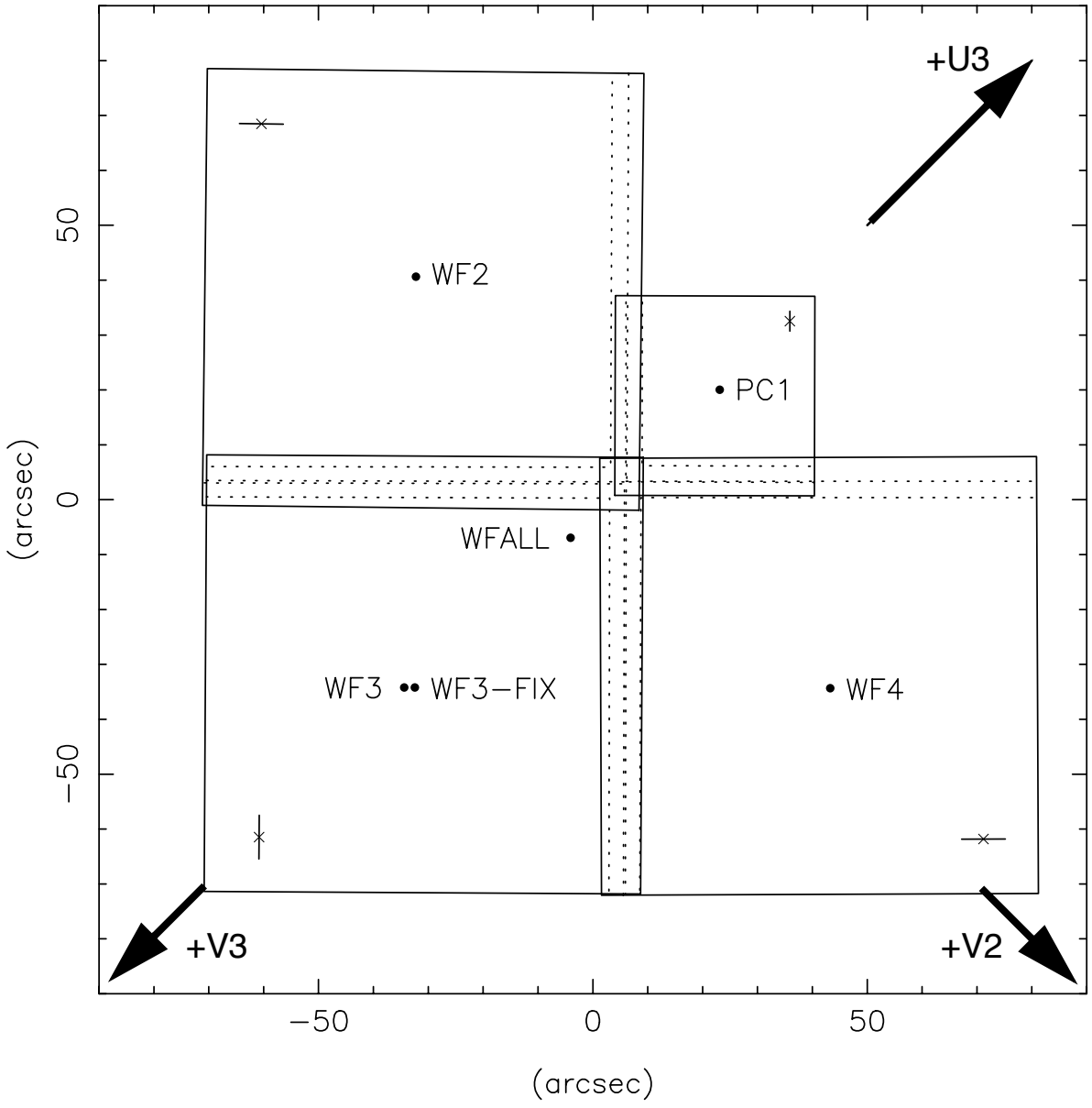

CHAPTER 4:

CCD Performance

In this chapter . . .

4.1 Introduction

The WFPC2 CCDs are thick, front-side illuminated devices, with a format of 800x800, 15x15μm multi-pinned phase (MPP). MPP allows CCD exposure with the total inversion of all phases. The Si-SiO_2 interface, at the surface of the CCD, is pinned at the substrate potential, directing signal charge away from the Si-SiO_2 interface states towards the buried n-channel. Figure 4.1 on page 78 shows a schematic which illustrates the principle of MPP (modified from Janesick, et al. 1989). The front-side Si-SiO_2 interface significantly affects the performance of CCDs, so MPP operation yields many practical benefits including reduced dark noise, better charge transfer efficiency (CTE), rapid removal of residual images, excellent pixel-to-pixel uniformity, and improved radiation hardness. MPP technology has been demonstrated and characterized in both Loral

(Janesick, et al., 1989) and Tektronix devices (Woodgate, et al., 1989). The CCD sensors for WFPC2 were made by Loral in 1991 and processed and packaged for flight at JPL.

Figure 4.1: MPP Operating Principle. A schematic showing the ideal potential profile through a frontside illuminated CCD whose front surface is inverted with multi-pinned phase (MPP). The CCD consists of a polysilicon gate, which forms part of the electrode structure, a surface layer of oxidized silicon (SiO_2) and the epitaxial layer which comprises p-doped silicon with an n-doped buried channel for charge transfer. MPP pins the surface potential by populating the Si-SiO_2 interface with holes. The holes passivate the Si-SiO_2 interface states and create an electric field which directs signal charge away from the interface towards the buried n-channel.

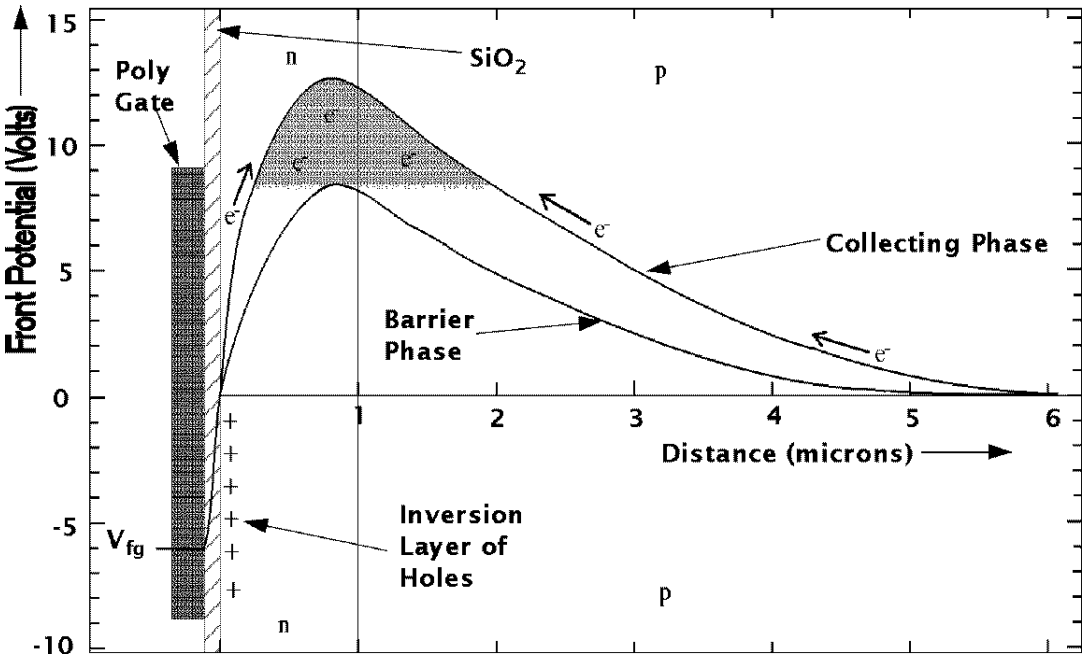

The Loral CCDs are illuminated from the 'front' surface, i.e., the light passes through the polysilicon gate structure overlying the 10μm thick active silicon layer. Because the WFPC2 devices are front-side illuminated and supported by a bulk silicon substrate, the CCD surface is flat, which has reduced the uncertainties in the astrometric calibration to about the 1/10 pixel level.

In this section the performance of the WFPC2 CCDs is reviewed, and compared to the earlier WF/PC-1 devices. A summary of device characteristics is given in Table 4.1 on page 79.

Table 4.1: Comparison of WF/PC-1 and WFPC2 CCDs.

Parameter	WF/PC-1[a]	WFPC2
Device	TI	Loral
Architecture	Thinned	Thick
Illumination	back-side	front-side
Format	800×800	800×800
Pixel size	152 μm	152 μm
UV Phosphor	Coronene	Lumogen
Dark rate	0.03 e^- $pixel^{-1}$ s^{-1}(-87°C)	~0.0045 e^- $pixel^{-1}$ s^{-1}(-88°C)
Read noise	13e^- RMS	5e^- RMS
Full well depth	40,000 e^-	~90,000 e^-
Gain	8e^- DN^{-1}	7e^- DN^{-1} or 14e^- DN^{-1}
ADC range	12 bits (4096 DN)	12 bits (4096 DN)
Full range (e^-)	~30,000e^-	~53,000e^-
QE 6000Å	50%	35%
QE 2500Å	12%	15%
WFC resolution	0.10″ $pixel^{-1}$	0.0996″ $pixel^{-1}$
PC resolution	0.043″ $pixel^{-1}$	0.0455″ $pixel^{-1}$

a. WF/PC-1 data are available through the STScI data archive.

4.2 Quantum Efficiency

The Loral CCDs are thick, front-side illuminated devices. This lowers their intrinsic QE, due to the absorption of incident light by the polysilicon electrode structure on the front-side surface of the CCD. We also note that due to its MPP operation, the QE of the Loral devices is stable without maintenance such as UV flooding.

The front surfaces of the CCDs are overcoated with a Lumogen phosphor, which serves as the primary detection medium for photons shortward of about 4800Å, down-converting these to 5100Å - 5800Å. Its long wavelength cutoff (4800Å) is also well matched to a CCD's intrinsic sensitivity. The QE of the four flight WFPC2 CCDs is shown in Figure 4.2 on page 80, which demonstrates the uniform UV response of 10-15% and a peak optical QE of 40%.

This phosphor coating also produces an enhancement of DQE at visual wavelengths, since it acts as an anti-reflection coating.

Figure 4.2: Pre-flight DQE Measurements on WFPC2 CCDs. The differences between the chips are probably due to systematic measurement error, and do not reflect a real difference in sensitivity.

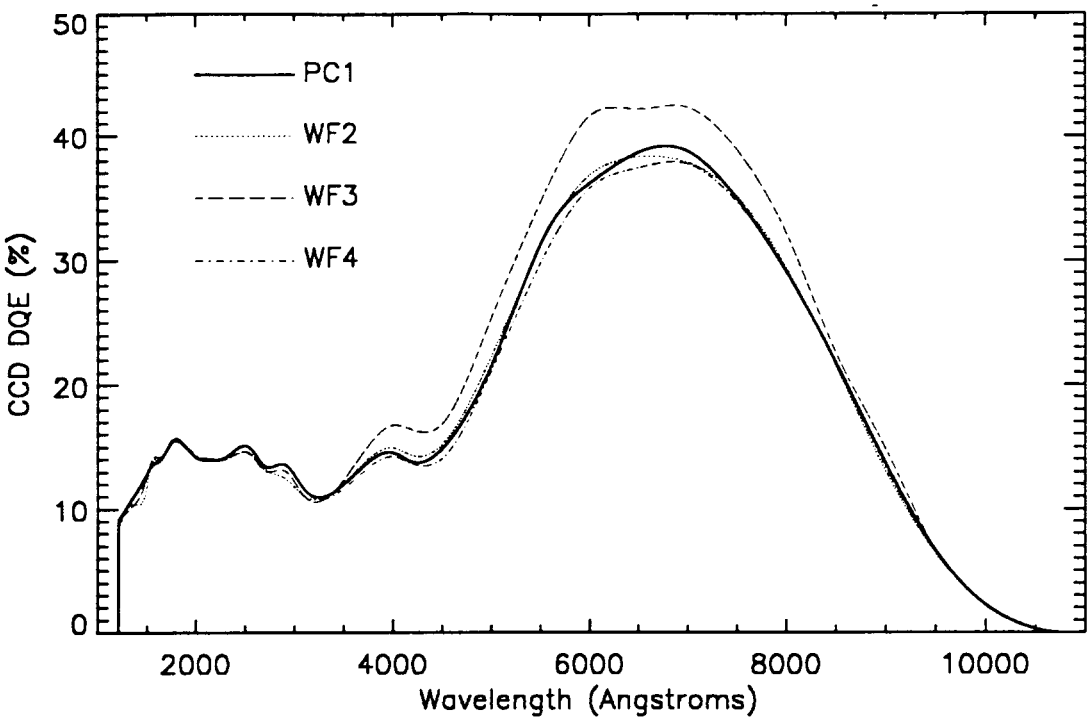

4.3 Dynamic Range

Linear full well capacity for these devices, clocked appropriately for the MPP mode, is approximately 90,000e^- $pixel^{-1}$. Flight qualified ADCs with higher dynamic range (>12 bits) were not available, so WFPC2 operates the two available ADCs at different gain factors, to take partial advantage of both the low read noise and large available full well depth.

One channel has a gain of 14e^- DN^{-1}, which significantly undersamples the CCD read noise (5 e^- $pixel^{-1}$ RMS), and gives a digital full well of about 53,000e^-. The other channel has a gain of 7e^- DN^{-1} which is comparable to the CCD read noise, and saturates at about 27,000e^-. The choice of gain factor is determined by the scientific objective. The 7 e^- DN^{-1} channel is best suited for faint object and UV imaging, where the lower CCD read noise will be most effective. For example, it should be used for UV imaging of planets or narrowband imaging of high redshift galaxies. The 14 e^- DN^{-1} channel has slightly higher effective read noise due to the quantization granularity, but can be used for programs where a signal level in excess of 27,000e^- is required. Even when imaging faint

sources, it may be desirable to retain the high signal-to-noise information on brighter field stars as a PSF reference.

Use of the 14 e^- DN^{-1} channel also allows reasonable recovery of counts for isolated, saturated point sources by summing over the saturated pixels (assuming that the charge bleeding does not extend to the edges of the CCD). See Gilliland (1994).

4.4 Bright Object Artifacts

4.4.1 Blooming

Blooming up and down a CCD column occurs when more than about 90,000e^- (the full well capacity) are collected in any pixel. When the pixel is full, the charge will flow into the next pixels along the column, and so on. The orientation of the bloomed column(s) on the sky depends on the readout direction of the particular CCD (see Figure 1.1 on page 2 or Figure 3.12 on page 76) and the roll angle of the spacecraft. This effect is visible in Figure 4.3 on page 83 which shows a logarithmic stretch of the image resulting from a 100s exposure on a star of V magnitude 2.6 through filter F502N in the PC.

Extreme overexposure of the Loral CCDs is not believed to cause any permanent effects, and therefore the WFPC2 does not have a bright object limit.

The WFPC2 CCDs can be operated in a non-standard mode during the integration phase of an exposure, in order to limit the blooming to only those columns containing the bright sources. This is accomplished by operating the serial transfer register clocks during the integration (using the optional parameter CLOCKS as specified in the Proposal Instructions). See Section 2.6, “Serial Clocks”, on page 33 for details.

4.4.2 Horizontal Smearing

During readout of a badly overexposed image, there is spurious charge detected by the readout electronics. The apparent brightness of the stellar halo is higher to the right of the saturated columns. This is particularly obvious at the bottom of the image in Figure 4.3 on page 83 which is a region in the shadow of the pyramid edge.

The horizontal “smearing” seen in highly saturated images can be modeled as an exponential function which decays over a few rows after a saturated pixel is encountered. The effect itself temporarily saturates after about ten saturated pixels (subsequent saturated pixels have no effect). The

effect is twice as bad with gain 7 e^- DN^{-1} than with gain 14 e^- DN^{-1}. This model only works on very highly saturated stellar images.

In Figure 4.3 on page 83, the image to the right side of the saturated columns is brighter than the left side; and the brightness increases as the number of saturated columns increases. This effect appears to be a signal which starts at a saturated pixel and decays over the next few rows, wrapping around as it does so. The signal is additive with each successive saturated pixel. Jumps are obvious when the number of saturated columns changes. The problem is a known characteristic of the amplifier electronics, and an effort was made to minimize it during design. The increase in signal in rows with saturated pixels is also seen in the over-scan region (the over-scans are provided in "`.x0d`" files from the pipeline).

An approach to calibrating out the horizontal smearing is described here. An exponential function fits the effect reasonably well. An appropriate algorithm creates an array to contain the signal model. It searches through the uncalibrated image (with the over-scan region included) in the sequence in which the pixels are read out. When it encounters a saturated pixel, it adds an exponential function to the model array, beginning at that pixel. The function has the form $s(x)=Ae^{-x/h}$, where x is the offset from the saturated pixel and only positive x values are included. The half-width, h, and amplitude, A, appear to vary from frame to frame and must be determined on the image itself. As more saturated columns are encountered in a row, the signal intensity builds up in the model image. The image can then be "improved" by subtracting the model from the raw image.

The amplitude and half-width parameters can be obtained by trial and error. The typical parameters vary slightly for each chip. The amplitude per saturated pixel is typically 1.75 DN (gain 7) or 0.2 DN (gain 14). On the other hand the half-width at a gain of 14 is larger (h=1800) than at 7 (h=350). So the total integrated effect is about twice as bad at gain 7. A straightforward application of the above algorithm cleaned up most of the signal in rows which had a few saturated columns, but over-subtracted in rows with a large number. The algorithm can be modified to saturate by making the parameter A, which gives the peak contribution from a single saturated pixel, depend on the current level of the effect: $A=A_0*(1-C/C_{max})$. This implies that the correction is never larger than C_{max} no matter how many saturated pixels are encountered. C_{max} is approximately 14 DN for a gain of 7 and 10 DN for a gain of 14.

The algorithm gives improvement only on highly saturated stellar images (where the star is saturated to 3 or 4 columns at the edges of the chip). On less saturated data, it over-subtracts significantly. This indicates that the problem is nonlinear, and therefore a general algorithm applicable to all data will be difficult to develop.

4.4.3 Diffraction Effects and Ghost Images

Several other artifacts that are common in saturated stellar images are also obvious in Figure 4.3 on page 83. The spider diffraction spikes caused by both the OTA spiders and internal WFPC2 spiders are at 45˚ to the CCD columns in all cameras.

The halo around the stellar image is well above the diffraction limit in intensity. Also there are ghost images which result from internal reflections in the filters and in the field-flatteners. These topics are discussed fully in the next Chapter.

Figure 4.3: Saturated Stellar Image Showing Horizontal Smearing.

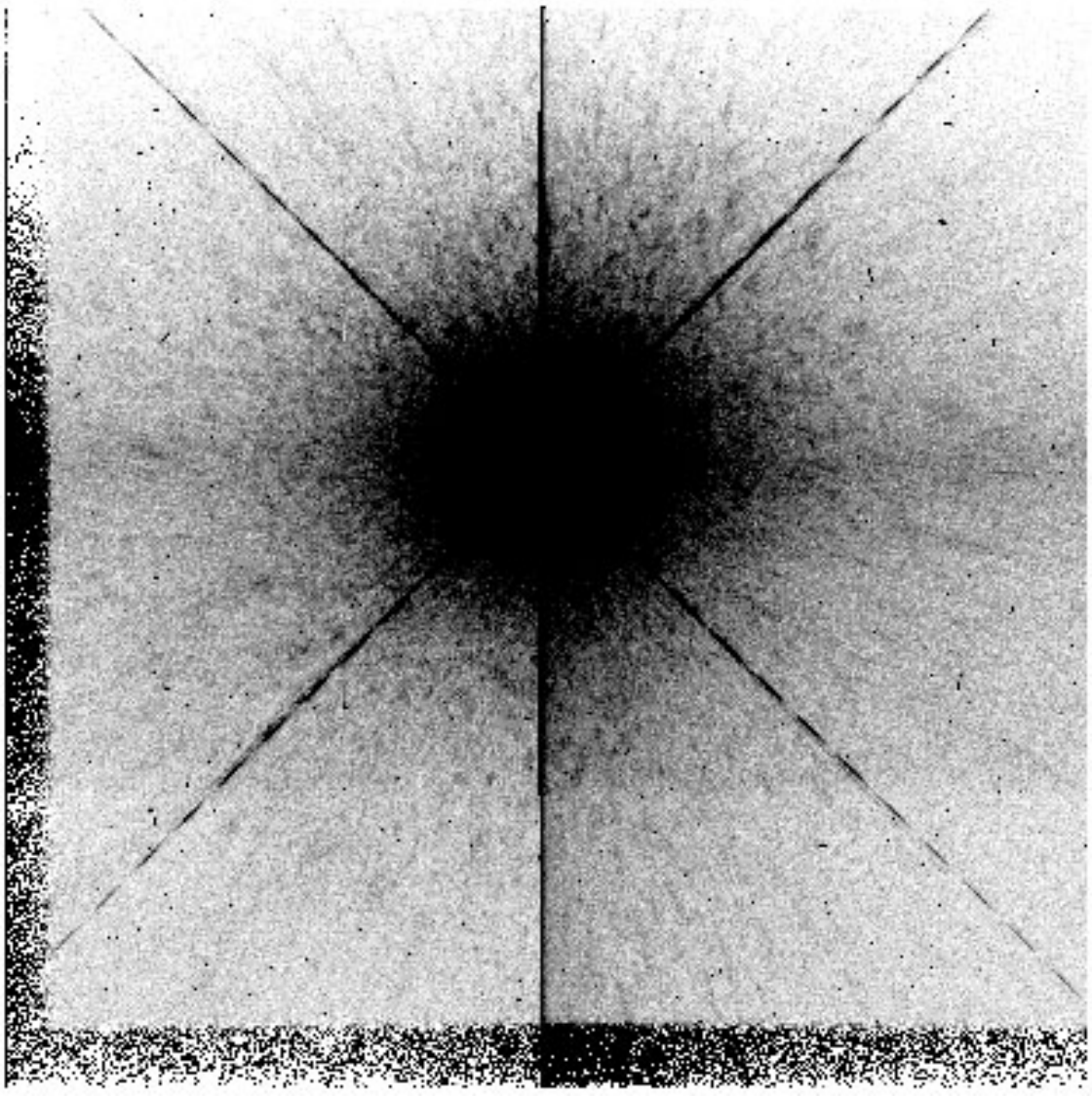

4.5 Residual Image

Residual images are seen in front-side-illuminated CCDs, and are associated with the front-side Si-SiO_2 surface interface. When the full well is exceeded, electrons can become trapped at the Si-SiO_2 interface. This trapped charge is slowly released giving rise to residual images. Inverted phase operation (MPP) allows holes to recombine with the trapped electrons at the front-side interface, and so residual images dissipate in a matter of minutes.

A second potential source of residual images, which occurs only in front-side-illuminated CCDs, is known as residual bulk image (RBI). Long wavelength photons can penetrate deeply enough to produce charge in the substrate. Most of this charge recombines rapidly (due to short carrier lifetimes), but some may diffuse into the epitaxial layer, where it can become trapped in epitaxial interface states. Residual images can occur as this charge is slowly released during an exposure. RBI is temperature sensitive since the bulk trapping time constants decrease with increasing temperature. The WFPC2 CCDs do exhibit RBI, but at -70˚C trapped charge rapidly escapes so that residual images disappear within 1000s (currently the CCDs are operated at -88˚C). Driven by the WFPC2 electronics, the CCDs recover quickly from large over-exposures (100 times full well or more), showing no measurable residual images a half hour after the overexposure.

For images exposed below the saturation level there is a very weak residual image due to charge trapping and charge transfer efficiency (CTE) problem. Measurements on 1800s dark frames interleaved with 2800s exposures of a star field yield a residual flux of 0.3% ± 0.1% of the original star flux, for stars with fluxes from 65 to 17,000 total counts. For typical star fields observed by WFPC2, these residual images are likely to be a problem only for stars that were saturated in a previous image, or for programs where long exposures in low throughput filters are taken immediately after highly exposed images. Hence, repeated exposures at the same CCD position should not lead to any appreciable systematic offset in photometry. CTE is further discussed in Section 4.12.

4.6 Quantum Efficiency Hysteresis

The problem of quantum efficiency hysteresis (QEH) due to back-side charge accumulation has been reviewed in detail by Griffiths, et al. (1989), and Janesick and Elliot (1991). QEH is not present in the Loral CCDs, because they are front-side illuminated and incorporate MPP operation. This has been verified in component tests at JPL. The absence of QEH means that the devices do not need to be UV-flooded, and so decontamination procedures are planned without the constraint of maintaining the UV-flood.

4.7 Flat Field Response

The flat field response is uniform within a few percent, with the exception of a manufacturing pattern defect which generates a 3% reduction in QE once every 34 rows. This pattern defect is caused by a manufacturing error in producing the CCDs; there was a 0.5μm overlap between adjacent 1024x0.5μm raster scans during the construction of the masks used to fabricate the chips. It is identical in all CCDs. The net effect is that every 34^{th} row on the CCD is approximately 3% too narrow. Photometry of point sources imaged onto these defects will be affected, since the error conserves counts, while flat fields (which are designed to produce a uniform image from a uniformly illuminated target) will effectively multiply the counts in these rows by 1.03. In applications requiring precision photometry across a wide field, it may be useful to correct the images for this flat field effect before performing photometry. There is also an astrometric offset of approximately 3% of the pixel height (0.003″ in the WFCs) every 34 rows. Anderson and King (1999) present a nice discussion of these effects.

WFPC2 flat fields also include instrumental effects such as vignetting and shadowing by dust particles, and illumination variations related to optical geometric distortion. For further discussion see Section 5.11.

Figure 4.4: WFPC2 CCD Flat Field.

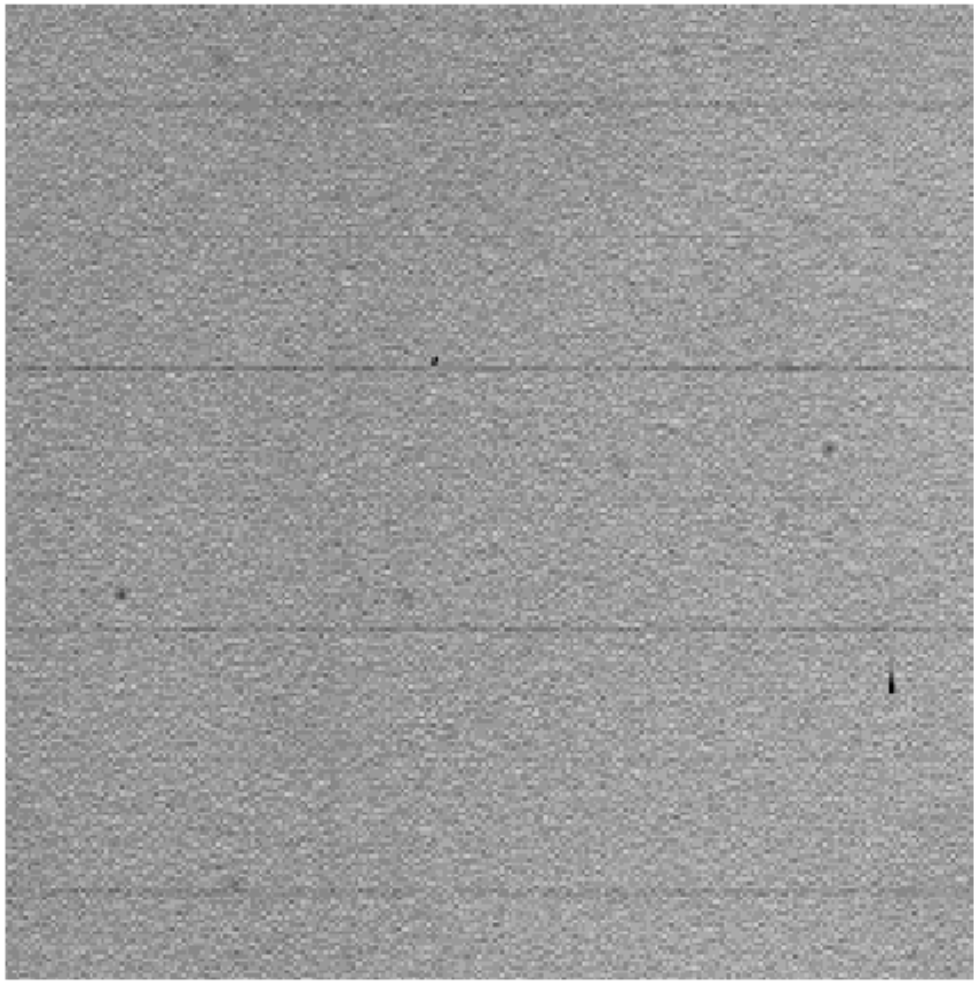

The WFPC2 CCDs have an intrinsically uniform flat field response since they are not thinned, so there are no large-scale chip non-uniformities resulting from the thinning process. MPP operation also improves pixel-to-pixel uniformity because charge transfer is driven deep into the buried n-channel, away from the influence of Si-SiO_2 interface states. The WFPC2 CCD flat fields show an overall pixel-to-pixel response having <2% non-uniformity. Figure 4.4 on page 86 shows a portion of a WFPC2 CCD flat field obtained during quantum efficiency measurements at JPL. The image illustrates the excellent pixel-to-pixel uniformity of the Loral devices. The 34 row defect is clearly visible, and its amplitude of 3% serves to calibrate the gray scale.

4.8 Dark Backgrounds

Low dark noise is one of the benefits of MPP, since inverted phase operation suppresses the dominant source of CCD dark noise production ($Si\text{-}SiO_2$ surface states). The remaining source of dark noise, thermal generation in the silicon bulk, is determined by the quality of the silicon used in chip fabrication. The intrinsic dark rate of WFPC2 CCDs is <0.01 e^- $pixel^{-1}$ s^{-1} at temperatures below -80°C.

Figure 4.5: Average Dark Rates vs. CCD Row.

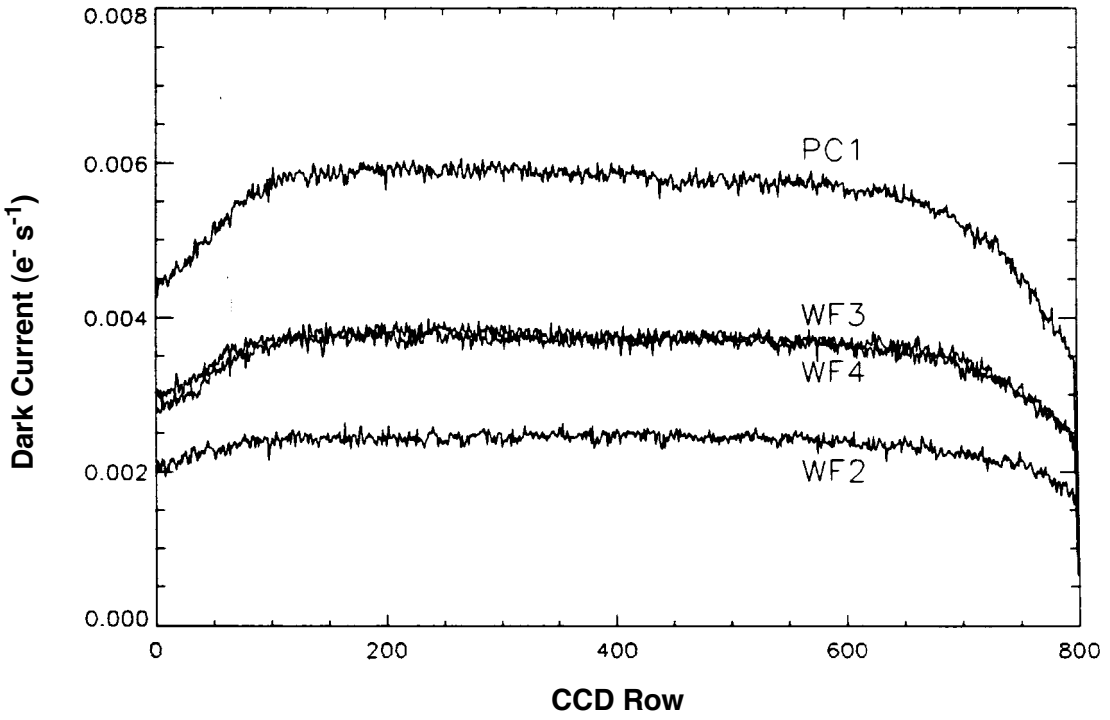

The temperature set-points for the WFPC2 TEC coolers are: -88, -83, -77, -70, -50, -40, -30 and -20 °C. The corresponding approximate median dark rates are given in Table 4.2 on page 88. For instrument health and safety reasons, GOs cannot command temperature changes.

4.8.1 Sources of Dark Current

The dark current appears to have two components: one from electronic sources in the CCD, and a second component whose strength correlates with the cosmic ray flux. The electronic dark current is ~0.001 e^- s^{-1}, consistent with the Thermal Vacuum Test data.

The second component of dark current appears only on-orbit, its strength drops towards the edges of each CCD, and it is both chip- and

time-dependent. At the current operating temperature, this non-electronic component constitutes up to 80% of the total signal measured in the PC. The fraction and overall level are lower in the other chips, and lowest in WF2. This second component ranges from 0.001 $e^- s^{-1}$ (WF2) to 0.005 $e^- s^{-1}$ (PC). The edge drop off is shown in Figure 4.5 on page 87, where the average of lines 200-600 for each chip (with hot pixels rejected) is plotted in $e^- s^{-1}$ as a function of column number. The drop near the edge is consistent with luminescence from the CCD windows, shadowed by a field stop mask just in front of the CCD.

Table 4.2: Dark Count Rates.

CCD Temperature (˚C)	Dark count rate ($e^- s^{-1}$ $pixel^{-1}$)
-20	10.0
-30	3.0
-40	1.0
-50	0.3
-70	0.03
-77	0.016
-83	0.008
-88	0.0045

A further indication of the possible origin of this second component is the correlation between its amplitude and the cosmic ray activity in the same exposure, as shown in Figure 4.6 on page 89. For example, the cosmic ray flux in the PC varies from $7x10^5$ to $13x10^5$ DN per 1000s, while the total dark signal in the PC varies concurrently between 0.0007 and 0.0010 DN s^{-1}. Similar, though slightly smaller effects are seen in the WFC CCDs. These clues point to cosmic-ray induced scintillation of the MgF_2 field-flattening windows as a likely source of the second dark current component. This might be caused by impurities in the MgF_2 windows; if so, the window of WF2 must contain substantially less impurities. However, other explanations cannot be completely ruled out at this point.

Figure 4.6: Dark Signal vs. Cosmic Ray Flux. Slopes and intercepts (“int”) are given on plots. Units are DN/1000s; 1 DN ~ 7 e^-.

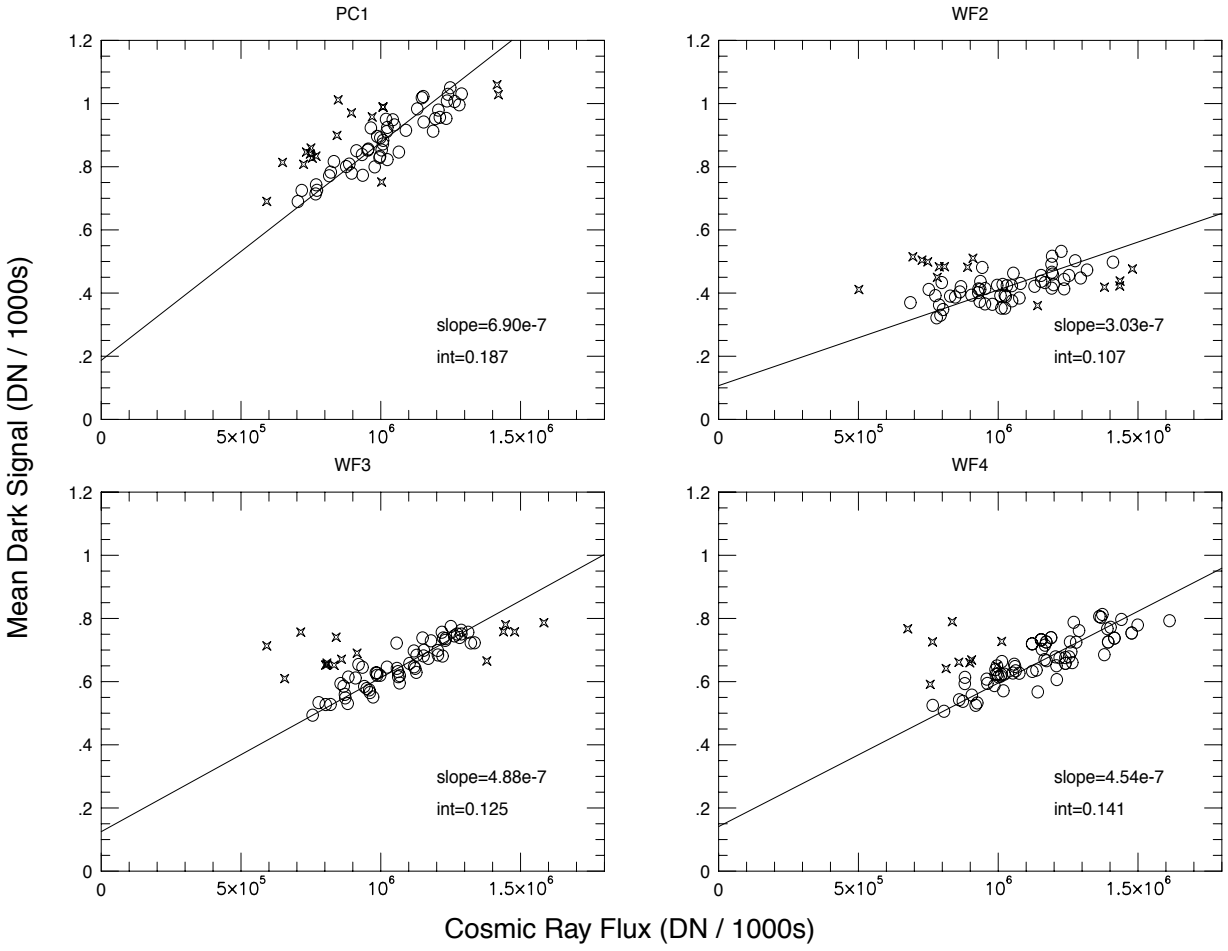

For the great majority of WFPC2 observations, this effect is negligible. In fact, it is noticeable mainly because the true dark rate is very low at the -88˚C operating temperature. However, observations for which the dark current is an important limiting factor, either due to noise or background flatness, will require special handling to remove the signature of the dark current properly, as its amplitude depends on the time-variable cosmic ray flux.

4.8.2 Darktime

As of this writing, the “*DARKTIME*” keyword in the WFPC2 image headers does not reflect correctly the actual time during which the CCD collects dark current. Instead, *DARKTIME* is merely set equal to *EXPTIME* (the exposure time) in the data headers, and this value is used for calibration. The error is small, and usually unimportant, but could be

significant for programs aimed at measuring the absolute level of the sky background. The actual darktime in seconds is given by

$$DARKTIME = 60 \times int\left(\frac{t + 16.4}{60}\right) + 43.6 + 13.6 \times (n - 1) + 60 \times (restart) \qquad (4.1)$$

where t is the requested exposure time in seconds, and n is the number of the CCD (PC1=1, WF2=2, etc.), and *int()* indicates the next lower integer. A duration of 16.4s is required to clear the CCDs before the exposure begins, and 13.6s is needed to read each CCD after the exposure. External exposures of 180s or longer made with the serial clocks off (CLOCKS=NO; the default setting) suffer an additional 60s of darktime (*restart*=1). This delay is associated with restarting the serial clocks for readout in exposures where the spacecraft AP-17 processor provides shutter control with loss-of-lock checking. Exposures made with the serial clocks on (CLOCKS=YES) avoid this extra 60s (*restart*=0).

We note that bias frames contain approximately $43.6 + 13.6 \times (n - 1)$ seconds of dark current. No attempt is made to subtract this from the bias images when creating calibration files for use in the calibration pipeline. This effect is unimportant for most observations, but could be significant if one averaged many undithered deep exposures of the same field, or if one is interested in measuring the absolute level of the sky background. If the dark current were constant in time, this could be corrected by merely changing the value of *DARKTIME* used during calibration. However, the hotpixels vary on monthly timescales, so this simple correction is only partially successful.

The timing of dark calibration frames is slightly different from that of external science exposures. Dark calibration frames always have *restart*=0 in Equation 4.1.

The dark calibration reference file in the pipeline is revised weekly to track variations in the hot pixels. The current method of generating these files is to combine the bright hot pixels from typically five on-orbit dark frames taken over the space of about one week, with the low-level dark current from the average of 120 on-orbit dark frames spanning a much longer time period. This method gives an optimal combination of low noise and accurate tracking of hot pixels. Care is also taken that the same super-bias reference files is used for both science data and generation of the dark reference file, as this tends to reduce the noise in long exposures. (Early dark reference files used a much simpler method, and were typically combinations of about ten dark frames taken over two weeks.)

4.8.3 Dark Current Evolution

The dark current in WFPC2 has had an interesting evolution over the lifetime of the instrument. Figure 4.7 on page 91 shows the median dark current for the central 400 x 400 pixels of each CCD at gain 7, each taken

just after WFPC2's monthly decontamination. Each data point represents the median of five raw 1800s dark frames (after rejection of cosmic rays and bias subtraction, normalized to units of DN/1000sec). As such, this plot reflects the uniform, low-level dark current near the center of each detector. During the first six years the dark current increased approximately linearly with time; the dark current increased by a factor of about 2 in the WFC CCDs and by a factor of ~1.3 in the PC. But after 1998 (MJD > 51200) the dark current leveled-off, and perhaps decreased somewhat.

Figure 4.7: Dark Evolution from 1994 to 2004.

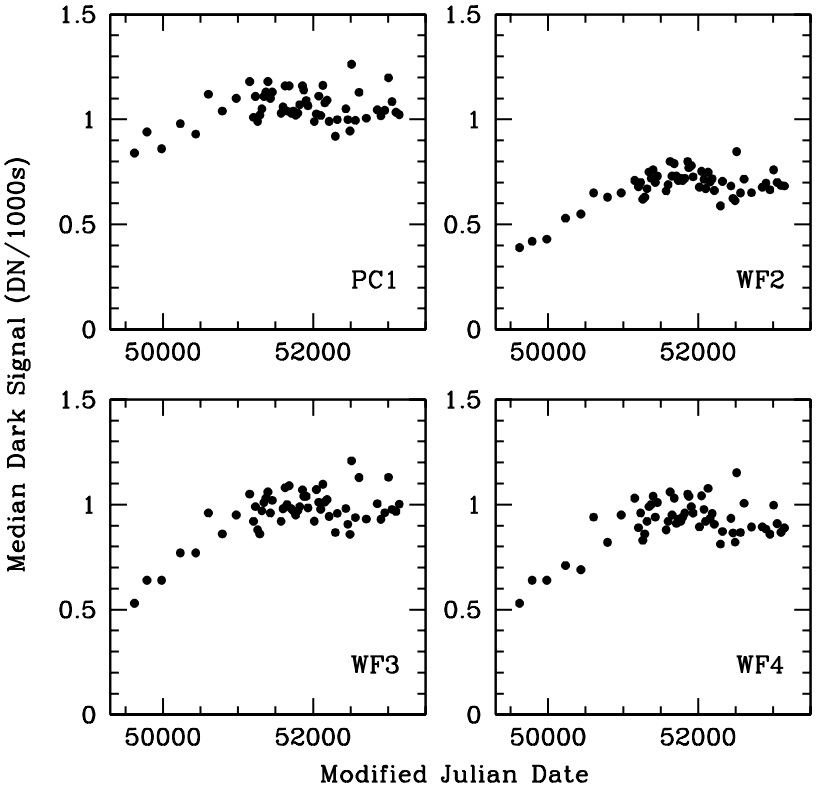

As mentioned before, there are two primary sources of dark current -- a dominant component which is strongly correlated with the cosmic ray flux in the image (probably due to scintillation in the MgF_2 CCD windows; see Figure 4.6 on page 89), and a smaller thermal dark current in the CCD itself. The dark current increase seen during early years was smaller in the optically vignetted regions near the CCD edges, which suggests much of this increase is related to scintillation effects in the CCD windows. Moreover, the ratio between the dark current at the CCD edge and the CCD center has remained nearly constant throughout the mission (within a range of ~5%; see WFPC2 ISR 2001-05), even though the dark current itself doubled in WF2, WF3, and WF4. Hence, it seems an inescapable conclusion that most of the long-term evolution is related to scintillation effects and variations in cosmic ray flux.

Long-term changes in the cosmic ray flux are perhaps most easily attributed to the solar cycle. The leveling-off of the dark current ~1998 is coincident with the approaching solar maximum which has the effect of reducing the cosmic ray flux at HST's low Earth orbit. Ground-based cosmic ray detectors show a gradual flux increase from 1992 to 1998, followed by a sharper decrease through early 2004. It is possible that other effects might also play some role. For example, portions of the HST orbit near the South Atlantic Anomaly experience higher cosmic ray rates, and it is possible that changes in the HST scheduling system could produce long-term changes in cosmic ray flux and hence dark current. It is also conceivable that long-term changes in the instrument itself might indirectly influence the sensitivity to scintillation effects (e.g. long-term radiation damage might modify the luminescence of camera components).

The thermal dark current of the CCD may also undergo long-term change (i.e. from radiation damage, etc.), and contribute some minor variation. A small increase in the CCD cold junction temperature was seen early in the mission; however, the temperature change can account for only a very small portion of the increase in dark current.

Since the dark current is generally a minor contributor to the total noise in WFPC2 images, its long-term variation is unlikely to impact the quality of WFPC2 observations, except perhaps in special cases (faint sources observed through narrow-band or UV filters, especially in AREA mode).

We note that the variation in dark signal reported here affects all pixels, and thus is distinct from hot pixels which vary in a more cyclic fashion. The hot pixels are highly localized, and are almost certainly due to radiation-damaged sites on the CCD detectors. Their number and intensity increase continuously, but are significantly reduced during decontamination procedures where the CCDs are warmed to +22˚C to clear the CCD windows of contaminants. These "decontaminations" were conducted monthly until June 2003, after which their frequency was reduced to 49-day intervals. Apparently the decontaminations anneal defects in the CCDs which produce hot pixels (see Section 4.11).

4.9 Cosmic Rays

HST is subjected to cosmic rays and protons from the Earth's radiation belts. The cosmic ray signature in the Loral CCDs is essentially the same as was seen in the WF/PC-1 devices. Electron-hole pairs generated in the thicker substrate by cosmic rays (and infrared photons) are usually removed by recombination in the low resistivity substrate material, because electrons do not diffuse efficiently up to the collecting phase.

Cosmic ray events usually deposit significant quantities of charge in more than one pixel. This is due partly to the finite thickness of the CCD

detectors, and partly to the less than perfect collection efficiency of each pixel. Figure 4.8 on page 93 shows a histogram of the number of affected pixels for each cosmic ray event. For the purposes of the figure, a cosmic ray is defined as having a peak pixel value more than 10 DN above the background; and an affected pixel is an attached pixel with a value more than 2 DN above the background. Cosmic ray events do have a clear lower cutoff at around 500 electrons of the total signal.

Cosmic ray events impact scientific imaging with WFPC2 differently from WF/PC-1, the previous generation camera. Firstly, the WFPC2 CCDs have an epitaxial thickness of about 10μm compared to 8μm for the thinned WF/PC-1 device, and a recombination length of 8-10μm in the substrate. These facts lead to a higher total number of electrons being deposited per event. WFPC2 CCDs also have lower read noise, and so the number of cosmic ray events apparently differs from that of the WF/PC-1 CCDs, since low amplitude events are detected. In practice, this means that the number of pixels apparently contaminated by cosmic rays in an image is higher in WFPC2, although the underlying event rate is similar to that experienced in WF/PC-1.

Figure 4.8: Histogram of Cosmic Ray Event Sizes. A cosmic ray event is defined by having a peak pixel of at least 10 DN (at gain 7).

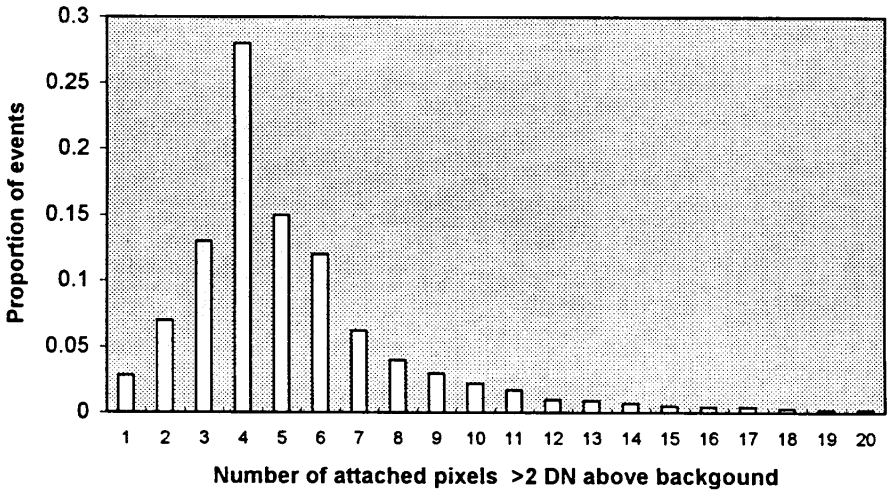

Secondly, stellar images are undersampled and much more difficult to separate from cosmic rays, as is shown in Figure 4.9 on page 94. Faint stellar images and low energy cosmic rays are often indistinguishable. Long science observations are therefore usually broken into at least two exposures (CR-SPLIT) to ensure that events can be identified.

The average properties of on-orbit cosmic ray events have been determined from examination of several dark exposures, each 2000s long. After bias and dark subtraction, “cosmic rays” were identified in each input

frame by first looking for pixels more than 5σ above the background, and then including in each event all adjacent pixels more than 2σ above the background. Very occasionally, two or more physically separate events will be merged into one as a result of this procedure; visual inspection confirms that in the vast majority of cases, this procedure correctly identifies each event and the area affected by it. The typical value of σ was 5 to 6 electrons, including both read and dark noise. The region near the borders of each CCD was excluded in order to avoid edge effects, but all results given here are rescaled to the full area of the CCD.

Figure 4.9: Comparison of Star Images and Cosmic Ray Events. An 80x80 pixel subimage of a 400 second F336W WF2 exposure in ω Cen.

One difficulty in this measurement is caused by hot pixels, for some of which the dark current has significant fluctuations from frame to frame; these can be mistakenly identified as cosmic rays when the dark current is at a maximum. Single-pixel events constitute 10% of the total number of events identified by our procedure, but at least half of them recur in the same position in several frames, thus identifying them as damaged (hot) pixels, rather than true cosmic rays. Also, unlike the majority of cosmic ray events, single-pixel events tend to have a very small total signal; the majority have a total signal of less than 200 electrons, as expected from hot pixels, while the signal distribution of multiple-pixel events peaks around 1000 electrons. For this reason, single-pixel events have been classified as “bad pixels" rather than “cosmic rays". While we cannot exclude that some true single-pixel events do occur, they are very rare, probably less than 2% of the total.

Cosmic ray events are frequent, occurring at an average rate of 1.8 events $chip^{-1}$ s^{-1}. The distribution of the total signal is shown in Figure 4.10 on page 95; it has a well-defined maximum at about 1000 electrons, and a cut-off at about 500 electrons. The latter is well above the detection threshold used for the above measurements (25 electrons in the central pixel of the cosmic ray), and is therefore undoubtedly real.

Figure 4.10: Histogram of Cosmic Ray Event Energies.

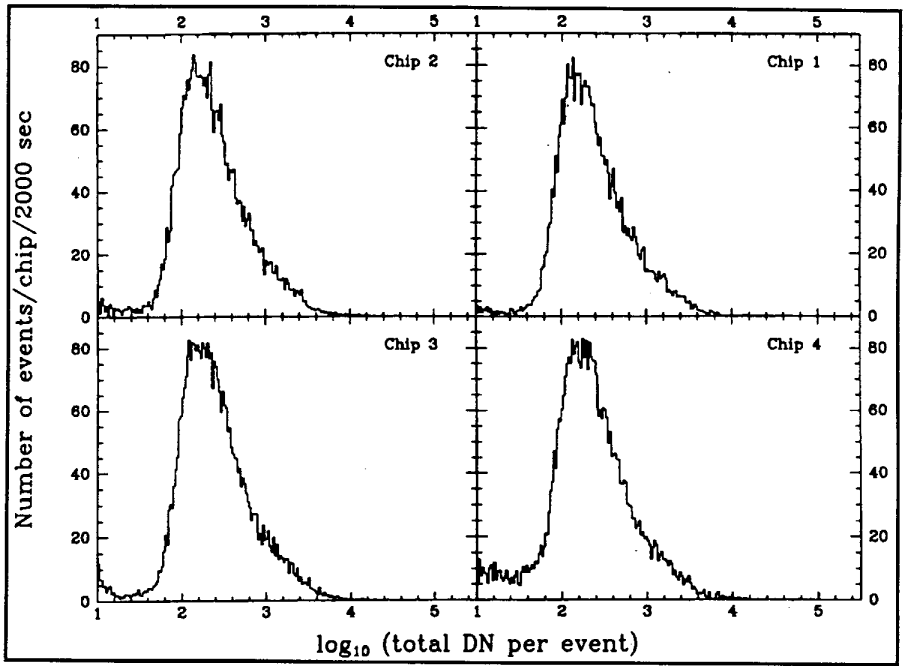

The histogram in Figure 4.10 on page 95 shows the distribution of the total energy of all cosmic ray events. One encouraging feature is the very small number of events below about 30 DN. This low energy drop is well above the energy level of excluded single-pixel events.

A good approximation to the cumulative distribution of events as a function of the total signal is given by a Weibull function with exponent 0.25. This function has the form:

$$N(>S) = N_0 \exp[-\lambda(S^{1/4} - S_0^{1/4})]$$

where N is the total number of events which generate a total signal larger than S. The best fit to the observed events gives N_0=1.4 events chip^{-1} s^{-1}, S_0=700 electrons, and $\lambda = 0.57$. The fit fails below S_0, and should not be extrapolated to low-signal events. The rate of events with the total signal below 700 electrons is 0.4 events chip^{-1} s^{-1} (i.e. total events per CCD per second is N_0+0.4≈1.8).

The number of pixels affected by cosmic ray events in a given exposure is a slightly more sensitive function of the threshold used. While there is a clear drop at low signal for both total and peak signal, neighboring pixels can be affected at low levels. Each event (defined as before) affects an average of 6.7 pixels, for about 12 affected pixels chip^{-1} s^{-1}. For a 2000s exposure, this results in about 24,000 affected pixels, or 3.8% of all pixels. As cosmic rays are expected to be randomly placed, a pair of such exposures would have about 900 pixels affected in both exposures; cosmic ray correction is impossible for such pixels. For a pair of 1000s exposures, about 220 pixels will be affected in both frames.

Cosmic ray activity varies as a function of time, geomagnetic latitude of the spacecraft, and other factors. The average numbers given here are subject to change in individual exposures. After studying about one month's worth of dark exposures, we estimate a total range of about a factor of two in cosmic ray rates.

4.10 SAA and Scheduling System Issues

Changes in the WFPC2 observation scheduling system were introduced early in 1999 primarily in order to increase the scheduling efficiency of HST observations starting with Cycle 8.

First, the South Atlantic Anomaly (SAA) contours used to limit WFPC2 observations were modified slightly. The SAA is a region where irregularities in the Earth’s magnetic field cause very high cosmic ray rates. WFPC2 imaging is generally not scheduled near the SAA, so as to avoid excessive cosmic ray hits which degrade images by obliterating data in numerous pixels. These adverse effects are usually minimized by operating each instrument only when HST is outside a designated “SAA avoidance contour.” (WFPC2 observations of time-critical phenomena can be taken inside the SAA avoidance contour, if necessary.) Biretta and Baggett (1998) analyzed available WFPC2 data, together with data from Air Force

satellites flying in similar orbits, and redefined the WFPC2 SAA avoidance contour. This resulted in a 3% increase in designated SAA-free orbits, which allows better scheduling efficiency, and negatively impacts less than 0.1% of WFPC2 science observations. The current (post-1999) contour is given by the M26 area in Figure 4.11 on page 97.

Figure 4.11: SAA Avoidance Contours.

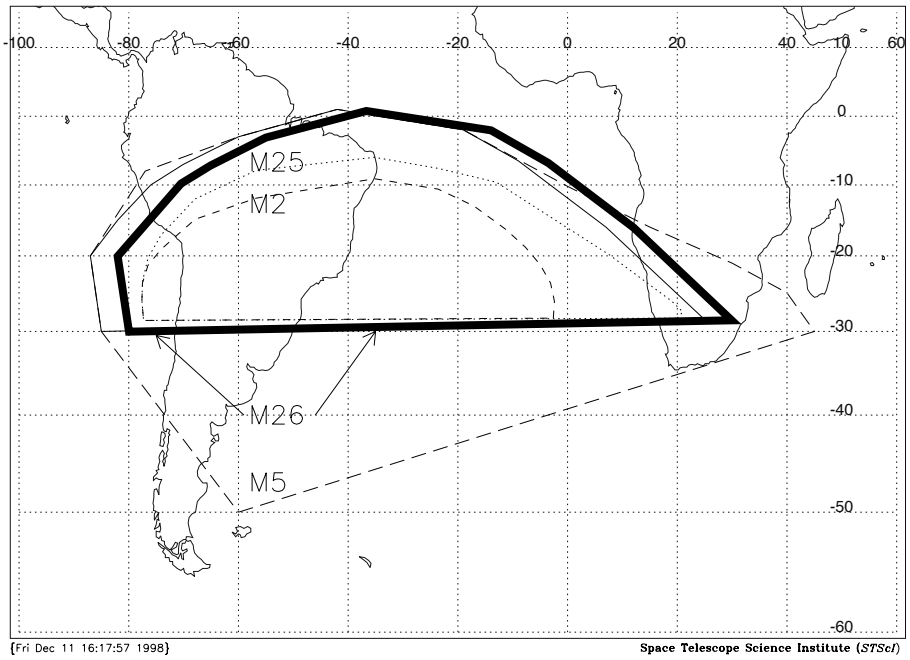

Second, WFPC2 visits are limited to a maximum length of 5 orbits. Very long visits (up to an earlier maximum of 8 orbits) have very limited opportunities for scheduling, reduce the efficiency of telescope use, and can cause long delays in execution, with long GO wait times. Shorter visits improve the scheduling opportunities for large proposals. One possible drawback is the lower pointing repeatability across visits; this is significant only for programs with special dithering requirements.

A third change since Cycle 8 is that an extra minute of overhead was added to each orbit, which allows splitting an orbit in the Phase II proposal into two separate spacecraft alignments. This one-minute “efficiency adjustment” allows much more efficient scheduling of HST orbits impacted by the SAA.

4.11 Radiation Damage and Hot Pixels

In low Earth orbit (LEO) the CCDs are subject to radiation damage from the Earth's radiation belts. The WFPC2 CCDs are shielded from energetic electrons and about half the incident energetic protons. Long term radiation damage to the CCDs from high energy protons leads to an increase in dark count rate (mainly from the creation of hot pixels), baseline shifts in the CCD amplifiers, and long term degradation of Charge Transfer Efficiency (CTE). There has not been a significant degradation in the amplifier baselines. CTE is discussed in the Section 4.12. On the other hand, one of the major radiation damage mechanisms is the creation of new Si-SiO_2 interface states, which cause increased dark current rates in affected pixels. In the MPP CCD these states immediately recombine with holes, reducing the gradual increase in dark noise by factors of about 25, compared to normal three-phase CCDs (Woodgate, et al. 1989, Janesick, et al. 1989b).

Figure 4.12 on page 99 is a histogram of the dark current distribution (in $e^- s^{-1}$) for hot pixels. It contains three curves: solid for the histogram of all hot pixels just before a decontamination (April 7, 1995); dashed only for the pixels that were hot just before the decontamination and were not hot at the beginning of the cycle (March 10); and long-dashed for pixels that were hot at the start of the cycle and were fixed by a decontamination. Thus, the dashed line represents the “new” hot pixels, and the long dashed line represents the fixed hot pixels. The fact that these two curves are very similar shows that the number of hot pixels is roughly in equilibrium. The majority of new hot pixels have low dark current. The hot pixels that constitute the accumulated legacy of previous periods, and thus survived one or more decontaminations, include higher-current pixels. The population of hot pixels increases at a rate of approximately 33 pixels CCD^{-1} day^{-1} above a threshold of 0.02 e^- $pixel^{-1}$ s^{-1}, while the camera remains at the normal operating temperature.

About 80% of the new hot pixels return to a normal state at decontamination events when the CCDs are warmed to a temperature of +22˚C for 6-12 hours. There is no evidence that the fraction of hot pixels that returns to normal is related to the length of the decontamination. Of those pixels that are not fixed, about half will be fixed after two or three additional decontaminations. After that, the rate of correction decreases. It is conceivable that all hot pixels will be repaired eventually. At the moment there is no evidence of a significant secular increase in the number of hot pixels, and we have a firm upper limit of 8% on the fraction of hot pixels that are not repaired after several decontamination cycles.

Figure 4.12: Hot Pixel Histogram.

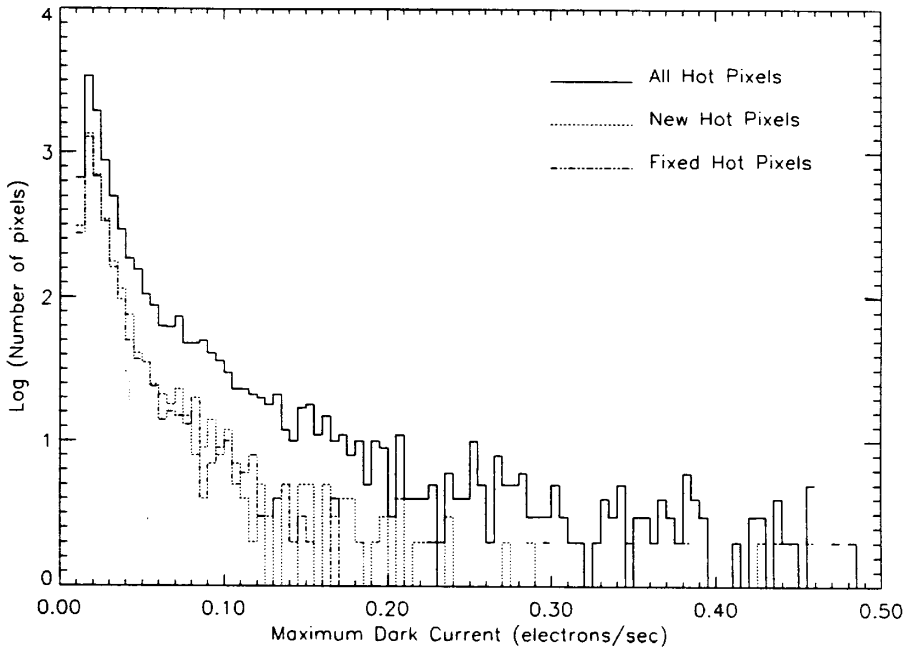

In order to deal with the hot pixel problem, we provide monthly lists of possible hot pixels via the World Wide Web. Look for hot pixels under WFPC2 Instrument News at:
http://www.stsci.edu/instruments/wfpc2/wfpc2_hotpix.html

These lists are best used to flag hot pixels as bad. While we do provide an estimate of dark current for each hot pixel as a function of time, there are indications that the noise in hot pixels is much higher than the normal shot noise, and thus dark current subtraction is unlikely to give good results.

4.12 Photometric Anomalies: CTE and Long vs. Short

There are two photometric anomalies which have now been extensively characterized. The first effect is due to the imperfect charge transfer efficiency (CTE) of the detectors, which causes sources at high row and column numbers to appear fainter than otherwise because the charge is transferred over a bigger fraction of the chip. This anomaly is increasing with time, especially for faint sources, presumably as a consequence of on-orbit radiation damage. In this section, we provide correction formula which reduce the impact of this anomaly to about 1-3% in typical cases. The second effect, called "long vs. short", causes sources to have a lower

count rate - and thus appear fainter - in short exposures than in longer exposures and appears independent of the position on the chip. This nonlinearity is very small (i.e. a few percent) or non-existent for uncrowded fields, with less than ~1000 stars per WFC chip. However, for crowded fields with ~10,000 stars per chip, apparent nonlinearities of tens of percent are possible in extreme cases (e.g., when comparing 10 sec. with 1000 sec. exposures). The most likely explanation is that this effect is the result of an overestimate of the sky measurement in the short exposure due to the presence of scattered light around bright stars. Because the magnitude of the "long vs. short" effect is highly dependent on the parameters of the photometric analysis, no standard correction formula have been provided. Both the CTE and "long vs. short" effect are more fully described below.

4.12.1 Charge Transfer Efficiency

The WFPC2 CCDs have a small but significant charge transfer efficiency (CTE) problem which causes some signal to be lost when charge is transferred down the chip during readout. This has the effect of making objects at higher row numbers (more charge transfers) appear fainter than they would if they were at low row numbers. The effect depends on the temperature of the CCDs. At the original temperature of -76˚C, as much as 10-15% of the light within a 0.5" radius aperture around a bright star could be lost for objects at the highest rows. As a result, the CCD operating temperature was changed to -88˚C on 23 April, 1994. This reduced the effect to a maximum amplitude of 4% for stars with more than 1,500 total detected electrons. This ~4% amplitude seems to remain in effect for stars up to 20,000 total electrons. However, for fainter stars (few electrons) seen against a low background, the effect appears to have grown much larger (up to tens of percent) over the last 8 years. We also note that the effect depends on the amount of background light on the chip. There is significantly less CTE effect in the presence of even a moderate (several tens of electrons) background. Hence, the effect is not well described by either a constant fractional loss or a constant additive loss per charge transfer, but must be calculated as a function of target counts, background light, and epoch.

Our basic understanding is that CTE problems are caused by electron traps in the CCD’s silicon. During the readout process these traps capture charge from the image electron packets as they are clocked across the CCD towards the readout amplifier. After some time delay, the charge is released from the traps, but by that time the affected electron packet has moved away, so the re-deposition occurs at some distance from the electron’s original position in the image. Hence this has the effect of producing “tails” on images. We believe that larger electron packets fill a larger volume in the bulk silicon, hence brighter images are able to access larger numbers of traps than faint ones. This simple paradigm also suggests that images with high background levels will tend to have less CTE problems, since the

background will fill some of the traps, and prevent them from robbing charge as the CCD is read out.

CTE: photometric effects

The primary observational consequence of CTE loss is that a point source at the top of the chip (Y=800) appears to be fainter than if observed at the bottom of the chip (Y=1), due to loss of electrons as the star is read out down the chip (see Figure 4.13 on page 102). This is called *Y-CTE*. There also appears to be a similar, but weaker tendency, for stars on the right side of the chip (X=800) to be fainter (called *X-CTE*). The effects also depend on the brightness of the star and the background level.

The photometric calibration of the instrument presented in this Handbook is based on Holtzman, et al. (1995b). It has been corrected for CTE by assuming a 4% loss across the 800 rows of the CCD (i.e. 2% correction for CCD centers). All of the frames considered in the primary photometric calibration are short exposures of bright stars. While correction formulae have been developed, as discussed below, the 4% ramp is still a reasonable approximation. Hence, for data taken at -88˚C, a 4% correction ramp was applied to the measured 0.5" radius aperture photometry, in the sense that objects at row 800 were made brighter by 4%, but the brightness of objects at the first row was not changed. The correction was applied to bring measurements to the values they would have had in the absence of CTE, or equivalently, the values they would have had if measurements had been made at row 0.

Several studies were done on the photometric effects of the Charge Transfer Efficiency (CTE) problem for WFPC2. This work was based on analysis of observations of the globular cluster ω Cen (NGC 5139). The first study provides a set of formulae that can be used to correct for CTE loss when doing aperture photometry, based on a data set taken on June 29, 1996 (Whitmore and Heyer 1997, ISR WFPC2 97-08), reducing the observational scatter in these test data from 4–7% to 2–3%, depending on the filter. The second study found evidence that CTE loss for faint stars has increased with time (Whitmore 1998).

Figure 4.13: Ratio of count rates observed for the same star (i.e., Throughput Ratio) as a function of the change in row position for stars in 4 different brightness ranges. The negative slope shows that a star appears brighter when it is at low row number, thus closer to the "bottom" of the chip and the readout amplifiers, than when it is at high row number. The effect is larger for fainter stars (top right panel) as compared to bright stars (bottom left panel). See Whitmore and Heyer (1997) for details.

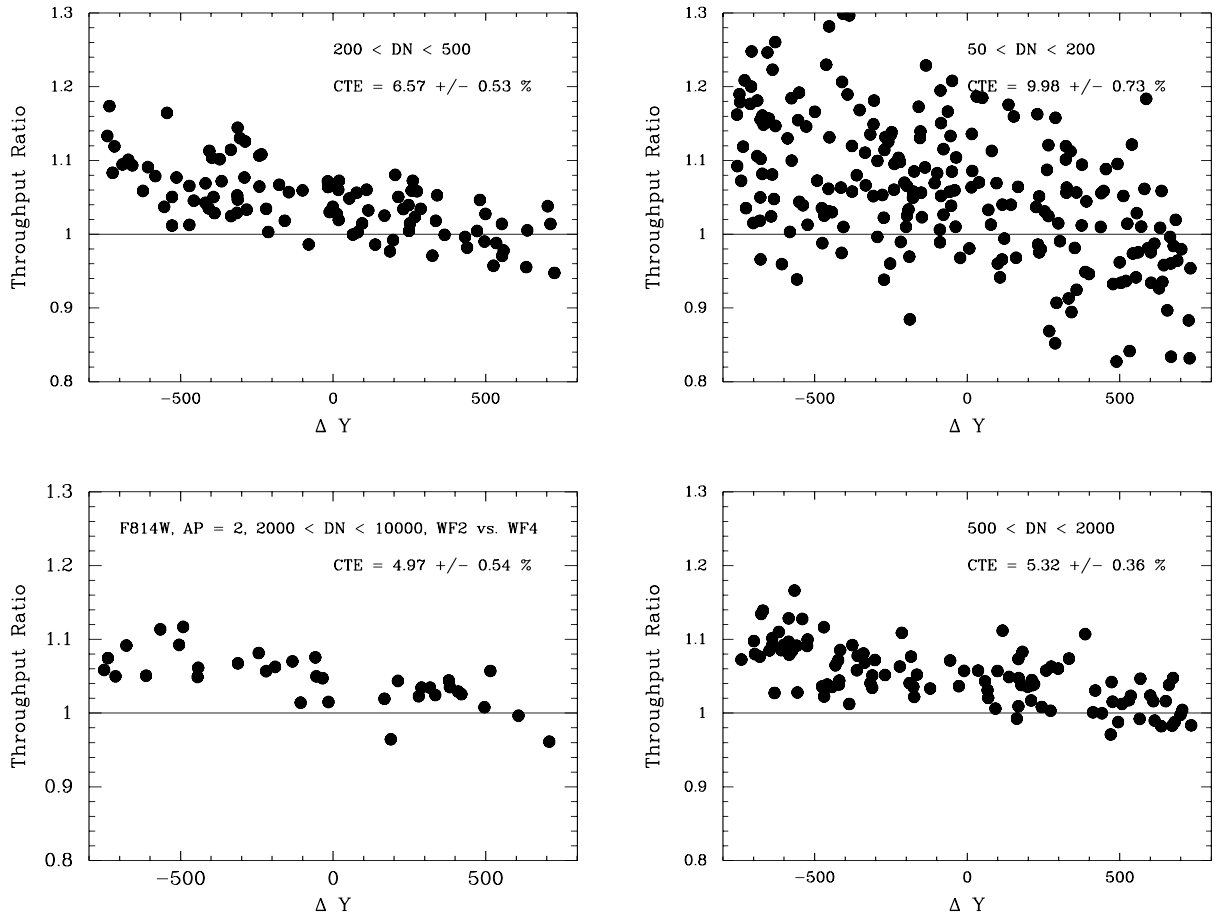

A continuation of this analysis using observations of ω Cen confirmed that the CTE loss for WFPC2 was time dependent (Whitmore, Heyer, and Casertano 1999). The datasets cover the time range from April 28, 1994 (shortly after the cooldown to -88˚C), to February 1999. For bright stars (i.e., brighter than 200 DN when using gain = 14 e^-/DN; equivalent to 400 DN for gain = 7 e^-/DN) there is only a modest increase in the amount of CTE loss as a function of time. However, for faint stars the CTE loss has increased more rapidly. For example, for very faint stars (i.e., 20–50 DN at a gain of 14 e^-/DN) the CTE loss has increased from 3% to 40% for a star at the top of the chip.

It should be noted that CTE loss is strongly dependent on the background level in an image. Figure 4.14 on page 103 illustrates CTE losses for background levels ranging from 0.03 to 70 DN/pixel. For

example, for faint targets (20 - 50 DN, top left panel) a low background of 0.03 DN/pixel results in ~40% CTE loss at late epochs, while a 14 DN/pixel background produces ~4% loss. The results in the previous Figure 4.13 on page 102 are based on very short (14s) exposures with very low background. By comparison, a typical WFPC2 exposure (300s in F555W) has ~3 DN/pixel background. Hence, the sky background will significantly reduce CTE loss for most science observations. CTE will primarily affect images in the UV and in narrow band filters, where the background is very low.

Figure 4.14: Y-CTE loss in stellar photometry as a function of epoch and background light. Each panel corresponds to a different range of target count levels (1 DN = 14 electrons). Different symbols correspond to different background levels; the larger plotting symbols indicate images with larger backgrounds. The straight lines represent the best-fit multilinear regression for Y-CTE as function of time, log counts (DN), and log background. See Whitmore et al. (1999).

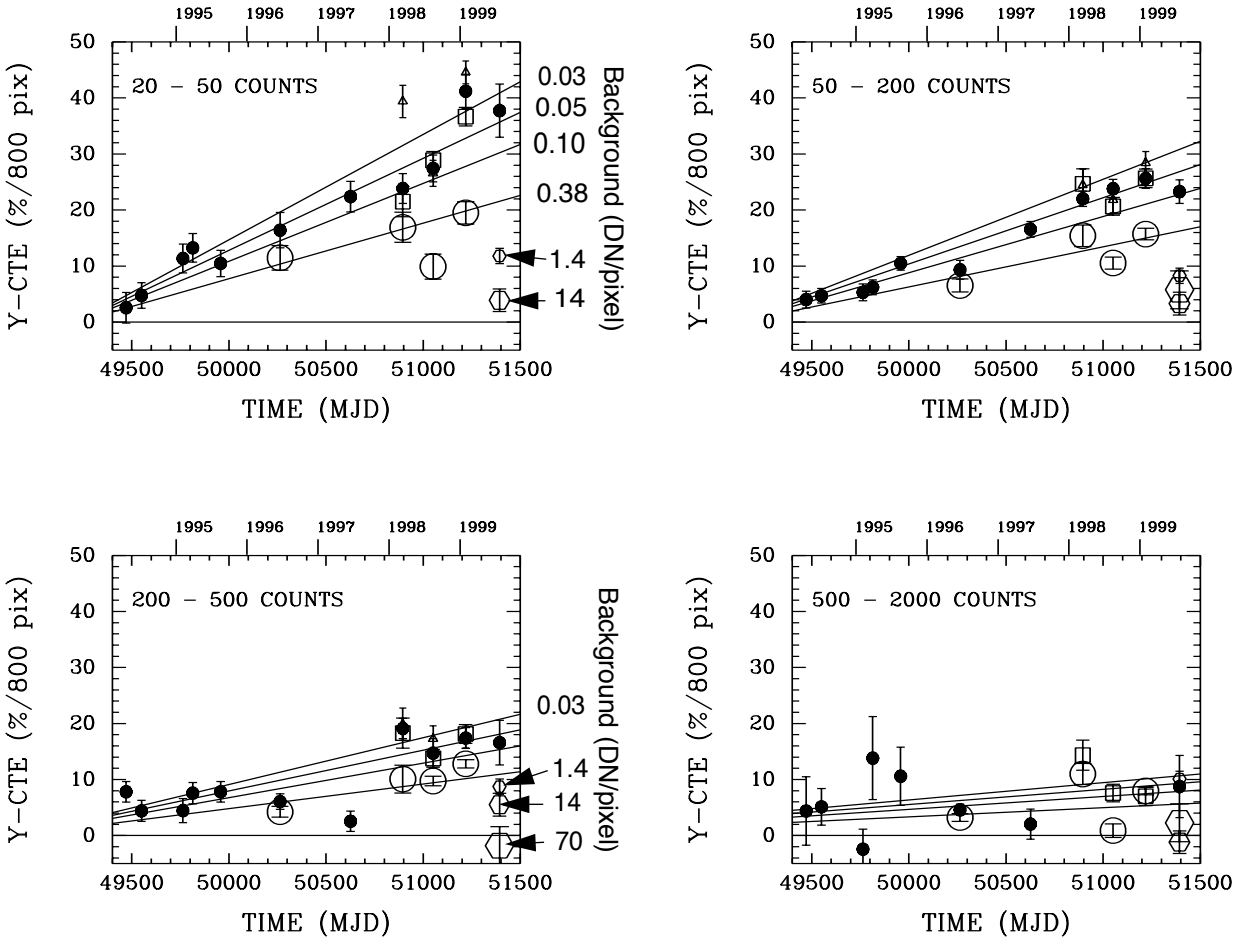

An approximate correction for stellar photometry is given by Whitmore, Heyer, and Casertano (1999) as follows for stellar photometry performed with a 2 pixel radius aperture. For $CTS_{obs} < 4000DN$ and $BKG > 0.1DN$ they give

$$Y-CTE = 2.3 \cdot 10^{-(0.256 \cdot \log(BKG))} \cdot [1 + 0.245(0.0313 - 0.0087 \log CTS_{obs})T]$$

$$X-CTE = 2.5 \cdot [1 + 0.341(0.00720 - 0.0020 \log CTS_{obs})T]$$

whereas for $CTS_{obs} > 4000DN$ and $BKG > 0.1DN$ they give

$$Y-CTE = 2.3 \cdot 10^{-(0.256 \cdot \log(BKG))}$$

$$X-CTE = 2.5$$

and finally the corrected stellar counts are given by

$$CTS = \left[1 + \frac{Y-CTE}{100} \cdot \frac{Y}{800} + \frac{X-CTE}{100} \cdot \frac{X}{800}\right] \cdot CTS_{obs}$$

where parameters are defined as:

CTS_{obs} = number of counts (DN) measured for the star.
$Y-CTE$ = percent loss over 800 pixels in Y-direction
$X-CTE$ = percent loss over 800 pixels in X-direction
X = X position of star in pixels
Y = Y position of star in pixels
BKG = mean background counts in image (DN)
$T = MJD - 49471$

Note that these equations are for gain = 7 e-/DN observations, since this is most commonly used for science observations. For gain = 14 e-/DN, multiply CTS_{obs} and BKG by 2 before using the above equations. For further details, please see Whitmore, Heyer, and Casertano (1999).

Another study analyzed CTE losses and developed formulae to correct them (Dolphin 2000). This paper compares WFPC2 observations with ground based observations of Omega Cen and NGC 2419 and derives CTE corrections using a baseline through March 2000, roughly a year longer than available for a similar study by Whitmore, Heyer, and Casertano (1999, PASP, 111, 1559). In general, Dolphin finds good agreement with the Whitmore et al. results (within a few hundredths of a magnitude) with less scatter in the residuals, except for relatively recent (1998 and later) data at low count levels. Dolphin updated his formula on September 17, 2002. For his most up-to-date formulas, the user is strongly encouraged to check his webpage at http://www.noao.edu/staff/dolphin/wfpc2_calib/. Figure 4.15 on page 106 shows data on Omega Cen which has been

corrected for CTE by the Dolphin (2002) formula. Based on this figure and the comparison presented in Whitmore and Heyer (2002), we find that the Dolphin formula provides better CTE corrections than that of Whitmore et al. formula. Our current recommendation is to use the Dolphin (2002) formula for the CTE loss correction, though caution should always be exercised at the faintest levels (e.g. approximately 4 DN in a 14 sec exposure). We list here Dolphin's "complex" equations which take into account the fact that the magnitude loss per pixel is not constant as the star reads out. These CTE correction equations, *expressed in magnitudes of CTE loss*, are given as follows:

First, calculate X-CTE, the CTE loss (in magnitudes) in the X readout:

$$X-CTE \;=\; 0.0202 \cdot e^{-(0.00083 \cdot bg)} \,.\, \frac{X}{800}$$

Second, calculate Y-CTE, the CTE loss (in magnitudes) in the Y readout:

$$c1 \;=\; 0.01785 \cdot (0.655 \cdot e^{-(0.402 \cdot lbg)} + 0.345 \cdot e^{-(0.0156 \cdot bg)}) \cdot (1.0 + 0.253 \cdot yr + 0.0082 \cdot yr^2) \cdot \frac{Y}{800}$$

$$c2 \;=\; 2.35 \cdot e^{-(0.517 \cdot lct) - (0.476 \cdot X-CTE)}$$

$$Y-CTE \;=\; \frac{\ln(e^{c1} \cdot (1.0 + c2) - c2)}{0.476}$$

where:

```
ct  = counts in electrons
lct = ln(ct) - 7
bg   = sqrt (background^2+1) - 10
lbg = ln( sqrt(background^2+1) ) - 1
yr  = (MJD - 50193) / 365.25
Counts and background are given in electrons.
```

Finally, the corrected magnitude of the star is then given by:

```
mag(corr) = mag - X-CTE - Y-CTE
```

Figure 4.15: The ratio of counts between a 14 sec. and 100 sec. exposure for stars in Omega Cen vs. the Y position for stars on all three WFC chips. The raw values (filled circles) fall below a ratio of 0.14 due to CTE loss. The different panels represent different target brightnesses (in DN), as selected on the 100 sec. exposure and described by the labels. The filled triangles show the values corrected using the Dolphin (2002) formula. Note that the extrapolation of the raw data to Y=0 (the sloped line) is consistent with the predicted value of the throughput ratio based on the exposure times; hence, the long-vs-short anomaly is not a problem for this data set (see Section 4.12.2 "The Long vs. Short Photometric Anomaly"). This figure courtesy of A. Dolphin (Dolphin 2002, private comm.).

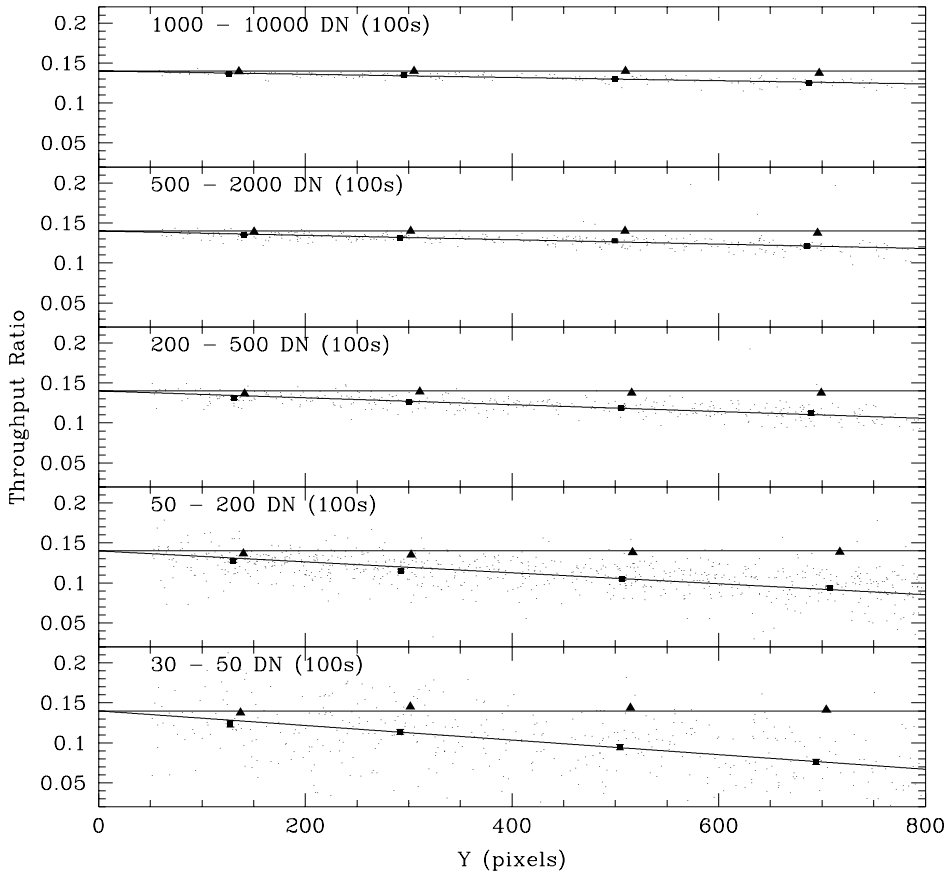

Physical effects of CTE

Late in 1999, efforts were made to better understand the detailed effects of CTE during the read out process (Biretta, Baggett, and Riess 2000). Figure 4.16 on page 109 illustrates the impact of CTE on a single pixel during the read out process. This image is the average of 700 hot pixels taken from WFPC2 dark frames from late 1999, and it effectively shows the system response to a single bright pixel at the center of a CCD. The CTE problem displaces counts into obvious "tails" extending in both the X and Y directions on the CCD. Three components of CTE can be discerned and characterized by the time delay for trapped charge to be released:

1. A rapidly decaying tail in the Y direction with a decay scale of a few pixels (decay time 10s of milliseconds)

2. A rapidly decaying tail in the X direction (decay time 10s of microseconds)
3. An extended tail in the Y direction which decays slowly over dozens of pixels (decay time 100s of milliseconds).

All of these components have the effect of robbing charge from typical small apertures (few pixel radius) used for stellar photometry. (A fourth component of CTE is responsible for long-lived residual images, and will be discussed later.)

The brightness profile along the Y-CTE tail is shown quantitatively in Figure 4.17 on page 110. While the count levels in the extended tail are low, they still make up approximately 2/3 of the total counts displaced from the hot pixel. Figure 4.17 also illustrates the effect in 1994, and gives a clear indication of the time evolution. Similar measurements made on hot pixels in separate intensity ranges are illustrated in Figure 4.18 on page 110; the total charge in the Y-CTE tail (in this case for late 1999 and background level ~1 DN) is approximately

$$I_{Y-CTE} = 1.2 \cdot I^{0.37}$$

where I is the hot pixel intensity in DN at gain 7 e^-/DN. This relationship together with Figure 4.17 and model PSFs can be used to predict stellar CTE, and the results appear to be in fair agreement with observations.

Cosmic rays in images are also impacted by CTE, and provide another useful probe of CTE effects. Much like the hot pixels, CTE causes tails to appear on the cosmic rays. Though cosmic rays themselves have complex shapes, these tails are still manifest as a statistical asymmetry, and this asymmetry can be used as a quantitative measure of CTE (Riess, Biretta, and Casertano 1999).

The total counts in these cosmic ray "tails" is a useful metric of CTE. As shown in the top panel of Figure 4.19 on page 111, no significant tail is apparent at low Y. But at high Y an exponentially declining tail is readily apparent with an e-fold decay of 2 pixels (indicating that charge is released on the 10's of milliseconds timescale). This Y dependence closely mimics that seen in stellar photometry. These tails are very similar to those seen for hot pixels.

Figure 4.20 on page 111 displays the temporal dependence of both parallel-read (Y) and serial-read (X) induced-tails for WFPC2 as measured with cosmic rays. This figure shows results from thousands of WFPC2 dark frames, and sharply delineates the degradation of CTE with time. There is even evidence for mild acceleration in the sense that the counts in the CR tails at late epochs are somewhat higher than expected by a linear extrapolation of the early data. The same growth trend is seen in Figure 4.20 for X-CTE tails except the X-tails are much weaker and have presently converged at 1/3 the size of the Y-tails. This is in good agreement with the relative strengths of X to Y stellar CTE measurements (Whitmore,

Heyer, & Casertano 1999).We note that using internal data, such as these cosmic rays in dark frames, saves external HST pointed time and provides a better time sampling, compared to more conventional stellar CTE monitoring.

As mentioned above, a fourth component of CTE is manifest as long-lived residual images. These residual images are seen as faint ghost images in exposures following a highly exposed target, and tend to decay with a timescale of roughly 10 to 20 minutes (Biretta and Mutchler 1997; Baggett, Biretta, and Hsu 2000). They usually appear at both the location of the bright target, and in pixels below the target (smaller Y values than target). Figure 4.21 on page 112 illustrates this phenomenon. The trail below the target is caused by charge which is trapped during read-out of the highly exposed image, which is then slowly released during subsequent exposures. The effect is most pronounced when long exposures in low throughput filters (narrow band or UV filters) immediately follow a highly exposed image (usually a broad band filter). These long-lived residual images may be related to surface traps on the CCD, whereas the other components are more likely related to traps in the bulk silicon.

Investigations reveal that CTE losses to extended sources are not uniform across the source (Riess 2000). Rather, they are proportionally greater on the side of the source which is closer to the read amplifier (i.e., low-Y), decrease in the direction away from the amplifier, and charge is regained at the opposite side (i.e., high-Y) of a source. The portion of an extended source which is far from the amplifier suffers little charge loss because charge traps encountered have been filled and in addition, charge is deferred. Our knowledge of how CTE affects galaxies and other extended sources is still growing and it is difficult at this point to provide a recipe to restore changes to the shape of a source. Nevertheless, we suggest that users consider that the total CTE loss expected for an extended source (Baggett et al. 2001; Whitmore, Heyer, & Casertano 1999) likely applies only to the side of the source near the amplifier (i.e., low-Y), with the opposite side (i.e., high-Y) facing smaller losses.

Figure 4.16: Average of 700 hot pixels illustrating the CTE effect. Data were taken from dark frames in late 1999 in all four CCDs in region 50<Y<750 and for hot pixels intensities in the range 100 to 4000 DN. The bottom panel is the same image enhanced to illustrate faint pixels.

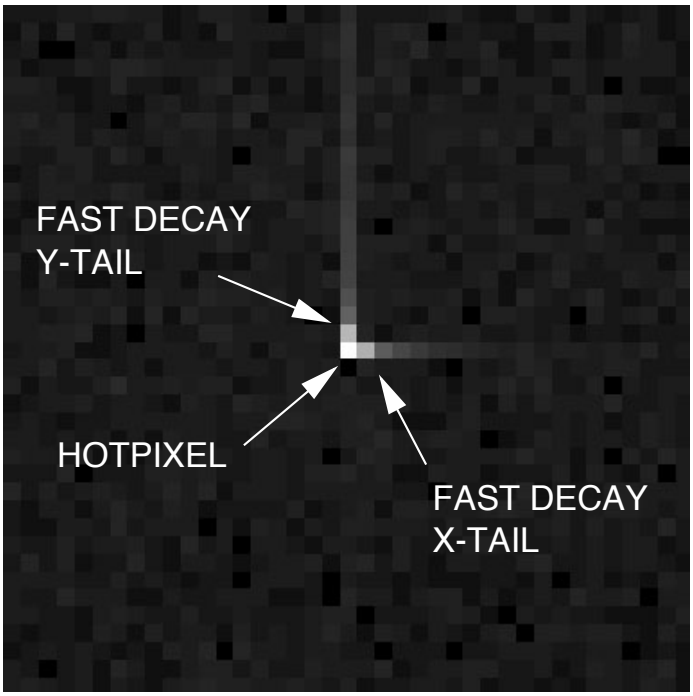

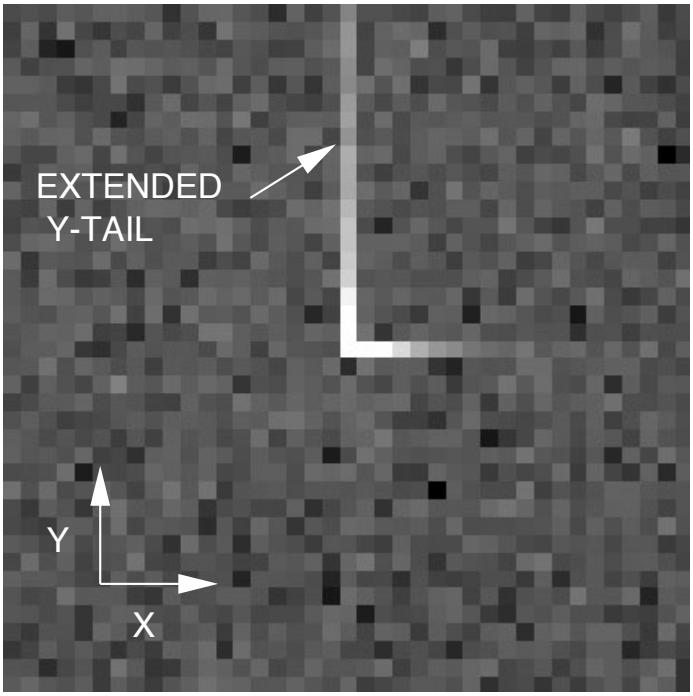

Figure 4.17: Intensity profile of CTE tail in Y direction for averaged hot pixel (~350 DN) in 1994 and 1999.

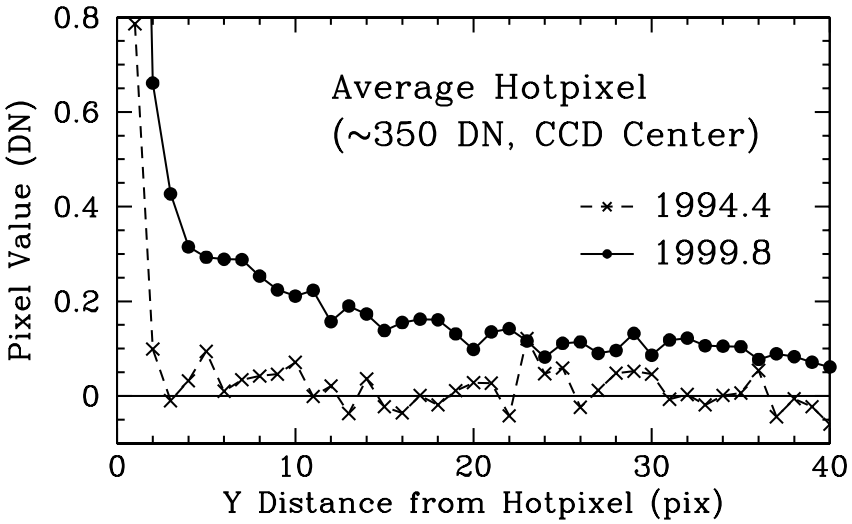

Figure 4.18: Dependence of Y-CTE tail on pixel intensity measured on late 1999 data.

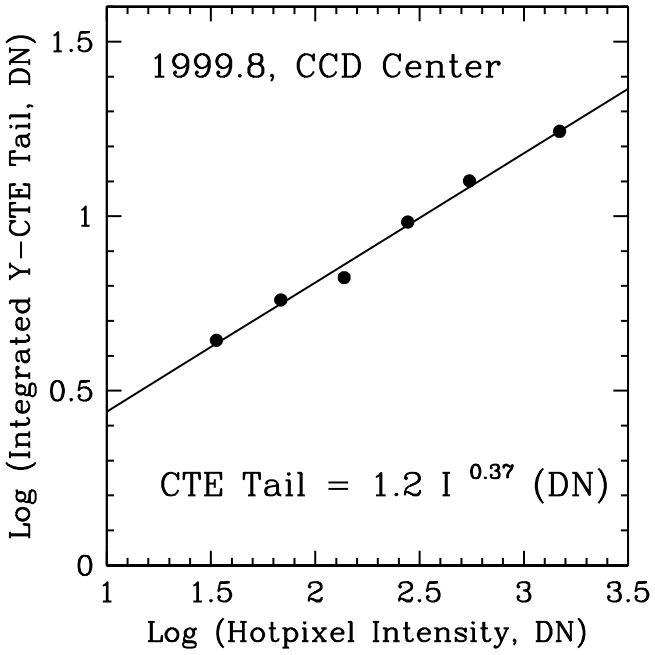

Figure 4.19: Cosmic ray tails in a single WFPC2 dark frame. Each individual point represents one cosmic ray and shows the differences between pixels which are equal distances from a cosmic ray pixel. The line is the median of the data. At low Y there are few charge transfers and hence minimal trailing of charge. At high Y the statistical cosmic ray tails are evident.

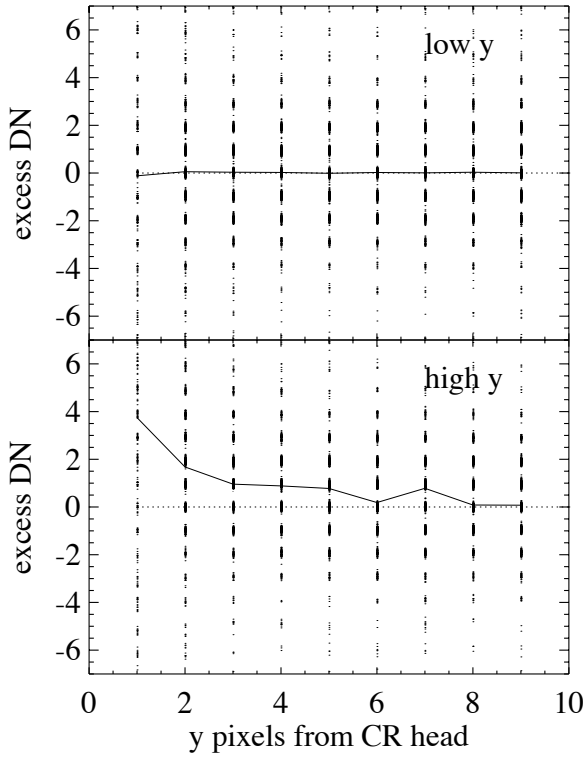

Figure 4.20: Counts in CTE tails measured on cosmic rays. Separate distributions are shown for the X-CTE and Y-CTE.

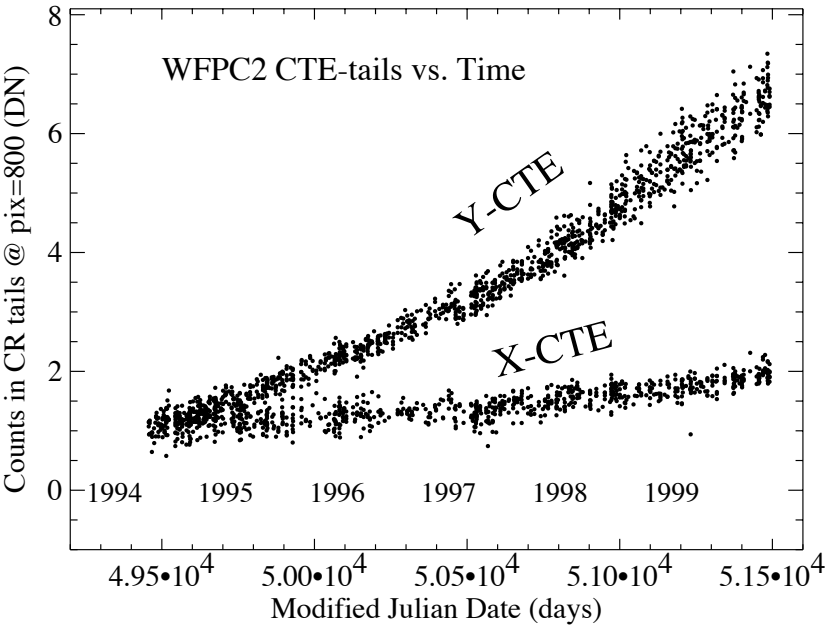

Figure 4.21: Images Illustrating CTE Residual Trail. (a) Image of star field taken in broad band filter on PC1. (b) 1500s dark exposure taken immediately following (a). Read out direction is towards bottom of image. Cosmic rays have been removed.

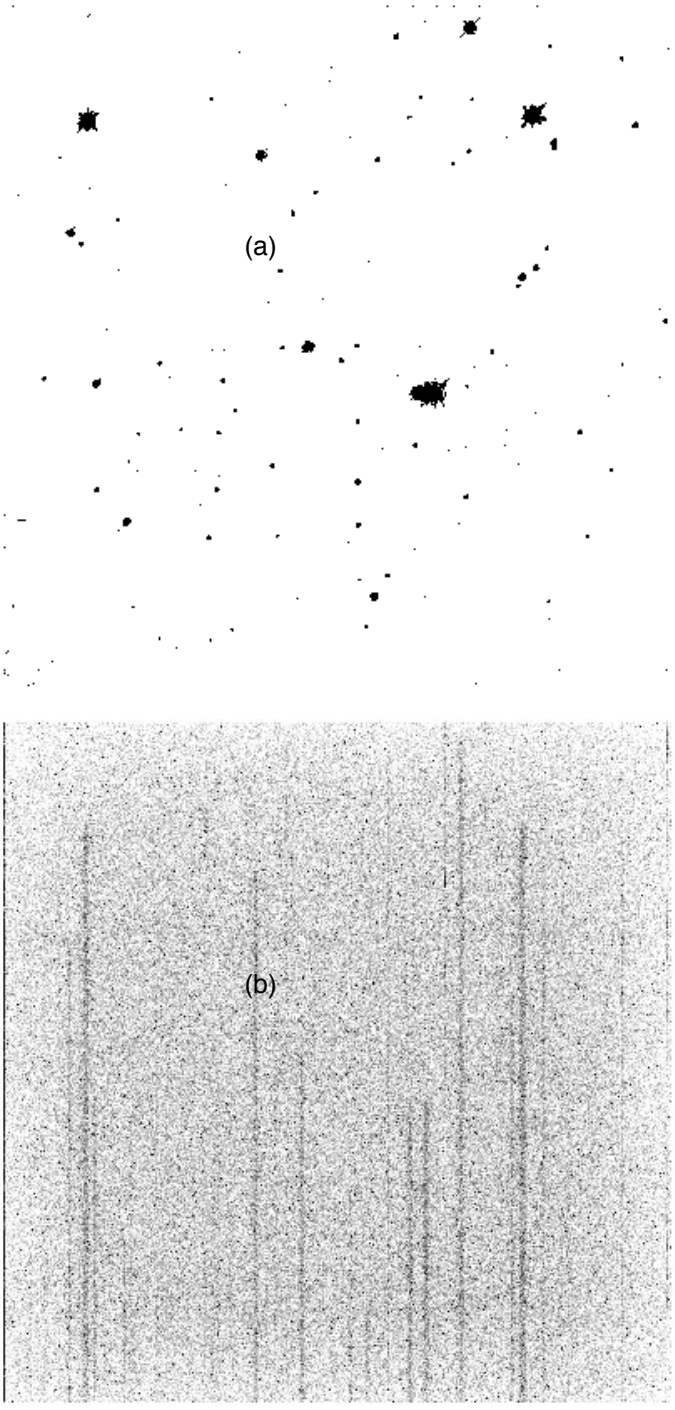

Mitigating CTE during observations

Observers can use a number of strategies to minimize the effect of CTE loss. Longer individual exposures help by increasing both background and source counts, both of which reduce CTE loss. Users thinking of dithering may wish to take this into account if they are considering shortened exposures to allow for more dither positions.

When observing a target significantly smaller than a single detector, it is advisable to place it towards the bottom of a chip (i.e., near the readout amplifier). For example, the aperture WFALL will place the target near the bottom of Chip 3. (Note, however, that targets larger than about 20" centered on WFALL will be split between chips, which itself may lead to photometric problems.) The resulting data can still be corrected using the CTE correction formulae, and the corrections will be smaller.

For faint point sources on low backgrounds, it is recommended that the target be imaged close to the pyramid apex at pixel location (150,150) to reduce the effects of CTE loss. When placing targets closer to the pyramid apex than this position, one risks the target landing near the vignetted regions and affecting the resulting photometry. For the wide field CCDs, aperture = WFALL is recommended. The aperture reference point for WFALL is at pixel (133,149) on the WF3 chip. Therefore, no movement of the target is required to reduce the effects of CTE loss when using this aperture. For PC1 imaging, it is recommended that a POS TARG be used to move the target from the aperture reference point (420.0,424.5) to the recommended position (150,150) using (POS TARG -12.292,-12.491). Table 4.3 on page 113 presents recommended POS TARGs to position a target at pixel location (150,150) in the respective CCD chip.

Table 4.3: Recommended POS TARGs to mitigate CTE.

Aperture	Reference Point X (pixel)	Reference Point Y (pixel)	POS TARG (arcsec)
PC1-FIX	420.00	424.00	-12.292, -12.491
WF2-FIX	423.00	414.00	27.213, -26.293
WF3-FIX	416.00	424.00	26.536, 27.307
WF4-FIX	423.00	421.00	-27.174, 27.001
WFALL	903.00	904.00	no POS TARG needed

When the very highest possible photometric accuracy is required, another possibility is to include a special calibration observation of ω Cen, taken close to the time of the science observations and designed so as to reproduce them as closely as possible in exposure and background levels.

A further possible strategy is to preflash the chip to raise the background level. However, tests indicate that the required level of preflash is so high that in general more is lost than gained by this method (due to overhead

times and added noise). A variation of this, called “noiseless” preflash, was tested where a flat field exposure is taken immediately prior to a science exposure.[1] However, it gave only very modest improvements in CTE (Schultz, et al. 2001).

As part of the Cycle 8 through 12 Calibration Plans, we continued to monitor the CTE for point sources by repeating the key observations of ω Cen every six months (Proposals 7629, 8447, 8821, 9254, 10076). This will be continued in Cycle 13 (Proposal 10364). We also added observations of a cluster of galaxies (Proposal 8456), which yielded a direct measurement of the effect of CTE for faint extended sources for more typical exposure times and background levels. A proposal in Cycle 10 (Proposal 9255) studied the astrometric effects of CTE.

4.12.2 The Long vs. Short Photometric Anomaly

The so-called "long vs. short" anomaly is a nonlinearity of WFPC2 which causes the recorded count rate to increase with exposure time for a given source - the source thus appears brighter in a long exposure than in a short exposure. Suggestions of this nonlinearity was first discussed by Stetson (1995) and then examined in more detail by Kelson et al. (1996), Saha et al. (1996), and Casertano & Mutchler (1998). More recent studies, however, have disputed the existence of the "long vs. short" problem (e.g., Dolphin 2000). Casertano & Mutchler (1998), Hill et al. (1998), and Dolphin (2000) suggest that the apparent "long vs. short" anomaly may be caused by overestimating the value of the sky by a few electrons in the shorter exposure.

We reexamined the “long vs. short” anomaly (Whitmore & Heyer 2002) using the same dataset as in Casertano & Mutchler (1998), that of the globular cluster NGC 2419 taken in 1997 (Proposal 7619). We have analyzed the stars on two chips, WF2 where the globular cluster was centered and WF4 where the stars are much less densely packed. Note that only chip WF2 was analyzed in Casertano & Mutchler (1998). For the uncrowded field (less than ~1000 stars per chip), the typical values of the “long vs. short” nonlinearity are small (a few percent) or nonexistent for stars in the range of 2-400 DN (i.e. 15-3000 electrons) as measured on the “short” exposure. We do not find the larger values (i.e. tens of percent) predicted by Casertano & Mutchler (1998). A re-analysis of WF2 with its densely-packed star field (~10,000 stars per chip) also indicates, in general, a smaller correction than Casertano & Mutchler. Although very large values of a “long vs. short” anomaly are possible for very faint stars in very crowded fields, it appears that the Casertano & Mutchler formula was tuned to fit the worst cases and, therefore, overestimates the values for more typical cases.

1. More details can be found in Biretta and Mutchler (1998) and Whitmore (1998).

We conclude that the “long vs. short” anomaly is very small or non-existent for relatively uncrowded fields (e.g., less than ~1000 stars per chip). However, we still find evidence for varying levels of a “long vs. short” nonlinearity associated with crowded fields, probably due to the subsequent difficulty of estimating accurately the sky background. In order to investigate this possibility further, we separated the measurement of the local sky and the measurement of the object for the crowded NGC 2419 field (WF2). The top panel of Figure 4.22 on page 116 shows the ratio of the counts in the object aperture of the 1000 sec. exposure relative to the counts in the 10 sec. exposure, *using constant values of the sky equal to 30 DN for the long exposure and 0.30 DN for the short exposure*. The dashed lines shows the linear fit to the data, with a slope due to the normal CTE effect. The intercept at Y=0 is within ~2 sigma of the theoretical value of 100. Hence, there appears to be little or no “long vs. short” problem for the ratio of the object observations. However, the ratio of the sky values (bottom panel of Figure 4.22) shows an obvious tendency to fall below the theoretical value of 100. This appears to be the cause of the “long vs. short” anomaly in the crowded NGC 2419 field. The sky values in the 10 sec. exposure appear to be overestimated by about 35%, relative to the predicted values based on the sky measurement of the 1000 sec. exposure. This overestimate of the sky background is enough to produce the large effect observed by Casertano & Mutchler (see Whitmore & Heyer 2002).

Because the sky measurement appears to be the cause of the apparent "long vs. short" anomaly, the magnitude of this effect is highly dependent both on the level of crowding in the image and on the specific reduction parameters (e.g., aperture size) used by the observer. Consequently, we do not provide any set formula to correct this effect. The user is referred to Whitmore & Heyer (2002) for more details on this apparent anomaly and for some possible recommendations for dealing with the most adversely affected datasets.

Figure 4.22: The ratios of the counts in the 1000 sec. exposure to the counts in the 10 sec. exposure for the crowded NGC 2419 field. The top panel shows the ratios in the object apertures using a constant sky value of 0.3 DN for the short exposure and 30 DN for the long exposure. The dashed lines shows the linear fit to the data, with a slope due to the normal CTE effect. The intercept at Y=0 is 102.6 +/- 1.2, within ~2 sigma of the theoretical value of 100. The bottom panel shows the ratio for the local sky measurements. The sky ratio is well below the predicted value of 100, with a median value of 74.1 (mean = 75.9 +/- 0.6). This result implies that the "long vs. short" effect is caused by sky measurements rather than object measurements.

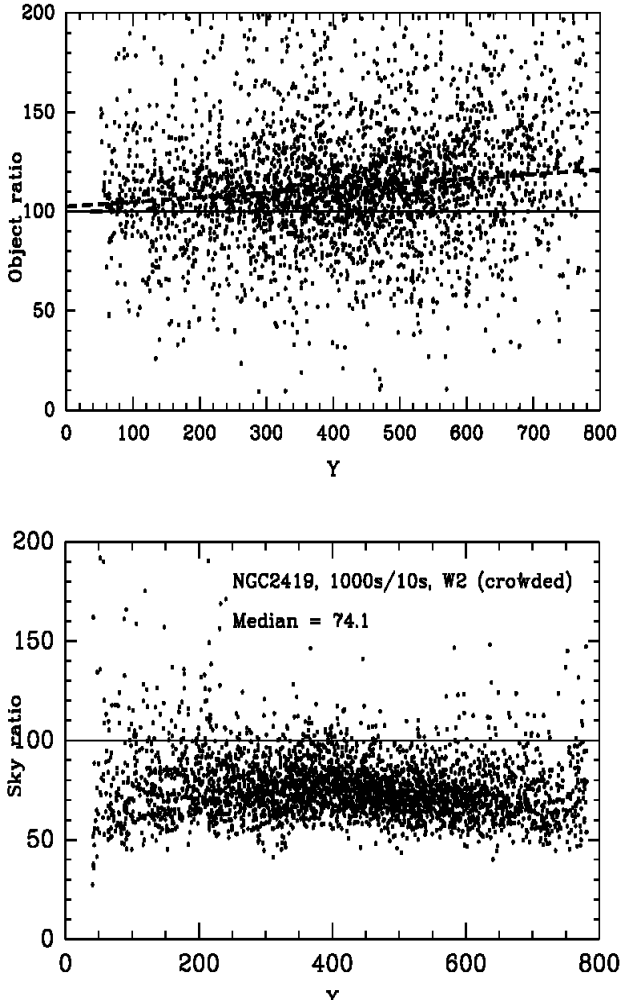

4.13 Read Noise and Gain Settings

The CCDs and their associated signal chains have readout noise levels (in the absence of signal shot noise or interference) of approximately $5e^-$. The analog-to-digital converter is highly accurate, and makes virtually no contribution to the read noise, other than the normal information loss caused by digitization of the signal.

The conversion factors from detected electrons (QE x number of incident photons) to data numbers (DN) are tabulated in Table 4.4 on page 117, as are read noise and linearity ("gamma" is the power law index relating detected DN to input flux). Note that all calculations of sensitivity in this manual assume gains of 7 and 14 for two gain channels, choices very close to the measured gains. The photometric calibration is based on an assumed exact gain of 14 in all CCDs. The measurements given here were derived from thermal vacuum testing. On-orbit measurements have confirmed that the gain ratios are correct to within a possible systematic error of 1%—which will feed directly into a photometric calibration error for gain 7 data, as most of the photometric calibration was done with gain 14 data. Note that the gain ratios are known much more accurately than the individual gains; they are derived from flat field ratios instead. Also, note that the Phase II proposal instructions refer to the ~14 e^- DN^{-1} setting as ATD-GAIN=15.

Table 4.4: Signal Chain Gains.

Parameter	Gain	PC1	WF2	WF3	WF4
Noise	"7"	5.2 4 ± 0.30	5.51 ± 0.37	5.22 ± 0.28	5.19 ± 0.36
	"15"	7.02 ± 0.41	7.84 ± 0.46	6.99 ± 0.38	8.32 ± 0.46
Gain	"7"	7.12 ± 0.41	7.12 ± 0.41	6.90 ± 0.32	7.10 ± 0.39
	"15"	13.99 ± 0.63	14.50 ± 0.77	13.95 ± 0.63	13.95 ± 0.70
Gamma	"7"	1.0015 ± 0.0006	1.0015 ± 0.0006	1.0020 ± 0.0006	1.0038 ± 0.0007
	"15"	1.0004 ± 0.0001	1.0023 ± 0.0004	1.0032 ± 0.0006	1.0018 ± 0.0012
14/7	ratio	1.987 ± 0.02	2.003 ± 0.02	2.006 ± 0.02	1.955 ± 0.02

CHAPTER 5:

Point Spread Function

In this chapter . . .

5.1 Effects of OTA Spherical Aberration

The OTA spherical aberration produces a Point Spread Function (PSF—the apparent surface brightness profile of a point source), as presented to the instruments, with broad wings. Briefly, the fraction of the light within the central 0.1″ was reduced by a factor of about 5. The resulting PSF had "wings" which extended to large radii (several arcseconds), greatly reducing the contrast of the images and degrading the measurements of sources near bright objects or in crowded fields. Burrows, et al. (1991, Ap. J. Lett. 369, L21) provide a more complete description of the aberrated HST PSF. Figure 5.1 on page 120 shows the PSF in three cases.

Figure 5.1: PSF Surface Brightness. The percentage of the total flux at 4000Å falling on a PC pixel as a function of the distance from the peak of a star image.

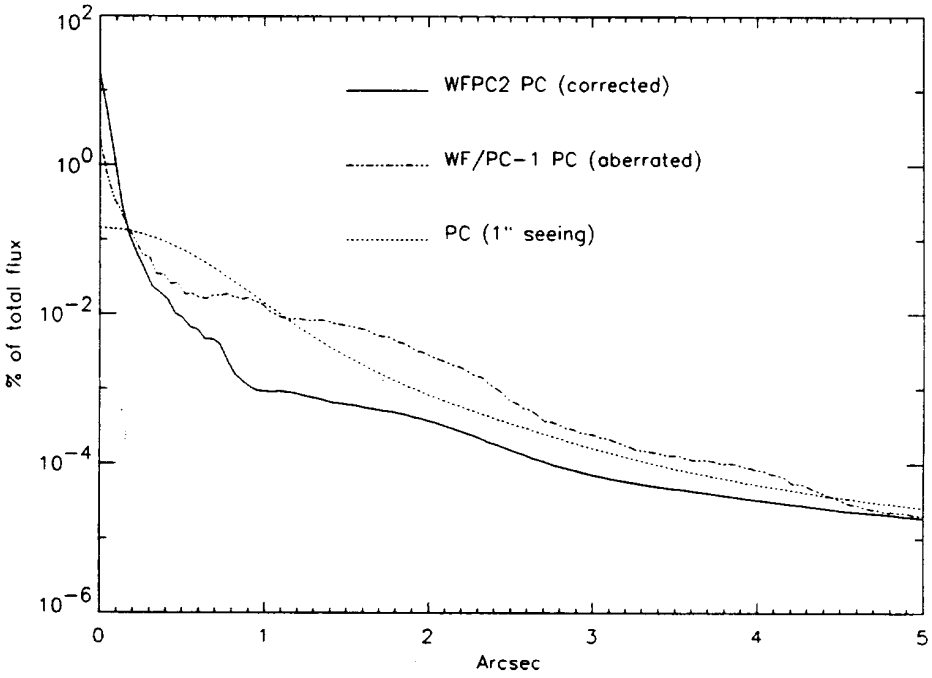

It shows the aberrated HST PSF, the WFPC2 PSF, and for comparison the PSF that would be obtained from a long integration if HST were installed at a ground based observatory with one arcsecond seeing. All of the PSFs were computed at 4000Å. The FWHM of the image both before and after the installation of WFPC2 is approximately proportional to wavelength, at least before detector resolution and MTF effects are considered. (The WF/PC-1 core was approximately 50% broader than the core that is obtained with WFPC2). Figure 5.2 on page 121 shows the encircled energy (EE), the proportion of the total energy from a point source within a given radius of the image center, for the same three cases.

Figure 5.2: Encircled Energy. The percentage of the total flux at 4000Å within a given radius of the image peak.

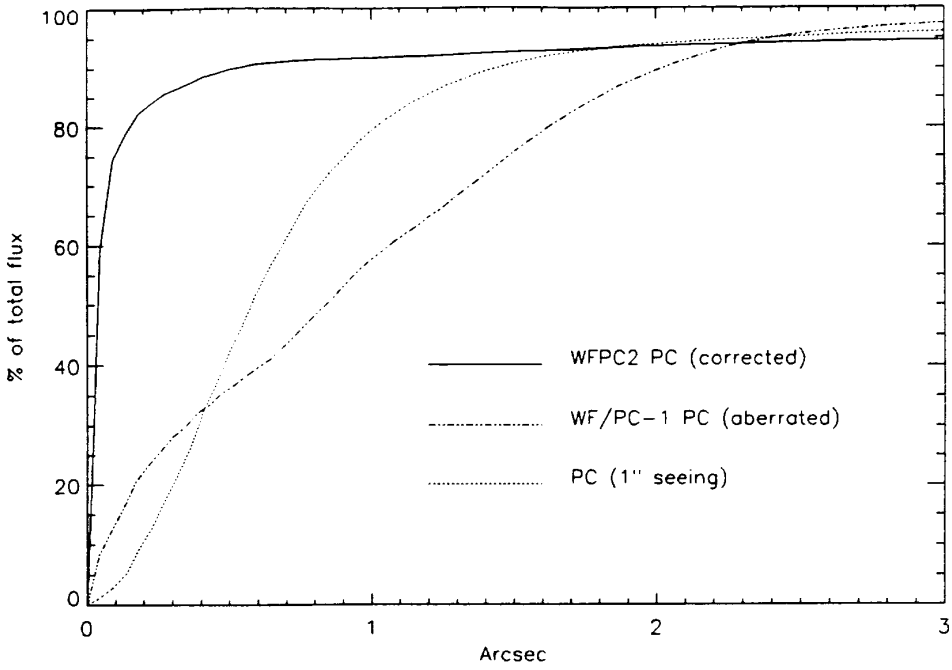

The WFPC2 curve shown is the average of measurements taken with F336W and F439W. It can be seen that the core of the image in WFPC2 contains most of the light. At this wavelength, 65% of the light is contained within a circle of radius 0.1″. However, this proportion is considerably less than the optics deliver. The reason for this is discussed in “CCD Pixel Response Function” on page 126. Encircled energy curves for other filters are shown in Figure 5.3 on page 122 and Figure 5.4 on page 123; note that these curves are normalized to unity at 1.0″ radius.

Figure 5.3: Encircled Energy for CCD PC1. The fraction of energy encircled is plotted vs. aperture radius for several filters. Curves are normalized to unity at a radius of 1.0″. From Holtzman, et al. 1995a.

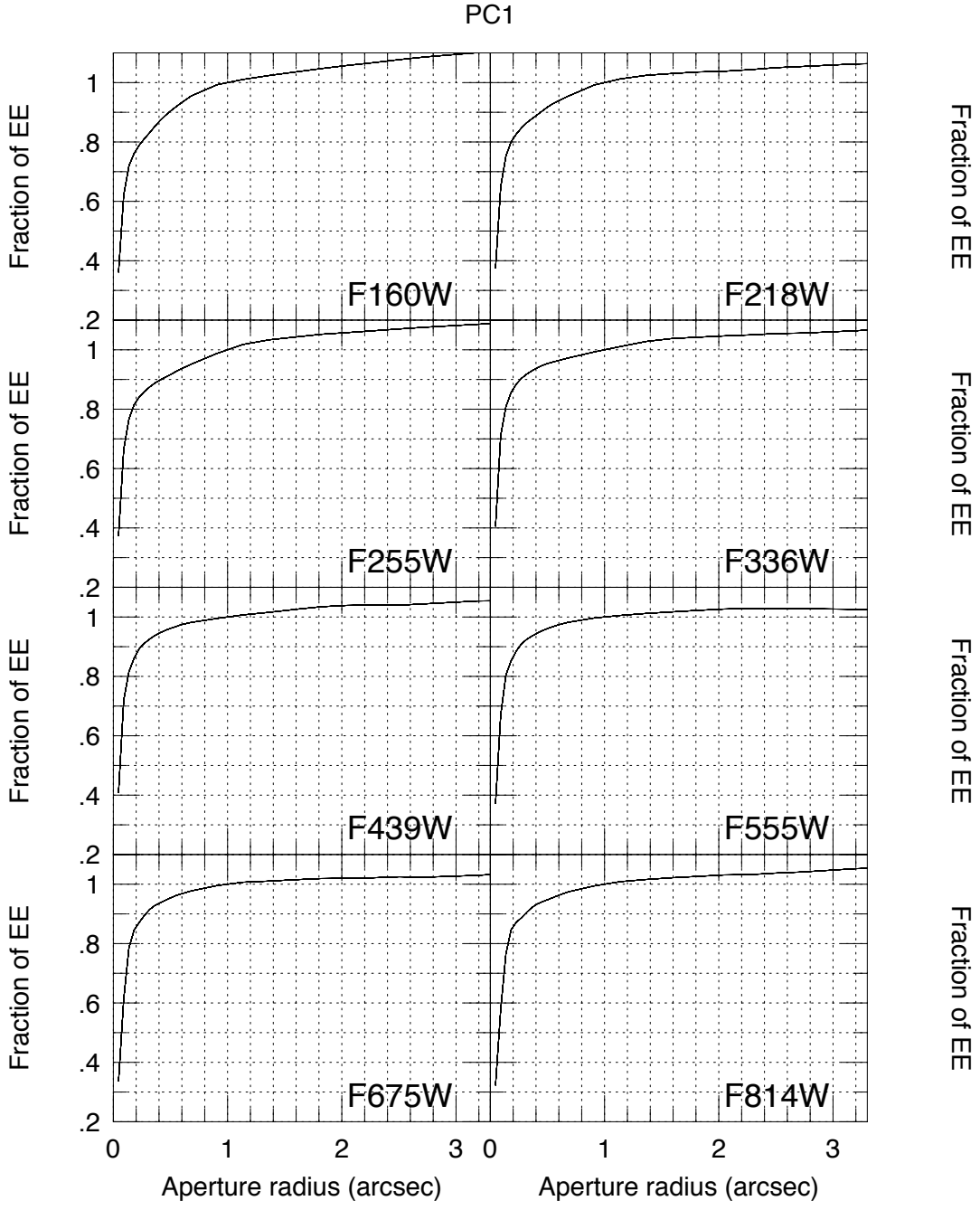

Figure 5.4: Encircled Energy for CCD WF3. The fraction of energy encircled is plotted vs. aperture radius for several filters. Curves are normalized to unity at a radius of 1.0″. From Holtzman, et al. 1995a.

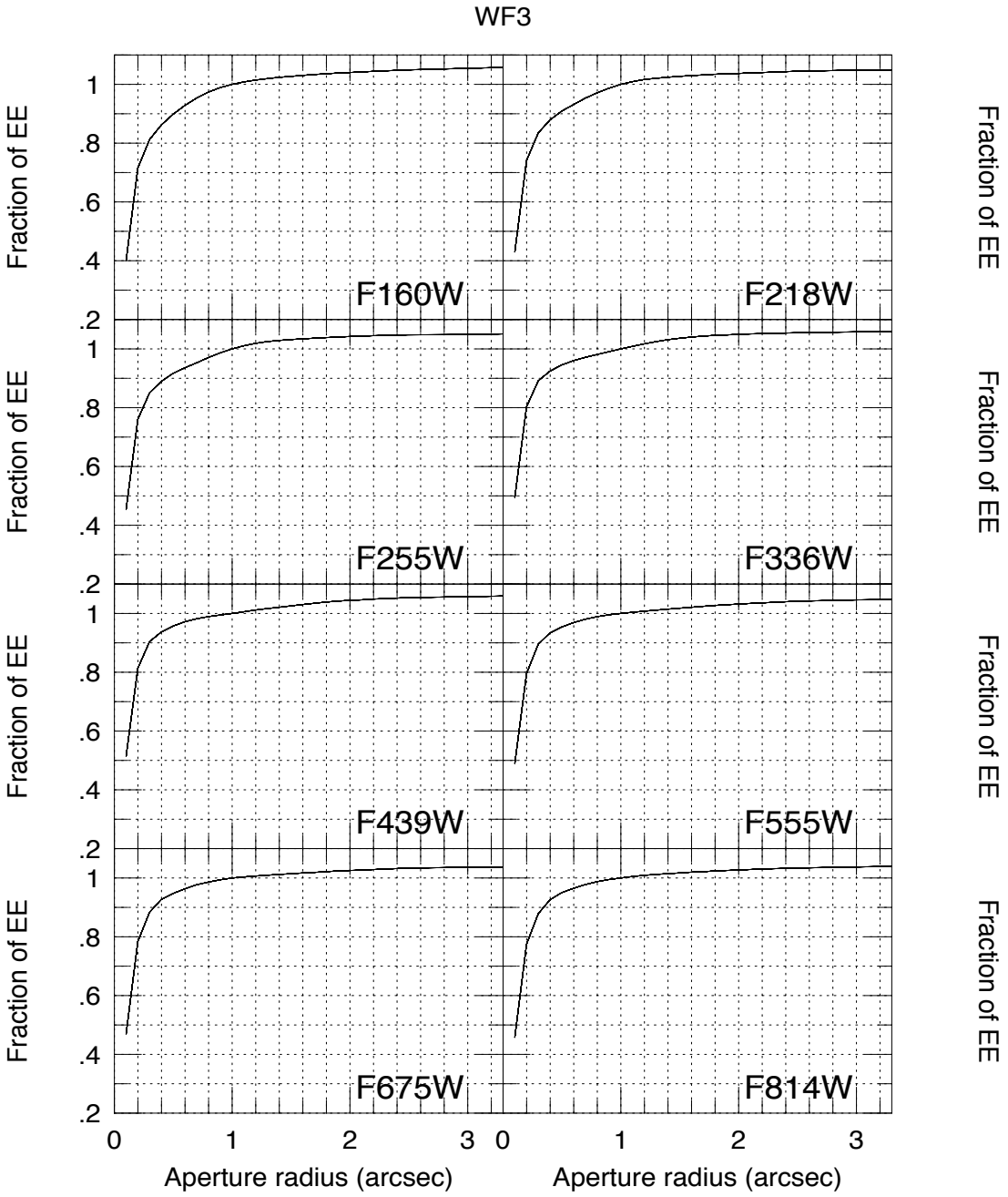

5.2 Aberration Correction

WFPC2 has corrective figures on the relay secondary mirrors where the primary mirror is imaged; this optical correction recovers near-diffraction limited images over the entire CCD fields-of-view. Proper correction requires tight optical alignment tolerances, which are facilitated on-orbit by actuated optics. The corrective optics enable essentially all of the scientific objectives of the original WF/PC-1 to be met.

Table 5.1: Wavefront Error Budget.

Camera	WFC (F/12.9)	PC(F/28.3)
Design error	λ/143	λ/50
Fabrication and alignment error	λ/14.7	λ/14.7
Alignment stability error	λ/25	λ/25
Total wavefront error	λ/12.6	λ/12.3

Through a number of independent analyses, based on investigations of star images obtained on-orbit, and the examination of fixtures used during the figuring of the primary mirror, the aberrations of the HST optics were accurately characterized. The primary mirror was figured to an incorrect conic constant: –1.0139±0.005 rather than the –1.0023 design requirement, resulting in a large amount of spherical aberration. The optical design of WFPC2 creates an image of the OTA primary mirror near the surface of the relay Cassegrain secondary mirror in each of its channels. This design minimizes vignetting in the relay optics, but more importantly, facilitates correction of spherical aberration in the OTA primary by application of the same error (but with opposite sign) to the relay secondary. The optical figure of the WFPC2 secondary mirrors contains a compensating “error” in the conic constant. By adopting a prescription within the error bars for the HST primary mirror, corrective secondary mirrors were made with sufficient accuracy that the residual spherical aberration in the WFPC2 wavefront is small compared to other terms in the WFPC2 optical wavefront budget.

On the other hand, new and stringent alignment requirements were created by the steep optical figure on the corrective relay secondary mirrors. The primary mirror image must be accurately centered on the corrective mirror, and must have the correct magnification. Centering is the most demanding requirement. A failure to center accurately would create a new aberration in the form of coma. A misalignment of 7% of the pupil diameter introduces as much RMS wavefront error as was present in the form of spherical aberration prior to the introduction of corrective optics. The new requirements for alignment accuracy and stability led to the

introduction of a tip-tilt mechanism on the pick-off mirror, to compensate for camera alignment uncertainties with respect to the OTA, and actuated fold mirrors which can compensate for internal misalignments. There was an additional term in the CEIS specification of the overall instrument wavefront error budget for alignment stability. It is λ/25 RMS at 6328Å, as shown in Table 5.1 on page 124.

"Design error" refers to the aberrations inherent in the design itself, which would be seen if the optics conformed perfectly to their specifications. All of the optics were fabricated and integrated into the WFPC2 optical bench. It was established on the basis of component tests, end-to-end optical interferometry, and through focus phase retrieval, that the WFPC2 optical system performed within the stated tolerances for "fabrication and alignment" in the laboratory environment. What remained was to demonstrate the stability of the optical alignment after launch vibration and in response to the thermal environment on-orbit. The "stability" line anticipated these uncertainties, and was verified during early science operations.

5.3 Wavefront Quality

The conclusion of the extensive optical testing in Thermal Vacuum was that the cameras are well corrected to within the specifications. The dominant problem was a small difference in focus between the four cameras (Krist and Burrows 1995). The actuated fold mirrors and pick-off mirror mechanism performed flawlessly in correcting residual coma aberrations in the image, and enabled the on-orbit alignment procedures. Using out-of-focus images, a very accurate alignment of the cameras was accomplished. A side product was that the aberrations in each camera were measured (Krist and Burrows, Applied Optics, 1995). The results are given in Table 5.2 on page 126. These values were used in generating the simulated PSFs given in "Model PSFs" on page 127. The WF3 wavefront error is higher than that of the other chips because it is the most out-of-focus relative to the PC (which is assumed to be in focus). It is the equivalent of about 10 microns of breathing out-of-focus.

Table 5.2: Aberrations in Each Camera. The numbers quoted are RMS wavefront errors in microns over the HST aperture (Zernike coefficients).

	Aberration	PC1	WF2	WF3	WF4
Z4	Defocus	0.0000	0.0410	0.0640	0.0480
Z5	0° Astig	0.0229	0.0109	0.0126	0.0163
Z6	45° Astig	0.0105	0.0041	0.0113	0.0190
Z7	V2 Coma	0.0000	0.0012	-0.0037	-0.0090
Z8	V3 Coma	-0.0082	0.0061	-0.0100	0.0019
Z9	X Clover	0.0063	0.0121	0.0010	0.0096
Z10	Y Clover	0.0023	0.0091	0.0130	0.0042
Z11	Spherical	-0.0131	-0.0215	-0.0265	-0.0247
Z22	5th Spherical	0.0034	0.0034	0.0036	0.0029
	Zonal Errors	0.0180	0.0180	0.0180	0.0180
	Total (RSS)	0.0353	0.0537	0.0755	0.0637
	Budget	0.0813	0.0794	0.0794	0.0794

5.4 CCD Pixel Response Function

From Thermal Vacuum testing, there was evidence that the images are not as sharp as expected, despite the good wavefront quality. The decrease in sharpness corresponds to a loss in limiting magnitude of about 0.5 magnitudes in the WF cameras, and less in the PC.

Further testing, by covering a flight spare CCD with a 2μm pinhole grid in an opaque metallic mask and illuminating it with a flat field source, showed that even when a pinhole was centered over a pixel only about 70% of the light was detected in that pixel.

For practical purposes, the effect can be modeled as equivalent to about 40 mas RMS gaussian jitter in the WFC, and 18 mas in the PC (as compared with the typical real pointing jitter of ~3 mas delivered by the excellent HST pointing control system). Alternatively, at least in the V band, it can be modeled by convolving a simulated image by the following kernel, which gives the pixel response function averaged within pixels:

$$K = \begin{bmatrix} 0.0125 & 0.050 & 0.0125 \\ 0.0500 & 0.750 & 0.0500 \\ 0.0125 & 0.050 & 0.0125 \end{bmatrix}$$

One clue is the wavelength dependence of the observed sharpness: the results from the 2μm pinhole grid test get worse at longer wavelengths. This may reflect the greater penetration into the silicon of low energy photons, which facilitates the diffusion of photoelectrons across the pixel boundaries defined by the frontside gate structure.

There is also evidence for sub-pixel QE variations at the 10% level. There is an implied dependence on pixel phase for stellar photometry. This has been seen at about the 1-3% level in on-orbit data. The work of Jorden, Deltorn, and Oates (Greenwich Observatory Newsletter 9/93) has yielded quite similar results, and suggests that sub-pixel response must be taken into account when seeking to understand the behavior of all CCD detectors forming undersampled images.

5.5 Model PSFs

Considerable effort has gone into the modeling of the HST point spread function (PSF), both in order to measure the optical aberrations in support of the WFPC2, COSTAR, and advanced scientific instruments, and to provide PSFs for image deconvolution in the aberrated telescope. Such PSFs are noise free and do not require valuable HST observing time. Software to generate model PSFs for any filter and at any location within the field-of-view is available from the STScI (TIM package, Hasan and Burrows 1993; TinyTIM package, Krist 1995). The results are illustrated in Table 5.3 on page 129 and Table 5.4 on page 130 for the PC1 and WF2 cameras, respectively. A representative PSF is on the left in each panel. It meets the wavefront error budget, with the measured mix of focus, coma, astigmatism, and spherical aberration. It has been degraded by the pixel response function as discussed in Section “CCD Pixel Response Function” on page 126. On the right is the diffraction limited case for comparison. In each case the percentage of the total flux in a central 5x5 pixel region of a point source is displayed. The peak of the star image can be at an arbitrary point relative to the boundaries of the CCD pixels. Two cases are shown: one where the star is approximately centered on a pixel, and one where it is approximately centered at a pixel corner. As a consequence of the under-sampling in the WFPC2, the limiting magnitude attainable in the background limit varies by about 0.5 magnitude, depending on the position of the source within the CCD pixel. This point is discussed in more detail in Chapter 6.

Neither observed nor modeled PSFs will provide a perfect match to the PSF in actual science observations, due to modeling uncertainties, the “jitter” in the HST pointing, and orbit to orbit variations in telescope focus (“breathing”—which seems to be generally limited to about 1/20 wave peak-to-peak). Jitter is not predictable but can be recovered to a reasonable

extent for observations obtained in Fine Lock. In long exposures, up to about 10 mas of apparent pointing drift may occur as a result of the breathing effects in the FGS, although smaller variations of ~3 mas are typical.

5.6 PSF Variations with Field Position

The WFPC2 PSFs vary with field position due to field-dependent aberrations, obscuration shifting, and scattering. This complicates photometry, PSF subtraction, and deconvolution (Krist, 1995).

The coma and astigmatism aberrations vary significantly within a camera across the field-of-view. These variations are simply part of the optical design. At the extreme corners of the WFC CCDs, away from the OTA axis, there is about 1/5 wave of astigmatism (referenced at 633 nm), which decreases to nearly zero at the CCD centers. Astigmatism at this level causes the PSF core to become elliptical and slightly less sharp; note the flattening of the PSF at pixel positions (54,777) and (605,148) in Figure 5.5 on page 131. Coma also varies, but to a much lesser extent. Coma and astigmatism variations are considerably smaller in PC1 (though we note the astigmatism at the center of PC1 is fairly significant - see Table 5.2 on page 126).

Table 5.3: PC Point Spread Functions. Shown as percentages (out of 100 percent) of the total flux in a 5 by 5 pixel region. On the left in each case is a model PSF with the observed wavefront errors and pixel response function. On the right is the diffraction limited case for comparison.

WFPC2 Model PSF					Diffraction Limited PSF				
2000 Å: Peak near corner of PC pixel									
0.9	2.3	2.3	0.9	0.3	0.2	0.6	0.5	0.3	0.1
2.5	10.3	12.7	2.5	0.5	0.6	17.6	20.9	0.5	0.1
1.9	11.2	13.3	2.6	0.5	0.5	20.9	26.0	0.6	0.2
0.9	2.1	2.7	1.4	0.3	0.3	0.5	0.6	0.3	0.1
0.3	0.5	0.5	0.4	0.2	0.1	0.1	0.2	0.1	0.2
Peak near center of pixel									
0.3	0.7	1.3	0.8	0.5	0.1	0.3	0.4	0.2	0.2
0.7	2.6	6.4	3.2	0.8	0.3	0.6	4.9	0.6	0.3
1.2	6.3	25.0	6.9	1.4	0.4	4.9	62.9	6.3	0.4
0.6	2.2	5.9	3.6	0.9	0.3	0.5	6.3	0.7	0.4
0.4	0.8	1.4	1.1	0.4	0.2	0.3	0.4	0.4	0.2
4000 Å: Peak near corner of PC pixel									
0.9	2.5	3.5	1.2	0.2	0.3	2.5	2.5	0.3	0.1
3.6	10.8	12.0	3.1	0.4	2.5	14.3	15.8	2.7	0.2
2.7	11.5	12.9	3.5	0.4	2.5	15.8	17.6	3.0	0.2
0.8	3.0	3.4	1.3	0.3	0.3	2.7	3.0	0.4	0.1
0.2	0.4	0.4	0.3	0.2	0.1	0.2	0.2	0.1	0.1
Peak near center of pixel									
0.3	0.6	0.8	0.9	0.3	0.1	0.2	0.3	0.2	0.1
0.9	4.0	6.6	4.9	0.8	0.2	3.8	4.4	3.8	0.2
0.9	6.9	26.1	7.0	0.8	0.3	4.5	49.4	5.1	0.4
0.5	3.4	6.8	4.9	0.9	0.2	3.8	5.0	4.3	0.2
0.2	0.6	0.8	0.9	0.4	0.1	0.2	0.4	0.2	0.1
6000 Å: Peak near corner of PC pixel									
2.0	2.6	3.4	2.4	0.5	2.1	2.3	2.0	2.1	0.2
3.4	9.8	10.4	2.9	0.6	2.2	11.4	12.8	2.1	0.6
2.8	10.6	11.2	3.2	0.6	2.0	12.9	14.1	2.1	0.6
1.6	2.8	3.1	2.4	0.5	2.0	2.0	2.1	2.3	0.2
0.4	0.6	0.7	0.5	0.2	0.2	0.5	0.6	0.2	0.1
Peak near center of pixel									
0.5	1.2	1.7	1.7	0.6	0.2	1.5	1.8	1.4	0.3
1.7	3.1	5.9	3.6	1.6	1.5	2.4	4.3	2.2	1.6
2.0	6.0	20.7	6.6	1.8	1.8	4.4	31.6	5.3	2.0
1.2	2.9	6.2	3.7	1.7	1.4	2.1	5.4	2.3	1.7
0.4	1.3	2.0	1.7	0.6	0.2	1.5	1.9	1.7	0.3
8000 Å: Peak near corner of PC pixel									
1.6	1.9	2.2	1.9	1.1	1.8	0.9	0.9	1.5	1.1
2.1	9.3	9.7	2.1	1.1	0.9	11.7	12.6	1.0	1.4
2.0	9.8	10.1	2.4	1.1	0.9	12.6	13.3	1.0	1.5
1.4	2.1	2.1	1.8	1.1	1.5	1.0	1.0	1.6	1.2
0.8	1.2	1.3	1.1	0.4	1.1	1.4	1.5	1.2	0.2
Peak near center of pixel									
1.2	1.4	1.5	1.8	1.4	1.3	1.8	1.1	1.6	1.4
1.8	2.5	6.0	2.8	1.6	1.8	1.5	6.2	1.7	1.6
1.6	6.0	15.4	6.6	1.5	1.1	6.2	22.5	7.1	1.0
1.3	2.7	6.3	3.0	1.7	1.6	1.7	7.1	1.9	1.7
1.0	1.4	1.5	1.7	1.4	1.4	1.6	1.0	1.7	1.5

Table 5.4: WFC Point Spread Functions. Shown as percentages (out of 100 percent) of the total flux in a 5 by 5 pixel region. On the left in each case is a model PSF with the observed wavefront errors and pixel response function. On the right is the diffraction limited case for comparison.

WFPC2 Model PSF					Diffraction Limited PSF				
2000 Å: Peak near corner of WF pixel									
0.5	1.8	2.1	0.8	0.3	0.4	0.4	0.4	0.3	0.1
1.5	9.9	13.6	3.1	0.5	0.4	15.4	21.5	0.4	0.1
1.5	9.8	24.0	4.7	0.5	0.4	21.5	33.4	0.4	0.1
0.5	2.1	3.6	1.3	0.3	0.3	0.4	0.4	0.4	0.1
0.2	0.4	0.4	0.2	0.2	0.1	0.1	0.1	0.1	0.1
Peak near center of pixel									
0.2	0.4	0.5	0.5	0.3	0.2	0.2	0.2	0.1	0.2
0.3	1.7	5.3	3.0	0.8	0.1	0.8	1.3	0.6	0.1
0.5	5.4	28.5	14.0	2.2	0.2	1.3	86.2	1.4	0.2
0.3	2.2	9.1	4.5	1.0	0.1	0.6	1.4	0.9	0.2
0.3	0.6	1.2	0.8	0.3	0.2	0.1	0.2	0.2	0.2
4000 Å: Peak near corner of WF pixel									
0.8	2.6	2.5	0.8	0.2	0.4	0.5	0.5	0.2	0.1
2.6	16.1	16.4	3.0	0.4	0.5	17.7	21.2	0.6	0.1
2.0	12.9	17.3	3.0	0.4	0.5	21.2	26.7	0.6	0.1
0.6	2.0	2.6	0.9	0.2	0.2	0.6	0.6	0.4	0.2
0.2	0.4	0.3	0.2	0.1	0.1	0.1	0.1	0.2	0.2
Peak near center of pixel									
0.3	0.6	0.7	0.5	0.3	0.3	0.2	0.3	0.2	0.2
0.6	3.1	7.2	3.4	0.7	0.2	0.7	3.7	0.7	0.2
0.9	8.5	33.3	10.2	1.2	0.3	3.7	68.8	5.3	0.4
0.4	2.5	8.8	3.0	0.6	0.2	0.7	5.3	0.8	0.2
0.2	0.5	0.9	0.5	0.3	0.2	0.2	0.4	0.2	0.3
6000 Å: Peak near corner of WF pixel									
0.7	2.6	2.6	0.9	0.3	0.2	0.5	0.4	0.2	0.2
3.0	14.9	15.6	3.3	0.5	0.5	18.3	20.7	0.5	0.3
2.2	13.7	16.3	3.2	0.4	0.4	20.7	24.2	0.6	0.2
0.6	2.3	2.9	0.7	0.2	0.2	0.5	0.6	0.2	0.2
0.2	0.3	0.3	0.2	0.2	0.2	0.3	0.2	0.2	0.2
Peak near center of pixel									
0.3	0.7	0.9	0.6	0.2	0.2	0.3	0.2	0.3	0.2
0.7	4.1	7.8	4.1	0.8	0.3	1.8	6.1	1.9	0.3
1.0	8.6	30.4	9.4	1.3	0.2	6.1	54.9	6.2	0.3
0.5	2.8	8.2	3.5	0.6	0.3	1.9	6.2	2.5	0.3
0.2	0.5	1.0	0.6	0.3	0.2	0.3	0.3	0.3	0.2
8000 Å: Peak near corner of WF pixel									
1.0	3.0	2.9	1.1	0.3	0.1	2.0	2.0	0.2	0.2
3.6	13.1	13.6	4.0	0.5	2.0	15.8	17.3	2.2	0.1
2.6	12.6	14.2	3.5	0.5	2.0	17.3	19.3	2.5	0.1
0.8	3.2	3.6	1.0	0.3	0.2	2.2	2.5	0.2	0.2
0.2	0.4	0.5	0.2	0.1	0.2	0.1	0.1	0.2	0.1
Peak near center of pixel									
0.2	0.8	0.8	0.7	0.3	0.1	0.2	0.3	0.2	0.1
0.9	4.6	6.9	4.4	1.0	0.2	3.5	4.6	3.4	0.2
0.9	7.5	30.8	8.1	1.2	0.3	4.6	52.0	5.0	0.3
0.5	3.1	7.3	3.7	0.7	0.1	3.4	5.1	3.9	0.2
0.2	0.5	1.0	0.7	0.2	0.1	0.2	0.3	0.2	0.1

Figure 5.5: PSF Variations with Field Position - Aberrations. Nine observed PSFs (filter F814W) are shown from a widely spaced grid on WF3. CCD pixel positions are labeled. Note the flattening of the PSF in the (54,777) and (605,148) positions.

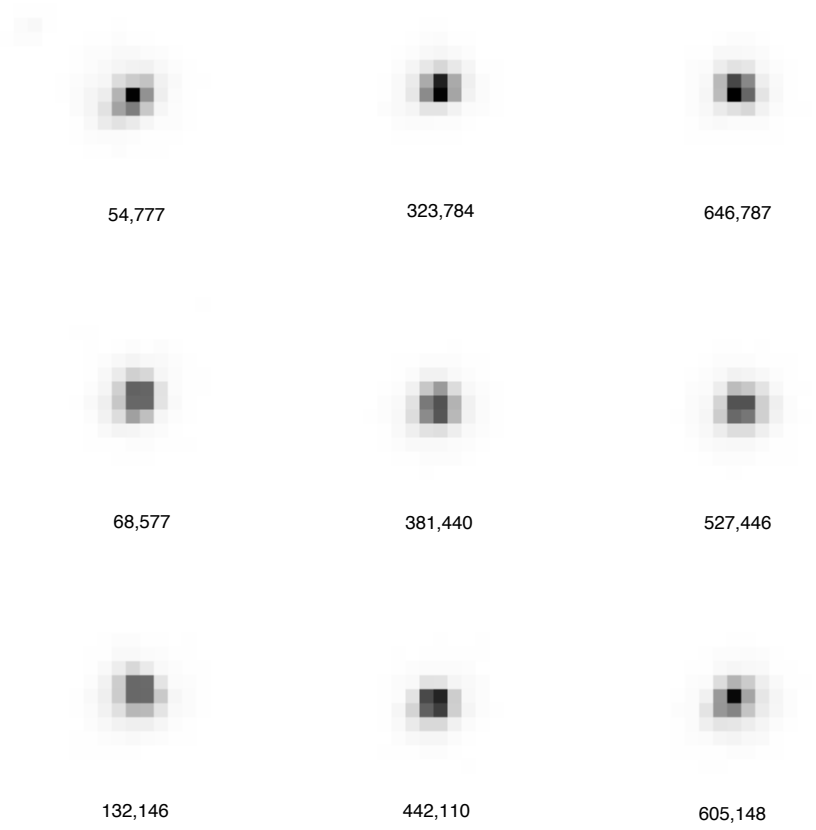

The obscuration patterns due to the camera optics (relay secondary mirror and spiders) appear to shift with respect to the OTA obscurations, depending on field position. The interacting diffraction patterns of the WFPC2 and OTA spiders cause ripples in the spider diffraction spikes, which vary with field position as the two spiders shift relative to each other. In Figure 5.6 on page 132 the OTA spider is hidden behind the WFPC2 spider at the field center and hence the diffraction spikes there have a simple, smooth appearance (c.f. position 446,425). At the CCD corners, however, one or more vanes of the OTA spider move out from behind the WFPC2 spider, and the double set of obscurations causes a “beating” pattern in the diffraction spikes.

The spiders also interact with light diffracted from zonal errors in the OTA mirrors, causing streaks in the scattering halo which vary in position and intensity.

Figure 5.6: PSF Variations with Field Position - Obscuration Shifts. Five saturated PSFs observed in F814W are shown from a widely spaced grid on WF4. Note the changes in the spider diffraction spikes. CCD pixel positions are labeled. The vertical feature is caused by saturation and blooming (see “Blooming” on page 81).

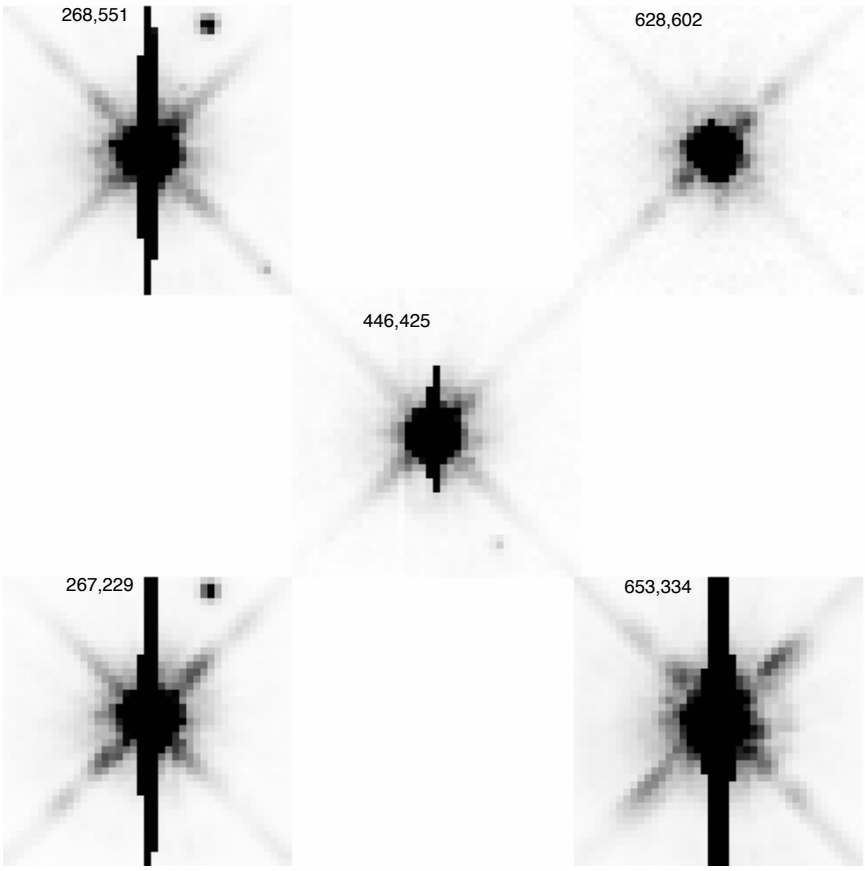

5.6.1 Aperture Corrections vs. Field Position

The amount of energy encircled by an aperture used for stellar photometry will depend on the aperture size, and on any variations in the PSF with field position, time, etc. In general, larger apertures will provide more stable results in the presence of PSF variations. However, large apertures will also exacerbate many problems: contamination from residual cosmic rays, scattered light from nearby stars, and the lower signal-to-noise (S/N) that typically results.

Gonzaga et al. (1999) have measured aperture corrections and characterized their change as a function of field position and filter. The differences in photometric magnitude between apertures with various radii (i.e. aperture corrections), and their mean and standard deviations for the F555W filter, are presented in Table 5.5 on page 133. For example, the first row of the table indicates that stars measured with a 1 pixel radius aperture will be about 0.887 magnitude fainter than if a 5 pixel radius aperture were

used (averaged over entire PC CCD), and this difference will vary by about 0.054 magnitudes RMS across the CCD.

Variations in the PSF with field position will, of course, cause a position dependence in the aperture corrections. Figure 5.7 on page 134 illustrates how the aperture correction varies with distance from the CCD center, R, for different pairs of aperture sizes. The scatter in the plots is due to contamination from residual cosmic rays and nearby faint stars within the larger aperture. While the data are somewhat incomplete, a clear trend is present: the aperture correction generally increases linearly as a function of distance from the CCD center. For example, the aperture correction between 1 to 5 pixel radius is about 0.82 magnitudes at the PC center, and increases to about 0.94 magnitude at the far corners of the CCD. (The average correction is about 0.89 magnitude, as given in the first line of Table 5.5.) The other WFPC2 CCD chips show results similar to the PC chip.

Table 5.5: Magnitude differences produced by different aperture sizes. Results given for PC, WF2, WF3, and WF4 in F555W.

Chip	Filter	Aperture Radii (pixels)	Number of Stars	Mean Magnitude Difference[a]	RMS of Magnitude Difference[b]
PC	F555W	1 vs. 5	116	0.887	0.054
PC	F555W	2 vs. 5	115	0.275	0.028
PC	F555W	2 vs. 10	115	0.401	0.075
PC	F555W	5 vs. 10	115	0.106	0.055
WF2	F555W	1 vs. 5	558	0.608	0.130
WF2	F555W	2 vs. 5	558	0.160	0.085
WF2	F555W	2 vs. 10	544	0.310	0.257
WF2	F555W	5 vs. 10	548	0.133	0.204
WF3	F555W	1 vs. 5	660	0.680	0.133
WF3	F555W	2 vs. 5	656	0.188	0.076
WF3	F555W	2 vs. 10	649	0.376	0.308
WF3	F555W	5 vs. 10	647	0.154	0.233
WF4	F555W	1 vs. 5	828	0.672	0.129
WF4	F555W	2 vs. 5	831	0.198	0.115
WF4	F555W	2 vs. 10	815	0.386	0.350
WF4	F555W	5 vs. 10	814	0.160	0.252

a. Magnitude difference averaged around CCD.
b. RMS magnitude difference around CCD.

In practice, the aperture correction also depends on defocus. The interplay between aperture correction and defocus may be complex, since the optimal focus changes with field position. A full correction has not been established, but the TinyTIM PSF model (see Section 5.7) can be used to estimate the extent of the variation in the aperture correction. In general, we recommend that a minimum aperture radius of 2 pixels be used whenever possible, in order to reduce the impact of variations of the aperture correction with focus and field position. If the field is too crowded and a smaller aperture is needed, we recommend that users verify the validity of the corrections on a few well-exposed stars.

The following section includes a discussion of aperture corrections as a function of OTA focus.

Figure 5.7: Aperture correction (delta) between two given apertures within the PC chip versus radial distance of the target from the center of the chip. Open symbols indicate spurious data.

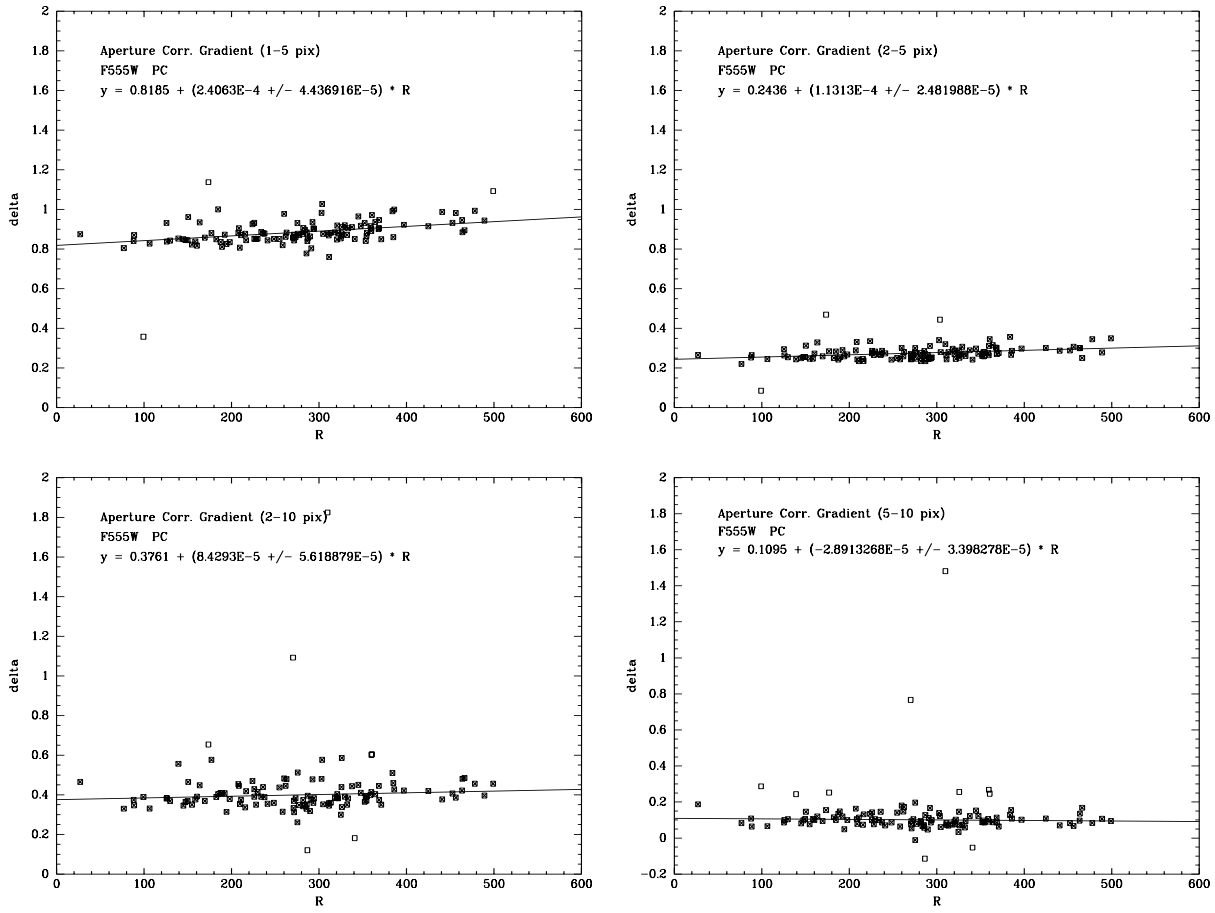

5.7 PSF Variations with Time / OTA Focus

The shape and width of observed PSFs varies slightly over time, due to the change in focus of the telescope. The focus variation consists of two terms: a secular change due to the ongoing shrinkage of the Metering Truss Assembly at an estimated rate of 0.25 μm per month in 1995 (Note: the shrinkage essentially stopped around 2000), and short-term variations, typically on an orbital time-scale (the so-called "breathing" of the telescope, see Figure 5.9 on page 136). The breathing is probably due to changes in the thermal environment as the telescope moves through its orbit, and has a typical peak-to-peak amplitude of 4 μm; larger variations are occasionally seen.

These small focus shifts will impact photometry performed with small (few pixel radius) apertures. Typical ±2 μm focus shifts will result in photometric variations in the PC1 of 6.8%, 4.5%, 2.0%, and 0.2% for aperture radii of 1, 2, 3, and 5 pixels, respectively, in F555W. This is based on the focus monitoring data taken over the period from January 1994 to February 2003 (see Figure 5.9 on page 136). Hence, "breathing" is often one of the major sources of errors for small-aperture photometry. However, relative photometry (i.e. the difference in magnitudes of stars in the same image) is less affected by this variation, since all the stars in an image tend to be impacted by the defocusing in a similar way.

Figure 5.8: HST Focus Trend over Mission Life.

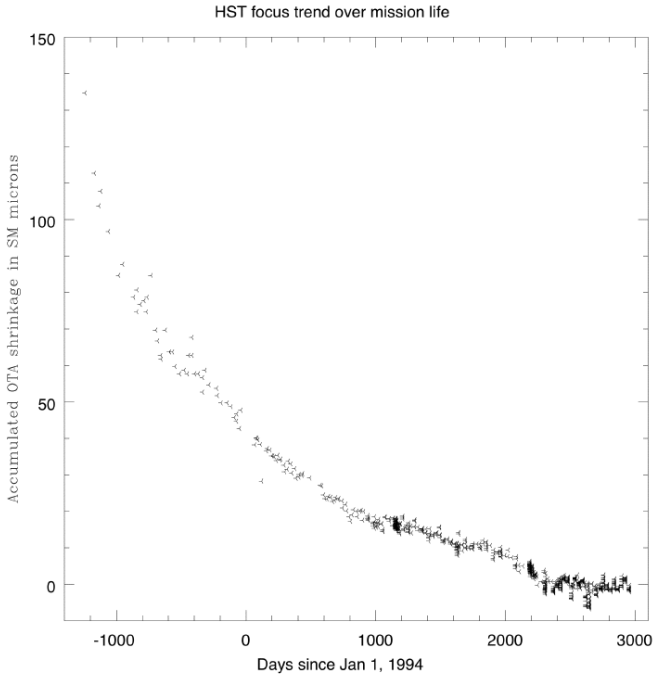

Up-to-date focus information is maintained on our web page at:

http://www.stsci.edu/instruments/observatory/focus

Figure 5.9: Measured OTA Focus Position (microns) as Function of Days since January 1, 1994. The focus position is defined as the difference between the optimal PC focus and the measured focus, in microns at the secondary mirror. Times and size of OTA focus adjustments are indicated along the bottom of the plot.

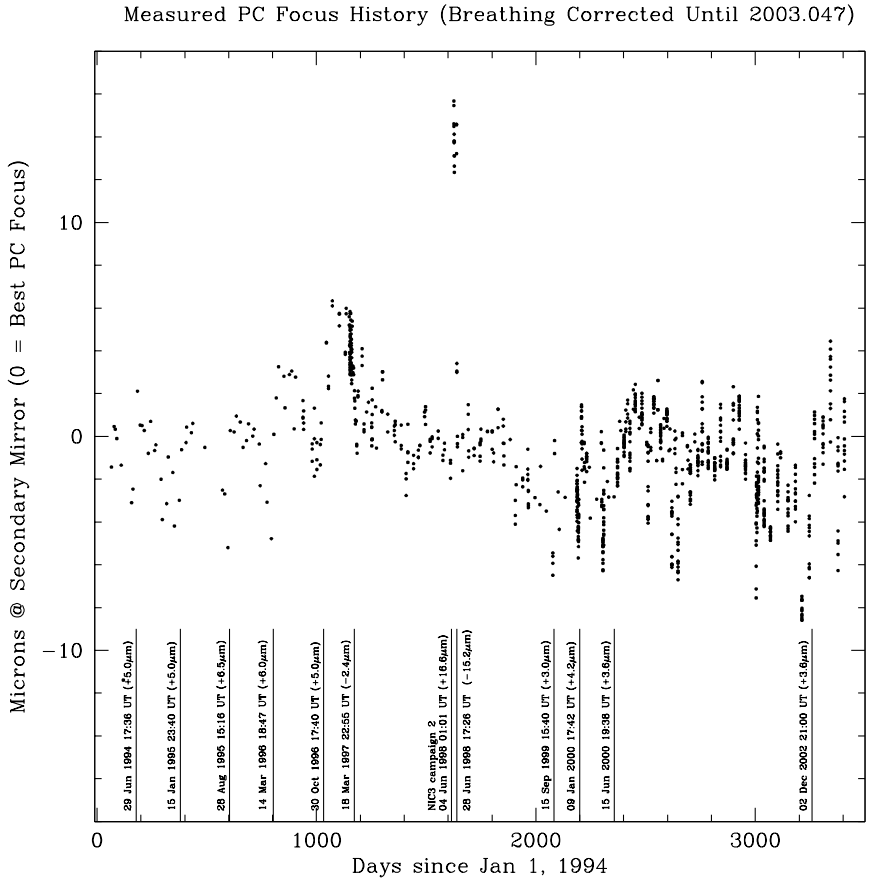

Figure 5.10: Measured Aperture Correction, V(r) - V(r=10 pix), in Magnitudes as Function of Shift from Optimal Focus. Data are given for aperture radii r=1, 2, 3, and 5 pixels for F555W filter on CCD PC1.

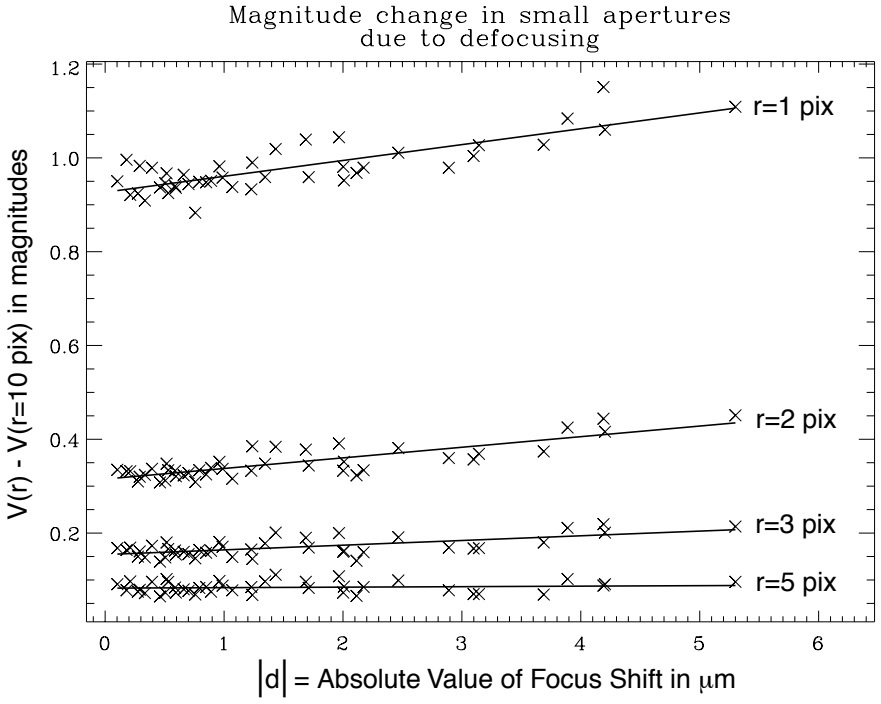

Systematic errors due to the secular focus drift can be corrected using aperture corrections as a function of focus change (see Figure 5.10 on page 137). The aperture correction adjusted for focus change is hence:

```
ap_corr = ap_corr_nominal + a(r) x d
```

where ap_corr_nominal is the nominal aperture correction (mag) as derived from Table 2a in Holtzman et al. (1995a), a(r) is the flux variation per 1 μm of focus drift (mag per micron) using an aperture with radius r (pixels), and d (μm) is the focus shift from the nominal position. The monitoring data mentioned above yield for PC1 and F555W, the following values for a(r):

$$a(1\ \text{pix}) = 0.0338 \pm 0.0038$$
$$a(2\ \text{pix}) = 0.0226 \pm 0.0024$$
$$a(3\ \text{pix}) = 0.0100 \pm 0.0018$$
$$a(5\ \text{pix}) = 0.00105 \pm 0.0015$$

Suchkov and Casertano (1997) provide further information on aperture corrections. They find that the aperture correction varies with focus by up to 10% for a 1-pixel radius in the PC, and is generally well-fitted by a quadratic function of focus position (see Figure 5.11 on page 138). A 10% change is measured only for 5 μm defocus, which is about the largest that is expected during normal telescope operations.

It is important to note that WF cameras can also have significant variations in their aperture corrections as the focus varies. While one would

naively expect the larger pixels on the WFC to produce weaker variations in the aperture corrections, in practice, the focus offsets between cameras, and the fact that the overall OTA focus is usually optimized for PC1, can lead to significant corrections in the WFC.

Suchkov and Casertano provide formulae that estimate the change in the aperture correction due to defocus for a variety of circumstances.

Figure 5.11: Magnitude change for a 1 pixel radius aperture as function of focus position. Derived from quadratic fits to observed data. Note offset between optimal focus for PC1 (solid line) and WF3 (dashed lines). From Suchkov and Casertano (1997).

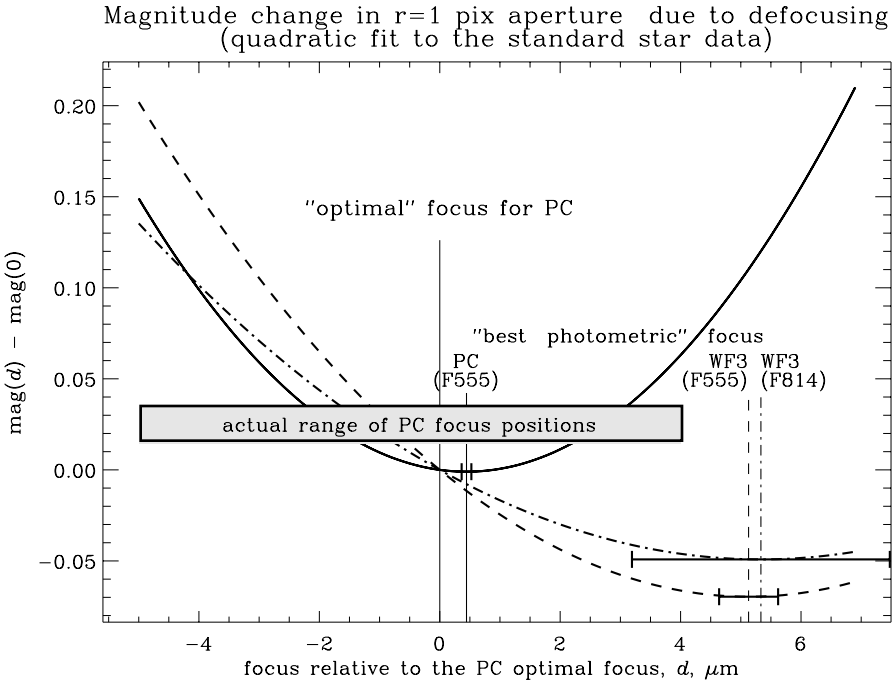

Large focus changes, with amplitudes up to 10μm, are seen occasionally (See Hasan and Bely 1993, Restoration of HST Images and Spectra II, p. 157). On May 1, 1994, and February 27, 1995, a short-lived defocusing of the telescope of up to 10μm was seen, probably due to extreme thermal conditions after the telescope was at an almost exact anti-sun pointing for an extended time. Such a defocusing causes an increase of the PSF width by about 5-10% and a significant change in its shape. This is especially evident in the PC both because of its higher resolution and its astigmatism, which makes the out-of-focus image appear elongated. The change in the PSF appears to be modeled adequately by the TinyTIM software. (See Hasan and Bely 1993, Restoration of HST Images and Spectra II, p. 157. Also see the sample PSF subtraction in Figure 7.2 on page 200).

For more information, see the HST focus web site at

http://www.stsci.edu/instruments/observatory/focus

Two- Gyro Mode: At some future date HST may be operated with only two gyros, hence causing additional spacecraft jitter and degradation of the effective PSF. Please see the Two-Gyro Mode Handbook for discussion of these effects.

5.8 PSF Anomaly in F1042M Filter

We note that the F1042M filter has an anomalous PSF containing additional light in a broad halo component. This is due to the CCD detector becoming transparent at these wavelengths, so that light is reflected and scattered by the back of the CCD producing a defocused halo. Figure 5.12 on page 139 compares the F1042M PSF with the more normal PSF seen slightly blueward in F953N. This scattering will impact photometry in the F1042M filter relative to other filters, since a greater fraction of the counts will lie outside the 1 arcsecond diameter aperture used herein for photometry on standard stars.

Figure 5.12: Comparison of azimuthal averages for observed F1042M and F953N PSFs. Courtesy of John Krist.

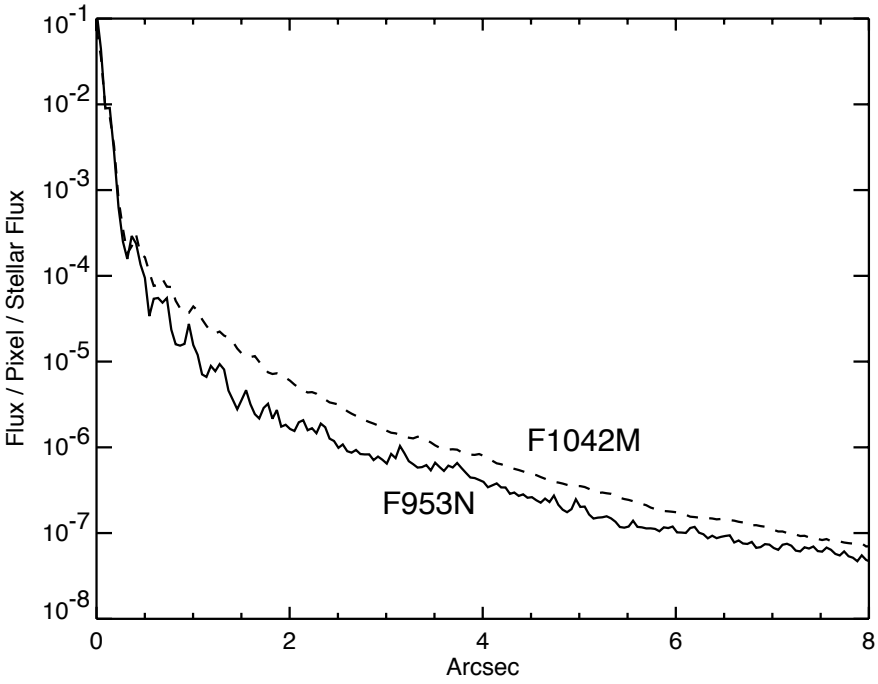

5.9 Large Angle Scattering

Analysis of the WFPC2 saturated star images indicate that the large angle scattering (>3″ from a star) is significantly higher than expected.

Three data sets were used to determine the WFPC2 scattering. The first set was from the SMOV Ghost Check Proposal 5615, in which 100-second images of δ Cas (V=2.7) were obtained at the center of each chip in F502N. The second set was a series of 6-second exposures of Vega (V=0.0) centered on WF2 through F410M (WFPC2 GTO Proposal 5205). The third set was ε Eridani (V=3.73) centered on the PC and taken through F631N (500s each) and F953N (2200s each). These were from GTO Proposal 5611.

WFPC2 scattering was determined by computing the azimuthal average and azimuthal median profiles. The regions near the diffraction spikes and saturated columns were not used. The profiles were determined using images corrected for horizontal smearing.

The measurements indicate that the average scatter in WFPC2 is an order of magnitude greater than in WF/PC-1. The increase is due to scattering in WFPC2, not due to the OTA. In the WFPC2 images, the pyramid edge shadow is not visible in the scattered light; the light is spread out to the chip edges, indicating that most of the scattering occurs after the pyramid. However, the light level in adjacent channels is back down at the WF/PC-1 levels as shown in Figure 5.13 on page 141.

The scattering does not show any strong dependence on wavelength between 410 nm and 953 nm, within the uncertainties of the measurements.

The scattered light is not uniform. There are high frequency spatial structures in the form of streaks radiating outwards from the star. These features are probably both wavelength and position dependent, and so cannot be readily subtracted.

The source of the WFPC2 scattering may be the CCDs. The WF/PC-l CCDs were back illuminated and had shiny surfaces. The electrode structure was not visible over most of the wavelength range. The WFPC2 CCDs, however, are front illuminated, so the electrode structure is visible and may be scattering the light. There was a large ghost in WF/PC-l due to a reflection between the CCD and filter, but no such feature has been seen in WFPC2. The flux from this missing ghost may instead constitute part of the scatter. (See also related material in “Observing Faint Targets Near Bright Objects” on page 198.)

Figure 5.13: Large Angle Scattering. The proportion of the total flux in F555W falling per square arcsecond as a function of the distance from the peak of a saturated stellar image. These curves are for a target in the PC. Note the large drop in the scattered light level when looking in an adjacent camera.

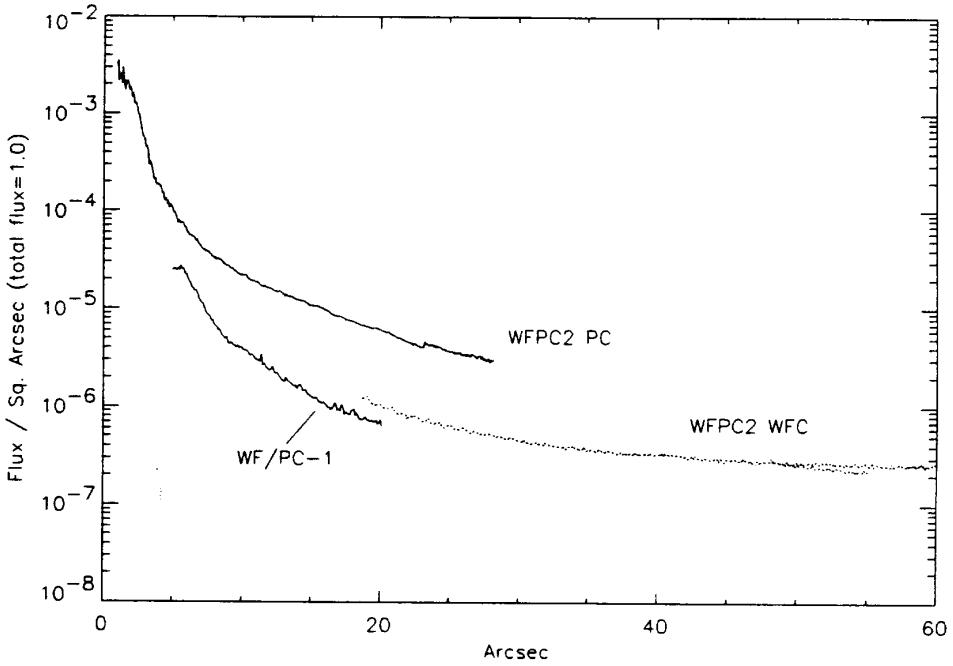

5.10 Ghost Images

Common ghost images result from internal reflections in the filters and in the field-flatteners. Two filter ghosts, caused by double (and quadruple) reflection inside the filter, are visible below and to the right of the star in Figure 5.14 on page 142. The position and brightness of these ghosts varies from filter to filter, typically being most obvious in interference filters. The comatic shape of the ghost is caused by the camera optics being effectively misaligned for the light path followed by the ghost. The relative position of these ghosts does not vary much over the field.

An additional ghost is caused by an internal reflection inside the MgF_2 field flattener lens immediately in front of each CCD (Figure 5.15 on page 143). The field flattener ghost is doughnut shaped (image of OTA pupil) in the WFC, but is smaller and more disk-like on the PC. This ghost contains ~0.15% of the total energy of the star. It is positioned on a line through the CCD center and the bright star; the distance from the ghost to the CCD center is 1.25 to 1.4 times the distance from the bright star to the CCD center. This geometry results from curvature of the field flattener lens.

The large ghost image expected to be caused by reflection off the CCD back to the filter and then back to the CCD is not seen. It was deliberately eliminated in the PC by tilting the CCD slightly.

Figure 5.14: Saturated Stellar Image Showing Filter Ghosts. Intensity scale is logarithmic.

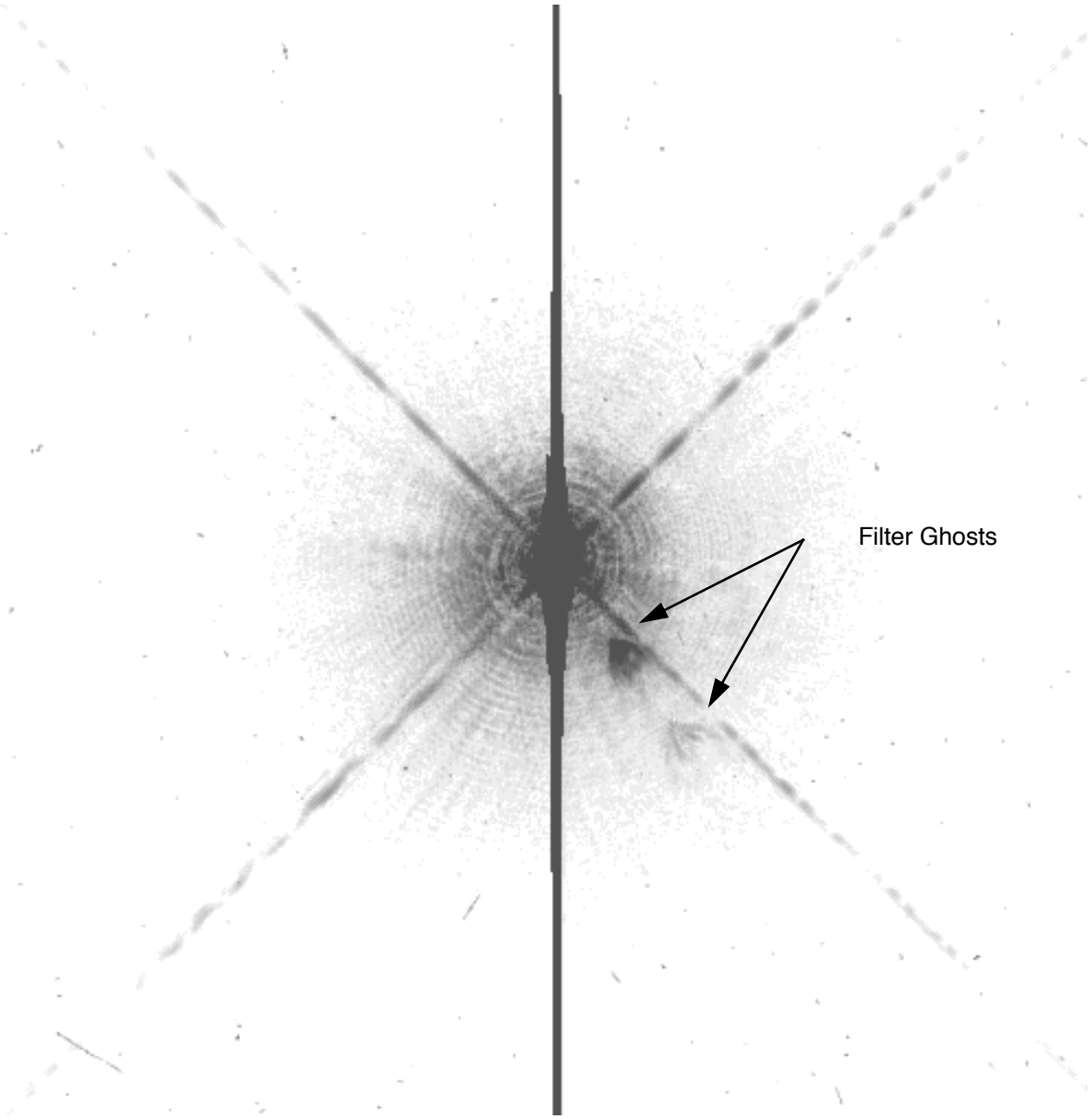

Figure 5.15: Saturated Stellar Image Showing Field Flattener Ghost on WF2.

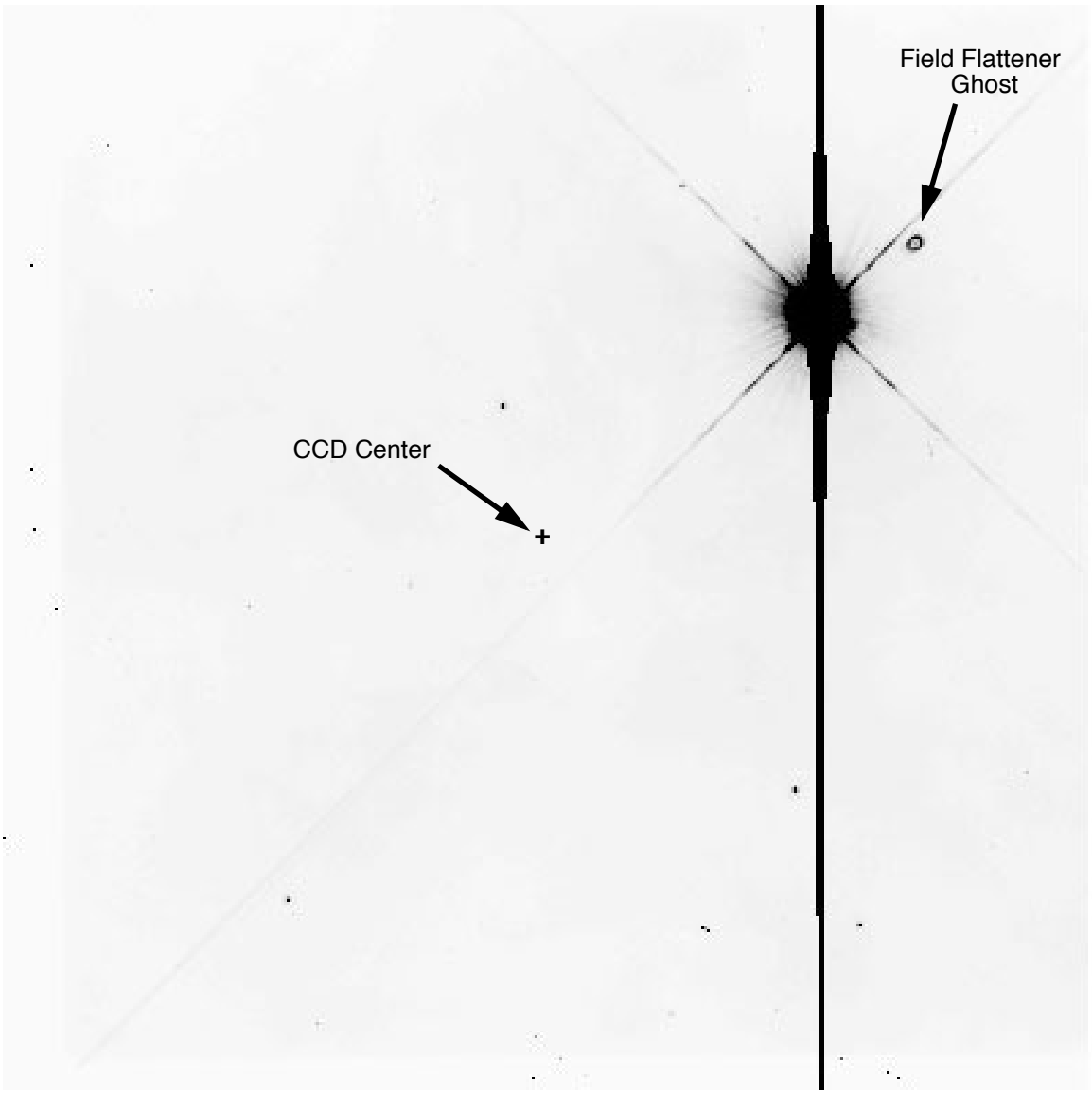

5.11 Optical Distortion

The geometric distortion of WFPC2 is complex since each individual CCD chip is integrated with its own optical chain (including corrective optics), and therefore each chip will have its own different geometric distortion. Apart from this, there is also a global distortion arising from the HST Optical Telescope Assembly (Casertano and Wiggs 2001).

Early attempts to solve the WFPC2 geometric distortion were made by Gilmozzi et al. (1995), Holtzman et al. (1995), and Casertano et al. (2001),

using third order polynomials for all chips in the PC system, i.e. the coordinates X,Y were transformed into one meta-chip coordinate system and fitted to find the offsets, rotation and scale for each of the four chips. These early meta-chip solutions failed to constrain the skew-related linear terms, which actually are responsible for ~0.25 pix residual distortion. These solutions did not have on-orbit data sets which were rotated with respect to each other.

In 2003, Anderson and King derived a substantially improved geometric distortion solution for WFPC2 in the F555W filter. First, the measured positions X_{obs},Y_{obs} were normalized over the range of (50:800) pixels excluding the pyramid edges (Baggett, S., et al. 2002) and adopting the center of the solution at (425,425) with a scale factor of 375, i.e:

$$X = (X_{obs} - (425)/375) \qquad (5.1)$$

$$Y = (Y_{obs} - 425)/375$$

The final solution was presented as a third-order polynomial:

$$X_g = a_1 + a_2X + a_3Y + a_4X^2 + a_5XY + a_6Y^2 + a_7X^3 + a_8X^2Y + a_9xXY^2 + a_{10}Y^3 \qquad (5.2)$$

$$Y_g = b_1 + b_2X + b_3Y + b_4X^2 + b_5XY + b_6Y^2 + b_7X^3 + b_8X^2Y + b_9XY^2 + b_{10}Y^3$$

where Xg and Yg are the corrected coordinates.

The coefficients of the polynomials for F555W filter are given in Table 5.6 on page 145 (Anderson and King 2003).

Figure 5.16 on page 145 shows the vector diagram of the geometric distortion in filter F555W.

Table 5.6: Polynomial Coefficients of the Geometric Distortion for F555W.

	APC	AWF2	AWF3	AWF4	BPC	BWF2	BWF3	BWF4
1	0.000	0.000	0.000	0.000	0.000	0.000	0.000	0.000
2	0.000	0.000	0.000	0.000	0.418	0.051	-0.028	0.070
3	0.000	0.000	0.000	0.000	-0.016	-0.015	-0.036	0.059
4	-0.525	-0.624	-0.349	-0.489	-0.280	-0.038	-0.027	-0.050
5	-0.268	-0.411	-0.353	-0.391	-0.292	-0.568	-0.423	-0.485
6	-0.249	-0.092	0.009	-0.066	-0.470	-0.444	-0.373	-0.406
7	-1.902	-1.762	-1.791	-1.821	-0.011	0.003	0.004	-0.015
8	0.024	0.016	0.006	0.022	-1.907	-1.832	-1.848	-1.890
9	-1.890	-1.825	-1.841	-1.875	0.022	0.011	0.006	0.022
10	-0.004	0.010	0.021	-0.006	-1.923	-1.730	-1.788	-1.821

Figure 5.16: The geometric distortion map for F555W filter using the Anderson and King solution (2003). The size of the longest arrows are 6.29 pixel for the PC (in PC pixels) and ~6 pixel for WF cameras (in WF pixels). The panels correspond to PC - upper right; WF2 - upper left; WF3 - lower left and WF4 - lower right. The size of the residuals are scaled by a factor of 10 relative to the pixel coordinates.

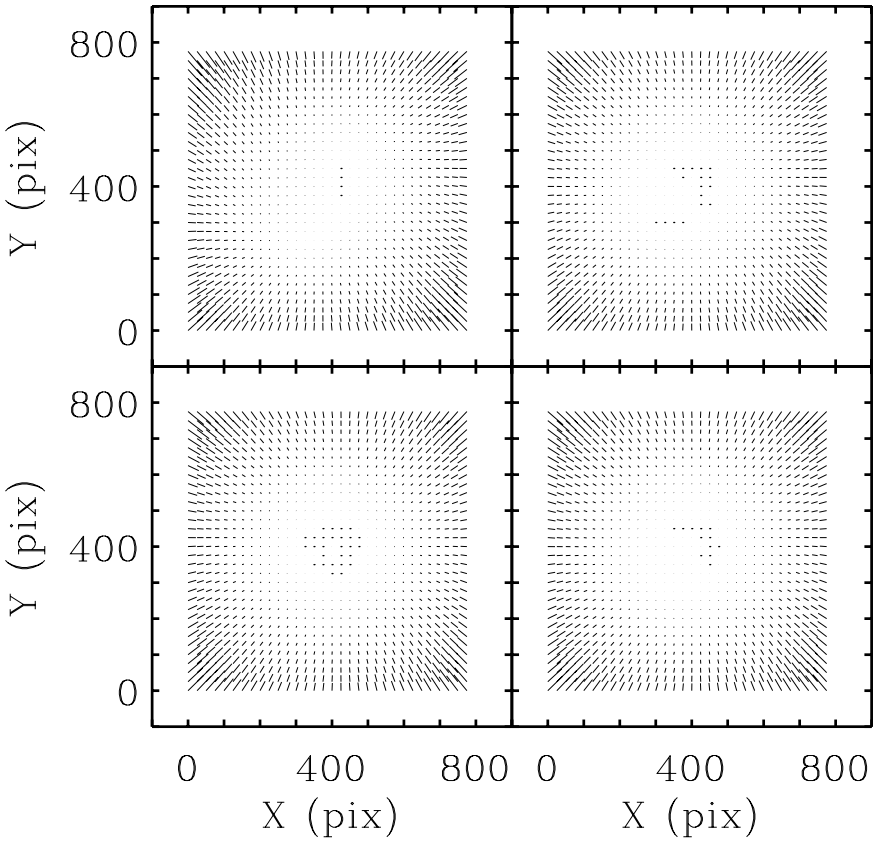

Trauger et al. (1995) showed that the geometric distortion for WFPC2 also depends on wavelength. This is due to the refractive MgF_2 field-flattener lens in front of each CCD. They computed the wavelength-dependent geometric distortion by analyzing the results of ray tracing, where the coefficients were represented as a quadratic interpolation function of the refractive index of the field-flattener lenses. Kozhurina-Platais et al. (2003), using the Anderson and King methodology (2003), derived the geometric distortion solutions for two other filters: F814W and F300W. Figure 5.17 on page 146 presents the difference in distortion between F555W and F300W, which clearly indicates a large amount of distortion in F300W, especially at the corners of the chips. An average increase of distortion in the F300W filters is ~3%, or 0.18 pixels in PC and 0.25 pixels in WF cameras. In contrast, there is only a small ~1% difference in distortion between F555W and F814W. Figure 5.18 on page 147 presents the difference between the filters F555W and F814W. The coefficients of the polynomials for filters F300W and F814W are given in Table 5.7 on page 148 and Table 5.7 on page 148, respectively.

Figure 5.17: Difference in the distortion correction between F555W and F300W (F555W-F300W). The size of the longest arrows are 0.18 pixel for PC (in PC pixel) and 0.25 pixel for WF cameras (in WF pixels). The panels are the same as in Figure 5.16, except the size of the residuals are scaled by a factor of 300.

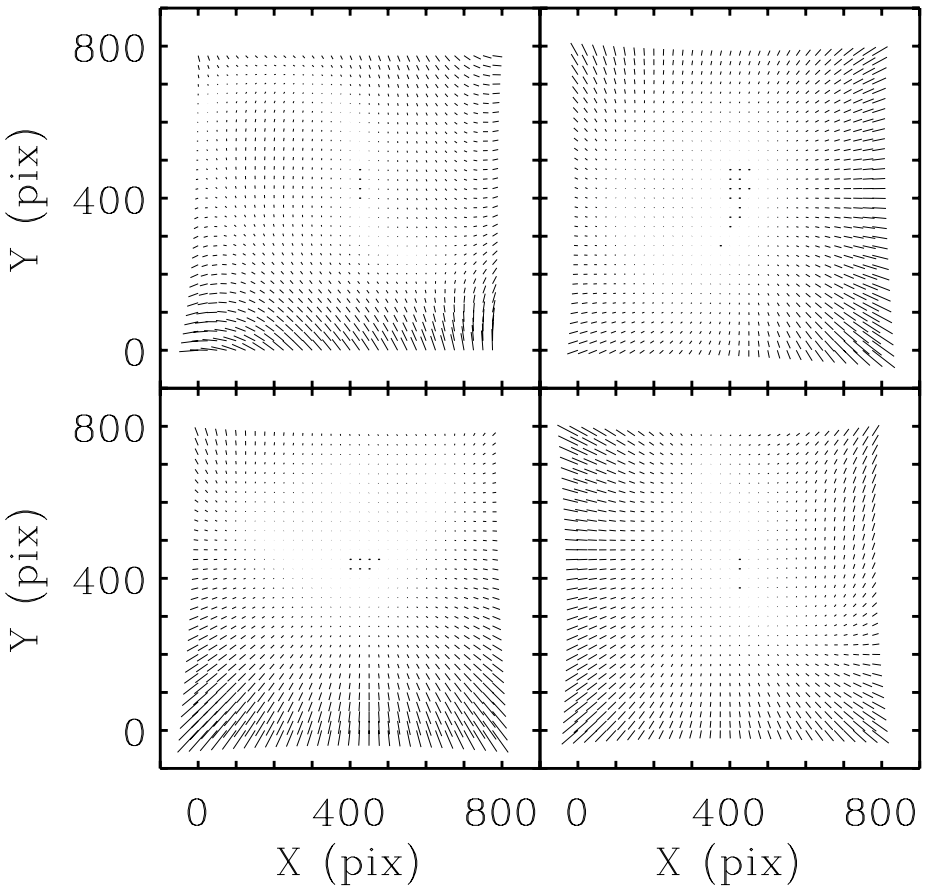

Figure 5.18: Difference in the distortion correction between F555W and F814W. The small amount of these differences along with fairly random pattern changing from chip to chip indicate that the differences are very small, if present at all. The size of the longest arrow is 0.04 PC pixels for the PC, and ~0.05 pixels for the WF cameras. The panels are the same as in Figure 5.16, except the size of the residuals are scaled by a factor of 300.

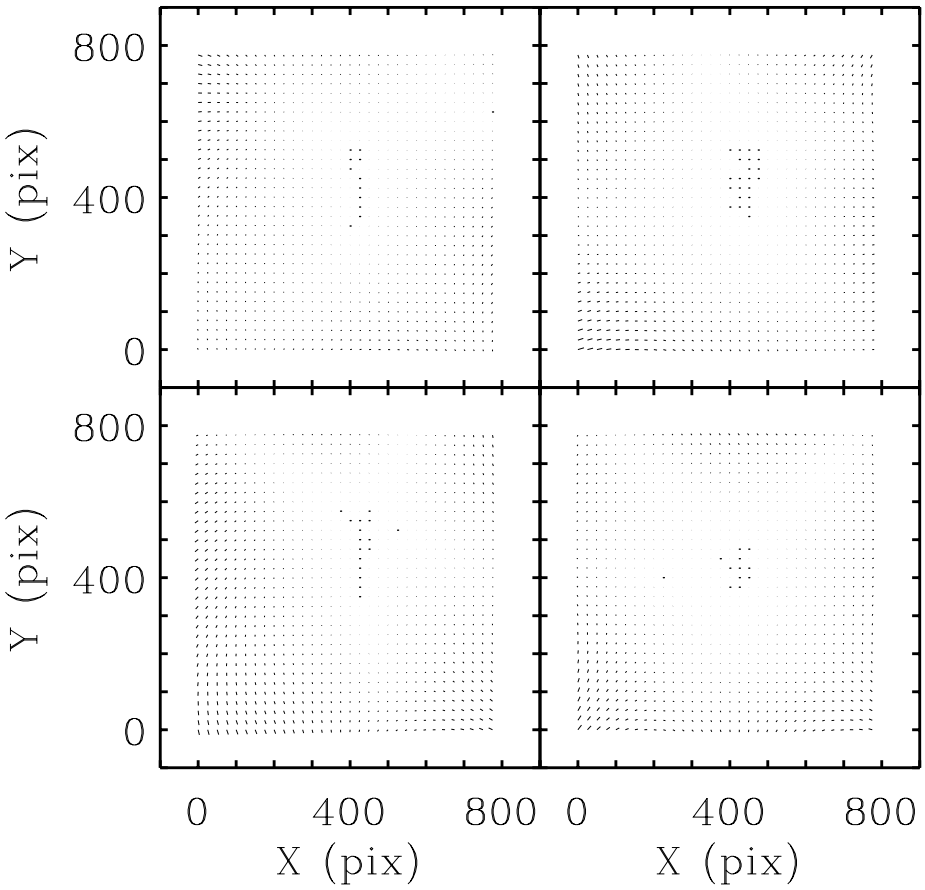

Application of the distortion coefficients are straight forward. To correct for geometric distortion, the measured raw coordinates should be normalized as in the equation 5.1 above. Then equation 5.2 above should be used, employing the coefficients from Table 5.6 on page 145, Table 5.7 on page 148 or Table 5.8 on page 148, depending on the filter used. Finally, the corrected coordinates Xg, Yg should then be shifted back to the natural system of the detector, with proper orientation and scale, specifically:

$$X = (X_g - 425)$$

$$Y = (Y_g - 425)$$

The constant terms a1 and b1 are offsets (or zero-points) between any two frames and can be ignored for most purposes. The linear coefficients a2 and b3 represent the plate scale and can be found in Anderson and King (2003) and Kozhurina-Platais et al. (2003). The FORTRAN code

developed by Anderson which correct the measured coordinates X and Y can be down-loaded from

http://www.stsci.edu/instruments/wfpc2/Wfpc2_memos/andersonking_distortion_routine.txt

The same program could be used to correct for distortion in filters F300W and F814W, using the coefficients from Table 5.7 on page 148 or Table 5.8 on page 148, respectively.

Table 5.7: Polynomial Coefficients of the Geometric Distortion for F300W.

	APC	AWF2	AWF3	AWF4	BPC	BWF2	BWF3	BWF4
1	0.374±0.047	0.149±0.010	-0.142±0.014	-0.072±0.012	0.267±0.021	-0.164±0.014	-0.113±0.011	0.174±0.014
2	0.999±0.091	0.999±0.009	0.999±0.009	0.999±0.015	0.480±0.069	0.042±0.010	-0.028±0.008	0.048±0.006
3	0.055±0.032	0.001±0.009	0.006±0.008	-0.027±0.009	0.999±0.101	0.999±0.010	0.999±0.013	0.999±0.012
4	-0.547±0.035	-0.687±0.009	-0.363±0.005	-0.469±0.007	-0.298±0.113	-0.043±0.006	-0.019±0.005	-0.078±0.005
5	-0.255±0.035	-0.394±0.008	-0.299±0.007	-0.386±0.010	-0.265±0.051	-0.592±0.011	-0.419±0.005	-0.489±0.006
6	-0.235±0.078	-0.098±0.007	0.015±0.008	-0.079±0.005	-0.479±0.052	-0.453±0.018	-0.335±0.006	-0.386±0.008
7	-1.937±0.139	-1.837±0.019	-1.838±0.011	-1.874±0.022	-0.079±0.126	0.006±0.015	0.007±0.008	-0.028±0.008
8	0.003±0.067	0.034±0.016	0.003±0.013	0.054±0.012	-1.913±0.113	-1.877±0.024	-1.891±0.014	-1.950±0.014
9	-1.909±0.056	-1.869±0.010	-1.875±0.015	-1.936±0.009	-0.021±0.083	0.040±0.016	0.016±0.008	0.049±0.018
10	-0.039±0.064	0.001±0.007	0.021±0.012	-0.011±0.017	-1.863±0.148	-1.773±0.018	-1.846±0.016	-1.852±0.014

Table 5.8: Polynomial Coefficients of the Geometric Distortion for F814W.

	APC	AWF2	AWF3	AWF4	BPC	BWF2	BWF3	BWF4
1	-0.029±0.009	0.075±0.009	0.081±0.003	0.046±0.006	0.048±0.007	0.075±0.004	0.055±0.008	-0.015±0.006
2	1.000±0.017	1.000±0.007	1.000±0.004	1.000±0.004	0.428±0.016	0.049±0.004	-0.037±0.004	0.066±0.004
3	0.002±0.014	-0.009±0.004	-0.011±0.002	-0.010±0.003	1.000±0.018	1.000±0.003	1.000±0.007	1.000±0.004
4	-0.526±0.009	-0.636±0.005	-0.344±0.002	-0.494±0.003	-0.281±0.005	-0.032±0.003	-0.018±0.002	-0.055±0.002
5	-0.264±0.008	-0.407±0.003	-0.365±0.004	-0.404±0.003	-0.305±0.008	-0.566±0.003	-0.401±0.003	-0.485±0.002
6	-0.253±0.009	-0.092±0.003	0.009±0.002	-0.059±0.002	-0.465±0.007	-0.439±0.004	-0.371±0.002	-0.408±0.003
7	-1.891±0.019	-1.769±0.005	-1.805±0.006	-1.832±0.004	-0.011±0.015	0.003±0.006	0.003±0.006	-0.013±0.003
8	0.005±0.013	0.027±0.004	0.005±0.005	0.017±0.005	-1.912±0.017	-1.809±0.005	-1.834±0.005	-1.858±0.004
9	-1.895±0.013	-1.806±0.004	-1.822±0.005	-1.853±0.005	0.014±0.017	0.017±0.005	0.009±0.003	0.029±0.006
10	0.004±0.016	0.016±0.004	0.018±0.004	0.000±0.003	-1.917±0.018	-1.735±0.007	-1.799±0.005	-1.837±0.006

Geometric distortion not only affects astrometry but photometry as well, since it induces an apparent variation in surface brightness across the field

of view. The effective pixel area can be derived from the geometric distortion coefficients, and is presented in Figure 5.19 on page 149. The pixel area map correction is necessary since the flat fields are uniformly illuminated, and do not explicitly conserve the total integrated counts for a discrete target, whereas the geometric distortion conserves the total counts and redistributes the counts on the CCD chip. Thus, for precise stellar photometry the raw flat fielded images require a correction for the pixel area -- raw flat-fielded images should be multiplied by the pixel area map so as to restore the proper total counts of the target. The pixel area map is available as a fits file in the HST archive. (Some additional discussion of the pixel area correction can be found in the ACS Instrument Handbook for Cycle 14.)

Figure 5.19: A map of the effective pixel areas of the WFPC2 chips. The areas are normalized to unity at the center of each chip. The contours are shown at half present level. The panel corresponds to PC -upper right; WF2 - upper left; WF3 - lower left and WF4 - lower right.

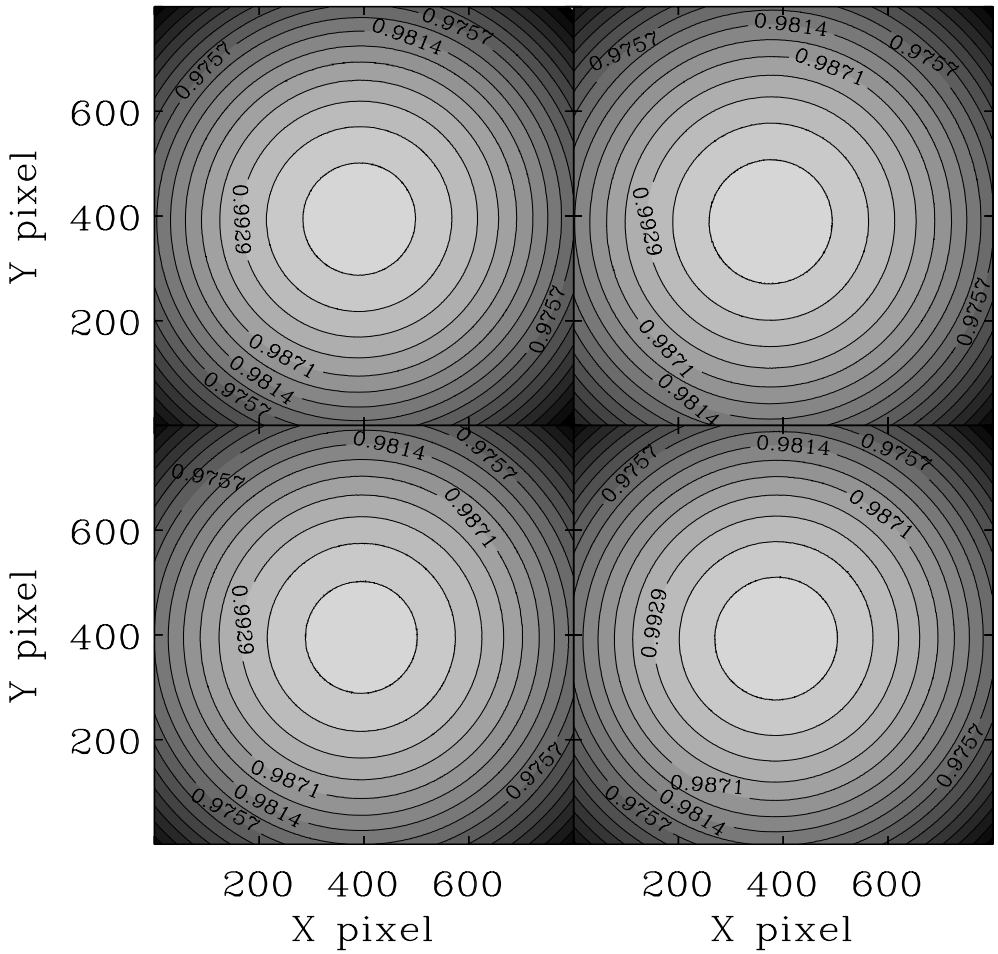

CHAPTER 6:

System Throughput and SNR / Exposure Time Estimation

In this chapter . . .

6.1 System Throughput

A decision on a suitable exposure time will require the combination of

- The overall spectral response of the system (Figure 2.4 on page 29).
- The spectral transmission of the filters (Chapter 3 and Appendix A).
- The spectral energy distribution and spatial profile of the target.
- The point response function and pixel size of the instrument (Chapter 5).
- Criteria for specifying desirable charge levels.

When the transmissions of filters $T(\lambda)$ are combined with the overall system response $Q(\lambda)$, we obtain detector quantum efficiency (DQE) plots (electrons-per-photon as a function of λ) for each filter. These DQE plots link the output of the CCD to the photon flux at the input to an unobscured 2.4 m telescope.

These calibrations exist in the STScI Calibration Data Base, and are accessible with the STSDAS SYNPHOT package or with the XCAL software. The XCAL and SYNPHOT Users Guides should be consulted for further details.

The throughput calibration presented here is accurate to at least 10%—which is sufficient for planning observations, but not for the analysis of many programs. Investigators wishing to do photometry on WFPC2 images should refer to the *HST Data Handbook* for an explanation of the conventions used in determining WFPC2 zeropoints and should use the zeropoints given in Table 5.1 of the WFPC2 Data Handbook (Version 4.0, January 2002). For the most accurate and up-to-date calibrations, users should examine the on-line version of the *Data Handbook* to verify that no numbers of interest have changed since the last paper publication. A recent study has examined the issue of WFPC2 zeropoints (Heyer, et al. 2004, WFPC2 ISR 04-01) and is recommending using the zeropoints of Dolphin (2002, private communication) on his web site at `http://www.noao.edu/staff/dolphin/wfpc2_calib/`

In Table 6.1 on page 154 the dimensionless efficiency and the mean wavelength for each filter are tabulated together with the effective width, the equivalent Gaussian dimensionless width, the maximum transmission, the derivative of the mean wavelength with respect to spectral index, the pivot wavelength, average wavelength, and wavelength of maximum transmission. The parameters are defined as follows. The dimensionless efficiency is

$$\int Q(\lambda)T(\lambda)d\lambda/\lambda$$

The mean wavelength is defined in Schneider, Gunn, and Hoessel (1993, ApJ 264, 337).

$$\bar{\lambda} = \exp\left[\frac{\int Q(\lambda)T(\lambda)\log_e(\lambda)d\lambda/\lambda}{\int Q(\lambda)T(\lambda)d\lambda/\lambda}\right]$$

This rather unconventional definition has the property that the correspondingly defined mean frequency is just $c/\bar{\lambda}$. It is in some sense halfway between the conventional frequency mean and the wavelength mean.

The pivot wavelength is defined as

$$\lambda_p = \left[\frac{\int Q(\lambda) T(\lambda) \lambda d\lambda}{\int Q(\lambda) T(\lambda) d\lambda / \lambda} \right]^{1/2}$$

The average wavelength $\langle \lambda \rangle$ is that defined in the simplest sense

$$\langle \lambda \rangle = \frac{\int Q(\lambda) T(\lambda) \lambda d\lambda}{\int Q(\lambda) T(\lambda) d\lambda}$$

The effective dimensionless Gaussian width is defined implicitly by

$$\sigma^2 = \left[\frac{\int Q(\lambda) T(\lambda) \left[\log_e \left(\frac{\lambda}{\bar{\lambda}} \right) \right]^2 \frac{d\lambda}{\lambda}}{\int Q(\lambda) T(\lambda) \frac{d\lambda}{\lambda}} \right]$$

The effective width of the bandpass is

$$\delta\bar{\lambda} = 2[2\log_e 2]^{1/2} \sigma\bar{\lambda}$$

We note that all of the above integrals have been evaluated over the range $\lambda = \bar{\lambda}(1 - 5\sigma)$ to $\bar{\lambda}(1 + 5\sigma)$ so as to avoid unrealistic contributions from imperfect blocking far from the bandpass. Where necessary, the integration range was further constrained to the range 1000Å to 11000Å.

Parameters QT_{max} and λ_{max} are the respective parameters at the peak throughput.

The parameter $d\bar{\lambda}/d\alpha$ is defined in section “Count Rates for Power Law Sources” on page 158.

The final two columns in Table 6.1 on page 154 are defined as follows. In the next-to-last column $m_{e/sec}$ is the zero-point magnitude for 1 e^- s^{-1} (with AB_V=0). The final column gives t_{wfsky}, which is the exposure time (in seconds) needed to make the sky noise equal to 5 e^- RMS (i.e. ~read noise) in the WFC for a sky level of V=23.3 mag arcsec^{-2}.

Table 6.1: System Efficiencies and Zeropoints. See Section 6.1 for definitions. [a]

Filter	$\int QT\, d\lambda/\lambda$	$\bar{\lambda}$	$\delta\bar{\lambda}$	σ	QT_{max}	$d\bar{\lambda}/d\alpha$	λ_p	$\langle\lambda\rangle$	λ_{max}	$m_{e/sec}$	t_{wfsky}
F122M	0.00010	1305.6	239.1	0.0778	0.00107	7.90	1321.6	1326.2	1260	18.48	1.1E+07
F130LP	0.10175	4285.9	4755.4	0.4712	0.13936	951.53	5814.6	6137.5	6398	26.01	1.9E+02
F160BW	0.00024	1473.0	449.1	0.1295	0.00074	24.69	1521.9	1534.9	1400	19.46	9.2E+05
F165LP	0.10091	4494.4	4528.9	0.4279	0.14066	823.00	5852.9	6155.6	6400	26.00	1.9E+02
F170W	0.00057	1707.7	545.1	0.1355	0.00169	31.37	1769.7	1786.3	1857	20.38	2.3E+06
F185W	0.00038	1941.6	334.3	0.0731	0.00196	10.38	1962.3	1967.7	1940	19.93	7.3E+06
F218W	0.00059	2177.4	395.0	0.0770	0.00286	12.92	2203.1	2209.6	2242	20.42	5.4E+06
F255W	0.00080	2577.7	395.1	0.0651	0.00462	10.92	2599.4	2604.9	2536	20.76	2.6E+06
F300W	0.00571	2919.8	740.2	0.1077	0.01974	33.84	2986.8	3004.3	2804	22.89	6.7E+04
F336W	0.00497	3329.3	374.3	0.0477	0.03558	7.59	3344.4	3348.2	3454	22.74	3.6E+04
F343N	0.00003	3426.9	23.5	0.0029	0.00397	0.03	3426.9	3427.0	3432	17.27	4.7E+06
F375N	0.00008	3732.2	24.4	0.0028	0.00983	0.03	3732.3	3732.3	3736	18.24	1.1E+06
F380W	0.00779	3940.5	681.8	0.0735	0.03752	21.27	3982.7	3993.1	3999	23.22	7.1E+03
F390N	0.00031	3888.0	45.0	0.0049	0.01999	0.09	3888.2	3888.2	3889	19.72	2.1E+05
F410M	0.00183	4085.7	146.8	0.0153	0.04027	0.95	4087.6	4088.1	4097	21.65	2.7E+04
F437N	0.00022	4369.1	25.2	0.0025	0.03065	0.03	4369.2	4369.2	4368	19.37	1.7E+05
F439W	0.00576	4292.6	473.2	0.0468	0.03903	9.41	4311.3	4316.0	4318	22.90	7.1E+03
F450W	0.01678	4483.6	950.8	0.0901	0.08671	36.36	4555.4	4573.0	5069	24.06	2.0E+03
F467M	0.00250	4667.7	166.5	0.0151	0.05582	1.07	4669.8	4670.4	4731	21.99	1.2E+04
F469N	0.00027	4694.4	25.0	0.0023	0.03784	0.02	4694.4	4694.4	4698	19.56	1.1E+05
F487N	0.00034	4865.1	25.9	0.0023	0.04811	0.02	4865.2	4865.2	4864	19.81	8.1E+04
F502N	0.00041	5012.4	26.9	0.0023	0.05800	0.03	5012.4	5012.4	5009	20.04	5.9E+04
F547M	0.01342	5467.8	483.2	0.0375	0.11515	7.70	5483.3	5487.1	5558	23.81	1.6E+03
F555W	0.03012	5336.8	1228.4	0.0977	0.11194	50.99	5439.0	5464.6	5550	24.69	7.3E+02
F569W	0.02343	5582.3	965.7	0.0735	0.11518	30.13	5642.0	5657.4	5549	24.42	8.9E+02
F588N	0.00145	5893.2	49.0	0.0035	0.13078	0.07	5893.5	5893.5	5896	21.40	1.3E+04
F606W	0.04513	5860.1	1502.4	0.1089	0.14220	69.46	5996.8	6030.8	6185	25.13	4.2E+02
F622W	0.02882	6137.4	917.1	0.0635	0.14096	24.71	6186.2	6198.6	6405	24.64	6.3E+02
F631N	0.00084	6306.4	30.9	0.0021	0.12632	0.03	6306.4	6306.4	6301	20.81	2.1E+04
F656N	0.00049	6563.8	21.5	0.0014	0.11273	0.01	6563.8	6563.8	6562	20.21	3.5E+04

Table 6.1: System Efficiencies and Zeropoints. See Section 6.1 for definitions. [a]

Filter	$\int QT\, d\lambda/\lambda$	$\bar{\lambda}$	$\delta\bar{\lambda}$	σ	QT_{max}	$d\bar{\lambda}/d\alpha$	λ_p	$\langle\lambda\rangle$	λ_{max}	$m_{e/sec}$	t_{wfsky}
F658N	0.00068	6590.8	28.5	0.0018	0.11443	0.02	6590.8	6590.8	6591	20.58	2.5E+04
F673N	0.00113	6732.2	47.2	0.0030	0.11978	0.06	6732.3	6732.3	6730	21.12	1.4E+04
F675W	0.02344	6677.4	866.8	0.0551	0.13604	20.29	6717.4	6727.6	6624	24.42	7.0E+02
F702W	0.03429	6818.0	1384.7	0.0862	0.14185	50.71	6918.5	6944.3	6513	24.83	4.6E+02
F785LP	0.00900	8627.9	1381.2	0.0680	0.04831	39.88	8707.0	8727.5	8226	23.38	1.3E+03
F791W	0.01694	7811.2	1230.7	0.0669	0.09530	34.97	7880.6	7898.4	7397	24.07	7.6E+02
F814W	0.01949	7904.8	1539.4	0.0827	0.10343	54.06	8012.2	8040.3	7255	24.22	6.5E+02
F850LP	0.00473	9086.1	1037.5	0.0485	0.03939	21.37	9128.8	9139.8	8810	22.68	2.4E+03
F953N	0.00016	9544.7	52.5	0.0023	0.02213	0.05	9544.9	9545.0	9525	19.00	6.9E+04
F1042M	0.00017	10220.5	448.9	0.0187	0.00481	3.56	10227.6	10229.4	10110	19.10	6.0E+04
FQUVN-A	0.00033	3764.4	73.2	0.0083	0.01326	0.26	3764.5	3764.6	3801	19.78	2.5E+05
FQUVN-B	0.00030	3829.3	57.3	0.0064	0.01557	0.15	3829.5	3829.6	3828	19.68	2.4E+05
FQUVN-C	0.00037	3912.6	59.5	0.0065	0.01900	0.16	3912.9	3913.0	3909	19.92	1.7E+05
FQUVN-D	0.00047	3991.8	63.6	0.0068	0.02329	0.18	3992.2	3992.3	3989	20.17	1.2E+05
FQCH4N-A	0.00076	5435.3	34.4	0.0027	0.09537	0.04	5435.4	5435.4	5442	20.70	2.9E+04
FQCH4N15-B	0.00088	6199.2	33.8	0.0023	0.12242	0.03	6199.4	6199.4	6202	20.85	2.0E+04
FQCH4N33-B	0.00087	6199.3	33.8	0.0023	0.12165	0.03	6199.4	6199.4	6202	20.85	2.0E+04
FQCH4N-C	0.00070	7278.5	38.1	0.0022	0.10275	0.04	7278.5	7278.5	7278	20.60	2.1E+04
FQCH4N-D	0.00021	8930.2	54.9	0.0026	0.02917	0.06	8930.2	8930.2	8930	19.31	5.0E+04
POLQ_par	0.06695	4978.4	4226.0	0.3605	0.09998	646.91	6099.9	6355.5	6493	25.56	–
POLQ_per	0.01494	6257.6	5233.7	0.3552	0.04268	789.39	7613.6	7843.4	8001	23.93	–

a. All values have been computed using the WF3 chip, except for the Quad filters.

6.2 On-Line Exposure Time Calculator

We note that most of the calculations below are incorporated in the on-line WFPC2 Exposure Time Calculator (ETC) program, which is available on the WFPC2 WWW pages at:
http://www.stsci.edu/instruments/wfpc2/Wfpc2_etc/wfpc2-etc.html.

To use this program, the user fills out an HTML form giving the target information (magnitude, color, and reddening), camera configuration (PC or WFC, desired gain setting, and filter), and either the exposure time or the desired signal-to-noise ratio. There are separate HTML forms for point sources, extended sources, point sources with a diffuse stellar background, and extended sources on a diffuse stellar background. After filling out the form the user then clicks on "calculate" and the program returns the resulting signal-to-noise ratio if the exposure time was specified, or vice versa. Examples of completed HTML forms and results are shown in "Sample SNR Calculations" on page 171. Note that clicking on any colored text on the HTML form will give a description of that item.

The ETC program handles sources with stellar spectra, power law sources, and emission line sources; point sources and extended sources; and sources superposed on a diffuse stellar background. The latest version (V4.0) includes calculations of exposure times and/or signal-to-noise ratios for point sources (plus background) using either the traditional "optimal PSF weighting" method or simple aperture photometry in a fixed aperture radius specified by the user. The latter option is more appropriate when comparing with the ACS ETC, which assumes the use of aperture photometry as a default.

In addition, the ETC allows for a flexible specification of the sky background. There are now three options. The first option uses a rough estimate of "average" or "high" or "low" sky background conditions. The second option estimates the sky background based on the position of the target and (optionally) an estimate for the heliocentric longitude of the target (sun angle). The last option allows the user to explicitly provide a value for the sky background, in magnitudes per square arcsecond. Finally, the program also returns advice on CR-SPLITing, use of CLOCKS=YES, and warnings about saturation, if appropriate. Results are typically accurate to a few percent.

While observers should familiarize themselves with the material below, most will find the ETC program faster and easier to use for actual calculations. The ETC program will also be updated to reflect any changes in instrument performance, so observers can be assured of up-to-the-minute information.

6.3 Target Count Rates

We now consider estimation of count rates for objects with stellar, power law, and emission line spectra.

6.3.1 Count Rates for Stellar Sources

To estimate the number of electrons collected from a point source of apparent visual magnitude V, one can use the equation:

$$N = 2.5 \times 10^{11} \cdot t \cdot [\int Q(\lambda) T(\lambda) d\lambda / \lambda] \times 10^{-0.4(V + AB_\nu)} \qquad (6.1)$$

where t is the exposure time in seconds, the QT integral is given in Table 6.1 on page 154, and AB_ν is given in Table 6.2 on page 157 as a function of spectral type and wavelength for some example spectral energy distributions. The quantity AB_ν is a color-dependent correction from V magnitude to AB magnitude at frequency ν. The AB magnitude system is defined as (Oke and Gunn 1983)

$$AB = V + AB_\nu = -2.5 \cdot \log F_\nu - 48.60$$

where F_ν is the flux in erg cm^{-2} s^{-1} Hz^{-1}.

Table 6.2: AB_ν as a Function of Wavelength. AB_ν is defined as a color-dependent correction from V magnitude to AB magnitude at frequency ν. Wavelength (Å) runs along the top; spectral classes run down the left most column. The second column contains B-V. See “Target Count Rates” on page 157.

	B-V	1500	2000	2500	3000	3500	4000	4500	5000	6000	7000	8000	9000	10000
sky	1.10	2.45	5.46	5.46	3.12	2.00	1.03	0.55	0.18	-0.11	-0.33	-0.55	-0.65	-0.75
B0	-0.31	-1.60	-1.50	-1.20	-0.78	-0.62	-0.46	-0.36	-0.22	0.16	0.46	0.76	0.96	1.17
A0	0.00	2.22	1.35	1.11	1.21	1.00	-0.23	-0.16	-0.09	0.11	0.22	0.33	0.36	0.4
F0	0.27	7.22	4.10	3.11	1.99	1.38	0.29	0.06	0.03	0.03	0.05	0.08	0.09	0.1
G0	0.58	8.9	6.35	4.61	2.46	1.63	0.67	0.26	0.08	-0.04	-0.12	-0.21	-0.23	-0.25
K0III	1.07	13	10.3	8.11	5.46	2.13	1.16	0.46	0.2	-0.24	-0.42	-0.61	-0.66	-0.72
M0III	1.60	15	12.3	9.36	6.21	4.63	2.26	0.96	0.51	-0.46	-0.76	-1.06	-1.12	-1.19
gE	1.00	6.82	6.41	5.43	3.63	2.49	1.40	0.55	0.21	-0.19	-0.52	-0.81	-1.07	-1.29
Sa	0.80	5.40	4.80	4.10	3.00	2.01	1.12	0.44	0.19	-0.17	-0.44	-0.7	-0.95	-1.16
Sbc	0.60	4.03	3.18	2.86	2.46	1.54	0.84	0.34	0.17	-0.14	-0.37	-0.6	-0.84	-1.04
Scd	0.45	2.67	2.29	2.15	1.76	1.35	0.65	0.28	0.13	-0.11	-0.26	-0.39	-0.47	-0.58
Ir I	0.30	1.77	1.40	1.36	1.24	0.94	0.43	0.34	0.17	0.13	-0.04	-0.21	-0.33	-0.45

Equation 6.1 may be trivially rewritten to give the count rate R_{object} in units of $e^- s^{-1}$ $pixel^{-1}$ for a target with a stellar spectrum as:

$$R_{object} = 2.5 \times 10^{11} \cdot [\int Q(\lambda) T(\lambda) d\lambda / \lambda] \cdot 10^{-0.4(V + AB_\nu)} \qquad (6.2)$$

6.3.2 Count Rates for Power Law Sources

If one knows the spectral index α (which is zero for a source with a flat continuum), $V+AB_\nu$ can also be calculated as the monochromatic Oke system magnitude at the corrected mean wavelength of the filter:

$$V + AB_\nu = -2.5 \log_{10}(S_\nu[\bar{\lambda} + \alpha(d\bar{\lambda}/d\alpha)]) - 48.6$$

where S_ν is the flux in ergs cm^{-2} s^{-1} Hz^{-1} as in Oke and Gunn, Ap. J., 266, 713 (1983) at the effective mean wavelength of the filter $\bar{\lambda} + \alpha(d\bar{\lambda}/d\alpha)$. It can be shown that

$$\frac{d\bar{\lambda}}{d\alpha} = \bar{\lambda}\sigma^2$$

if the integrands are weighted by a source with spectral index α in the definition of λ. See also Koornneef, J., et al. "Synthetic Photometry and the Calibration of the Hubble Space Telescope" in Highlights of Astronomy (7, 833, J.-P. Swings Ed (1983). Combining the above equations gives

$$R_{object} = 6.9 \times 10^{30} \cdot [\int Q(\lambda) T(\lambda) d\lambda / \lambda] \cdot S_\nu\left(\bar{\lambda} + \alpha \frac{d\bar{\lambda}}{d\alpha}\right) \qquad (6.3)$$

6.3.3 Count Rates for Emission Line Sources

The count rate in units of $e^- s^{-1}$ for a monochromatic emission line is given by

$$R_{object} = 2.3 \times 10^{12} \cdot (QT) \cdot F \cdot \lambda \qquad (6.4)$$

where F is the emission line flux in units of ergs cm^{-2} s^{-1}, and λ is the wavelength of the line in Angstroms. The quantity QT is the (system + filter) quantum efficiency at the wavelength of the line, which can be determined from inspection of the figures in "F622W, F631N, F656N" on page 345. For lines near the maxima of the filter transmission curves, it should be sufficient to use QT_{max} from Table 6.1 on page 154. Note that the integrated filter efficiency is not relevant for the signal calculation.

In cases where the width of the line approaches that of the filter, it will be necessary to convolve the line shape and filter bandpass using either the SYNPHOT or XCAL programs.

For example, H_α emission at 6563Å, with total source flux $F=10^{-16}$ erg s^{-1} cm^{-2}, observed through the F656N filter (total system throughput T=0.11 from the plots "F622W, F631N, F656N" on page 345), will produce a target count rate R_{object}=0.17 e^- s^{-1} integrated over the entire source.

6.4 Sky Background

The sky background can contribute significant Poisson noise in broad and medium band filters, and must be taken into account during noise calculations. The actual sky brightness depends on the heliocentric ecliptic coordinates (latitude and longitude) in a manner summarized in Table 6.3 on page 160. The appropriate AB_V can be taken from Table 6.2 on page 157. To convert mag $arcsec^{-2}$ to mag $pixel^{-1}$ one needs to add 5 magnitudes (WFC) or 6.7 magnitudes (PC1). These values are actually lower limits on the effective sky-brightness that will be seen, because light from the bright Earth limb can scatter into the aperture.

If your observations are sky background limited, and signal-to-noise is a driver, consider the use of the special requirement LOW-SKY as described in the *Call for Proposals* or the *Phase II Proposal Instructions*. LOW-SKY has two effects:

- It causes the observation to be scheduled at the time of year when the zodiacal background light is no more than 30% greater than the minimum possible background value for the target, and
- It requires that the observation be made when the bright Earth limb is more than 40° from the OTA axis, which greatly reduces scattered light.

For many targets LOW-SKY will have minimal impact on the observing efficiency. Note, however, that targets in the Continuous Viewing Zone (CVZ) cannot be observed if LOW-SKY is specified. See "Observing Faint Targets" on page 195 for more information.

Table 6.3: Sky Brightness (V mag arcsec^{-2}) as a Function of Heliocentric Ecliptic Latitude and Longitude. “SA” denotes that the target is unobservable due to solar avoidance.

Heliocentric Ecliptic Longitude	Ecliptic Latitude						
	0°	15°	30°	45°	60°	75°	90°
180°	22.1	22.4	22.7	23.0	23.2	23.4	23.3
165°	22.3	22.5	22.8	23.0	23.2	23.4	23.3
150°	22.4	22.6	22.9	23.1	23.3	23.4	23.3
135°	22.4	22.6	22.9	23.2	23.3	23.4	23.3
120°	22.4	22.6	22.9	23.2	23.3	23.3	23.3
105°	22.2	22.5	22.9	23.1	23.3	23.3	23.3
90°	22.0	22.3	22.7	23.0	23.2	23.3	23.3
75°	21.7	22.2	22.6	22.9	23.1	23.2	23.3
60°	21.3	21.9	22.4	22.7	23.0	23.2	23.3
45°	SA	SA	22.1	22.5	22.9	23.1	23.3
30°	SA	SA	SA	22.3	22.7	23.1	23.3
15°	SA	SA	SA	SA	22.6	23.0	23.3
0°	SA	SA	SA	SA	22.6	23.0	23.3

Another option for reducing the sky brightness, is the special requirement SHADOW, which forces the observation to be made when HST is in the Earth’s shadow. This usually has a large negative impact on the observing efficiency, and is recommended only when attempting to avoid geocoronal lines when observing far-UV emission lines (e.g. Ly α and OI 1304Å). Moreover, it does not attempt to minimize zodiacal emission, which dominates at visible wavelengths.

Table 6.4 on page 161 shows approximate sky count rates for the WFC and PC1 for filters with significant sky count rates. An average sky brightness of V=22.9 mag arcsec^{-2} is assumed. Filters not listed in the table have sky count rates below that of the dark current, so the sky contribution will generally be unimportant. Values for other filters or sky brightnesses can be computed from Table 6.2 on page 157, Table 6.1 on page 154, Table 6.3 on page 160, and Equation 6.2.

Table 6.4: Sky Count Rate per Pixel (P_{sky}). An average sky brightness of V = 22.9 mag arcsec^{-2} is assumed. Filters not listed have sky rate significantly below the dark current.

Filter	Sky Count Rate (P_{sky}) ($e^- s^{-1}$ pixel^{-1})	
	WFC	PC1
F336W	0.0009	0.0002
F380W	0.005	0.001
F439W	0.005	0.0011
F450W	0.018	0.004
F467M	0.003	0.0006
F547M	0.021	0.0045
F555W	0.052	0.010
F588N	0.002	0.0006
F569W	0.040	0.0081
F606W	0.090	0.020
F622W	0.060	0.012
F673N	0.002	0.0006
F675W	0.056	0.012
F702W	0.082	0.0016
F785LP	0.024	0.0050
F791W	0.048	0.010
F814W	0.054	0.011
F850LP	0.012	0.0024

6.5 Signal-to-Noise Ratio Estimation

The signal-to-noise ratio (SNR) for a point source depends on both the Poisson noise of the object, and on noises associated with the background. Sources of background noise include “read noise” of the CCDs, and

Poisson noise in the dark current, sky background, and any smooth galaxy light superposed on the target.

Two-Gyro Mode: At some future date HST may be operated with only two gyros, hence causing additional spacecraft jitter and degradation of the effective PSF. While this could potentially degrade the signal-to-noise ratio for point sources, we expect to see very little impact for WFPC2 due to its large pixel sizes. Please see the Two-Gyro Mode Handbook for additional discussion.

The SNR obtained for photometry of a point source will depend on the analysis technique used. The optimum SNR will be obtained when the pixels of the point source PSF are weighted in proportion to their expected intensity by PSF fitting. Aperture photometry will tend to give lower SNR, especially for sources where the background is important, but nonetheless is widely used. We now consider both methods.

6.5.1 Point Sources -- PSF Fitting

In the bright target limit, Poisson noise sets the SNR and

$$SNR = (S)^{1/2} = (R_{object} \cdot t)^{1/2}$$

where S is the number of detected photons, and R_{object} is given by the above Equations 6.2 through 6.4, and t is the exposure time.

In the background limited case (e.g. read noise, dark current, or sky noise limited) the SNR is a function not only of the expected number of detected photons S from the source but also of the average effective background count rate B in each pixel, the point spread function $(PSF)_{i,j}$, and the weights used to average the signal in the pixels affected by the source. It is easy to show that the signal-to-noise ratio for optimal weights (which are proportional to the point spread function) is given by:

$$SNR = \frac{S}{\sqrt{B}} \cdot \left(\sum (PSF)_{i,j}^{\,2}\right)^{1/2} = \frac{S}{\sqrt{B}} \cdot (sharpness)^{1/2} \qquad (6.5)$$

where *sharpness* is effectively the reciprocal of the number of pixels contributing background noise. The summation is tabulated for a few representative cases in Table 6.5 on page 163. To estimate the signal-to-noise, multiply the signal-to-noise obtained, assuming all the flux is in one pixel, by the square root of the value in the table.

Table 6.5: Sharpness as a Function of Wavelength, Camera, and Location of the Star Center with Respect to the Pixel Grid. The "Obs." columns represent the values for the real OTA, WFPC2 optics, and CCD MTF function. The "Diff." column represents values for the theoretical diffraction limit with perfect optics and detectors. Target location refers to both the camera used (PC or WFC), and the location of the star center on the pixel grid.

Target Location	2000 Å		4000 Å		6000 Å		8000 Å	
	Obs.	Diff.	Obs.	Diff.	Obs.	Diff.	Obs.	Diff.
PC Pixel Center	0.084	0.409	0.095	0.259	0.066	0.115	0.046	0.073
PC Pixel Corner	0.063	0. 186	0.065	0.107	0.054	0.072	0.045	0.068
WFC Pixel Center	0.120	0.745	0.145	0.482	0.128	0.318	0.124	0.285
WFC Pixel Corner	0.102	0.228	0.105	0.193	0.098	0.178	0.081	0.126

We note that PSF fitting is equivalent to convolving the image with the PSF, and then measuring the peak counts for stellar objects. Also, the location of the star on the pixel grid will be impossible to know in advance of the observation (i.e. pixel center vs. pixel corner in Table 6.5 on page 163). In general, the lower "pixel corner" values should be used, so as to insure adequate SNR.

The average effective background counts per exposure and per pixel can be expanded to include various sources:

$$B = readnoise^2 + P_{dark} \cdot (t + 46) + P_{sky} \cdot t + P_{background} \cdot t$$

where terms include the read out noise of the CCD (*readnoise*), the dark current (P_{dark}), sky background count rate (P_{sky}), and the count rate of any diffuse background light from astrophysical sources ($P_{background}$). Herein we will use "*P*" to represent count rates **per pixel**, and "*R*" to represent the **total** counts for an object. The exposure time is represented by *t*.

For example, Table 2.2 on page 30 lists the faintest V magnitude star, V=28.19, measurable with a signal-to-noise ratio of 3 in a 3000s integration in F569W in the Wide Field Cameras. The calculation to check this goes as follows. The efficiency of the filter is 0.02343 from Table 6.1 on page 154. The sky background in each pixel is 23.3+5=28.3, assuming an ecliptic latitude of 90˚ from Table 6.3 on page 160, and the pixel area correction for the WFC given in that section. The total sky background collected per pixel in 3000 seconds is given by Equation 6.1 as 84.1 electrons. Note that the AB_ν color correction required for the sky in the wavelength range of the filter is 0.0 from Table 6.2 on page 157. From Table 4.4 on page 117, the read noise for WF3 is 5.2 electrons. From Table 4.2 on page 88, the median dark current at -88 ˚C is 0.0045. Therefore the

total dark current (on which there will be shot noise) is only 13.5 electrons. The equivalent background per pixel is then given as B=84.1+5.2^2+13.5=124.5. The total number of detected electrons from a star with V=28.19 is S=93 electrons, again using Equation 6.1. (We note that AB_v is approximately zero at this wavelength, so the spectral class is unimportant.) The expected peak count is 28 detected electrons using Table 5.4 on page 130 (peak near pixel center), which is much less than B, requiring the use of Equation 6.5 for the background limited case. The sharpness for the WF camera in the best case, when the star is centered on a pixel, is given in Table 6.5 on page 163 as 0.128. Then Equation 6.5 above gives the signal-to-noise as 3.0:

$$SNR = \left(\frac{93}{\sqrt{124.5}} \cdot \sqrt{0.128}\right) = 3.0$$

If, instead, the peak count rate comes out much greater than the background, the observation is photon noise limited, and the signal-to-noise should be computed as the square root of the signal S in electrons.

In principle, one should also include contributions in the signal-to-noise for flat fielding uncertainties, noise in the bias and dark calibration files, and quantization noise. Flat fielding errors will be of order 1%, and will limit SNR in the large-signal limit. Noise in the bias and dark calibration files will be unimportant in most pixels, although these could become important if many (>10) non-dithered frames of the same field are combined.

Quantization noise can be estimated as $gain/\sqrt{12}$ (i.e., $\sqrt{4.1}$ in the 7 e^- DN^{-1} channel, and $\sqrt{16.3}$ in the 14 e^- DN^{-1} channel). In nearly all situations it can be ignored. In the weak signal case, the quantization noise is effectively included in the read noise values given throughout this Handbook; in the strong signal case it is very small compared to the Poisson noise and can be ignored.

A generalized equation for estimating point source signal-to-noise ratio per exposure is given below (Equation 6.6). It is exact in both the bright and faint object limits, and is a reasonable approximation to the intermediate case. $P_{background}$ represents any generalized source of diffuse background light (e.g. galaxy on which target is superposed). Table 6.6 on page 165 gives rough values for some of the parameters, along with references for more accurate values.

$$SNR = \frac{R_{object} \cdot t}{\sqrt{R_{object} \cdot t + \frac{readnoise^2 + P_{dark} \cdot (t + 46) + P_{sky} \cdot t + P_{background} \cdot t}{sharpness}}} \qquad (6.6)$$

Note that in this formulation, $sharpness^{-1}$ is the equivalent number of pixels the weighted signal is integrated over. In the event that multiple exposures are taken (e.g. to remove cosmic rays), the signal-to-noise ratio for the final averaged image is approximately given by:

$$SNR_{total} = SNR \cdot \sqrt{N}$$

where N is the number of images averaged.

Table 6.6: Parameters for Point Source SNR Estimation - PSF Fitting

Parameter	Description	Units	Approx. Value	Better Value
R_{object}	object count rate	$e^- s^{-1}$		Equation 6.1, 6.2, or 6.3
P_{dark}	dark count rate	$e^- s^{-1}$ pixel^{-1}	0.004	Table 4.2 on page 88; Eqn 4.1 on page 90
P_{sky}	sky count rate	$e^- s^{-1}$ pixel^{-1}	Table 6.4 on page 161	Table 6.2 on page 157, Table 6.1 on page 154, Table 6.3 on page 160; Eqn 6.1
$P_{background}$	count rate from background light (if any)	$e^- s^{-1}$ pixel^{-1}		Table 6.2 on page 157, Table 6.1 on page 154; Eqn 6.1
read noise		e^-	ATD-GAIN=7 use 5.3[a] ATD-GAIN=15 use 7.5	Table 4.4 on page 117
sharpness			WFC use 0.11 PC1 use 0.06	Table 6.5 on page 163
t	exposure time	s		

a. ATD-GAIN defaults to 7 unless otherwise specified on Phase II proposal.

6.5.2 Point Sources -- Aperture Photometry

When aperture photometry is used, one must consider the fraction of the object counts encircled by the aperture, as well the background noise in the aperture. In the bright target limit the SNR is given by

$$SNR = (S \cdot f(r))^{1/2} = (R_{object} \cdot f(r) \cdot t)^{1/2}$$

where S is the number of detected photons, $f(r)$ is the fraction of the total counts encircled by the aperture with radius r, and R_{object} is target count rate. Representative values of $f(r)$ are given in Table 6.7 on page 166; values for other aperture sizes and filters can be estimated from Figure 5.3 on page 122, or Figure 5.4 on page 123.

In the faint target limit the noise contributed by background counts determines the SNR

$$SNR = \frac{S \cdot f(r)}{\sqrt{B \cdot \pi r^2}}$$

where B represents the effective background counts per pixel, and r is the aperture radius in pixels.

In the generalized case the SNR per exposure for aperture photometry is given approximately by:

$$SNR = \frac{f(r) \cdot R_{object} \cdot t}{\sqrt{(f(r) \cdot R_{object} \cdot t) + \left[readnoise^2 + P_{dark} \cdot (t + 46) + P_{sky} \cdot t + P_{background} \cdot t\right] \cdot \pi r^2}} \quad (6.7)$$

where the parameters are summarized in Table 6.8 on page 167.

Table 6.7: Encircled Energy for Representative Filters. Encircled energy values are normalized to unity at large radius.

CCD	Aperture Radius (r)	Encircled Energy f(r)		
		F218W	F555W	F814W
PC1	0.1″	0.60	0.67	0.53
	0.2″	0.73	0.85	0.78
	0.5″	0.84	0.96	0.87
	1.0″	0.92	1.00	0.92
WF3	0.1″	0.40	0.46	0.44
	0.2″	0.69	0.76	0.74
	0.5″	0.85	0.90	0.91
	1.0″	0.94	0.94	0.96

Table 6.8: Parameters for Point Source SNR Estimation - Aperture Photometry.

Parameter	Description	Units	Approx. Value	Better Value
R_{object}	object count rate	$e^- s^{-1}$		Equation 6.1, 6.2, or 6.3
P_{dark}	dark count rate	$e^- s^{-1}$ $pixel^{-1}$	0.004	Table 4.2 on page 88; Eqn 4.1 on page 90
P_{sky}	sky count rate	$e^- s^{-1}$ $pixel^{-1}$	Table 6.4 on page 161	Table 6.2 on page 157, Table 6.1 on page 154, Table 6.3 on page 160; Eqn 6.1
$P_{background}$	count rate from background light (if any)	$e^- s^{-1}$ $pixel^{-1}$		Table 6.2 on page 157, Table 6 on page 151; Eqn 6.1
readnoise		e^-	ATD-GAIN=7 use 5.3[a] ATD-GAIN=15 use 7.5	Table 4.4 on page 117
f(r)	encircled energy		table 6.7	Figure 5.3 on page 122 or Figure 5.4 on page 123
r	aperture radius	pixels		
t	exposure time	s		

a. ATD-GAIN defaults to 7 unless otherwise specified on Phase II proposal.

6.5.3 Extended Sources

The calculations for extended sources are nearly identical to those for point sources. The easiest procedure is to compute the SNR per detector pixel, and then adjust this value if the total SNR is required for an area encompassing many pixels.

In general, one will have the target magnitude or flux per square arcsecond. To compute the flux per pixel for the PC one merely multiplies the flux per square arcsecond by 0.00207, or instead, adds the value 6.7 to the magnitude per square arcsecond to get the necessary magnitude per PC pixel. For the WFC, one either multiplies the flux per square arcsecond by 0.00993, or adds 5.0 to the magnitude per square arcsecond. Equations 6.2, 6.3, and 6.4 can be rewritten including these factors as below.

PC Camera

For the PC camera, sources with stellar spectra, and V surface brightness per square arcsecond σ_V we have a count rate in $e^- s^{-1}$ $pixel^{-1}$ of

$$P_{object} = 2.5 \times 10^{11} \cdot [\int Q(\lambda) T(\lambda) d\lambda / \lambda] \cdot 10^{-0.4(\sigma_V + AB_v + 6.7)} \quad (6.8)$$

For power law sources where B_ν is the target flux in units of ergs cm^{-2} s^{-1} Hz^{-1} arcsec^{-2} we have

$$P_{object} = 1.4 \times 10^{28} \cdot [\int Q(\lambda)T(\lambda)d\lambda/\lambda] \cdot B_\nu\left(\bar{\lambda} + \alpha\frac{d\bar{\lambda}}{d\alpha}\right) \qquad (6.9)$$

And finally for emission line sources where I_ν is the flux in ergs cm^{-2} s^{-1} arcsec^{-2} we have

$$P_{object} = 4.8 \times 10^{9} \cdot (QT) \cdot I_\nu \cdot \lambda \qquad (6.10)$$

where the emission line wavelength λ is in Angstroms.

WFC Cameras

For the WFC cameras and stellar sources with V surface brightness per square arcsecond σ_V we have a count rate in e$^-$ s^{-1} pixel^{-1} of

$$P_{object} = 2.5 \times 10^{11} \cdot [\int Q(\lambda)T(\lambda)d\lambda/\lambda] \cdot 10^{-0.4(\sigma_V + AB_\nu + 5)} \qquad (6.11)$$

For power law sources where B_ν is the target flux in units of ergs cm^{-2} s^{-1} Hz^{-1} arcsec^{-2} we have

$$P_{object} = 6.9 \times 10^{28} \cdot [\int Q(\lambda)T(\lambda)d\lambda/\lambda] \cdot B_\nu\left(\bar{\lambda} + \alpha\frac{d\bar{\lambda}}{d\alpha}\right) \qquad (6.12)$$

And finally for emission line sources where I_ν is the flux in ergs cm^{-2} s^{-1} arcsec^{-2} we have

$$P_{object} = 2.3 \times 10^{10} \cdot (QT) \cdot I_\nu \cdot \lambda \qquad (6.13)$$

where the emission line wavelength λ is in Angstroms.

SNR

The generalized SNR per pixel per exposure for an extended source is then obtained simply by setting the sharpness to unity in Equation 6.5:

$$SNR = \frac{P_{object} \cdot t}{\sqrt{P_{object} \cdot t + (readnoise^2 + P_{dark} \cdot (t + 46) + P_{sky} \cdot t + P_{background} \cdot t)}} \qquad (6.14)$$

Table 6.9: Parameters for Extended Source SNR Estimation.

Parameter	Description	Units	Approx. Value	Better Value
P_{object}	object count rate	$e^- s^{-1} pixel^{-1}$		Equations 6.9 to 6.12
P_{dark}	dark count rate	$e^- s^{-1} pixel^{-1}$	0.004	Table 4.2 on page 88; Eqn 4.1 on page 90
P_{sky}	sky count rate	$e^- s^{-1} pixel^{-1}$	Table 6.4 on page 161	Table 6.2 on page 157, Table 6.1 on page 154, Table 6.3 on page 160; Eqn 6.7 (PC) or 6.10 (WFC)
$P_{background}$	count rate from background light (if any)	$e^- s^{-1} pixel^{-1}$		Table 6.2 on page 157, Table 6.1 on page 154; Eqn 6.7 (PC) or 6.10 (WFC)
readnoise		e^-	ATD-GAIN=7 use 5.3[a] ATD-GAIN=15 use 7.5	Table 4.4 on page 117
t	exposure time	s		

a. Default value is ATD-GAIN=7.

Since many observations of extended sources are for galaxies in broad-band filters, a few rules of thumb can be useful. Saturation is seldom a concern, except in very bright spots such as the inner core of ellipticals and of some bulges. Count rates for spiral galaxies range typically from 2 to 0.01 $e^- pixel^{-1} s^{-1}$ (and lower) for filters such as F555W, F606W, F702W, and F814W; the lower end of the range corresponds roughly to the de Vaucouleurs D_{25}. Count rates are significantly lower in blue and UV filters. Spiral structure can typically be traced reasonably well with total exposures of 3000 seconds or longer in the above filters.

For galaxies of very small angular size at redshifts of cosmological interest, the image may cover a small number of pixels; thus the detection of such objects follows rules similar to those of point sources. However, the fraction of light falling in the central pixel is smaller for most galaxies than it is for true point sources. The approximate magnitude difference between the light falling in the central pixel and the entire galaxy is plotted in Figure 6.1 on page 170 for a typical giant elliptical galaxy, as a function of redshift. For other types of galaxies, a morphological term can be added to the values (for example, 0.6 magnitudes for lenticulars, 0.7 for S, 0.8 for Sab, 0.9 for Sbc, 1.2 for Scd, and 1.8 for Irr). These values must be increased by an additional 1.7 magnitudes for the PC.

Figure 6.1: Giant Elliptical Galaxy.

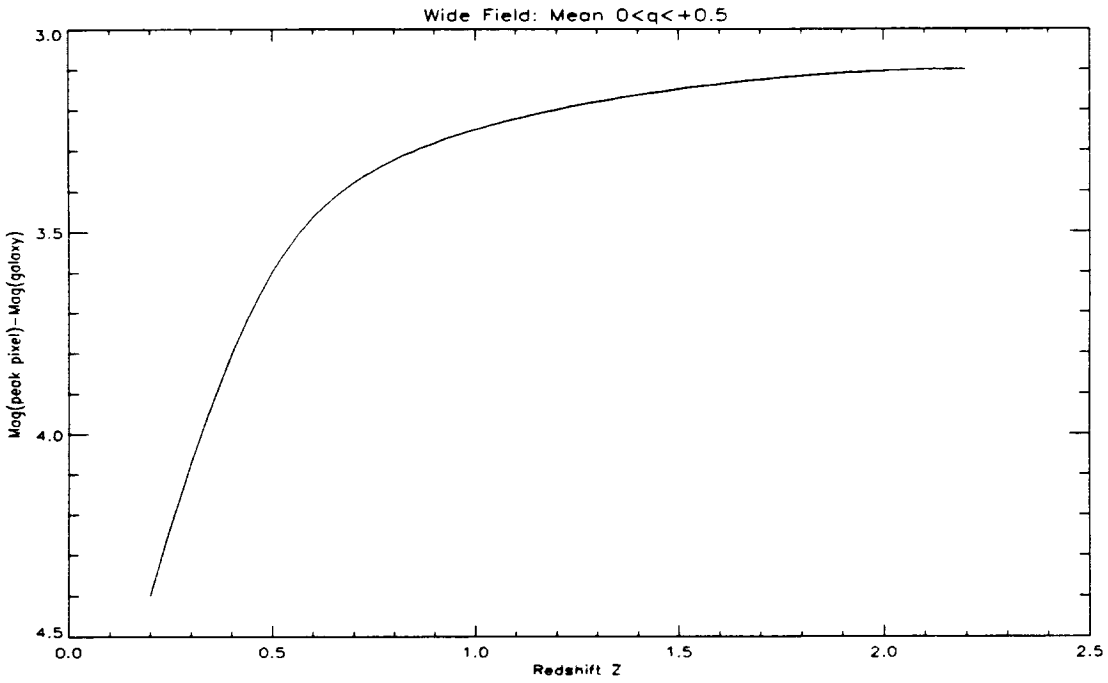

6.6 Exposure Time Estimation

In many instances one desires a certain SNR, and wishes to solve for the corresponding exposure time. Given the SNR, Equations 6.6, 6.7, or 6.14 can be solved for the exposure time, *t*. Since there are time-dependent and time-independent noise sources, quadratic equations are obtained. For example, we may solve Equation 6.6 for the point source exposure time:

$$t = \frac{1}{2Y} \cdot (b + \sqrt{b^2 + 4aY})$$

where the term *A* contains the time-independent noise sources

$$a = \frac{readnoise^2 + 46P_{dark}}{sharpness}$$

and *B* contains the time-dependent noise sources

$$b = \frac{P_{dark} + P_{sky} + P_{background}}{sharpness} + R_{object}$$

and

$$Y = \left(\frac{R_{object}}{SNR}\right)^2$$

Equations for aperture photometry (6.7) and extended sources (6.12) can be solved with similar results. Parameters are as described in Table 6.6 on page 165, Table 6.8 on page 167, and Table 6.9 on page 169. We again note that the on-line WFPC2 Exposure Time Calculator program provides an easy method for these calculations.

6.7 Sample SNR Calculations

Below we give further examples of SNR calculations. Appendix B also contains SNR plots for a wide range of representative cases.

6.7.1 Point Sources

Simple Star, Manual Calculation, PSF Fitting

We begin with the simple example of a V=20 star of spectral class G0. We want to observe with the PC using filter F555W. The star is somewhere near the ecliptic pole. We want to know the SNR for a 1200s CR-SPLIT exposure. Default ATD-GAIN=7 is used. We plan to use PSF fitting to analyze the data.

First we estimate the count rate for our target. Consulting Equation 6.2, Table 6.1 on page 154, and Table 6.2 on page 157 we have:

$$R_{object} = 2.5 \times 10^{11} \cdot \left[\int Q(\lambda)T(\lambda)d\lambda/\lambda\right] \cdot 10^{-0.4(V + AB_V)}$$

$$= 2.5 \times 10^{11} \cdot [0.030] \cdot 10^{-0.4(20 + 0.02)} = 74$$

in units of $e^- s^{-1}$. Next we fill out Equation 6.6. To keep things simple we just use values from Table 6.6 on page 165, and get the sky count rate from Table 6.4 on page 161. There is no background light (i.e. no superposed

galaxy), so $P_{background}$=0. The exposure time t=600 for each exposure of the CR-SPLIT:

$$SNR = \frac{R_{object} \cdot t}{\sqrt{R_{object} \cdot t + \frac{readnoise^2 + P_{dark} \cdot (t+46) + P_{sky} \cdot t + P_{background} \cdot t}{sharpness}}}$$

$$= \frac{74 \cdot 600}{\sqrt{74 \cdot 600 + \frac{(5.3)^2 + 0.004 \cdot (600+46) + (0.01 \cdot 600) + (0 \cdot 600)}{0.06}}}$$

$$= \frac{44400}{\sqrt{44400 + 611}} = 209$$

The SNR for the total 1200s exposure, i.e. both halves of the CR-SPLIT, would simply be:

$$SNR_{total} = SNR \cdot \sqrt{N} = 209 \cdot \sqrt{2} = 296$$

At these high SNR levels, it is likely that flat fielding would limit the photometric accuracy, rather than the noise. If we have a look at the terms in the SNR equation, we can see that the Poisson noise dominates; the term containing the sharpness and background noise sources is unimportant.

Just for fun, let us see what happens if we keep everything the same, but give the target V=25. Now we have R_{object}=0.74 $e^- s^{-1}$, and:

$$SNR = \frac{0.74 \cdot 600}{\sqrt{0.74 \cdot 600 + \frac{(5.3)^2 + 0.004 \cdot (600+46) + (0.01 \cdot 600) + (0 \cdot 600)}{0.06}}}$$

$$= \frac{444}{\sqrt{444 + 611}} = 13.7$$

We see that now the term with the background noise (in particular, the read noise) limits the SNR. For the full 1200s exposure the SNR_{total}=19.3.

Simple Star, Manual Calculation, Aperture Photometry

What if we now want to observe this same V=25 star, but we plan to reduce the data by measuring counts in a 0.5″ radius aperture? We now use

Equation 6.7 instead, consult Table 6.7 on page 166 for the encircled energy *f(r)*, and note that 0.5″ corresponds to *r*=11.6 PC pixels:

$$SNR = \frac{f(r) \cdot R_{object} \cdot t}{\sqrt{(f(r) \cdot R_{object} \cdot t) + [readnoise^2 + P_{dark} \cdot (t + 46) + P_{sky} \cdot t + P_{background} \cdot t] \cdot \pi r^2}}$$

$$= \frac{0.96 \cdot 0.74 \cdot 600}{\sqrt{(0.96 \cdot 0.74 \cdot 600) + ((5.3)^2 + 0.004(600 + 46) + 0.01 \cdot 600 + 0 \cdot 600) \cdot \pi(11.6)^2}}$$

$$= \frac{426}{\sqrt{426 + 15500}}$$

$$= 3.4$$

Apparently using aperture photometry with a 0.5″ radius aperture reduces the SNR by a factor ~4 as compared to PSF fitting, for this background limited case.

Simple Star, SNR Plots, PSF Fitting

We now repeat the first calculation above for the V=20 star using the SNR plots in Appendix B. We look up the G0 spectral class and F555W filter (5500Å) in Table B.1, and obtain AB_V=0.02. For the V=20 star, we thus have V+AB_V=20.02. We look at Figure B.10 and find this value on the horizontal axis. We locate exposure time 600s (one-half of the total 1200s CR-SPLIT exposure), and find SNR~200. For the total 1200s exposure the SNR would be $200\sqrt{2} = 280$.

Simple Star, On-Line Calculator, PSF Fitting

The above calculation for a V=20 G0 star may also be performed using the WFPC2 Exposure Time Calculator program, which is available on the WFPC2 WWW pages at:

http://www.stsci.edu/instruments/wfpc2/Wfpc2_etc/wfpc2-etc.html

Figure 6.2: Sample Fill-out Form for WFPC2 On-Line Exposure Time Calculator..

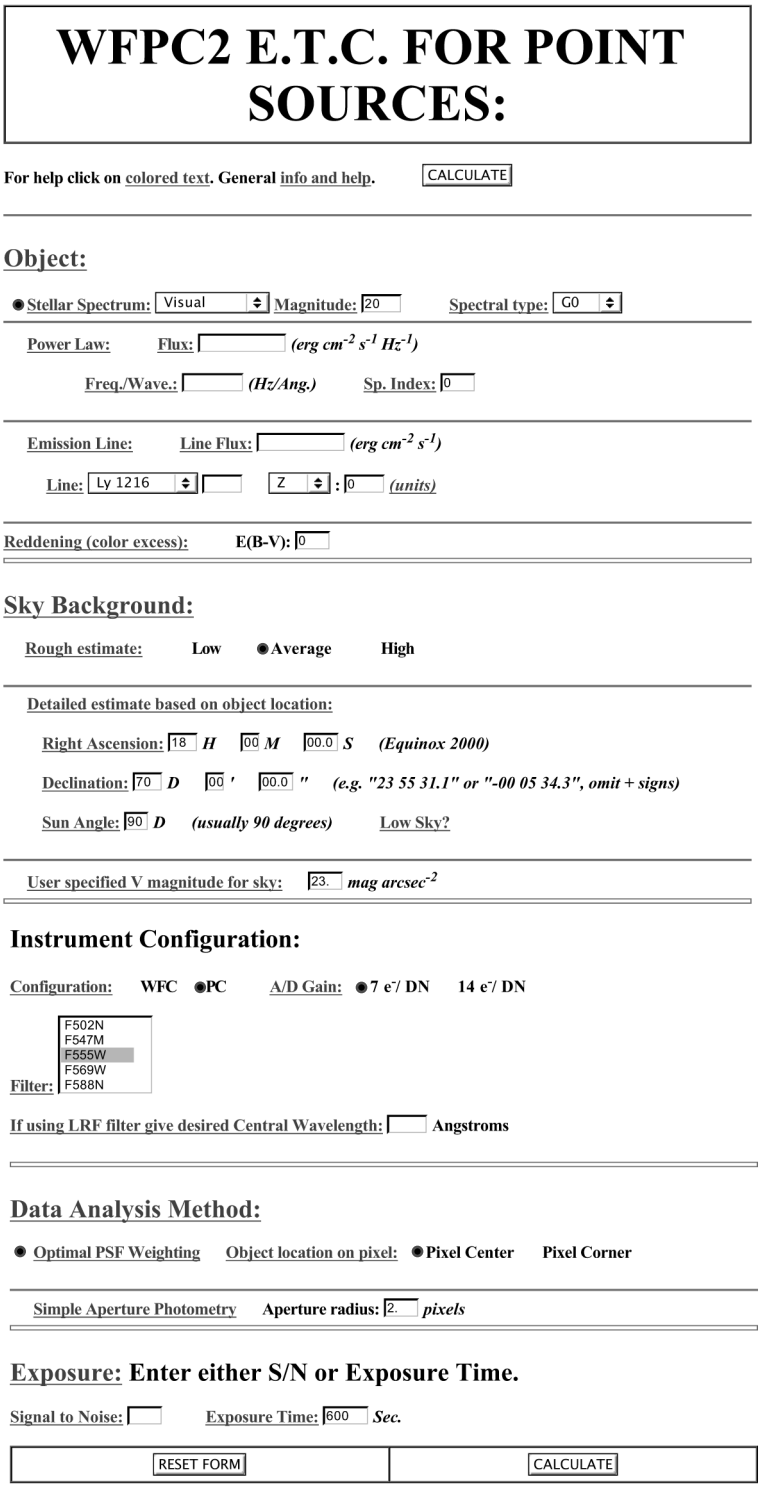

To use this program, access the above address with Netscape, or a similar program. Once in the WFPC2 area, select the “Software Tools” page, and then the “ETC” page. For the first example above, choose the

"Point Source" form and complete it as shown in Figure 6.2 on page 174 for the 600s sub-exposure. Then click the "calculate" button and after a few seconds the result is displayed (Figure 6.3 on page 175). The answer, SNR=208, is comparable to that obtained by the manual calculation above for the 600s sub-exposure (SNR=209). Alternatively, one can input the total exposure time (1200s), and then use the result farther down the output page for "No. Sub-Exposures = 2" (see Figure 6.4 on page 175), thereby obtaining SNR=291 for the total 1200s CR-SPLIT exposure.

Figure 6.3: Sample Results from WFPC2 On-Line Exposure Time Calculator.

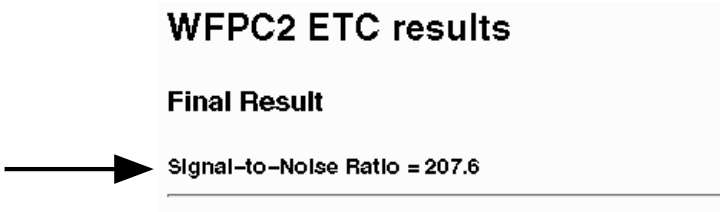

Figure 6.4: Sample Results on CR-SPLITing from WFPC2 On-Line Exposure Time Calculator Results Page.

No. Sub-Exposures	Total SNR	Pixels Lost
(No Split)	294.2	3.981250%
2	290.7	0.039626%
3	291.1	0.000234%
4	291.0	0.000001%
6	290.3	0.000000%
8	289.4	0.000000%
12	287.4	0.000000%
16	285.3	0.000000%
32	277.1	0.000000%

Star Superposed on Galaxy, Manual Calculation

We now consider a B=25 point source of spectral class B0, which is superposed on an elliptical galaxy with σ_V=22 mag arcsecond^{-2}. We want to compute the SNR obtained from a one-orbit (40 min.) non-CR-SPLIT observation in filter F300W on the WFC. PSF fitting will be used for the photometry.

We begin by computing the total count rate for the target. Using Table Table 6.2 on page 157 we see that this target will have V=25.31. From Table 6.1 on page 154 we obtain the filter efficiency and mean wavelength.

Interpolating by mean wavelength in Table 6.2 on page 157 we obtain AB_V=-0.83 for the B0 star. Using Equation 6.2 we have:

$$\begin{aligned} R_{object} &= 2.5 \times 10^{11} \cdot \left[\int Q(\lambda)T(\lambda)d\lambda/\lambda\right] \cdot 10^{-0.4(V + AB_V)} \\ &= 2.5 \times 10^{11} \cdot [0.00571] \cdot 10^{-0.4(25.31 - 0.83)} \\ &= 0.23 \end{aligned}$$

in units of e^- s^{-1}. Next we consider the background light from the superposed galaxy. We set σ_V=22 mag arcsecond^{-2} in Equation 6.11, and AB_V=3.63 for a gE galaxy at λ=3000Å (filter F300W) from Table 6.2 on page 157. Hence the count rate per pixel due to the background light is:

$$\begin{aligned} P_{background} &= 2.5 \times 10^{11} \cdot \left[\int Q(\lambda)T(\lambda)d\lambda/\lambda\right] \cdot 10^{-0.4(\sigma_V + AB_V + 5)} \\ &= 2.5 \times 10^{11} \cdot [0.00571] \cdot 10^{-0.4(22 + 3.63 + 5)} \\ &= 0.00080 \end{aligned}$$

For the sky background, we note that Table 6.4 on page 161 has no entry for F300W, so that the sky must be unimportant. If we wanted to calculate it anyway, as a check, we would use Table 6.3 on page 160 for the sky brightness, Table 6.2 on page 157 for the sky's AB_V, and again Equation 6.11. We will assume the target is near the ecliptic pole.

$$\begin{aligned} P_{sky} &= 2.5 \times 10^{11} \cdot \left[\int Q(\lambda)T(\lambda)d\lambda/\lambda\right] \cdot 10^{-0.4(\sigma_V + AB_V + 5)} \\ &= 2.5 \times 10^{11} \cdot [0.00571] \cdot 10^{-0.4(23.3 + 3.12 + 5)} \\ &= 0.00039 \end{aligned}$$

For the sharpness function we will use "pixel corner" values (least optimistic choice) from Table 6.5 on page 163. Using read noise and dark current from Table 6.6 on page 165, and Equation 6.6 for point source SNR:

$$\begin{aligned} SNR &= \frac{R_{object} \cdot t}{\sqrt{R_{object} \cdot t + \dfrac{readnoise^2 + P_{dark} \cdot (t + 46) + P_{sky} \cdot t + P_{background} \cdot t}{sharpness}}} \\ &= \frac{0.23 \cdot 2400}{\sqrt{0.23 \cdot 2400 + \dfrac{(5.3)^2 + 0.004 \cdot (2400 + 46) + (0.00039 \cdot 2400) + (0.00080 \cdot 2400)}{0.103}}} \\ &= \frac{552}{\sqrt{552 + 395}} \\ &= 17.9 \end{aligned}$$

for this single exposure. The SNR for multiple 40 min. exposures would be simply $17.9(N^{1/2})$, where N is the number of exposures.

Star Superposed on Galaxy, On-Line Calculator

The above calculation could also be performed with the on-line WFPC2 Exposure Time Calculator. One would select the "Point source + stellar background" form, and complete it as in Figure 6.5 on page 177, and then click on "calculate." Figure 6.6 on page 178 shows some of the results.

Figure 6.5: Point Source + Stellar Background Fill-out Form for WFPC2 On-Line Exposure Time Calculator. SNR is calculated for B=25 star (class B0) superposed on an elliptical galaxy (gE) with σ_V=22. WFC is used with F300W.

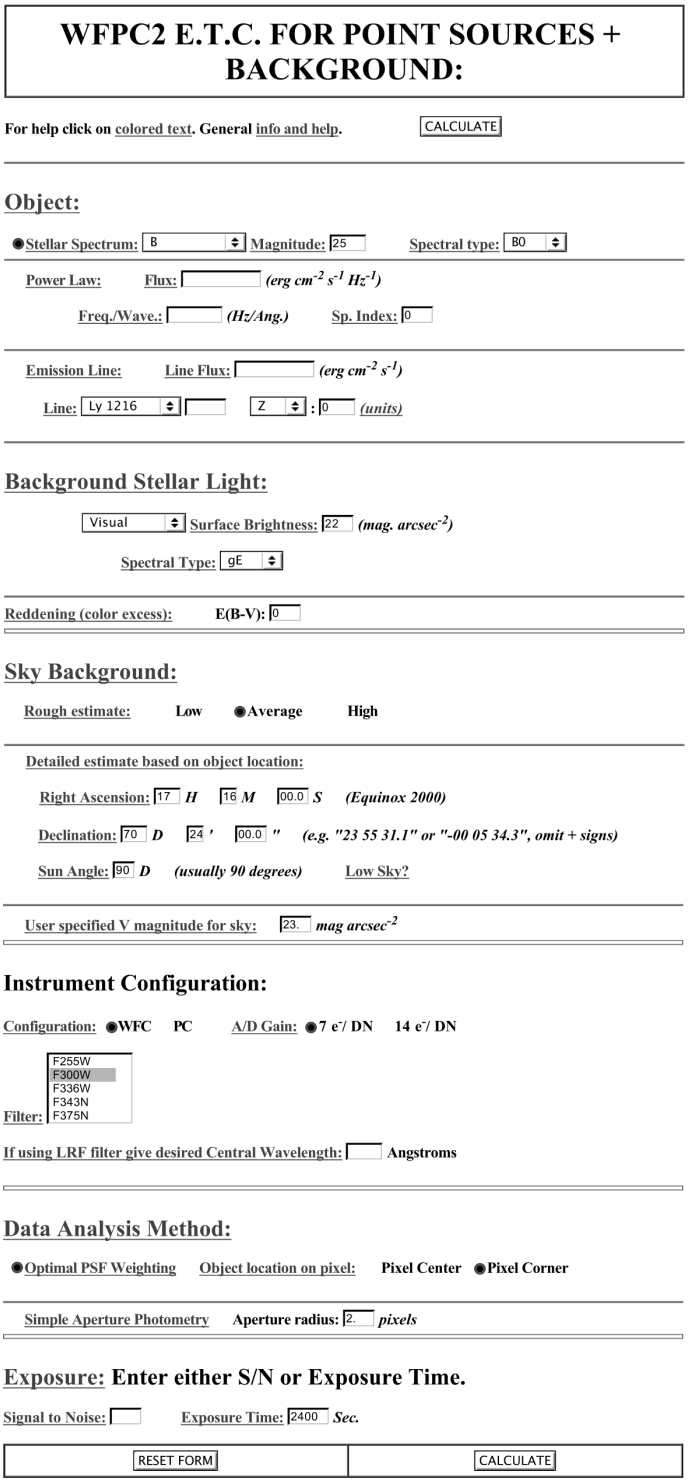

WFPC2 E.T.C. FOR POINT SOURCES + BACKGROUND:

For help click on colored text. General info and help. CALCULATE

Object:

● Stellar Spectrum: B Magnitude: 25 Spectral type: B0

Power Law: Flux: *(erg cm^{-2} s^{-1} Hz^{-1})*

Freq./Wave.: *(Hz/Ang.)* Sp. Index: 0

Emission Line: Line Flux: *(erg cm^{-2} s^{-1})*

Line: Ly 1216 Z : 0 *(units)*

Background Stellar Light:

Visual Surface Brightness: 22 *(mag. arcsec^{-2})*

Spectral Type: gE

Reddening (color excess): E(B-V): 0

Sky Background:

Rough estimate: Low ● Average High

Detailed estimate based on object location:

Right Ascension: 17 *H* 16 *M* 00.0 *S* *(Equinox 2000)*

Declination: 70 *D* 24 ' 00.0 " *(e.g. "23 55 31.1" or "-00 05 34.3", omit + signs)*

Sun Angle: 90 *D* *(usually 90 degrees)* Low Sky?

User specified V magnitude for sky: 23. *mag arcsec^{-2}*

Instrument Configuration:

Configuration: ● WFC PC A/D Gain: ● 7 e$^-$/ DN 14 e$^-$/ DN

Filter: F255W / F300W / F336W / F343N / F375N

If using LRF filter give desired Central Wavelength: Angstroms

Data Analysis Method:

● Optimal PSF Weighting Object location on pixel: Pixel Center ● Pixel Corner

Simple Aperture Photometry Aperture radius: 2. *pixels*

Exposure: Enter either S/N or Exposure Time.

Signal to Noise: Exposure Time: 2400 *Sec.*

RESET FORM CALCULATE

Figure 6.6: Sample Output from WFPC2 On-Line Exposure Time Calculator.

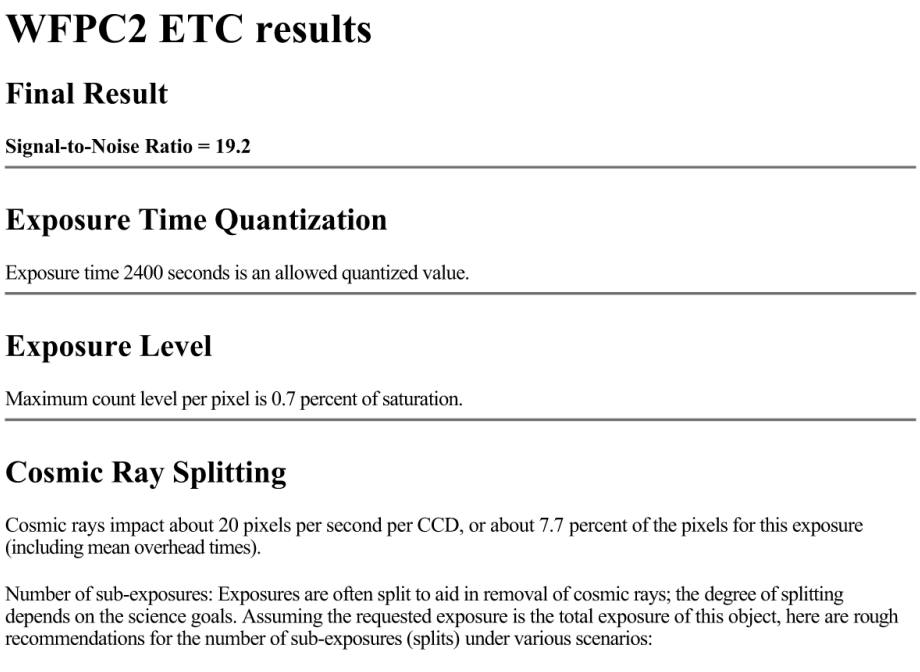

WFPC2 ETC results

Final Result

Signal-to-Noise Ratio = 19.2

Exposure Time Quantization

Exposure time 2400 seconds is an allowed quantized value.

Exposure Level

Maximum count level per pixel is 0.7 percent of saturation.

Cosmic Ray Splitting

Cosmic rays impact about 20 pixels per second per CCD, or about 7.7 percent of the pixels for this exposure (including mean overhead times).

Number of sub-exposures: Exposures are often split to aid in removal of cosmic rays; the degree of splitting depends on the science goals. Assuming the requested exposure is the total exposure of this object, here are rough recommendations for the number of sub-exposures (splits) under various scenarios:

6.7.2 Extended Sources

In general, the signal-to-noise level for extended sources can be computed by comparing the expected signal, S, in each pixel, determined from Equations 6.8 through 6.13, to the noise $N=(S+B)^{1/2}$, where B is the equivalent background, determined in a manner similar to that for point sources. Unlike for point sources, the calculation does not, in a first approximation, involve the sharpness of the point spread function. For example, let us consider the observation of a source with a V surface brightness of 24 mag arcsec^{-2}, assuming the F569W filter, WFC camera, and sky background V=23.3 mag arcsec^{-2}. The signal-to-noise estimate goes as follows. The signal in each WFC pixel is 24.0+5.0 = 29.0 magnitude. By Equation 6.11, the total signal collected from the source in a 3000 second integration is S = 44.1 electrons, neglecting the small AB color correction. The sky signal per pixel is 84.1 electrons. The dark current is ~12 electrons. The total equivalent background is thus B = $84.1+5.3^2+12$ = 124.2 electrons, larger than the signal detected, thus the noise is background-dominated. The noise is $N=(S+B)^{1/2}$= 13.0 electrons, and the signal-to-noise *per pixel* expected in this case is 3.4. Similar calculations can be carried out for other filters; for observations in narrow-band filters and in the UV, the sky background signal will usually be unimportant. For very long observations of faint objects, other noise

terms, such as flat field uncertainty, and errors in dark (and possibly bias) subtraction, must be considered more carefully.

If the scale of features in the target is larger than one pixel, the signal-to-noise can sometimes be improved by smoothing the observed image or - if read noise is a significant contributor - by reading the image out in AREA mode (see “CCD Orientation and Readout” on page 37).

6.7.3 Emission Line Sources

The signal-to-noise ratio calculation for point-like or extended emission-line sources is similar to that for continuum sources. However, the details of the calculation are different, because of the units used for the line flux, and because the flux is in a narrow line. The integrated filter efficiency is not relevant for the signal calculation; what matters is the total system throughput QT at the wavelength of the line, which can be determined from inspection of the figures in Appendix A. For lines near the center of the filter bandpasses the QT_{max} values from Table 6.1 on page 154 can be used. The total signal expected for a point source of line strength F, expressed in erg s^{-1} cm^{-2}, is S=2.28x10^{12} λ t QT F, where t is the exposure time in seconds, and λ the wavelength of the line in Angstroms. Thus, H_α emission at 6563Å, with flux F=10^{-16} erg s^{-1} cm^{-2}, observed for 1000 seconds through the F656N filter (total system throughput QT=0.11 from the plots of “F622W, F631N, F656N” on page 345), will produce a total signal of S=165 electrons. The equivalent background per pixel is read-noise dominated: B=1+5.3^2+4=33, for a background noise of ~6 electrons. The total noise is dominated by photon noise from the signal itself, and the signal-to-noise ratio achieved in this observation is ~27.

If the source is extended, the expected signal *per arcsecond* must be multiplied by the effective pixel area: 0.0099 $arcsec^2$ for the WF, 0.0021 for the PC. For a line flux of, say, F = 10^{-15} erg s^{-1} cm^{-2} $arcsec^{-2}$, this corresponds to 16 electrons in 1000 seconds for a WFC pixel. The noise is now dominated by the background, and the single-pixel signal-to-noise ratio is $16/(33 + 16)^{1/2} \sim 2.3$.

Extended Line Emission Source, Manual Calculation

We now consider a detailed example of a planetary nebula observed on the PC with the F502N filter. The nebula has a diameter of 5″ and a total flux F=4x10^{-13} erg s^{-1} cm^{-2} in the [OIII] 5007Å line. We want to estimate the SNR for an 1800s exposure, which will be CR-SPLIT.

First we must estimate the flux per square arcsecond. Using the nebula diameter, the average brightness is I_ν = 2.0x10^{-14} erg s^{-1} cm^{-2} $arcsec^{-2.}$

From the plots in Appendix A, we see that QT=0.058. Using Equation 6.10 for the target count rate per pixel:

$$\begin{aligned} P_{object} &= 4.8 \times 10^9 \cdot (QT) \cdot I_\nu \cdot \lambda \\ &= 4.8 \times 10^9 \cdot (0.058) \cdot 2.0 \times 10^{-14} \cdot 5007 \\ &= 0.028 \end{aligned}$$

Next we estimate the SNR for each 900s sub-exposure using Equation 6.14 and Table 6.9 on page 169. For this narrow filter the sky background can be ignored. We presume there is no background light from astrophysical sources:

$$\begin{aligned} SNR &= \frac{P_{object} \cdot t}{\sqrt{P_{object} \cdot t + (readnoise^2 + P_{dark} \cdot (t + 46) + P_{sky} \cdot t + P_{background} \cdot t)}} \\ &= \frac{0.028 \cdot 900}{\sqrt{0.028 \cdot 900 + (5.3^2 + 0.004 \cdot (900 + 46) + 0 \cdot 900 + 0 \cdot 900)}} \\ &= 3.3 \end{aligned}$$

Hence SNR=3.1 per pixel for each 900s sub-exposure. The SNR per pixel for the total 1800s is

$$\begin{aligned} SNR_{total} &= SNR\sqrt{N} \\ &= 3.3 \cdot \sqrt{2} \\ &= 4.7 \end{aligned}$$

The SNR for the entire nebula is this SNR per pixel times the square root of the number of pixels in the image, or ~460. In actuality, uncertainties in the photometric calibration and flat fields, would limit the SNR to ~100.

Extended Line Emission Source, On-Line Calculator

The above example could be calculated with the "Extended Source" form of the ETC program. The fill-out form would be completed as shown in Figure 6.7 on page 181.

Figure 6.7: Extended Source Form for WFPC2 On-Line Exposure Time Calculator. Here the target is a galactic [OIII] 5007 line emission source and is observed on PC with filter F502N. SNR is computed for 1800s exposure.

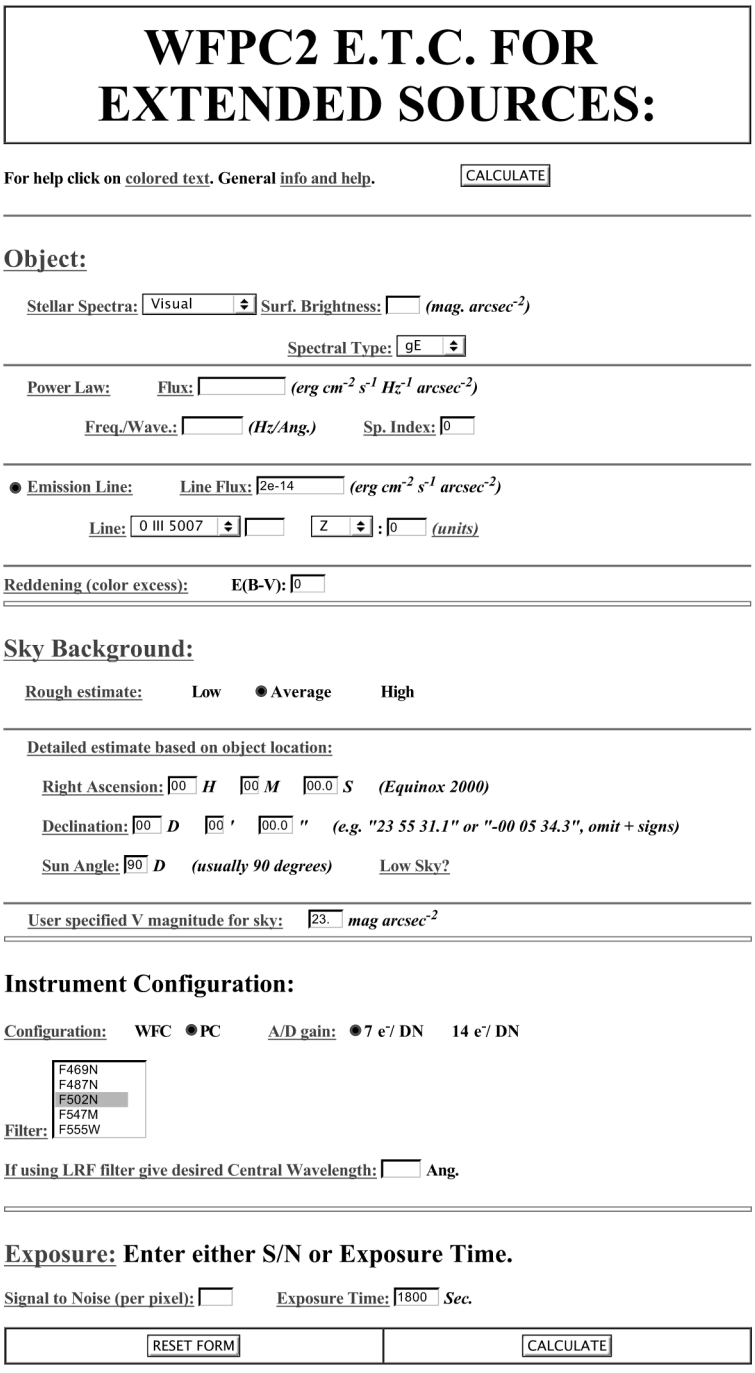

We have selected “[OIII] 5007” on the emission line menu, and have left the redshift (z) set to zero. The PC and F502N filter are selected. Note we have entered the exposure time as 1800s. Scrolling down through the

output page we find a table of SNR for various CR-SPLITings of the exposure (See Figure 6.8). “No. Sub-Exposures = 2” gives the answer we want, SNR=4.6 per pixel.

Figure 6.8: Sample Results on CR-SPLITing from WFPC2 On-Line Exposure Time Calculator Results Page.

No. Sub-Exposures	Total SNR	Pixels Lost
(No Split)	5.3	5.856250%
2	4.6	0.085739%
3	4.1	0.000744%
4	3.8	0.000005%
6	3.3	0.000000%
8	3.0	0.000000%
12	2.5	0.000000%
16	2.2	0.000000%
32	1.6	0.000000%

Line Emission Point Source w/ LRF, Manual Calculation

In this example we consider an unresolved source of H_α emission in a galaxy at redshift z=0.22 with flux F=1.5x10^{-16} erg s^{-1} cm^{-2}. We want the SNR for a 2400s exposure without CR-SPLITing.

Since the redshift is significant, we cannot observe with the F656N filter. Instead we will use the Linear Ramp Filter (LRF). The observed wavelength will be 8007Å. From Table 3.7 on page 58 we see that this will be observed using the FR868N filter on CCD WF3. Combining the LRF transmission from Figure 3.3 on page 54 and the “WFPC2 + OTA System Throughput” from Figure 2.4 on page 29 we estimate QT=0.054. We compute the count rate using Equation 6.4.

$$\begin{aligned} R_{object} &= 2.3 \times 10^{12} \cdot (QT) \cdot F \cdot \lambda \\ &= 2.3 \times 10^{12} \cdot (0.054) \cdot (1.5 \times 10^{-16}) \cdot 8007 \\ &= 0.15 \end{aligned}$$

To estimate the SNR we use Equation 6.6, which assumes that PSF fitting will be used to analyze the image. Since the filter is narrow, we will ignore the sky emission. We use Table 6.6 on page 165 for the WFC sharpness and also the read noise.

$$SNR = \frac{R_{object} \cdot t}{\sqrt{R_{object} \cdot t + \frac{readnoise^2 + P_{dark} \cdot (t + 46) + P_{sky} \cdot t + P_{background} \cdot t}{sharpness}}}$$

$$= \frac{0.15 \cdot 2400}{\sqrt{0.15 \cdot 2400 + \frac{5.3^2 + 0.004(2400 + 46) + 0 \cdot 2400 + 0 \cdot 2400}{0.11}}}$$

$$= \frac{360}{\sqrt{360 + 344}}$$

$$= 14$$

which is for an un-split 2400s exposure. The Poisson noise and background noises contribute nearly equally. For three such exposures over three orbits

$$SNR_{total} = SNR\sqrt{N}$$

$$= 14\sqrt{3}$$

$$= 23.$$

Line Emission Point Source w/ LRF, On-Line Calculator

The above calculation can be performed using the ETC program. The "Point Source" form is used. "Emission Line" source and the "H 6563" line are selected; the redshift is set to 0.22. The program will automatically choose between PC and WFC, depending on the LRF setting. The least optimistic case of placing the object on a "pixel corner" is selected. The filter "LRF" is selected from the filter menu, and 8007Å is given for the central wavelength. The exposure time is specified as 2400s. (See Figure 6.9 on page 184 for example of completed form.)

Figure 6.9: Point Source Form for WFPC2 On-Line Exposure Time Calculator. The target is an unresolved galaxy (z=0.22) nucleus with Hα line emission which is observed with LRF. SNR is computed for 2400s exposure.

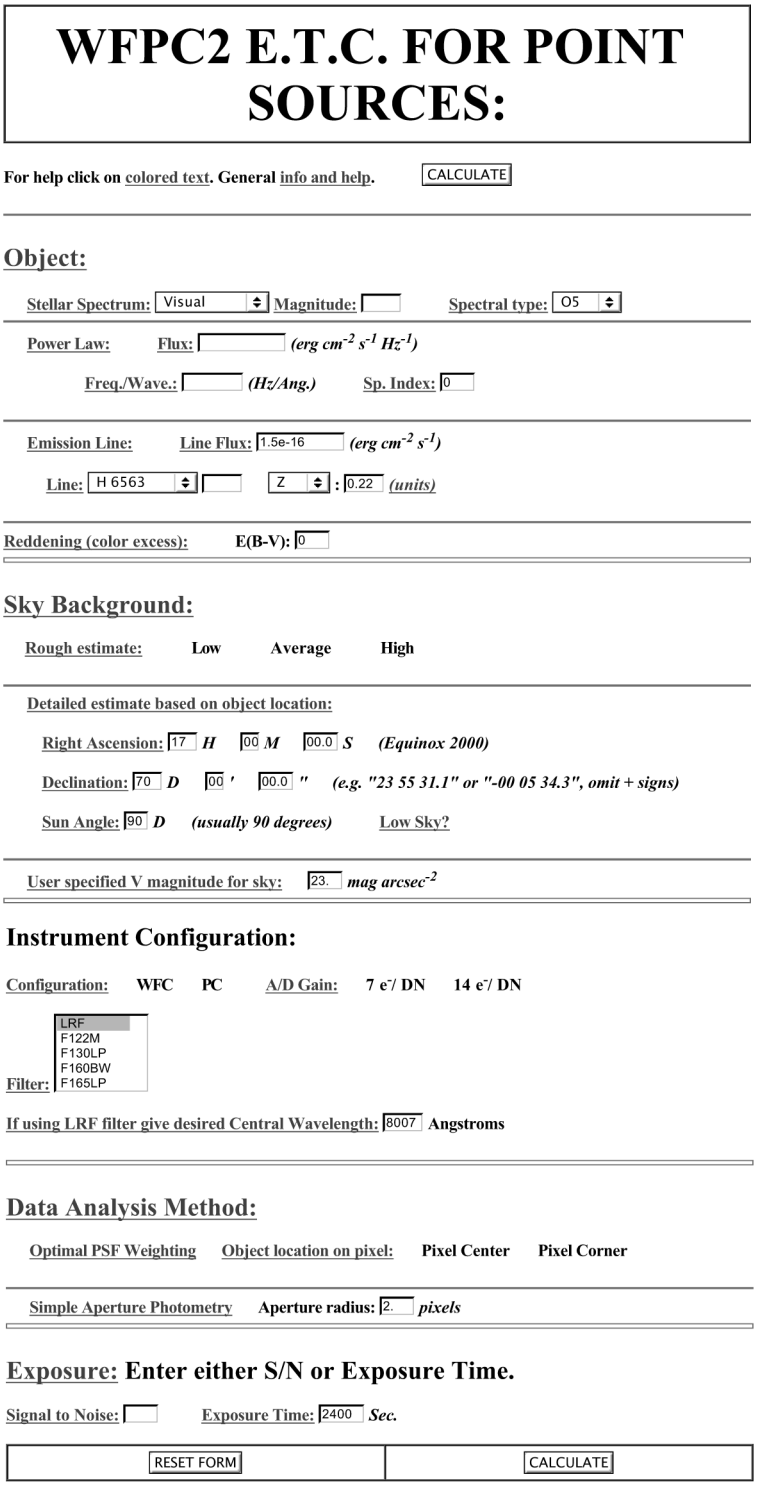

WFPC2 E.T.C. FOR POINT SOURCES:

For help click on colored text. General info and help. CALCULATE

Object:

Stellar Spectrum: Visual Magnitude: Spectral type: O5

Power Law: Flux: *(erg cm^{-2} s^{-1} Hz^{-1})*

Freq./Wave.: *(Hz/Ang.)* Sp. Index: 0

Emission Line: Line Flux: 1.5e-16 *(erg cm^{-2} s^{-1})*

Line: H 6563 Z : 0.22 *(units)*

Reddening (color excess): E(B-V): 0

Sky Background:

Rough estimate: Low Average High

Detailed estimate based on object location:

Right Ascension: 17 *H* 00 *M* 00.0 *S* *(Equinox 2000)*

Declination: 70 *D* 00 ′ 00.0 ″ *(e.g. "23 55 31.1" or "-00 05 34.3", omit + signs)*

Sun Angle: 90 *D* *(usually 90 degrees)* Low Sky?

User specified V magnitude for sky: 23. *mag arcsec^{-2}*

Instrument Configuration:

Configuration: WFC PC A/D Gain: 7 e$^-$/ DN 14 e$^-$/ DN

Filter: LRF F122M F130LP F160BW F165LP

If using LRF filter give desired Central Wavelength: 8007 Angstroms

Data Analysis Method:

Optimal PSF Weighting Object location on pixel: Pixel Center Pixel Corner

Simple Aperture Photometry Aperture radius: 2. *pixels*

Exposure: Enter either S/N or Exposure Time.

Signal to Noise: Exposure Time: 2400 *Sec.*

RESET FORM CALCULATE

The result is SNR=13.1 for the un-split 2400s exposure (Figure 6.10 on page 185), which is comparable to the manual calculation of SNR=14.

Figure 6.10: Sample Output for WFPC2 On-Line Exposure Time Calculator.

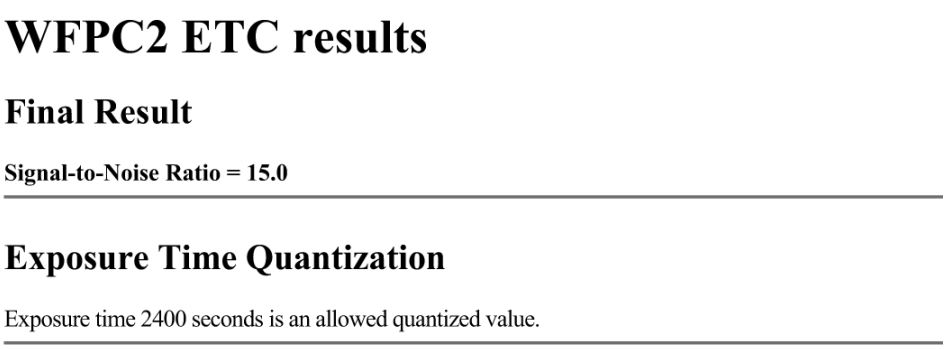

WFPC2 ETC results

Final Result

Signal-to-Noise Ratio = 15.0

Exposure Time Quantization

Exposure time 2400 seconds is an allowed quantized value.

6.8 Photometric Anomalies

There are two photometric anomalies resulting from nonlinearities of the WFPC2 detectors. The first is due to the imperfect charge transfer efficiency (CTE) of the detectors, which causes sources at high row and column numbers to appear fainter because the charge is transferred over a bigger fraction of the chip. This anomaly is increasing with time, especially for faint sources, presumably as a consequence of on-orbit radiation damage. We have developed correction formulae which appear to reduce the impact of this anomaly to about 1-3% for faint sources. The second, called “long vs. short”, causes sources to have a lower count rate - and thus appear fainter - in short exposures than in longer exposures, and appears independent of the position on the chip. The most likely explanation is that this effect is due to an overestimate of the sky measurement in the short exposure due to the presence of scattered light around bright stars. For further discussion, see “Photometric Anomalies: CTE and Long vs. Short” on page 99.

We also note the F1042M filter has an anomalous PSF which can impact aperture photometry. See “PSF Anomaly in F1042M Filter” on page 139.

6.9 Red Leaks in UV Filters

The presence of significant red leaks in the UV filters, together with the much greater sensitivity and wavelength coverage in the red part of the spectrum, can make UV observation and calibration difficult. Observers must sometimes be prepared to take additional frames at red wavelengths, in order to estimate the contribution of red leak to the UV counts. The counts contributed by red leak can be a significant noise source, and must also be taken into account during SNR and exposure time estimation. See "Red Leaks in UV Filters" on page 68 for detailed information. Note that the SYNPHOT synthetic photometry package can be used to estimate counts due to red leak for particular filter / target combinations.

6.10 Long-term Photometric Stability

The long-term photometric stability of WFPC2 has been evaluated by examining the photometric monitoring data collected over the lifetime of the instrument. Our primary standard, GRW+70D5824, has been observed roughly every four weeks, before and after decontamination procedures, both in the far UV and in the standard photometric filters. Early observations were taken monthly in both the PC and WF3. Later observations (since Cycle 6) were on a rotating schedule, where observations are taken in a different chip each month. Overall, a baseline of over ten years is available for the PC and WF3, and about eight years in WF2 and WF4. The data have been analyzed and reported by Baggett and Gonzaga (1998); here we summarize their main conclusions.

Overall, the WFPC2 photometric throughput, as measured via our primary standard, has remained remarkably stable throughout. Its long-term behavior in filters longward of F336W is characterized by small fluctuations (2% peak-to-peak) which appear to have no specific pattern, and there is no significant overall sensitivity trend. Aside from contamination corrections, which are only significant shortward of F555W, the same photometric zeropoints can be applied to non-UV data throughout the life of WFPC2.

In contrast, the UV photometric throughput of WFPC2 has changed measurably over the years. In most cases, the throughput has increased slowly, perhaps as a result of continuing evaporation of low-level contaminants. In F170W, the best-characterized UV filter on WFPC2, the clean throughput (immediately after a decontamination) has *increased* in the PC by about 12% from 1994 to 1998. Not all UV filter / detector combinations show this behavior; some combinations show a modest *decline* in throughput (e.g. 3% in F255W). Baggett and Gonzaga (1998)

report the details of the secular throughput changes for the filters we monitor.

Finally, the contamination rates - the rate at which the camera throughput declines after a decontamination, due to the gradual buildup of contaminants on the cold CCD windows - have generally decreased since installation of WFPC2, possibly also because the environment has become cleaner with time. (This excludes brief periods of increased contamination just after servicing missions.) For example, the contamination rate in F170W in the PC has decreased from ~0.56%/day to ~0.45%/day. See "Short-term Time Dependence of UV Response" on page 187 for additional discussion of the UV response variations.

Baggett and Gonzaga (1998) suggest a number of ways users can correct long-term changes in WFPC2 photometry. While these changes are generally small, users wishing to achieve high-precision photometry, especially in the UV, should follow their recommendations.

6.11 Short-term Time Dependence of UV Response

The UV throughput of the WFPC2 degrades in a predictable way after each monthly decontamination. The photometric calibration given in "System Throughput" on page 151 is applicable at the start of each cycle, and measurements taken at other times must be corrected to account for the change in sensitivity since the last decontamination. In addition, a long-term change in sensitivity is present for the F160BW and F170W filter observations on the PC, and may be present to a lesser degree at other wavelengths.

Figure 6.11 on page 190 shows the photometric monitoring data for the standard star GRW+70D5824 (a white dwarf classified DA3; B-V = -0.09) in the WF3 and PC1 for the set of filters which are routinely monitored. Only data after April 24, 1994, when the CCD operating temperatures were lowered from -76˚C to -88˚C, are shown. Figure 6.11 on page 190 shows that the effect of contamination on the F675W and F814W filter observations is essentially negligible. However, at UV wavelengths contamination effects are readily apparent; the upper envelope of points indicate measurements made shortly *after* a decontamination, while the lower envelope are data taken shortly *prior* to a decontamination. Contamination effects are largest for the F160BW filter where they cause a 30% - 40% modulation in throughput. Table 6.10 on page 188 shows the monthly decline in throughput based on this data. The values in parentheses are based on similar observations of the globular cluster ω Cen (NGC 5139; mean B-V ~ 0.7 mag). In general, the values derived from the ω Cen data are in good agreement with the values derived from GRW+70D5824 data.

Table 6.10: Change in WFPC2 Throughput Over 30 Days[a].

Filter	PC1	WF2	WF3	WF4
F160BW	-0.263 ± 0.030		-0.393 ± 0.051	
F170W	-0.160 ± 0.011	-0.284 ± 0.005	-0.285 ± 0.006	-0.232 ± 0.006
F218W	-0.138 ± 0.009		-0.255 ± 0.010	
F255W	-0.070 ± 0.007		-0.143 ± 0.009	
F336W	-0.016 ± 0.008		-0.057 ± 0.011	
	(-0.038 ± 0.018)	(-0.043 ± 0.010)	(-0.046 ± 0.008)	(-0.047 ± 0.007)
F439W	-0.002 ± 0.007		-0.021 ± 0.010	
	(0.002 ± 0.014)	(-0.022 ± 0.007)	(-0.023 ± 0.009)	(-0.023 ± 0.007)
F555W	-0.014 ± 0.006		-0.016 ± 0.008	
	(0.007 ± 0.013)	(-0.007 ± 0.007)	(-0.009 ± 0.009)	(-0.008 ± 0.008)
F675W	-0.001 ± 0.006		-0.001 ± 0.006	
	(-0.020 ± 0.020)	(0.001 ± 0.011)	(0.002 ± 0.011)	(0.004 ± 0.011)
F814W	0.007 ± 0.007		0.003 ± 0.008	
	(0.013 ± 0.019)	(-0.002 ± 0.009)	(-0.000 ± 0.009)	(-0.002 ± 0.010)

a. Values in parentheses are from the ω Cen observations.

A slight difference between the throughput declines for GRW+70D5824 and ω Cen might be expected due to differences in spectral shape, especially for filters like F336W which have a substantial red leak. However, even in the case of F336W the effect should be less than 0.01 mag based on SYNPHOT simulations.

Figure 6.12 on page 191 and Figure 6.13 on page 192 show the throughput decline for the F170W filter in all four chips as a function of days since the last decontamination. The contamination rate is remarkably constant during each decontamination cycle, and can be accurately modeled by a simple linear decline following the decontaminations, which appear to return the throughput to roughly the nominal value each month. While the contamination rates are similar for the three WF chips, the values for the PC are significantly lower.

In addition to the monthly changes in throughput there is evidence for a long-term variation in the F170W data on the PC, where the throughput has *increased* at the rate of approximately 3.3% ± 0.2% per year. This is evident in Figure 6.11 on page 190, but is much clearer in the top panel of Figure 6.12 on page 191 where lines are fitted separately to the epoch ~1994 (dotted line) and ~1998 data (solid line). The effect is most evident in Figure 6.14 on page 193 where only data taken 4 days or less after a decontamination are shown. The F160BW filter shows an even stronger

trend but with larger uncertainties (i.e., an increase of 9.0% ± 1.7% per year). The WF chips do *not* show this effect, nor do the observations on the PC at longer wavelengths. One possible explanation of the throughput increase is that WFPC2 was flown with some initial contaminant on the PC1 optics which is slowly evaporating on-orbit. The pre-launch thermal vacuum test gave evidence of elevated contamination in PC1, which is consistent with this hypothesis.

A second long-term effect is also apparent in Figure 6.12 on page 191 and Figure 6.13 on page 192. In all four CCDs the line fitted to the later data show a shallower slope, which indicates a slower throughput decline. The decline rate is reduced by 19% (PC) to 30% (WF4) over the four-year interval between the dotted and solid lines in each panel. This is likely caused by contamination slowly escaping the camera.

ISRs WFPC2 96-4 and WFPC2 98-3 describe detailed results of this monitoring (available from our WWW site). Observers are advised to consult the STScI WFPC2 WWW page for the latest information at the following address:

`http://www.stsci.edu/instruments/wfpc2/wfpc2_top.html`

Figure 6.11: Photometric Monitoring Data for WFPC2.

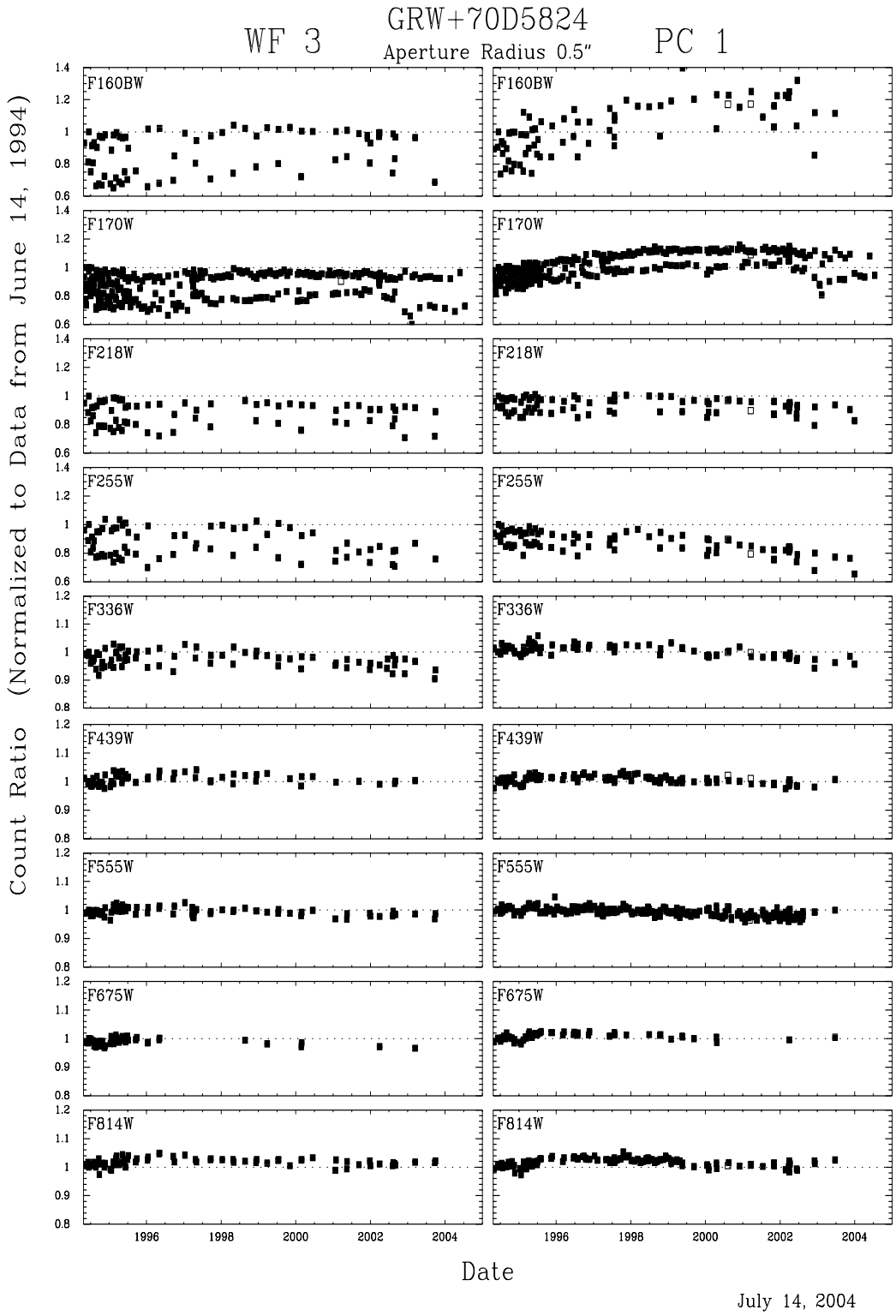

Figure 6.12: Post-decontamination Throughput for F170W Filter in PC and WF2.

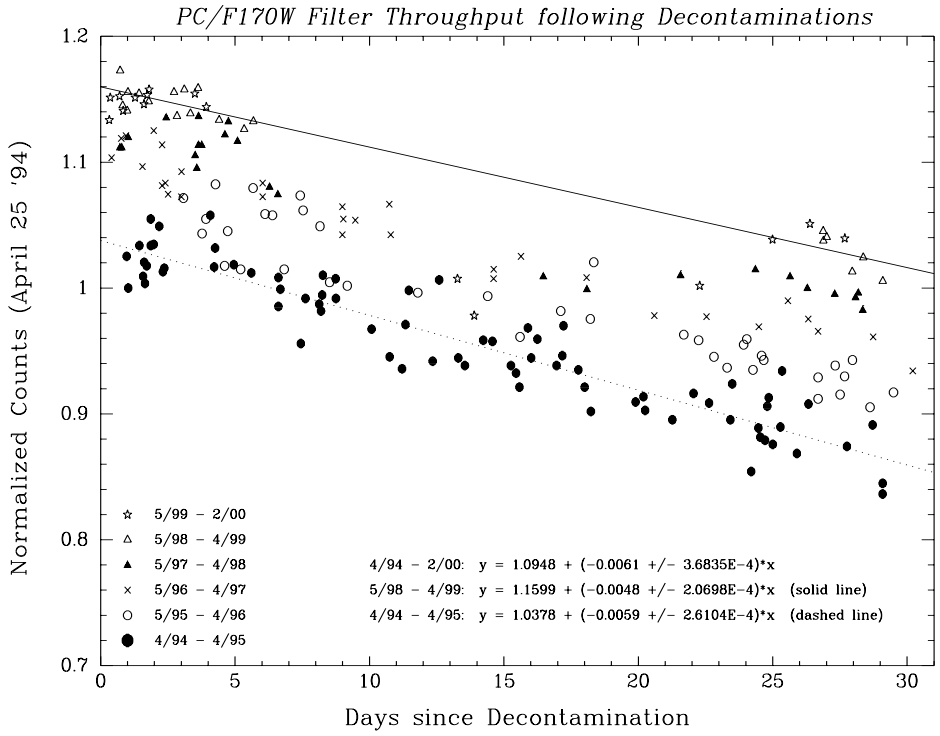

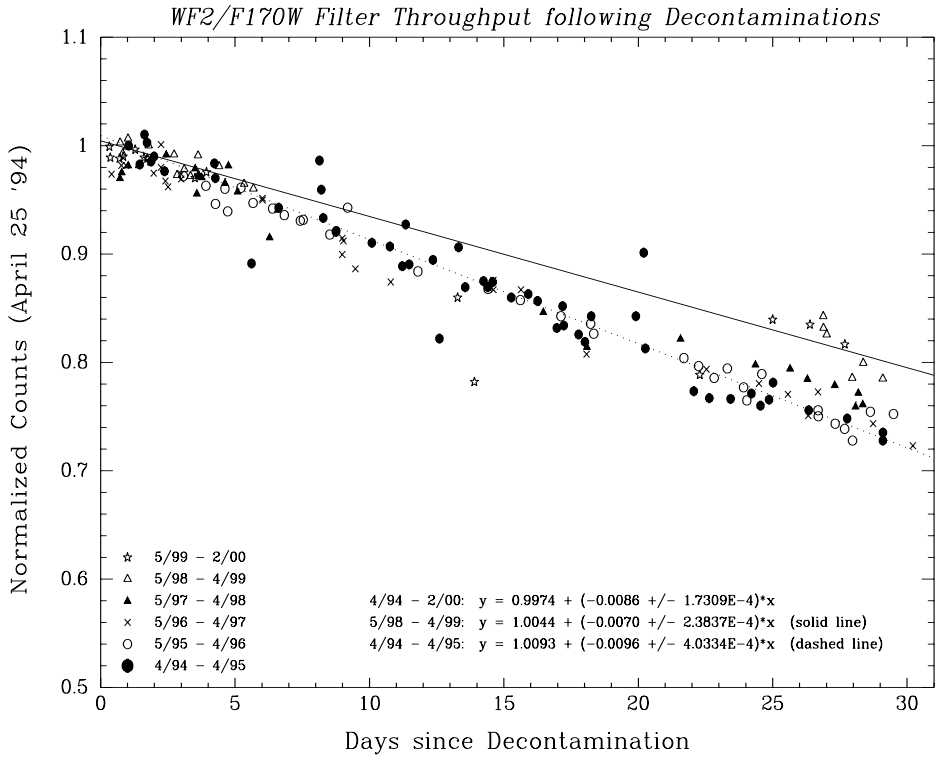

Figure 6.13: Post-decontamination Throughput for F170W Filter in WF3 & WF4.

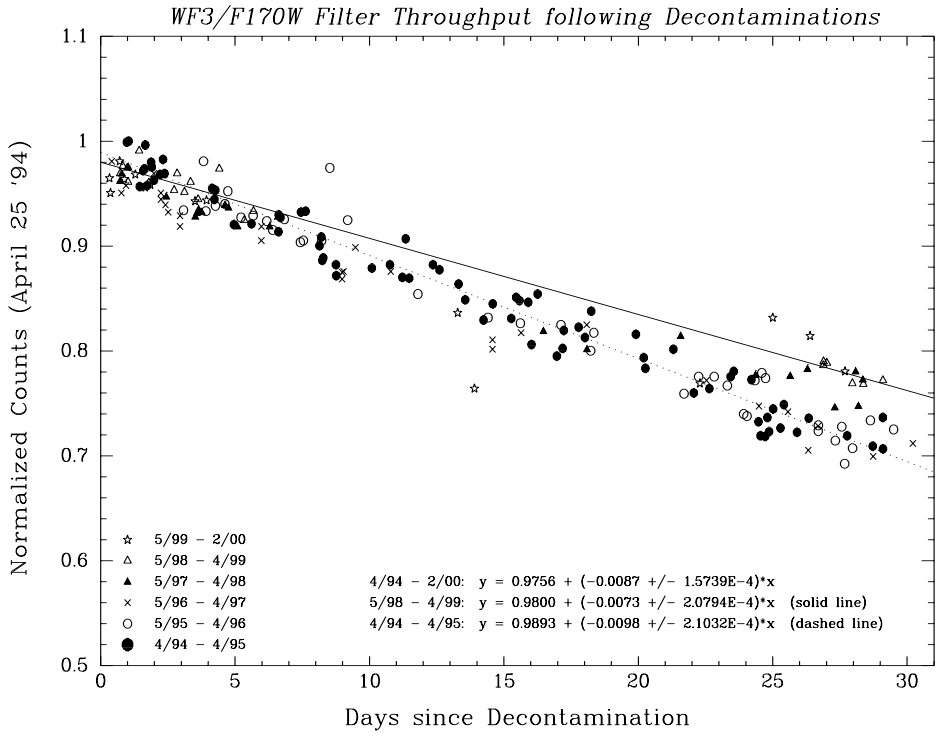

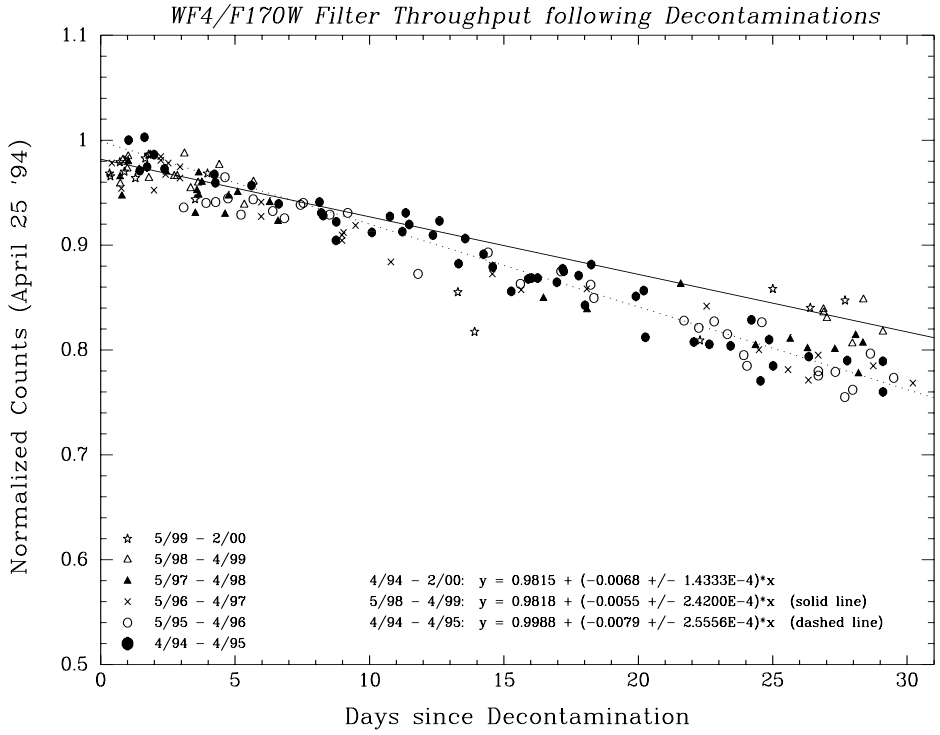

Figure 6.14: Change in Throughput vs. Time.[1]

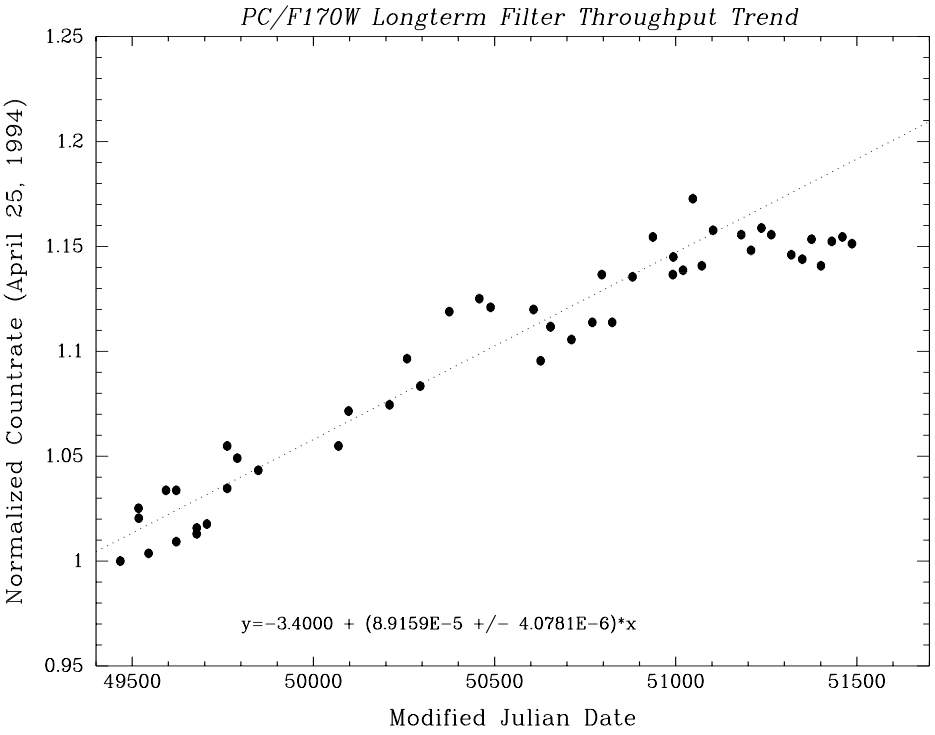

1. Only data taken 4 days or less after a decontamination are shown. Data taken 0 to 60 days after service missions are also excluded. The fit is to data prior to MJD 51100.

CHAPTER 7:

Observation Strategies

In this chapter . . .

7.1 Observing Faint Targets

For broad band filters the sky background will limit the detection of faint targets. For example, an 8-orbit observation in F555W gives a ~5σ detection limit at Johnson V=28.6 for an average sky level of 23 mag arcsec^{-2} in V. Note that the sky background is a strong function of position, especially for targets near the ecliptic; the sky level can vary from V=23.3 mag arcsec^{-2} at the ecliptic pole to about V=20.9 mag arcsec^{-2} on the ecliptic near the solar avoidance limit. (See Table 6.3 on page 160 for sky level as function of ecliptic coordinates.)

If these higher sky levels would severely impact the science data, observers should consider specifying the special requirement LOW-SKY on the Phase II proposal. This parameter forces the observation to be made when the sky background is within 30% of the minimum value for the target. Note, however, that this will also reduce the number of HST

calendar windows available to the observation, and so could result in scheduling delays or may even make the observation infeasible if there are other constraints such as ORIENTs. A minor decrease in the per-orbit visibility period also results from LOW-SKY, but for background limited programs this is a minor price to pay for the guarantee of a much lower background. In summary, LOW-SKY will reduce the sky background, but should only be used if the science goals *require* it.

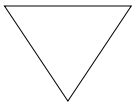

Note that LOW-SKY cannot be used for CVZ targets, as they imply mutually exclusive pointing constraints.

Scattering of bright Earth light in the OTA can produce non-uniformities in the background which may hamper analysis of faint target images. Most often these take the form of diagonal bars of suppressed background light in several of the CCDs. These effects tend to occur for broad band filters when the OTA axis is about 25˚ from the bright Earth. This effect is most often seen in observations of targets in the CVZ (continuous viewing zone), since the Earth limb is never very far from the OTA axis when observing in the CVZ. Figure 7.1 on page 197 shows a typical case. LOW-SKY will eliminate this effect for non-CVZ targets, as it places the OTA axis more than 40˚ from the bright Earth. Alternatively, one can place the target away from the CCD center to avoid these artifacts.

Another option for reducing the sky brightness, is the special requirement SHADOW, which forces the observation to be made when HST is in the Earth's shadow. This usually has a large negative impact on the observing efficiency, and is recommended only when observing far-UV emission lines (e.g. Ly α and OI 1304Å). Its primary goal is only to reduce geocoronal emission lines. Moreover, it does not attempt to minimize zodiacal emission, which dominates at visible wavelengths.

Figure 7.1: Example of Scattered Earth Light. Scattered light contributes ~100 e^- of background throughout this image. The camera spiders block some of this scattered light along CCD diagonals, hence forming "X" patterns and bars where the background is reduced by ~40% in this image.

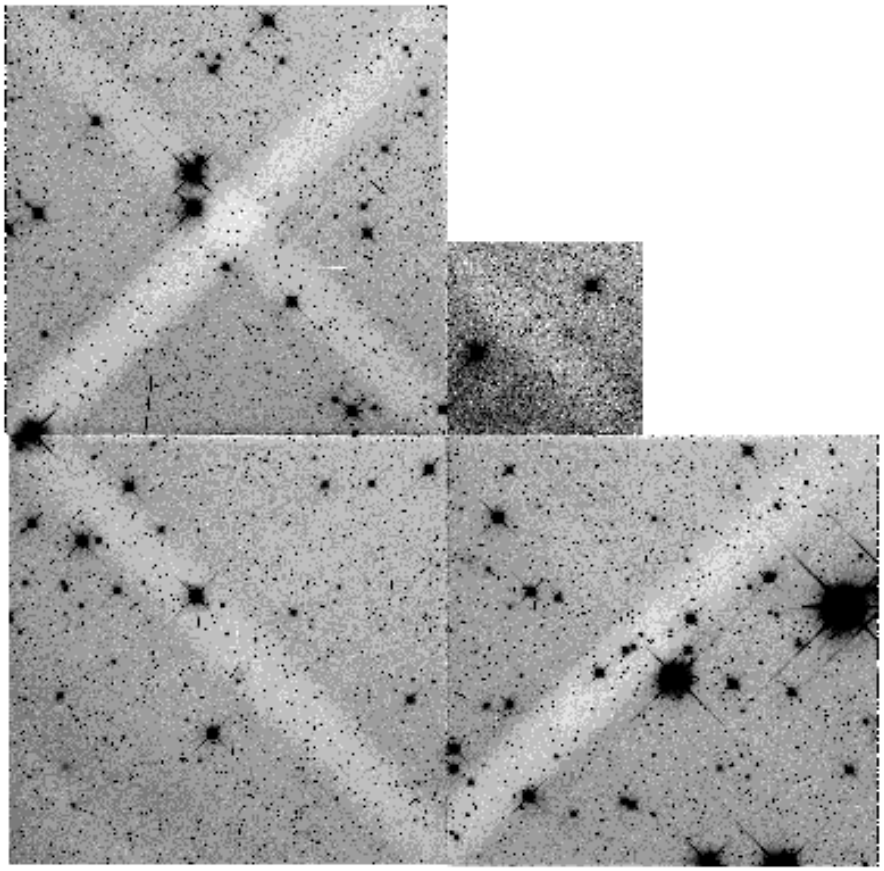

7.2 Observing Bright Targets

Saturation is the primary concern when observing bright targets. The analog-to-digital converter will run out of bit codes at ~28,000 e^- $pixel^{-1}$ in the ATD-GAIN=7 (default) setting, and at ~53,000 e^- $pixel^{-1}$ in the ATD-GAIN=15 setting. Count levels above these are merely reported as 4095 DN in the data. Hence ATD-GAIN=15 is recommended for targets approaching 28,000 e^- $pixel^{-1}$. The disadvantage of this setting is that the read noise is poorly sampled by this coarse digitization, and hence the read noise is slightly increased.

At count levels above ~90,000 e^- $pixel^{-1}$ charge will overflow the potential well of each pixel, and begin to bloom up and down the CCD columns. For example, this occurs in the F555W filter at about V=13.5 for a 10s exposure on the WFC, and at about V=13.0 on the PC1.

At very high count levels, above ~10^8 e^- per CCD column, the charge bloom will reach the top and bottom of the CCD and flow into the serial registers. CLOCKS=YES will dispose of this charge as it reaches the ends of the CCD, and thus prevent it from leaking back into adjacent CCD columns. This exposure level corresponds roughly to a 10s exposure of a V=7 star in F555W. Note that CLOCKS=YES offers no benefit unless the bloom reaches the ends of the CCD, and that it may slightly compromise the bias and dark calibration. Moreover, CLOCKS=YES will result in anomalous exposure times; exposure times are rounded to the nearest integral second, minus a delay time of up to 0.25s for the shutter to open. (See "Serial Clocks" on page 33 for further discussions about the use of CLOCKS=YES.)

Besides setting ATD-GAIN=15, the PC CCD can be used to reduce saturation effects for stellar objects. The peak of the PSF will be spread over more pixels on the PC (vs. WFC), so stars can be exposed about 50% longer on the PC before saturation sets in.

Note that the narrow band filters may be useful when observing very bright targets. For example, stars as bright as V~4.4 can be observed without saturation in F502N using the PC at ATD-GAIN=15 with a 0.11s exposure time.

7.3 Observing Faint Targets Near Bright Objects

The concerns here are similar to those for observing bright targets; saturation and blooming of the bright companion PSF must not impact the faint target. Also, one may need to consider subtracting the PSF of the bright object, and effects which limit the accuracy of that subtraction.

If the bright companion will saturate and bloom, it will be necessary to rotate the CCD so that blooming along the CCD columns does not obliterate the faint target. See Figure 7.9 on page 216 for an illustration of the bloom directions. It may also be useful to orient the field so that the OTA diffraction spikes from the bright companion (along diagonal lines on the CCDs) avoid the faint target. Table 7.1 on page 199 summarizes ORIENTs which can be used to avoid CCD blooming tracks and OTA diffraction spikes caused by bright objects. For example, if a faint companion is at PA 60° on the sky relative to a bright companion, it would be advantageous to observe on PC1 with ORIENT= PA + 45° = 105°. Ideally, some range in ORIENT would be specified to ease scheduling, hence "ORIENT=90D TO 120D" might be specified on the Phase II

proposal. Note that "ORIENT=270D TO 300D" is also feasible, and should be indicated in the visit level comments.

Table 7.1: ORIENTs for Avoiding Bloom Tracks and Diffraction Spikes. "PA" is the position angle of the faint target relative to the bright object. Note that ORIENT should be between 0D and 360D, so subtract 360°, if necessary. In the proposal these are specified as, e.g., "ORIENT=231D TO 261D".

CCD	ORIENT
PC1	PA+30° to PA+60°, PA+210° to PA+240°
WF2	PA+120° to PA+150°, PA+300° to PA+330°
WF3	PA+30° to PA+60°, PA+210° to PA+240°
WF4	PA+120° to PA+150°, PA+300° to PA+330°

If instead of observing a known companion, one is *searching* for companions, it is advisable to observe at several ORIENTs so that the CCD bloom track and OTA diffraction spikes will not hide possible companions. For example, three ORIENTs, each separated by 60°, would give good data at all possible companion position angles.

If PSF subtraction will be needed during data analysis, then the PC CCD may have some advantage, since it provides better sampling of fine undulations in the PSF. It may also be useful to obtain observations of a second bright star for PSF calibration, though these may be of limited utility since thermal effects and OTA "breathing" can modify the telescope focus, and hence the PSF, on time scales of less than one hour. Any such PSF star should be similar in color to the target, and should be observed at the same CCD position (within 1″) and with the same filter. Sub-pixel dithering may also be useful, so as to improve sampling of the PSF (see "Dithering with WFPC2" on page 208).

Figure 7.2 on page 200 illustrates the effect of OTA breathing, and periodic focus adjustments, on PSF subtraction. It shows the difference between an "in focus" PSF and one where the OTA secondary mirror has been moved by 5μm. This amount of focus change is comparable to the range of OTA "breathing" effects (time scale <1 hour), and the periodic (semi-annual) focus adjustments of the OTA. Each panel shows a different contrast setting; the percentages indicate the energy per pixel which is plotted as white, expressed as a fraction of the total (un-subtracted) PSF energy. For example, features which are just white in the "0.003%" panel contain 0.003% of the total PSF energy in each pixel. In other words, the feature labeled "a" is, in effect, ~10 magnitudes fainter than the PSF of the bright object, so that it may be very difficult to detect a "real" companion object ~10 magnitudes fainter than the bright object, at this distance from the bright object. In a real PSF subtraction situation, other effects including PSF sampling, noise, and pointing instability would further degrade the

subtraction. (The elongated appearance of the residuals in the PSF core is due to astigmatism in PC1).

Figure 7.2: Impact of OTA Focus Shift on PSF Subtraction. Each image shows the difference between an “in focus” and a 5 micron defocused PSF at different contrast settings. Numbers indicate the energy per pixel which is plotted as white, as a percentage of total energy in the un-subtracted PSF. Based on TinyTIM models for PC1 in F555W filter.

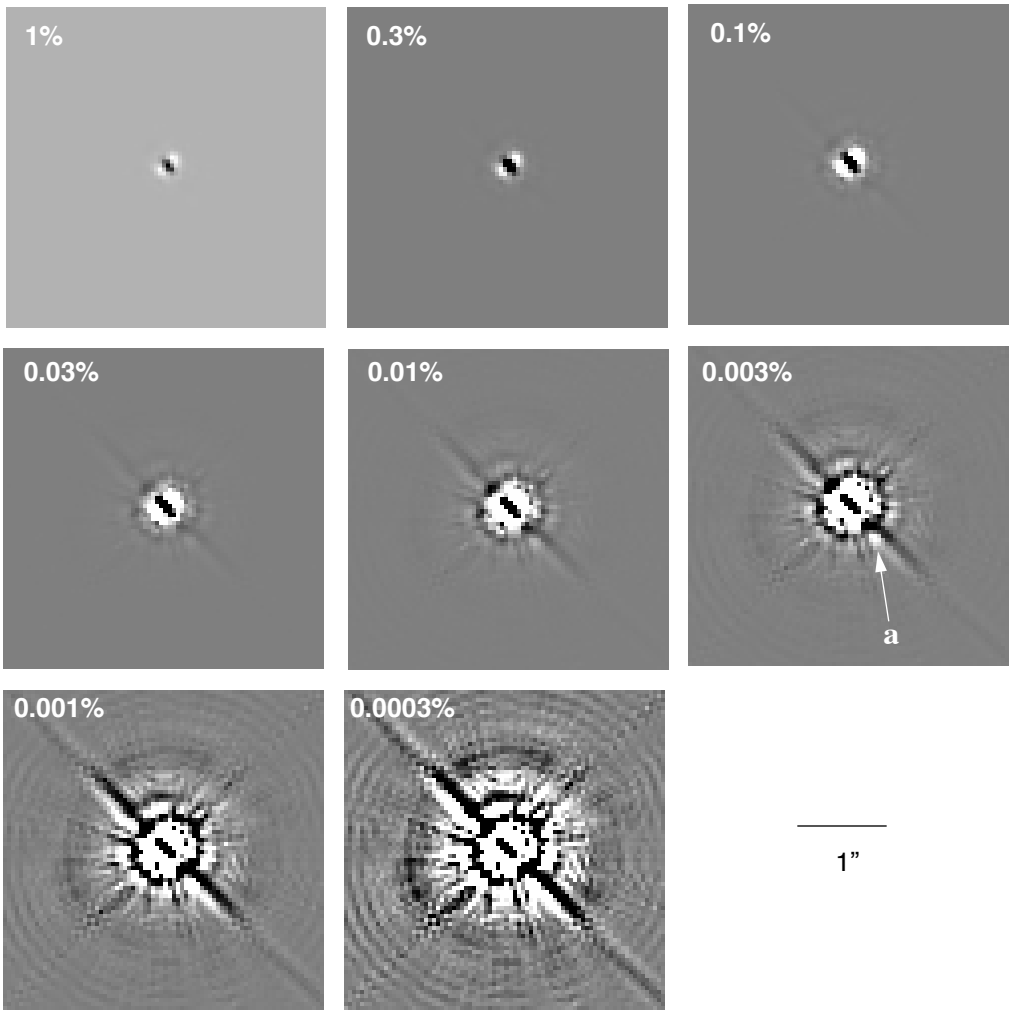

Table 7.2 on page 201 gives some quantitative indication of the performance expected for PSF subtractions in the high signal-to-noise limit. It gives the magnitude of “star-like” artifacts remaining in the subtracted image, as a function of distance from the bright object, and magnitude m_{bright} for the bright object. The right-most column gives an effective magnitude limit imposed by artifacts from the PSF subtraction. These results are derived for the 5μm focus shift described above, and are for PC1 and filter F555W. It may be possible to do somewhat better than these limits by subtracting accurate model PSFs, or by finding an observed PSF with matching focus.

Table 7.2: Approx. PSF Subtraction Artifact Magnitudes and Magnitude Limits.

Distance from Bright Object	Effective Magnitude of Subtraction Artifacts	Effective Faint Object Detection Limit (3σ)
0.1″	m_{bright}+4.7	m_{bright}+3.5
0.3″	m_{bright}+8.6	m_{bright}+7.4
1″	m_{bright}+11.4	m_{bright}+10.2
3″	m_{bright}+13.2	m_{bright}+12.0

Results indicate that PSF subtraction and detection of faint objects very close to bright objects can be improved by using a composite PSF from real data, especially dithered data. Table 7.3 on page 201 indicates limits that may be obtained for well-exposed sources (nominal S/N > 10 for the faint object) where a dithered PSF image has been obtained.

Table 7.3: Limiting Magnitudes for PSF Subtraction Near Bright Objects.

Separation in arcsec (on PC)	Limiting Δm (without PSF subtraction)	Limiting Δm (with PSF subtraction)
0.15	2.5	5.0
0.25	4.5	6.4
0.4	6.5	7.3
1.0	8.9	10.7
3.0	10.7	12.9

A technique that has been used with some success to search for nearby neighbors of bright stars is to image the source at two different roll angles, and use one observation as the model PSF for the other. In the difference image, the secondary source will appear as a positive residual at one position and a negative residual at a position separated by the change in roll angles. PSF artifacts generally do not depend on roll angle, but rather are fixed with respect to the telescope. Thus, small changes in the PSF between observations will not display the positive or negative signature of a true astrophysical object. Again, it is recommended that the observations at each roll angle be dithered.

Large angle scattering may also impact identification of very faint objects near very bright ones. This scattering appears to occur primarily in the camera relay optics, or in the CCD. Hence, if a faint target is more than ~10″ from a bright object (i.e. very highly saturated object), it would be advisable to place the bright object on a different CCD, so as to minimize large angle scattering in the camera containing the faint target. See the

section on “Large Angle Scattering” on page 140. Note also that highly saturated PSFs exist for PC1 in filters F439W, F555W, F675W, and F814W, and for F606W on WF3; these may be useful when attempting to subtract the large-angle scattered light. As of this writing TinyTIM does not accurately model the large angle scattering, and should be used with caution when analyzing highly saturated images (Krist 1996). To obtain available PSFs please visit the PSF Library page at:

http://www.stsci.edu/instruments/wfpc2/Wfpc2_psf/wfpc2-psf-form.html

It is generally unwise to place bright companions or other bright objects just outside the area imaged by the CCDs. The region of the focal plane just outside the CCDs (within about 6″ of the CCDs) contains a number of surfaces which can reflect light back onto the CCDs, hence placing bright targets there can have undesired results. Also, the un-imaged “L” shaped region surrounding PC1 should be avoided, since incomplete baffling of the relay optics allows out-of-focus images of objects in this region to fall on the CCDs. Figure 7.3 on page 202 illustrates various bright object avoidance regions near the WFPC2 field-of-view; the indicated avoidance magnitudes will produce 0.0016 e^{-} s^{-1} $pixel^{-1}$ in the stray light pattern for F555W. Figure 7.4 on page 203 and Figure 7.5 on page 204 show examples of artifacts which can result from bright stars near the PC1 CCD. The report “A Field Guide to WFPC2 Image Anomalies” (ISR WFPC2 95-06, available on the WFPC2 WWW pages and from (help@stsci.edu) gives more detailed discussions of artifacts associated with bright objects, and their avoidance.

Figure 7.3: Bright Object Avoidance Regions Near WFPC2 FOV.

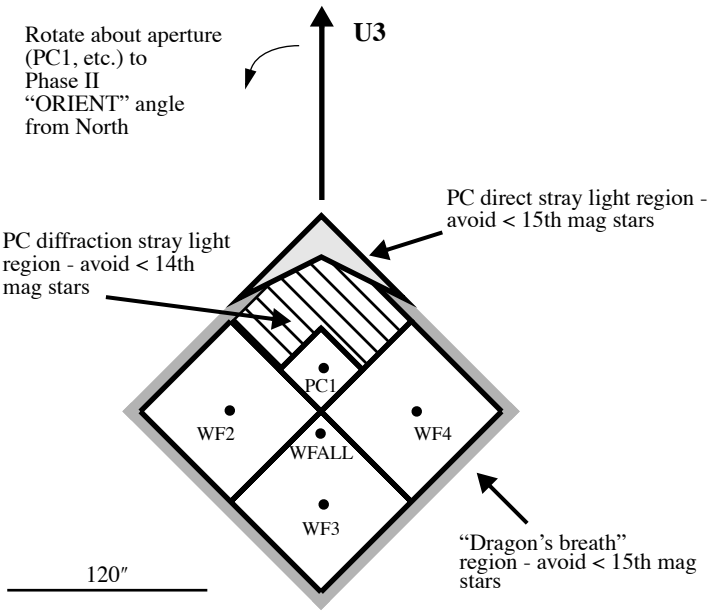

Figure 7.4: Example of PC1 “Direct” Stray Light Ghost.

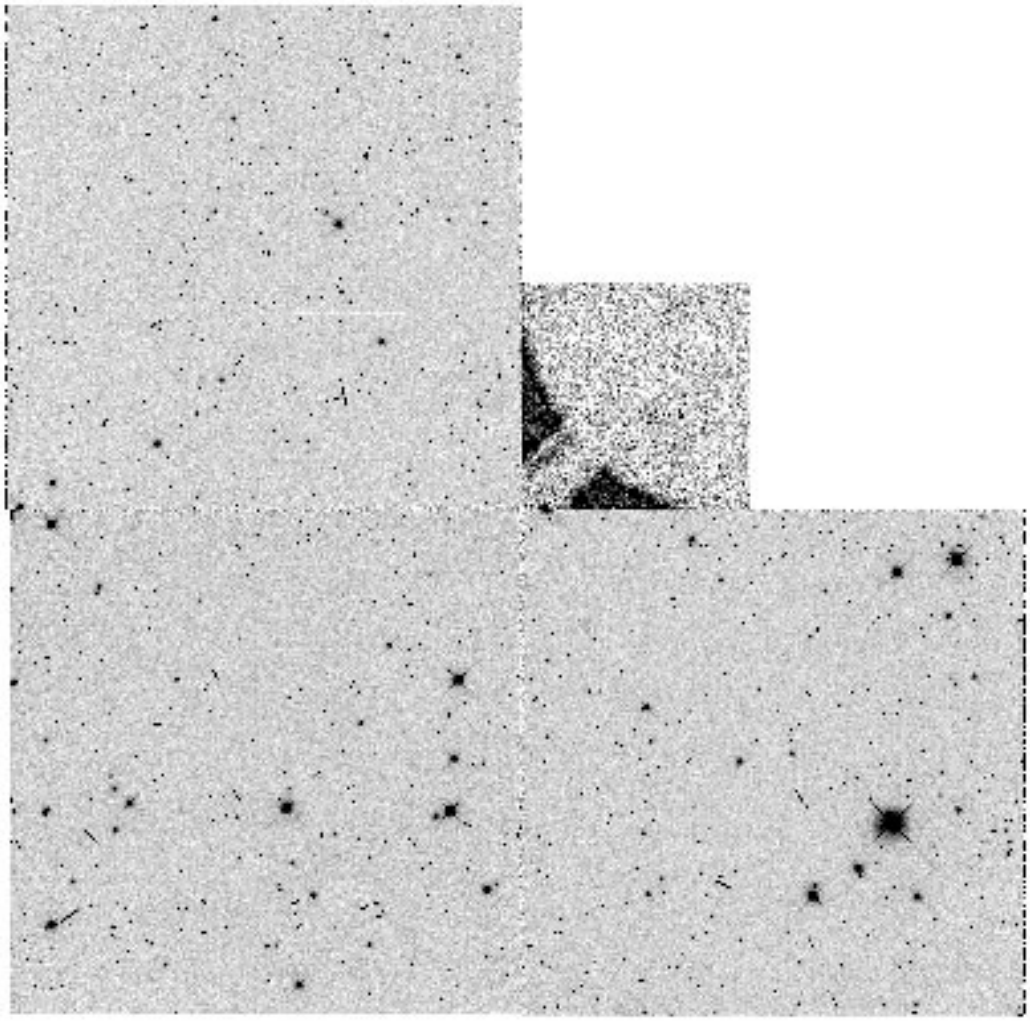

Figure 7.5: Example of PC1 “Diffraction” Stray Light Ghost.

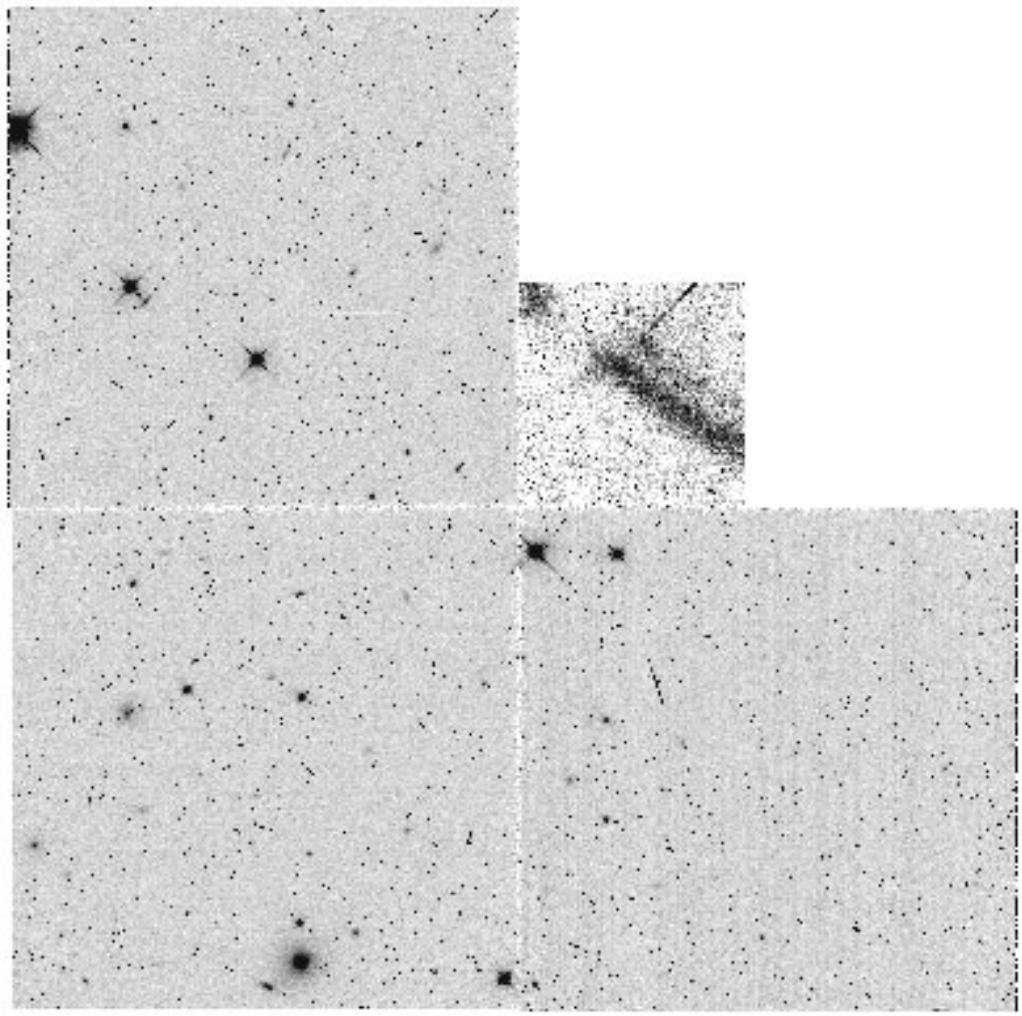

7.4 Cosmic Rays

Cosmic rays will obliterate ~20 pixels per second per CCD. It is imperative that two or more images be obtained at each pointing position, if these artifacts are to be removed from the data. The default action by the Phase II proposal processing software is to split exposures longer than 600s into two nearly equal parts, so as to allow removal of the cosmic ray tracks. The CR-SPLIT and CR-TOLERANCE optional parameters on the Phase II proposal allow observers to adjust this behavior. CR-SPLIT can be set to either DEF (default), NO, or a numeric value (0.0 to 1.0) giving the fraction of the total exposure allotted to the first sub-exposure of the pair. CR-TOLERANCE indicates the spread allowed in dividing the exposure,

as a fraction of the total exposure time. For example, the default CR-TOLERANCE=0.2 allows the first sub-exposure to range from 0.3 to 0.7 of the total exposure. Setting CR-TOLERANCE=0 will force equal-length sub-exposures.

The required degree of cosmic-ray avoidance will depend on the science goals of the proposal; observations of a single small target will usually suffer much less impact from cosmic rays than programs needing very "clean" data over a large area. Table 7.4 on page 205 gives very rough recommendations for the number of sub-exposures for a given total exposure time. Note that splitting into *many* sub-exposures introduces additional overhead time and will increase the noise for "read noise" limited exposures (usually exposures in UV or narrow band filters), and hence one should not use more sub-exposures than are truly required by the science goals.

Table 7.4: Recommended Exposure Splittings.

Total Exposure Time (s)	Rough Recommended Number of Sub-exposures	
	Programs with Single Small Target	Wide-area Search Programs
<300	1	3
300 - 600	1 or 2	4
600 - 1600	2 or 3	4
1600 - 5000	3	5
5000 - 10000	4	6
>10000	One exposure per orbit (2400s each)	

7.5 Choosing Exposure Times

The choice of exposure time generally depends on the signal-to-noise ratio required to meet the science goals. This can be assessed using information in Chapter 6 or plots in Appendix B herein, or by using the on-line WWW Exposure Time Calculator tool.

However, when packing orbits, one must often compromise somewhat and decide which exposures to lengthen or shorten. Table 7.5 on page 207 may be helpful in this regard. It shows the total time required to execute a single CR-SPLIT=NO exposure, *excluding* any time needed to change filters.

Note that the most efficient exposure times are those whose length approaches or equals, but does not exceed, an integral number of minutes

plus 40s. Figure 7.6 on page 206 illustrates event timings during a typical 60s WFPC2 exposure, similarly, Figure 7.7 on page 206 illustrates events during a (more efficient) 100s exposure. (See "Overhead Times" on page 35 for more information about exposure timings).

Figure 7.6: Event Timings During a 60s WFPC2 Exposure. All events, except shutter opening, start on 1 minute spacecraft clock pulses. Both the CCD clear and readout of each CCD require 13.6s. This 60s exposure, including the filter change, requires 4 minutes.)

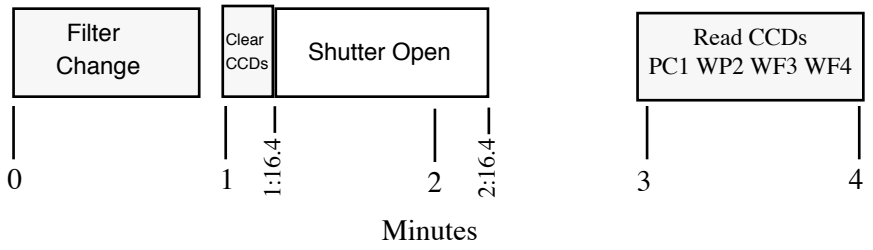

Figure 7.7: Event Timings During a 100s WFPC2 Exposure. This exposure, including the filter change, requires 4 minutes.

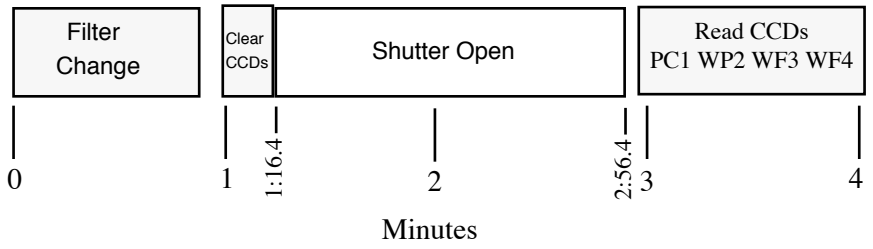

Due to the various overheads, shortening or lengthening an exposure can have unexpected effects on the orbit packing. For example, shortening an exposure from 400s to 350s has no effect on orbit packing; they both require 9 minutes to execute (CLOCKS=NO, the default setting). On the other hand, shortening an exposure from 180s to 160s trims the execution time by 2 minutes (again CLOCKS=NO, the default setting).

CLOCKS=YES may have some advantage in a long series of exposures whose lengths are 180s or somewhat greater. Each savings of 1 minute can add up to a few more exposures per orbit. The down side is that most calibrations are derived for exposures with CLOCKS=NO, so the calibration may be slightly compromised. The largest calibration error is expected to occur in the dark current, where there may be a slight increase near the top and bottom of each CCD. In many situations this error may be acceptable, such as a small target near a CCD center, or broad band filter images where the sky completely dominates the dark current. CLOCKS=YES will have more impact on calibration of narrow filters, or situations requiring an extremely flat background. (Also, see "Serial Clocks" on page 33 for discussion of exposure time anomalies associated

with CLOCKS=YES, though these are most important for exposures <30s.)

An exposure with CR-SPLIT=YES would simply require the total time for each sub-exposure as given by Table 7.5 on page 207, again, plus any time needed to change filter before the first exposure. However, the default CR-SPLITting allows schedulers some latitude in dividing the exposures (CR-TOLERANCE=0.2 is the default) so the exact overheads are unpredictable. For example, a 700s exposure with CR-SPLIT=0.5 (the default) could be split into a pair of 350s exposures totaling 18 minutes, or a 300s and 400s exposure totaling 17 minutes.

Table 7.5: Basic Time to Execute Single Non-CR-SPLIT Exposure. This includes time to prep the CCD, execute the exposure, and read out the CCDs. Times needed to change filter (1 minute), or insert a second filter (1 minute), are *excluded*. See "Overhead Times" on page 35 for more discussion and other overheads.

Exposure Time (s)	Total Execution Time (min.)	
	CLOCKS=NO (default)	CLOCKS=YES
0.11 to 30	2	(not recommended)
35, 40	2	2
50,60,70,80,100	3	3
120,140,160	4	4
180,200	6	5
230,260	7	6
300	8	7
350,400	9	8
500	11	10
600	13	12
700	14	13
800	16	15
900	18	17
1000	19	18
1100	21	20
1200	23	22

7.6 Dithering with WFPC2

Dithering is the technique of displacing the telescope between observations either on integral pixel scales (to assist in removing chip blemishes such as hot pixels) or on sub-pixel scales (to improve sampling and thus produce a higher-quality final image). Here we briefly discuss observation and data analysis for dithered data.

7.6.1 Dither Strategies

There is no single observing strategy that is entirely satisfactory in all circumstances for WFPC2. One must consider cosmic rays, hot pixels (i.e. pixels with high, time variable dark count), spatial undersampling of the image, and large-scale irregularities such as the few arcsecond wide region where the CCDs adjoin. One strategy that can be used to minimize the effects of undersampling and to reduce the effects of hot pixels and imperfect flat fields is to dither, that is, to offset the telescope by either integer-pixel or sub-pixel steps. The best choice for the number and size of the dithers depends on the amount of time available and the goals of the project. In the following we will address a few issues related to dithering:

1. **Undersampling:** Individual images taken with ***sub-pixel*** offsets can be combined to form an image with higher spatial resolution than that of the original images. A single dither from the original pixel position -- call it (0,0) -- to one offset by half a pixel in both x and y, (0.5,0.5) will produce a substantial gain in spatial information. On the other hand very little extra information is gained from obtaining more than four positions, if the standard four point dither is used, and if the telescope has successfully executed the dither. Therefore the recommended number of sub-pixel dither positions is between 2 and 4.

2. **Hot Pixels:** There are three ways to deal with hot pixels: correct them by using "dark frames" that bracket the observation, dither by an ***integer*** amount of pixels, or use a task such as "WARMPIX" within STSDAS to filter out the known hot pixels. Note that the integer dither strategy would ideally use six images, i.e. two CR-SPLIT images at each of three different dither positions. This is because in addition to hot pixels, low or "cold" pixels[1] can be present and simple strategies selecting the minimum of two pixel values can fail. However, even four images (two each at two dither positions) will greatly aid in eliminating hot pixel artifacts.

1. Cold pixels usually result from hot pixels in the dark calibration file which do not actually appear in the science data.

3. **Cosmic Rays:** Although dithering naturally provides many images of the same field, it is better to take several images at each single pointing in order to remove cosmic rays. The dither package (see further below) has been developed to allow cosmic ray removal from dithered data. This, for example, might allow single images at each pointing, which will be important if observing time is quite limited (e.g. less than one orbit). This capability has now been tested and appears to work fairly well. For effective cosmic ray removal we generally recommend obtaining a minimum of three to four images, and preferably more if practical. For very long integrations it is convenient to split the exposure into *more than two separate images*. As an example, for two 1500s exposures, about 1500 pixels per chip will be hit in both images and will therefore be unrecoverable. However, dividing the same observation into 3x1000s results in only about 20 pixels on each chip that would be hit by cosmic rays in all three exposures. Moreover, since CR events typically affect 7 pixels per event, these pixels will not be independently placed, but rather will frequently be adjacent to other unrecoverable pixels.

4. **Accuracy of dithering**: The telescope pointing accuracy is typically better than 10 mas, but on occasion can deviate by much more, depending on the quality of the guide stars. For example, during the Hubble Deep Field, nearly all dithers were placed to within 10 mas (during ±1.3″ offsets and returns separated by multiple days), although in a few cases the dither was off by more than 25 mas, and on one occasion (out of 107 reacquisitions) the telescope locked on a secondary FGS peak causing the pointing to be off by approximately 1″ as well as a field rotation of about 8 arcminutes. The STSDAS "drizzle" software (initially developed by Fruchter and Hook for the Hubble Deep Field, and now used generally for many other programs) is able to reconstruct images even for these non-optimal dithers, still gaining in resolution over non-dithered data.

The recommended way to schedule dithers is to specify dither patterns WFPC2-LINE (e.g. for two-point diagonal dithers) or WFPC2-BOX (for four-point dithers). An alternative approach is to use POS TARGs. Note that when the WF3 is specified as an aperture, the POS TARG axes run exactly along the WF3 rows and columns. For the other chips, they only run approximately along the rows and columns due to the small amount of rotation between CCDs. For small dithers (less than a few pixels) these rotations are unimportant.

Some specific offsets allow one to shift by convenient amounts both the PC and the WFC chips. For instance an offset of 0.5″ is equivalent to 5 WFC pixels and 11 PC pixels. Likewise, the default WFPC2-LINE spacing of 0.3535″ along the diagonal is equivalent to shifts of (2.5,2.5) pixels for the WFC and (5.5,5.5) pixels for the PC.

Dithers larger than a few pixels will incur errors due to the camera geometric distortion which increases toward the CCD corners and alters the image scale by about 2% at the corners. Hence a 1.993″ offset will be 20.3 WF pixels at the field center, but suffer a 0.4 pixel error at the CCD corners. Large dithers may also occasionally require a different set of guide stars for each pointing, thus greatly reducing the expected pointing accuracy (accuracy only ~1″ due to guide star catalogue).

The most up-to-date information about dither strategies and related issues can be found on the general WFPC2 dither web page:

http://www.stsci.edu/instruments/wfpc2/dither.html

7.6.2 Analysis of Dithered Data

The software we recommend for combining dithered data is known as "MultiDrizzle" (Koekemoer, et al. 2002), which is based on the "drizzle" program (Fruchter and Hook 2002). This method has been incorporated into the IRAF/STSDAS **dither** package, and allows effective cosmic ray removal from dithered data.

In order to help users reduce dithered images, we have prepared the *HST Dither Handbook* (Koekemoer et al. 2002), available from the above WFPC2 dither web site. This document gives a general outline of the reduction of dithered images and provides step-by-step instructions for six real-life examples that cover a range of characteristics users might encounter in their observations. The data and scripts needed to reproduce the examples are also available via the same URL. (This handbook expands upon the original *Drizzling Cookbook* by Gonzaga et al. 1998.)

Despite all the improvements in the combination of dithered images, users should be mindful of the following cautionary notes:

- Processing singly dithered images can require substantially more work (and more CPU cycles) than processing data with a number of images per pointing.
- Removing cosmic rays from singly dithered WFPC2 data requires good sub-pixel sampling; therefore one should probably not consider attempting this method with WFPC2 using fewer than four images and preferably no fewer than six to eight if the exposures are longer than a few minutes and thus subject to significant cosmic ray flux.
- It is particularly difficult to correct stellar images for cosmic rays, due to the undersampling of the WFPC2 (particularly in the WF images). Therefore, in cases where stellar photometry better than a few percent is required, the user should take CR-split images, or be prepared to use the combined image only to find sources, and then extract the photometry from the individual images, rejecting entire stars where cosmic ray contamination has occurred.

Figure 7.8: On the left, a single 2400s F814W WF2 image taken from the HST archive. On the right, the drizzled combination of twelve such images, each taken at a different dither position.

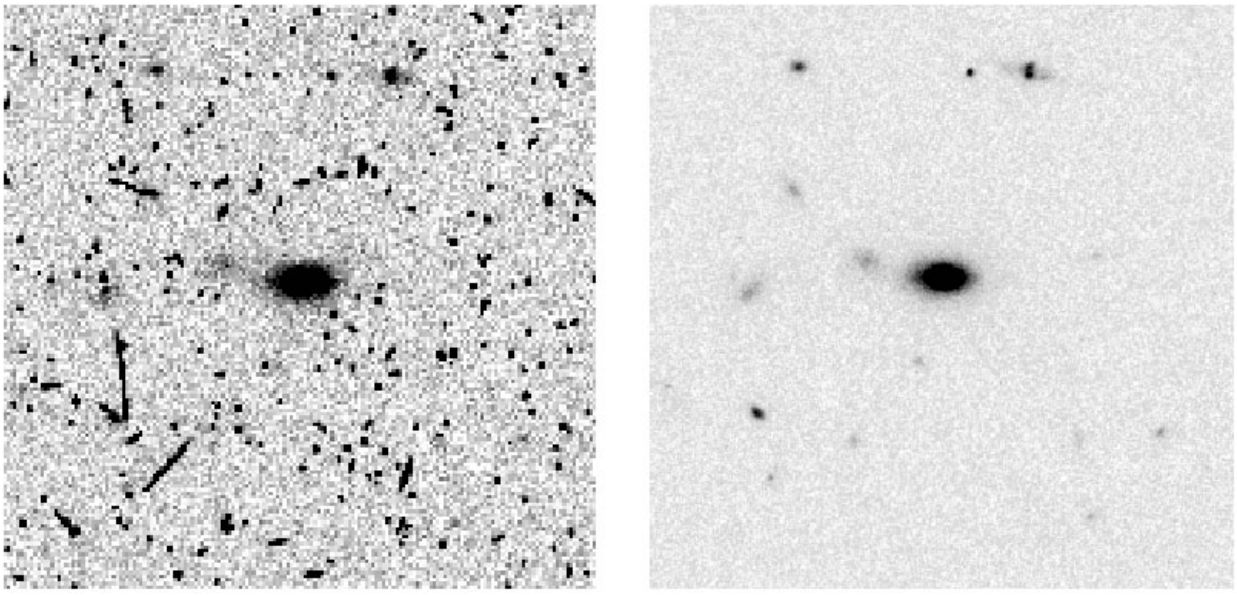

- Offsets between dithered images must be determined accurately. The jitter files, which contain guiding information, cannot always be relied upon to provide accurate shifts. Therefore, the images should be deep enough for the offsets to be measured directly from the images themselves (typically via cross-correlation). In many cases, the observer would be wise to consider taking at least two images per dither position to allow a first-pass removal of cosmic rays for position determination.
- Finally, and perhaps most importantly, dithering will provide little additional spatial information unless the objects under investigation will have a signal-to-noise per pixel of at least a few at each dither position. In cases where the signal-to-noise of the image will be low, one need only dither enough to remove detector defects.

7.7 Pointing Accuracy

Some WFPC2 programs have critical target positioning constraints (i.e. the target must be as close as possible to a specified aperture). A sure way to meet such requirements is to include an interactive acquisition. However, INT ACQs are costly in terms of allotted orbits. A variation of the Reuse Target Offset (RTO) capability can be used to acquire and position a target in the WFPC2 FOV. However, the user must request an additional orbit for the acquisition. The first orbit is used for the acquisition and the second orbit for the science observations.

7.7.1 Absolute Pointing Accuracy

We have looked carefully at a sequence of images to assess the absolute pointing performance that HST delivers to WFPC2. The apertures used in the observations studied were either PC1, PC1-FIX, or WF2. The observed positions of stars on WFPC2 images were measured and compared with the proposed coordinates and apertures. Where necessary, coordinate and proper motion errors were accounted for (with the assumption that SAO catalog coordinates are exact - they form the astrometric basis for the guide star coordinate system). The typical residual pointing error is 0.86″, with 1.84″ being the largest error seen. This study did bring out several easy-to-make target coordinate errors (which we corrected in the analysis, but which frequently dominated the pointing error), so we discuss these first.

In a number of cases studied, the proposal coordinates were from the printed version of the Yale Bright Star Catalog. One problem is that the equinox 2000 positions in the BSC are given in the FK4 (Besselian) reference system. The proposal system assumes that equinox 2000 and later coordinates are in the FK5 (Julian) reference frame, and that earlier ones are in the FK4 frame. This can be overridden by specifying B2000 instead of J2000 for the equinox in the proposal. The latest digital version of the BSC (BSC5) is in J2000. The 1950 edition of the SAO catalog is in B1950 (FK4), and a digital version is available for J2000 (FK5). An error of up to 1.5″ can result from assuming BSC positions are J2000 instead of B2000 in the proposal.

Another common problem with target coordinates is that they lack precision. For example, in the BSC, RA is given to the nearest 0.1^s and DEC to the nearest arcsecond. This can cause an error of up to 0.75″ in RA and 0.5″ in DEC. The SAO coordinates have higher precision, 0.001^s in RA and 0.01″ in DEC, and should be used when possible.

A common error source is not specifying proper motion or specifying it in the wrong units. It is critical to follow the latest version of the proposal

instructions on this. Even small proper motions are significant at the resolution of HST images.

Residual pointing errors (after coordinate errors and aperture location changes) range from 0.26″ to 1.84″. The average is 0.93″ and the median is 0.86″. There are no obvious trends in any coordinate system. These are errors which cannot be accounted for by a proposer, being due to guide star position errors, FGS alignment uncertainties, and residual aperture location errors. Using Guide Star Catalog positions may help reduce the error between target and guide stars. Most of the targets used in this study were too bright to have true Guide Star Catalog positions.

In summary, a target with good coordinates (and proper motion) referenced to the SAO catalog can typically be placed within 0.9″ of a specified aperture. However, errors of around 1.5″ occasionally happen.

7.7.2 Updates to Aperture / Coordinate Systems

On 11 April, 1994, an update was made to the spacecraft database which tells HST where to place targets relative to the FGSs. This update affected both the location of targets in the WFPC2 field-of-view, and the position reference frame in the image headers. The nominal (or intended) pixel locations of the apertures in the WFPC2 focal plane did not change. Only the (V2,V3) coordinates of the apertures changed, as their locations relative to the FGSs became better known. For example, PC1 and PC1-FIX are designated to be at pixel (420,424.5). Before April 1994, this aperture was thought to be at (V2,V3) =(4.95″,-30.77″), which, using the most current information, was actually located at pixel (X,Y) = (459.8,377.3). Since April 1994, the aperture in the spacecraft's database has been at (V2,V3) = (1.87″,-30.96″) or, assuming the current best estimate is exactly correct, at (X,Y) = (414.9,428.1). Thus, for the same coordinates and aperture, the pixel position of a target in an image taken before April 1994, could be nearly 3″ different from its position in later images, due to aperture updates. Similar corrections apply to all WFPC2 data taken before this date.

This update also affects the position information placed in the image headers, which maps sky coordinates onto each individual CCD. Observations taken before April 11, 1994, have preliminary plate scales, rotations, and reference pixel locations in their image headers. Thus, the sky coordinates associated with a given pixel will be different for otherwise identical images taken before and after April 11, 1994, due to improvements in the aperture locations. The change is primarily an approximate 3″ shift, as well as a small rotation. There is a 0.8˚ rotation for WF2, and smaller rotations for the other chips (0.28˚ in PC1, 0.46˚ in WF3, and 0.06˚ in WF4). We note that the On-The-Fly Calibration System initiated in 2000 does not correct for these offsets, since the pointing information is set upstream of the pipeline calibration; the On-The-Fly

Reprocessing System installed in May 2001 does, however, correct the pointing offsets.

The STSDAS tasks METRIC/INVMETRIC and WMOSAIC use this header information; hence, images taken before April 11, 1994, required header updates in order for these tasks to produce optimum results. In this situation, observers were advised to run the STSDAS task UCHCOORD, to update the headers, prior to running METRIC/INVMETRIC and/or WMOSAIC.

The On-The-Fly Calibration System (OTFC), in place from Dec. 1999 to May 2001, did not correct for these offsets. Observers submitting requests to the archive prior to May 16, 2001 received data processed through OTFC; this data would benefit from running UCHCOORD.

As of May 16, 2001, however, the On-The-Fly Reprocessing System (OTFR) is in place and OTFR data does contain the most up-to-date header information.

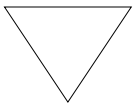

UCHCOORD should not be run on OTFR data.

OTFR data can be identified by the presence of the keyword PROCTIME in the header. Please see "On-The-Fly Reprocessing Systems" on page 231 for more details on OTFC, OTFR, and the use of UCHCOORD.

We also note, that in April and May 1996, two updates were made to the (V2,V3) coordinate system. This update should not affect observers. The purpose was to remove a slow drift in the position of WFPC2 in the HST focal plane; the largest change was 0.6″. (See Table 3.15 on page 75 for details.) An additional update of 0.2″ was made on December 1, 1997. All the apertures are now thought to be correct to within 0.3″, and future updates should be small. Please also see the section on the "ORIENT Anomaly" on page 219.

7.7.3 Pointing Repeatability

The Hubble Deep Field (HDF) afforded an opportunity to study the repeatability of pointing over many images and acquisitions of the same field. The pointing appears to have been stable to better than 5 mas accuracy while taking many images of the same field without interruption over several orbits. The accuracy for full-up acquisition of the same field after slewing to other targets appeared to be ~10 mas typically, with occasional 20 mas errors seen. However, a few large errors were seen; in about 1 in 100 acquisitions the FGSs locked-up incorrectly resulting in a ~1″ error.

Other programs report similar 3 mas pointing accuracy if simple re-acquisitions are done between orbits. Approximately once per day a "full-up" acquisition is usually required (for engineering reasons) where the dominant FGS is fixed in position, but the sub-dominant FGS performs a spiral search for the guidestar and tracks wherever the star is found. On rare occasion these full-up acquisitions produce position errors of several hundred mas, and field rotations of up to ~0.1˚, relative to previous images of the same field. This may impact long sequences of exposures requiring half a day or more to execute.

7.7.4 Tracking Modes

Two guiding modes are available: Gyro Hold, and Fine Lock. Fine Lock (PCS MODE FINE) is used by default, since use of Coarse Track may be harmful to the Fine Guidance Sensors. Use of Gyro Hold (PCS MODE GYRO) is not generally recommended, even for snapshot (SNAP) observations, since the pointing accuracy is only 14″. Also the drift rate is 0.0014″ s^{-1} so exposures >100s can result in smeared images. However, if the reduced pointing accuracy can be tolerated, and the exposures are only a few seconds or less, Gyro Hold can give a significant savings in the target acquisition overhead time.

7.8 CCD Position and Orientation on Sky

During observation the target is placed at the aperture (PC1, WF2, WFALL, etc.) specified on the Phase II proposal. Locations of the principal apertures are shown in Figure 7.9 on page 216 (Table 3.14 on page 74 gives a complete list of apertures; the (V2,V3) system here is post 1996 day 127).

The POS TARG special requirement can be used when a position offset is needed. The target is positioned with offset "POS TARG x,y", measured in arcseconds, from the specified aperture. The approximate directions (within 1˚) of the POS TARG offsets are shown in Figure 7.9 on page 216. The exact directions of the offsets are parallel to the rows and columns of the CCD on which the aperture is specified. There are small rotations (few tenths of a degree) between the CCDs. (For detailed information see "Dithering: Relationship Between POS TARGs and CCD Rows/Columns" obtainable from the WFPC2 WWW pages or help@stsci.edu.)

It is often useful to explicitly specify the desired rotation of the WFPC2 field-of-view on the sky. This is specified in the Phase II proposal using the ORIENT special requirement. It is defined as the PA (measured from North through East) of the +U3 axis on the sky. Figure 7.9 on page 216 shows the CCD orientation and aperture locations relative to the U3 axis.

Figure 7.9: ORIENT Definition, Aperture Positions, and CCD Alignments. “FIX” apertures are in same locations, unless otherwise indicated. Dashed lines show vignetted regions along CCD boundaries. Short lines and “X”s in outer CCD corners indicate directions of bloom and OTA diffraction spikes, respectively. Origin of the (V2, V3) system is at the origin of the plot axes, with V2 and V3 exactly along diagonal lines as marked. POS TARGs are offsets measured from the aperture specified on the proposal (PC1, WF2, WFALL, etc.); their directions are as indicated. CCDs have pixel (1,1) where the four CCDs overlap.

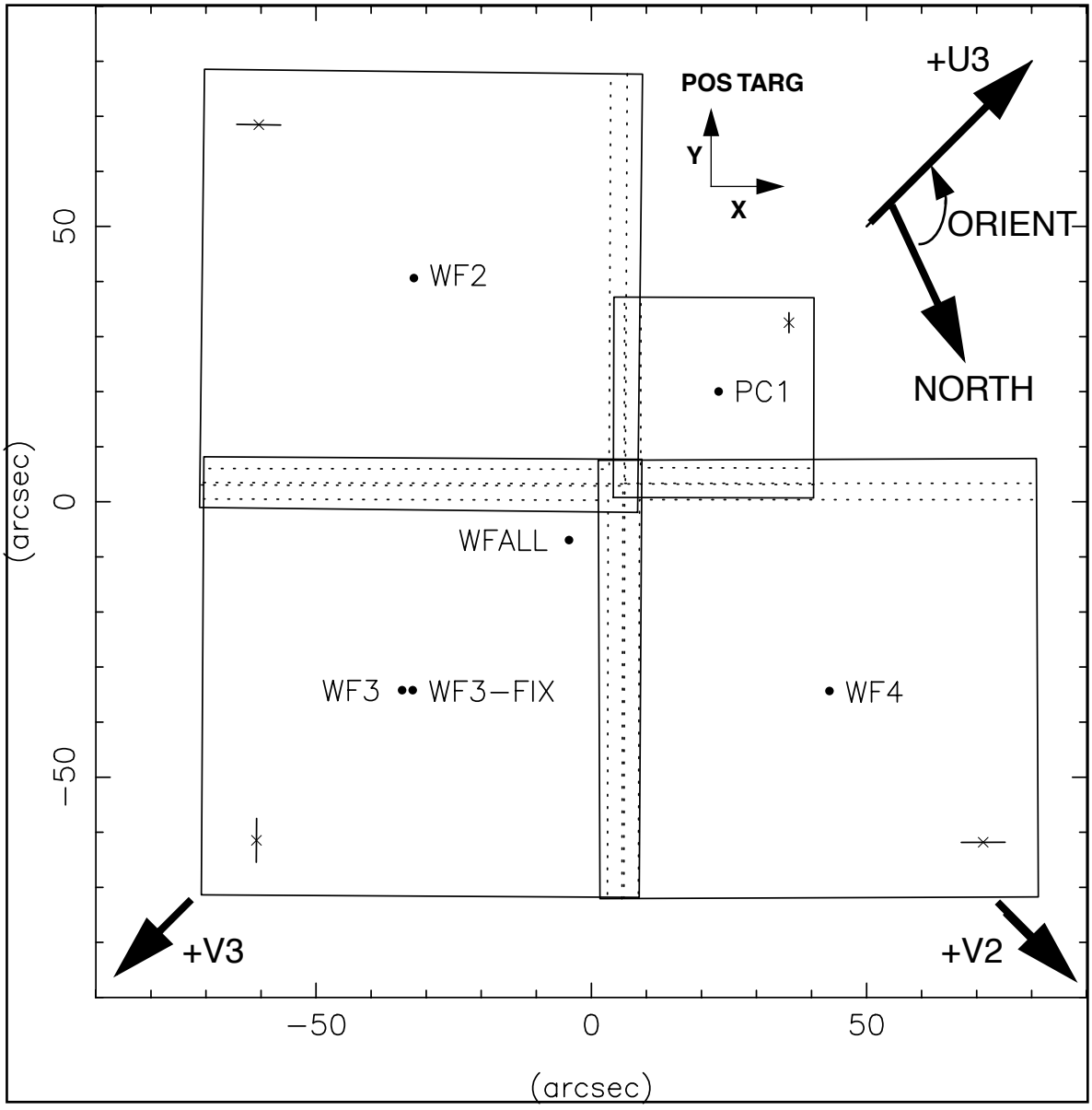

ORIENT is defined as the Position Angle of the +U3 Axis on the Sky.

In effect, the sequence of events is to first move the target to the desired aperture, then offset by any specified POS TARG from the aperture, and finally to rotate the target “in place” on the CCDs to the desired ORIENT.

Observers should try to specify all possible ORIENTs which would give the desired data, since having a range of values, or several ranges, will make the observation much easier to schedule. Often two ORIENTs separated by 180˚ will both give useful data. Sometimes ORIENTs separated by 90˚ will also give similar data.

The ORIENT for any observation can be computed as follows:

1. Obtain the Position Angle (PA) of the source axis on the sky, measured in the standard way, North through East.
2. Look at Figure 7.9 on page 216 and decide what angle you want, measured clockwise, from the +U3 axis to the source axis.
3. Sum the angles in steps 1 and 2.
4. ORIENT must be between 0˚ and 360˚, so subtract 360˚, if necessary. The result is the ORIENT you should specify on the proposal.

Another way to select the ORIENT, is to place Figure 7.9 on page 216 on an image of the target, shift and rotate to get the desired alignment, and then simply measure the position angle of the +U3 axis relative to North.

Note that the +V3 axis is quite different from the +U3 axis. They are exactly parallel, but oppositely directed. The +U3 axis is used for specifying orientation (ORIENT) in the proposal, while the +V3 axis is used in the data headers to indicate field orientation. Data header keyword PA_V3 gives the position angle of the +V3 axis on the sky.

We now give two examples of how the POS TARG and ORIENT special requirements might be used. The first example (Figure 7.10 on page 218) shows placement of a 100″ long jet along the CCD diagonals in PC1 and WF3 (i.e. along the -U3 direction). The coordinates of the nucleus are given on the proposal. Aperture PC1 together with POS TARG +10, +10 are used to place the nucleus near the outer corner of PC1. We want to rotate the WFPC2 field-of-view about the nucleus so the jet is diagonal on PC1 and WF3. We can thus compute the desired orientation as

```
ORIENT = (source PA on sky)
+ (desired source angle in field-of-view measured CW from
+U3 axis)
= 290˚ + 180˚ = 470˚ - 360˚ = 110˚
```

On the Phase II proposal we would allow some range in the angle (to ease scheduling), hence “ORIENT 105D TO 115D” might be specified.

Figure 7.10: Example of ORIENT and POS TARG Selection. (A) A jet at PA=290° is observed using PC1 and WF3; the position of the nucleus is used for the target position. (B) The aperture is specified as "PC1" and the nucleus is placed near the outer corner of PC1 using "POS TARG +10,+10." To place the jet across PC1 and WF3 "ORIENT 105D TO 115D" is specified.

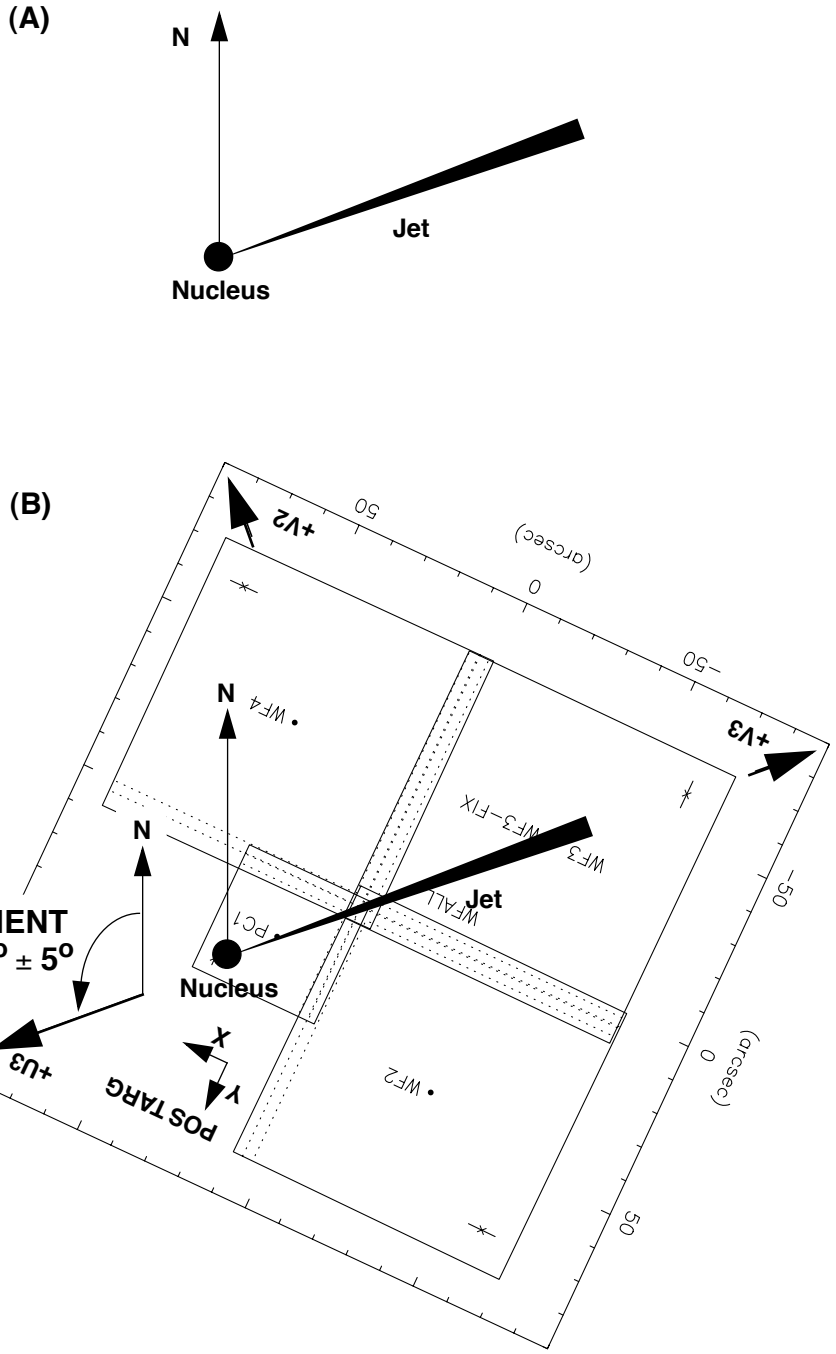

The second example (Figure 7.11 on page 220) shows placement of a galaxy across WF2 and WF3, with the nucleus on WF3 safely away from

the vignetted region. Aperture WF3 together with POS TARG +20, 0 is used to place the nucleus near the outer edge of WF3. We want to rotate the WFPC2 field-of-view about the nucleus so the galaxy's major axis is across WF2 and WF3. We can thus compute the desired orientation as

```
ORIENT = (source PA on sky)
+ (desired source angle in field-of-view measured CW from
+U3 axis)
= 60° + 315° = 375° - 360° = 15°
```

On the Phase II proposal we would again allow some range in the angle (to ease scheduling), hence "ORIENT 5D TO 25D" would be specified. Note that "ORIENT 185D TO 205D" is also feasible, and should be indicated in the visit level comments. Note also, that WF3 and WF4 could be used with either "ORIENT 95D TO 115D" or "ORIENT 275D TO 295D".

7.8.1 Software to Aid ORIENT Selection

The Visual Target Tuner (VTT) allows observers to select ORIENTs via a graphical user interface. The VTT will display Digitized Sky Survey images, NASA/IPAC Extragalactic Database (NED) images, HST images, or other suitable FITS images. It will then superpose HST instrument apertures and allow observers to manipulate their ORIENT and position. For more information see http://apt.stsci.edu/vtt/.

7.8.2 ORIENT Anomaly

We note that a minor anomaly was discovered in the data header values pertaining to image orientation (i.e. rotation about the target aperture) for data taken prior to September 15, 1997. Specifically the header keywords PA_V3 and ORIENTAT were affected. During long visits their values were incremented by up to 0.05 degree per hour whenever the telescope pointing was changed, when in fact these header values should have remained fixed. Observers requiring highly accurate image orientations should check values in the so-called jitter files (*jit.fits and *jif.fits), which were not affected by the bug. Data extracted from the HST archive using the On-The-Fly Reprocessing system implemented in mid-2001 is automatically corrected for this problem.

Figure 7.11: Example of ORIENT and POS TARG Selection. (A) A galaxy with major axis at PA=60° is to be placed across WF2 and WF3. (B) The aperture is specified as “WF3” and the nucleus is placed near the outer edge of WF3 using “POS TARG +20,0.” To place the major axis across WF2 and WF3 “ORIENT 5D TO 25D” is specified. Note that “ORIENT 185D TO 205D” is also feasible.

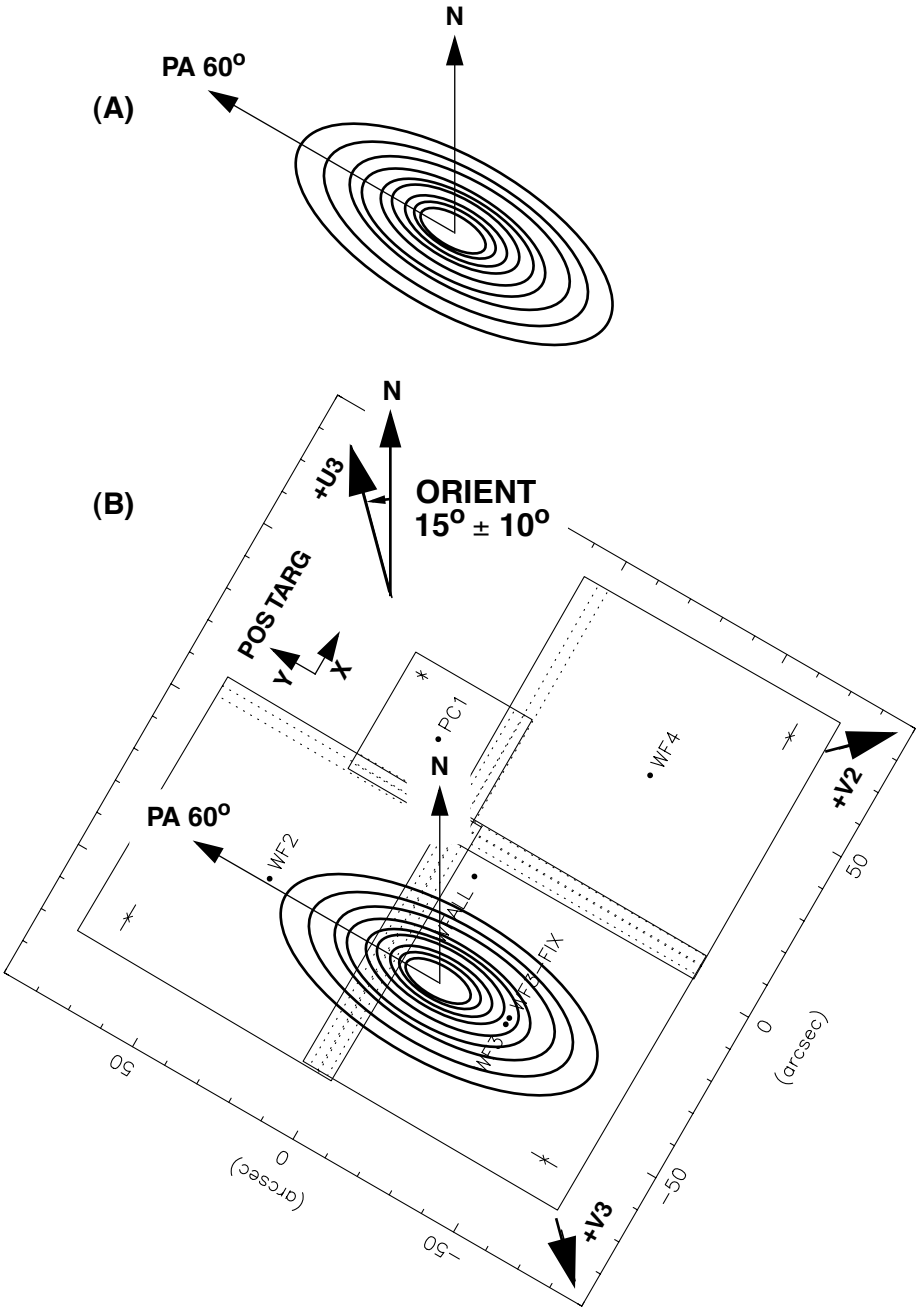

7.9 Polarization Observations

Polarization observations require three or more images with the polarizing filter spanning a large range of position angles on the sky. For WFPC2, this may be achieved by using different quads of the polarizing filter (each quad being oriented 45° to the others), by rotating the spacecraft though different angles, or by a combination of these methods. Rotating the spacecraft through use of ORIENTs provides the simplest calibration, as a single polaroid can be used for all images. However, in practice, it will be the most difficult method to schedule. For further information see Biretta and Sparks (1995, ISR WFPC2 95-01).

We note that WFPC2 has significant instrumental polarizations which will make measurements on targets with less than 3% polarization difficult. The pick-off mirror introduces about 6% instrumental polarization. Furthermore, the pair of mirrors in the calibration channel, which is used to generate the polarizer flat fields, introduces ~12% polarization. In principle these effects can be calibrated out, but this has yet to be demonstrated.

The polarizers are most effective in the range from 3000Å to 6500Å; this corresponds roughly to filters in the range F255W to F675W. At shorter wavelengths the transmission decreases sharply, and at longer wavelengths they cease to polarize the incoming light.

7.10 Observing with Linear Ramp Filters

The Linear Ramp Filters (LRFs) provide a narrow band ($\Delta\lambda/\lambda = 0.013$) imaging capability which is continuously tunable from 3710Å to 9762Å. These are essentially a collection of narrow band interference filters whose central wavelength varies with position on the filter glass. The filter and aperture should be specified as LRF on the Phase II proposal, and the desired central wavelength should also be specified. The HST scheduling software will then select the target position so as to provide the desired wavelength.

Note that it is not possible to choose between PC1 and WFC for the LRFs; one must use whatever CCD is automatically assigned by the scheduling software. If it is necessary to know which CCD will be used, observers can consult Table 3.7 on page 58 or Table 3.8 on page 60, or use the on-line LRF calculator tool on the WFPC2 WWW pages at http://www.stsci.edu/instruments/wfpc2/Wfpc2_lrf/wfpc2_lrfcalc.html.

It is possible to use POS-TARGs with LRF observations; the offsets are made from the default pointing for the specified wavelength. Observers should be mindful that the unvignetted field-of-view has a minimum size of ~10″ in diameter, so that only small POS-TARGs (<4″) should be used.

While it is recommended that observers assume a 10″ diameter field-of-view when using the LRFs, larger elongated (e.g. 15″ x 10″) targets can sometimes be accommodated by placing the target's major axis along the direction of the wavelength variation on the filter. This will result in a small reduction in throughput (i.e. small central wavelength offset) at the outer edges of the target. However, placing targets outside the central 10″ of each ramp is strongly discouraged; outside the central 10″ width the light will pass through more than one ramp segment, hence mixing light from different wavelengths, and making the data very difficult to calibrate. (See "Linear Ramp Filters" on page 48 for further details on LRFs.)

A common situation is one in which observers desire to make observations through an LRF filter, and then repeat the observation in a standard broad or narrow band filter at the same position on the CCD. The LRF Calculator Tool, available on the WFPC2 WWW pages, will tell observers the aperture (PC1-FIX, WF2-FIX, etc.) and POS-TARG for any wavelength setting of the LRFs. Observers merely need to use this same aperture and POS-TARG for the exposure through the other filter. If it is necessary to calculate the POS-TARG manually, one can do this using the information in Table 3.7 on page 58, Table 3.8 on page 60, Table 3.14 on page 74, and Figure 7.9 on page 216. For example an LRF observation at 5034Å would be made on WF2 at pixel (673.4, 235.7) (from interpolation by wavelength between X1 and X2, and between Y1 and Y2 in Table 3.7 on page 58). These offsets are referred to the WF2-FIX aperture which is located (Table 3.14 on page 74) at pixel (423.5,414). From Figure 7.9 on page 216 we can deduce that pixel X direction is parallel to POS-TARG "+Y" on WF2, and that pixel Y direction runs in the POS-TARG "-X" direction. Using the pixel scale in "Optical Distortion" on page 143, we have

POS-TARG "X" = -0.09961 (235.7-414) = 17.76″, and

POS-TARG "Y" = 0.09961 (673.4-423.5) = 24.89″,

hence POS-TARG=+17.76,+24.89 would be requested for the non-LRF exposure.

We note that analysis of FR533N VISFLAT images has revealed an apparently randomly occurring offset in the filter position (Gonzaga et al. 2001, WFPC2 ISR 01-04). This anomalous offset corresponds to one step in the filter wheel rotation, or about 0.5 degrees. We expect no significant impact on point-source observations; any photometric effect is less than 1%. But caution needs to be exercised for extended sources greater than about 5 arcseconds. (A cursory check of several other filters on other filter wheels shows no similar problems.) Figure 7.12 on page 223 shows throughput plotted against CCD pixels in the direction of the anomalous offset/rotation. The two curves in each plot show the throughput effect of the filter offset. Several points in the wavelength mapping (from actual GRW+70D5824 observations in proposals 6939, 8054, and 8454) are indicated for illustrative purposes. At this time, the source of this anomaly,

whether it is mechanical or due to a software error, is not known. This anomaly was investigated further as part of the WFPC2 Cycle 10 Calibration Plan.

Figure 7.12: Linear Ramp Filter Anomaly.

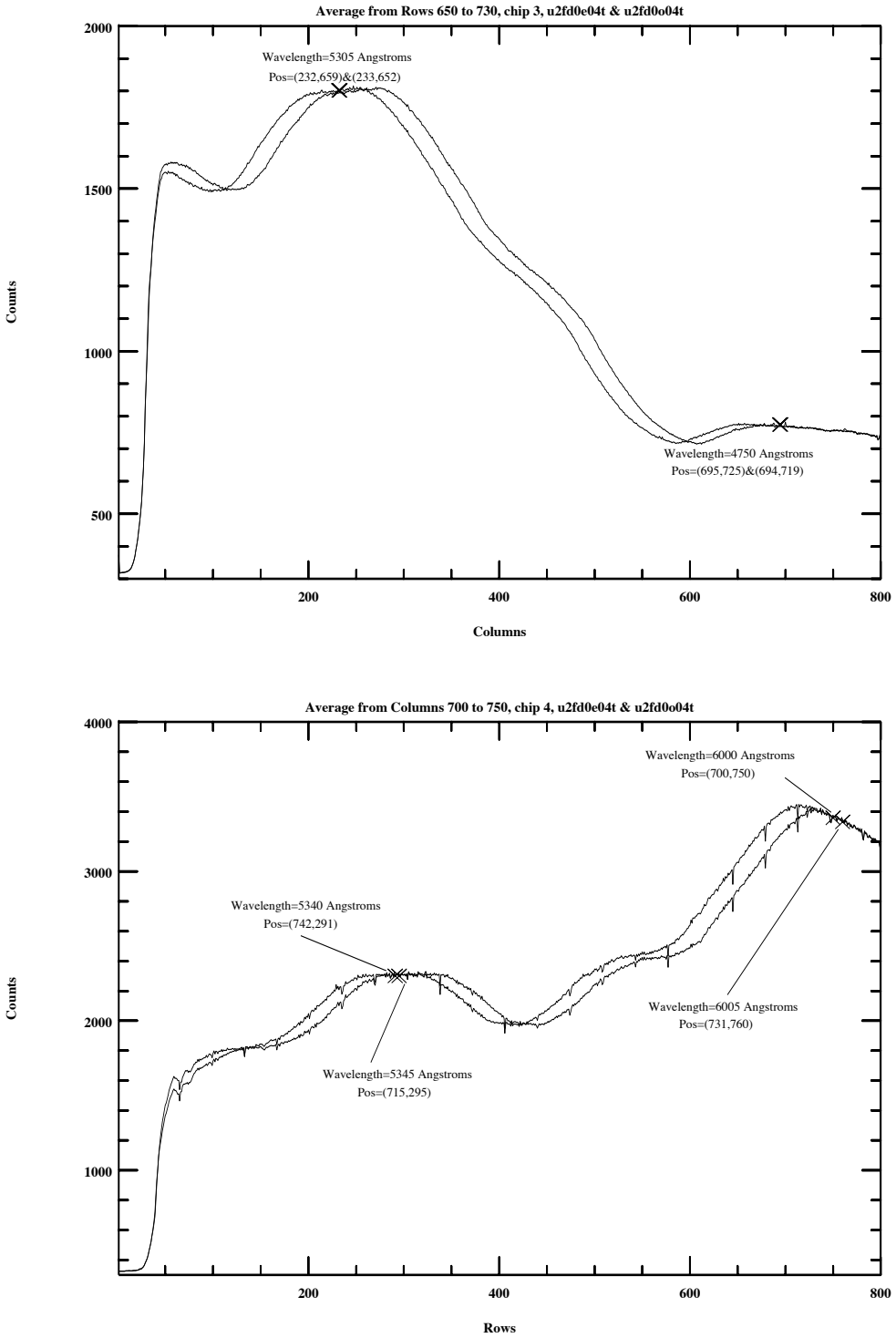

7.11 Emission Line Observations of Galaxy Nuclei

Saturation is a common problem for narrow band filter images of galaxy nuclei. Often the surface brightness of the emission line is estimated from ground based images with 1″ resolution; sometimes line fluxes are quoted for apertures several arcseconds in radius. However, at HST resolution, much of this flux may occur in a single unresolved spot at the galaxy nucleus, thus leading to saturated images. Observers should be cautious and consider this possibility when estimating exposure times.

7.12 Two-Gyro Mode

At some future date HST may be operated with only two gyros, hence causing additional spacecraft jitter and degradation of the effective PSF. Other potential impacts of operating in two-gyro mode are decreased visibility periods between occultations, and restricted target availability during the year. It is also possible that the pointing stability between exposures may be slightly poorer.

Please see the Two-Gyro Mode Handbook for additional discussion.

CHAPTER 8:

Calibration and Data Reduction

In this chapter . . .

8.1 Calibration Observations and Reference Data

Standard calibration observations are obtained and maintained in the HST archive at the STScI, and can be retrieved by external users using StarView. This includes those flat field, dark, and bias reference files needed to operate the Post Observation Data Processing System (PODPS; now called OPUS, and usually just called the "pipeline"), photometric calibration derived from standard star observations and the measured filter profiles, and derived determinations of the plate scale, distortion, and so on. The first set of these calibrations was provided to the STScI by the WFPC2 IDT from the Servicing Mission Observatory Verification (SMOV) and System Level Thermal Vacuum (SLTV) testing periods, and has been maintained and updated thereafter by the STScI with assistance from the IDT as part of the long term calibration program. For measurements requiring more precise calibrations, special calibration observations may need to be obtained as part of the observing proposal. Please consult the STScI WFPC2 Contact Scientists for guidance if the routine calibration appears unlikely to support the requirements of a proposed observation, or email help@stsci.edu. Individual GO programs requiring special calibrations must directly request these observations as part of their Phase I proposal.

A database of laboratory characterizations of optical components, CCD sensors, filters, and the flat field channel has been collected to support the instrument calibration. On-orbit pointed calibrations require large HST resources, taking time that could otherwise be used for direct scientific observations. They can also be unsatisfactory due to the limitations of the available astronomical reference sources. For WFPC2, the inherent stability and uniformity of the CCD sensors, the well-calibrated filters, the internal flat field calibration system, and an archive populated with flat field images obtained in SLTV prior to launch improve the scientific data analysis and productivity. Hence the need for on-orbit calibrations has been minimized.

8.2 Flat Fields

The process of correcting for the effect of the variation in the sensitivity of the WFPC2 with field position is known as flat-fielding, or flattening. For ground based observations, usually a "flat field" (an exposure of a spatially uniform source) is observed through the telescope with the desired filter. Unfortunately, there is no uniformly illuminated target available on-orbit. Instead, several assets are available to estimate the flat field and monitor any changes -- these include pre-launch SLTV optical

stimulus flats, Earth flats, calibration channel flats (VISFLATS), and internal flats (INTFLATS).

During SLTV (System Level Thermal Vacuum) ground tests of WFPC2, flat fields were obtained using both the calibration channel and the WFPC2 optical stimulus (HST simulator). The later provided a close approximation to a uniform target as viewed through HST, and are a prime ingredient for the final calibration flats.

The Earth is an imperfect flat field target because it is too bright for the WFPC2 in the broad-band green and red filters. In addition, the rapid motion of the HST creates streaks across the flat field images, though the streaks can be removed by combining multiple Earth observations with the streaks at different angles on the CCDs. An extensive discussion of the generation of Earth flat fields is available in Chapter 6 of the WF/PC-1 IDT OV/SV Report, as well as in the History records of the flat field reference files themselves.

While imperfect, Earth flats are an important part of the flat field calibration; they provide corrections to the SLTV flats for any differences between the SLTV optical stimulus illumination, and the OTA illumination pattern. Flat fields in narrow bandpass filters are obtained using the sunlit Earth (Target = EARTH-CALIB) as part of routine calibration. These are used primarily to remove the low spatial frequency effects in the calibration flats.

Flat field calibration files have been generated for all filters by combining information from the SLTV test flats (which are good for all but the lowest spatial frequencies), and on-orbit Earth flats obtained for a small subset of narrow band filters (F375N, F502N and F953N). These Earth flats are used to correct low spatial frequency errors in the ground based SLTV flats, which result from imperfect simulation of the HST OTA illumination pattern. These Earth flats taken regularly during available occultation time periods (i.e., no impact to science observations).

There are also two types of on-board flats available in WFPC2, which can be used to monitor changes in the flat field. The calibration channel (VISFLAT system) produces a reasonably flat illumination pattern down to about 1800Å. It works by imaging an illuminated diffuser plate onto the WFPC2 exit pupil (relay secondary) by means of an MgF_2 lens. Two lamps provide optical and FUV illumination, yielding a flat field which resembles the input beam from the OTA between 1600Å and 10000Å. The system is mounted outside, but adjacent to, WFPC2, and light is directed into WFPC2 via a mechanically actuated flip mirror. A second system is much cruder, but provides a measure of redundancy: the internal flat system (INTFLAT system) consists of small lamps which, when commanded on, illuminate the back side of the shutter blade. The INTFLAT illumination pattern is not very uniform, but provides a robust backup capability.

The calibration channel data (VISFLATS) are used to monitor time dependent changes in the flat fields; only small changes have been seen to

date in the visible filters. INTFLATS are also taken on a routine basis, and provide a redundant monitor capability. As of this writing (June 2001), both types on internal flats have been used only as monitors, with no corrections being made to the actual calibration files.

A major update of the flat field reference files for all standard filters redward of 300nm (F300W) was completed, using on-orbit data from Earthflat exposures covering the period from September 1995 to May 2001 (Koekemoer, Biretta & Mack 2002). The flat fields have been divided into epochs depending on the appearance of new dust spots, as well as long-term changes in existing features. The new correction flats are accurate for pixel-to-pixel variations down to an intrinsic level of approximately 0.3% for the PC and 0.1% for the WF chips, and they result in an improved rms noise of many of the flats by a factor of two or more. Since early 2002, the new flat fields are automatically applied to any WFPC2 data in relevant filters when the data are retrieved from the archive.

Note that the flat fields presently used in the pipeline are based on gain 14 data. The gain ratios are not constant from chip to chip, and therefore a small correction to photometric results derived from gain 7 data should be applied (see Table 4.4 on page 117). (See Biretta 1995 for further discussion of WFPC2 flat fields; also see the *HST Data Handbook*.)

8.3 Dark Frames

Dark frames are long exposures that are taken with no light incident on the CCDs. They are used to detect CCD counts (the dark current) caused by thermal processes at the interfaces between the silicon and oxide layers, as well as charged particle and secondary radiation events. Estimated dark current and cosmic ray event rates are given in “Dark Backgrounds” on page 87 and “Cosmic Rays” on page 92, respectively. Observers are cautioned that the calibration provided by the pipeline may not use the most up-to-date dark frames until several weeks after the observation is taken. The time delay is the time it takes for coeval dark frames to be taken, archived, and processed into dark reference files, and delivered for use in the pipeline and OTFC. Use of optimal darks can be important due to the new hot pixels continually being generated. Each week of observations typically has one applicable (optimum) dark reference file.

8.4 Bias Frames

The WFPC2 bias correction is performed in the pipeline in two steps: a pedestal level is removed and a bias image subtracted. The pedestal level is

determined from the overscan columns in each science image; the specific values subtracted are documented in the bias-even / bias-odd science image header keywords. However, the value of the pedestal can also vary with position across the chip. Therefore, after the pedestal correction is performed, the pipeline removes any position-dependent bias pattern by subtracting a bias reference file. This reference file is typically generated from a stack of 120 bias frames (CCD readouts without an exposure); new bias reference files are usually installed in the pipeline about once a year.

8.5 Data Products and Data Reduction

The routine processing of WFPC2 science data consists of the pipeline functions described below. The resulting images will be available in FITS format on magnetic tape or via FTP transfer, and as grey scale images in PDF format. The reformatted raw data will also be available, along with the relevant calibration data. The *HST Data Handbook* or *STSDAS Calibration Guide* should be consulted for a more complete description than the summary presented here.

The following data are supplied to observers on FITS tapes:

- Edited Image and DQF (uncalibrated): `.d0h`,`.q0h`
- Standard Header Packet: `.shh`
- Extracted Engineering Data and DQF: `.x0h`,`.q1h`
- Trailer File (ASCII file): `.trl`
- Calibrated Image and DQF: `.c0h`,`.c1h`

In addition, a histogram file used for monitoring of the signal chain (`.c2h` file), and a calibration table containing the throughput curve (`.c3t` file) used in populating the photometric keywords are included.

Further data reduction and analysis can be performed under the STScI's science data analysis software system (STSDAS). Standard routines are available, operating under IRAF, for the analysis of data for image photometry, spectral analysis, astrometry, and the generation of the calibration data files.

8.6 Pipeline Processing

The pipeline processing of WFPC2 data sets reformats the telemetry received from HST into group FITS format images, generates headers containing a large number of keywords taken from both the HST and WFPC2 telemetry streams, in addition to various STScI ground system databases, and applies the corrections described below. This calibration is done with a software module known as "CALWP2" which is written in the IRAF SPP language and is available, in identical form, to users of the STSDAS system. Therefore, off-line recalibration of observations is fairly easy, and will use the same program as the OPUS system. Documentation is available in the *HST Data Handbook*, and the *STSDAS User's Guide*.

CALWP2 performs the following operations if required by the observation:

- A-to-D correction (depending on ATODGAIN)
- Bias pedestal level removal
- Bias image subtraction (depending on the gain and mode [FULL or AREA])
- Dark image scaling and subtraction (depending on gain, serials, and mode)
- Shutter shading correction (depending on exposure time and shutter in place at the beginning of the observation)
- Flat field image correction (depending on filters and mode used)
- Population of various photometric calibration keywords

In addition, the following conditions are flagged in the Data Quality File (DQF):

- Transmission failures and other possible failures
- Known bad pixels (e.g. blocked columns)
- Pixels at or above the maximum A/D converter level (i.e. saturated)
- Bad pixels in calibration reference files

8.7 On-The-Fly Reprocessing Systems

The On-The-Fly Calibration (OTFC) system, publicly released in Dec. 1999, calibrated data at the time a user requested data from the archive. The advantages to using OTFC included the automatic application of improved calibration files and switches, use of most recent calibration software (allowing for rapid access to improved algorithms, new capabilities, and software fixes), and correction of header keywords if needed. An additional benefit is that only the uncalibrated data needs to be stored in the archive.

The On-The-Fly Reprocessing (OTFR) system replaced OTFC on May 16, 2001. *The change is transparent to most HST archive users*. Requests for data are submitted as usual via StarView or WWW; raw and freshly-calibrated data will be delivered. There is no need to explicitly ask for OTFR: all requests for WFPC2 data are handled by the OTFR system.

The primary difference between the two systems is that OTFR begins earlier in the data path. It uses the original telemetry files ("POD" files) received from Goddard Space Flight Center and performs all pipeline processing steps; OTFC performed only the last pipeline processing step (calibration), on raw files retrieved from the archive. An overview of the data flow for both systems is summarized in the table below. The benefits of the OTFR system encompass the benefits in the OTFC system; in addition, OTFR data needs fewer header corrections (most problems are fixed as part of the pre-calibration pipeline processing) and the system as a whole requires significantly less maintenance effort than OTFC.

UCHCOORD and OTFR.

Improved knowledge of the detector plate scales and chip rotations, as well as changes in reference pixel locations, have resulted in periodic changes to the pointing parameters, especially early in the instrument's lifetime. These header parameters, which define the mapping between the pixel and world coordinate systems, can be updated using the STSDAS task UCHCOORD. The keywords affected include the reference pixel locations (crpix*), the values of the world coordinate system at the reference location (crval*), the partial derivatives of the world coordinate system with respect to the pixel coordinates (cd*), and the orientation of the chip (orientat).

Prior to OTFR (released to the public on May 16, 2001), observers requiring the most up-to-date pointing information in their science image headers ran UCHCOORD on their calibrated images. Since the implementation of OTFR in May 2001, all WFPC2 data retrieved from the archive, regardless of its observation date, has had these corrections applied automatically before being delivered, thus we have discouraged running the UCHCOORD task on OTFR data since it is no longer needed (as described in WFPC2 STAN 45, March 2001 by Baggett, Hsu & Gonzaga). In fact, running UCHCOORD (versions prior to September 2003) on

OTFR data would apply unnecessary corrections and corrupt the astrometry (for example, Section 4.3.3 in WFPC2 Data Handbook, Version 4.0, 2002, S. Baggett et al.).

The new version of UCHCOORD in the September 2003 STSDAS release will correctly check whether or not the images have been processed through OTFR, and will no longer modify the header astrometric keywords in such cases. We remind users that it is no longer necessary to run the UCHCOORD task on any WFPC2 data that is retrieved via OTFR, and we recommend that any old WFPC2 data should rather be re-retrieved via OTFR since many other calibrations are also improved.

Table 8.1: Comparison of Dataflow in On-The-Fly Systems.

OTFC	OTFR
Request for data is submitted to the archive via StarView or WWW interface; archive responds with acknowledgement email.	Same as OTFC.
Raw files are retrieved from the HST archive and passed to the OTFC system. For WFPC2, the raw files include d0, q0, q1, x0, and trl files.	POD file (original telemetry file) is retrieved from HST archive and passed to OTFR system. For WFPC2, there is typically 1 POD file for each image. Pre-calibration OPUS processing is performed: data partitioning, data editing, and generic conversion; these steps generate the raw files (d0, q0, q1, x0, and trl files).
Any problems in the header keywords are fixed by special lookup table.	*Same as OTFC* although the OPUS pre-calibration processing will have fixed the majority of keyword problems automatically (i.e., significantly fewer header corrections required in OTFR).
The best calibration files & switches are determined by separate standalone task, and header keywords updated accordingly.	*Not needed*. The best calibration files & switches are set by the pre-calibration OPUS code (generic conversion).
Images are calibrated by STSDAS calxxx module and sent back to the archive system.	Same as OTFC.
Archive delivers raw + calibrated data and emails completion notification to the requestor.	Same as OTFC.

8.8 Fluxes and Standard Magnitudes

The pipeline calibrated data are not flux calibrated and the data are in units of Data Numbers (DN). However, a flux calibration is supplied in the header keywords. To obtain the flux density, multiply DN by the value of the keyword PHOTFLAM in the calibrated (`.c0h`) science header file, and divide by the value of the keyword EXPTIME.

The magnitude of an object can be determined using the photometric zero-point keyword PHOTZPT as:

$$m = -2.5\log_{10}\left(PHOTFLAM \times \frac{DN}{EXPTIME}\right) + PHOTZPT$$

where *m* is in the STMAG system which is based on a spectrum with constant flux per unit wavelength set to roughly match the Johnson system at V. The more conventional systems are based on Vega's spectrum. Table 8.2 on page 233 was generated using SYNPHOT to provide rough conversions from STMAG to the Johnson UBVRI and Cousins RI systems. Typical uncertainties are 5%, and probably much worse for the U filter. The correction depends on the spectrum of the object, hence the table was generated using a wide range of Bruzual models.

For example, to convert to the Cousins I band for an object on WF4, get PHOTZPT=-21.1 and PHOTFLAM=2.6044 x 10^{-18} from the header. Then convert from WFPC2 counts to magnitudes in Cousins I using:

$$I_c = -2.5\log_{10}\left(2.6044 \times 10^{-18}\frac{DN}{EXPTIME}\right) - 21.2 - 1.21$$

Note that the Cousins I filter is much closer to the F814W filter than Johnson I, as shown by the nearly constant correction as a function of spectral type (i.e. color term).

Table 8.2: Conversion from STMAG to Johnson UBVRI and Cousins RI.

	U-F336W	B-F439W	V-F555W	R_J-F675W	I_J-F814W	R_C-F675W	I_C-F814W
O5V	0.53	0.67	0.05	-0.67	-1.11	-0.71	-1.22
B0V	0.46	0.66	0.05	-0.67	-1.13	-0.70	-1.22
A0V	-0.08	0.67	0.02	-0.68	-1.22	-0.67	-1.21
F2V	-0.03	0.62	-0.00	-0.69	-1.28	-0.63	-1.22
G0V	-0.02	0.58	-0.01	-0.70	-1.31	-0.60	-1.23
K0V	-0.10	0.53	-0.01	-0.69	-1.32	-0.58	-1.23
M0V	-0.04	0.43	-0.00	-0.78	-1.48	-0.54	-1.22
M6V	0.05	0.29	-0.03	-1.05	-1.67	-0.56	-1.21

This procedure will provide typical accuracies of about 0.05 mag, worse in the UV. More accurate photometry will require a variety of corrections (e.g., CTE effect, contamination and red leaks for the UV filters, variable gains on different chips, color terms, geometric distortions) which are

discussed in detail in Holtzman et al. (P.A.S.P., 1995b) and in the HST Data Handbook.

8.9 Color Transformations of Primary Filters

The WFPC2 UBVRI system is fairly close as regards effective wavelengths to the Johnson UBVRI system, but cross-calibration is necessary to convert to Johnson magnitudes. See the IDT OV/SV Report and Harris, et al., A.J. 101, 677 (1991) for examples in the case of WF/PC-1. Figure 8.1 on page 234 through Figure 8.5 on page 237 show the results of regression fits between these two systems on the main sequence stars in the Bruzual, Persson, Gunn, Stryker atlas that is installed in the calibration database system (CDBS). This atlas, and others, are available via the WWW from the WFPC2 Documentation page, or directly via

`http://www.stsci.edu/instruments/observatory/cdbs/astronomical_catalogs.html`

Figure 8.1: F336W-F439W against Johnson U-B for the BPGS atlas of MS dwarf spectra. The change in slope in the transformation for U-B greater than about 0.1 is due to red leak in the F336W filter. For hotter stars, the transformation is quite linear.

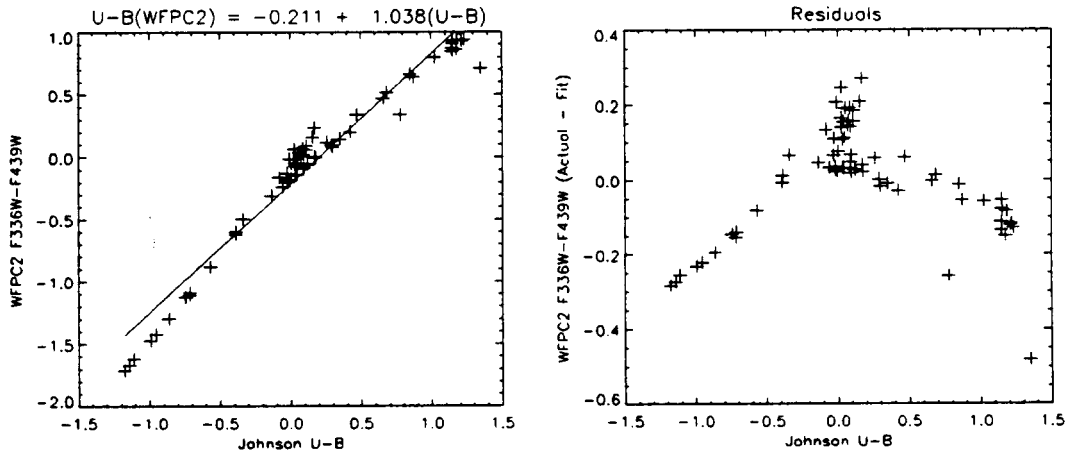

Figure 8.2: F439W-F555W against Johnson B-V. The residuals from the best linear fit are quite similar to those that apply if F569W (instead of the preferred F555W) is chosen for a WFPC2 passband.

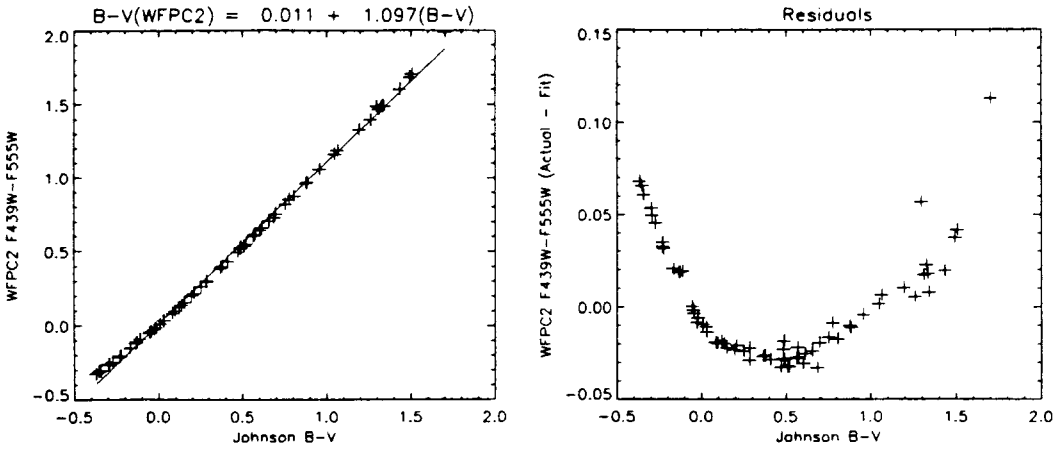

Figure 8.3: F555W-F814W against Johnson V-I_C. The residuals from the best linear fit are generally very small. This particular color combination is widely used.

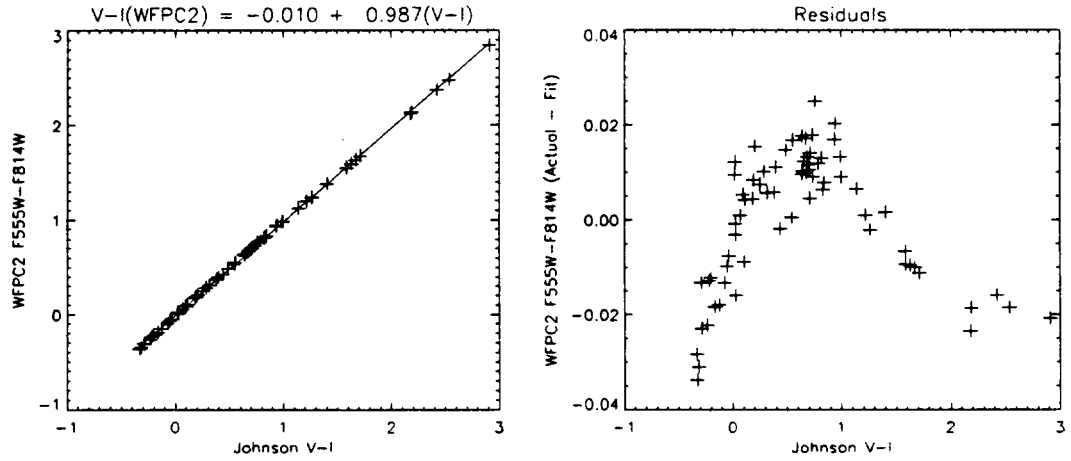

Figure 8.4: F555W-F675W against Johnson V-R_C. The residuals from the best linear fit are somewhat larger for blue stars than those that apply if F569W is chosen.

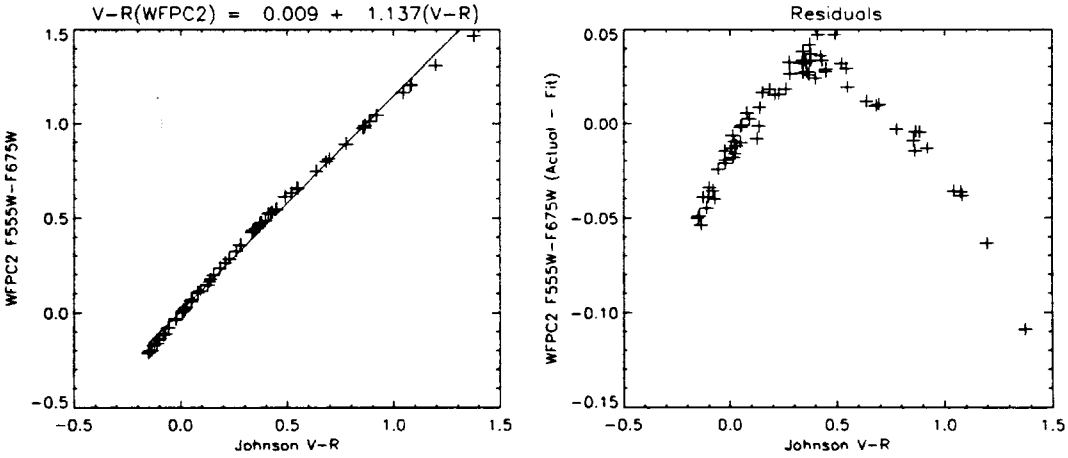

These fits should be used with caution for quantitative work. The zero-points in all cases are defined so that Vega's spectrum integrated over the bandpass is exactly magnitude zero (VEGAMAG in XCAL). The zero-points of the canonical Johnson-Cousins system differ from this by up to 0.02 magnitudes. The zero-points thus defined for the HST filters do not coincide with the STMAG definition used in the previous section. In addition, the ground based filter curves used, which are taken from Bessel (P.A.S.P. 102, 1181), give a good approximation to the standard Johnson-Cousins system, but are not as accurate as taking Landolt's curves and applying his color corrections to transform to the standard system. The latter procedure was used to derive the transformations given in Holtzman et al. (P.A.S.P., 1995b), which also discusses the changes in the transformations that result from source spectrum variations (such as metallicity and gravity effects).

Figure 8.5: F675W-F814W against Cousins R_C-I_C. The residuals from the best linear fit are similar to those that apply if F791W is chosen for a WFPC2 I passband. For spectral type M8V and later (not shown) the transformation will not work as well.

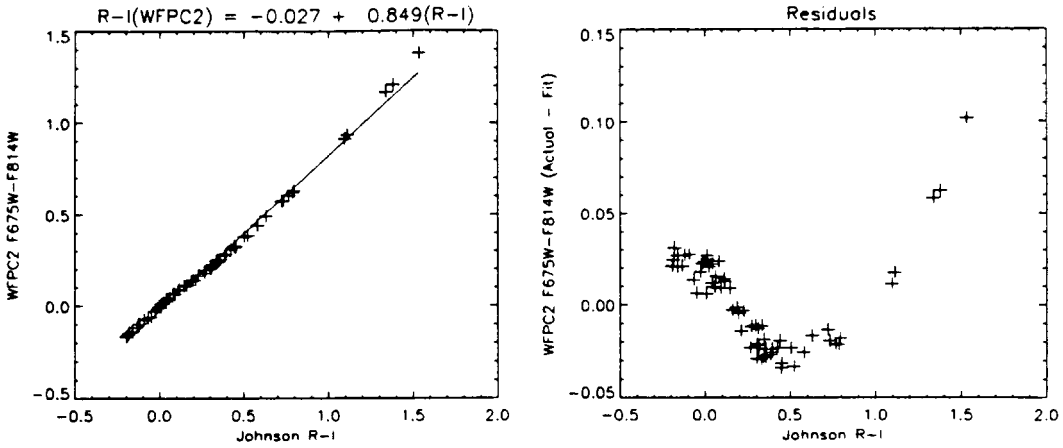

8.10 Calibration Plan Summary

Table 8.3 on page 238 summarizes the nominal proposal cycle boundaries. The dates are intended as a rough guideline only, since in reality, of course, there are no sharp cycle boundaries. Some GO proposals are identified as candidates for early execution while other proposals take longer to complete due to various scheduling constraints. Additional observatory restrictions factor in as well, for example, the acceleration of the NICMOS observations in Cycle 7 (due to the limited lifetime of the NICMOS cryogen) caused many WFPC2 and other programs to be delayed. Cycle 7, initially set to span July 1997 to July 1998 was initially extended to October 1998 (due to Servicing Mission requirements), then later extended to July 1999, due to acceleration of NICMOS programs and the additional NICMOS programs solicited during the "Cycle 7N - NICMOS only" call for proposals.

Table 8.3: Nominal Proposal Cycle Boundaries.

cycle	start date	end date
4	May 28, 1994	July 1, 1995
5	July 1, 1995	July 1, 1996
6	July 1, 1996	July 1, 1997
7	July 1, 1997	July 1, 1999
8	July 1, 1999	July 1, 2000
9	July 1, 2000	July 1, 2001
10	July 1, 2001	July 1, 2002
11	July 1, 2002	October 1, 2003
12	October 1, 2003	October 1, 2004
13	October 1, 2004	October 1, 2005

8.11 Cycle 4 Calibration Plan

The primary goal of the Cycle 4 calibration plan was to provide an instrument calibration for Cycle 4 GO and GTO science programs as well as monitor internal health, photometric and optical stability of the instrument. This report briefly summarizes the WFPC2 calibration proposals as they were implemented during Cycle 4. Table 8.4 on page 239 outlines the proposal contents as well as the approximate frequency of execution while the following section presents more details of the justification and intent for each proposal.

Table 8.4: Summary of Cycle 4 Calibration Plans.

ID	Title	Frequency	notes
Internals			
5568	Decontaminations	1 x month	internals plus decon itself
5560	Internal Monitor 1.	2 x week	intflats, biases, kspots
5561 5655	Internal Monitor 2. - Flats	~2 x month	darks, visflats. UVflats suspended after June 12; one set of uvflats run as a test (Oct. 1994)
5562	Internal Monitor 3. - Darks	5 per week	serials=ON taken in 5561/5655
5569 5764	Internal Flats	once	intflats & visflats, in variety of filters
6140	Ramps: Internals & Earthcals	once	internals to aid in LRF calibration
Photometry			
5563	Photometric Monitor - UV Std.	2 x month	GRW+70D5824, std.filters. Clocks OFF except Dec. 1994, 1994 (ON).
5565 5663	Photometric Monitor - Fields	2 x month	Usually NGC5139. Clocks OFF except Dec. 1994 (ON).
5629	Photometric Monitor - Four Chip Std.	1 x week	GRW+70D5824; 4 CCDs, F170W
5572	Photometric Filter Calibration	run twice during Cycle 4	GRW+70D5824 in all filters used by GO/GTOs during Cycle 4; NGC5139 done in subset of broadbands.
5646	CTE Dither Test	run once	Omega Cen, nine 40 sec images in F555W, offset in 15” steps
5659	CTE Dither Test - Part 2	run once	same as 5646 but in F439W, F814W
5564	Photometric Calibration: 4-CCD	to be run once	GRW+70D5824, in 4 CCDs, standard broadband filters
Earth Flats			
5570	Earth flats - Large Set	~ 40 per week	200 Earthflats in each of four filters: F375N, F502N, F656N and F953N
5571	Earth flats - Small Set	~14-20 per week	20 Earthflats in each of ~20 filters
Other			
5643	Partially Rotated Filters	done once	GRW+70D5824 & visflats, FQUVN, FQCH4N and partial rotations
5632	Preflash Test	done twice	Omega Cen in broadband filters; includes preflash done with intflat; replaced 5565 during Apr. 1994
5778	Lyman Alpha Throughput Check	do twice	target: BD+75D325
5573	Ramp Calibration		
5574	Polarization Calibration	done once	G191B2B, BD+64D106, RMon, NGC 4147, and visflats

Table 8.4: Summary of Cycle 4 Calibration Plans.

ID	Title	Frequency	notes
Placeholders/Contingency (no plans to execute, may not be run at all)			
5627	Photometric Monitor 1a: Std. in UV		Not needed.
5628	Photometric Monitor 1b: Std. in Vis.		Not needed.
5645	Optimum Preflash Test		Not needed.
5648	Charge Transfer Test		Withdrawn.
5566 5567	UV Campaign Photometry UV Campaign Flats		Not needed; no UV campaigns run
5575	Dither Test		Not needed.

8.11.1 Internal Monitors

These proposals monitor the instrument's health throughout the cycle, including the stability of the cameras, their signal chain electronics, and the internal optical alignment of the WFPC2. The internal flat fields are intended as delta-flats, in order to monitor the stability for the main photometric filter set as well as provide data for the generation of high S/N flat fields. The darks are required not only for the generation of darks for the pipeline but also for tracking the evolution of hot pixels and mapping low-level CCD defects such as traps.

The internal visflats obtained in most of the visible WFPC2 filters will be used with the thermal vacuum test flat fields and the Earth flats to generate "superflats"; the intflats are obtained as a backup for the visflats (for example, if the cal-channel should fail).

8.11.2 Photometric Monitors

These proposals provide a regular monitor of the instrument's QE stability from the FUV to the near-IR, allow tracking of the UV throughput decline due to contaminant buildup, and provide observational PSFs. The standard star observations provide a baseline for the standard field photometry and allow updates to SYNPHOT. The standard field measurements will allow calibration of the filter sets' color terms, as well as enabling a mapping of the geometric distortions across the field of view. The four CCD photometry program provides the relative CCD-to-CCD sensitivities for the filter set and allows the regular PC1/WF3 standard star photometry to be applied to WF2 and WF4.

8.11.3 Earth Flats

These are divided into two proposals: the first to obtain a large number of Earth cals (observations of the bright Earth) in just four filters and the second to obtain a small set of Earth cals in a larger number of (primarily narrowband) filters. The superflats generated from the first proposal's data map the OTA illumination pattern and are combined with the thermal vacuum test data flats (and possibly cal-channel flat fields) to provide a set of flat fields which remove both the OTA illumination pattern and the pixel-to-pixel response of the cameras. The images from the second proposal will also help determine the OTA illumination pattern, but used in conjunction with the Earth superflats (and cal-channel flats), will provide delta corrections to the superflats applicable to the narrow- and medium-band filters.

8.12 Cycle 5 Calibration Plan

A summary of the Cycle 5 calibration plan follows as a general guide to the calibration and monitoring program in place for WFPC2. The full proposals are available through STScI's proposal status web page.

http://presto.stsci.edu/public/propinfo.html

The data that the calibration and monitoring program produced have no proprietary period and are immediately available through the HST archive.

Calibration information obtained by the start of Cycle 5 consisted primarily of the System Level Thermal Vacuum (SLTV) tests, the initial on-orbit tests conducted in SMOV, and the Cycle 4 calibration. These tests have shown that the instrument is stable with some important exceptions and have provided an initial calibration sufficient for routine processing of most data.

The Cycle 5 calibration was designed to enable users to maximize the scientific usefulness of their data, while at the same time minimizing the use of spacecraft time. This was done by designing efficient proposals that:

A. Improved the existing calibration - in particular towards the goal of 1% absolute photometric accuracy.

B. Assessed the accuracy of the existing and new calibrations.

C. Recalibrated important known time variable features of the instrument.

D. Calibrated some important instrumental effects that are not well understood.

E. Monitored the instrument and telescope to ensure that no new problems or variability in their performance are missed.

F. Maintained the instrument in a healthy state and ensured that in the event of partial instrumental failures, the calibration can be maintained when possible.

The calibration of the instrument is seen in a larger context than simply preparing reference files for a pipeline reduction and assessing the errors in them. Several calibrations (such as geometric distortion, CTE correction, PSF calibration, chip-to-chip alignments, polarization calibration) are very important to some observers, yet are not included in the pipeline. Other corrections frequently need to be done to the data after it is ADC, bias, dark, and flat field corrected, with a photometric calibration included in the header. These other calibrations are made available to users through this Instrument Handbook, journal publications, instrument science reports, and postings linked to the Institute's WFPC2 WWW home page. The address is:

http://www.stsci.edu/instruments/wfpc2/wfpc2_top.html

A list of the most important calibrations consists of the following items:

1. Photometric zero-point: converting count rates to flux units.
2. Photometric transformations: converting DN values to magnitudes in standard systems. Two separate photometric calibrations can be used for this, a direct approach and a synthetic approach.
3. Photometric temporal variations: particularly important in the UV where significant variability is seen.
4. Photometric spatial variation: flat fields and charge transfer efficiencies.
5. Dark current: including its time variability and hot pixels.
6. Bias.
7. Analog-to-Digital converter errors.
8. PSF: crucial for PSF fitting photometry, PSF subtraction, PSF modeling, and deconvolution efforts. Because PSF subtraction of very saturated sources is specialized to a few very diverse programs, PSF calibration in the image halo (beyond about 0.5 arcsecond) is not supported and must be requested with the program as a special calibration.
9. Polarization and Linear Ramp Filter calibrations.
10. Geometric calibration.

The Cycle 5 program consisted of 15 proposals which used a total of 63 orbits of spacecraft time (compared to a total of about 1550 orbits of approved Cycle 5 GO time). The proposal summaries and their associated Phase II files largely speak for themselves. Table 8.5 on page 243 lists all of the proposal numbers, titles, the schedule for the calibration execution, an

indication of whether the output forms part of the pipeline data reduction (CDBS) or provides other information, usually documented in Instrument Science Reports (ISRs), the approximate calibration accuracy expected (see the summary forms for the interpretation of these numbers), the primary areas from the above 10 calibration types they address and in what ways (A-F from the above list). Following the table there are more details on each proposal individually, including purpose, observing description, accuracy, and data products. For a report on the final results from these programs, please see ISR WFPC2 97-02 ("Cycle 5 Closure Report") to be found at:

http://www.stsci.edu/instruments/wfpc2/Wfpc2_isr/wfpc2_isr9702.html.

Table 8.5: Summary of Cycle 5 Calibration Plans.

ID	Proposal Title	Schedule	Results	Accuracy	External Time (orbits)	Notes[a]
6179	Photomet. Zero.	Late 95	CDBS	1%	8	1ABE, 2AB
6182	Photomet. Trans.	9/95, 3/96	CDBS	2%	6	2ABE
6183	Decontamination	1x per 4 wks.	ISR	N/A	0	F
6184	Photometric Mon.	2x per 4 weeks	ISR	1%	24	3E
6186	UV Throughput	Early in Cyc. 5	CDBS	10%	6	1AB, 3C
6187	Earth Flats	Continuous	CDBS	1%	0	4ABE
6188	Darks	Weekly	CDBS	6%	0	5ABC
6189	Visflat Monitor	2x per 4 weeks	ISR	0.6%	0	4E
6190	Internal Flats	Early Cyc. 5	CDBS	0.6%	0	4F,7E
6191	UV flats	2x in Cyc. 5	ISR	2%	0	4ABE
6192	CTE Calibration	Early Cyc. 5	TIPS	<1%	4	4ABD
6193	PSF	CTE+2m	TIM	10%	5	8ABD
6194	Polarizers+Ramps	TBD	CDBS	3%+2%	8	9DE, 1AB
6195	Flat field Check	Late 95	CDBS	1%	2	4B
6250	Internal Monitor	2x per week	ISR	N/A	0	5,6,10F
	TOTALS				63	

a. Letters and numbers are keyed to lists in text.

6179: Photometric Zero-point

- **Purpose**: Set synthetic zero points of all WFPC2 filters.
- **Description**: GRW+70D5824 is observed through all filters not in the photometric calibration monitors and longward of F336W (inclusive). It is observed in both PC1 and WF3. This data-set is directly comparable to the corresponding results for Cycle 4 (program 5572).

Because of possible errors in the spectrophotometry for this target, and in order to check synthetic color transformations over a reasonably wide range of colors, the observations are repeated with 3 red standards, and 2 other blue standards in WF3 only. This time, most of the 18 broad and medium bandpass filters longward of F336W are included (restricted to 1 orbit/target). If CTE calibration fails, this proposal may need to be run with preflash (and take more time or do less targets). This proposal is needed by all GO proposals that want to do quantitative photometry at the few percent level.

- **Accuracy**: Overall discrepancies between the synthetic photometric products and the results of this test should be reduced to 1% rms. Part of the point of the test is to measure this accuracy, which will largely depend on the accuracy of the spectrophotometric calibration sources.
- **Products**: After pipeline processing, each image will be reduced by aperture photometry to measure the throughput of each filter. These numbers can be directly compared to SYNPHOT predictions. Systematic differences will be corrected in the throughput database by tweaking the filter normalizations (already done for the primary target in Cycle 4), overall system response (which is quite uncertain particularly longward of 8000Å), and finally bandpass shapes. Residual differences will give an idea of the intrinsic accuracy of the calibration.

6182: Photometric Transformation

- **Purpose**: Update photometric transformations to Johnson-Cousins system.
- **Description**: A photometric standard star field in ω Cen is observed twice, once at the September 1994 orientation and once rotated by 180˚ degrees (to correct to first order for residual CTE effects). All broad and medium bandpass filters are used. Based on Cycle 4 program 5663, this proposal also gives a check on the long term full field photometric stability of the instrument.
- **Accuracy**: Independent of the synthetic photometry results this test gives direct transformations to the Johnson-Cousins system for a wide range of source colors (but excluding very blue stars). These transformations should be accurate to 2%. The stability of these transformations will be measured to the sub-percent level (because then errors in the ground based photometry do not enter significantly).
- **Products**: A comparison with the corresponding Cycle 4 monitor (which ran monthly) will verify the photometric stability of the camera. Direct transformations to the Johnson-Cousins photometry sys-

tem can be derived for all filters. The observations also provide a check of the astrometric and PSF stability of the instrument over its full field of view.

6183: Decontamination

- **Purpose**: Remove UV blocking contaminants from CCD windows.
- **Description**: A sequence of observations is defined that is run twice - once before and once after a DECON when the CCDs are heated to +20˚C for 6 hours. The sequence consists of 2 bias frames at each gain setting, 5 1800 second darks, 2 INTFLATS through F555W at each gain, and two K-spot images. The observations are arranged so that the first sequence occurs about 33 hours before the DECON, and the second follows it by 12 hours. The proposal is run every 4 weeks. This is based on Cycle 4 program 5568 with bias frames added.
- **Accuracy**: This proposal is mainly designed to test aliveness, and monitor the instrument to ensure that no untoward effects from the DECON have occurred. It will identify all hot pixels that are annealed by the DECON.
- **Products**: The data is examined and checked for anomalies. The dark frames are processed to yield plots showing the growth and annealing of hot pixels.

6184: Photometric Monitor

- **Purpose**: Monthly external check of instrumental stability.
- **Description**: GRW+70D5824 is observed through F170W in all four chips. It is then observed in one chip for filters F160BW, F185W, F218W, F255W, F300W, F336W, F439W, F555W, F675W, F814W to fill out the orbit. The chip chosen is changed each month, so each chip is used three times during the year. One extra F555W exposure is taken through the PC to allow for focus monitoring. The proposal is run once before and once after each monthly decontamination, with the same chip selected. Based on Cycle 4 programs 5629 + 6143 + (5563) + 5564.
- **Accuracy**: Overall discrepancies between the results of this test should be less than 1% rms. The point of the test is to measure this variation.
- **Products**: After pipeline processing, each image will be reduced by aperture photometry to measure the throughput of the filters. These numbers can be directly compared to results for previous months. This will allow the long term performance of the instrument to be checked for changes, and verify that the decontaminations are satis-

factory. This proposal will be run every 4 weeks in association with the DECON. Results reported in Baggett et al., ISR WFPC2 96-02 and Whitmore, et al., ISR WFPC2 96-04.

6186: UV Throughput

- **Purpose**: Update SYNPHOT database for UV throughput.
- **Description**: GRW+70D5824 is observed shortly before and after a DECON through all of the UV filters in each chip and through F160BW crossed with F130LP, F185LP, and F165LP (where applicable) to determine the wavelength dependence of the throughput across the bandpass (hence color terms). Based on no particular Cycle 4 program, this program is designed to characterize better the spectral response curve in the UV, and the spectral shape introduced by the contamination.
- **Accuracy**: Overall discrepancies between the updated synthetic photometric products and the results of this test should be 1-2% rms. This does not mean that the UV throughput will be known to this accuracy, primarily because of uncertainties in the flux calibration of the standard used (5%), uncertainties in the UV flat fields (maybe 3% near the chip center), and time dependent contamination corrections (3% error), and uncertainties in the CTE correction (2%). The derived UV absolute photometric accuracy at the center of the chips should therefore be about 10%.
- **Products**: After pipeline processing, each image will be reduced by aperture photometry. The throughput curves and their normalizations can be updated by trial and error.

6187: Earth Flats

- **Purpose**: Generate flat fields.
- **Description**: Four sets of 200 Earth streak-flats are taken to construct high quality narrow-band flat fields with the filters F375N, F502N, F656N, and F953N. Of these 200 perhaps 50 will be at a suitable exposure level for de-streaking. The resulting Earth superflats map the OTA illumination pattern, and will be combined with SLTV data (and calibration channel data in case of variation) for the WFPC2 filter set, to generate a set of superflats capable of removing both the OTA illumination and pixel-to-pixel variations in the flat field. In addition, more limited observations are made in F160BW and the broad bandpass photometric filters.
- The Cycle 4 plan is being largely repeated except: (1) UV filters are dropped because the measurement is generally only of the red leak. (2) F160BW is retained in order to check for developing pinholes. (3) Crossed filters used as neutral densities are eliminated (illumination

pattern is wrong). (4) An attempt will be made to schedule some broad bandpass measurements on the dark Earth. This is based on Cycle 4 programs 5570 + 5571 + 6142.

- **Accuracy**: Overall accuracy of the flats derived from this test and the corresponding Cycle 4 observations should be below 1% RMS. Discrepancies between the results of this test and those from Cycle 4 should be 1% RMS. Differences between the two datasets analyzed separately will measure the flat field variability to this level. This data, together with the flat field check proposal should enable similar accuracy in the broad bandpass flats.
- **Products**: This proposal provides medium and narrow bandpass streak flats which can be combined with the high frequency information in the TV flats to yield accurate flat fields. The ratio of the TV and derived flats provides a correction that can also be applied to the TV broad bandpass data. We may also get broad band flat fields directly for comparison from the sky or from this proposal's exposures on the Earth's shadow.

6188: Darks

- **Purpose**: Provide dark frames for pipeline reduction, and hot pixel lists.
- **Description**: Five dark frames are taken every week to provide ongoing calibration of the CCD dark current rate and to monitor the characteristics and the evolution of hot pixels. Over an extended period, these data provide a monitor of radiation damage to the CCDs. The dark frames will be obtained with the CLOCKS=OFF. In addition, four darks are taken per month with CLOCKS=ON (although there is no effect such as amplifier glow expected from running the serial register for these CCDs).
- Changes from the Cycle 4 program 5562 are that each group of five darks is constrained to be taken within a 2-day period, in order to simplify the data analysis (because fewer new hot pixels are involved), and the CLOCKS=ON exposures have been added.
- **Accuracy**: The accuracy of the super-dark computed from these data depends on the number of frames combined. The present practice is to combine them in groups of 10 frames for pipeline super-darks. This gives a median signal-to-noise of 16 and higher signal-to-noise on hotter pixels than the median (with the somewhat shaky assumption that the dark noise is Poisson). This means that the residual systematic error after super-dark subtraction on an 1800-second exposure is about 3 electrons - much less than the read noise. In prin-

ciple, this residual can be further reduced to 0.4 electrons if a super-dark is generated from all of the dark frames, with suitable masking based on hot pixel lists.

- **Products**: The data is grouped into sets of 10 frames every two weeks. These are combined into super-darks for use in the pipeline. In addition, hot pixel lists can be generated with a time resolution of one week.

6189: VISFLAT Monitor

- **Purpose**: Monitor internal flat fields of instrument.
- **Description**: All use of the VISFLAT channel is concentrated in this proposal. It is based on Cycle 4 programs 5568 and 5655. The program takes one complete set of exposures using the visible calibration channel lamp (VISFLATS) at the start of the cycle through all visible filters. Monthly, VISFLATS will be obtained with the photometric filter set (F336W, F439W, F555W, F675W, and F814W) both before and after the DECON. A monthly VISFLAT exposure with the Wood's filter, F160BW, allows its visible transmission to be monitored. Two monthly VISFLAT exposures obtained through the LRF (FR533N), one at each gain, provide a monitor of the ADC's performance. The VISFLAT exposures should be packed together to optimize use of each lamp-on cycle.
- **Accuracy**: The internal flats, when well exposed, are each accurate to 0.6% in terms of the pixel-to-pixel (high frequency) variations in the CCDs. Thus, high frequency flat field stability can be verified to 1%. When the results from several filters are combined it will be possible to check that the CCDs are indeed relatively stable to much better than 1%.
- **Products**: The complete filter-set sweep will be compared to the corresponding Cycle 4 data-set primarily to verify that none of the filters are developing problems. Ratios of these flats will primarily indicate the stability of the channel itself, unless there are strong variations from filter to filter. Unless time dependence in the filters is seen, it is likely that flat fields for pipeline calibration will continue to be made by combining Earth-flat, SLTV-flats, and eventually sky-flats.
- The bi-monthly photometric filter-set observations will be used to monitor WFPC2's flat field response and to build a high S/N flat field database (primarily useful in tracking any changes in the pixel-to-pixel response of the instrument and any possible long term contamination induced changes). Histograms generated from the ramp filter flats will be used to trace the ADC transfer curve. F160BW can be checked monthly for pinholes. Results reported in Stiavelli and Baggett, ISR WFPC2 96-01.

6190: Internal Flats

- **Purpose**: Provide backup database of INTFLATS, in case VISFLAT channel fails.
- **Description**: Based on Cycle 4 program 5568. A complete set of illuminated shutter blade flats (INTFLATS) is taken close to the complete set of VISFLATS. Each filter is exposed on each shutter blade (A or B) at each gain setting (7 or 15). Thus, there are four exposures per filter which should be uninterruptedly sequenced as (A7, A15, B15, B7). There is a possible concern on thermal control, where an out-of-limit condition was almost reached when 5568 was run. This will be avoided by spacing the exposures suitably.
- **Accuracy**: The signal-to-noise per pixel is similar to that obtained in the VISFLAT program (0.6%) but there are much larger spatial and wavelength variations in the illumination pattern. As a result, this data-set will not form any part of the pipeline calibration. This baseline is necessary in case the VISFLAT channel fails, and there are temporal variations in the camera flat fields at the 1% level. The test does give a good measurement of the gain ratios and their stability, which should be accurate to much better than 1%, when all of the data is analyzed.
- **Products**: INTFLAT/VISFLAT ratios can be generated if there is a failure in the calibration channel. Gain ratios and stability will be assessed. Results reported in Stiavelli and Baggett, ISR WFPC2 96-01.

6191: UV Flats

- **Purpose**: Use UV calibration channel to monitor long term internal UV stability.
- **Description**: UV flat fields will be obtained with the calibration channel's ultraviolet lamp (UVFLAT) using the limited FUV filter set (F122M, F170W, F160BW, F185W, and F336W) twice in the cycle immediately after a DECON. The UV lamp is degrading with use, so its use must be minimized. The UV flats will be used to monitor the FUV flat field stability and the stability of the Wood's filter, F160BW, by using F170W as a reference. The VISFLAT/UVFLAT ratio from the F336W filter will provide a diagnostic of the UV flat field stability, and tie the UVFLAT and VISFLAT flat field patterns together. This program represents the entire use of the UV lamp in Cycle 5. This proposal is based on the Cycle 4 program 5568, but with two extra filters (F122M and F185W).

- **Accuracy**: Should verify stability of the UV filters and flat field to 2%. The overall flat field response is not measured because the lamp output is not uniform, and temporal variations in throughput are not measured because the lamp output varies.
- **Products**: Ratio images with the corresponding data-set from Cycle 4 and future cycles will verify the UV flat field stability.

6192: CTE Calibration

- **Purpose**: Calibrate CTE effect for a range of star brightness and background.
- **Description**: The crowded ω Cen field is observed for 40 seconds through F555W with gain 7 and preflashes of 0, 5, 10, 20, 40, 80 and 160 electrons. As a gain check and calibration, it is observed at the same orientation with gain 15 twice at preflash levels of 0 and 160 electrons. The whole sequence is repeated with filter F814W. Then a whole orbit is filled with 1 second exposures, in order to investigate the effect of CTE on low signal level stars (but with high accumulated signal-to-noise). This last orbit is repeated with a preflash of 40 electrons. This is based on Cycle 4 programs 5645 + 5646 + 5659.
- **Accuracy**: As this test is a differential measurement of the CTE slope, it should be very accurate (much better than 1%). As a large number of stars are involved, and the photon noise on each measurement is of order 1%, the slope derived should be much more accurate. The largest remaining uncertainty will be the absolute level of the slope, not differential effects caused by varying background.
- **Products**: After pipeline processing, each image will be reduced by aperture photometry to measure the stellar brightness and how it depends on the preflash level. This is a differential measurement and gives no direct information about the slope of the CTE effect at high background levels. The absolute CTE can be estimated from 5646 (already run once with a raster in this field).

6193: PSF Characterization

- **Purpose**: Provide a sub-sampled PSF over the full field to allow PSF fitting photometry.
- **Description**: This proposal measures the PSF over the full field in photometric filters in order to update the TIM and TinyTIM models and to allow accurate empirical PSFs to be derived for PSF fitting photometry. With one orbit per photometric filter, a spatial scan is performed over a 4x4 grid on the CCD. The step size is 0.025 arcseconds. This gives a critically sampled PSF over most of the visible range. The crowded ω Cen field is used. 40 sec images are taken through each of the photometric filters (F336W, F439W, F555W,

F675W, F814W). Data volume will be a problem, so special tape recorder management will be called for. This is based partially on Cycle 4 program 5575, which used the same field. The proposal also allows a check for sub-pixel phase effects on the integrated photometry.

- **Accuracy**: The chosen field will have hundreds of well exposed stars in each chip. Each star will be measured 16 times per filter at different pixel phases. In principle, the proposal therefore provides a high signal-to-noise critically sampled PSF. This would leave PSF fitting photometrists in a much better position than now where pixel undersampling clearly limits the results. The result will be largely limited by breathing variations in focus. It is hard to judge the PSF accuracy that will result. If breathing is less than 5 microns peak-to-peak, the resulting PSFs should be good to about 10% in each pixel. PSF fitting results using this calibration would, of course, be much more accurate. In addition, the test gives a direct measurement of sub-pixel phase effects on photometry, which should be measured to much better than 1%.
- **Products**: This program provides sub-sampled PSFs for photometry codes, data for comparison with PSF codes, and measurement of pixel phase effect on photometry (sub-pixel QE variations exist).

6194: Polarization and Ramps

- **Purpose**: Perform residual calibration and check for stability of polarizer and ramp filters.
- **Description**: This proposal does not duplicate the existing ramp wavelength calibration or polarization calibration (Cycle 4 programs 5574 and 6140). Instead, it provides a full polarization calibration for a filter that was not supported in Cycle 4 (F300W), a check for polarization stability, and a throughput calibration for the linear ramp filters, by scanning the spectrophotometric standard along the ramps.
- **Accuracy**: The proposal should support polarimetry at the 3% level and measure the ramp throughput at the 2% level.

6195: Flat field Check

- **Purpose**: Check quality of flat fields and estimate errors in them.
- **Description**: The crowded ω Cen field is positioned with a bright star at the center of each CCD in turn. 40 second images are taken through each of the photometric filters (F336W, F439W, F555W, F675W, F814W) and as many supplementary filters (from F450W, F606W, F702W and F547M) as can be fitted in. If data volume is a problem, single chip readout is acceptable, but should be avoided as much as possible. This is based on Cycle 4 programs 5659 and 5646.

- **Accuracy**: Overall discrepancies between the existing flat fields and the results of this test should be 1-2% rms. Part of the point of the test is to measure this accuracy.
- **Products**: After pipeline processing, each image will be reduced by aperture photometry to measure the RMS errors in the flat fields. The RMS error will be determined by the additional noise in the independent measurements over the expected variance of less than 1% from photon statistics. The single bright star at the center of each chip independently estimates the chip to chip normalization error.

6250: Internal Monitor

- **Purpose**: Check for short term stability of instrument.
- **Description**: The routine internal monitor, to be run twice weekly for WFPC2 during Cycle 5, obtains two bias frames at each gain, two INTFLATs with the F555W filter at each gain, and two Kelsall spot images with exposure times optimized for the WF and PC, respectively. It is identical to the Cycle 4 program 5560.
- **Accuracy**: This monitor is not involved in generating quantitative calibration information.
- **Products**: The test provides a biweekly monitor of the integrity of the CCD camera chain electronics both at gain 7 and 15, a test for quantum efficiency hysteresis in the CCDs, and an internal check on the alignment of the WFPC2 optical chain. Stiavelli and Baggett, ISR WFPC2 96-01.

8.13 Cycle 6 Calibration Plan

The Cycle 6 calibration plan is similar to that for Cycle 5, and is summarized in Table 8.6 on page 253. Important differences include the addition of programs to check the astrometric calibration (6941), more detailed checking of the camera electronics (6942), and measurements of narrow band filter throughputs (6943). Also, it is expected that there will be reduced usage of the calibration channel VISLAMP, so as to prolong the lamp lifetime. More detailed program descriptions are given below. For a report on the final results from these programs, please see ISR WFPC2 98-01 ("Cycle 6 Closure Report") at:

http://www.stsci.edu/instruments/wfpc2/Wfpc2_isr/wfpc2_isr9801.html

Table 8.6: Summary of Cycle 6 Calibration Plan.

ID	Proposal Title	Schedule	Results	Accuracy	External Time (orbits)	Notes
			Routine Monitoring Programs			
6902	Photometric Monitor	2x per 4 weeks	SYNPHOT	2%	26	
6903	Decontamination	1x per 4 weeks	CDBS	n/a	0	(darks, internals)
6904	Darks	Weekly	CDBS	1 e/hr	0	WWW hot pixel lists
6905	Internal Monitor	Weekly	CDBS	0.8 e	0	
6906	Visflat Monitor	2x per 4 weeks	ISR	0.3%	0	(monitor lamp health)
6907	Intflat Monitor	1x per 4 weeks	ISR	0.3%	0	
6908	UV Flat Field Monitor	2x in Cyc. 6	ISR	2-8%	0	
6909	Earth Flats	Continuous	CDBS	0.3%	0	
			Special Calibration Programs			
6934	Photometric Zeropoint	1x in Cyc. 6	SYNPHOT	2%	6	Add 2 new standards
6935	Photometric Trans.	2x in Cyc. 6	ISR	2-5%	9	Three targets
6936	UV Throughput & Ly α	2x in Cyc. 6	SYNPHOT	3-10%	12	Include BD+75D325
6937	CTE Calibration	1x in Cyc. 6	ISR	1%	2	
6938	PSF Characterization	1x in Cyc. 6	CDBS	10%	7	
6939	Linear Ramp Filters	1x in Cyc. 6	CDBS	3%	4	
6940	Polarizers	1x in Cyc. 6	CDBS	3%	4	
6941	Astrometry Verification	1x in Cyc. 6	STSDAS	0.01″	4	
6942	Camera Elect. Verification	1x in Cyc. 6	ISR	0.5%	1	
6943	Narrow Band Throughput	SNAP	SYNPHOT	3%	8	SNAP
	TOTALS				83	

6902: Photometric Monitor

- **Purpose:** Monthly external check of instrumental stability.
- **Description:** The standard star GRW+70D5824 is observed before and after each decontamination (i.e. twice in a four-week period). Each observation consists of three sequences: (1) F170W in all four chips to monitor contamination in the far UV; (2) F439W, F555W, F814W on the PC to monitor focus; and (3) F160W, F185W, F218W, F255W, F300W, F336W, F439W, F555W, F675W, F814W in a dif-

ferent chip each month. Some filters may be cut because of lack of time (F185W cut first, then F300W, then F675W, then F218W). This proposal is based largely on Cycle 5 program 6184; focus monitoring in F439W and F814W is added at the expense of some UV filters.

- **Accuracy:** Overall discrepancies between the results of this test need to be measured to better than 2% and are expected to be less than 1% rms. The point of the test is to measure this variation.
- **Products:** Documents produced are Instrument Handbook, TIPS, WWW (sensitivity trends). Updates in UV sensitivity variation used in SYNPHOT are provided.

6903: Decontamination

- **Purpose:** UV blocking contaminants are removed by warming the CCDs.
- **Description:** The decon itself is implemented via use of the DECON mode, in which the TECs are turned off and the CCD and heat pipe heaters are turned on to warm the detectors and window surfaces. Keeping WFPC2 warm for ~6 hours has been shown in previous Cycles to be sufficient to remove the contaminants and anneal many hot pixels; continuation of 6-hour decons is anticipated for Cycle 6. The internal observations taken before and after each decontamination consist of: four biases (two at each gain setting), four INTFLATs (two at each gain setting), two kspots (both at gain 15, one short and one long exposure, optimized for PC and WF), and finally, five darks (gain 7, CLOCKS=NO). To minimize time-dependent effects, each set of internals will be grouped within two days and performed no more than one day before the DECON and no later than 12 hours after the DECON. To protect against residual images in the darks (which results in the irretrievable loss of the critical pre-DECON hot-pixel status), the darks will be executed NON-INT and requested to be done at least 30 minutes after any WFPC2 activity.
- **Special Requirements:** This requires scheduling at four-week intervals. It prevents WFPC2 from being used for several hours, although other instruments can be used most of that time. Dark frames taken before decontaminations need to be protected from possible residual images from overexposed sources.
- **Accuracy:** This proposal is mainly designed to maintain the health of the instrument. Biases, darks and other internals taken with this proposal are used in generating appropriate reference files.
- **Products:** Those obtained from use of darks, biases and other internals (see Proposals 6904 and 6905).

6904: Darks

- **Purpose:** Measure dark current on individual pixels and identify hot pixels at frequent intervals.
- **Description:** Every week, six 1800s exposures are taken with the shutter closed (five with clocks=OFF, and one with clocks=ON). The length of the exposures is chosen to fit within an occultation period. The weekly frequency is required because of the high formation rate of new hot pixels (about 70/CCD/day). Five darks (clocks=OFF) a week are required for cosmic ray rejection, to counterbalance losses due to residual images, and to improve the noise of individual measurements. Even with these measures, there are some weeks when no usable darks will be available because of residual images. Normally this results only in a longer-than-usual gap in the hot pixel lists, but in a decontamination week, information on pixels that became hot and then annealed would be lost irretrievably. For this reason, pre-DECON darks are to be executed NON-INT and at least 30 minutes after any WFPC2 activity (see Proposal 6903). Non-decon-week darks do not need to be protected in this fashion.
- **Accuracy:** Superdarks should be accurate to better than 1 e^-/hour and are expected to reach errors of about 0.05 e^-/hour (single-pixel rms). Systematic errors due to dark glow (a spatially and temporally variable component of dark signal) and hot pixels may exceed these limits significantly.
- **Products:** Weekly dark reference files are delivered to CDBS and monthly tables of hot pixels are posted on the Web.

6905: Internal Monitor

- **Purpose:** Verification of short-term instrument stability for both gain settings.
- **Description:** The internal observations will consist of eight biases (four at each gain, and four INTFLATs (two at each gain). The entire set should be run once per week (except for DECON weeks) on a non-interference basis. This proposal is similar to the Cycle 5 Internal Monitor (6250), except that the K-spot images have been removed (these are being taken with the DECON Proposal). The execution frequency during Cycle 6 has also been reduced, from twice a week to once a week, although the total number of biases has been increased to continue to provide an adequate number of frames for pipeline reference file generation.
- **Accuracy:** Approximately 120 bias frames will be used for each pipeline reference file; accuracy is required to be better than 1.5 e^-/pixel, and is expected to be 0.8 e^-/pixel.

- **Products:** Superbiases are delivered every 6-12 months to CDBS. TIPS reports are made on possible buildup of contaminants on the CCD windows (worms) as well as gain ratio stability, based on INTFLATs. ISRs document any changes.

6906: Visflat Monitor

- **Purpose:** Monitor the stability of the camera and filter responses via the VISFLAT channel.
- **Description:** Twice a month, internal flat fields (VISFLATs) will be obtained using the visible calibration channel lamp with the photometric filter set plus a couple of narrow-band filters. The images will be used to monitor WFPC2's flat field response as well as to build a high S/N flat field database, which will provide information on the pixel-to-pixel response in the cameras and any possible long-term contamination-induced changes. The LRF (FR533N) exposures, one at each gain, taken after DECON will provide a monitor of the ADC's performance. Histograms generated from the ramp filter flats will be used to trace the ADC transfer curve. ON HOLD: In addition to the monitor observations, an initial filter-sweep is done to obtain VISFLATs in all visible filters. These will be compared to the Cycle 5 filter-sweep data to verify that none of the filters are developing any problems, and to provide a check of the calibration channel's long-term stability.
- **Special Requirements:** Uses the VISFLAT calibration channel, whose Welch-Allyn bulb is apparently wearing out. (A back-up exists for the Welch-Allyn bulb.) The Cycle 6 proposal has been redesigned to limit the number of ON/OFF cycles placed on this channel to a level believed safe over 10-15 years. The sweep part of the proposal, which puts the heaviest usage on the lamp, is on hold, pending verification of the lamp health from the short monthly executions. The INTFLAT Monitor (Proposal 6907) can obtain similar information if necessary.
- **Accuracy:** The VISFLAT response is stable to about 0.3%, both in overall level (lamp degradation aside) and in spatial variations. The point of this proposal is to verify this stability on a regular basis and to monitor the lamp degradation.
- **Products:** ISR and TIPS reports will be prepared.

6907: Intflat Monitor

- **Purpose:** Provide backup database of INTFLATS in case VISFLAT channel fails.

- **Description:** This proposal consists of two parts: 1) an INTFLAT filter sweep and, 2) a series of exposure to test the linearity of the camera. 1) The sweep is a complete set of internal flats cycling through both shutter blades and both gains. Signal-to-noise per pixel is estimated to be similar to the VISFLATs (0.6%) but the spatial and wavelength variations in the illumination pattern are much larger. However, the INTFLATs will provide a baseline comparison of INTFLAT vs. VISFLAT, in the event of a calibration channel system failure and temporal variations in the flat fields at the 1% level. In addition, these images will provide a good measurement (better than 1%) of the stability of the gain ratios. 2) The linearity test portion is aimed at obtaining a series of INTFLAT with both gains and both shutters. Since the INTFLATs have significant spatial structure, any non-linearity would appear as a non-uniform ratio of INTFLATs with different exposure times. A set of exposures is also taken with gain 7, shutter B, and CLOCKS=YES.
- **Accuracy:** The signal-to-noise per pixel is similar to that obtained in the VISFLAT program (0.6%) but there are much larger spatial and wavelength variations in the illumination pattern. As a result, this dataset will not form any part of the pipeline calibration. This baseline is necessary in case the VISFLAT channel fails and there are temporal variations in the camera flat fields at the 1% level.
- **Products:** TIPS reports and ISRs will be prepared if any significant variations are observed.

6908: UV Flat Field Monitor

- **Purpose:** Monitor the stability of UV flat field.
- **Description:** UV flat fields will be obtained with the calibration channel's ultraviolet lamp (UVFLAT) using the UV filter set (F122M, F170W, F160BW, F185W, and F336W). The UV flats will be used to monitor UV flat field stability and the stability of the Woods filter (F160BW) by using F170W as the control. The F336W ratio of VISFLAT (Cycle 6 proposal 6906)/UVFLAT ratio will provide a diagnostic of the UV flat field degradation and tie the UVFLAT and VISFLAT flat field patterns together. Two supplemental dark frames must be obtained immediately after each use of the lamp, in order to check for possible afterimages.
- **Special Requirements:** This uses the limited life UV lamp. In order to prevent excessive degradation of the lamp, the SU duration for each UVFLAT visit should be kept the same as the durations used during Cycle 5 (proposal 6191); the lamp should not remain on for periods of time longer than those used in Cycle 5. To be executed once before and once after the refurbishment mission, shortly after a decontamination.

- **Accuracy:** About 2-8% pixel-to-pixel are expected (depending on filter).
- **Products:** New UV flat fields are made if any changes are detected.

6909: Earth Flats

- **Purpose:** Monitor flat field stability.
- **Description:** As in Cycle 5 program 6187, four sets of 200 Earth streak-flats are taken to construct high quality narrow-band flat fields with the filters F160BW, F375N, F502N, F656N and F953N. Of these 200 perhaps 50 will be at a suitable exposure level for de-streaking. The resulting Earth superflats map the OTA illumination pattern and will be combined with SLTV data (and calibration channel data in case of variation) for the WFPC2 filter set to generate a set of superflats capable of removing both the OTA illumination and pixel-to-pixel variations in flat field. The Cycle 4 plan is being largely repeated except: (1) UV filters are dropped because measurement is generally only of the read leak; (2) F160BW is retained in order to check for developing pinholes; and (3) Crossed filters used as neutral densities are eliminated (illumination pattern is wrong). Specific observations for the Methane Quad filters will also be included.
- **Accuracy:** The single-pixel noise expected in the flat field is 0.3%.
- **Products:** New flat fields to CDBS if changes detected.

6934: Photometric Zeropoint

- **Purpose:** Verify synthetic zeropoint of WFPC2 filters.
- **Description:** Standard stars are observed through all filters longward of F336W (inclusive) with the limit of one orbit per target. Targets include: the spectrophotometric standard GRW+70D5824 in PC and WF3; two stars chosen as standards by other instruments on HST; and two standard star fields, containing 3-4 stars each, commonly used in ground based photometry. Observations of GRW+70D5824 will be directly comparable to the corresponding observations for Cycles 4 and 5 (programs 5572 and 6179) and will verify the stability of the filters as well as improve the accuracy of the calibration. The other standards are observed to provide cross-instrument calibration and in order to increase the range of colors used for photometric verification. This proposal will help all observers who want to do quantitative photometry at the 2% level.
- **Special Requirements:** Specific orientations will be required for the two fields of standards in order to fit the maximum number of stars. All observations should be executed within a week after decontamination.

- **Accuracy:** 2% required, 1% expected for our main spectrophotometric standard GRW+70D5824. Expected accuracy for the other standards is between 2% and 5%, depending on spectral type and filter; most of the error derives from limited knowledge of the transformations between ground based and WFPC2 photometric systems.
- **Products:** TIPS reports, SYNPHOT updates if necessary, and ISRs will be prepared.

6935: Photometric Transformation

- **Purpose:** (1) Update photometric transformations to Johnson-Cousins system and Strömgren system; (2) Determine spatial dependence of contamination; (3) Check the astrometric solution using M67; (4) Spot check of gain=7 vs. gain=15 ratios; 5) Spot check short vs. long exposure zeropoints.
- **Description:** Three photometric standard star fields in NGC 5139 (ω Cen; metal rich), NGC 2682 (M67; metal poor), and NGC 2100 (young cluster) are observed before and after a decontamination. Four different filter sets are used: (1) The five filters generally used to match the Johnson-Cousins system (F336W, F439W, F555W, F675W, F814W); (2) The wide-band equivalents for the Johnson-Cousins system (F300W, F380W, F450W, F606W, F702W); (3) The Strömgren equivalents (F336W, F410M, F467M, F547M); and (4) Two filters farther toward the UV (F255W, F170W), so that contamination over the full field of view can be measured. F255W is not used for the reddest cluster (NGC 5139). F170W is only used for the bluest cluster (NGC 2100). For the brighter clusters (NGC 2682 and NGC 2100) long and short exposures are taken in the UBVRI equivalents both to extend the dynamic range and to check for differences in photometric zeropoints. A spot check is included to compare gain=7 and gain=15 is also included for NGC 5139 and NGC 2682.
- **Special Requirements:** The first visit for each target must be taken within 3 days after a decontamination. The second visit, including only the UV filters, must be taken more than 25 days after the first visit, but before the next decontamination.
- **Accuracy:** The photometric transformations should be accurate to 2-5%. The stability of these transformations will be measured to the 1% level. The astrometry should be good to 0.1″ (absolute) and 0.05″ (relative).
- **Products:** ISR and Instrument Handbook. It will also be part of a planned paper on the possibility to do 1% photometry.

6936: UV Throughput and Lyman-α Verification

- **Purpose:** Verify throughput for all UV filters, including Lyman-α test to monitor possible contamination on pick-off mirror.
- **Description:** Spectrophotometric standards are observed shortly before and after a DECON through all the UV filters in each chip and through F160BW crossed with F130LP, F185LP, and F165LP to determine the wavelength dependence of the throughput across the bandpass (for color terms). This proposal is based on the Cycle 5 UV Throughput proposal (6186) but includes also the standard BD+75D325 used in Cycle 4 (proposal 5778) to establish the Lyman-α throughput calibration.
- **Special Requirements:** Timing requirements with respect to decontaminations.
- **Accuracy:** The UV throughput will be measured to better than 3%. Accuracy in Lyman-α throughput is expected to be between 5 and 10%, because of the residual uncertainty of the red leak correction after observations with crossed F122M and F130LP.
- **Products:** TIPS reports, SYNPHOT updates, and ISRs will be prepared if necessary.

6937: CTE Calibration

- **Purpose:** (1) Test if the exposure-time dependence of the photometric calibration is due to CTE (long vs. short exposure problem); (2) refine flux and background-level dependent aperture corrections.
- **Description:** The globular cluster NGC 2419 will be observed through F555W with a combination of exposure times (between 5 and 1400 s) and preflash levels (0 to 500 e^-). Analysis of Cycle 5 CTE calibration (proposal 6192) suggests that magnitude errors due to charge transfer effects are greatly reduced (if not entirely eliminated) at background levels of 160 e^- or greater. CTE effects have been proposed as the solution to reported differences in the magnitudes of stars measured on frames with short exposures vs. long exposures. If CTE is the cause, then the differences should disappear with preflash. We will re-observe the cluster NGC 2419 with and without preflash to test this hypothesis. This dataset will also provide a large number of stars with which to refine existing measurements of the effects of CTE on the wings of the PSF. A range of preflash levels will be explored at the 60 sec exposure time.
- **Special Requirements:** Observations should be made at the same position and roll angle as the previous NGC 2419 LONG exposures (proposal GO-5481).

- **Accuracy:** The reported short vs. long effect is ~0.05 mag. We wish to reduce this to less than 0.01 mag.
- **Products:** An ISR will be prepared. If appropriate, a special task to correct the CTE effect will be generated.

6938: PSF Characterization

- **Purpose:** Provide a sub-sampled PSF over the full field to allow PSF fitting photometry, test PSF subtraction as well as dithering techniques (c.f. effects of the OTA breathing and CCD gain).
- **Description:** Measure PSF over full field in photometric filters in order to update the TIM and TinyTIM models and to allow accurate empirical PSFs to be derived for PSF fitting photometry. These observations will also be useful in order to test PSF subtraction and dithering techniques at various locations on the CCD chips. With one orbit per photometric filter, a spatial scan is performed over a 4X4 grid on the CCD. The step size is 0.025 arcseconds; this gives a critically sampled PSF over most of the visible range. This program uses the same specially chosen field in ω Cen as the Cycle 5 proposal 6193, but with a few arcsec shift in order to map the PSF variation better. The standard 'photometric' filters are used. Two additional orbits are used to explore the effects of OTA breathing and CCD gain onto dithering and PSF subtraction techniques. Data volume will be a problem, so special tape recorder management will be called for. The proposal also allows a check for sub-pixel phase effects on the integrated photometry.
- **Special Requirements:** This needs the same pointing and orientation as Cycle 5 observations for proposal 6193, thus should be scheduled within a similar time frame.
- **Accuracy:** It provides measurement of pixel phase effect on photometry (sub pixel QE variations exist). The chosen field will have tens of well exposed stars in each chip. Each star will be measured 16 times per filter at different pixel phases. The proposal therefore provides, in principle, a high signal-to-noise, critically sampled PSF. This would leave PSF fitting photometrists in a much better position than now, where pixel undersampling clearly limits the results. The result will be largely limited by breathing variations in focus. It is hard to judge the PSF accuracy that will result. If breathing is less than 5 microns peak-to-peak, the resulting PSFs should be good to about 10% in each pixel. Breathing effects will be investigated (one additional orbit) as well as the gain dependence (one additional orbit). PSF fitting results using this calibration would of course be much more accurate. In addition, the test gives a direct measurement of sub-pixel phase effects on photometry, which should be measured to better than 1%.

- **Products:** A PSF library (CDBS) will be assembled, and an ISR will be issued as needed.

6939: Linear Ramp Filters

- **Purpose:** Verify throughput calibration for Linear Ramp Filters at selected wavelengths.
- **Description:** Throughput calibration is obtained by observing the spectrophotometric standard GRW+70D5824 at several filter rotations and wavelengths. This completes the program carried out in Cycle 5, in which some wavelength ranges and rotations could not be covered.
- **Accuracy:** Throughput accuracy should be verified to better than 3%; 1-2% can be achieved.
- **Products:** SYNPHOT throughput tables will be updated if necessary.

6940: Polarizers

- **Purpose:** Verify stability of polarization calibration.
- **Description:** The goal of this proposal is to check for any changes in the polarization calibration since Cycle 5. Observations are made in F555W+POLQ of both polarized and unpolarized stars, in addition to VISFLATs. Data are taken in all four quads of the polarizer, as well as in three rotated positions of the POLQ.
- **Special Requirements:** Requires specific orientations.
- **Accuracy:** 3%.
- **Products:** Update throughput tables if necessary

6941: Astrometry Verification

- **Purpose:** Verify accuracy and stability of geometric transformation and relative astrometry solution.
- **Description:** A very rich star field in ω Cen will be observed in five different positions with relative shifts of 40″ in each coordinate. Positions of more than 2000 stars per chip will be compared between pointings using the three different astrometric solutions provided by Gilmozzi, Holtzman, and Trauger, in order to verify and refine their accuracy. (Differences of up to 1 PC pixel exist in some regions of the field of view.) A very densely populated field is chosen in order to achieve better coverage of the field of view, even if at the expense of the accuracy of individual position measurements. Observations will be carried out in three filters, F555W, F300W, and F814W, to provide a verification and/or correction of the wavelength dependence of the solution. The F555W observation is repeated with smaller shifts of 15″ to ensure a better coverage of the PC.

- **Accuracy:** We expect better than 0.01″ and require better than 0.05″ (full field of view).
- **Products:** Improvements will be noted in METRIC and in the aperture reference file if required. An ISR will be issued as needed.

6942: Camera Electronics Verification

- **Purpose:** Verify several aspects of the WFPC2 camera electronics: linearity, gain ratios, effect of CLOCKS, and effect of CTE on extended sources.
- **Description:** Observing a very extended non-uniform target represented by the giant elliptical galaxy NGC 4472. The linearity test is carried out by taking exposures of NGC 4472, centered in WFALL, with a variety of exposure times. Since the galaxy is non-uniform, the ratio of these exposures is directly related to the camera linearity. The exposures will be taken with GAIN=7. However, one exposure will also be taken with GAIN=15. Additional exposures will be taken with CLOCKS=YES and with a preflash. These observations complement those of the internal calibration proposal 6907. The two major advantages of these observations compared to the 6907 ones are the possibility of studying the effect of preflash (since the light distribution of the preflash is different from that of NGC 4472) and the possibility of measuring an absolute response curve, since NGC 4472, unlike the INTFLAT lamp, does not have variations in luminosity. NGC 4472 has been chosen as target galaxy because it is large enough to produce significant signal in all chips and bright enough to allow us to explore the highest counts without excessive integration times.
- **Accuracy:** We expect 0.5% for linearity and CTE, 0.1-0.2% for gain ratios and CLOCKS. We require less than 1% on each item.
- **Products:** ISRs and TIPS reports will be prepared as needed.

6943: Throughput Verification for Narrow Band Filters

- **Purpose:** Direct verification of throughput of narrow band filters through observations of emission line objects.
- **Description:** The current throughput calibration of narrow-band filters is based on filter profiles from data obtained before launch and on observations of continuum sources. This program will verify the accuracy of the calibration, and indirectly the stability of the filters, by observing eight planetary nebulae with strong lines and well-established ground based spectra. The observations can be executed in SNAPSHOT mode since they will be short and none is specifically required. Some planetary nebulae with existing Cycle 4 and 5 observations will be included for stability verification.

- **Accuracy:** We expect 2% and require 3%.
- **Products:** SYNPHOT tables will be updated and an ISR issued if required.

8.14 Cycle 7 Calibration Plan

8.14.1 Overview

The main goals of the WFPC2 Calibration Plans for Cycle 7 are:

- verify that the instrument remains stable in its main characteristics.
- address its photometric accuracy.

These goals are achieved by a mix of monitoring programs, which verify the stability and continued performance of the camera by repeating routine observations on a regular basis, and special calibrations, which have the goal to enhance the WFPC2 calibration in specific areas.

Standard Monitoring Programs

The stability of WFPC2 is mainly verified through the Photometric Monitoring program and the set of internal monitoring programs. The Photometric Monitoring program (7618) consists of regular one-orbit visits of our photometric standard GRW+70D5824, executed immediately before and after decontaminations. These observations allow us to monitor efficiently four main areas: the overall photometric throughput of the camera, the contamination of the CCD windows, especially in the UV, the PSF properties at different wavelengths, and the OTA focus. We continue to rely heavily on internal observations for some instrument maintenance and for many other types of monitoring: decontaminations (7619) to clear the contaminants from the CCD windows and to limit the growth in hot pixels; darks (7620) in order to produce up-to-date, high-quality dark reference files and to identify new hot pixels in a timely manner; biases, INTFLATs, and K-spots (decontamination programs, plus 7622, 7623), to verify the integrity of the camera's optics and electronics chain, and the pixel-to-pixel response in the visible; Earth Flats (7625) to follow variations in the large-scale flat field; and UV flats using the internal UV lamp (7624), to monitor the pixel-to-pixel response in the UV. The planned observations have remained largely the same as in previous cycles, except that internal flats place an increasing emphasis on the INTFLAT channel because of the continuing degradation of the VISFLAT channel.

Other Monitoring Programs

Some additional monitoring programs introduced in Cycles 7 deserve special mention. The Supplemental Darks program (7621, 7712, 7713) aims at obtaining a large number of relatively short darks on a very frequent basis, with the main goal of helping users identify hot pixels in their observations. The program has been designed to place the least possible burden on the scheduling system; that these additional darks have a low priority, and are scheduled whenever feasible. Under normal circumstances, this program provides up to 21 additional 1000s darks per week, providing users a good chance of having a dark within half a day of their observations. The Astrometric Monitor program (7627) measures the relative placement of the four WFPC2 CCD in the focal plane; we have evidence that shifts of up to 150 mas have occurred since 1994, and the Astrometric Monitor program is designed to track the continuing motion of the detectors. Finally, the CTE Monitor (7929), introduced late in Cycle 7, measures the photometric impact of the loss in charge transfer efficiency of the WFPC2 detectors, which continues to increase with time.

Special Calibration Programs

Special calibration programs address specific areas of WFPC2 calibration that require dedicated calibration measurements. They include substantial photometric, CTE, and PSF characterization programs, of interest to the majority of WFPC2 users, as well as a number of smaller programs which address areas of more limited interest.

The Photometric Characterization program, a continuation of the Cycle 6 program of the same name, is designed to improve the link between WFPC2 and ground based photometry. The Cycle 7 program (7628) includes additional observations of NGC 2100, a young LMC cluster, and NGC 2419, a very distant globular cluster in the Milky Way, which allows good coverage of the bright red giants, too bright and rare in nearby clusters. We also carry out a filter sweep on both our primary standard, GRW+70D5824, and our reference rich field in ω Cen. In Cycle 8 (8451) we repeat the filter sweep of the primary standard.

The Cycle 7 CTE Characterization program (7630) has provided a thorough exploration of the various parameters that could affect the so-called “long vs. short” anomaly, that is, the observed difference in count rates between long and short exposures. This extensive set of dedicated observations, in which each of the potentially critical parameters is varied in turn, has enabled us to characterize the anomaly and to suggest a correction formula that removes its impact almost completely.

The PSF Characterization program (7629) continues our accumulation of data for the WFPC2 PSF library, by addressing often-used filters such as F300W, F450W, F702W which were not included in previous cycles.

Table 8.7 on page 267 summarizes the relevant data for Cycle 7 programs, followed by summary descriptions of each program. For a report

on the final results from these programs, please see ISR WFPC2 99-05 (Cycle 7 Closure Report) at:

http://www.stsci.edu/instruments/wfpc2/Wfpc2_isr/wfpc2_isr9905

Details on individual proposals can be found through the HST Program Information page at URL

http://presto.stsci.edu/public/propinfo.html

Table 8.7: WFPC2 Cycle 7 Calibration Plan.

ID	Proposal Title	Frequency	Estimated Time (orbits)		Products	Accuracy	Notes
			"External"	"Internal"			
			Routine Monitoring Programs				
7618	Photometric Monitor	1–2/4 weeks	36		SYNPHOT	1–2%	Also focus monitor
7619	Decontamination	1/4 weeks		288	CDBS	n/a	Used together with darks, internals
7620	Standard Darks	weekly		360	CDBS, WWW	1 e/hr	Also hot pixel lists on WWW
7621, 7712, 7713	Supplemental Darks	weekly		2016		n/a	No analysis provided
7622	Internal Monitor	2/4 weeks		72	CDBS, TIR	0.8 e/pixel	New superbias (with 7619)
7623	Internal Flats	1/4 weeks		75	TIR	0.3%	Mostly INTFLATs
7624	UV Flat Field Monitor	2/cycle	4	8		2-8%	Before and after decon
7625	Earth Flats	continuous		155	CDBS	0.3%	Also LRF, Methane quads
7626	UV Throughput	2/cycle	4		SYNPHOT	3–10%	
7627	Astrometric Monitor	2/cycle	2	2	TIPS, TIR	0.″05	Also K-spots
			Special Calibration Programs				
7628	Photometric Characterization	1	10		ISR	2–5%	Also test zeropoint differences between chips, UV vignetting, astrometry
7629	PSF Characterization	1	5		WWW	10%	Covers widely used, high-throughput filters
7630	CTE Characterization	1	14		ISR	0.01 mag	Extensive coverage of preflash levels and exposure times in F555W, spot checks in F555W, F300W, hysteresis, CTE ramp
7929	CTE Monitor	4	4		ISR	0.02 mag	Measure changes in CTE ramp
8053	Supplemental Earth Flats	1		155	CDBS	0.3%	Repeat Earth Flats towards end of cycle
8054	LRF Calibration	1	10		ISR	3–5%	Complete LRF calibration, test stability
	TOTAL TIME (including all executions)		89	3131			

7618: WFPC2 Cycle 7: Photometric Monitor

- **Purpose**: Regular external check of instrumental stability. Based on Cycle 6 program 6902.
- **Description**: The standard star GRW+70D5824 is observed before and after a decontamination using three different strategies:
- F170W in all four chips to monitor contamination in the far UV.
- F439W, F555W, F814W on the PC to monitor focus.
- F160BW, F218W, F255W, F300W, F336W, F439W, F555W, F675W, F814W in a different chip each month. Some filters may be cut because of lack of time.
- Observations are taken after each decontamination and before every other decontamination, resulting in 36 orbits for 24 decontamination cycles.
- **Accuracy**: Overall discrepancies between the results of this test need to be measured to better than 2% and are expected to be less than 1% rms. This has been the case in Cycles 4 through 6. The point of the test is to measure this variation. Focus measurements have an expected accuracy of 1.5 micron, and a goal of 1 micron; the uncertainty in the focus determination is dominated by external factors, such as OTA breathing.
- **Products**: Instrument Handbook, reports at monthly TIPS meetings, WWW (sensitivity trends); updates in UV sensitivity variation used in SYNPHOT.

7619: WFPC2 Cycle 7: Decontamination

- **Purpose**: UV blocking contaminants are removed, and hot pixels cured, by warming the CCDs to +20C for six hours.
- **Description**: The decontamination itself is implemented via the DECON mode, in which the TECs are turned off and the CCD and heat pipe heaters are turned on to warm the detectors and window surfaces. Keeping WFPC2 warm for ~6 hours has been shown in previous Cycles to be sufficient to remove the contaminants and anneal many hot pixels.
- The internal observations taken before and after each decontamination consist of: four biases (two at each gain setting), four INTFLATs (two at each gain setting), two K-spots (both at gain 15, one short and one long exposure, optimized for PC and WF), and finally, five darks (gain 7, clocks off). To minimize time-dependent effects, each set of internals will be grouped within two days and performed no more than one day before the decon and no later that 12 hours after the decon. To protect against residual images in the darks (which results

in the irretrievable loss of the critical pre-decon hot pixel status), the darks will be executed as a non-interruptible sequence at least 30 minutes after any other WFPC2 activity.

- **Accuracy**: This proposal is mainly designed to maintain the health of the instrument. Biases, darks and other internals taken with this proposal are used in generating appropriate reference files (see Proposals 7620 and 7622).
- **Products**: Those obtained from use of darks, biases and other internals (see Proposals 7620 and 7622).

7620: WFPC2 Cycle 7: Standard Darks

- **Purpose**: Measure dark current on individual pixels and identify hot pixels at frequent intervals.
- **Description:** Every week, six 1800s exposures are taken (five with clocks=OFF and one with clocks=ON) with the shutter closed. The length of the exposures is chosen to fit nicely within an occultation period. The weekly frequency is required because of the high formation rate of new hot pixels (several tens per CCD per day). Five darks a week are required for cosmic ray rejection, to counterbalance losses due to residual images, and to improve the noise of individual measurements. Even with these measures, some weeks no usable darks will be available because of residual images. Normally this results only in a longer-than-usual gap in the hot pixel lists, but in a decontamination week, information on pixels that became hot and then annealed would be lost irretrievably. For this reason, pre-decon darks are to be executed in a non-interruptible sequence, at least 30 minutes after any WFPC2 activity (see Proposal 7619). Normal darks do not need to be protected in this fashion. The Supplemental Darks program (7621, 7712, 7713) will provide additional information on hot pixels.
- **Accuracy**: The required accuracy for darks is about 1 e^-/hour (single-pixel rms) for the vast majority of science applications. The expected accuracy in a typical superdark is 0.05 e^-/hour for normal pixels. The need for regular dark frames is driven by systematic effects, such as dark glow (a spatially and temporally variable component of the dark signal) and hot pixels, which cause errors that may exceed these limits significantly.
- **Products**: Weekly dark frames delivered to CDBS and monthly tables of hot pixels on the Web.

7621, 7712, 7713: WFPC2 Cycle 7: Supplemental Darks

- **Purpose**: Obtain very frequent monitoring of hot pixels.
- **Description**: This program is designed to provide up to three short (1000s) darks per day, to be used primarily for the identification of hot pixels. Shorter darks are used so that observations can fit into almost any occultation period, making automatic scheduling feasible. Supplemental darks will be taken at low priority, and only when there is no other requirement for that specific occultation period. This program is complementary with 7620, Standard Darks, whose longer individual observations are better suited to produce high-quality pipeline darks and superdarks, and are also carried out at higher priority. Note that hot pixels are often a cause of concern for relatively short science programs, since they can mimic or mask key features of the observations, and about 400 new hot pixels per CCD are formed between executions of the Standard Darks program (7620). These observations will be made available as a service to the GO community, and there is no plan to use them in our standard analysis and products. This program has become feasible starting in Cycle 7, due to the placement of a solid state recorder on-board HST.
- **Accuracy**: N/A
- **Products**: None

7622: WFPC2 Cycle 7: Internal Monitor

- **Purpose**: Verification of short-term instrument stability for both gain settings.
- **Description**: The internal observations will consist of eight biases (four at each gain) and four INTFLATs (two at each gain). The entire set should be run once per week, except for decon weeks, on a non-interference basis. This proposal is similar to the Cycle 6 Internal Monitor (6905).
- **Accuracy**: Approximately 120 bias frames will be used for each superbias pipeline reference file, generated once a year; accuracy is required to be better than 1.5 e^-/pixel, and is expected to be 0.8 e^-/pixel.
- **Products**: Superbiases delivered yearly to CDBS; TIPS reports on possible buildup of contaminants on the CCD windows (worms) as well as gain ratio stability, based on INTFLATs. A Technical Instrument Report will be issued if significant changes occur.

7623: WFPC2 Cycle 7: Internal Flats

- **Purpose**: Monitor the pixel-to-pixel flat field response and the VISFLAT lamp degradation as well as detect any possible changes due to contamination. This program is a combination and continuation of the Cycle 6 VISFLAT Monitor and INTFLAT Monitor proposals (6906, 6907, respectively). The VISFLAT portion has been minimized to conserve the lifetime of the CAL channel lamp.
- **Description**: This proposal contains an INTFLAT filter sweep, a VISFLAT mini-sweep, linearity tests, and monitoring images. Monitoring is carried out by taking INTFLATs with the photometric filter set after each decon. The VISFLAT mini-sweeps (before and after decon, twice during the cycle) will include the photometric filter set at gain 7, plus the linear ramp filter FR533N at both gains to test the camera linearity. The INTFLAT sweep, taken within a two-week period, includes almost all filters, some with both blades and gains (F336W, F439W, F547M, F555W, F569W, F606W, F622W, F631N, F502N, F656N, F675W, F673N, F702W, F785LP, F814W, F1042M), others with just one blade and gain (F487N, F467M, F588N, F380W, F658N, F791W, F850LP, F953N, F450W, F300W, F390N, F410M, F437N, F469N, and F160BW). The linearity test is done at both gains and blades using F555W, and an additional set with one blade and gain with clocks on.
- **Accuracy**: Assuming Cycle 7 results will be similar to those from previous cycles, the VISFLATs should be stable to better than 1%, both in overall level and spatial variations (after correcting for lamp degradation), and contamination effects should be < 1%. For the INTFLATs, the signal-to-noise ratio per pixel is estimated to be similar to the VISFLATs, but the spatial and wavelength variations in the illumination pattern are much larger. However, the INTFLATs will provide a baseline comparison of INTFLAT vs. VISFLAT, in the event of a complete failure of the CAL channel system. Temporal variations in the flat fields can be monitored at the 1% level. Gain ratios should be stable to better than 0.1%.
- **Products**: TIPS report, Technical Instrument Report if any significant variations are observed.

7624: WFPC2 Cycle 7: UV Flat field Monitor

- **Purpose**: Monitor the stability of UV flat field.
- **Description**: UV flat fields will be obtained with the CAL channel's ultraviolet lamp (UVFLAT) using the UV filters F122M, F170W, F160BW, F185W, and F336W. The UV flats will be used to monitor UV flat field stability and the stability of the Wood's filter (F160BW) by using F170W as the control. The F336W ratio of VISFLAT (Cycle

6 proposal 6906) to UVFLAT will provide a diagnostic of the UV flat field degradation and tie the UVFLAT and VISFLAT flat field patterns together. Two supplemental dark frames must be obtained immediately after each use of the lamp, in order to check for possible after-images.

- **Accuracy**: About 2-8% pixel-to-pixel expected (depending on filter).
- **Products**: New UV flat fields if changes are detected.

7625: WFPC2 Cycle 7: Earth Flats

- **Purpose**: Monitor flat field stability.
- **Description**: As in Cycle 6 program 6909, sets of 200 Earth-streak flats are taken to construct high quality narrow-band flat fields with the filters F160BW, F375N, F502N, F656N, and F953N. Of these 200 perhaps 50 will be at a suitable exposure level for de-streaking. The resulting Earth superflats map the OTA illumination pattern and will be combined with SLTV data (and calibration channel data in case of variation) for the WFPC2 filter set to generate a set of superflats capable of removing both the OTA illumination and pixel-to-pixel variations in the flat fields. The general plan of Cycles 5 and 6 is repeated.
- **Accuracy**: The single-pixel signal-to-noise ratio expected in the flat field is 0.3%.
- **Products**: New flat fields to CDBS if any changes are detected.

Proposal ID 7626: WFPC2 Cycle 7: UV Throughput

- **Purpose**: Verify throughput for all UV filters. Loosely based on the Cycle 5 and 6 UV throughput proposals (6186, 6936).
- **Description**: GRW+70D5824 will be observed shortly before and after a DECON through all the UV filters in PC and WF3. Observations should be taken roughly mid-way through the cycle.
- **Accuracy**: The UV throughput will be measured to better than 3%.
- **Products**: TIPS, SYNPHOT update if necessary, Technical Instrument Report to document any changes if necessary.

7627: WFPC2 Cycle 7: Astrometric Monitor

- **Purpose**: Verify relative positions of WFPC2 chips with respect to one another. Repeats parts of Cycle 6 proposal 6942 twice during Cycle 7.
- **Description**: The rich field in ω Cen used for the Astrometry Verification (6942) is observed with large shifts (35″) in F555W only, at two different times during Cycle 7. This will indicate whether there

are shifts in the relative positions of the chips or changes in the astrometric solution at the subpixel level. Kelsall spot images will be taken in conjunction with each execution. The K-spots data and some external data indicate that shifts of up to 1 pixel may have occurred since mid-1994.

- **Accuracy**: At least 0.″1 in the relative shifts, with a goal of 0.″02–0.″05.
- **Products**: TIPS, Technical Instrument Report; update of chip positions in PDB and of geometric solution in STSDAS task **metric** if any changes are found.

7628: WFPC2 Cycle 7: Photometric Characterization

- **Purpose**: (1) Determine if any changes in the zeropoint, or in the spatial dependence of the zeropoint or contamination, have occurred; (2) include another globular cluster (NGC 2419) in order to extend the parameter space for determinations of photometric transformation. Combines and continues Cycle 6 proposals 6934, 6935.
- **Description**: Observations of the primary photometric standard GRW+70D5824 will be compared against baseline observations. The cluster fields in ω Cen and NGC 2100 will be compared to previously obtained data in order to test for spatial variations in the throughput, using most broad-band and intermediate-width filters, including the far UV set for NGC 2100 (very young, many blue stars). A contamination test using UV filters will also be performed for NGC 2100. New observations of the Galactic globular cluster NGC 2419 will be compared with good ground based photometry; this cluster is very distant (100 kpc) and will provide a large color spread on giant branch and HB.
- **Accuracy**: Photometric stability expected to be better than 2%. Photometric transformations to be defined to 2–5%, depending on filter; most of the error derives from limited knowledge of the transformations between ground based and WFPC2 photometric systems.
- **Products**: ISR; SYNPHOT updates if necessary.

7629: WFPC2 Cycle 7: PSF Characterization

- **Purpose**: Provide a subsampled PSF over the full field to allow PSF fitting photometry, test PSF subtraction as well as dithering techniques. Based on Cycle 6 program 6938.
- **Description**: Measure the PSF over the full field in often-used, high-throughput filters in order to update the Tim and TinyTIM models and to allow accurate empirical PSFs to be derived for PSF fitting photometry. Compared to Cycles 5 and 6, we will repeat F814W to provide a continuing baseline, and will replace the other filters with

F300W, F450W, F606W and F702W, which are often used because of their high throughput but are not as well characterized as the photometric set (F336W, F439W, F555W, F675W) used in previous Cycles. These observations will also be useful in order to test PSF subtraction and dithering techniques at various locations on the CCD chips. With one orbit per photometric filter, a spatial scan is performed over a 4 x 4 grid on the CCD. The step size is 0.025 arcseconds; this gives a critically sampled PSF over most of the visible range. This program uses the same specially chosen field in ω Cen as the Cycle 5 proposal 6193. The proposal also allows a check for sub-pixel phase effects on the integrated photometry.

- **Accuracy**: Provides measurement of pixel phase effect on photometry (sub-pixel QE variations exist). The chosen field will have tens of well exposed stars in each chip. Each star will be measured 16 times per filter at different pixel phase. The proposal therefore provides, in principle, a high signal-to-noise, critically sampled PSF. This will improve the quality of PSF fitting photometry for the filters used. The result will be largely limited by breathing variations in focus. It is difficult to predict the PSF accuracy that will result. If breathing is less than 5 microns peak-to-peak, the resulting PSFs should be good to about 10% in each pixel. In addition, the test gives a direct measurement of sub-pixel phase effects on photometry, which should be measured to better than 1%.
- **Products**: PSF library (WWW).

7630: WFPC2 Cycle 7: CTE Calibration

- **Purpose**: Conduct a thorough examination of the variation in photometric zeropoint as a function of exposure length, background (via preflash), and position in the chip. Include spot checks for the dependence of zeropoint variations on filter, order of exposures, and camera shifts (CTE ramp).
- **Description**: A well-studied field in the globular cluster NGC 2419 will be observed through F814W with a combination of exposure times (10, 40, 100, 300, 1000s) and preflash levels (0, 5, 10, 100, and 1000 e^-). Completes Cycle 6 proposal 6937, which was shortened substantially because of SM constraints. Will also include several observations in reverse order (to test for hysteresis), in F555W and F300W (filter dependence), and after a pointing shift (to test for x, y dependence), as well as a series of equal-length exposures to test the effect of noiseless preflash. This proposal should improve substantially our understanding of CTE and of the long vs. short anomaly.
- **Accuracy**: The reported short vs. long effect is ~0.05 mag. We want to determine it to better than 0.02 mag, with a goal of 0.01 mag.

- **Products**: ISR, paper; if appropriate, a special task to correct the CTE effect will be generated.

7929: WFPC2 Cycle 7: CTE Monitor

- **Purpose**: Monitor variations in CTE ramp for bright and faint targets.
- **Description**: Analysis of Cycle 6 CTE data shows that the CTE ramp depends strongly on stellar magnitude and background, and that its amplitude varies in time for faint stars. However, most measurements have been taken so far under slightly different conditions from one another. This program will take four one-orbit measurements of the CTE at four month intervals, under the same conditions as the best data taken so far. It will provide an accurate and efficient tracer of changes in the CTE ramp, and show to what extent WFPC2 remains a photometric instrument for faint objects. Observations of the standard field in NGC 5139 (ω Cen) will be taken at the same roll angle, but centered in each of the WF chips in turn, thus reversing the x and y positions of each star. No preflash test is included.
- **Accuracy**: The measurements will enable tracking of the CTE ramp with an accuracy requirement of 0.02 mag, and a goal of 0.01 mag.
- **Products**: ISR.

8053: WFPC2 Cycle 7: Supplemental Earth Flats

- **Purpose**: Repeat the sequence of Earth flats late in Cycle 7 to verify stability of flat field.
- **Description**: As in previous cycles and earlier in Cycle 7, sets of 200 Earth-streak flats are taken to construct high quality narrow-band flat fields with the filters F160BW, F375N, F502N, F656N and F953N. Of these 200 perhaps 50 will be at a suitable exposure level for de-streaking. The resulting Earth superflats map the OTA illumination pattern and will be combined with SLTV data (and calibration channel data in case of variation) for the WFPC2 filter set to generate a set of superflats capable of removing both the OTA illumination and pixel-to-pixel variations in the flat fields. A repeat is requested because of the length of Cycle 7 and the fact that low-level temporal variations are typically discerned on time scales of about a year.
- **Accuracy**: Large-scale flat field variations can be tracked to about 0.3%.
- **Products**: New flat fields will be generated and delivered.

8054: WFPC2 Cycle 7: LRF Calibration

- **Purpose**: Complete the analysis of LRF properties: throughput and wavelength scale.

- **Description**: The primary spectrophotometric standard GRW+70D5824 will be observed at several locations on the three most used Linear Ramp Filters to verify its throughput as a function of wavelength. In addition, exposures of the Orion Nebula at two different pointings will be used to verify the wavelength calibration of the LRF at the wavelengths of major nebular lines. Previous executions of the LRF calibration have demonstrated a throughput consistent with the expectations based on laboratory filter tracings, with a scatter of 8% rms. The series of observations of GRW+70D5824 will: 1) measure the temporal stability of the difference between measured and predicted throughput; 2) demonstrate whether the scatter is due to measurement errors or to intrinsic variations in the filter; 3) complete the wavelength coverage (some of the observations from previous programs were lost); and 4) and provide more closely spaced points in the most often used ramp filter. The observations of the Orion Nebula, at two carefully optimized pointings, will provide a direct test of the wavelength calibration and vignetting of the LRF at the wavelengths of Hα, Hβ, [OIII], [NII] and [SII].
- **Accuracy**: Measure throughput to 5%, wavelength position to about 5–10 pixels.
- **Products**: ISR, new SYNPHOT tables.

8.15 Cycle 8 Calibration Plan

8.15.1 Introduction

The Cycle 8 calibration program is aimed at maintaining the calibration of WFPC2 via monitoring programs, as well as continuing some proposals from previous Cycles into Cycle 8 and performing new tests to improve our understanding in several key areas. A brief overview of the Cycle 8 program as a whole is provided in the next section, followed by a table summarizing the proposals, and finally, detailed descriptions of each program (including proposal numbers, statement of purpose, observing description, products, and accuracy expected).

8.15.2 Overview

Standard Monitoring Programs

As in previous cycles, a substantial part of the program consists of the routine monitors and decontamination (decon) procedures. In Cycle 8, the decons will continue to be performed on a monthly basis, to remove the

UV contaminants and anneal hot pixels. The monitoring observations associated with the decons are similar to those from previous Cycles, allowing us to efficiently track the overall long-term photometric throughput of the camera, the monthly throughput decline rates due to contaminant buildup on the CCD windows, the return to nominal throughput after the decons, the PSF properties at different wavelengths, the OTA focus, and the general health and performance of the cameras. A new aspect this cycle is that a handful of programs tied to a decon (internals, photometric monitor, focus check, UV throughput) have been combined into the decon proposal, to help minimize scheduling problems. For convenience, the resulting decon proposal was split into two pieces (8441, 8459; see Table 8.8 on page 279), to run before and after SM3a in Oct. 1999.

In addition to the decon proposal and its associated observations, we will continue the standard darks program (six darks per week, used for reference files), the supplemental darks program (0-3 darks per day, low priority, for archive only), and the weekly internal monitor (biases and kspots). The Earth flat program will also be continued, to allow tracking and correction for changes in the flat field. Following the general plans of previous cycles, streak flats in a subset of filters will be obtained to construct superflats which are used to generate the pipeline flats.

The other monitoring proposals include the astrometric monitor, the CTE monitor, the INTFLAT/VISFLAT sweeps, and the UV internal flats. The astrometry program, along with the internal kspots, will allow measurement of any chip position shifts or changes in the astrometry. The CTE monitor program will allow tracking of the CTE problem, which continues to worsen with time. The internal flats programs will provide verification of the pixel-to-pixel flat field response; as in Cycle 7, the emphasis will be on the INTFLATS, so as to minimize shortening the VISFLAT lamp lifetime.

Special Programs - Continuations from Previous Cycles

The remaining proposals planned for Cycle 8 will be used to verify and improve the existing WFPC2 calibration in key areas. Several special programs which were executed in previous cycles will be run as shorter versions in Cycle 8: the photometric and PSF characterization proposals, the polarization check, and the linear ramp filter proposal. Cycle 7 included a thorough test of the photometric zeropoints and contamination rates; the Cycle 8 proposal will be a spot-check of those results, with a comparison to the baseline observations to identify any time dependencies. The PSF characterization proposal will be similar to that of Cycle 6, but only two filters will be checked (F555W and F814W), instead of the full suite of filters. The polarization proposal will allow us to verify the stability of the polarization calibration from Cycle 5 via observations of polarized and unpolarized standards; a small set of VISFLATs will be obtained to check for flat field changes. The linear ramp filter proposal is at present only a

placeholder, pending receipt and analysis of the Cycle 7 data; however, the plan is to merely spot-check a subset of wavelengths in Cycle 8.

Special Programs - New

There are five new special programs, designed to address the remaining photometric issues (CTE and long vs. short) as well as user concerns from previous cycles.

The noiseless preflash proposal will test if illuminating the detectors prior to an exposure reduces the impact of the CTE and long vs. short anomalies. The preflash will be accomplished via INTFLATs which will be read out prior to the external exposures, thereby minimizing additional noise in the observations. Darks will be taken before the visit and during occultations, to insure that no prior exposures will effectively preflash the non-preflashed images.

The CTE for extended sources proposal will, for the first time, allow a direct measurement of the CTE effect on small (2″-3″) extended sources; the tentative target, selected from the archive, is galaxy cluster 135951+621305. The cluster will be positioned at a variety of chip locations; images will be obtained in F606W and F814W to match those in the archive, thereby allowing an assessment of any temporal changes in the CTE.

The Cycle 8 special programs also include a check of the photometric calibration for very red stars (two late M dwarfs, VB8 and VB10) in BVRI. The current zeropoints (based on a white dwarf UV standard and verified via solar analog data) and the color transformations from HST BVRI to ground based BVRI are highly uncertain for stars this red; this program will provide straightforward empirical calibration. In addition, a short single-orbit program will allow us to measure variations in the plate scale with wavelength, particularly in the UV, where the index of refraction in the MgF window increases rapidly. Finally, a special program is being developed to help improve the quality of the UV flat fields: the Earth flats will be obtained in a variety of UV filters as well as some crossed filter combinations to account for any read leak contributions. Several of these special programs have been designated as candidates for “calibration outsourcing”, where external groups would be funded to perform the analysis.

Table 8.8: WFPC2 Cycle 8 Calibration Plan.

ID	Proposal Title	Frequency	Estimated Time (orbits)		Scheduling Required	Products	Accuracy Required	Notes
			"External"	"Internal"				
				Routine Monitoring Programs				
8441 8459	WFPC2 Decons & Associated Observations	1-2/4 weeks	32	72	every 28 days	Synphot, CDBS	1-2%	Includes decons, photometric monitor, focus monitor, internals, UV throughput.
8442	Standard Darks	weekly		324	every 7 days	CDBS	1 e/hr	Also hot pixel lists on WWW.
8443	Supplemental Darks (8460, 8461)	0-3/day		1308	anytime		n/a	For archive only, no analysis provided.
8444	Internal Monitor	3/4 weeks		45	every 7days	CDBS	0.8e/pixel	New superbiases, not run on decon weeks.
8445	Earth Flats	continuous		442	mid-cycle	CDBS	0.3%	Also LRF, Methane quads.
8446	Astrometric Monitor	2/cycle	2		early & late	ISR	0.05"	Also K-spots & plate scale check in red.
8447	CTE Monitor	2/cycle	4		mid- & late	ISR	0.01 mag	
8448	Intflat and Visflat Sweeps	1/cycle		43	mid-cycle	TIR	0.3%	Mostly intflats.
8449	UV Flats Internal Monitor	1/cycle	2		mid-cycle	TIR	2-8%	Uses UV cal channel lamp.
				Special Calibration Programs				
8451	Photometric Characterization	1	2		mid-cycle	ISR	2.5%	Subset of Cycle 7 proposal, as check.
8452	PSF Characterization	1	2		late in cycle	CDBS	10%	Subset of standard broadband filters.
8453	Polarization	1	6	10	early in cycle	CDBS	3-5%	Subset of Cycle 6, as check.
8454	Linear Ramp Filters	1	4		late in cycle	CDBS	3%	Placeholder, pending results from Cycle 7.
8450	Noiseless Preflash	1	5		early in cycle	TIR	0.01 mag	Test scheme to reduce CTE problem.
8455	Photometry of Very Red Stars	1	2		mid-cycle	ISR	2-5%	Outsourcing candidate.
8456	CTE for Extended Sources (2-3")	1	4		mid-cycle	ISR	0.01 mag	Outsourcing candidate.
8457	UV Earth Flats	continuous		720	early in cycle	CDBS	10%	Outsourcing candidate.
8458	Plate Scale Verification	1	1		mid-cycle	ISR	0.05%	Outsourcing candidate.
	~10% reserve for unexpected items		7					Placeholder.
TOTAL TIME (including all executions)			73	2964				

8441, 8459: WFPC2 Cycle 8: Decontaminations and Associated Observations

- **Purpose**: Monthly WFPC2 decons. Instrument monitors tied to decons: photometric stability check, focus monitor, pre- and post-decon internals -- bias, intflats, K-spots, & darks, UV throughput checks.
- **Description:** *Decontamination:* UV-blocking contaminants removed and hot pixels annealed, by warming the CCDs to +20C for 6 hours. *Internals:* intflats, biases, darks & K-spots, before/after decons. *Photometric and Focus Monitor:* Standard star GRW+70D5824 is observed after each decon and before every other decon: (1) F170W in all chips to monitor far UV contamination. (2) PC focus monitor observations in F439W, F555W, F814W. (3) F160BW, F218W, F255W, F336W, F439W, F555W, F814W observed in a different chip each month.
  UV Throughput: PC & WF3 UV observations in all UV filters, popular UV filters in all chips, to verify that the UV spectral response curve is unchanged. Also check Methane quads.
- **Products**: SYNPHOT, CDBS, Instrument Handbook, TIPS meetings, WWW reports, TIR, ISR.
- **Accuracy**: *Photometry*: less than 2% discrepancy between results, 1% rms expected. *Focus measurement:* 1.5 μ accuracy, with a goal of 1 μ. *UV throughput:* better than 3%. *Flat Field:* temporal variations monitored at 1% level. *Gain ratios:* stable to better than 0.1%.

8442: WFPC2 Cycle 8: Standard Darks

- **Purpose**: Measure dark current and identify hot pixels.
- **Description**: Six 1800s exposures/week with the shutter closed, five with clocks off, one with clocks on. This frequency is required due to the high formation rate of new hot pixels (several tens/CCD/day). Five darks per week are required for cosmic ray rejection, counterbalancing losses due to residual images, and improving the noise of individual measurements. Sometimes, no usable darks are available for a given week due to residual images, resulting in a longer-than-usual gap in the hot pixel lists. In a decon week, information on hot pixels that became hot and then annealed would be lost irretrievably. As a result, pre-decon darks (see Decon proposal) are executed in a non-interruptible sequence, at least 30 min after any WFPC2 activity.
- **Products**: Weekly darks delivered to CDBS and monthly tables of hot pixels on the WWW. Superdark reference files.

- **Accuracy**: Require ~1 e^-/hour (single-pixel rms) accuracy for most science applications. Expected accuracy in a typical superdark is 0.05 e^-/hour for normal pixels. The need for regular darks is driven by systematic effects, such as dark glow (a spatially and temporally variable component of dark signal) and hot pixels, which cause errors that may exceed these limits significantly.

8443, 8460, 8461: WFPC2 Cycle 8: Supplemental Darks

- **Purpose**: Obtain very frequent monitoring of hot pixels.
- **Description**: This program (a continuation of Cycle 7 programs 7621, 7712, and 7713) is designed to provide up to three short (1000s) darks per day, to be used primarily for the identification of hot pixels. Shorter darks are used so that observations can fit into almost any occultation period, making automatic scheduling feasible. Supplemental darks will be taken at low priority, and only when there is no other requirement for that specific occultation period. This program is complementary with the higher priority Standard Darks proposal that has longer individual observations for producing high-quality pipeline darks and superdarks. Note that hot pixels are often a cause of concern for relatively short science programs, since they can mimic stars or mask key features of the observations. (About 400 new hot pixels/CCD are formed between executions of the Standard Darks program.) These observations will be made available as a service to the GO community; there is no plan to use them in our standard analysis and products.
- **Products**: None.
- **Accuracy**: n/a

8444: WFPC2 Cycle 8: Internal Monitor

- **Purpose**: Verify the short-term instrument stability at both gain settings.
- **Description**: Each set of internal observations consists of eight biases (four at each gain) and four INTFLATs (two at each gain). The entire set should be run once per week, except for decon weeks, on a non-interference basis.
- **Products**: Superbiases delivered annually to CDBS; TIPS reports on possible buildup of contaminants on the CCD windows (worms) as well as gain ratio stability, based on INTFLATs. A Technical Instrument Report will be issued if significant changes occur.
- **Accuracy**: Approximately 120 bias frames are used for each superbias pipeline reference file, generated once a year; accuracy is required to be better than 1.5 e-/pixel, and is expected to be 0.8 e^-/pixel.

8445: WFPC2 Cycle 8: Earth Flats

- **Purpose**: Monitor flat field stability.
- **Description**: As in Cycle 7 programs 7625 and 8053, sets of 200 Earth-streak flats are taken to construct high quality narrow-band flat fields with the filters F375N, F502N, F656N and F953N. Of these 200 perhaps 50 will be at a suitable exposure level for de-streaking. The resulting Earth superflats map the OTA illumination pattern and are combined with SLTV data (and calibration channel data in case of variation) for the WFPC2 filter set to generate a set of superflats capable of removing both the OTA illumination and pixel-to-pixel variations in the flat fields. The general plans of Cycles 5, 6, and 7 are repeated.
- **Products**: New flat fields generated and delivered to CDBS if changes detected.
- **Accuracy**: The single-pixel signal-to-noise ratio expected in the flat field is 0.3%.

8446: WFPC2 Cycle 8: Astrometric Monitor

- **Purpose**: Verify relative positions of WFPC2 chips with respect to one another.
- **Description**: The rich field in ω Cen (same positions as Cycle 7 proposal 7627) is observed with large shifts (35″) in F555W only, at two different times during Cycle 8. This will indicate whether there are shifts in the relative positions of the chips or changes in the astrometric solution at the sub-pixel level. Kelsall spot images will be taken in conjunction with each execution. The K-spots data and some external data indicate that shifts of up to 1 pixel may have occurred since mid-1994.
- **Products**: TIPS, Technical Instrument Report, update of chip positions in PDB and of geometric solution in STSDAS tasks metric and wmosaic if significant changes are found.
- **Accuracy**: relative positions determined to 0.05″; variations to 0.01″.

8447: WFPC2 Cycle 8: CTE Monitor

- **Purpose**: Monitor CTE changes during Cycle 8.
- **Description**: Observations of ω Cen (NGC 5139) are taken every six months during Cycle 8 to monitor changes in Charge Transfer Efficiency (CTE) of the WFPC2 (extension of Cycle 7 proposal 7929). The principal observations will be in F814W at gain 15 in WF2 and WF4. Supplemental observations at gain 7, in WF3, and with a pre-

flash will be performed if time permits, along with observations in F439W and F555W. For each visit, observations will be done in single guide star mode.

- **Products**: Instrument Science Report
- **Accuracy**: 0.01 magnitudes.

8448: WFPC2 Cycle 8: Intflat and Visflat Sweeps

- **Purpose**: Monitor the pixel-to-pixel flat field response and the VISFLAT lamp degradation, as well as detect any possible changes due to contamination. The linearity test obtains a series of INTFLATs with both gains and both shutters. Since the INTFLATs have significant spatial structure, any nonlinearity would appear as a non-uniform ratio of INTFLATs with different exposure times.
- **Description**: *VISFLAT mini-sweep:* pre- and post-decon observations using the photometric filter set at gain 7, and FR533N at both gains to test the camera linearity. *INTFLAT sweep:* taken within a two-week period. Almost all filters used, some with both blades and gains, others with just one blade and gain. *Linearity test:* done at both gains and blades using F555W, and an additional set with one blade and gain with clocks=on.
- **Products**: TIPS, TIR if any significant variations are observed.
- **Accuracy**: *VISFLATs:* stable to better than 1% in overall level and spatial variations (after correcting for lamp degradation). Contamination effects should be < 1%. *INTFLATs:* signal-to-noise ratio per pixel similar to the VISFLATs, but spatial and wavelength variations in the illumination pattern are much larger. (INTFLATs will provide a baseline comparison of INTFLAT vs. VISFLAT if the CAL channel system fails.)

8449: WFPC2 Cycle 8: UV Flats Internal Monitor

- **Purpose**: Monitor the stability of UV flat field.
- **Description**: UV flat fields obtained with the CAL channel's ultraviolet lamp (UVFLAT) using the UV filters F122M, F170W, F160BW, F185W, and F336W. The UV flats are used to monitor UV flat field stability and the stability of the F160BW filter by using F170W as the control. The F336W ratio of VISFLAT to UVFLAT provides a diagnostic of the UV flat field degradation and ties the UVFLAT and VISFLAT flat field patterns. Two supplemental dark frames must be obtained immediately after each use of the lamp to check for possible after-images.
- **Products**: New UV flat fields if changes are detected.
- **Accuracy**: About 2-8% pixel-to-pixel expected (depending on filter).

8451: WFPC2 Cycle 8: Photometric Characterization

- **Purpose**: Determine if any changes in the zeropoint, the spatial dependence of the zeropoint, or contamination rates have occurred, by comparing with the baseline measurements for GRW+70D5824 (single photometric standard with 13 filters)
- **Description**: Observe the standard star GRW+70D5824 in PC1 and WF3 using filters F380W, F410M, F450W, F467M, F547M, F569W, F606W, F622W, F702W, F785LP, F791W, F850LP, and F1042M. Observations should be done within seven days after a decon. These observations will be compared with data from the Cycle 7 program 7628.
- **Products**: TIR, SYNPHOT update if necessary.
- **Accuracy**: 2% photometry.

8452: WFPC2 Cycle 8: PSF Characterization

- **Purpose**: Provide a check of the subsampled PSF over the full field.
- **Description**: Observations using only two of the standard broadband filters (F555W and F814W). With one orbit per photometric filter, DITHER-LINE and POS TARG observations are performed in a 4x4 parallelogram. The dither-line-spacing is 0.177, and POS TARG steps are 0.125; this yields a critically sampled PSF over most of the visible range. Each star is measured 16 times per filter at different pixel phase, providing a high S/N, critically sampled PSF. This will improve the quality of PSF fitting photometry.
- **Products**: PSF library (WWW). Updates for TIM and TinyTIM. Accurate empirical PSFs to be derived for PSF fitting photometry.
- **Accuracy**: Results will be limited by breathing variations in focus, so predicting PSF accuracy is difficult. (For breathing < 5 micron peak-to-peak, PSFs should be good to ~10% in each pixel.) Proposal provides a measurement of pixel phase effect on photometry (sub-pixel QE variations exist), and gives a direct measurement of sub-pixel phase effects on photometry, measured to better than 1%.

8453: WFPC2 Cycle 8: Polarization

- **Purpose**: Verify stability of polarization calibration.
- **Description**: The data from this proposal will be used to identify any changes that may have occurred since the polarizer calibration in Cycle 5. Two stars will be observed, G191B2B and BD+64D106, a non-polarized and polarized standard star, respectively. The unpolarized star will be observed in two visits with the ORIENT changed by 90 degrees between visits, so as to sample any residual polarization of the star. The polarized star will be observed in four visits with the

ORIENT changed by 45 degrees between visits, so as to fully sample the properties of each polarizer quad. Each visit consists of F555W exposures in PC1 and WF3, followed by F555W+POLQ exposures in PC1, WF2, WF3, and WF4. Other popular broadband filters (F300W, F439W, F675W, and F814W) will be checked using only the unrotated polarizer. Finally, a small set of VISFLATs (with a minimum of lamp cycles) will be included to check for flat field changes.

- **Products**: TIR or ISR report. If necessary, update SYNPHOT tables, WWW polarization calibration tools, and CDBS flat fields.
- **Accuracy**: Expected accuracy is <3%.

8454: WFPC2 Cycle 8: Linear Ramp Filter

- **Purpose**: Check wavelength and throughput calibration for LRFs at selected wavelengths.
- **Description**: A thorough check of the linear ramp filters (LRFs) is being done as part of the Cycle 7 calibration program, where the UV spectrophotometric standard (GRW+70D5824) is observed at 75 different wavelengths and an extended source (Orion Nebula) is observed for one orbit as well. This proposal is currently a placeholder, pending data analysis results from the Cycle 7 program. We anticipate requiring four orbits to spot-check some of the more popular wavelengths as well as cover any wavelengths requested by Cycle 8 GOs that were not observed as part of the Cycle 7 calibration program.
- **Products**: Updates to SYNPHOT tables if necessary and an ISR.
- **Accuracy**: Throughput accuracy should be better than 3%.

8450: WFPC2 Cycle 8: Noiseless Preflash

- **Purpose**: Test effectiveness of “Noiseless” preflash in reducing CTE and long vs. short Photometric effects.
- **Description**: A globular cluster is observed both before and after a preflash that has been read out (i.e. noiseless). The preflash will be tailored to expose the CCDs to about 3000 DN without saturation. The hypothesis is that the traps in the CCD will remain filled even though the preflash has been read out, thereby minimizing the effects of CTE. The observation sequence is repeated at two detector positions and exposure times, so as to test for CTE and long vs. short effects. The four orbits are done in one non-interruptible visit, which is preceded by a pair of 1800s darks and includes single darks during occultation periods, to insure that no prior exposures will effectively preflash the non-preflash exposures.
- **Products**: Improved observing strategies; ISR.
- **Accuracy**: 1% photometry

8455: WFPC2 Cycle 8: Photometry of Very Red Stars

- **Purpose**: Verify the photometric calibration of WFPC2 filters and obtain estimated color terms (HST to Johnson) for late M stars.
- **Description**: WFPC2 imaging (F439W, F555W, F675W, F814W) of two well-known M dwarfs, VB8 and VB10, for which ground based measurements in the Johnson filters exist. Use two different y positions to account for CTE. The current calibration is based on white dwarf and solar analog data, which are insufficient to produce an accurate calibration for cool red stars (late K and M) in broad-band filters. The calibration of cool stars is especially difficult at the red end (F814W), because their spectra can rise quickly where the DQE drops substantially (increasing the uncertainty in the synthetic magnitude calibration). The observations of two well-studied late M stars, VB8 and VB10, will provide a direct empirical calibration of these effects and reduce the uncertainties in the photometric response of WFPC2 for very red stars.
- **Products**: N/A
- **Accuracy**: Better than 0.03 mag.

8456: WFPC2 Cycle 8: CTE for Extended Sources

- **Purpose**: Determine the effect of Charge Transfer Efficiency (CTE) on small extended sources.
- **Description**: Previous CTE proposals have all focused on stellar targets. This proposal is aimed at observing small (~2-3") extended sources in a suitable galaxy cluster. The target (tentatively cluster 135951+621305, at z=0.3) will be observed in WF2 and WF4, in F606W and F814W. The filter F606W is chosen instead of the F555W used for stellar CTE measurements, to allow a comparison to archival images for estimation of any possible time-dependence. One orbit is needed for each pointing for each filter, for a total of four orbits.
- **Products**: ISR
- **Accuracy:** 10%

8457: WFPC2 Cycle 8: UV Earth Flats

- **Purpose**: Improve quality of pipeline UV flat fields.
- **Description**: Earth streak-flats are taken in UV filters (F170W, F185W, F218W, F255W, F300W, F336W, and F343N). Those UV filters with significant read leak will also be observed crossed with selected broadband filters (F450W, F606W, F675W, and F814W), in

order to assess and remove the read leak contribution. Earth Flats required: 100 for each of the seven UV filters plus 20 with each of the crossed filter sets (16 combinations).

- **Products**: Updated flat fields for pipeline via CDBS.
- **Accuracy**: 10%

8458: WFPC2 Cycle 8: Plate Scale Verification

- **Purpose**: Check of the WFPC2 plate scale in the UV and red.
- **Description**: UV and F953N observations of the bright cluster NGC2100. Data will be taken in F170W, F218W, F300W, F555W (to allow tie-in to previous observations) and F953N. To minimize orbits required, the program is designed around short exposures in the filters listed above; the data will provide a verification the plate scale in the UV but exposure times will not be long enough to allow a full distortion solution.
- **Products**: ISR
- **Accuracy**: Better than 0.05% (0.4 pixels over 1 chip), or 0.05 mas/pixel in WF.

8.16 Cycle 9 Calibration Plan

The Cycle 9 calibration program is aimed at maintaining the calibration of WFPC2 via monitoring programs, as well as continuing two proposals from previous Cycles into Cycle 9 (photometric and PSF characterizations) and performing several new tests (on-orbit red leak check, CTE, wavelength stability check of narrowbands and linear ramp filters). Table 8.9 on page 288 summarizes the programs proposed for calibrating WFPC2 in Cycle 9, followed by detailed descriptions of each program (including proposal numbers, statement of purpose, observing description, products, and accuracy expected).

Table 8.9: WFPC2 Cycle 9 Calibration Plan.

ID	Proposal Title	Frequency	Estimated Time (orbits) "External"	Estimated Time (orbits) "Internal"	Scheduling Required	Products	Accuracy Required	Notes
			Routine Monitoring Programs					
8822-8825	WFPC2 Decons & Associated Observations	1-2/4 wks	30	82	every 28 d	Synphot, CDBS	1-2%	Decons, phot. & focus monitor, internals, UV throughput, VISFLATs, and UV FLATs
8811	Standard Darks	weekly		366	every 7 d	CDBS	1 e^-/hr	Also hot pixel lists on WWW.
8826-8828	Supplemental Darks (8460, 8461)	0-3/day		1282	anytime		n/a	For archive only, no analysis provided
8812	Internal Monitor	weekly		76	every 7d	CDBS	0.8e/pixel	Includes INTFLAT monitor, for possible future preflashed observations.
8815	Earth Flats	continuous		210	mid-cycle	CDBS	0.3%	
8816	UV Earth Flats	continuous		400	mid-cycle	CDBS	3-10%	Outsourcing candidate.
8813	Astrometric Monitor	2/cycle	2		early & late	ISR	0.05''	Omega Cen as well as K-spots.
8817	Intflat Sweep and Linearity Test	1/cycle		21	mid-cycle	TIR	0.3%	
			Special Calibration Programs					
8818	Photometric Characterization	1	2		mid-cycle	ISR	2-3%	GRW+70D5824; nonstandard filters.
8819	PSF Characterization	1	6		late in cycle	CDBS	10%	Omega Cen; standard broadband filters.
8814	Read Leak Check	1	2		mid-cycle	Synphot, CDBS	2%	Solar analogs used to measure UV filter read leaks.
8821	CTE - Monitor and Absolute Calibration	1	15		mid/late	ISR	0.01 mag	Includes monitor as well as follow up to ground based observations. Outsourcing candidate.
8820	Wavelength Stability of Narrow-band and Linear Ramp Filters	1	4	15	mid/late	CDBS, ISR	2Å	Check of wavelength/aperture mapping and test for changes in LRFs.
	~10% reserve		6					Placeholder.
	TOTAL TIME (including all executions)		**67**	**2452**				

8822, 8823, 8824, 8825: Decontaminations and Associated Observations

- **Purpose:** Monthly WFPC2 decons. Other programs tied to decons are also included: photometric stability check, focus monitor, pre- and post-decon internals, UV throughput checks, VISFLAT sweep, and internal UV flat check.
- **Description:** *Decontamination:* UV-blocking contaminants removed and hot pixels annealed by warming the CCDs to +20C for 6 hours.
  Internals: intflats, biases, darks & kspots, before/after decons.
  Photometric Monitor: GRW+70D5824 is observed after each decon and before every other decon: (1) F170W in all chips to monitor far UV contamination. (2) As many as possible of F160BW, F218W, F255W, F336W, F439W, F555W, F814W will be observed in a different chip each month.
  Focus Monitor: two PC, F555W observations of GRW+70D5824 will be taken during every photometric monitoring orbit (one at orbit start, one near orbit end).
  UV Throughput: PC & WF3 UV observations in most UV filters, popular UV filters in all chips, to verify that the UV spectral response curve is unchanged. In addition, two PC, F555W observations will be included as an extra focus monitor.
  Internal UV flat fields: obtained with the CAL channel's ultraviolet lamp (UVFLAT) using the UV filters F122M, F170W, F160BW, F185W, & F336W. The UV flats are used to monitor UV flat field stability and the stability of the F160BW filter by using F170W as the control. The F336W ratio of VISFLAT to UVFLAT provides a diagnostic of the UV flat field degradation & ties the UVFLAT and VISFLAT flat field patterns. Two supplemental dark frames must be obtained immediately after each use of the lamp to check for possible after-images.
- **Products:** SYNPHOT, CDBS, Instr. Handbook, TIPS meetings, WWW reports, TIR, ISR; new UV flat fields if changes are detected.
- **Accuracy Goals:** *Photometry*: less than 2% discrepancy between results, 1% rms expected. *Focus measurement:* 1.5 μm accuracy with a goal of 1 μm. *UV throughput:* better than 3%. *Flat field:* temporal variations monitored at 1% level. *Gain ratios:* stable to better than 0.1%. *UV flats*: About 2-8% pixel-to-pixel expected (filter dependent). *VISFLATs:* stable to better than 1% in overall level and spatial variations (after correcting for lamp degradation). Contamination effects should be < 1%.

8811:WFPC2 Cycle 9 Standard Darks

- **Purpose:** Measure dark current & identify hot pixels.

- Description: Six 1800s exp/week with the shutter closed, five with clocks off, one with clocks on. This frequency is required due to the high formation rate of new hot pixels (several tens/CCD/day). Five darks per week are required for cosmic ray rejection, counterbalancing losses due to residual images, & improving the noise of individual measurements. Sometimes, no usable darks are available for a given week due to residual images, resulting in a longer-than-usual gap in the hot pixel lists, but in a decon week, information on hot pixels that became hot and then annealed would be lost irretrievably. As a result, pre-decon darks (see Decon proposal) are executed NON-INT and at least 30 min after any WFPC2 activity.
- **Products:** Weekly darks delivered to CDBS and monthly tables of hot pixels on the WWW. Superdark reference files.
- **Accuracy Goals:** Require ~1 e^-/hr (single-pixel rms) accuracy for most science applications. Expected accuracy in a typical superdark is 0.05 e^-/hour for normal pixels. The need for regular darks is driven by systematic effects, such as dark glow (a spatially and temporally variable component of dark signal) and hot pixels, which cause errors that may exceed these limits significantlly.

8826, 8827, 8828: WFPC2 Cycle 9 Supplemental Darks

- **Purpose:** Images will allow for frequent monitoring of hot pixels.
- **Description:** This program is designed to provide up to three short (1000s) darks per day, to be used primarily for the identification of hot pixels. Shorter darks are used so that the observations can fit into almost any occultation period, making automatic scheduling feasible. These supplemental darks are low priority, and should be taken only when there is no other requirement for that specific occultation period. This program complements the higher priority Standard Darks proposal that has longer individual observations for producing high-quality pipeline darks and superdarks. Hot pixels are often a cause of concern for relatively short science programs, since they can mimic stars or mask key features of the observations: about 400 new hot pixels/CCD are formed between executions of the Standard Darks program. The supplemental darks are available to the GO community from the archive; there is no plan to use them in our standard analysis and products.
- **Products:** None.
- **Accuracy Goals:** For archive only, no STScI analysis provided.

8812: WFPC2 Cycle 9 Internal Monitor

- **Purpose:** Verify the short-term instrument stability at both gain settings and provide INTFLATs for calibrating preflashed observations.
- **Description:** Each set of internal observations consists of 8 biases (4 at each gain) and 4 INTFLATs (2 at each gain). The entire set should be run once per week, except for decon weeks, on a non-interference basis. During the decon week, INTFLATs in F502N will be taken, with each shutter blade and at a variety of exposure times to test for linearity. The F502N filter is likely to be the recommended filter for preflashing observations.
- **Products:** Superbiases delivered annually to CDBS; TIPS reports on possible buildup of contaminants on the CCD windows (worms) as well as gain ratio stability, based on INTFLATs. A Technical Instrument Report will be issued if significant changes occur. Possible preflash correction images will be generated.
- **Accuracy Goals:** Approximately 120 bias frames are used for each superbias pipeline reference file, generated once a year; accuracy is required to be better than 1.5 e^-/pixel, and is expected to be 0.8 e^-/pixel.

8815: WFPC2 Cycle 9 Earth Flats

- **Purpose:** Monitor flat field stability. This proposal obtains sequences of Earth streak flats to construct high quality flat fields for the WFPC2 filter set. These flat fields will allow mapping of the OTA illumination pattern and will be used in conjunction with previous internal and external flats to generate new pipeline superflats. These Earth flats will complement the Earth flat data obtained during SMOV and Cycles 4-8.
- **Description:** Observations of the bright Earth (earthcals) are obtained in a variety of filters. Approximately 200 exposures in each of four narrowband filters (F375N, F502N, F656N, F953N) are required, as well as about 50 exposures in other filters (F160BW, F336W, F343N, F390N, F437N, F469N, F487N, F631N, F658N, F673N -- the F160BW filter is included to provide pinhole information). In addition, if dark-earth pointing becomes available, some of the broadband filters are requested (F336W, F439W, F555W, F675W, and F814W; all marked as on-hold for now), 10 exposures in each filter.
- **Products:** New flat fields generated and delivered to CDBS if changes detected.
- **Accuracy Goals:** The single-pixel signal-to-noise ratio expected in the flat field is 0.3%.

8816: WFPC2 Cycle 9 UV Earth Flats

- **Purpose:** Monitor flat field stability. This proposal obtains sequences of earth streak flats to improve the quality of pipeline flat fields for the WFPC2 UV filter set. These Earth flats will complement the UV earth flat data obtained during Cycle 8.
- **Description:** Earth streak-flats are taken in UV filters (F170W, F185W, F218W, F255W, F300W, F336W, and F343N). Those UV filters with significant read leak will also be observed crossed with selected broadband filters (F450W, F606W, F675W, and F814W), in order to assess and remove the read leak contribution. Earthflats required: 100 for each of the 7 UV filters plus 20 with each of the crossed filter sets (16 combinations). The entire proposal should be done within 7 months, with the observations evenly distributed over that period of time. The observations are divided into 10 batches, with each batch done 21 days apart.
- **Products:** Updated flat fields for pipeline via CDBS.
- **Accuracy Goals:** 3-10%. Outsourcing candidate.

8813: WFPC2 Cycle 9 Astrometric Monitor

- **Purpose:** Verify relative positions of WFPC2 chips with respect to one another.
- **Description:** The positions of the WFPC2 chips with respect to each other appear to be shifting slowly (by about 1 pixel, since 1994). The rich field in ω Cen (same positions as Cycle 8 proposal 7627) is observed with large shifts (35”) in F555W only, every ~six months. This will allow monitoring of shifts in the relative positions of the chips or changes in the astrometric solution at the sub-pixel level. Kelsall spot images will be taken in conjunction with each execution.
- **Products:** TIPS reports, ISR, update of chip positions in PDB and of geometric solution in STSDAS tasks metric and wmosaic if significant changes are found.
- **Accuracy Goals:** At least 0.01” in relative shifts; 0.05” or better for absolute.

8817: WFPC2 Cycle 9 Intflat Sweeps and Linearity Test

- **Purpose:** Using INTFLAT observations, this WFPC2 proposal is designed to monitor the pixel to pixel flat field response and provide a linearity check. The INTFLAT sequences, to be done once during the year, are similar to those from the Cycle 8 program 8448. The images will provide a backup database in the event of complete failure of the VISFLAT lamp as well as allow monitoring of the gain ratios. The

sweep is a complete set of internal flats, cycling through both shutter blades and both gains. The linearity test consists of a series of INTFLATs in F555W, in each gain and each shutter.

- **Description:** *Intflat sweep* -- flat fields are obtained with a variety of filters (F336W, F439W, F547M, F555W, F569W, F606W, F622W, F631N, F502N, F656N, F675W, F673N, F702W, F785LP, F814W, F1042M) using shutters A and B, and gains 7 and 15; the BLADE optional parameter is used throughout. A smaller set is obtained only at gain 7 using any shutter blade (F160BW, F300W, F380W, F390N, F410M, F437N, F450W, F469N, F487N, F467M, F588N, F658N, F791W, F850LP, F953N).
  Linearity test -- flat fields are taken with F555W at a variety of exposure times, using shutters A & B, and gains 7 & 15. In addition, a set is done with clocks=YES (only gain 7, shutter A; gain 7 shutter B set was taken during Cycle 8). Since the INTFLATs have significant spatial structure, any non-linearity should appear as a non-uniform ratio of INTFLATs with different exposure times.
- **Products:** TIPS, TIR if any significant variations are observed.
- **Accuracy Goals:** *INTFLATs:* Stable to better than 1%. (INTFLATs will provide a baseline comparison of INTFLAT vs. VISFLAT (taken in decon proposal) if the CAL channel system fails.)

8818: WFPC2 Cycle 9 Photometric Characterization

- **Purpose:** Provide a check of the zeropoints and contamination rates in non-standard WFPC2 filters.
- **Description:** Observations of the standard star GRW+70D5824 in PC1 and WF3 will be made using filters that are not routinely monitored (F380W, F410M, F450W, F467M, F547M, F569W, F606W, F622W, F702W, F785LP, F791W, F850LP, and F1042M). Images should be taken within 7 days after a decon, to minimize any contamination effects. Results from this program will be compared with data from the Cycle 7 program 7628 and Cycle 8 program 8451.
- **Products:** TIR, SYNPHOT update if necessary.
- **Accuracy Goals:** 2% photometry.

8819: WFPC2 Cycle 9 PSF Characterization

- **Purpose:** Provide a subsampled PSF over the full WFPC2 field of view in order to support PSF fitting photometry and provide data to test PSF subtraction as well as dithering techniques (e.g., effects of OTA breathing and gain).

- **Description:** Measure PSF over full field in photometric filters in order to update the TIM and TinyTIM models and to allow accurate empirical PSFs to be derived for PSF fitting photometry. These observations will also be useful in order to test PSF subtraction and dithering techniques at various locations on the CCD chips. With ~1 orbit per photometric filter, each star is measured 16 times per filter at different pixel phase, providing a high S/N, critically sampled PSF. This will improve the quality of PSF fitting photometry. The step size is 0.125 arcseconds, very close to 1.25 pixels in the WFs and 2.75 pixels in the PC - so that fractional steps of 0.25, 0.5, and 0.75 pixels are used in each camera. This provides a critically sampled PSF over most of the visible range. The crowded ω Cen field is used, with 40 sec (gain = 15) images taken through each of the wide standard photometric filters (F336W, F439W, F555W, F675W and F814W). The Cycle 9 observations use the same pointings as in Cycles 7 and 8. The proposal also allows a check for subpixel phase effects on the integrated photometry.
- **Products:** PSF library (WWW). Updates for TIM and TinyTIM. Accurate empirical PSFs to be derived for PSF fitting photometry.
- **Accuracy Goals:** If breathing is less than 5 microns peak to peak, the resulting PSFs should be good to about 10% in each pixel. PSF fitting results using this calibration would of course be much more accurate. In addition, the test gives a direct measurement of sub-pixel phase effects on photometry, which should be measured to better than 1%.

8814: WFPC2 Cycle 9 Red Leak Check

- **Purpose:** Obtain an on-orbit verification of the red leak in WFPC2 UV filters by observing solar analog standards in the UV.
- **Description:** Two targets, for which FOS spectrophotometry is available, will be chosen from those used in the solar analog photometric verification program (P041-C, P177-D, or P330-E; Cycle 6 proposal 6934 and 6179). Observed count rates will be compared to SYNPHOT predictions of the expected count rates from the UV proper and from the red leak. A robust verification of the red leak will benefit programs that rely on precision multicolor photometry and comparison with model spectra. Some discrepancies seen thus far could be explained by a significant (> 10%) error in the estimated red leak.
- **Products:** TIR and SYNPHOT update if necessary.
- **Accuracy Goals:** 2% on the flux measurements; accuracy of read leak determination will vary by filter.

8821: WFPC2 Cycle 9 CTE - Monitor and Absolute Calibration

- **Purpose:** Monitor CTE changes during Cycle 9 and provide complementary suite of observations to ground based CTE proposal.
- **Description:** *Monitor*: Observations of ω Cen (NGC 5139) are taken every 6 months during Cycle 9 to monitor changes in the CTE (charge transfer efficiency) of WFPC2. An extension of proposals 7629 and 8447, the principal observations will be at gain 7, in F814W and F555W, in WF2 and WF4, at a variety of preflash (background) levels (20 to 1000 electrons).
  Absolute Calibration: Observations of three of the globular clusters Eridanus, NGC 2419, Pal 3, Pal 4, and Pal 14 are planned, to match the targets selected for a companion ground based proposal - subject to approval of the latter. Direct comparison with ground based observations permits a direct verification of the absolute photometric calibration of WFPC2 in observations that may be affected by CTE, and therefore a more robust determination of the zero point for many WFPC2 observations. While there is no evidence that the current WFPC2 zero point is inapplicable to faint sources, enough corrections need to be applied that a direct verification is extremely desirable. Comparison to a well-populated field observed from the ground can also yield a direct, independent determination of the CTE effect in such observations (Stetson 1998). Five suitable fields with existing WFPC2 observations have been selected, and a WYIN 3.5m proposal (PI Whitmore) has been submitted for ground based observations of these fields with exposure times sufficient to reach 1% photometric accuracy at V=22. The ground based proposal asks for observations of three of these five fields, to be chosen on the basis of their RA and the time of the observations.
- **Products:** Instrument Science Report. Outsourcing candidate?
- **Accuracy Goals:** 0.01 magnitudes.

8820: WFPC2 Wavelength Stability of Narrowband and Linear Ramp Filters

- **Purpose:** Verify the mapping of wavelength as a function of CCD position on LRFs; check for changes in central wavelengths of narrow band filters.
- **Description:** On-orbit VISFLATs taken through the ramps crossed with the narrow band filters will constrain the wavelength calibration of the ramps filters relative to the narrow band filters. Comparison with similar Cycle 4 data will show whether the filter properties have evolved with time due to annealing / shrinkage of the thin film materials. The uncrossed VISFLATs can also be used to constrain the transverse (cross-wavelength) placement of the ramp filters. In addi-

tion, 4 external orbits are required for external observations of an extended line emission source (planetary nebula) through ramp filters. These will provide an absolute test for changes in the ramp filters.

- **Products:** New aperture locations if necessary. Updated wavelengths / throughput curves for both ramp and narrow band filters in SYNPHOT.
- **Accuracy Goals:** Central wavelengths to 2Å.

8.17 Cycle 10 Calibration Plan

As in previous cycles, the Cycle 10 calibration program is aimed at maintaining the calibration of WFPC2 via the internal and external monitoring programs as well as performing several new tests. The standard suite of calibrations will be continued, including those used to monitor the health of the instrument as well as the programs to collect data for calibration reference files. In addition, several new proposals will be implemented: a measurement of the effect of CTE on astrometry, a characterization of the PSF wings, a calibration check of the clocks ON mode, and a test of the methane quad filter throughput. The total spacecraft time required for the Cycle 10 plan is 61 externals orbits and 2294 occultation periods. This estimate does not include any calibrations associated with Servicing Mission (SM3b), which occurred in March 2002.

We also note that two "calibration outsourcing" programs are underway to improve the UV flatfields and test for a position-independent component of CTE. See “Future Calibrations, Calibration by Observers, and Calibration Outsourcing” on page 332 for details.

Table 8.10: WFPC2 Cycle 10 Calibration Plan.

ID	Proposal Title	Frequency	Estimated Time (orbits) "External"	Estimated Time (orbits) "Internal"	Scheduling Required	Products	Accuracy Required	Notes
			Routine Monitoring Programs					
8932-8934	WFPC2 Decons & Associated Observations	1-2/4 wks	19 photmon 2 UV thru.put 2 UV flats	82	every 28 d	CDBS, IHB, Synphot, WWW reports	1-2%	Decons, phot. & focus monitor, internals, UV throughput, visflats and uvflats.
8935	Standard Darks	weekly		318	every 7 d	CDBS	1 e/hr	Also for WWW hot pixel lists.
8836-8838	Supplemental Darks	0-3/day		1095	every day		n/a	For archive only, no analysis.
8839	Internal Monitor	weekly		76	every 7 d	CDBS	$0.8e^-$/pix	Incl. intflats for preflash.
8840	Earth Flats	continuous		210	mid to late	CDBS	0.3%	
8841	UV Earth Flats	continuous		400	early to mid	CDBS	3-10%	Outsourcing candidate.
8842	Intflat & Visflat Sweeps	1/cycle		61	mid-cycle	TIR	0.3%	Incl. filter rotation offset check.
			Special Calibration Programs - Continuations					
9253	Astrometric Monitor	2/cycle	2	2	early & late	ISR, STSDAS	0.05''	ω Cen as well as K-spots.
9254	CTE Photometric Monitor	2 x 3 orbits	6		mid & late	ISR	0.01 mag	Continuation of monitors.
9251	Photometric Characterization	1	4		mid-cycle	ISR, Synphot	2-3%	All four chips.
			Special Calibration Programs - New					
9255	Astrometric Effects of CTE	1	12		late	ISR	1-2 mas	Target kept on 1 chip.
9257	Super-PSF	1	6		mid-cycle	CDBS, STS-DAS, ISR	10%	PSF wing characterization.
9252	Clocks ON Verification	1	1	50	early	ISR, Synphot	2-3%	Closure calibration.
9256	Methane Quad Filter Check	1	1		mid-cycle	Synphot, ISR	5%	Test of transmission curve across aperture (GO suggestion). Out-sourcing candidate.
	~10% reserve		6					Placeholder for unexpected items.
	TOTAL TIME (including all executions)		**61**	**2294**				

8932, 8933, 8934: WFPC2 Decontaminations and Associated Observations

- **Purpose:** Monthly WFPC2 decons. Other programs tied to decons are also included: photometric stability check, focus monitor, pre- and post-decon internals, UV throughput checks, visflat sweep, and internal UV flat check.
- **Description:** D*econtamination:* UV-blocking contaminants removed and hot pixels annealed by warming the CCDs to +20C for 6 hours.
  Internals: intflats, biases, darks & kspots, before/after decons.
  Photometric Monitor: GRW+70D5824 is observed after each decon and before every other decon: (1) F170W in all chips to monitor far UV contamination. (2) As many as possible of F160BW, F218W, F255W, F336W, F439W, F555W, F814W will be observed in a different chip each month.
  Focus Monitor: two PC, F555W observations of GRW+70D5824 will be taken during every photometric monitoring orbit (one at orbit start, one near orbit end).
  UV Throughput: PC & WF3 UV observations in most UV filters, popular UV filters in all chips, to verify that the UV spectral response curve is unchanged. In addition, two PC, F555W observations will be included as an extra focus monitor.
  Internal UV flatfields: obtained with the CAL channel's UV lamp using the filters F122M, F170W, F160BW, F185W, & F336W. The uvflats are used to monitor UV flatfield stability and the stability of the F160BW filter by using F170W as the control. The F336W ratio of visflat to uvflat provides a diagnostic of the UV flatfield degradation & ties the uvflat and visflat flatfield patterns. Two supplemental dark frames must be obtained immediately after each use of the lamp to check for possible after-images.
- **Products:** SYNPHOT, CDBS, Instr. Handbook, TIPS meetings, WWW reports, TIR, ISR; new UV flatfields if changes are detected.
- **Accuracy Goals:** *Photometry*: less than 2% discrepancy between results, 1% rms expected. *Focus measurement:* 1.5 micron accuracy with a goal of 1 mic. *UV throughput:* better than 3%. *Flatfield:* temporal variations monitored at 1% level. *Gain ratios:* stable to better than 0.1%. *UV flats*: About 2-8% pixel-to-pixel expected (filter dependent). *Visflats:* stable to better than 1% in overall level and spatial variations (after correcting for lamp degradation). Contamination effects should be < 1%.

8935: WFPC2 Cycle 10 Standard Darks

- **Purpose:** Measure dark current & identify of hot pixels.
- **Description:** Six 1800s exp/week with the shutter closed, five with clocks off, one with clocks on. This frequency is required due to the high formation rate of new hot pixels (several tens/CCD/day). Five darks per week are required for cosmic ray rejection, counterbalancing losses due to residual images, & improving the noise of individual measurements. Sometimes, no usable darks are available for a given week due to residual images, resulting in a longer-than-usual gap in the hot pixel lists, but in a decon week, information on hot pixels that became hot and then annealed would be lost irretrievably. As a result, pre-decon darks (see Decon proposal) are executed NON-INT and at least 30 min after any WFPC2 activity.
- **Products:** Weekly darks delivered to CDBS and monthly tables of hot pixels on the WWW. Superdarks for use in generating pipeline dark reference files.
- **Accuracy Goals:** Require ~1 e^-/hr (single-pixel rms) accuracy for most science applications. Expected accuracy in a typical superdark is 0.05 e^-/hour for normal pixels. The need for regular darks is driven by systematic effects, such as dark glow (a spatially and temporally variable component of dark signal) and hot pixels, which cause errors that may exceed these limits significantly.

8936, 8937, 8938: WFPC2 Cycle 10 Supplemental Darks

- **Purpose:** Images will allow for frequent monitoring of hot pixels.
- **Description:** This program is designed to provide up to three short (1000s) darks per day, to be used primarily for the identification of hot pixels. Shorter darks are used so that the observations can fit into almost any occultation period, making automatic scheduling feasible. These supplemental darks are low priority, and should be taken only when there is no other requirement for that specific occultation period. This program complements the higher priority Standard Darks proposal that has longer individual observations for producing high-quality pipeline darks and superdarks. Hot pixels are often a cause of concern for relatively short science programs, since they can mimic stars or mask key features of the observations: about 400 new hot pixels/CCD are formed between executions of the Standard Darks program. The supplemental darks are available to the GO community from the archive; there is no plan to use them in our standard analysis and products.
- **Products:** None, though some daily darks may occasionally be used for hot pixel lists if standard darks were lost.

- **Accuracy Goals:** For archive only, no STScI analysis provided.

8939: WFPC2 Cycle 10 Internal Monitor

- **Purpose:** Verify the short-term instrument stability at both gain settings and provide intflats for calibrating preflashed observations.
- **Description:** Each set of internal observations consists of 8 biases (4 at each gain) and 4 intflats (2 at each gain). The entire set should be run once per week, except for decon weeks, on a non-interference basis. During the decon week, intflats in F502N will be taken, with each shutter blade and at a variety of exposure times to test for linearity. The F502N filter is likely to be the recommended filter for preflashing observations.
- **Products:** Superbiases delivered annually to CDBS; TIPS reports on possible buildup of contaminants on the CCD windows (worms) as well as gain ratio stability, based on intflats. A Technical Instrument Report will be issued if significant changes occur. Preflash correction images may be generated.
- **Accuracy Goals:** Approximately 120 bias frames are used for each superbias pipeline reference file, generated once a year; accuracy is required to be better than 1.5 e^-/pixel, and is expected to be 0.8 e^-/pixel.

8940: WFPC2 Cycle 10 Earth Flats

- **Purpose:** Monitor flatfield stability. This proposal obtains sequences of Earth streak flats to construct high quality flat fields for the WFPC2 filter set. These flat fields will allow mapping of the OTA illumination pattern and will be used in conjunction with previous internal and external flats to generate new pipeline superflats. These Earth flats will complement the Earth flat data obtained during SMOV and Cycles 4-9.
- **Description:** Observations of the bright Earth (Earthcals) are obtained in a variety of filters. Approximately 200 exposures in each of four narrowband filters (F375N, F502N, F656N, F953N) are required, as well as about 50 exposures in other filters (F160BW, F336W, F343N, F390N, F437N, F469N, F487N, F631N, F658N, F673N -- the F160BW filter is included to provide pinhole information).
- **Products:** New flatfields generated and delivered to CDBS if changes detected.
- **Accuracy Goals:** The single-pixel signal-to-noise ratio expected in the flatfield is 0.3%.

8941: WFPC2 Cycle 10 UV Earth Flats

- **Purpose:** Monitor flatfield stability. This proposal obtains sequences of Earth streak flats to improve the quality of pipeline flat fields for the WFPC2 UV filter set. These Earth flats will complement the UV Earth flat data obtained during Cycles 8-9.
- **Description:** Earth streak-flats are taken in UV filters (F170W, F185W, F218W, F255W, F300W, F336W, and F343N). Those UV filters with significant read leak will also be observed crossed with selected broadband filters (F450W, F606W, F675W, and F814W), in order to assess and remove the read leak contribution. Earth flats required: 100 for each of the 7 UV filters plus 20 with each of the crossed filter sets (16 combinations). The entire proposal should be done within 7 months, with the observations evenly distributed over that period of time. The observations are divided into 10 batches, with each batch done 21 days apart.
- **Products:** Updated flatfields for pipeline via CDBS.
- **Accuracy Goals:** 3-10%. Outsourcing candidate.

8942: WFPC2 Cycle 10 Intflat Sweeps and Linearity Test

- **Purpose:** Using intflat observations, this WFPC2 proposal is designed to monitor the pixel-to-pixel flatfield response and provide a linearity check. The intflat sequences, to be done once during the year, are similar to those from the Cycle 9 program 8817. The images will provide a backup database in the event of complete failure of the visflat lamp as well as allow monitoring of the gain ratios. The sweep is a complete set of internal flats, cycling through both shutter blades and both gains. The linearity test consists of a series of intflats in F555W, in each gain and each shutter. New this cycle will be extra visflat exposures to test the repeatability of filter wheel motions.
- **Description:** *Intflat sweep* -- flatfields are obtained with a variety of filters (F336W, F439W, F547M, F555W, F569W, F606W, F622W, F631N, F502N, F656N, F675W, F673N, F702W, F785LP, F814W, F1042M) using shutters A and B, and gains 7 and 15; the BLADE optional parameter is used throughout. A smaller set is obtained only at gain 7 using any shutter blade (F160BW, F300W, F380W, F390N, F410M, F437N, F450W, F469N, F487N, F467M, F588N, F658N, F791W, F850LP, F953N).
  Linearity test -- flatfields are taken with F555W at a variety of exposure times, using shutters A & B, and gains 7 & 15. In addition, a set is done with clocks ON (only gain 7, shutter B; gain 7 shutter A set was taken during Cycle 9). Since the intflats have significant spatial structure, any non-linearity will appear as a non-uniform ratio of intflats with different exposure times.

Filter rotation check -- 10 visits of visflats will be taken to test the repeatability of the filter wheel positioning. A problem is known to exist in FR533N; other filters will be used, to determine whether the problem is limited to the one filter or is present in other filters/wheels.

- **Products:** TIPS. TIR/ISR if any significant variations are observed or if any new filter problems are noted.
- **Accuracy Goals:** *Intflats:* Stable to better than 1%. (intflats will provide a baseline comparison of intflat vs visflat (taken in decon proposal) if the CAL channel system fails.)

9253: WFPC2 Cycle 10 Astrometric Monitor

- **Purpose:** Verify relative positions of WFPC2 chips with respect to one another.
- **Description:** The positions of the WFPC2 chips with respect to each other appear to be shifting slowly (by about 1 pixel, since 1994). The rich field in ω Cen (same positions as Cycle 9 proposal 8813) is observed with large shifts (35'') in F555W only, every ~six months. This will allow tracking of the shifts in the relative positions of the chips or changes in the astrometric solution at the sub-pixel level. Kelsall spot images will be taken in conjunction with each execution.
- **Products:** TIPS reports, ISR, update of chip positions in PDB and of geometric solution in STSDAS tasks metric and wmosaic if significant changes are found.
- **Accuracy Goals:** At least 0.01'' in relative shifts; 0.05" or better for absolute.

9254: WFPC2 Cycle 10 CTE Photometric Monitor

- **Purpose:** Monitor CTE changes during Cycle 10.
- **Description:** Obtain observations of ω Cen (NGC 5139) to continue tracking changes in the CTE (charge transfer efficiency) losses in WFPC2. A continuation of proposals in earlier cycles (7629, 8447, and 8821), the principal observations will be at gain 7, in F814W and F555W, taken with and without a variety of preflash (background) levels (20 to 1000 e^-). The same pointing is used at WF2 and WF4; along with the relative orientation of the chips, this results in stars at the bottom of one chip falling near the top of the other chip.
- **Products:** ISR and updates to published CTE correction formulae.
- **Accuracy Goals:** 0.01 magnitudes.

9251: WFPC2 Cycle 10 Photometric Characterization

- **Purpose:** Provide a check of the zeropoints and contamination rates in non-standard WFPC2 filters.
- **Description:** Observations of the standard star GRW+70D5824 in all four chips will be made using filters that are not routinely monitored (F380W, F410M, F450W, F467M, F547M, F569W, F606W, F622W, F702W, F785LP, F791W, F850LP, and F1042M). Images should be taken within 7 days after a decon, to minimize any contamination effects. Results from this program will be compared with archival data from earlier cycles.
- **Products:** ISR, SYNPHOT update if necessary.
- **Accuracy Goals:** 2-3% photometry.

9255: WFPC2 Cycle 10 Astrometric Effects of CTE

- **Purpose:** This proposal attempts to quantify the astrometric effects of CTE by measuring (1) the relative separation of a bright source vs. a faint target at different positions on the PC1 CCD, and (2) the relative motion of a source on the CCD compared to very precise slews performed with the FGSs. These tests will be conducted for point and extended targets at several different intensity levels.
- **Description:** While the photometric effects of CTE have been well studied, and correction algorithms have been developed, very little is known about the astrometric effects of CTE. Riess (2000; WFPC2 ISR 00-04) has shown that extended sources suffer some degree of distortion due to CTE, indicating that the astrometry of sources must also be affected. E.g., the relative separation of a faint source from a bright source may depend on all the factors that influence CTE (position on detector, observing epoch, brightness in electrons, and image background).
  Targets will be observed in PC, 2x2 grid, 20” on a side, in the first orbit; the second orbit is a repeat with a small pointing offset (dither of N+1/2 PC pixels). The 2-orbit sequence will be done at different background light levels, using exposures from 100s in F450W to 1200s in F622W, repeated three times for two targets (total ~12 orbits).
  Targets will be the dense star field in ω Cen, and a field of faint galaxies (from extended target CTE proposal 8456). Both fields in both targets will be chosen to have a bright star surrounded by fainter objects. While most of the test is performed on the PC, the WFC CCDs will also be important, as they can provide a sanity check on the motions made with the FGSs. The motions on the WFC CCDs will be a smaller number of pixels, and hence less subject to CTE variations. (Though the larger WFC pixels will make astrometry

more difficult). Hence some care should be taken to have stars available on the WFC CCDs, though PC1 is the detector of primary interest.

- **Products:** ISR.
- **Accuracy Goals:** The relative separations of the faint targets from the bright star will be measured with millarcsecond accuracy as a function of target position on the CCD and background level. The measured sizes of the large slews (~20”) will also be compared to the sizes of commanded slews as a function of background intensity. It will be necessary to correct for image scale effects (i.e. geometric distortion) with care to insure that optical and CTE effects do not become confused.

9257: WFPC2 Cycle 10 Super-PSF

- **Purpose:** Obtain deep images of the WFPC2 PSF in several broadband filters in order to investigate the 2-dimensional structure in the PSF wings and characterize the change in structure with varying focus and target color.
- **Description:** This program will provide deep observations of the PSF wings by obtaining highly saturated images which are stepped in exposure time, allowing the creation of a "Super-PSF". STScI is currently developing software that will be able to accurately blend these larger-scale empirical PSF wings together with model PSF cores from TinyTIM. The new software will then perform 2-dimensional fitting and subtraction of the blended PSF from science images. The deep images proposed here are crucial for the new software to be effective: the majority of PSFs in the library have poor S/N in the wings and the TinyTIM models, while excellent for PSF cores, are inadequate beyond ~2”, primarily due to scattering by the WFPC2 detectors.
  Since the shape and width of the PSF varies over time due to the change in telescope focus, the observations are split into 3 visits, 2 orbits each. The majority of archival programs which would benefit from these observations have placed the target on the PC chip, therefore, the PC1-FIX aperture will be used. Targets will be an A0V and a G0V star (TBD), to allow characterization of the color dependence of the PSF. Each star will be observed for an entire orbit, cycling through several broadband filters (F450W, F606W, F702W and F814W), 2 images per filter, at low and high saturation levels.
- **Products:** Accurate empirical PSFs to be derived for PSF fitting photometry, intended for use with STSDAS software currently under development. Observed PSFs and blended PSFs to be archived in on-line PSF library in CDBS. ISR.

- **Accuracy Goals:** Enable PSF subtraction with ~10% residuals at ~2".

9252: WFPC2 Cycle 10 Clocks ON Verification

- **Purpose:** Closure calibration for clocks ON mode.
- **Description:** This proposal will provide a check of the existing photometric and dark calibration for the clocks ON mode. An initial analysis was performed on photometric data taken Dec 1994; additional standard star observations using a small number of filters were taken and checked in Nov. 2000. The Cycle 10 external orbit will be used to observe a standard star in as many of the most frequently used filters and apertures not covered by prior observations. The results will be compared with clocks OFF data, in order to determine whether any significant differences exist between the two modes (none are expected). The new images will serve as a final verification of the calibration of this mode.
  The requested occultation periods will be used to obtain sufficient clocks ON darks over a time span of a few months to allow for generation of a clocks ON superdark.
- **Products:** SYNPHOT update; new clocks ON superdark and reference files, if necessary. ISR.
- **Accuracy Goals:** Photometric accuracy 2-3%. Expected accuracy in resulting superdark ~0.08 e^-/hour for normal pixels.

9256: WFPC2 Cycle 10 Methane Quad Filter Check

- **Purpose:** Verify FQCH4N-D methane filter characteristics.
- **Description:** Based on results from Jupiter and Uranus archival WFPC2 data, the extended wings of the methane filter transmission curve appear to vary across the field of view (Karkoshka, priv. comm.). While this is unimportant for objects with flat spectra, it can have a major impact on photometry of objects with methane bands, where a significant fraction of photons comes from the wings. To provide data to check the methane filter, a set of eight 40-sec Saturn images will be taken in a 3x3 grid around the FQCH4W3 methane quad filter aperture (one of the 9 positions falls outside of the filter). The magnitude and direction of the effect will be quantified by comparing results from the rings of Saturn (flat spectrum) to results from Saturn itself (deep methane band spectrum).
- **Products:** Outsourcing candidate. Expected product would be an updated filter transmission curve, to be installed in SYNPHOT and an ISR, if the project is not outsourced.
- **Accuracy Goals:** 5%.

8.18 Cycle 11 Calibration Plan

Due to the significant decrease in WFPC2 observations in Cycle 11 (with the advent of ACS becoming operational), the WFPC2 calibration plan for Cycle 11 has been scaled back. Forty external orbits will be used for WFPC2 calibration this cycle, compared to 61 orbits used in Cycle 10.

Routine calibrations from previous cycles, such as the photometric monitor, darks, and flat fields, will continue in Cycle 11. There is, however, one significant change in these routine monitors: the interval between decontaminations has been increased from 28 days to 49 days. A requirement for WFPC2 UV observations is that the decrease in throughput due to contamination never drops below 70% of the total (post-decon) throughput. Over the past few years, UV photometric monitor data of the standard star GRW+20D5824 has shown that the contamination rates have been decreasing, making it safer to implement longer intervals between decons.

Other scaled-back programs include the Earth flats and astrometric monitor. There was a major update to flat field reference files, as documented by Koekemoer et al. in ISR-2002-02: *Updated WFPC2 Flatfield Reference Files for 1995 - 2001*. For Cycle 11, fewer Earth flats are being executed, and these will be used primarily to track possible small-scale changes in order to update the current flat field reference files.

Astrometric monitor observations will be done once a year, compared to twice a year in past cycles. Since the astrometric properties of the chips are changing more slowly with time, decreasing the frequency to once per year is sufficient to track the changes. An improved astrometric solution for F555W was published by Casertano et al. in ISR-2001-10: *An Improved Geometric Solution for WFPC2*. The WFPC2 group expects to derive additional solutions for other filters in the future.

The CTE characterization program continues the CTE monitor of previous cycles. In addition, two new components have been added. One is to better characterize the "long-vs-short" anomaly since there are indications that this effect is only relevant for very crowded fields. The second component is a test of 2x2 pixel-binned observations to see if binning reduces CTE. A test of this technique could also be useful for ACS observations.

Data from the Photometric Characterization program will, as in past cycles, be used to verify photometric stability to 1-2%. Observations from

this and previous cycles will also be used to update photometric zeropoints used in SYNPHOT.

A new program added to the calibration plan is the WFPC2-ACS Photometric Cross-Calibration. Observations of the primary ACS standard star, two globular clusters spanning a wide range of metallicities, as well as Sloan standard stars, will be taken in WFPC2 with a wide range of the more commonly-used filters.

The WFPC2 group is also beginning to lay out plans for closure of WFPC2 calibration work, making sure all major aspects of WFPC2 are well-characterized. A better idea of what needs to be done will emerge during the WFPC2 session of the upcoming Calibration Workshop (October 2002), where user feedback will provide additional guidance. One primary item for closure will be an accurate cross-calibration between WFPC2 and ACS, an effort that is being coordinated with ACS starting this cycle.

Details about the Cycle 11 calibration plan are outlined in the following pages. For additional details on the WFPC2 calibration plan, please email to help@stsci.edu.

Table 8.11: WFPC2 Cycle 11 Calibration Plan.

ID	Proposal Title	Frequency	Estimated Time (orbits)		Scheduling Required	Products	Accuracy Required	Notes
			"External"	"Internal"				
Routine Monitoring Programs								
9589	WFPC2 Decons & Associated Observations	Decons every 49d (from 28d)	20 (13 photmon, 5 UV thruput, 2 UV flats)	124	every 49d, UV thruput early	CDBS, Inst Hbk, Synphot, WWW reports	1-2%	Decons, phot.monitor, internals, UV throughput, VISFLATS and UVFLATS.
9592	Standard Darks	weekly, except decon week		294	every 7 days, except decon wk.	CDBS	1 e-/hr	Also for WWW hot pixel lists.
9593, 9594, 9595	Supplemental Darks	0-3/day		1182	every day		n/a	For archive only, no analysis.
9596	Internal Monitor	weekly, except decon week		53	every 7 days, except decon week	CDBS	0.8e-/pix	
9598	Earth Flats	continuous		150	mid-to-late	CDBS	0.3%	
9599	UV Earth Flats	continuous		200	early-to-mid	CDBS	3-10%	
9597	Intflat & Visflat Sweeps, Filter Anomaly Check	1/cycle		166	mid-cycle	TIR	0.3%	
Special Calibration Programs								
9600	Astrometric Monitor	1/cycle	1	1	mid-cycle	ISR, STSDAS	0.05"	ω Cen as well as K-spots.
9591	CTE Characterization	1/cycle	5		early, late	ISR	0.03 mag	Continuation of monitors, new tests (2x2 binning & long vs. short).
9590	Photometric Characterization	1/cycle	3		early	ISR, Synphot	1%	Std. star in all 4 chips. Non-monitor broadband filters, not UV.
9601	WFPC2-ACS Photometric Cross-Calibration	1/cycle	8		early	ISR, Synphot	1%	Cross-calibration with ACS, using NGC2419, 47 Tuc, ACS calib star, & Sloane Calibration Field.
	~10% reserve		3					Placeholder for unexpected items.
TOTAL TIME (including all executions)			**40**	**2171**				

9589: WFPC2 Cycle 11: Decontaminations and Associated Observations

- **Purpose:** Monthly WFPC2 decons. Other programs tied to decons are also included: photometric stability check, focus monitor, pre- and post-decon internals, UV throughput checks, visflat sweep, and internal UV flat check.
- **Description:** UV-blocking contaminants removed and hot pixels annealed by warming the CCDs to +20C for 6 hours. Done every 49 days.
  Internals: intflats, biases, darks & kspots, before/after decons.
  Photometric Monitor: GRW+70D5824 is observed after each decon and before every other decon: (1) F170W in all chips to monitor far UV contamination. (2) As many as possible of F160BW, F218W, F255W, F336W, F439W, F555W, F814W will be observed within 1 orbit in a different chip each month.
  UV Throughput: pre-decon PC & WF3 UV observations in most UV filters, post-decon observations of same filters in all 4 chips. Used to verify that the UV spectral response curve is unchanged.
  Internal UV flatfields: obtained with the CAL channel's UV lamp using the filters F122M, F170W, F160BW, F185W, & F336W. The uvflats are used to monitor UV flatfield stability and the stability of the F160BW filter by using F170W as the control. The F336W ratio of visflat to uvflat provides a diagnostic of the UV flatfield degradation & ties the uvflat and visflat flatfield patterns. Two supplemental dark frames must be obtained immediately after each use of the lamp to check for possible after-images.
  VISFLAT mini-sweep: Taken before and after a decon, once during the cycle. VISFLATs will also be taken with a ramp filter, one at each gain, to be done at the post-decon visit, to provide a check of the A-to-D correction.The F336W ratio of VISFLAT to UVFLAT provides a diagnostic of the UV flatfield degradation & ties the UVFLAT and VISFLAT flatfield patterns.
- **Products:** SYNPHOT, CDBS, Instrument Handbook, TIPS meetings, WWW reports, TIR, ISR; new UV flatfields if changes are detected.
- **Accuracy Goals**: *Photometry:* less than 2% discrepancy between results, 1% rms expected.
  UV throughput: better than 3%.
  Flatfields: temporal variations monitored at 1% level. Gain ratios: stable to better than 0.1%.
  UV flats: About 2-8% pixel-to-pixel expected (filter dependent). *Visflats:* stable to better than 1% in overall level and spatial variations (after correcting for lamp degradation). Contamination effects should be < 1%.

9592: WFPC2 Cycle 11: Standard Darks

- **Purpose:** Measure dark current & identify hot pixels.
- **Description:** Six 1800s exp/week with the shutter closed, five with clocks off, one with clocks on. This frequency is required due to the high formation rate of new hot pixels (several tens/CCD/day). Five darks per week are required for cosmic ray rejection, counterbalancing losses due to residual images, & improving the noise of individual measurements. Sometimes, no usable darks are available for a given week due to residual images, resulting in a longer-than-usual gap in the hot pixel lists, but in a decon week, information on hot pixels that became hot and then annealed would be lost irretrievably. As a result, pre-decon darks (see Decon proposal) are executed NON-INT and at least 30 min. after any WFPC2 activity.
- **Products:** Weekly darks delivered to CDBS and monthly tables of hot pixels on the WWW. Superdarks for use in generating pipeline dark reference files.
- **Accuracy Goals:** Require ~1 e-/hr (single-pixel rms) accuracy for most science applications. Expected accuracy in a typical superdark is 0.05 e-/hour for normal pixels. The need for regular darks is driven by systematic effects, such as dark glow (a spatially and temporally variable component of dark signal) and hot pixels, which cause errors that may exceed these limits significantly.

9593, 9594, 9595: WFPC2 Cycle 11: Supplemental Darks

- **Purpose:** Images will allow for frequent monitoring of hot pixels.
- **Description:** This program is designed to provide up to three short (1000s) darks per day, to be used primarily for the identification of hot pixels. Shorter darks are used so that the observations can fit into almost any occultation period, making automatic scheduling feasible. These supplemental darks are low priority, and should be taken only when there is no other requirement for that specific occultation period. This program complements the higher priority Standard Darks proposal that has longer individual observations for producing high-quality pipeline darks and superdarks. Hot pixels are often a cause of concern for relatively short science programs, since they can mimic stars or mask key features of the observations: about 400 new hot pixels/CCD are formed between executions of the Standard Darks program. The supplemental darks are available to the GO community from the archive; there is no plan to use them in our standard analysis and products.
- **Products:** None, though some daily darks may occasionally be used for hot pixel lists if standard darks were lost.

- **Accuracy Goals:** For archive only, no STScI analysis provided.

9596: WFPC2 Cycle 11: Internal Monitor

- **Purpose:** This calibration proposal is the Cycle 11 routine internal monitor for WFPC2, to be run weekly to monitor the health of the cameras. A variety of internal exposures are obtained in order to provide a monitor of the integrity of the CCD camera electronics in both bays (gain 7 and gain 15), a test for quantum efficiency in the CCDs, and a monitor for possible buildup of contaminants on the CCD windows.
- **Description:** The internal observations consist of:
  at gain=7: 4 biases, 2 F555W intflats
  at gain=15: 4 biases, 2 F555W intflats
  The entire set should be run once a week (except on decon weeks), on a non-interference basis. Proposal should start near the beginning of Cycle 11 (early August 2002), replacing Cycle 10 Internal Monitor proposal 8939. This proposal should not be run during Decon weeks as the decon proposal will contain the necessary internal images for those weeks. Each visit should be somewhat evenly spaced, i.e. they should be scheduled about 1 week +/- 2 days apart. Due to the change in DECON schedule for Cycle 11, this program should start during the week beginning with August 5, 2002. All visits in 8939 after the start of this program will be withdrawn.
- **Products:** CDBS (superbias created annually)
- **Accuracy Goals:** 0.8 e-/pix for superbias reference file.

9598: WFPC2 Cycle 11: Earth Flats

- **Purpose:** Monitor flatfield stability. This proposal obtains sequences of Earth streak flats to construct high quality flat fields for the WFPC2 filter set. These flat fields will allow mapping of the OTA illumination pattern and will be used in conjunction with previous internal and external flats to generate new pipeline superflats.
- **Description:** Observations of the bright Earth (Earthcals) are obtained in a variety of filters: F375N, F502N, F656N, F953N, F160BW, F336W, F343N, F390N, F437N, F469N, F487N, F631N, F658N, and F673N.
- **Products:** New flatfields generated and delivered to CDBS if changes detected. (Most recent update was delivered to CDBS in early 2002.)
- **Accuracy Goals:** The single-pixel signal-to-noise ratio expected in the flatfield is 0.3%.

9599: WFPC2 Cycle 11: UV Earth Flats

- **Purpose:** Monitor flatfield stability. This proposal obtains sequences of Earth streak flats to improve the quality of pipeline flat fields for the WFPC2 UV filter set.
- **Description:** Earth streak-flats are taken in UV filteLrs (F170W, F185W, F218W, F255W, F300W, F336W, and F343N). Those UV filters with significant read leak will also be observed crossed with selected broadband filters (F450W, F606W, F675W, and F814W), in order to assess and remove the read leak contribution.
- **Products:** Updated flatfields for pipeline via CDBS. (Most recent delivery to CDBS made in early 2002.)
- **Accuracy Goals:** 3-10%.

9597: WFPC2 Cycle 11: Intflat and Visflat Sweeps, and Filter Rotation Anomaly Monitor

- **Purpose:** Using intflat observations, this WFPC2 proposal is designed to monitor the pixel-to-pixel flatfield response and provide a linearity check. The intflat sequences, to be done once during the year, are similar to those from the Cycle 10 program 8942. The images will provide a backup database in the event of complete failure of the visflat lamp as well as allow monitoring of the gain ratios. The sweep is a complete set of internal flats, cycling through both shutter blades and both gains. The linearity test consists of a series of intflats in F555W, in each gain and each shutter. As in Cycle 10, we plan to continue to take extra visflat, intflat, and earthflat exposures to test the repeatability of filter wheel motions.
- **Description:** This proposal contains the intflat filter sweep, linearity and filter rotation tests.
  Linearity test: flatfields are taken with F555W at a variety of exposure times, using shutters A & B, and gains 7 & 15. Since the intflats have significant spatial structure, any non-linearity will appear as a non-uniform ratio of intflats with different exposure times.
  Filter rotation check: visflats will be taken to test the repeatability of the filter wheel positioning. A problem is known to exist in several filters.
- **Products:** TIR, ISR
- **Accuracy Goals:** 0.3%

9600: WFPC2 Cycle 11: Astrometric Monitor

- **Purpose:** Verify relative positions of WFPC2 chips with respect to one another.
- **Description:** The positions of the WFPC2 chips with respect to each other appear to be shifting slowly (by about 1 pixel, since 1994). The rich field in ω Cen (same positions as cycle 9 proposal 8813) is observed with large shifts (35”) in F555W only, once in the cycle. This will allow tracking of the shifts in the relative positions of the chips or changes in the astrometric solution at the sub-pixel level. Kelsall spot images will be taken in conjunction with each execution.
- **Products:** TIPS reports, ISR, update of chip positions in PDB and of geometric solution in STSDAS tasks metric and wmosaic if significant changes are found.
- **Accuracy Goals:** At least 0.01’’ in relative shifts; 0.05” or better for absolute.

9591: WFPC2 Cycle 11: CTE Characterization

- **Purpose:** Monitor CTE changes during Cycle 11; test whether 2X2 binning affects CTE (may be relevant for ACS) and perform a high S/N long-vs-short test in an uncrowded field.
- **Description:** Obtain observations of Omega Cen (NGC 5139) to track changes in the CTE (charge transfer efficiency) in WFPC2. A continuation of proposals in earlier cycles (7629, 8447, and 8821, 9254), the principal observations will be at gains 7 and 15, in F814W and F555W. The same pointing is used on WF2 and WF4. The relative orientation of the chips then results in stars at the bottom of one chip falling near the top of the other chip, hence providing a measurement of the CTE loss. We will make similar observations using 2X2 binning. This may reduce CTE loss since the largest loss is to the adjoining pixel, which gets included in the 2X2 bin in 50% of the cases. This may be relevant for ACS. We will also obtain a high S/N measurement of the long-vs-short anomaly for uncrowded fields by taking 10 X 10s exposures in Omega Cen, in order to test the recent finding that the long-vs.-short problem is only relevant for crowded fields.
- **Products:** ISR and updates to published CTE correction formulae.
- **Accuracy Goals:** 0.03 magnitudes for the majority (90%) of cases

9590: WFPC2 Cycle 11: Photometric Characterization

- **Purpose:** Provide a check of the zeropoints and contamination rates in non-standard WFPC2 filters.
- **Description:** Observations of the standard star GRW+70D5824 in all four chips will be made using filters that are not routinely monitored but are still used in cycle 11(F467M, F547M, F569W, F606W, F675W, F791W, F850LP, and F1042M). Images should be taken within 7 days after a decon, to minimize any contamination effects. Results from this program will be compared with archival data from earlier cycles.
- **Products:** ISR, SYNPHOT update.
- **Accuracy Goals:** 2-3% photometry.

9601: WFPC2 Cycle 11: WFPC2-ACS Photometric Cross-Calibration

- **Purpose:** This proposal is aimed at providing photometric zeropoint cross-calibration between the commonly used WFPC2 photometric filter sets and those that will be used for ACS programs.
- **Description:** Observations of two globular clusters spanning a wide range in metallicity (NGC 2419 and 47 Tuc). Also WFPC2 observations of the primary ACS standard star, as well as observations of a Sloan Standard Field. These observations will produce a valuable tie-in between the WFPC2, ACS and Sloan filter photometric systems.
- **Products:** ISR, Synphot, WFPC2 and ACS Handbooks
- **Accuracy Goals:** 1%

8.19 Cycle 12 Calibration Plan

Until Cycle 10, WFPC2 was the most heavily used instrument on HST (~40-60% of the total of ~3000 orbits available for science in a given Cycle), with much of the observing being carried out in prime mode. Since the installation of the Advanced Camera for Surveys (ACS) in Cycle 11, there has been a dramatic change in the usage pattern for WFPC2. The instrument is still used quite heavily by the community (~800 - 1200 orbits/Cycle), though somewhat less than before, but the main difference is that now almost all the WFPC2 observing is carried out in parallel mode. Thus about 40% of prime HST science orbits during Cycles 11 and 12 have WFPC2 observations of parallel targets, while the number of prime WFPC2 science observations have decreased to ~5% and 2% of the total

awarded time in each of Cycles 11 and 12 respectively, as demonstrated in Table 8.14.

Table 8.12: WFPC2 Science Program Usage During Cycles 10 - 12.

WFPC2 Science Program Usage	Cycle 10	Cycle 11	Cycle 12
Primary Orbits	1080	153	56
Coordinated Parallel Orbits	40	200	381
Pure Parallel Orbits	300	500	844

In addition to the change in emphasis by the community from prime to parallel observing, there has also been a change in emphasis on the types of WFPC2 science programs that are carried out. Specifically, WFPC2 remains competitive with ACS in the following three areas:

- A comparatively broad selection of filters in a total of 48 optical elements, consisting of 18 narrow-band and medium-band filters, 23 broad-band and long-pass filters, as well as 2 quad filters (each giving 4 different narrow-band wavelengths on the 4 WFPC2 chips), one polarizing filter, and 4 linear ramp filters (LRFs).
- A relatively high discovery efficiency in the near-UV (essentially the product of the instrument area and its UV throughput); while the ACS/HRC is ~3-4 times more sensitive than WFPC2 in the 2000-3500A wavelength range (i.e. short wards of the blue cutoff of ACS/WFC), the area of WFPC2 is ~30 times larger than the ACS/HRC.
- A long history of on-orbit performance (10 years as of December 2003) and well-characterized behavior, making WFPC2 suitable for long-term monitoring studies of objects that are variable in their photometric or astrometric properties.

Thus, the majority of Cycle 12 science programs making use of WFPC2 in prime mode have consisted of either narrow-band filter observations, or the continuation of long-term monitoring programs. On the other hand, the WFPC2 parallel science tends to consist mostly of observations through a subset of the broad-band filters, often in the near-UV.

- Considering both the reduced observing time for WFPC2 in Cycle 12, as well as the change in its usage patterns, this has necessitated a change in the calibration strategy for the instrument during this Cycle. The principal emphasis of routine calibration continues to be two-fold:
- Monitor and maintain the basic health and safety of the instrument in all its modes.

- Maintain the required calibration accuracies for science modes used in Cycle 12, while also streamlining the calibration process to remove unnecessary observations of modes that are not used during this Cycle.

In addition, during Cycles 11 and 12 we have begun implementation of a class of special Close-Out Calibration Programs, taking into account community input to carry out programs that will increase the value of the WFPC2 archival scientific legacy. In Cycle 12, these include the following programs:

- Photometric cross-calibration with other instruments and systems, in particular ACS and SDSS, by observing a range of different photometric standards through the widest possible range of WFPC2 filters.
- Improving our knowledge of the astrometric distortion of WFPC2 in the UV, by carrying out observations on our standard astrometric field ω Centauri using the near-UV F255W filter.
- Improving characterization of the long-term stability of the narrow-band / LRF filter set, by observing an emission-line source in a range of narrow-band filters, by themselves and crossed with LRFs. This will enable verification of the constancy of the central wavelength of the narrow-band filter, as well as providing a check on its throughput.

These changes to the calibration philosophy are reflected in the orbit allocations for the Cycle 12 calibration programs, as shown in Table 8.16. The number of external orbits for routine monitoring programs are reduced compared with previous cycles, with the dominant remaining components being the verification of UV throughput before and after decontaminations, as well as a number of CTE and photometric monitoring exposures. Likewise, the internal orbit allocation is reduced somewhat to account for the fact that we are no longer calibrating filter modes that are not used for science during this Cycle. However, the Special and Close-Out programs remain at a level of ~50% of the entire external orbit allocation budget, reflecting our emphasis on carrying out these programs that are needed to provide final calibration data to enhance the long-term archival legacy of the instrument.

The total time allocated for Cycle 12 calibrations is 25 external orbits (compared to 40 orbits in cycle 11), and 1681 internal/occultation orbits. This allocation spans October 1, 2003 to September 30, 2004. As always, about 10% of the total external orbit time allocation has been set aside for

calibration issues that arise during Cycle 12, amounting to 2 external orbits.

Table 8.13: WFPC2 Calibration Program Orbit Allocations During Cycles 10 - 12.

WFPC2 Calibration Program Usage	Cycle 10		Cycle 11		Cycle 12	
	Ext.	Int.	Ext.	Int.	Ext.	Int.
Monitors: Decons, darks, internal flats	23	2242	19	2170	12	1677
Special / Close-Out Programs	32	52	17	1	13	4
Reserve (Unexpected Items)	6		3		2	
Total	**61**	**2294**	**40**	**2171**	**25**	**1681**

Table 8.14: WFPC2 Cycle 12 Calibration Plan.

ID	Proposal Title	Frequency	Estimated Time (orbits)		Scheduling Required	Products	Accuracy Required	Notes
			"External"	"Internal"				
Routine Monitoring Programs								
10067	WFPC2 Decons & Associated Observations	Decons every 49d	8	124	every 49d	CDBS, IHB, Synphot, WWW reports	1-2%	Decons, phot.monitor, internals, UV throughput, VISFLATS and UVFLATS.
10068	Standard Darks	weekly, exc. decon wk		264	every 7 days, exc.decon wk	CDBS	1 e-/hr	CDBS updates and weekly WWW hot pixel lists.
10069, 10070, 10071	Supplemental Darks	0-3/day		1195	every day		n/a	For archive only, no analysis. Schedule at a low priority. Useful for calibrating WFPC2 parallels.
10072	Internal Monitor	weekly, exc. decon wk		44	every 7 days, exc.decon wk	CDBS	0.8e-/pix	BIAS, INTFLATS in F555W for gain and throughput stability measurements
10073	Visible Earth Flats	continuous		50	mid-to-late	CDBS	0.3%	Reduce to 1 filter (time dep. only)
10074	UV Earth Flats	continuous		20	mid-to-late	CDBS	0.3%	
10075	Intflat & Visflat Sweeps, Filter Anomaly Check	1/cycle		80	mid-cycle	TIR	0.3%	Flats in all the filters used in Cycle 12, both gain settings/shutters.
10076	CTE Monitor	1/cycle	2		mid-to-late	ISR	0.03 mag	Continue CTE monitor.
10077	Photometric Monitor	1/cycle	2		mid-cycle	ISR, Synphot	1%	GRW+70D5824 in filter/chip combos used for science in Cycle 12.
Close-Out Calibration Programs								
10078	Photometric Cross-Calibration	once	6		mid-cycle	ISR, Synphot	1%	Several standard stars in a range of WFPC2 filters, for ACS & WFC3 cross-calibration.
10079	UV Astrometric Characterization	once	3	1	mid-cycle	ISR, Synphot	0.05"	Determine astrometric solution in new UV filters (not done before), and K-spots.
10080	Narrow-Band/LRF Characterization	once	2	3	mid-to-late	ISR, Synphot	1-2%	Check filter wavelength stability: observe emission-line source in narrow-band filters, and crossed with LRFs
	~10% reserve		2					Placeholder for unexpected items.
TOTAL TIME (including all executions)			**25**	**1601**				

10067: WFPC2 Cycle 12: Decontaminations and Associated Observations

- **Purpose:** WFPC2 decons every 49 days. Other programs tied to decons are also included: photometric stability check, focus monitor, pre- and post-decon internals, UV throughput checks, visflat sweep, and internal UV flat check.
- **Description:** UV-blocking contaminants removed and hot pixels annealed by warming the CCDs to +20C for 6 hours. Done every 49 days.
  Internals: intflats, biases, darks & kspots, before/after decons.
  Photometric Monitor: GRW+70D5824 is observed either before or after a decon, rotating chips: (1) F170W in all chips to monitor far UV contamination. (2) As many as possible of F218W, F255W, F300W, F336W will be observed within 1 orbit in a different chip each time.
  UV Throughput: Observations in most UV filters (F122M, F185W, F343N, F375N, F390N) added to each the photometric monitor. Used to verify that the UV spectral response curve is unchanged.
  Internal UV flatfields: obtained with the CAL channel's UV lamp using the filters F122M, F170W, F160BW, F185W, & F336W. The uvflats are used to monitor UV flatfield stability and the stability of the F160BW filter by using F170W as the control. The F336W ratio of visflat to uvflat provides a diagnostic of the UV flatfield degradation & ties the uvflat and visflat flatfield patterns. Two supplemental dark frames must be obtained immediately after each use of the lamp to check for possible after-images.
  VISFLAT mini-sweep: Taken before and after a decon, once during the cycle. VISFLATs will also be taken with a ramp filter, one at each gain, to be done at the post-decon visit, to provide a check of the A-to-D correction.The F336W ratio of VISFLAT to UVFLAT provides a diagnostic of the UV flatfield degradation & ties the UVFLAT and VISFLAT flatfield patterns.
- **Products:** SYNPHOT, CDBS, Instrument Handbook, TIPS meetings, WWW reports, TIR, ISR; new UV flatfields if changes are detected.
- **Accuracy Goals**: *Photometry:* less than 2% discrepancy between results, 1% rms expected.
  UV throughput: better than 3%.
  Flatfields: temporal variations monitored at 1% level. Gain ratios: stable to better than 0.1%.
  UV flats: About 2-8% pixel-to-pixel expected (filter dependent). *Visflats:* stable to better than 1% in overall level and spatial variations (after correcting for lamp degradation). Contamination effects should be < 1%.

10068: WFPC2 Cycle 12: Standard Darks

- **Purpose:** Measure dark current & identify hot pixels.
- **Description:** Six 1800s exp/week with the shutter closed, five with clocks off, one with clocks on. This frequency is required due to the high formation rate of new hot pixels (several tens/CCD/day). Five darks per week are required for cosmic ray rejection, counterbalancing losses due to residual images, & improving the noise of individual measurements. Sometimes, no usable darks are available for a given week due to residual images, resulting in a longer-than-usual gap in the hot pixel lists, but in a decon week, information on hot pixels that became hot and then annealed would be lost irretrievably. As a result, pre-decon darks (see Decon proposal) are executed NON-INT and at least 30 min. after any WFPC2 activity.
- **Products:** Weekly darks delivered to CDBS and monthly tables of hot pixels on the WWW. Superdarks for use in generating pipeline dark reference files.
- **Accuracy Goals:** Require ~1 e-/hr (single-pixel rms) accuracy for most science applications. Expected accuracy in a typical superdark is 0.05 e-/hour for normal pixels. The need for regular darks is driven by systematic effects, such as dark glow (a spatially and temporally variable component of dark signal) and hot pixels, which cause errors that may exceed these limits significantly.

10069, 10070, 10071: WFPC2 Cycle 12: Supplemental Darks

- **Purpose:** Images will allow for frequent monitoring of hot pixels.
- **Description:** This program is designed to provide up to three short (1000s) darks per day, to be used primarily for the identification of hot pixels. Shorter darks are used so that the observations can fit into almost any occultation period, making automatic scheduling feasible. These supplemental darks are low priority, and should be taken only when there is no other requirement for that specific occultation period. This program complements the higher priority Standard Darks proposal that has longer individual observations for producing high-quality pipeline darks and superdarks. Hot pixels are often a cause of concern for relatively short science programs, since they can mimic stars or mask key features of the observations: about 400 new hot pixels/CCD are formed between executions of the Standard Darks program. The supplemental darks are available to the GO community from the archive; there is no plan to use them in our standard analysis and products.
- **Products:** None, though some daily darks may occasionally be used for hot pixel lists if standard darks were lost.

- **Accuracy Goals:** For archive only, no STScI analysis provided.

10072: WFPC2 Cycle 12: Internal Monitor

- **Purpose:** This calibration proposal is the Cycle 12 routine internal monitor for WFPC2, to be run weekly to monitor the health of the cameras. A variety of internal exposures are obtained in order to provide a monitor of the integrity of the CCD camera electronics in both bays (gain 7 and gain 15), a test for quantum efficiency in the CCDs, and a monitor for possible buildup of contaminants on the CCD windows.
- **Description:** The internal observations consist of:
  at gain=7: 4 biases, 2 F555W intflats
  at gain=15: 4 biases, 2 F555W intflats
  The entire set should be run once a week (except on decon weeks), on a non-interference basis. Proposal should start near the beginning of Cycle 12 (early August 2003), replacing Cycle 11 Internal Monitor proposal 9596. This proposal should not be run during Decon weeks as the decon proposal will contain the necessary internal images for those weeks. Each visit should be somewhat evenly spaced, i.e. they should be scheduled about 1 week +/- 2 days apart.
- **Products:** CDBS (superbias created annually)
- **Accuracy Goals:** 0.8 e-/pix for superbias reference file.

10073: WFPC2 Cycle 12: Visible Earth Flats

- **Purpose:** Monitor flatfield stability. This proposal obtains sequences of Earth streak flats to construct high quality flat fields for the WFPC2 filter set. These flat fields will allow mapping of the OTA illumination pattern and will be used in conjunction with previous internal and external flats to generate new pipeline superflats.
- **Description:** Observations of the bright Earth (Earthcals) are obtained in F502N to monitor time-dependence of flatfield features. In Cycle 12, we will continue monitoring only F502N; prior to Cycle 12, all 12 narrow-band filters have been used. A detailed study of Earthflats (Koekemoer 2001) showed that there was no time evolution in the color dependence of flatfields, i.e. the time evolution of flatfields is monochromatic.
- **Products:** New flatfields generated and delivered to CDBS if changes detected. (Most recent update was delivered to CDBS in early 2002.)
- **Accuracy Goals:** The single-pixel signal-to-noise ratio expected in the flatfield is 0.3%.

10074: WFPC2 Cycle 12: UV Earth Flats

- **Purpose:** Monitor flatfield stability. This proposal obtains sequences of Earth streak flats to improve the quality of pipeline flat fields for the WFPC2 UV filter set.
- **Description:** Earth streak-flats are taken in UV filteLrs (F170W, F185W, F218W, F255W, F300W, F336W, and F343N). Those UV filters with significant read leak will also be observed crossed with selected broadband filters (F450W, F606W, F675W, and F814W), in order to assess and remove the read leak contribution.
- **Products:** Updated flatfields for pipeline via CDBS. (Most recent delivery to CDBS made in early 2002.)
- **Accuracy Goals:** 3-10%.

10075: WFPC2 Cycle 12: Intflat and Visflat Sweeps, and Filter Rotation Anomaly Monitor

- **Purpose:** Using intflat observations, this WFPC2 proposal is designed to monitor the pixel-to-pixel flatfield response and provide a linearity check. The intflat sequences, to be done once during the year, are similar to those from the Cycle 11 program 9597. The images will provide a backup database in the event of complete failure of the visflat lamp as well as allow monitoring of the gain ratios. The sweep is a complete set of internal flats, cycling through both shutter blades and both gains. The linearity test consists of a series of intflats in F555W, in each gain and each shutter. As in Cycle 11, we plan to continue to take extra visflat, intflat, and earthflat exposures to test the repeatability of filter wheel motions.
- **Description:** This proposal contains the intflat filter sweep, linearity and filter rotation tests.
  Linearity test: flatfields are taken with F555W at a variety of exposure times, using shutters A & B, and gains 7 & 15. Since the intflats have significant spatial structure, any non-linearity will appear as a non-uniform ratio of intflats with different exposure times.
  Filter rotation check: visflats will be taken to test the repeatability of the filter wheel positioning. A problem is known to exist in several filters.
- **Products:** TIR, ISR
- **Accuracy Goals:** 0.3%

10076: WFPC2 Cycle 12: CTE Monitor

- **Purpose:** Monitor CTE changes during Cycle 12; test whether 2X2 binning affects CTE (may be relevant for ACS) and perform a high S/N long-vs-short test in an uncrowded field.

- **Description:** Obtain observations of Omega Cen (NGC 5139) to track changes in the CTE (charge transfer efficiency) in WFPC2. A continuation of proposals in earlier cycles (7629, 8447, and 8821, 9254), the principal observations will be at gains 7 and 15, in F814W and F555W. The same pointing is used on WF2 and WF4. The relative orientation of the chips then results in stars at the bottom of one chip falling near the top of the other chip, hence providing a measurement of the CTE loss. We will make similar observations using 2X2 binning. This may reduce CTE loss since the largest loss is to the adjoining pixel, which gets included in the 2X2 bin in 50% of the cases. This may be relevant for ACS. We will also obtain a high S/N measurement of the long-vs-short anomaly for uncrowded fields by taking 10 X 10s exposures in Omega Cen, in order to test the recent finding that the long-vs.-short problem is only relevant for crowded fields.
- **Products:** ISR and updates to published CTE correction formulae.
- **Accuracy Goals:** 0.03 magnitudes for the majority (90%) of cases

10077: WFPC2 Cycle 12: Photometric Monitor

- **Purpose:** Provide a check of the zeropoints and contamination rates in non-standard, less-used, or WFPC2 filters F439W and long-ward.
- **Description:** Observations of the standard star GRW+70D5824 in all four chips will be made using filters that are not routinely monitored but are still used in cycle 12 (F439W, F450W, F547M, F555W, F569W, F606W, F675W, F791W, F814W, F850LP, and F1042M). F675W, F850LP and F1042M are observed in the PC1 chip only. Images should be taken within 7 days after a decon, to minimize any contamination effects. Results from this program will be compared with archival data from earlier cycles.
- **Products:** ISR, SYNPHOT update.
- **Accuracy Goals:** 2-3% photometry.

10078: WFPC2 Cycle 12: Close-Out Photometric Cross-Calibration

- **Purpose:** This proposal is aimed at providing photometric zeropoint cross-calibration between the commonly used WFPC2 photometric filter sets and those that will be used for ACS programs.
- **Description:** Observations of two globular clusters spanning a wide range in metallicity (NGC 2419 and 47 Tuc). Also WFPC2 observations of the primary ACS standard star, as well as observations of a Sloan Standard Field. These observations will produce a valuable tie-in between the WFPC2, ACS and Sloan filter photometric systems.

- **Products:** ISR, Synphot, WFPC2 and ACS Handbooks
- **Accuracy Goals:** 1%

10079: WFPC2 Cycle 12: Close-Out UV Astrometric Characterization

- **Purpose:** Verify relative positions of WFPC2 chips with respect to one another.
- **Description:** The positions of the WFPC2 chips with respect to each other appear to be shifting slowly (by about 1 pixel, since 1994). The rich field in ω Cen (same positions as cycle 9 proposal 8813) is observed with large shifts (35") in F555W only, once in the cycle. This will allow tracking of the shifts in the relative positions of the chips or changes in the astrometric solution at the sub-pixel level. Kelsall spot images will be taken in conjunction with each execution.
- **Products:** TIPS reports, ISR, update of chip positions in PDB and of geometric solution in STSDAS tasks metric and wmosaic if significant changes are found.
- **Accuracy Goals:** At least 0.01'' in relative shifts; 0.05" or better for absolute.

10080: WFPC2 Cycle 12: Close-Out Narrow-Band/LRF Characterization

- **Purpose:** This proposal is aimed at measuring the wavelength stability of the LRFs, which may have changed over time due to annealing or shrinkage of the thin films.
- **Description:** On-orbit VISFLATs taken through the LRFs crossed with narrow-band filters to constrain the LRF wavelength calibration, as well as uncrossed LFRF VISFLAT exposures to contain the transverse (cross-wavelength) placement of the LRFs. External observations of a planetary nebula (2 orbits) to provide an absolute test of the LRF wavelength calibration.
- **Products:** ISR, Synphot, WFPC2 and ACS IHB.
- **Accuracy Goals:** 1%.

8.20 Cycle 13 Calibration Plan

The overall goals of the Cycle 13 WFPC2 Calibration Programs are to monitor health and safety of the instrument and to maintain required calibration accuracies for the science modes used in Cycle 13. We will also streamline routine monitoring programs and remove unnecessary observations. Specifically, we are discontinuing the supplemental darks program as they were little used. Eliminating them will help prolong the life of the data transmitter aboard HST. We will further implement special close-out calibration programs to increase the value of the WFPC2 archive scientific legacy, such as photometric cross-calibration with other instruments.

Until the end of Cycle 10, WFPC2 was most heavily used in prime mode. During Cycles 11-13, WFPC2 prime orbits have decreased dramatically and parallel usage is now the dominant mode for WFPC2 science operation. Table 8.15 on page 325 shows the recent history of science program and calibration program usage.

Table 8.15: Recent Science and Calibrations Program Usage

WFPC2 Science Program Usage	Cycle 10	Cycle 11	Cycle 12	Cycle 13
Primary Orbits	1080	153	56	21
Coordinated Parallel Orbits	40	200	381	890
Pure Parallel Orbits	300	500	844	0

WFPC2 Calibration Program Usage	Cycle 10		Cycle 11		Cycle 12		Cycle 13	
	Ext.	Int.	Ext.	Int.	Ext.	Int.	Ext.	Int.
Monitors: decons, darks, internals, flats	23	2242	19	2170	12	1677	13	582
Special / Close-Out Programs	32	52	17	1	13	4	2	0
Reserve (Unexpected Items)	6	0	3	0	2	0	2	0
Total	**61**	**2294**	**40**	**2171**	**25**	**1681**	**17**	**582**

WFPC2 Cycle 13 Calibration Plan.

ID	Proposal Title	Frequency	Estimated Time (orbits)		Scheduling Required	Products	Accuracy Required	Notes
			"External"	"Internal"				
				Routine Monitoring Programs				
10356	WFPC2 Decons & Associated Observations	Decons every 49d	8	124	every 49d	CDBS, IHB, Synphot, WWW reports	1-2%	Decons, phot.monitor, internals, UV throughput, VISFLATS and UVFLATS.
10359	Standard Darks	weekly, exc. decon wk		264	every 7 days, exc.decon wk	CDBS	1 e-/hr	CDBS updates and weekly WWW hot pixel lists.
10360	Internal Monitor	weekly, exc. decon wk		44	every 7 days, exc.decon wk	CDBS	0.8e-/pix	BIAS, INTFLATS in F555W for gain and throughput stability measurements
10361	Visible Earth Flats	continuous		50	mid-to-late	CDBS	0.3%	F502N only (time dependence only)
10362	UV Earth Flats	continuous		20	mid-to-late	CDBS	0.3%	F255W only
10363	Intflat & Visflat Sweeps, Filter Anomaly Check	1/cycle		80	mid-cycle	TIR	0.3%	Flats in all the filters used in Cycle 12, both gain settings/shutters.
10364	CTE Monitor	1/cycle	2		mid-to-late	ISR	0.03 mag	Continue CTE monitor.
10365	Photometric Monitor	1/cycle	3		mid-cycle	ISR, Synphot	1%	GRW+70D5824 in filter/chip combos used for science in Cycle 13.
				Close-Out Calibration Programs				
10366	Photometric Cross-Calibration	once	2		mid-cycle	ISR, Synphot	1%	T-dwarf star in a range of WFPC2 filters, for ACS & WFC3 cross-calibr.
	~10% reserve		2					Placeholder for unexpected items.
TOTAL TIME (including all executions)			**17**	**582**				

10356: WFPC2 Cycle 13: Decontaminations and Associated Observations

- **Purpose:** WFPC2 decons every 49 days. Other programs tied to decons are also included: photometric stability check, focus monitor, pre- and post-decon internals, visflat sweep, and internal UV flat check.
- **Description:** *Decontamination:* UV-blocking contaminants removed and hot pixels annealed by warming the CCDs to +20C for 6 hours. Done every 49 days.
  Internals: intflats, biases, darks & kspots, before/after decons.
  Photometric Monitor: GRW+70D5824 is observed alternately before or after each decon, rotating chips: (1) F170W in all chips to monitor far UV contamination. (2) As many as possible of F122M, F185W, F218W, F255W, F300W, F336W, F343N, F375N, F390N, and F555W will be observed within 1 orbit in a different chip each time.
  UV Throughput: pre-decon PC & WF3 UV observations in most UV filters, post-decon observations of same filters in all 4 chips. Used to verify that the UV spectral response curve is unchanged.
  Internal UV flatfields: obtained with the CAL channel's UV lamp using the filters F122M, F170W, F160BW, F185W, & F336W. The UVFLATs are used to monitor UV flatfield stability and the stability of the F160BW filter by using F170W as the control. The F336W ratio of VISFLAT to UVFLAT provides a diagnostic of the UV flat-field degradation & ties the UVFLAT and VISFLAT flatfield patterns. Two supplemental dark frames must be obtained immediately after each use of the lamp to check for possible after-images.
  VISFLAT mini-sweep: Taken before and after a decon, once during the cycle. VISFLATs will also be taken with a ramp filter, one at each gain, to be done at the post-decon visit, to provide a check of the A-to-D correction.The F336W ratio of VISFLAT to UVFLAT provides a diagnostic of the UV flatfield degradation & ties the UVFLAT and VISFLAT flatfield patterns.
- **Products:** SYNPHOT, CDBS, Instrument Handbook, TIPS meetings, WWW reports, TIR, ISR; new UV flatfields if changes are detected.
- **Accuracy Goals**: *Photometry:* less than 2% discrepancy between results, 1% rms expected.
  UV throughput: better than 3%.
  Flatfields: temporal variations monitored at 1% level. Gain ratios: stable to better than 0.1%.
  UV flats: About 2-8% pixel-to-pixel expected (filter dependent). *Visflats:* stable to better than 1% in overall level and spatial variations (after correcting for lamp degradation). Contamination effects should be < 1%.

10359: WFPC2 Cycle 13: Standard Darks

- **Purpose:** Measure dark current & identify hot pixels.

- **Description:** Six 1800s exp/week with the shutter closed, five with clocks off, one with clocks on. This frequency is required due to the high formation rate of new hot pixels (several tens/CCD/day). Five darks per week are required for cosmic ray rejection, counterbalancing losses due to residual images, & improving the noise of individual measurements. Sometimes, no usable darks are available for a given week due to residual images, resulting in a longer-than-usual gap in the hot pixel lists, but in a decon week, information on hot pixels that became hot and then annealed would be lost irretrievably. As a result, pre-decon darks (see Decon proposal) are executed NON-INT and at least 30 min. after any WFPC2 activity.
- **Products:** Weekly darks delivered to CDBS and monthly tables of hot pixels on the WWW. Superdarks for use in generating pipeline dark reference files.
- **Accuracy Goals:** Require ~1 e-/hr (single-pixel rms) accuracy for most science applications. Expected accuracy in a typical superdark is 0.05 e-/hour for normal pixels. The need for regular darks is driven by systematic effects, such as dark glow (a spatially and temporally variable component of dark signal) and hot pixels, which cause errors that may exceed these limits significantly.

10360: WFPC2 Cycle 13: Internal Monitor

- **Purpose:** This calibration proposal is the Cycle 13 routine internal monitor for WFPC2, to be run weekly to monitor the health of the cameras. A variety of internal exposures are obtained in order to provide a monitor of the integrity of the CCD camera electronics in both bays (gain 7 and gain 15), a test for quantum efficiency in the CCDs, and a monitor for possible buildup of contaminants on the CCD windows.
- **Description:** The internal observations consist of:
  at gain=7: 4 biases, 2 F555W intflats
  at gain=15: 4 biases, 2 F555W intflats
  The entire set should be run once a week (except on decon weeks), on a non-interference basis. Proposal should start near the beginning of Cycle 13 (early August 2004), replacing Cycle 12 Internal Monitor proposal 10072. This proposal should not be run during Decon weeks as the decon proposal will contain the necessary internal images for those weeks. Each visit should be somewhat evenly spaced, i.e. they should be scheduled about 1 week +/- 2 days apart.
- **Products:** CDBS (superbias created annually)
- **Accuracy Goals:** 0.8 e-/pix for superbias reference file.

10361: WFPC2 Cycle 13: Visible Earth Flats

- **Purpose:** Monitor flatfield stability. This proposal obtains sequences of Earth streak flats to construct high quality flat fields for the WFPC2 filter set. These flat fields will allow mapping of the OTA illumination pattern and will be used in conjunction with previous internal and external flats to generate new pipeline superflats.
- **Description:** Observations of the bright Earth (Earthcals) are obtained in F502N to monitor time-dependence of flatfield features. In Cycle 13, we will continue monitoring only F502N (as was done in Cycle 12; prior to Cycle 12, all 12 narrow-band filters have been used). A detailed study of Earthflats (Koekemoer 2001) showed that there was no time evolution in the color dependence of flatfields, i.e. the time evolution of flatfields is monochromatic.
- **Products:** New flatfields generated and delivered to CDBS if changes detected.
- **Accuracy Goals:** The single-pixel signal-to-noise ratio expected in the flatfield is 0.3%.

10362: WFPC2 Cycle 13: UV Earth Flats

- **Purpose:** Monitor flatfield stability. This proposal obtains sequences of Earth streak flats to improve the quality of pipeline flat fields for the WFPC2 UV filter set.
- **Description:** Earth streak-flats are taken in UV filter F255W, in order to measure time dependence of flatfield due to changes in the camera geometry as well as any possible long-term changes from permanent evaporation of contaminants.
- **Products:** Updated flatfields for pipeline via CDBS.
- **Accuracy Goals:** 3-10%.

10363: WFPC2 Cycle 13: Intflat and Visflat Sweeps, and Filter Rotation Anomaly Monitor

- **Purpose:** Using INTFLAT observations, this WFPC2 proposal is designed to monitor the pixel-to-pixel flatfield response and provide a linearity check. The INTFLAT sequences, to be done once during the year, are similar to those from the Cycle 10 program 8942. The images will provide a backup database in the event of complete failure of the VISLFAT lamp as well as allow monitoring of the gain ratios. The sweep is a complete set of internal flats, cycling through both shutter blades and both gains. The linearity test consists of a series of INTFLATs in F555W, in each gain and each shutter. As in Cycle 12, we plan to continue to take extra VISLFAT, INTFLAT, and Earthflat exposures to test the repeatability of filter wheel motions.

- **Description:** This proposal contains the INTFLAT filter sweep, linearity and filter rotation tests.
  Linearity test: flatfields are taken with F555W at a variety of exposure times, using shutters A & B, and gains 7 & 15. Since the INTFLATs have significant spatial structure, any non-linearity will appear as a non-uniform ratio of intflats with different exposure times.
  Filter rotation check: VISFLATs and Earthflats will be taken to test the repeatability of the filter wheel positioning. A problem is known to exist in several filters.
- **Products:** TIR, ISR
- **Accuracy Goals:** 0.3%

10364: WFPC2 Cycle 13: CTE Monitor

- **Purpose:** Monitor CTE changes during Cycle 13; test whether 2X2 binning affects CTE (may be relevant for ACS) and perform a high S/N long-vs-short test in an uncrowded field.
- **Description:** Obtain observations of Omega Cen (NGC 5139) to track changes in the CTE (charge transfer efficiency) in WFPC2. A continuation of proposals in earlier cycles (7629, 8447, 8821, 9254, 10076), the principal observations will be at gains 7 and 15, in F814W and F555W. The same pointing is used on WF2 and WF4. The relative orientation of the chips then results in stars at the bottom of one chip falling near the top of the other chip, hence providing a measurement of the CTE loss. We will also obtain a high S/N measurement of the long-vs-short anomaly for uncrowded fields by taking 10 X 10s exposures in Omega Cen, in order to test the recent finding that the long-vs.-short problem is only relevant for crowded fields.
- **Products:** ISR and updates to published CTE correction formulae.
- **Accuracy Goals:** 0.03 magnitudes for the majority (90%) of cases

10365: WFPC2 Cycle 13: Photometric Monitor

- **Purpose:** Provide a check of the zeropoints and contamination rates in non-standard WFPC2 filters.
- **Description:** Observations of the standard star GRW+70D5824 in all four chips will be made using filters that are not routinely monitored but are still used in Cycles 12 and 13. The filters are PC1: F439W, F450W, F467M, F487N, F502N, F547M, F555W, F588N, F606W, F631N, F656N, F658N, F673N, F675W, F791W, F814W, F850LP, F953N, F1042M, and FQCH4N15; WF2: same as PC1 but omitting F467M, F675W, F791W, F850LP, F1042M, and FQCH4N15 -- and adding F410M; WF3 and WF4: same as WF2. Images should be

taken within 7 days after a decon, to minimize any contamination effects. Results from this program will be compared with archival data from earlier cycles.

- **Products:** ISR, SYNPHOT update.
- **Accuracy Goals:** 2-3% photometry.

10366: WFPC2 Cycle 13: Close-Out Photometric Cross-Calibration

- **Purpose:** Tie WFPC2 photometry to other systems (ACS, WFC3, STIS, NICMOS, and ground based) for extremely red targets.
- **Description:** Observe T-dwarf star (2M0559-14) in as many WFPC2 filters as possible, essentially replicating ACS calibration program 10056 visit 4. The plan is to spend 2 orbits exposing on PC1 in single chip read-out mode (to minimize overheads), cycling through filters F606W, F622W, F675W, F702W, F785LP, F791W, F814W, F850LP, F1042M. Images should be taken within 7 days after a Decon, to minimize any contamination effects.
- **Products:** ISR, Synphot update
- **Accuracy Goals:** 2-3% photometry

8.21 Future Calibrations, Calibration by Observers, and Calibration Outsourcing

It is expected that the calibrations outlined here for recent cycles and the current Cycle 13 will be maintained for Cycle 14. However, it is possible that as the number WFPC2 users decreases further with the availability of ACS, some WFPC2 calibrations maybe curtailed. For example, monitoring observations may become less frequent, and special modes (e.g. ramp filters) may not receive further calibration. It is the intention of STScI to develop a calibration program that effectively balances the needs of the community for obtaining excellent science results from the instrument with the limited resources available (e.g., a nominal limit of 10% time available for calibration). As always, frequently used modes of the instrument will be fully calibrated.

In special situations it is possible that observers may find the STScI calibration programs do not meet their needs. For example, they may require an accuracy better than outlined in Table 8.16, or may require calibration of some unique mode or observation strategy. In these cases observers may propose to obtain their own calibration data. Such observations may be proposed in one of two ways.

The first type of special calibration would be to simply request additional orbits within a GO program for the purpose of calibrating the proposed science data (see section 4.3 of the CP). In this case the extra calibration would only need to be justified on the basis of the expected science return of the GO's program.

The second type of special calibration would be performed as a general service to the community via Calibration Proposals (section 3.7 of CP, sometimes called "Calibration Outsourcing"). These proposals are to obtain calibration data and/or support analysis of data (including archival data) for the purpose of improving calibrations. New observations obtained for calibration programs will generally be flagged as non-proprietary, and will be immediately released to the community. These proposals will generally be judged on their value to the scientific community and scientific impact they are likely to make (see the Call for Proposals for details). These programs, if approved, will usually carry a requirement to provide separately negotiated deliverables (e.g. results, reference files, documentation) so as to support other members of the community.

Proposers interested in obtaining either type of special calibration should consult with Instrument Scientists from the WFPC2 Group via the Help Desk at least 14 days before the proposal deadline in order to ascertain if the proposed calibrations would be done at STScI in the default program.

During Cycles 9 and 10, two WFPC2 Calibration Outsource programs were awarded. The first (Karkoshka, PI) sought to improve the

signal-to-noise ratio of the UV flatfields. While the standard UV flats provided by STScI are adequate for most observers, people with bright targets (e.g. planets) have sometimes found their signal-to-noise ratio was limited by the calibration flats rather than photon noise. We anticipate this program will provide new flatfields in the UV which reduce noise in certain observations by up to a factor ~3. The second program (Saha, PI) tested for a position independent component of CTE by comparing ground based and WFPC2 observations of several fields containing faint standard stars. This program could potentially improve the photometric accuracy for faint targets, and impact scientifically important problems such as the extragalactic distance scale. Results of both programs will be disseminated via the WFPC2 WWW site, as results become available.

8.22 Calibration Accuracy

Table 8.16 summarizes the accuracy to be expected from WFPC2 observations in several areas. The numbers in the table should be used with care, and only after reading the relevant sections of this handbook and the documents referenced therein; they are presented in tabular form here for easy reference.

Table 8.16: Accuracy Expected in WFPC2 Observations.

Procedure	Estimated Accuracy	Notes
Calibration (flatfielding, bias subtraction, dark correction)		
Bias subtraction	0.1 DN rms	Unless bias jump is present
Dark subtraction	0.1 DN/hr rms	Error larger for warm pixels; absolute error uncertain because of dark glow
Flatfielding	<1% rms large scale	Visible, near UV
	0.3% rms small scale	
	~10%	F160BW; however, significant noise reduction achieved with use of correction flats
Relative photometry		
Residuals in CTE correction	< 3% for the majority (~90%) of cases	
	up to 10% for extreme cases (e.g., very low backgrounds)	
Long vs. short anomaly (uncorrected)	< 5%	Magnitude errors <1% for well-exposed stars but may be larger for fainter stars. Some studies have failed to confirm the effect
Aperture correction	4% rms focus dependence (1 pixel aperture)	Can (should) be determined from data
	<1% focus dependence (> 5 pixel)	
	1-2% field dependence (1 pixel aperture)	
Contamination correction	3% rms max (28 days after decon) (F160BW)	
	1% rms max (28 days after decon) (filters bluer than F555W)	
Background determination	0.1 DN/pixel (background > 10 DN/pixel)	May be difficult to exceed, regardless of image S/N
Pixel centering	< 1%	
Absolute photometry		
Sensitivity	< 2% rms for standard photometric filters	Red leaks are uncertain by ~10%
	2% rms for broad and intermediate filters in visible	
	< 5% rms for narrow-band filters in visible	
	2-8% rms for UV filters	
Astrometry		
Relative	0.005" rms (after geometric and 34th-row corrections)	Same chip
	0.1" (estimated)	Across chips
Absolute	1" rms (estimated)	

APPENDIX A:

Passband Plots

In this appendix . . .

A.1 Filter Passbands, with and w/out Total System

In this Appendix we give two plots for each filter -- one for the filter in isolation (left panel), and for the filter together with all other system elements (HST and WFPC2 optics and WF3 CCD; right panel). Quantities labeled on the plots are defined in "System Throughput" on page 151.

Note that $\overline{\lambda}$ deviates from λ_p and $<\lambda>$ by progressively larger amounts for the wider filters, which is simply a consequence of the way in which $\overline{\lambda}$ is defined.

A.1.1 F122M, F130LP, F160BW

F122M (Wheel:1 Pos:4)

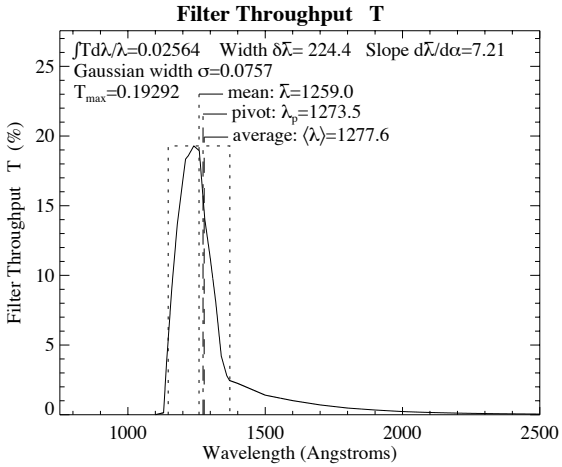

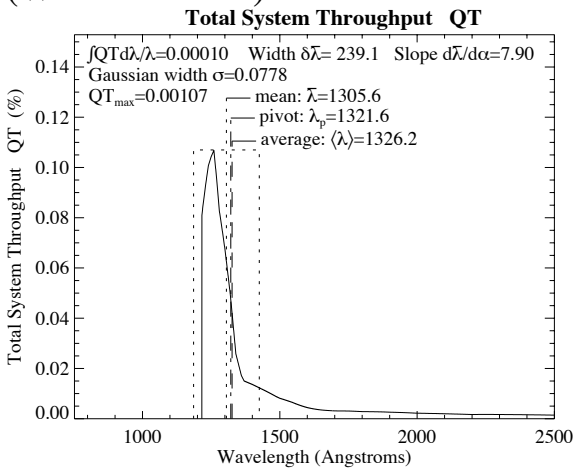

F130LP (Wheel:2 Pos:1)

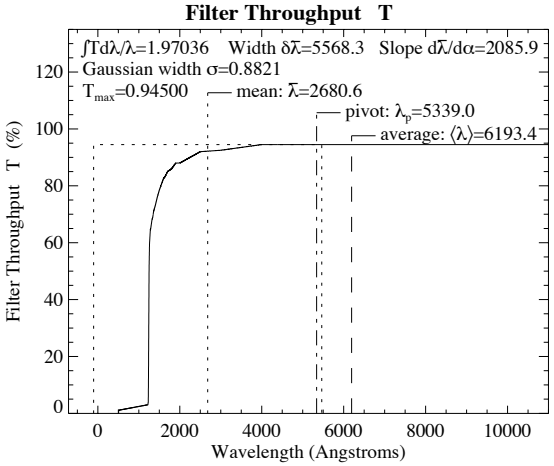

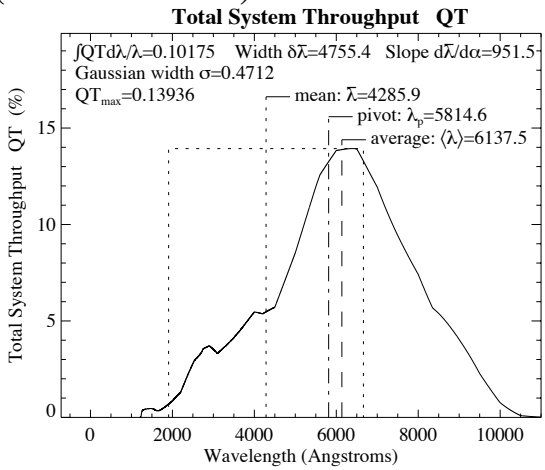

F160BW (Wheel:1 Pos:2)

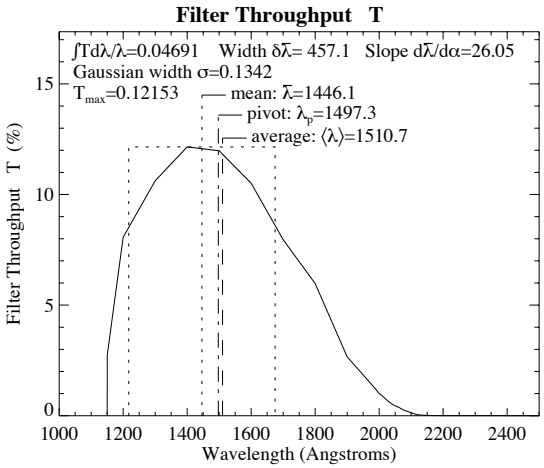

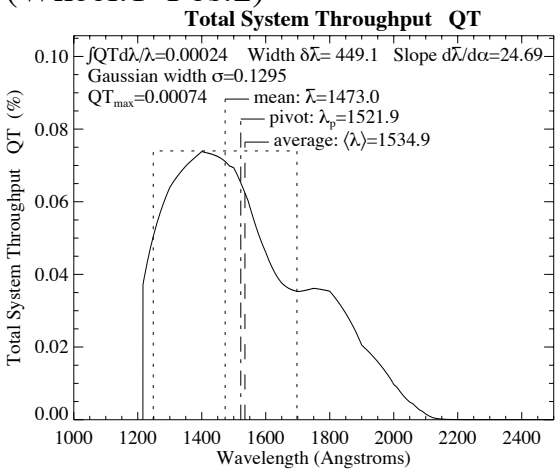

A.1.2 F165LP, F170W, F185W

F165LP (Wheel:2 Pos:2)

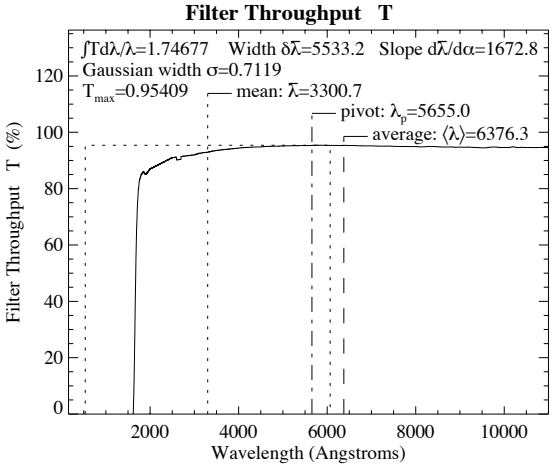

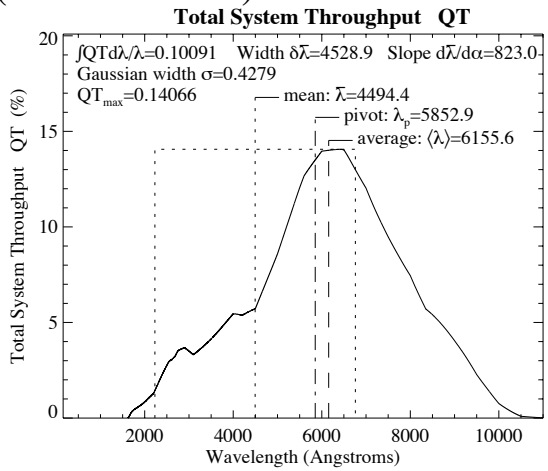

F170W (Wheel:8 Pos:1)

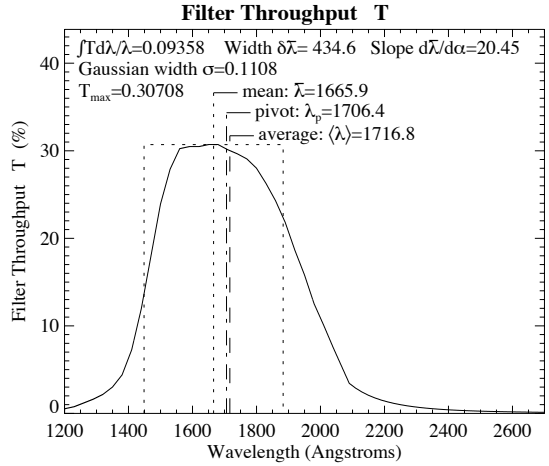

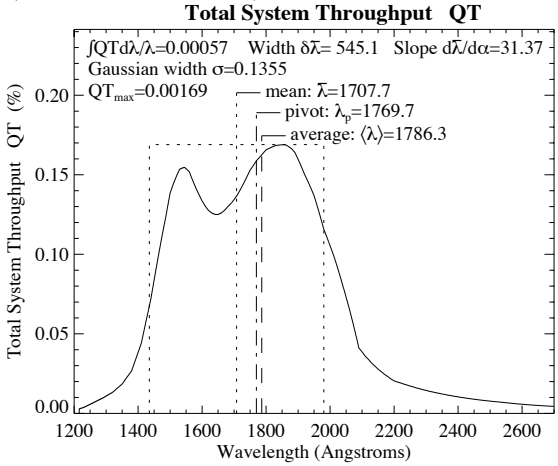

F185W (Wheel:8 Pos:2)

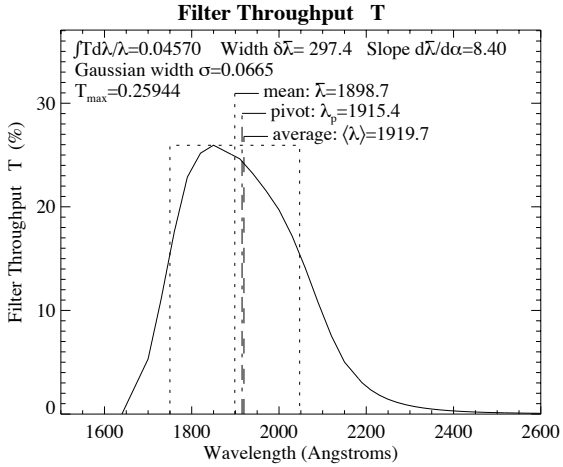

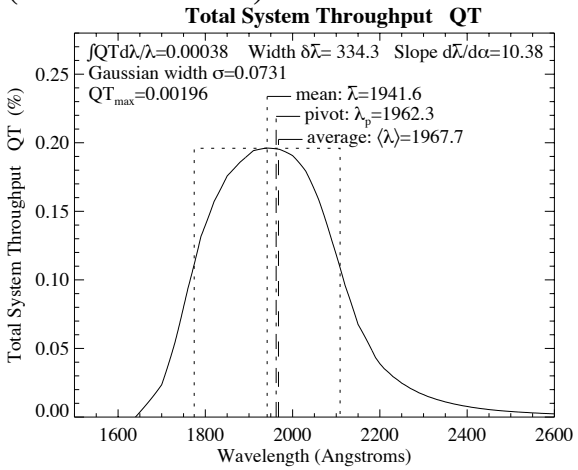

A.1.3 F218W, F255W, F300W

F218W (Wheel:8 Pos:3)

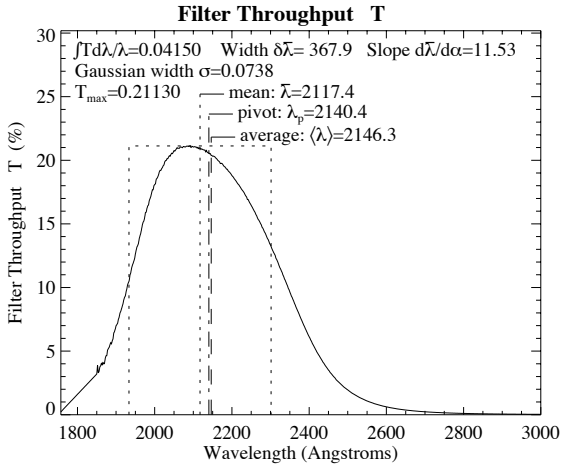

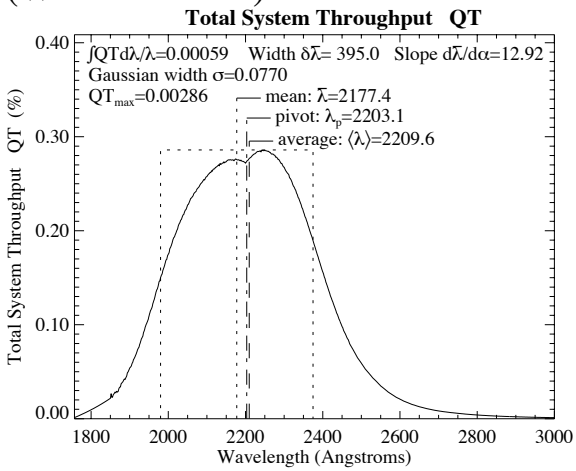

F255W (Wheel:8 Pos:4)

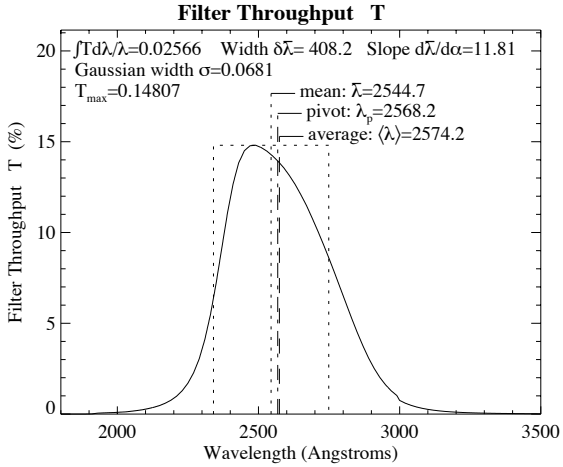

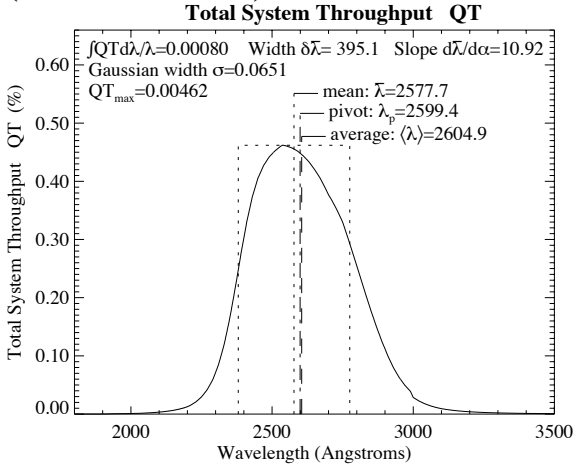

F300W (Wheel:9 Pos:4)

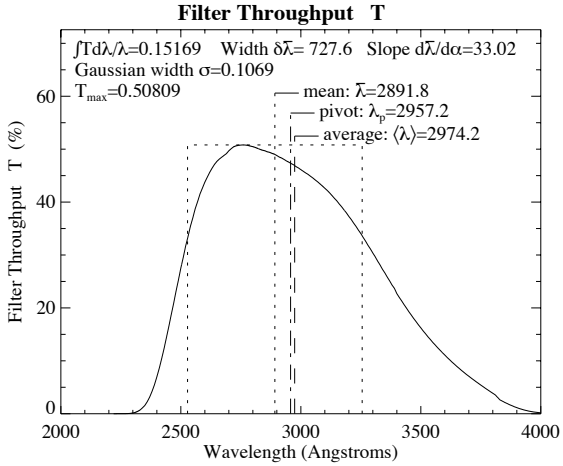

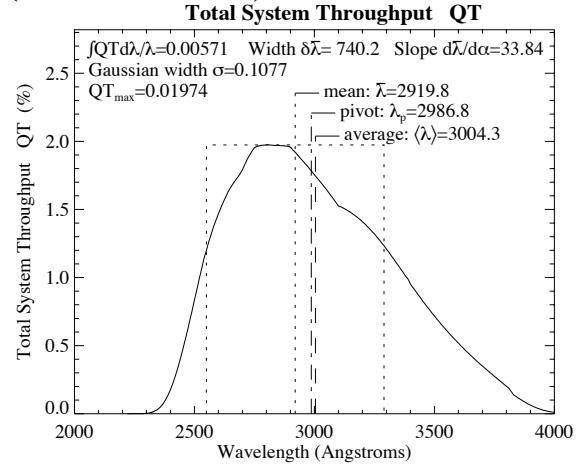

A.1.4 F336W, F343N, F375N

F336W (Wheel:3 Pos:1)

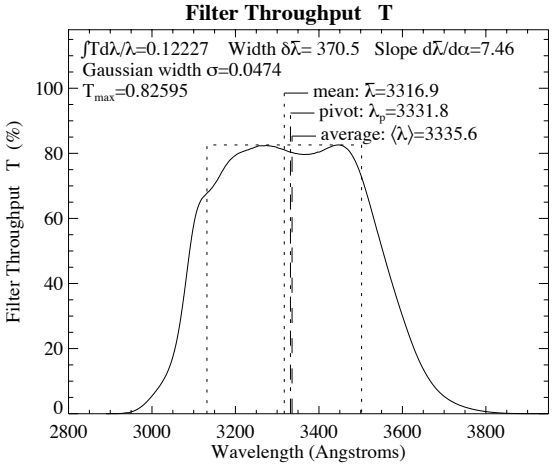

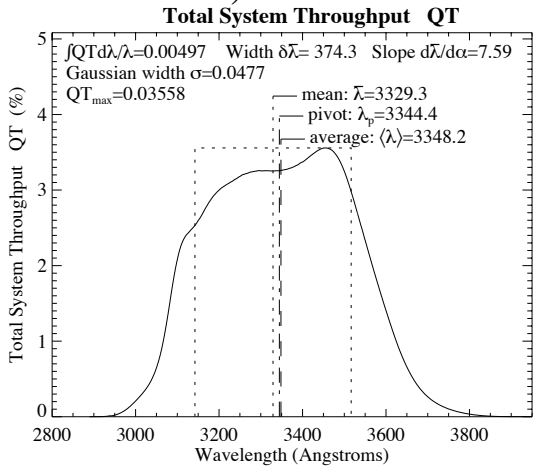

F343N (Wheel:5 Pos:1)

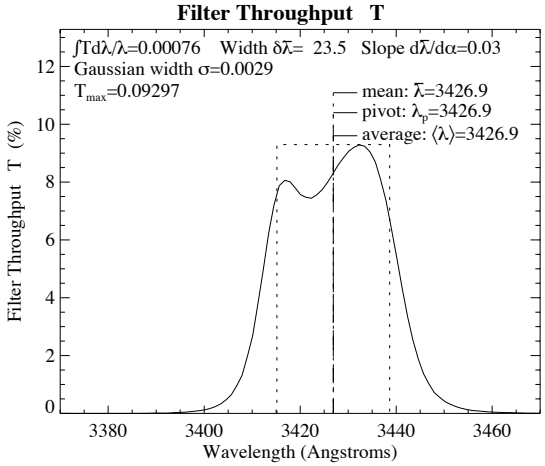

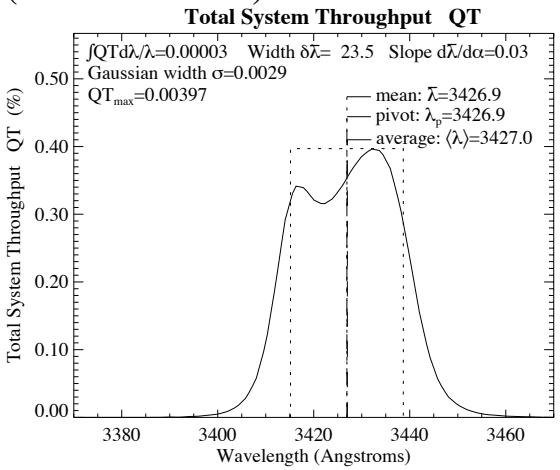

F375N (Wheel:5 Pos:2)

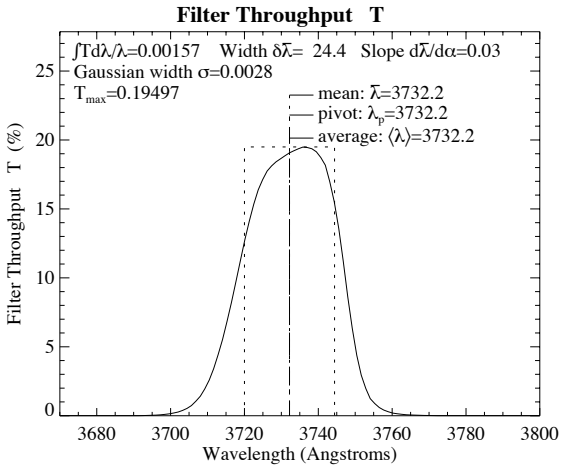

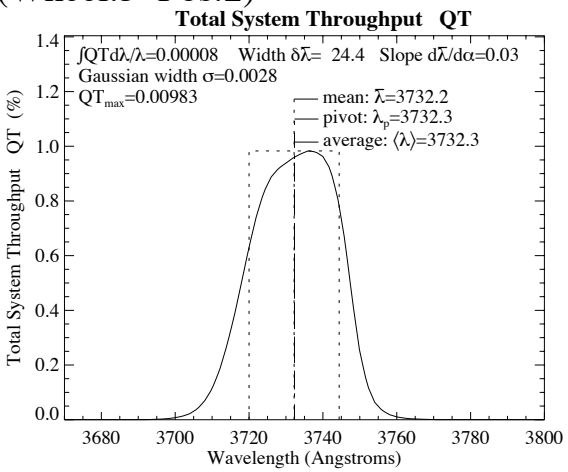

A.1.5 F380W, F390N, F410M

F380W (Wheel:9 Pos:1)

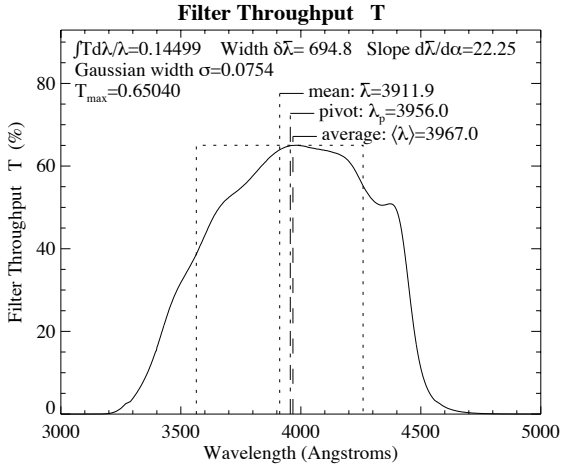

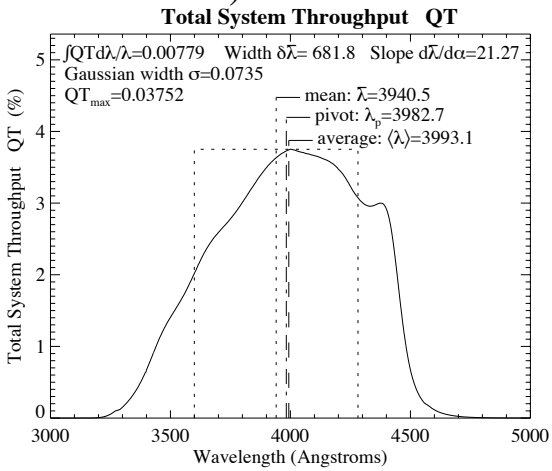

F390N (Wheel:5 Pos:3)

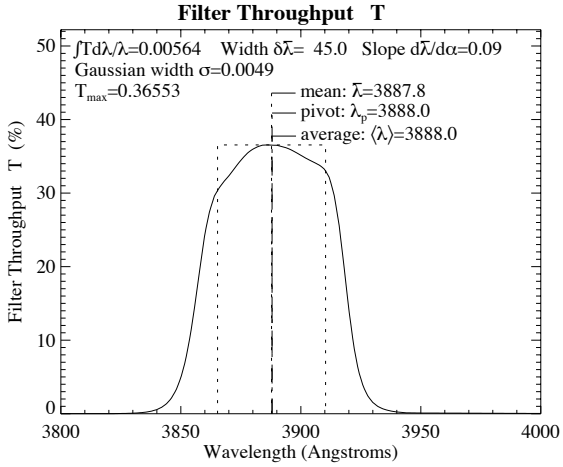

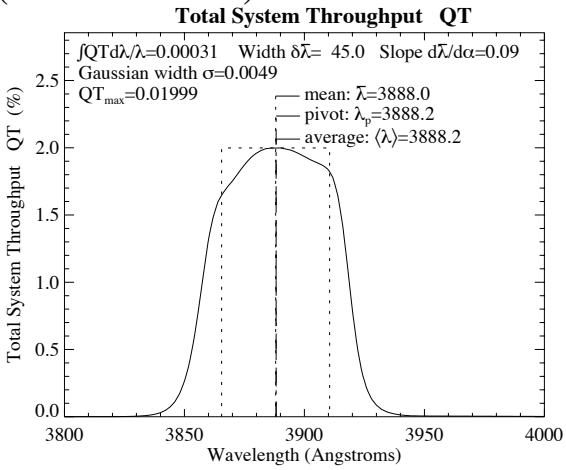

F410M (Wheel:3 Pos:2)

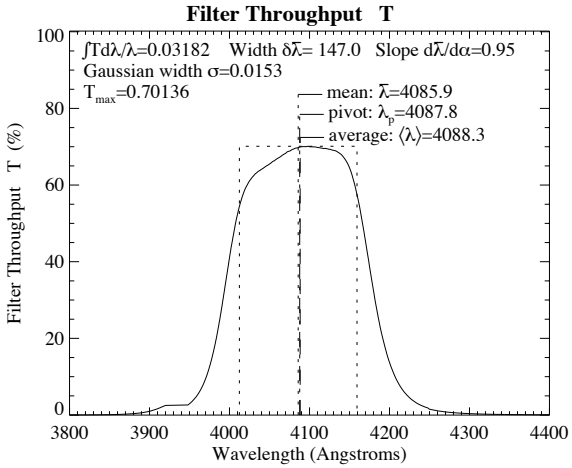

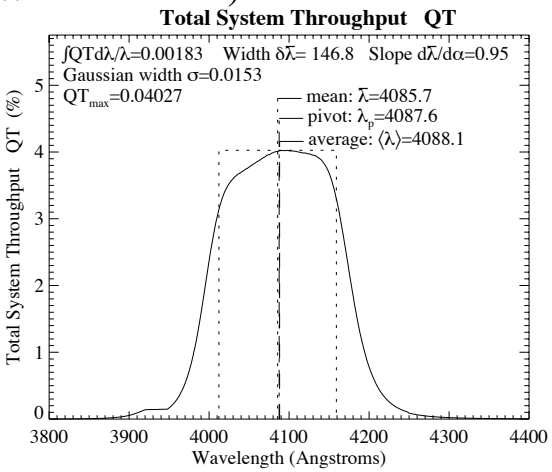

A.1.6 F437N, F439W, F450W

F437N (Wheel:5 Pos:4)

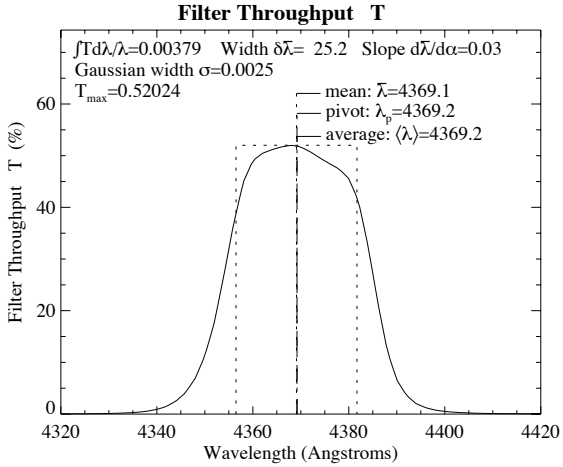

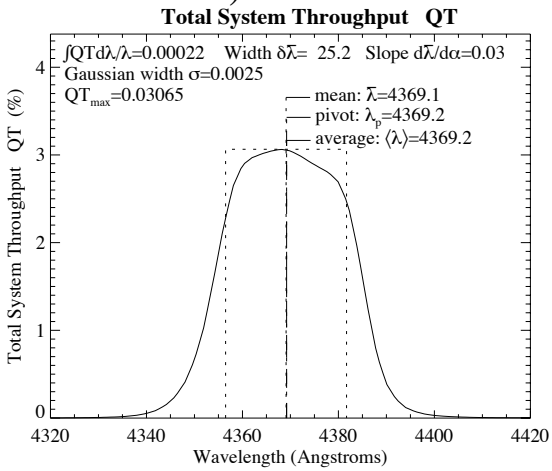

F439W (Wheel:4 Pos:4)

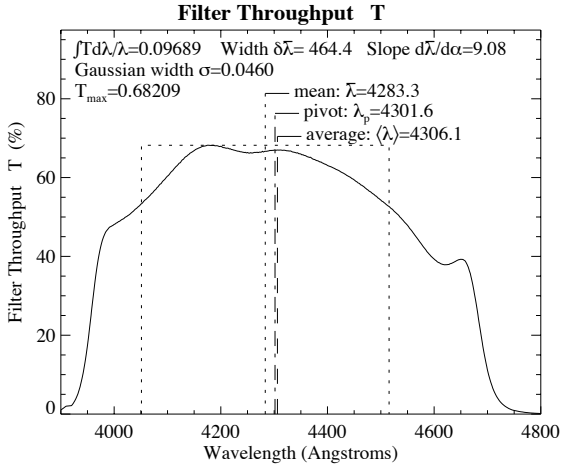

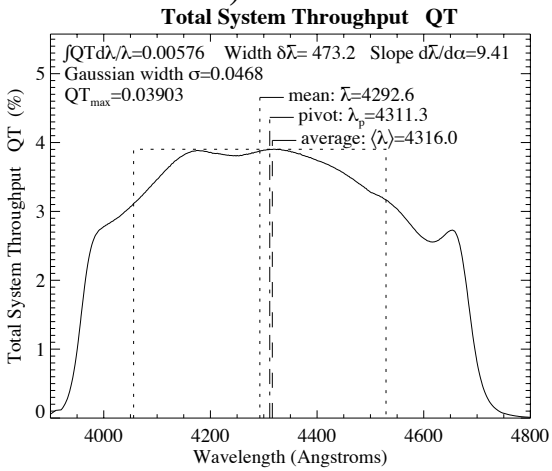

F450W (Wheel:10 Pos:4)

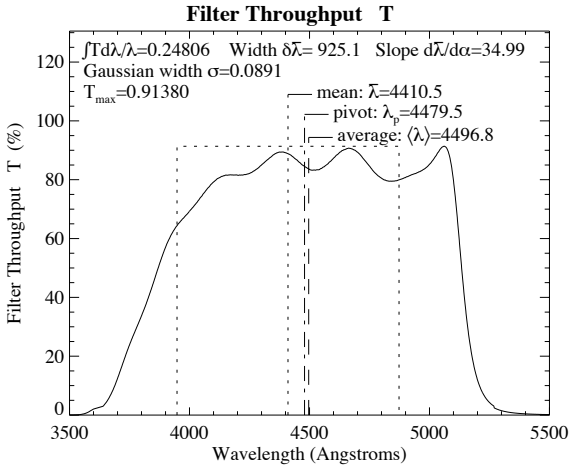

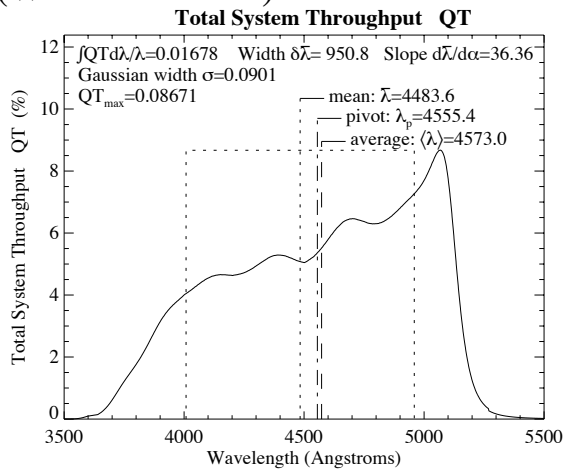

A.1.7 F467M, F469N, F487N

F467M (Wheel:3 Pos:3)

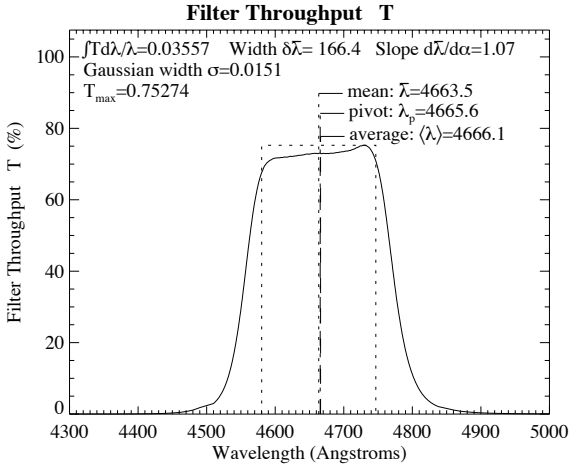

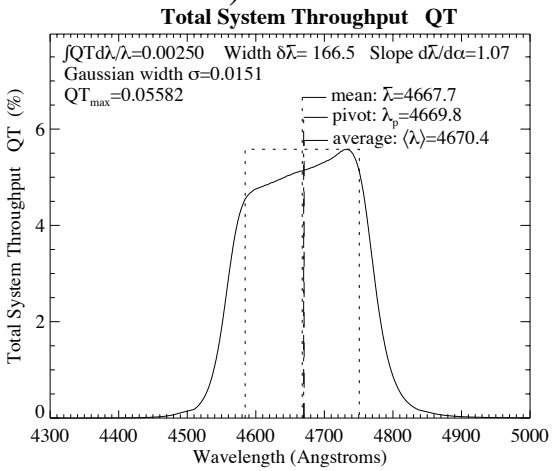

F469N (Wheel:6 Pos:1)

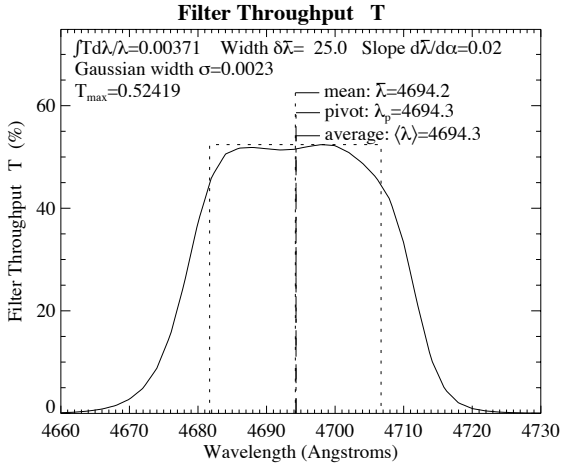

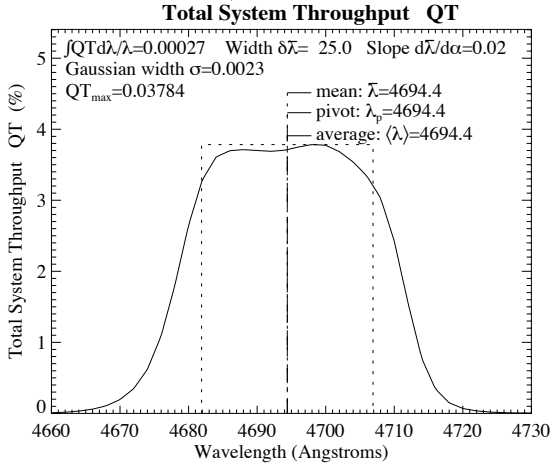

F487N (Wheel:6 Pos:2)

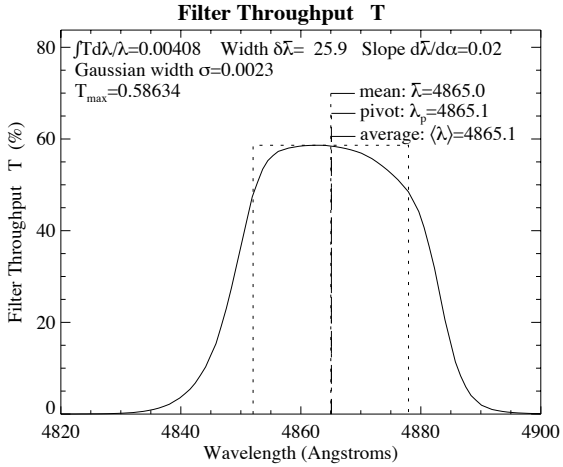

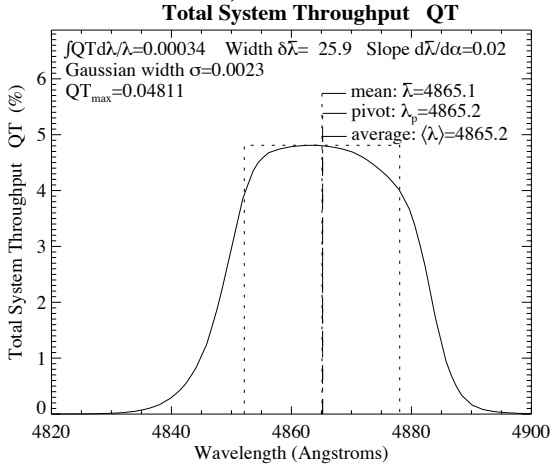

A.1.8 F502N, F547M, F555W

F502N (Wheel:6 Pos:3)

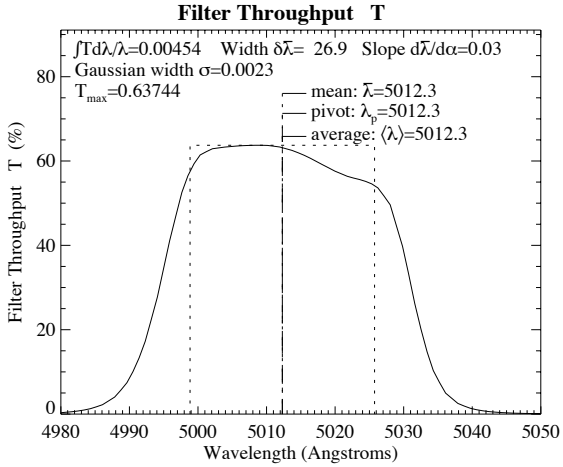

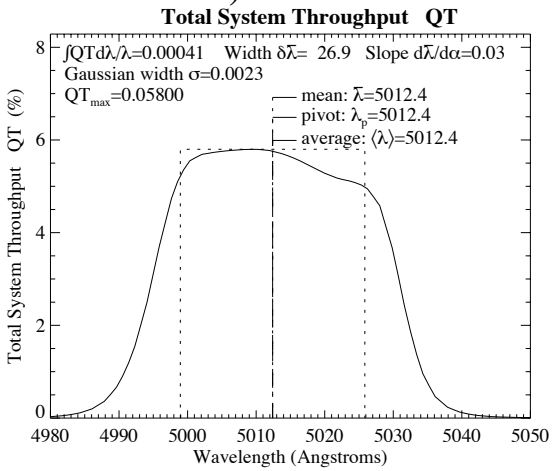

F547M (Wheel:3 Pos:4)

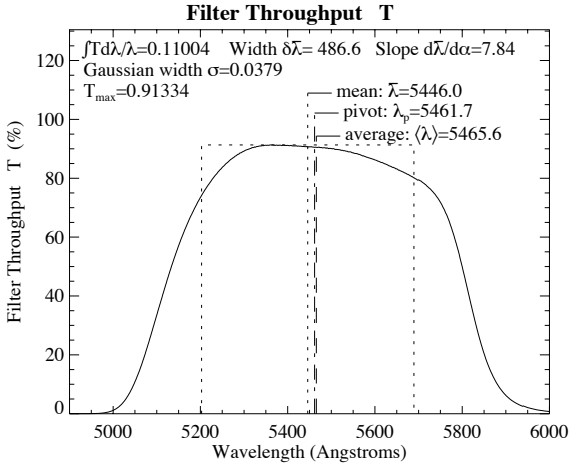

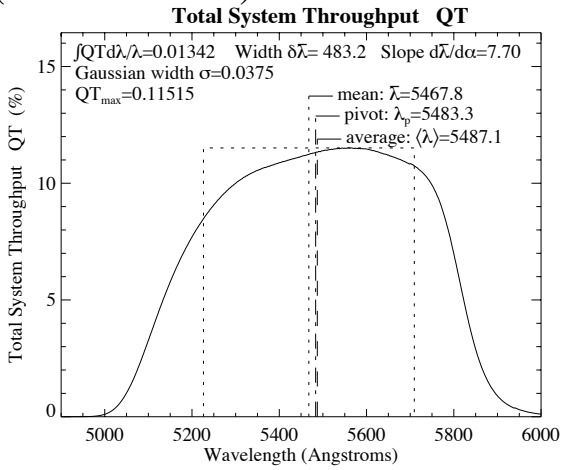

F555W (Wheel:9 Pos:2)

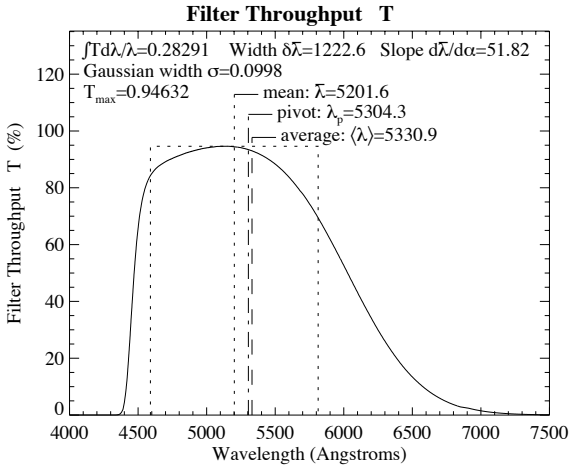

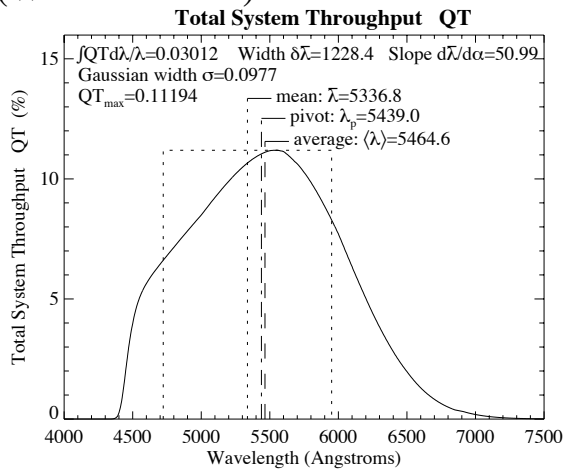

A.1.9 F569W, F588N, F606W

F569W (Wheel:4 Pos:2)

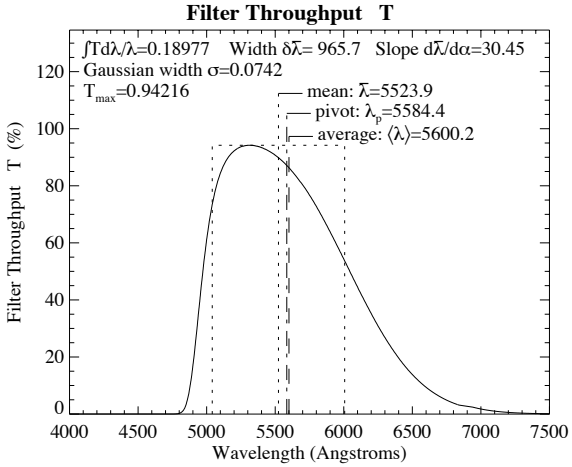

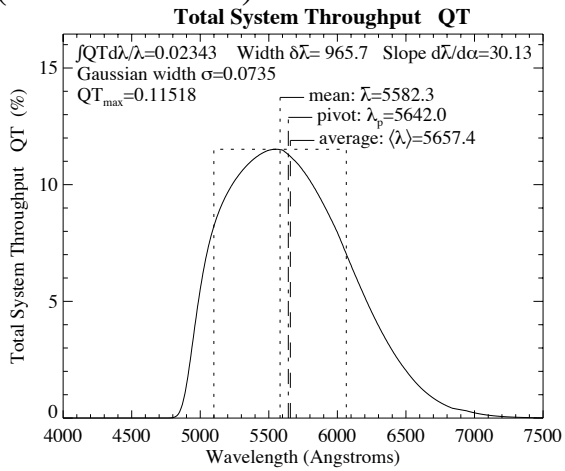

F588N (Wheel:6 Pos:4)

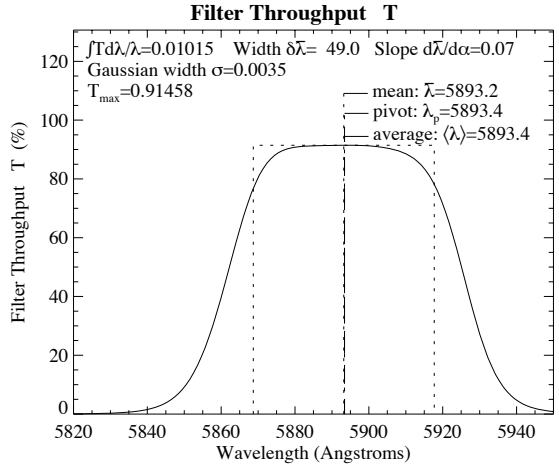

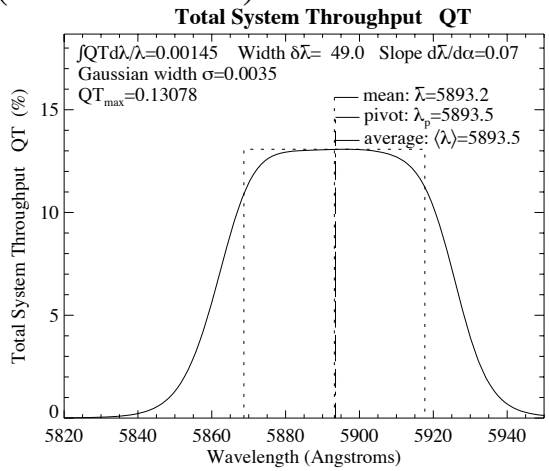

F606W (Wheel:10 Pos:2)

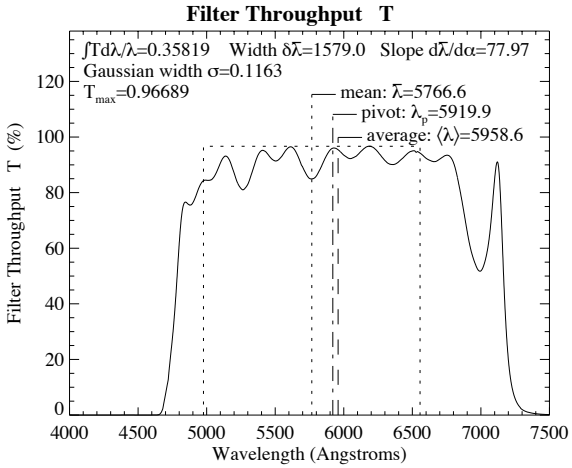

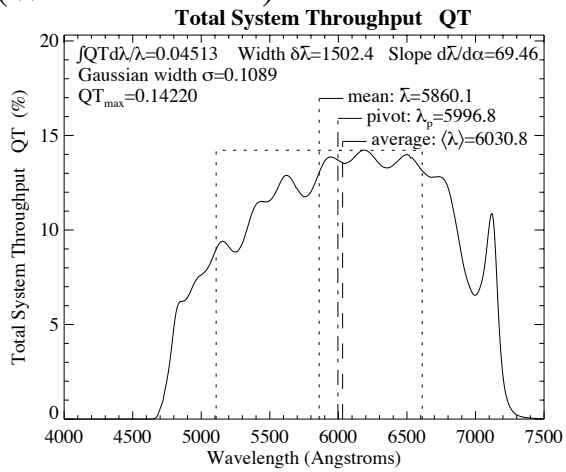

A.1.10 F622W, F631N, F656N

F622W (Wheel:9 Pos:3)

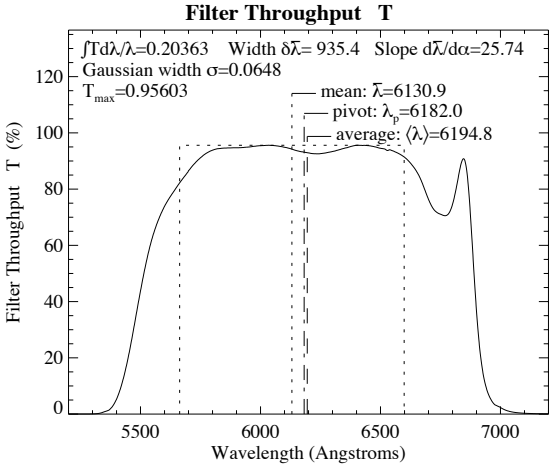

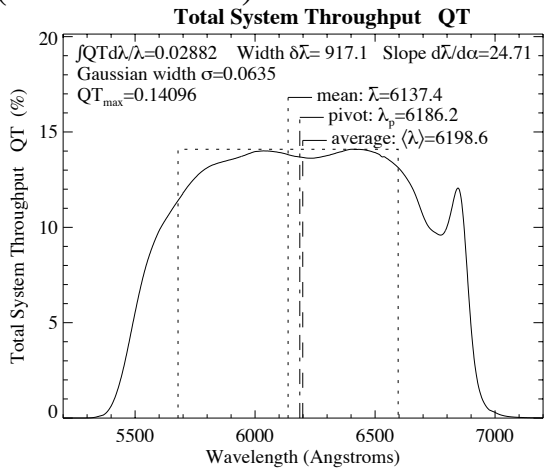

F631N (Wheel:7 Pos:1)

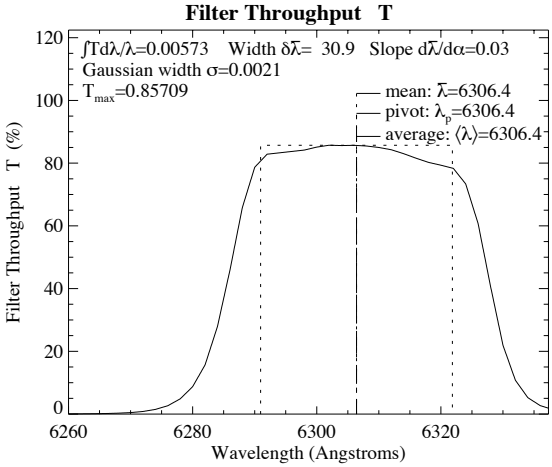

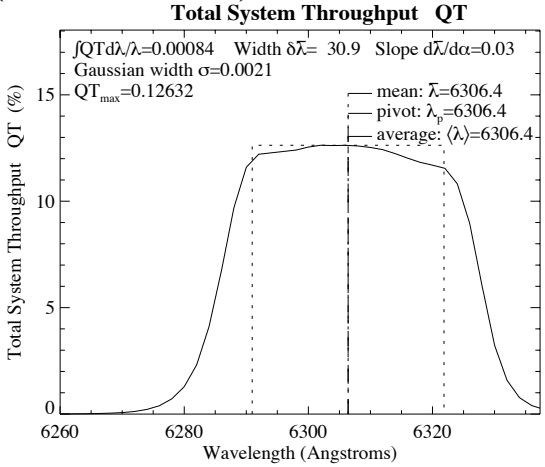

F656N (Wheel:7 Pos:2)

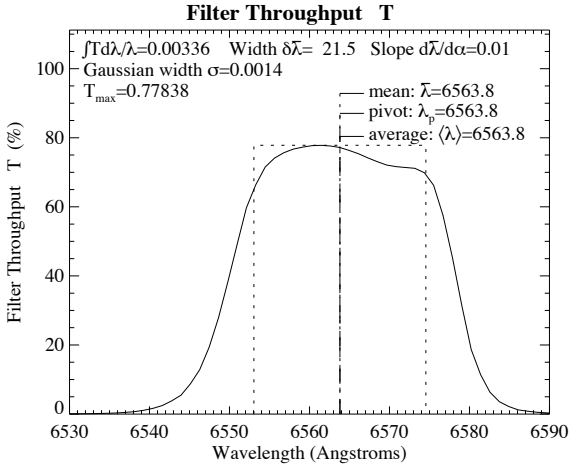

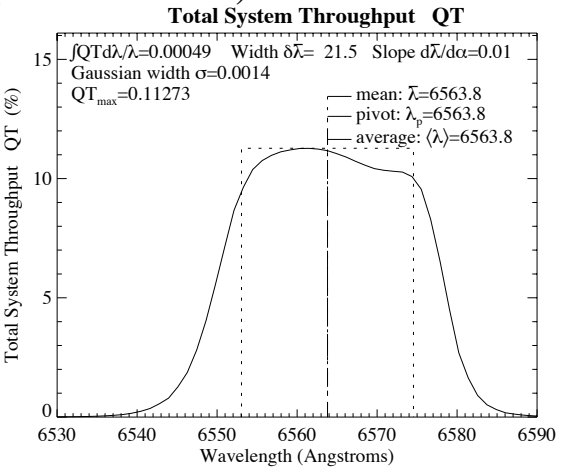

A.1.11 F658N, F673N, F675W

F658N (Wheel:7 Pos:3)

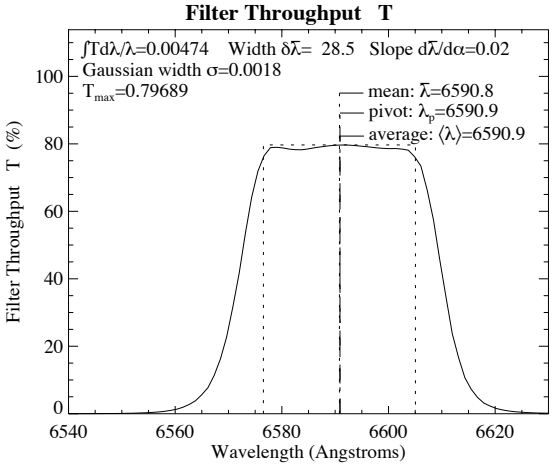

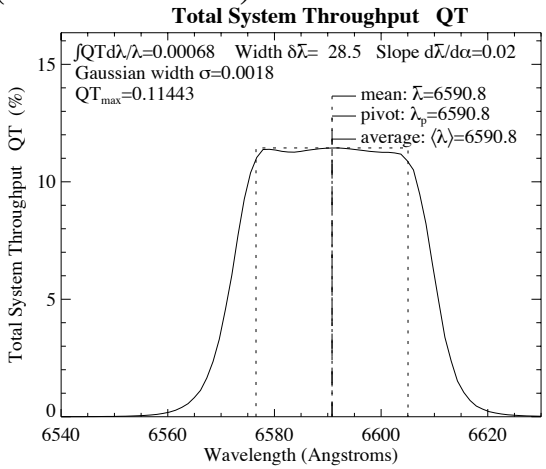

F673N (Wheel:7 Pos:4)

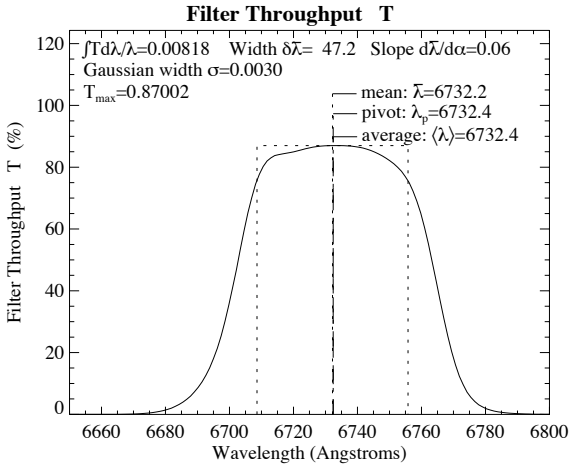

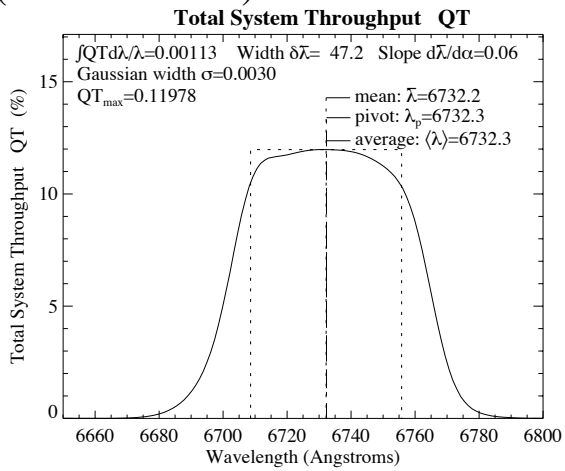

F675W (Wheel:4 Pos:3)

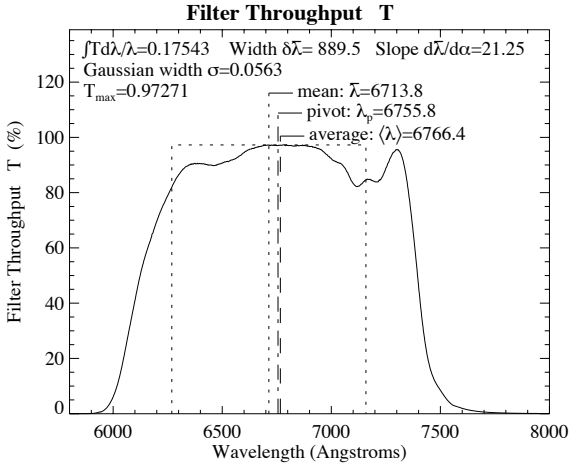

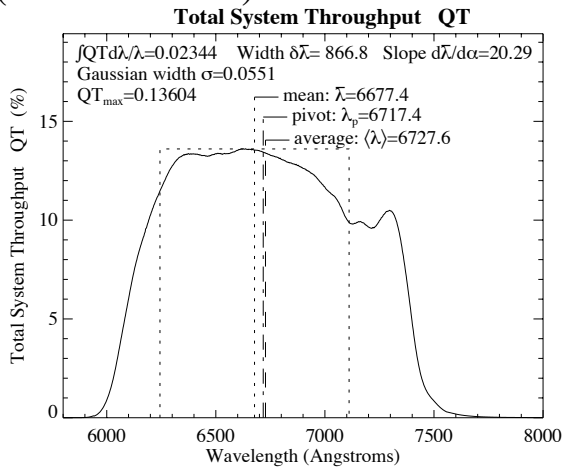

A.1.12 F702W, F785LP, F791W

F702W (Wheel:10 Pos:3)

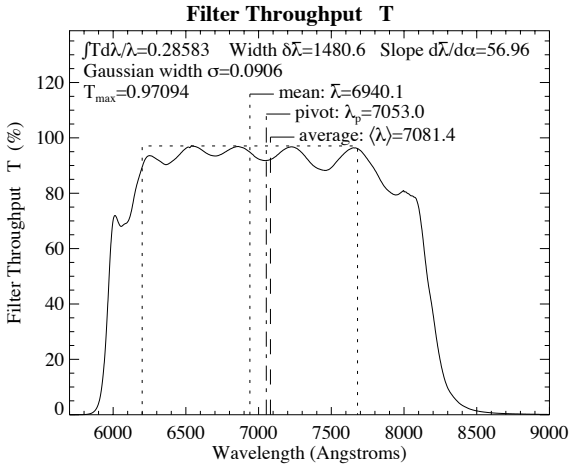

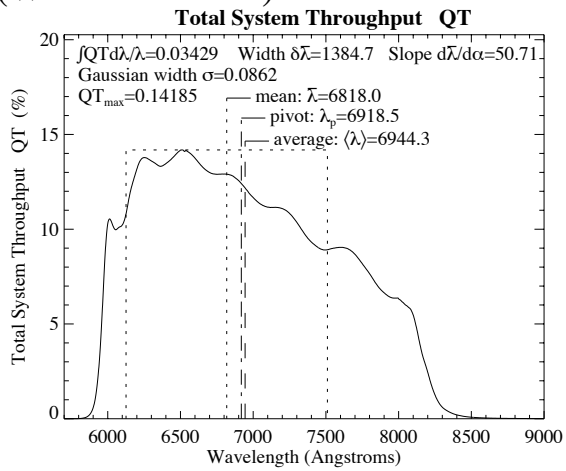

F785LP (Wheel:2 Pos:3)

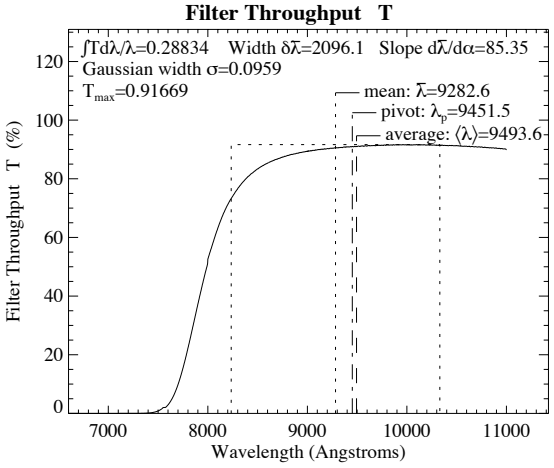

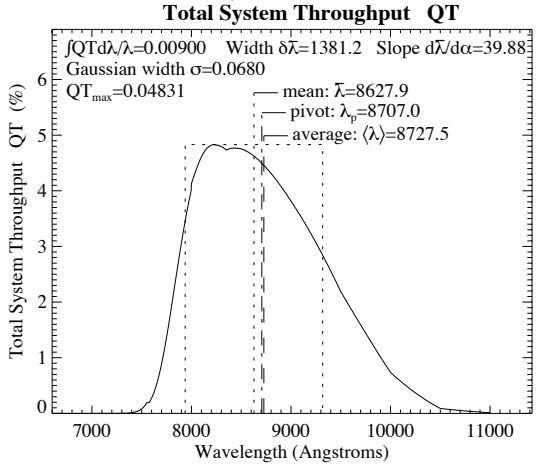

F791W (Wheel:4 Pos:1)

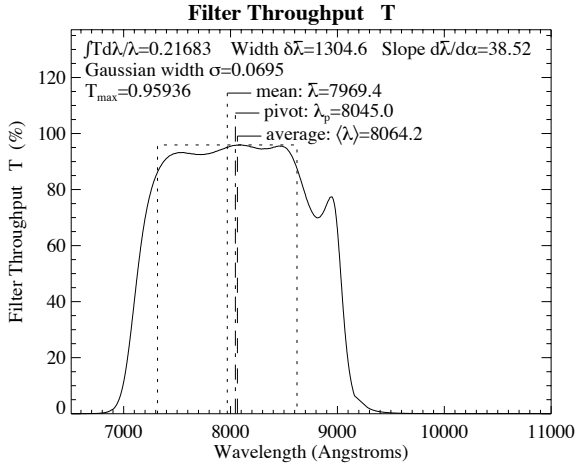

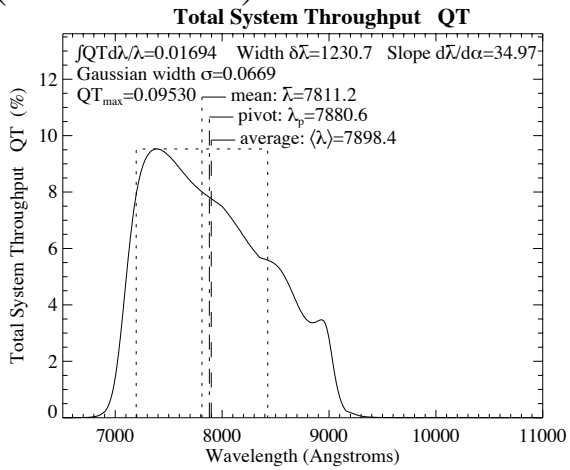

A.1.13 F814W, F850LP, F953N

F814W (Wheel:10 Pos:1)

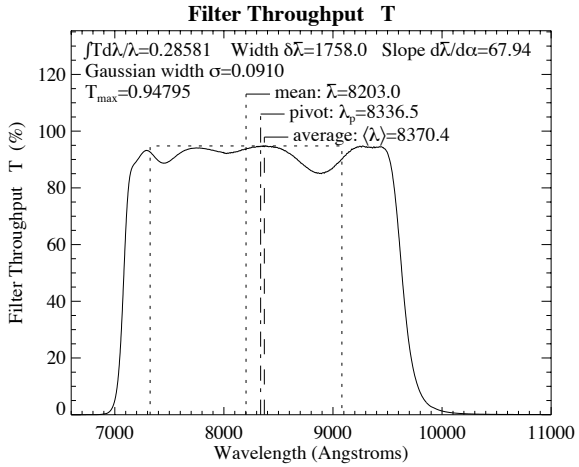

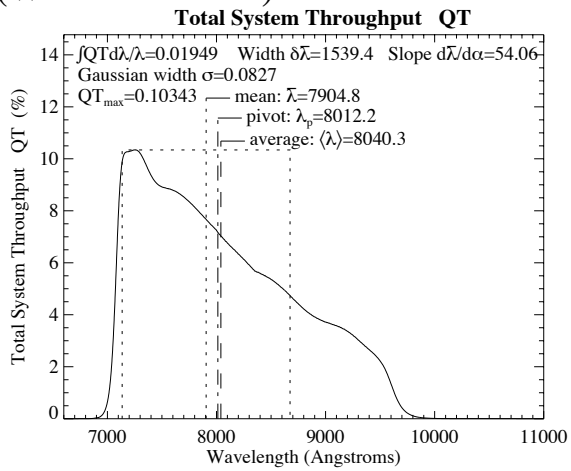

F850LP (Wheel:2 Pos:4)

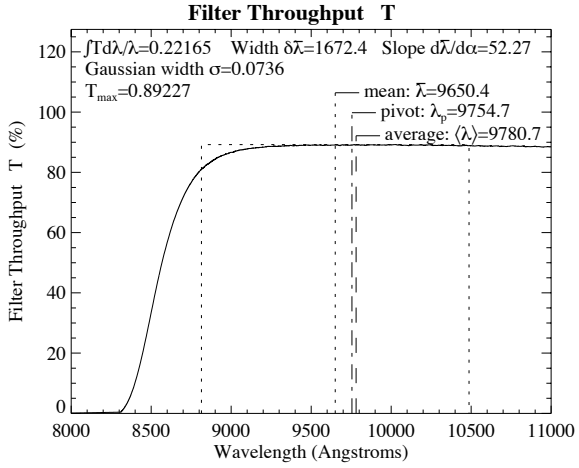

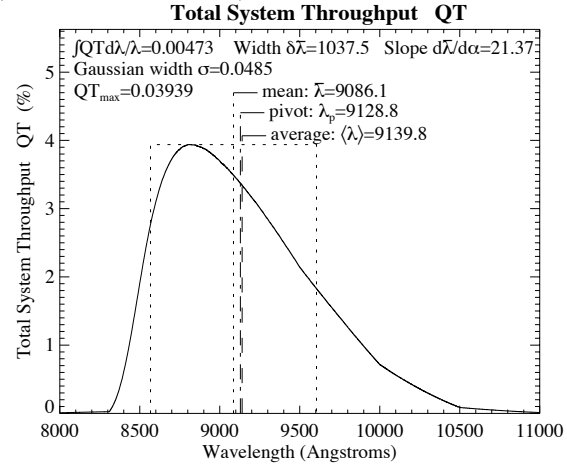

F953N (Wheel:1 Pos:1)

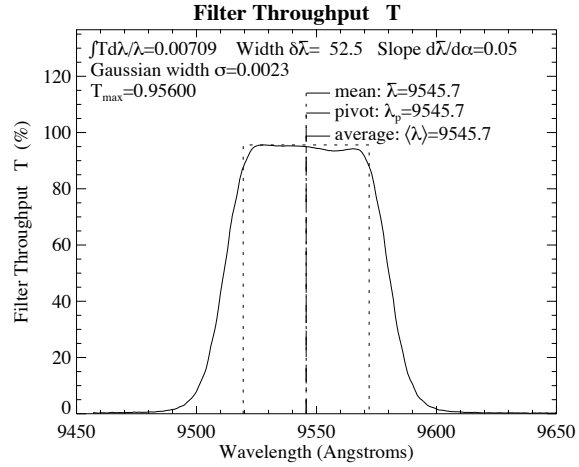

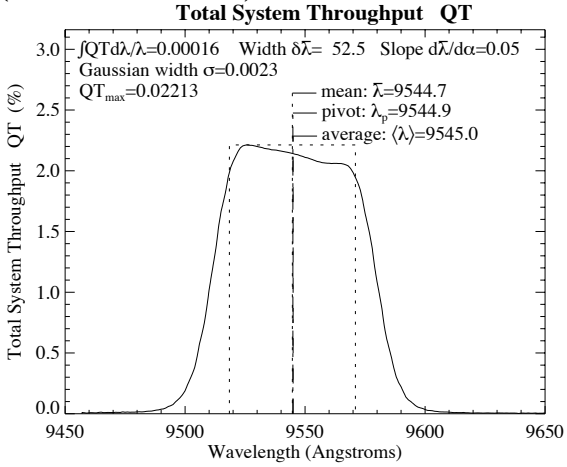

A.1.14 F1042M, FQUVN-A, FQUVN-B

F1042M (Wheel:11 Pos:2)

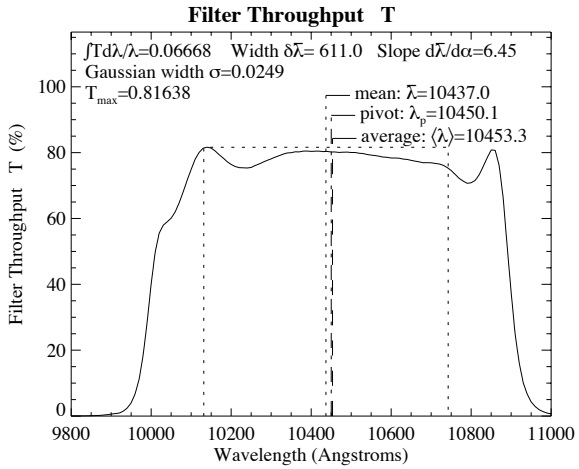

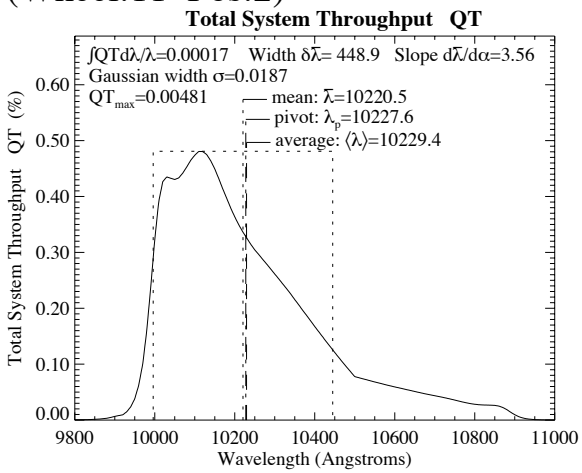

FQUVN-A (Wheel:11 Pos:3)

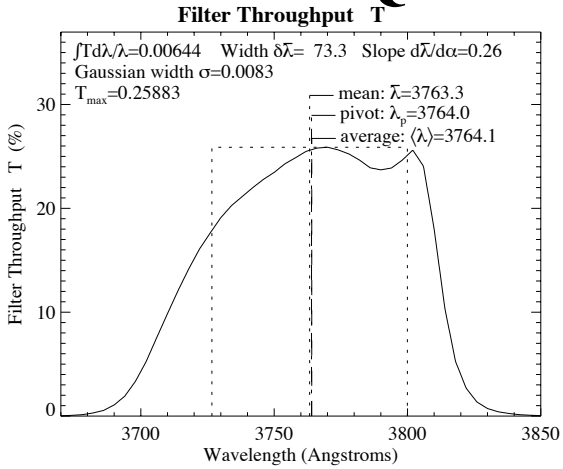

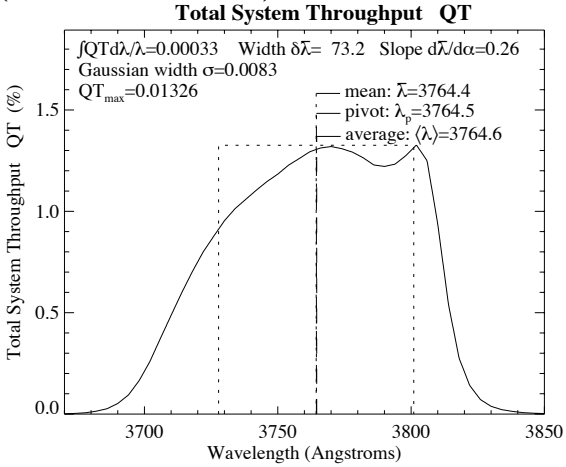

FQUVN-B (Wheel:11 Pos:3)

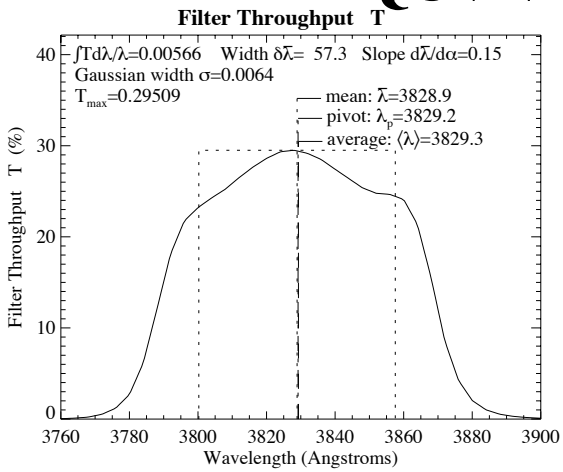

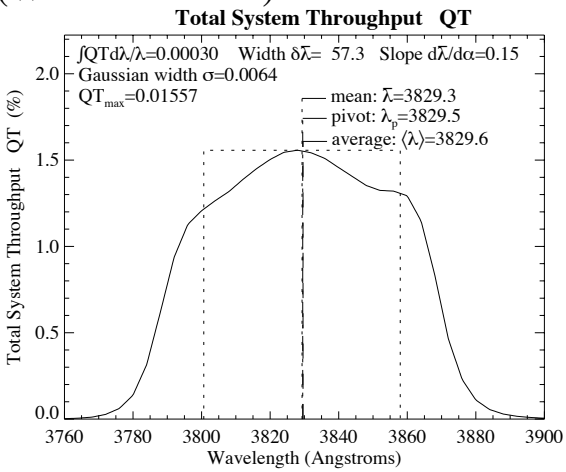

A.1.15 FQUVN-C, FQUVN-D, FQCH4N-A

FQUVN-C (Wheel:11 Pos:3)

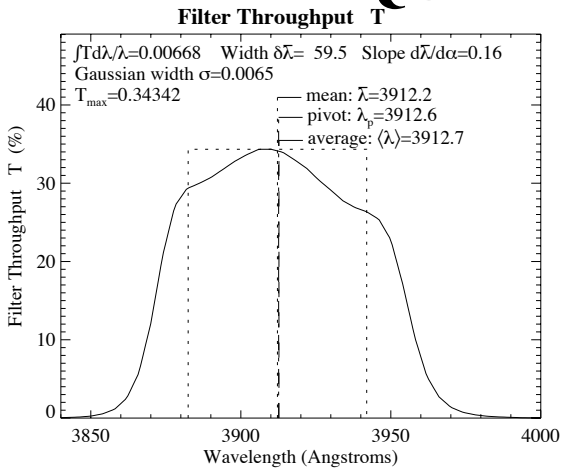

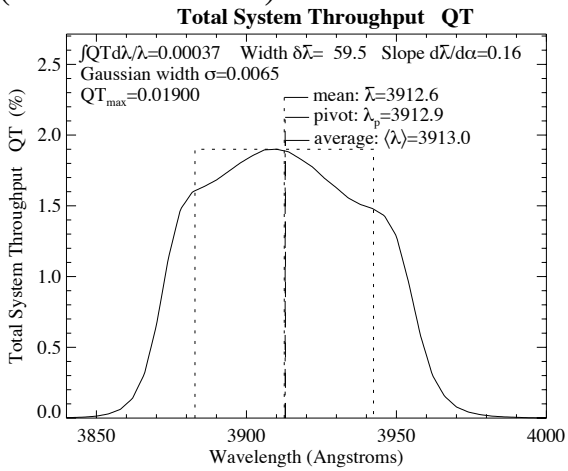

FQUVN-D (Wheel:11 Pos:3)

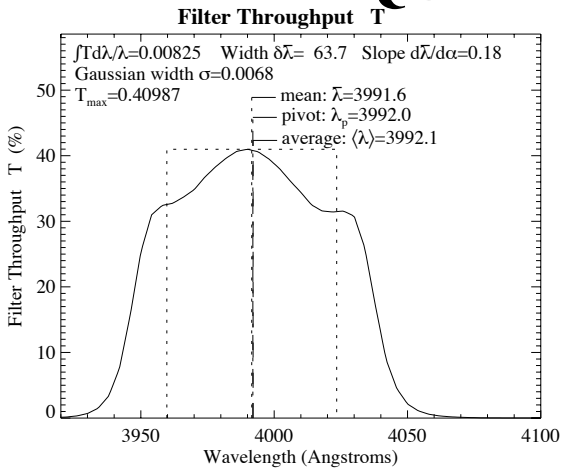

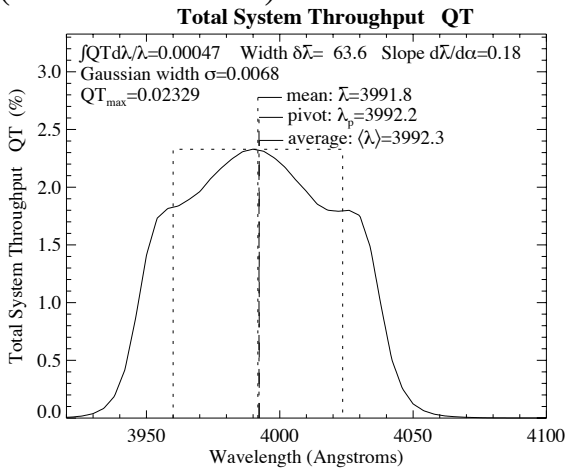

FQCH4N-A (Wheel:11 Pos:4)

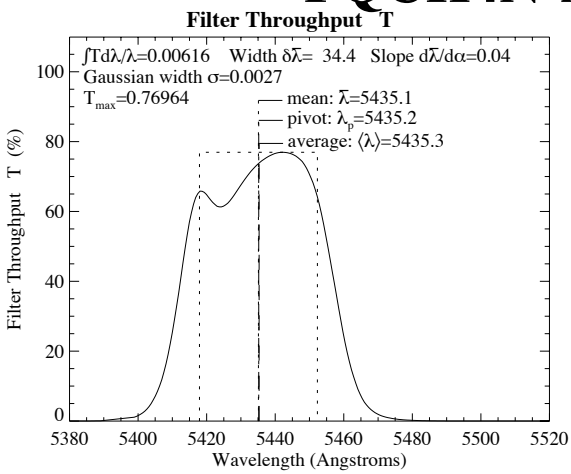

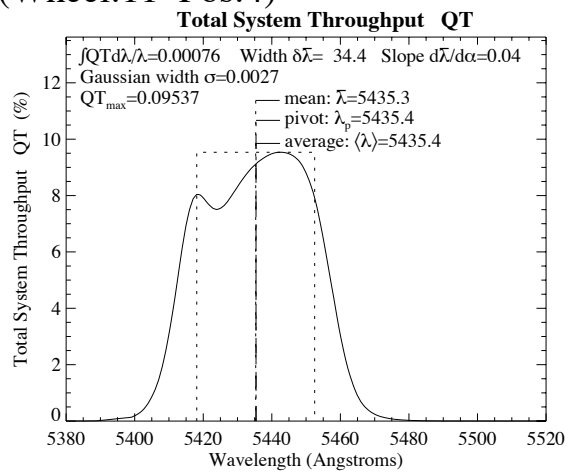

A.1.16 FQCH4N15-B, FQCH4N33-B, FQCH4N-C

FQCH4N15-B (Wheel:11 Pos:4)

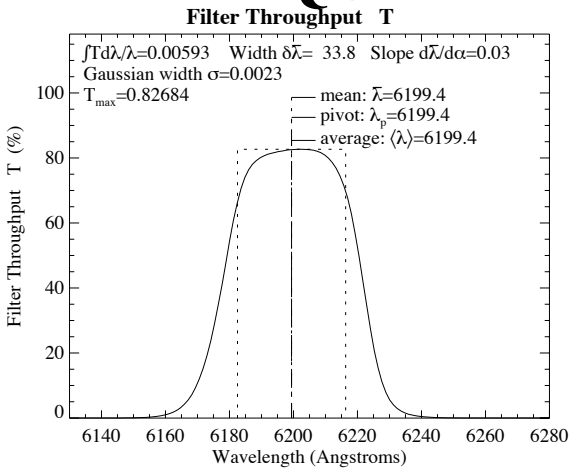

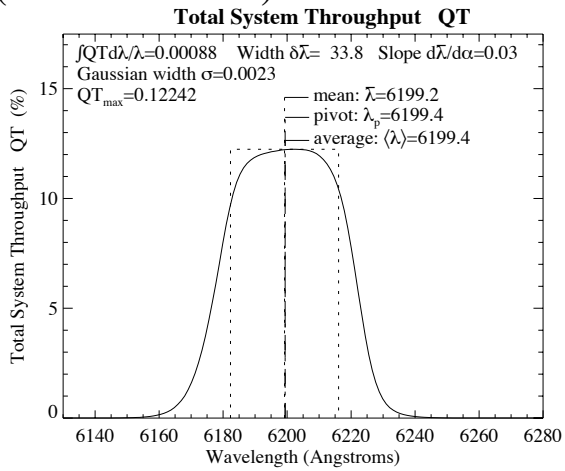

FQCH4N33-B (Wheel:11 Pos:4)

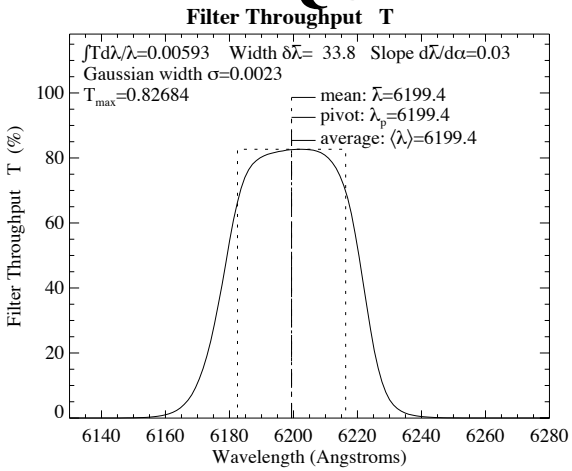

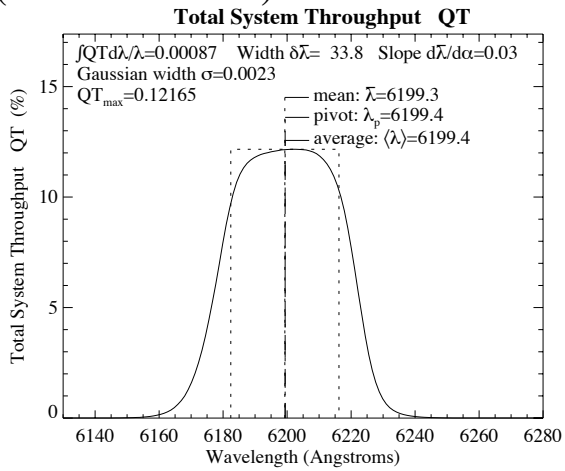

FQCH4N-C (Wheel:11 Pos:4)

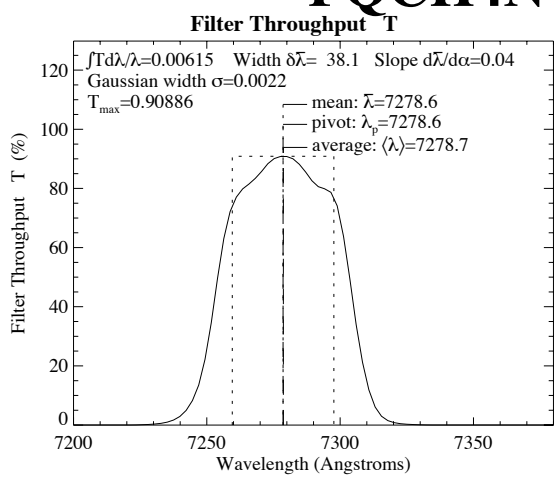

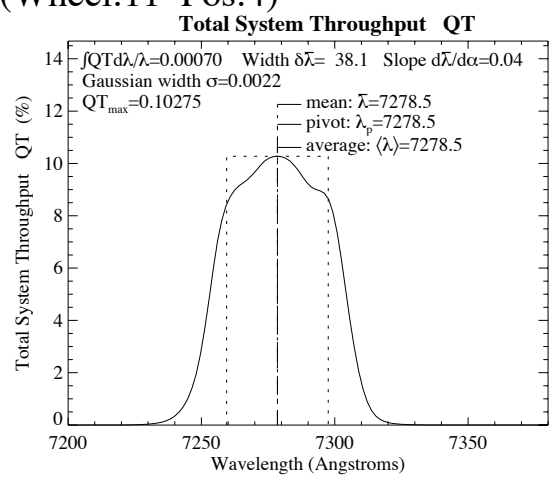

A.1.17 FQCH4N-D, Parallel and Perpendicular Polarizers

FQCH4N-D (Wheel:11 Pos:4)

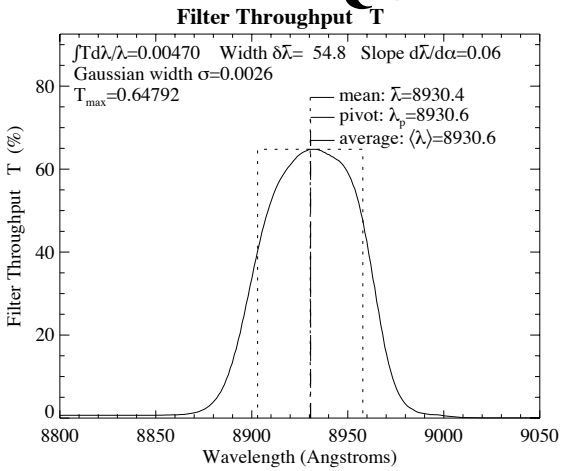

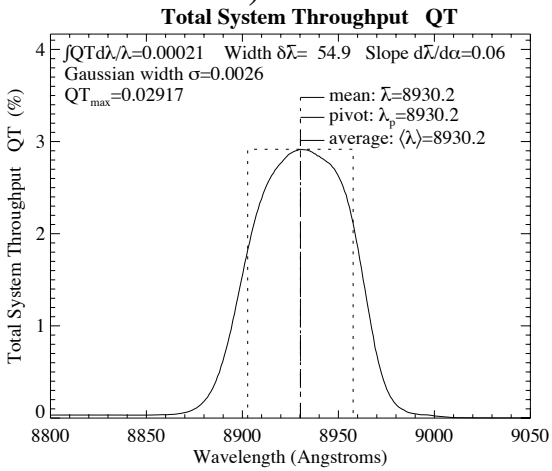

POLQ_par (Wheel:11 Pos:1)

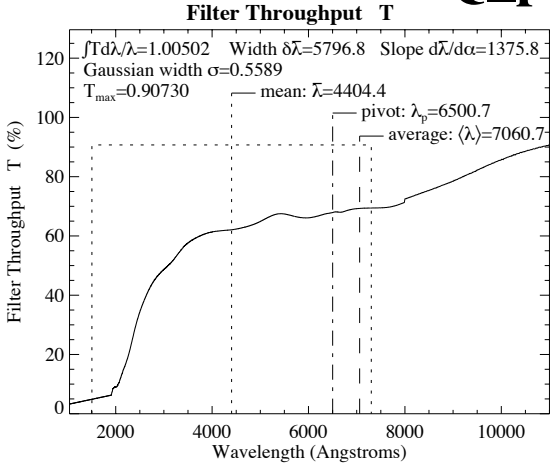

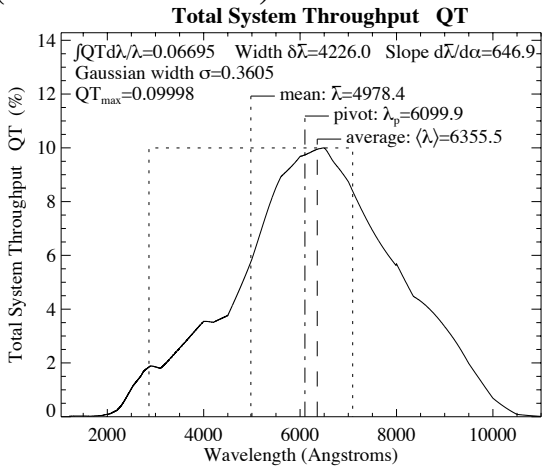

POLQ_per (Wheel:11 Pos:1)

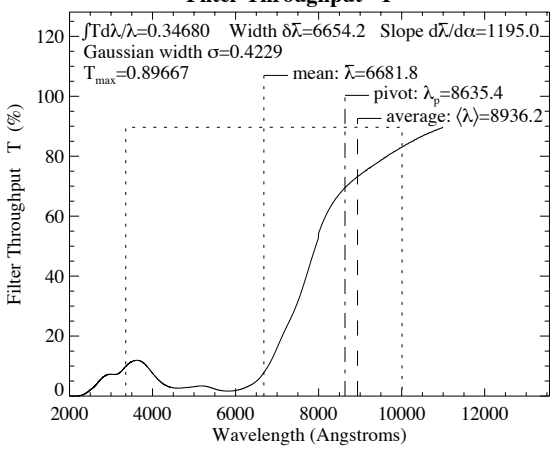

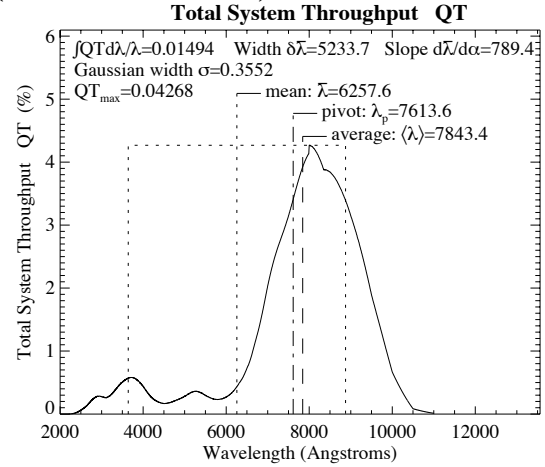

A.2 Normalized Passbands including System Response

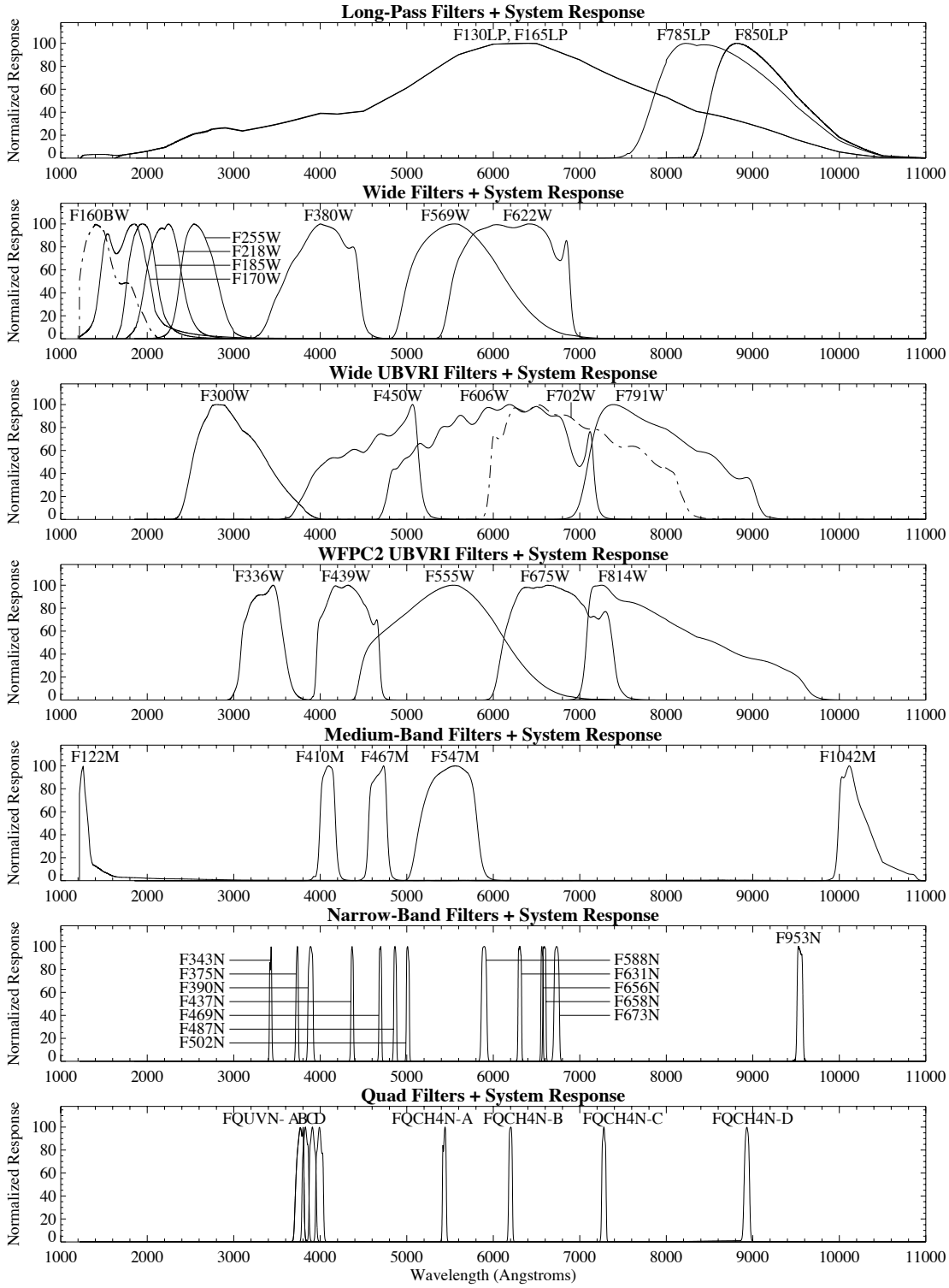

APPENDIX B:

Point Source SNR Plots

In this section we present plots which may be used to rapidly estimate signal-to-noise ratio (SNR) for point sources with stellar spectra observed through popular WFPC2 filters. Plots are given for filters F160BW, F218W, F255W, F300W, F336W, F410M, F439W, F502N, F547M, F555W, F606W, F675W, F702W, and F814W. These plots assume that the data will be analyzed by PSF fitting, which optimizes the SNR in the background noise limited case. They also assume an average sky background of V=22.9 mag arcsec^{-2}. These plots do not explicitly include SNR reduction due to CR-SPLITing when the read noise dominates, but this effect is easily included as described below.

In situations requiring more detailed calculations (non-stellar spectra, extended sources, other sky background levels, don't know target V magnitude, etc.), the WFPC2 Exposure Time Calculator tool, located on the WFPC2 WWW pages, should be used instead.

One uses these plots as follows:

1. Examine Table B.1 and find the spectral type and wavelength of the desired filter (e.g. F555W ≈5500Å). Interpolate in the table to get AB_V.
2. Sum the V magnitude of the target and AB_V derived from the table.
3. Find the appropriate plot for the filter in question, and locate $V+AB_V$ on the horizontal axis. Then read off the SNR for the desired exposure time, or vice-versa.
4. To get accurate values for CR-SPLIT exposures, one should use the sub-exposure time when consulting the plot, and then multiply the resulting SNR by $\sqrt{N}$, where N is the number of sub-exposures to be averaged.

There are separate lines for PC1 (light lines) and the WFC (heavy lines), as well as for ATD-GAIN=7 (default, solid lines), and ATD-GAIN=15 (dashed lines).

Dotted lines across the top of each plot indicate the onset of saturation. There are lines for saturation of the ATD-GAIN=7 setting (G=7), saturation of the ATD-GAIN=15 setting (G=15), and finally a line where blooming starts (top-most line for given camera).

We now give a sample SNR calculation using these plots. Consider a V=20 star of spectral class G0, for which we want to derive the SNR for 1200s CR-SPLIT exposure in F555W on PC1. We look up the G0 spectral class and F555W filter (5500Å) in Table B.1, and obtain AB_V=0.02. We thus have V+AB_V=20.02. We look at Figure B.10 and find this value on the horizontal axis. We locate exposure time 600s (one-half of the total 1200s CR-SPLIT exposure), and find SNR~200. For the total 1200s exposure the SNR would be $200\sqrt{2} = 280$. This exposure is well below the saturation lines in the plot, so saturation is not a concern. If instead, the star had V=19, we would be approaching the “Saturate G=7 PC” line indicating A-to-D converter saturation at gain 7, and so would want to specify ATD-GAIN=15.

Table B.1:AB_ν as a Function of Wavelength. AB_ν is defined as a color-dependent correction from V magnitude to AB magnitude at frequency ν. Wavelength (Å) runs along the top; spectral classes run down the left most column. The second column contains B-V. See Section “Target Count Rates” on page 157.

	B-V	1500	2000	2500	3000	3500	4000	4500	5000	6000	7000	8000	9000	10000
sky	1.10	2.45	5.46	5.46	3.12	2.00	1.03	0.55	0.18	-0.11	-0.33	-0.55	-0.65	-0.75
B0	-0.31	-1.60	-1.50	-1.20	-0.78	-0.62	-0.46	-0.36	-0.22	0.16	0.46	0.76	0.96	1.17
A0	0.00	2.22	1.35	1.11	1.21	1.00	-0.23	-0.16	-0.09	0.11	0.22	0.33	0.36	0.4
F0	0.27	7.22	4.10	3.11	1.99	1.38	0.29	0.06	0.03	0.03	0.05	0.08	0.09	0.1
G0	0.58	8.9	6.35	4.61	2.46	1.63	0.67	0.26	0.08	-0.04	-0.12	-0.21	-0.23	-0.25
K0III	1.07	13	10.3	8.11	5.46	2.13	1.16	0.46	0.2	-0.24	-0.42	-0.61	-0.66	-0.72
M0III	1.60	15	12.3	9.36	6.21	4.63	2.26	0.96	0.51	-0.46	-0.76	-1.06	-1.12	-1.19
gE	1.00	6.82	6.41	5.43	3.63	2.49	1.40	0.55	0.21	-0.19	-0.52	-0.81	-1.07	-1.29
Sa	0.80	5.40	4.80	4.10	3.00	2.01	1.12	0.44	0.19	-0.17	-0.44	-0.7	-0.95	-1.16
Sbc	0.60	4.03	3.18	2.86	2.46	1.54	0.84	0.34	0.17	-0.14	-0.37	-0.6	-0.84	-1.04
Scd	0.45	2.67	2.29	2.15	1.76	1.35	0.65	0.28	0.13	-0.11	-0.26	-0.39	-0.47	-0.58
Ir I	0.30	1.77	1.40	1.36	1.24	0.94	0.43	0.34	0.17	0.13	-0.04	-0.21	-0.33	-0.45

Figure B.1: Point Source SNR vs. V+AB$_\nu$ for F160BW Filter.

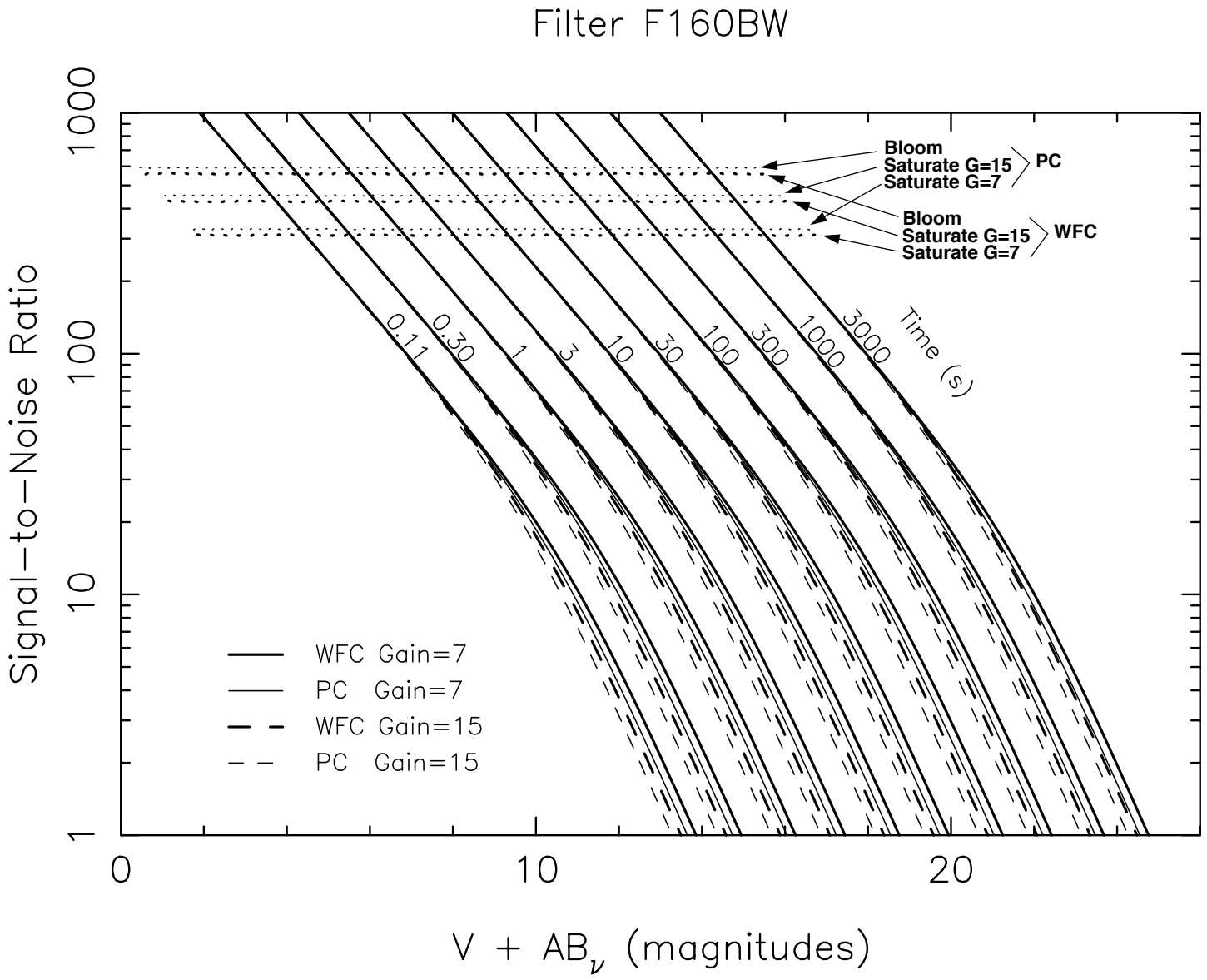

Figure B.2: Point Source SNR vs. V+AB$_\nu$ for F218W Filter.

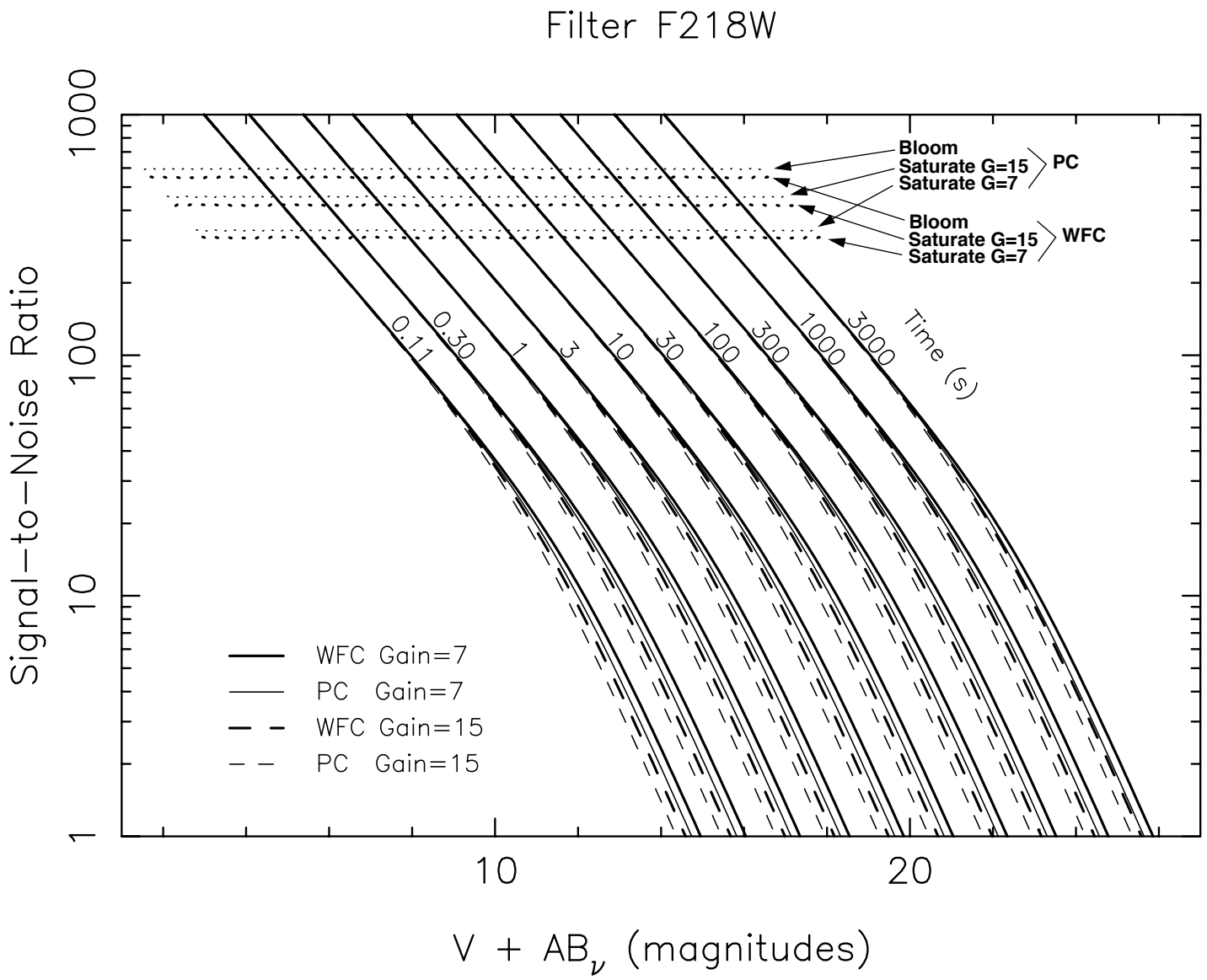

Figure B.3: Point Source SNR vs. V+AB$_\nu$ for F255W Filter.

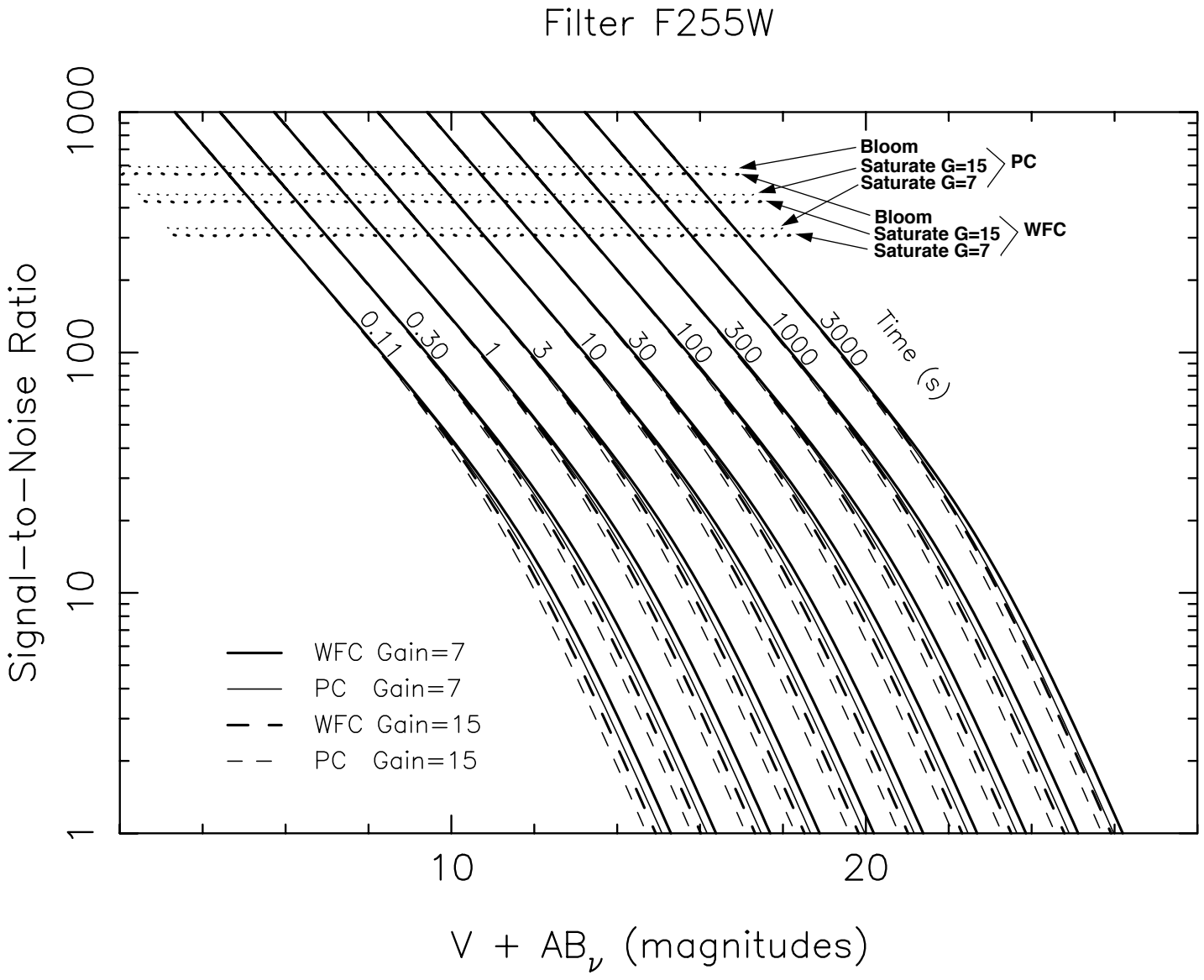

Figure B.4: Point Source SNR vs. V+AB$_\nu$ for F300W Filter.

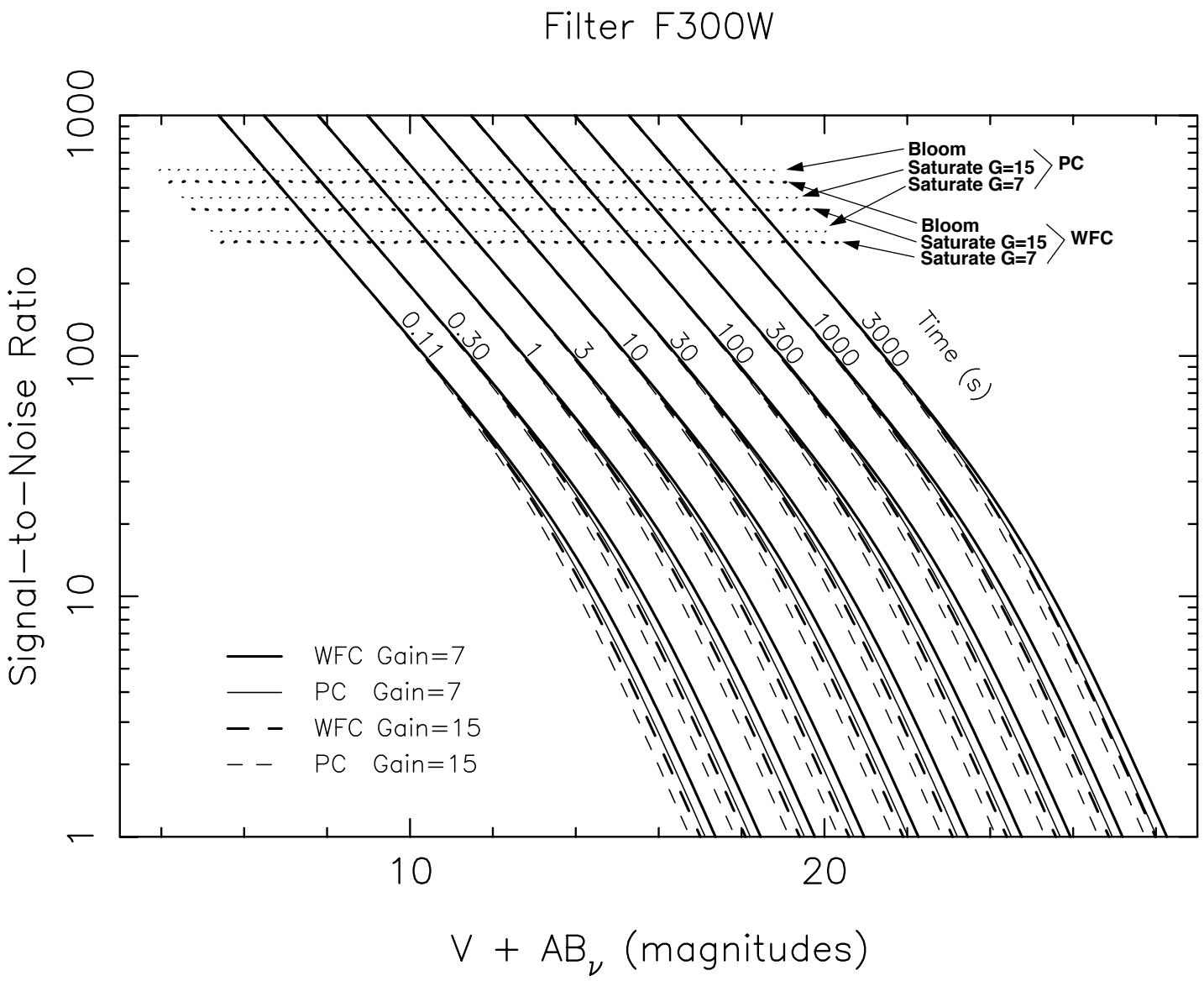

Figure B.5: Point Source SNR vs. V+AB$_\nu$ for F336W Filter.

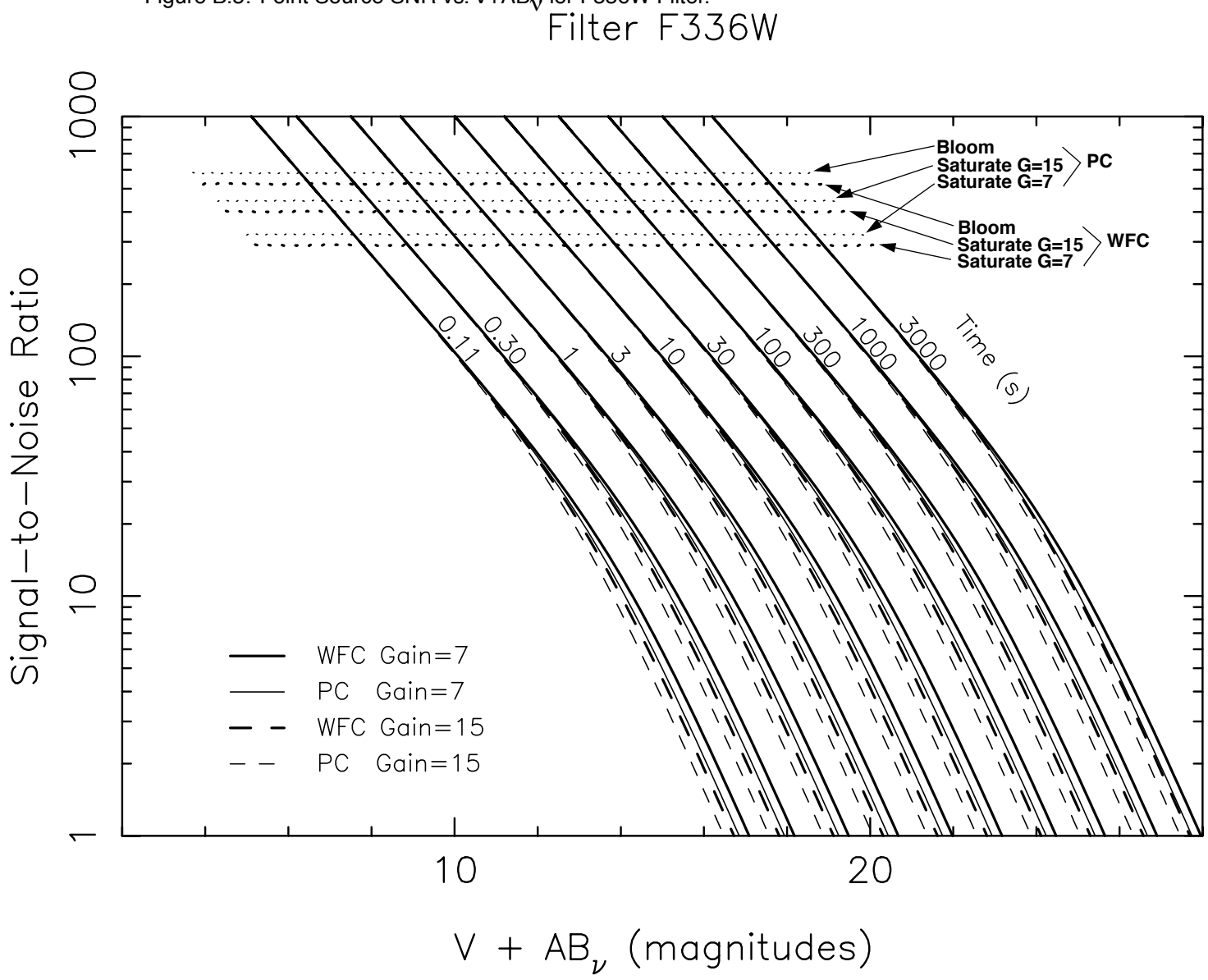

Figure B.6: Point Source SNR vs. V+AB$_\nu$ for F410M Filter.

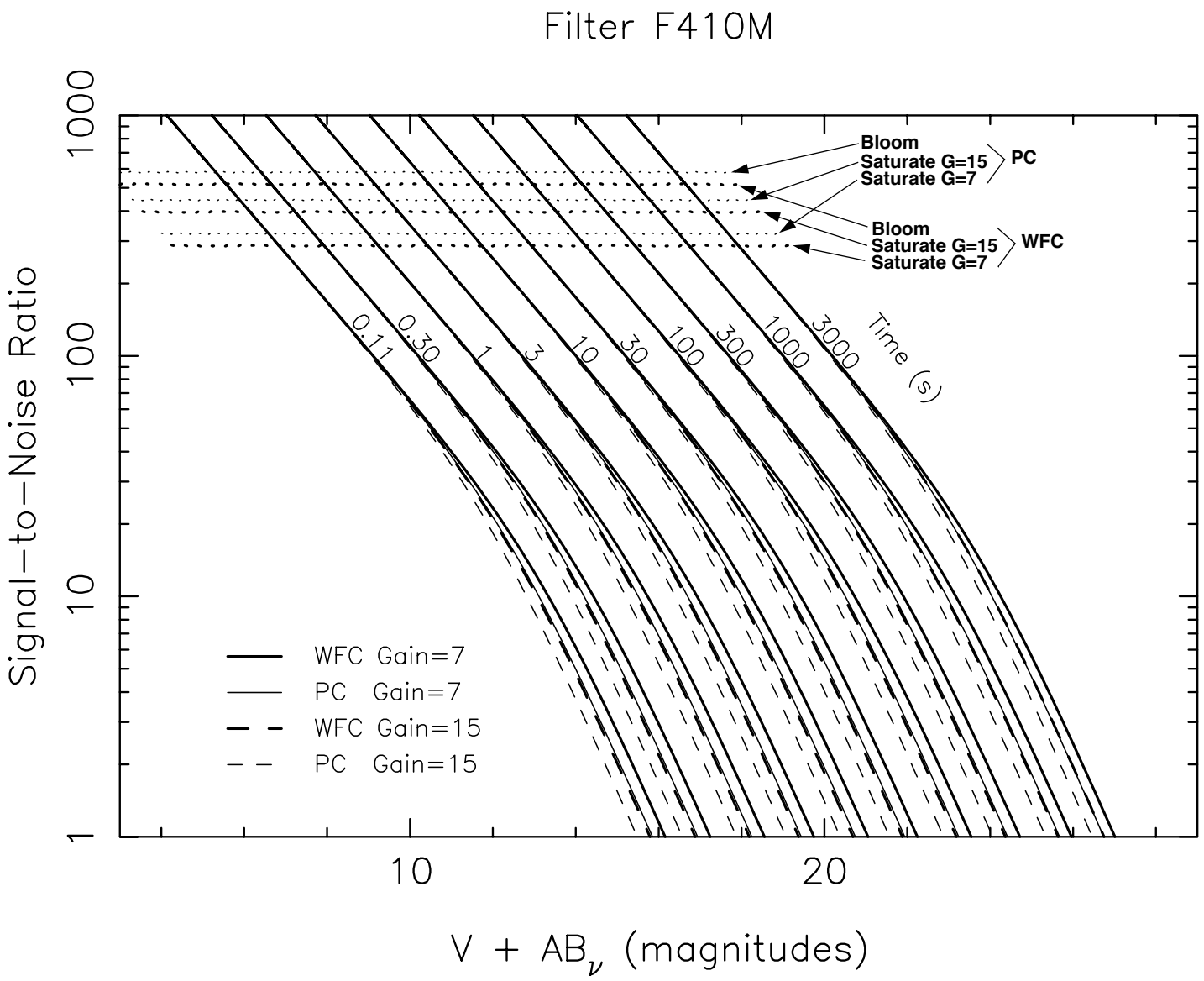

Figure B.7: Point Source SNR vs. V+AB$_\nu$ for F439W Filter.

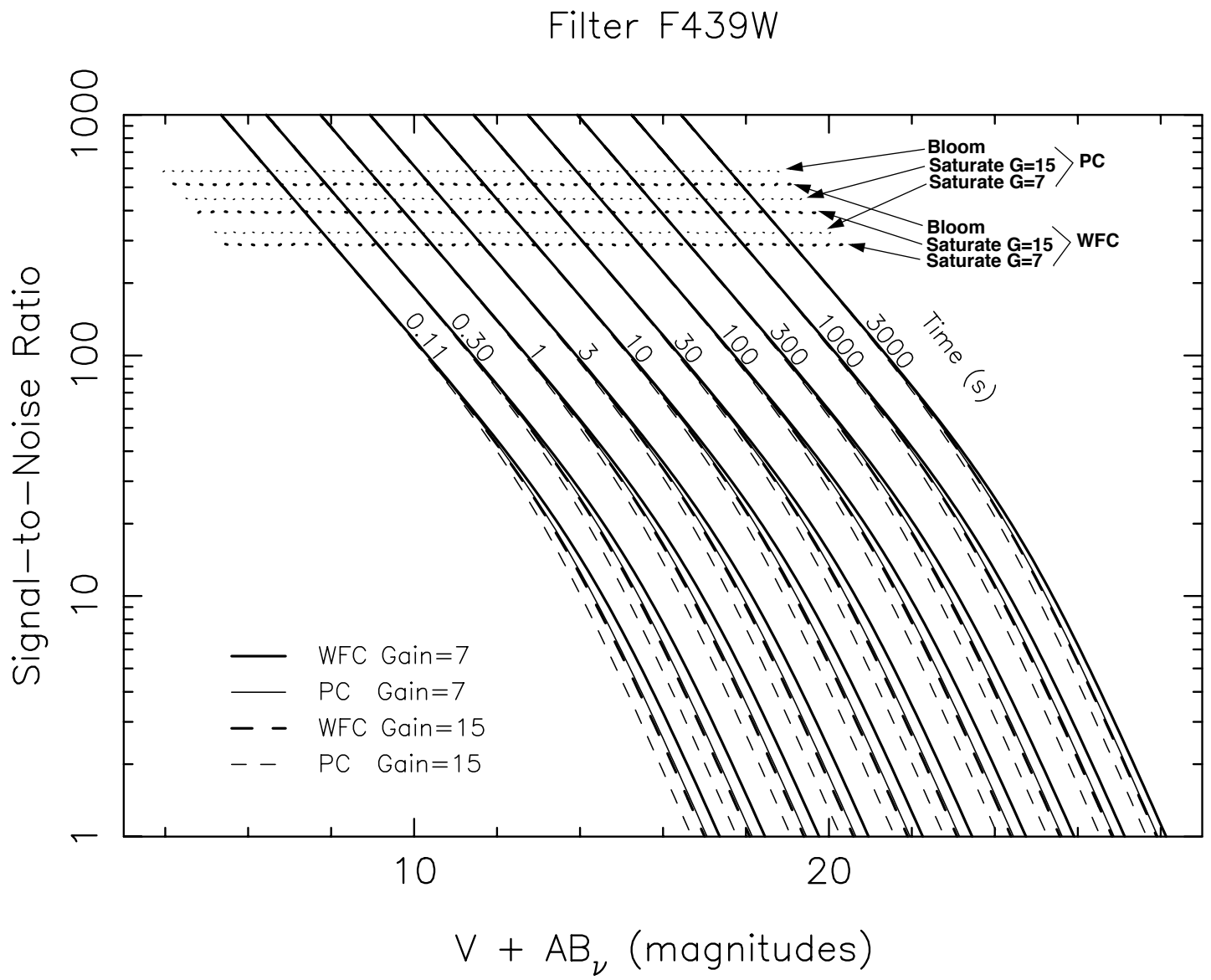

Figure B.8: Point Source SNR vs. V+AB$_\nu$ for F502N Filter.

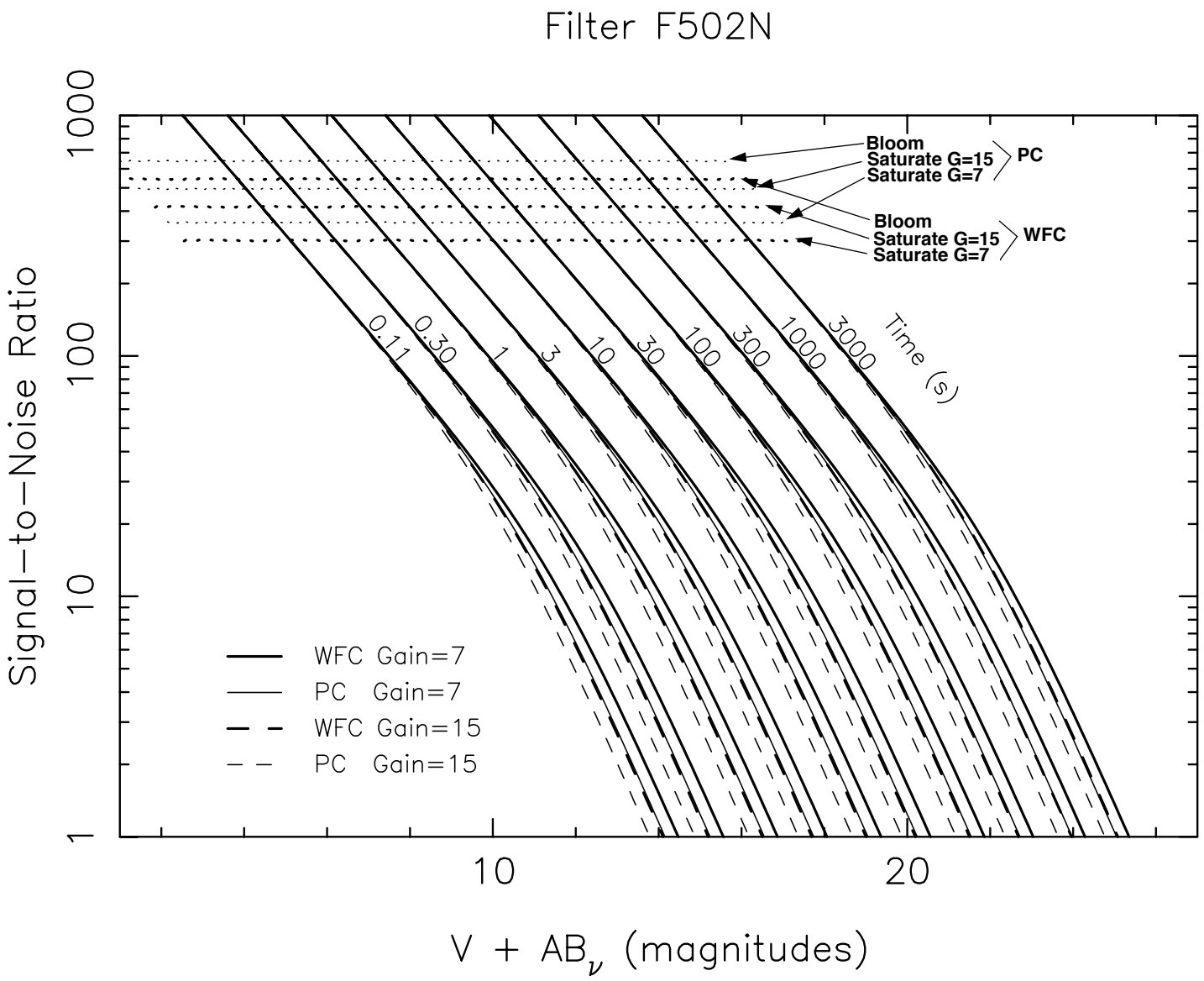

Figure B.9: Point Source SNR vs. V+AB$_\nu$ for F547M Filter.

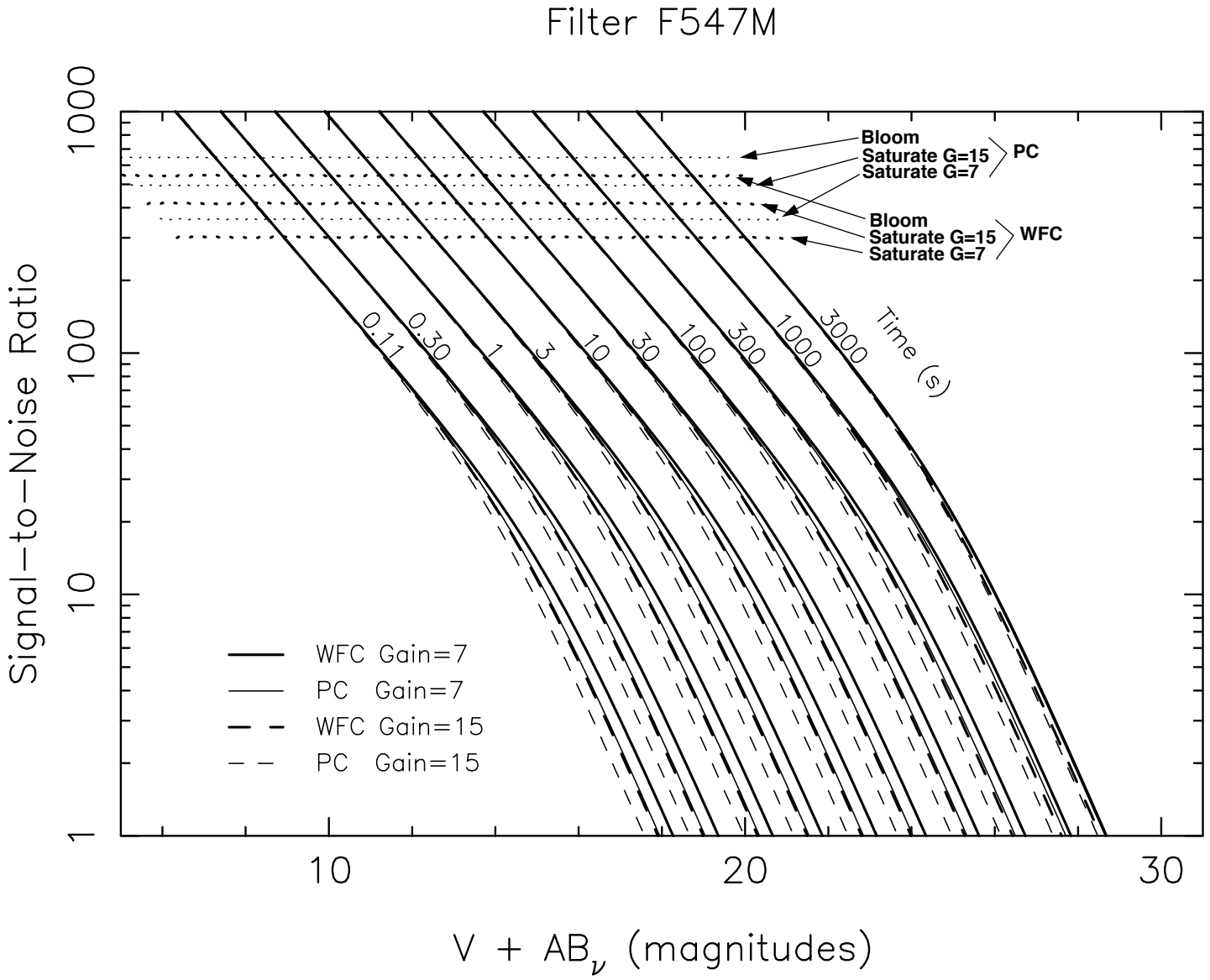

Figure B.10: Point Source SNR vs. V+AB$_\nu$ for F555W Filter.

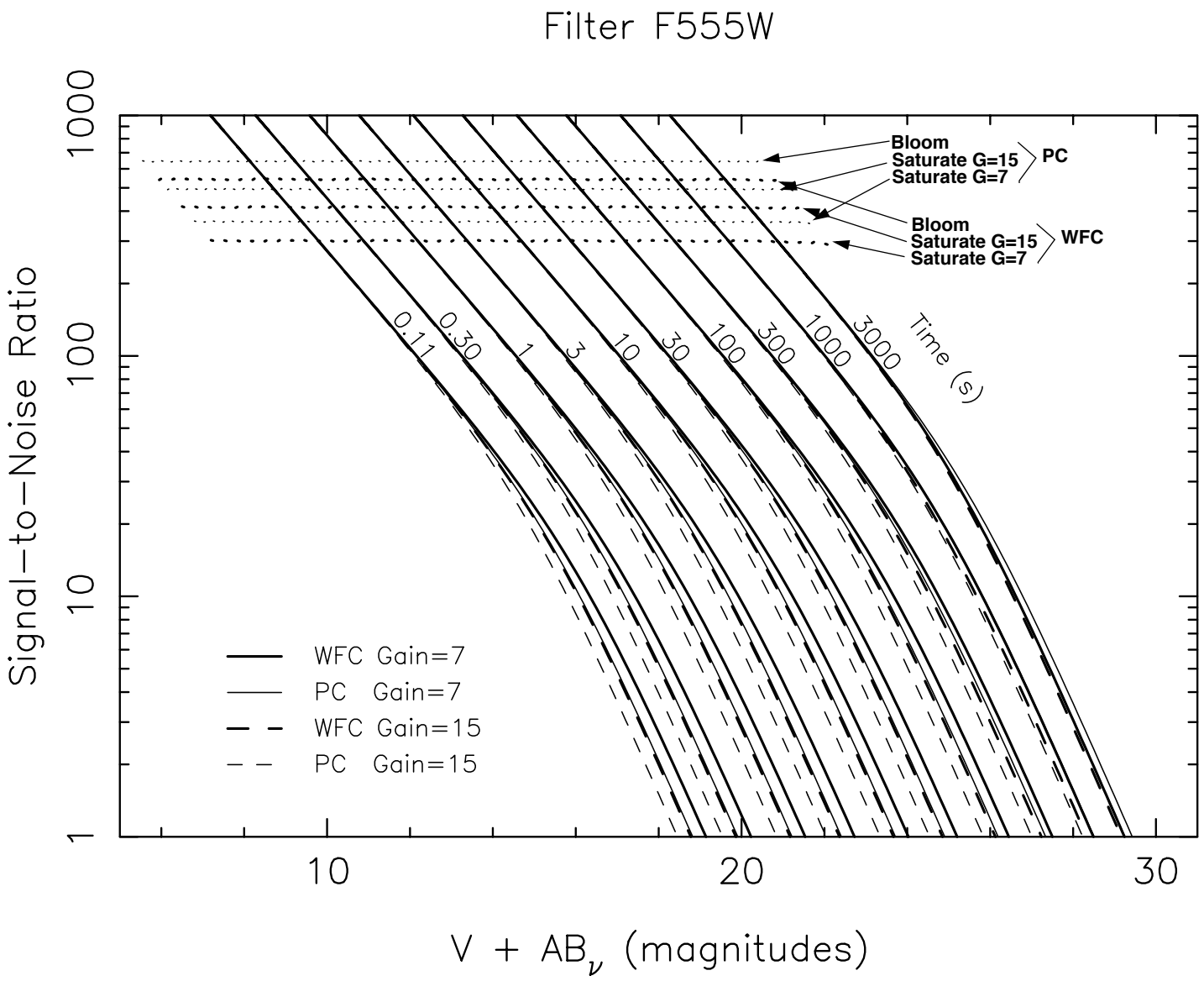

Figure B.11: Point Source SNR vs. V+AB$_\nu$ for F606W Filter.

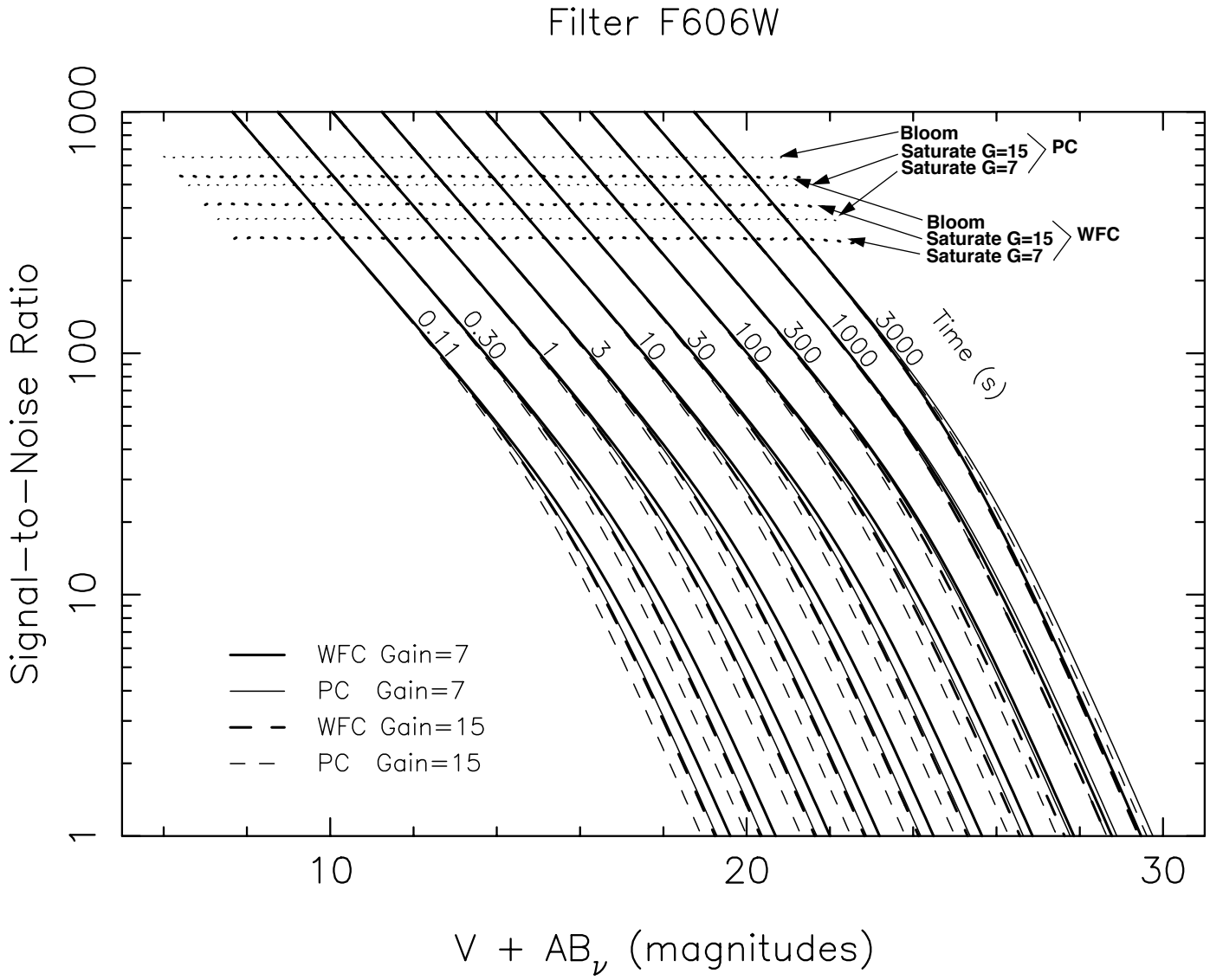

Figure B.12: Point Source SNR vs. V+AB$_\nu$ for F675W Filter.

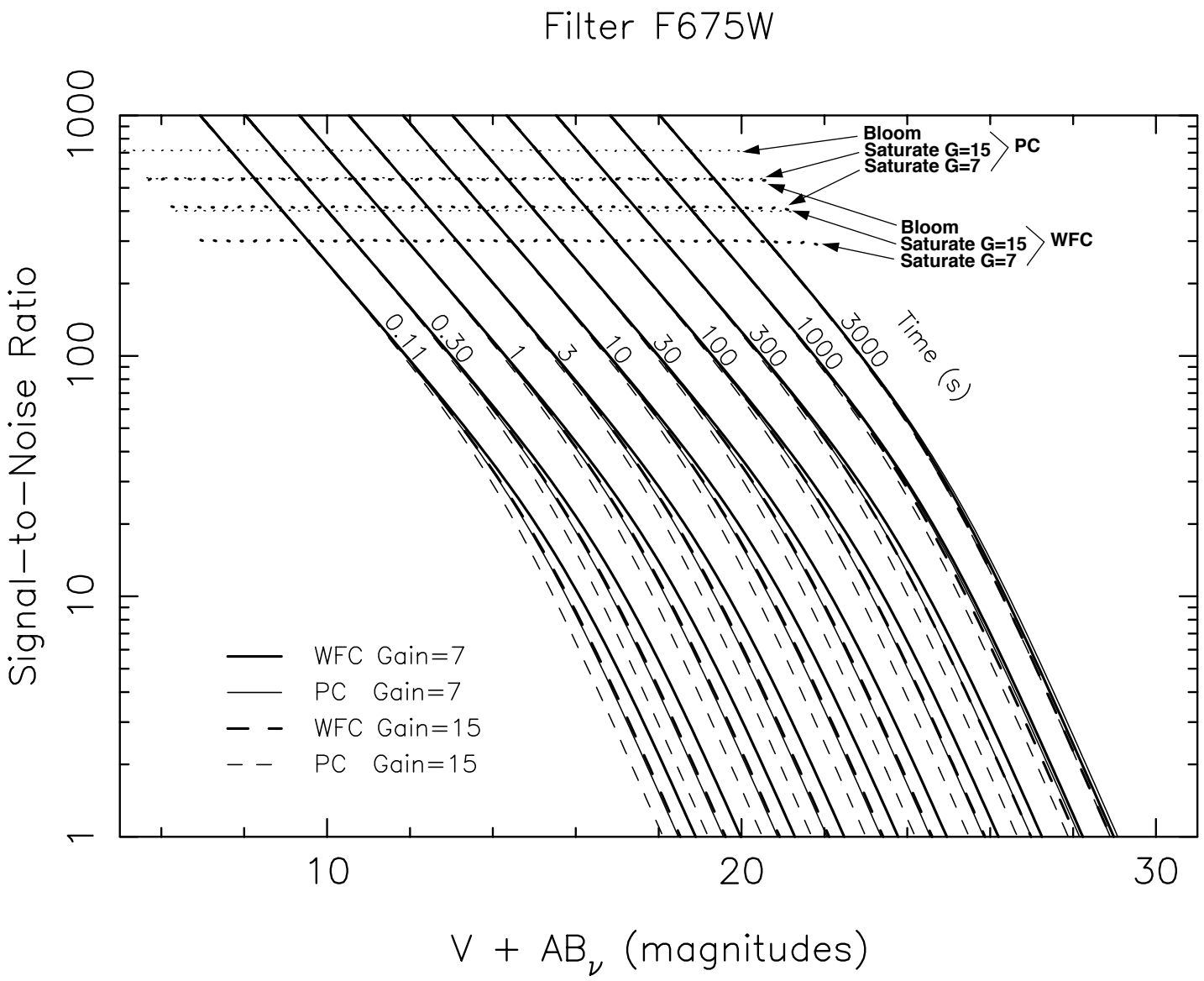

Figure B.13: Point Source SNR vs. V+AB$_\nu$ for F702W Filter.

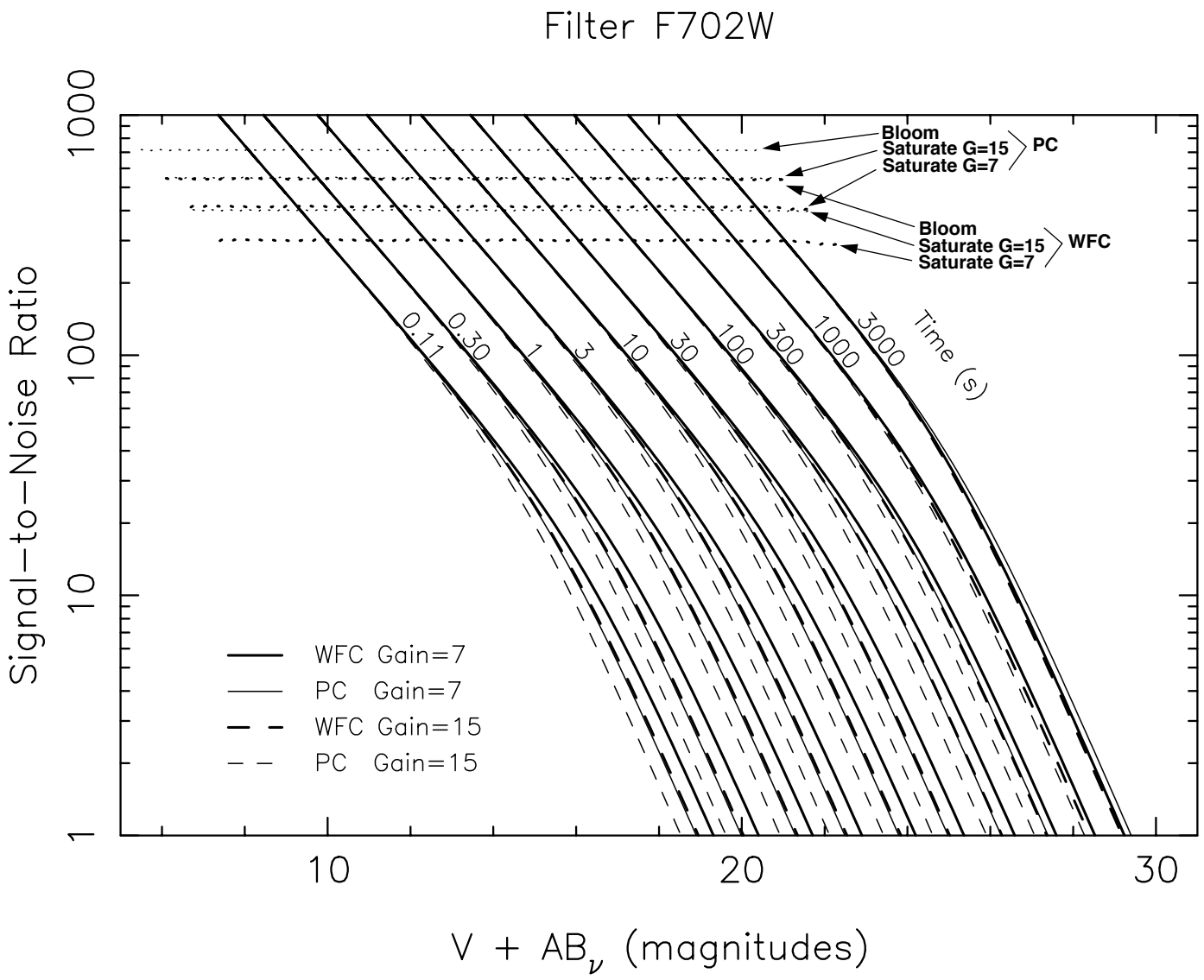

Figure B.14: Point Source SNR vs. V+AB$_\nu$ for F814W Filter.

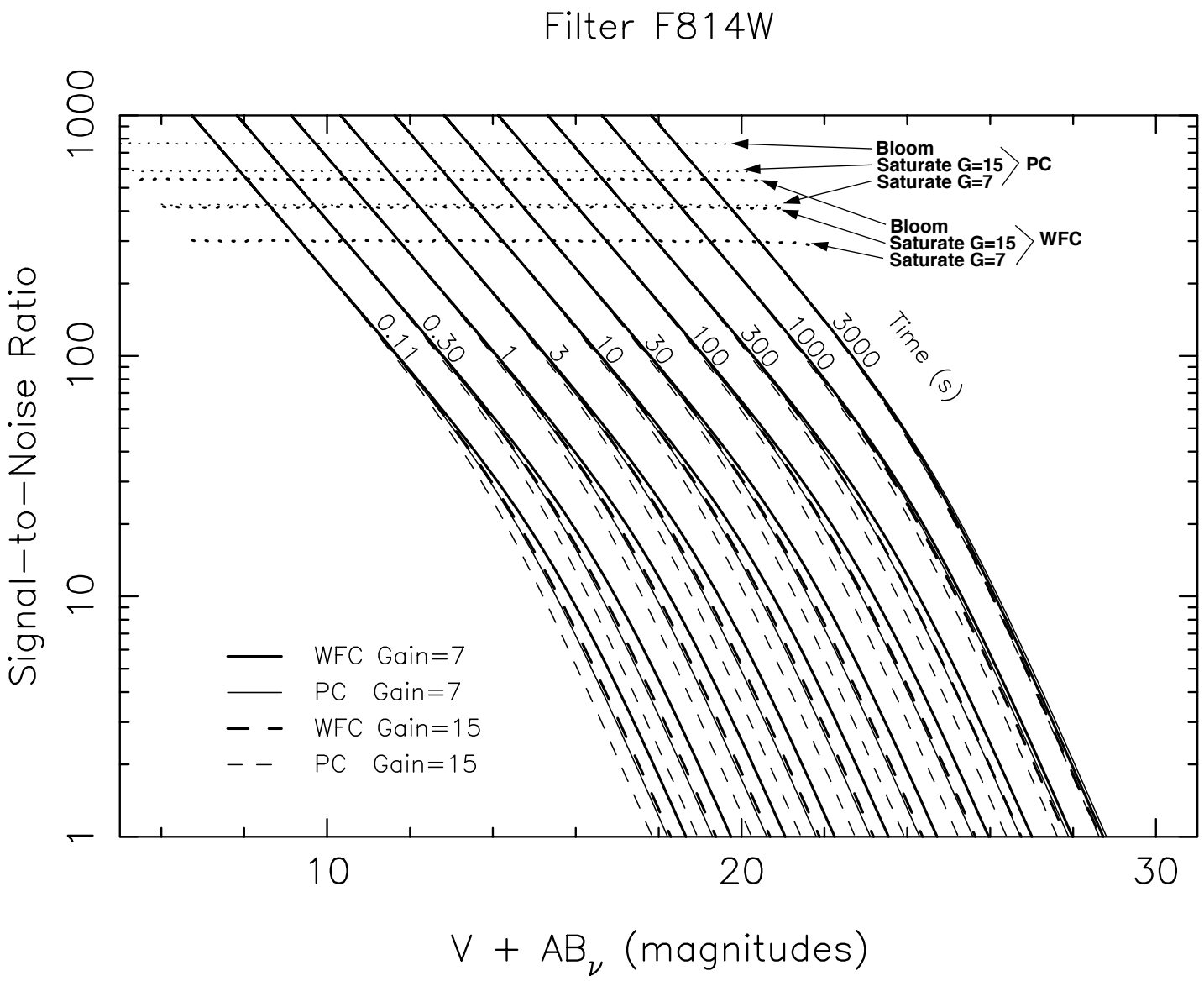

Acronyms

ACS	Advanced Camera for Surveys
ADC	Analog-to-Digital Conversion
ADU	Analog-to-Digital Units (see DN)
CCD	Charge-Coupled Device
CDBS	Calibration DataBase System
CEIS	Contract End Item Specification
CVZ	Continous Viewing Zone
DQE	Detector Quantum Efficiency
DN	Data Number (output of A-to-D converter)
EE	Encircled Energy
FITS	Flexible Image Transport System
FOC	Faint Object Camera
FOV	Field of View
GEIS	Generic Edited Information Set
GO	General Observer
GSFC	Goddard Space Flight Center
GTO	Guaranteed-Time Observer
HDF	Hubble Deep Field
HST	Hubble Space Telescope
ICD	Interface Control Document
IDT	Instrument Definition Team
IR	Infrared
ISR	Instrument Science Report
JPL	Jet Propulsion Laboratory
LEO	Low Earth Orbit

mas	milliarcsecond
MPP	Multi-Pinned Phase
MTF	Modulation Transfer Function
NICMOS	Near-IR Camera and Multi-Object Spectrograph
OTA	Optical Telescope Assembly
PC	Planetary Camera
PI	Principal Investigator
PODPS	Post Observation Data Processing System
PSF	Point Spread Function
QEH	Quantum Efficiency Hysteresis
RBI	Residual Bulk Image
RMS	Root Mean Square
RTO	Reuse Target Offset
SAA	South Atlantic Anomaly
SLTV	System Level Thermal Vacuum Test
SMOV	Servicing Mission Orbital Verification
SNR	Signal-to-Noise Ratio
STAN	Space Telescope [Data] Analysis Newsletter
STEIS	Space Telescope Electronic Information Service
STIS	Space Telescope Imaging Spectrograph
STScI	Space Telescope Science Institute
STSDAS	Space Telescope Science Data Analysis System
TIPS	Telescope and Instruments Performance Summary
TIR	Technical Instrument Report
UV	Ultraviolet
WF/PC-1	Wide Field and Planetary Camera
WFC	Wide Field Camera
WFPC2	Wide Field and Planetary Camera 2
WWW	World Wide Web

References

In this chapter . . .

References

Anderson, J, and King, I. R. 1999, *Astrometric and Photometric Corrections for the 34th Row Error in HST's WFPC2 Camera*, PASP 111, 1095.

- Anderson, J., King, I. 2003, PASP, 115, 113.
- Baggett, S., et al. 1998, *WFPC2 Dark Current Evolution*, TIR WFPC2 98-03.
- Baggett, S., Gonzaga, S. 1998, *WFPC2 Long-Term Photometric Stability*, ISR WFPC2 98-03.
- Baggett, S., Gonzaga, S., Biretta, J. 2000, *CTE Effects on Aperture Photometry of Extended Sources*, (private communication).
- Baggett, S., McMaster, M., et al. 2002, in HST WFPC2 Data Handbook, V.4.0, ed. B. Mobaster, Baltimore, STScI
- Bessell, M. S. 1990, *UBVRI Passbands*, PASP 102, 1181.
- Biretta, J. A, and Sparks, W. B. 1995, *WFPC2 Polarization Observations: Strategies, Apertures, and Calibration Plans*, WFPC2 ISR 95-01.
- Biretta, J. A. 1995, "WFPC2 Flat Field Calibration," in *Calibrating Hubble Space Telescope: Post Servicing Mission*, eds. A. Koratkar and C. Leitherer, p. 257.

- Biretta, J., Baggett, S., 1998, *Proposed Modification to the WFPC2 SAA Avoidance Contour,* TIR WFPC2 98-04 (plus update).
- Biretta, J., McMaster, M. 1997, *WFPC2 Polarization Calibration*, ISR WFPC2 97-11.
- Biretta, J., Mutchler, M. 1998, *Charge Trapping and CTE Residual Images in the WFPC2 CCDs*, ISR WFPC2 97-05.
- Blouke, D. P. 1991, eds. Janesick, J. and Elliot, T., PASP, 8, 153.
- Burrows, C. et al. 1991, *The Imaging Performance of the Hubble Space Telescope*, ApJL 369, L21.
- Casertano, S. 1998, *The Long vs. Short Anomaly in WFPC2 Images*, ISR WFPC2 98-02.
- Casertano, S., et al., editors, *The 1997 HST Calibration Workshop Proceedings*, STScI, 1998.[1]
- Casertano, S., Wiggs, M. 2001, WFPC2 ISR 01-10, Baltimore, STScI.
- Clarke, J.T. and the WFPC2 IDT 1992, *White Paper for WFPC2 Far-Ultraviolet Science*.[2]
- *Dithering: Relationship Between POS TARG's and CCD Rows/Columns*.[1]
- Dolphin, A., 2000, PASP 112, 1397.
- Evans, R. E. 1992, JPL Memorandum, DFM #2031.
- Fruchter, A. S., Hook, R. N. 1997, "A Novel Image Reconstruction Method Applied to Deep Hubble Space Telescope Images", in *Applications of Digital Image Processing XX*, Proc. SPIE, Vol. 3164, A. Tescher, editor, p.120.
- Fruchter, A.S., Hook, R.N. 2002, "Drizzle: A Method for the Linear Reconstruction of Undersampled Images", PASP 114, 144.
- Gilliland, R. L. 1994, ApJ 435, L63.
- Gilmozi, R., et al. 1995, WFPC2 ISR 95-02, Baltimore, STScI
- Gonzaga, S., et al. 1998, *The Drizzling Cookbook*, ISR WFPC2 98-04.
- Gonzaga, S., et al. 1999, *WFPC2 Aperture Photometry Corrections as a Function of Chip Position*, TIR WFPC2 99-01.

1. Available at http://www.stsci.edu/stsci/meetings/cal97/proceedings.html

2. These documents may be requested by e-mail from help@stsci.edu.

- Gonzaga, S., Baggett, S., Biretta, J. 2001, *Preliminary Assessment of the FR533N Filter Anomaly*, ISR WFPC2 01-04.
- Gonzaga, S., Baggett, S., Biretta, J. 2002, *An Analysis of WFPC2 Filter Positional Anomalies*, ISR WFPC2 02-04.
- Gonzaga, S., Biretta, J. 2002, *Predicting Photometry Errors due to Linear Ramp Filters*, TIR WFPC2 02-06.
- Groth, E. and Shaya, E. 1991, in *Wide Field/Planetary Camera Final Orbital/Science Verification Report*, S., M., Faber, Ed.
- Griffiths, R. Ewald, S. and MacKenty, J. W. 1989, in *CCDs in Astronomy*, PASP 8, 231, ed. G. Jacoby.
- Gunn, J. E., and Oke, J. B. 1983, ApJ 266, 713.
- Harris, H. C., et al. 1991, *Photometric Calibration of the HST WF/PC-1 Camera: I. Ground Based Observations of Standard Stars*, AJ 101, 677.
- Hasan, H. and Bely, P. 1993, *Restoration of HST Images and Spectra II,* p.157.
- Hasan, H. and Burrows, C. J. 1993, "Calibrations of the Hubble Space Telescope Optical Telescope Assembly" in *Calibrating Hubble Space Telescope,* eds. C. Blades and S. Osmer, p. 395.
- Harris, et al. 1991, AJ 101, 677.
- Holtzman, J., et al. 1995a, "The Performance and Calibration of WFPC2 on the Hubble Space Telescope," PASP, 107, 156.
- Holtzman, J., et al. 1995b, "The Photometric Performance and Calibration of WFPC," PASP, 107, 1065.
- *HST Data Handbook*, C. Leitherer, ed., (Version 2.0, December 1995).[1]
- *HST Phase II Proposal Instruction*, (Version 8.0, 15 December 1995).[1]
- Interface Control Document (ICD) 19, "PODPS to STSDAS".
- Interface Control Document (ICD) 47, "PODPS to CDBS".
- Janesick, J., Elliot, T., Bredthauer, R., Cover, J., Schaefer, R. and Varian, R. 1989, in *Optical Sensors and Electronic Photography*, SPIE Proc. 1071.
- Janesick, J., Elliot, T., Blouke, M. and Corrie, B. 1989b, in *Optical Sensors and Electronic Photography*, SPIE Proc. 1071, 115, ed. B. Pophal.
- Jordan, Deltorn, and Oates 1993, *Greenwich Observatory Newsletter*, Sept. 1993.

- Koekemoer, A. M., et al. 2002, *HST Dither Handbook* (Version 2.0)
- Koekemoer, A. M., Fruchter, A.S., Hook, R.N., Hack, W. 2002, "MultiDrizzle: An Intergrated Script for Registering, Cleaning and Combining Images", *2002 HST Calibration Workshop,* eds. S. Arribas and A.M. Koekemoer and B. Whitmore, p. 339.
- Koekemoer, A.M., Biretta, J., Mack, J. 2002, *Updated WFPC2 Flat-field Reference Files for 1995 - 2001*, ISR WFPC2 02-02.
- Koornneef, J. et al. 1983, "Synthetic Photometry and the Calibration of the Hubble Space Telescope," in *Highlights of Astronomy*, 7, 833, ed. J.-P. Swings.
- Kozhurina-Platais, V., Anderson J., Koekemoer, A. 2003, WFPC2 ISR 03-02, Baltimore, STScI
- Krist, J., Burrows, C. 1995, *Applied Optics* 34, 4951.
- Krist, J. E. 1995, "WFPC2 Ghosts, Scatter, and PSF Field Dependence," in *Calibrating Hubble Space Telescope: Post Servicing Mission*, eds. A. Koratkar and C. Leitherer, p. 311.
- Lauer, T. 1989, *The Reduction of WF/PC Camera Images*, P.A.S.P. 101, 445.
- Lauer, T. 1991, in *Wide Field/Planetary Camera Final Orbital/Science Verification Report*, ed. S. M. Faber.
- Oke, J.B. and Gunn, J. 1983, ApJ 266, 713.
- Riess, A. 2000, *How CTE Affects Extended Sources*, ISR WFPC2 00-04.
- Riess, A., Biretta, J., Casertano, S. 1999, *Time Dependence of CTE from Cosmic Ray Trails*, ISR WFPC2 99-04.
- *STSDAS Calibration Guide* (November 1991).[1]
- STDAS Users' Guide.
- Schneider, D. P., Gunn, J. E., and Hoessel, J. G. 1983, ApJ 264, 337.
- Schultz, A., Heyer, I., Biretta, J. 2001, *Noiseless Preflashing of the WFPC2 CCDs,* ISR WFPC2 01-02.
- Schultz, A., Baggett, S., Biretta, J. 2002, *WFPC2 Clocks-ON Close Out*, ISR WFPC2 02-01.
- Suchkov, A., Casertano, S. 1997, *Impact of Focus Drift on Aperture Photometry*, ISR WFPC2 97-01.
- Trauger, J. T. 1989, in *CCDs in Astronomy*, PASP 8, 217, ed. G. Jacoby.

- Trauger, J. T., ed. 1993, *The WFPC2 Science Calibration Report*, Pre-launch Version 1.2. [IDT calibration report]
- Trauger, J. T., Vaughan, A.H., Evans, R.W., Moody, D.C. 1995, "Geometry of the WFPC2 Focal Plane" *Calibrating Hubble Space Telescope: Post Servicing Mission*, eds. A. Koratkar and C. Leitherer, p. 379.
- Voit, M., ed., *HST Data Handbook*, (Version 3.0, October 1997).[3]
- WF/PC-1 IDT OV/SV Report, WFPC2 World Wide Web page at address:

  `http://www.stsci.edu/instruments/wfpc2/wfpc2_top.html`
- Westphal, J., et al. 1982, *The Wide Field/Planetary Camera in The Space Telescope Observatory*, IAU 18th General Assembly, Patras, NASA CP-2244.
- Whitmore, B. 1998, "Time Dependence of the Charge Transfer Efficiency on the WFPC2."[4]
- Whitmore, B., Heyer, I. 1997, *New Results on Charge Transfer Efficiency and Constraints on Flat-Field Accuracy*, ISR WFPC2 97-08 (updated in 1998).
- Whitmore, B., Heyer, I., Casertano, S. 1999, PASP 111, 1559.
- Whitmore, B., Heyer I. 2002, *Charge Transfer Efficiency for Very Faint Objects and a Reexamination of the Long-vs-Short Problem for the WFPC2*, ISR WFPC2 02-03.
- Woodgate, B. E. 1989, in *CCDs in Astronomy*, PASP 8, 237, ed. G. Jacoby.

Instrument Science Reports

These documents may be requested by e-mail from help@stsci.edu or online at:

`http://www.stsci.edu/instruments/wfpc2/wfpc2_bib.html`.

- ISR WFPC2 04-01: *The Accuracy of WFPC2 Photometric Zeropoints,* Heyer, I., Richardson, M., Whitmore, B., Lubin, L.

3. Available at: http://www.stsci.edu/instruments/wfpc2/Wfpc2_dhb/WFPC2_longdhbcover.html

4. Available at: http://www.stsci.edu/instruments/wfpc2/Wfpc2_isr/cte_vs_time_post.ps

- ISR WFPC2 03-03: *WFPC2 Cycle 12 Calibration Plan*, Koekemoer, A. M., Heyer, I., Brammer, G., Kozhurina-Platais, V., Rhoads, J., Whitmore, B.
- ISR WFPC2 03-02: *Toward a Multi-Wavelength Geometric Distortion Solution for WFPC2*, Kozhurina-Platais, V., Anderson, J., Koekemoer, A. M.
- ISR WFPC2 03-01: *WFPC2 Cycle 9 Closure Report*, Koekemoer, A. M., Baggett, S., Casertano, S., Gonzaga, S., Heyer, I., and the WFPC2 Group.
- ISR WFPC2 02-07: *Updated Contamination Rates for WFPC2 UV Filters*, McMaster, M., Whitmore, B.
- ISR WFPC2 02-06: *Results of the Observatory Verification for WFPC2 after Servicing Mission 3B*, Koekemoer, A. M., and the WFPC2 Group.
- ISR WFPC2 02-05: *WFPC2 Cycle 11 Calibration Plan*, Gonzaga, S., and the WFPC2 Group.
- ISR WFPC2 02-04: *An Analysis of WFPC2 Filter Positional Anomalies*, Gonzaga, S., Baggett S., Biretta, J.
- ISR WFPC2 02-03: *Charge Transfer Efficiency for Very Faint Objects and a Reexamination of the Long-vs-Short Problem for the WFPC2*, Whitmore, B., Heyer I.
- ISR WFPC2 02-02: *Updated WFPC2 Flatfield Reference Files for 1995 - 2001*, Koekemoer, A.M., Biretta, J., Mack, J.
- ISR WFPC2 02-01: *WFPC2 Clocks-ON Close Out*, Schultz, A., Baggett, S., Biretta, J.
- ISR WFPC2 01-11: *Summary of WFPC2 SM3B Plans,* A. M. Koekemoer, S. Gonzaga, I. Heyer, L. M. Lubin, and V. Kozhurina-Platais.
- ISR WFPC2 01-10: *An Improved Geometric Solution for WFPC2,* S. Casertano and M. Wiggs
- ISR WFPC2 01-09: *The WFPC2 Photometric CTE Monitor*, I. Heyer.
- ISR WFPC2 01-08: *Creating WFPC2 Dark Reference Files: Addendum*, J. Mack, S. Baggett, and J. Biretta.
- ISR WFPC2 01-07: *WFPC2 Flatfields with Reduced Noise*, E. Karkoschka and J. Biretta.
- ISR WFPC2 01-06: W*FPC2 Cycle 8 Closure Report,* S. Baggett, S. Gonzaga, J. Biretta, S. Casertano, I. Heyer, A. M. Koekemoer, J. Mack, M. McMaster, A. Riess, A. Schultz, and M. S. Wiggs.

- ISR WFPC2 01-05: *WFPC2 Dark Current vs. Time,* Mack, J., Biretta, J., Baggett, S., Proffitt, C.
- ISR WFPC2 01-04: *Preliminary Assessment of the FR533N Filter Anomaly,* Gonzaga, S., Baggett, S., Biretta, J.
- ISR WFPC2 01-03: *WFPC2 Cycle 10 Calibration Plan,* Baggett, S., et al.
- ISR WFPC2 01-02: *Noiseless Preflashing of the WFPC2 CCDs,* Schultz, et al.
- ISR WFPC2 01-01: *Creating WFPC2 Dark Reference Files,* Mack and Wiggs.
- ISR WFPC2 00-04: *How CTE Affects Extended Sources,* Riess.
- ISR WFPC2 00-03: *Update on Charge Trapping and CTE Residual Images in WFPC2,* Baggett, et al.
- ISR WFPC2 00-02: *Results of the WFPC2 Observatory Verification after SM3a,* Casertano, et al.
- ISR WFPC2 00-01: *WFPC2 Cycle 9 Calibration Plan,* Baggett, et al.
- ISR WFPC2 99-05: *WFPC2 Cycle 7 Closure Report*, Baggett, et al.
- ISR WFPC2 99-04: *Time Dependence of CTE from Cosmic Ray Trails*, Riess, et al.
- ISR WFPC2 99-03: *Summary of WFPC2 SM3a Plans*, Casertano, et al., (revised: December 20, 1999).
- ISR WFPC2 99-02: *WFPC2 Cycle 8 Calibration Plan*, Baggett, et al.
- ISR WFPC2 99-01: *Internal Flat Field Monitoring II. Stability of the Lamps, Flat Fields, and Gain Ratios*, O'Dea, Mutchler, Wiggs.
- ISR WFPC2 98-04: *The Drizzling Cookbook*, Gonzaga, et al.
- ISR WFPC2 98-03: *WFPC2 Long-Term Photometric Stability*, Baggett and Gonzaga.
- ISR WFPC2 98-02: *The Long vs. Short Anomaly in WFPC2 Images*, Casertano and Mutchler.
- ISR WFPC2 98-01: *WFPC2 Cycle 6 Calibration Closure Report*, Baggett, et al.
- ISR WFPC2 97-11: *WFPC2 Polarization Calibration*, Biretta and McMaster.
- ISR WFPC2 97-10: *WFPC2 SYNPHOT Update*, Baggett, et al.
- ISR WFPC2 97-09: *Results of the WFPC2 Post-Servicing Mission-2 Calibration Program*, Biretta, et al.

- ISR WFPC2 97-08: *New Results on Charge Transfer Efficiency and Constraints on Flat-Field Accuracy*, Whitmore and Heyer.
- ISR WFPC2 97-07: *WFPC2 Electronics Verification*, Stiavelli and Mutchler.
- ISR WFPC2 97-06: *WFPC2 Cycle 7 Calibration Plan*, Casertano, et al.
- ISR WFPC2 97-05: *Charge Trapping and CTE Residual Images in the WFPC2 CCDs*, Biretta and Mutchler.
- ISR WFPC2 97-04: *Properties of WFPC2 Bias Frames*, O'Dea, et al.
- ISR WFPC2 97-03: *Summary of WFPC2 SM97 Plans*, Biretta, et al.
- ISR WFPC2 97-02: *WFPC2 Cycle 5 Calibration Closure Report,* Casertano and Baggett.
- ISR WFPC2 97-01: *Impact of Focus Drift on Aperture Photometry*, Suchkov and Casertano.
- ISR WFPC2 96-02: *Contamination Correction in SYNPHOT for WFPC2 and WF/PC-1,* Baggett, et al.
- ISR WFPC2 96-01: *Internal Flat Field Monitoring,* Stiavelli and Baggett.
- ISR WFPC2 95-07: *WFPC2 Cycle 4 Calibration Summary,* Baggett, Casertano, and Biretta.
- ISR WFPC2 95-06: *A Field Guide to WFPC2 Image Anomalies,* Biretta, Ritchie, and Rudloff.
- ISR WFPC2 95-05: *Wavelength / Aperture Calibration of the WFPC2 Linear Ramp Filters,* Biretta, Ritchie, Baggett, MacKenty.
- ISR WFPC2 95-04: *Demonstration Analysis Script for Performing Aperture Photometry*, Whitmore and Heyer.
- ISR WFPC2 95-03: *Charge Transfer Traps in the WFPC2*, Whitmore and Wiggs.
- ISR WFPC2 95-02: *The Geometric Distortion of the WFPC2 Cameras*, Gilmozzi, R. et al.
- ISR WFPC2 95-01: *WFPC2 Polarization Observations: Strategies, Apertures, and Calibration Plans,* Biretta and Sparks.
- ISR WFPC2 94-03: *WFPC2 Pipeline Calibration*, Burrows, C.
- ISR WFPC2 94-01: *Large Angle Scattering in WFPC2 and Horizontal "Smearing" Correction*, Krist, J. and Burrows, C.
- ISR WFPC2 93-01: *Polarizer Quad Nomenclature*, Clampin, M.
- ISR WFPC2 92-06: *WFPC2 CCDs,* Clampin, M.

- ISR WFPC2 92-05: *WFPC2 AFM and POMM Actuation Algorithm,* Burrows, C.
- ISR WFPC2 92-04: *Science with the Second Wide Field and Planetary Camera*, Trauger, J.T. et al.
- ISR WFPC2 92-03: *WFPC2 Science Observation and Engineering Modes*, Trauger, J.T. and Brown, D.I.
- ISR WFPC2 92-02: *System Level Contamination Issues for WFPC2 and COSTAR*, Clampin, M.

Technical Instrument Reports

Internal memos, available by request to help@stsci.edu.

- TIR WFPC2 02-06: *Predicting Photometry Errors due to Linear Ramp Filters*, Gonzaga, S., Biretta, J.
- TIR WFPC2 02-05: *SMOV3B WFPC2 Lyman-Alpha Throughput Check*, L.M. Lubin, B. Whitmore, A.M. Koekemoer, I. Heyer.
- TIR WFPC2 02-04: *SMOV3B WFPC2 Photometry Check*, B. Whitmore, I. Heyer.
- TIR WFPC2 02-03: *SMOV3B WFPC2 UV Contamination Monitoring and Throughput Check*, A. M. Koekemoer, S. Gonzaga, L. Lubin, B. Whitmore, I. Heyer.
- TIR WFPC2 02-02: *SMOV3B Flat Field Verification,* A. M. Koekemoer and I. Heyer.
- TIR WFPC2 02-01: *SMOV3b Check of the WFPC2 Point-Spread-Function*, V. Kozhurina-Platais, L.M. Lubin, and A.M. Koekemoer.
- TIR WFPC2 01-02: *Testing the On-The-Fly-Reprocessing System with WFPC2 Data,* S. Gonzaga, S. Baggett, J. Biretta.
- TIR WFPC2 01-01: *Shutter Jitter History Measured from INTFLATs*, Riess, A., Casertano, S., and Biretta, J.
- TIR WFPC2 00-05: *Testing the On-The-Fly-Calibration System with WFPC2 Data*, Wiggs, M.S., and Baggett, S.
- TIR WFPC2 00-04: *WFPC2 Internal Monitoring*, O'Dea C., Heyer I., and Baggett, S.
- TIR WFPC2 00-03: *SM3a SMOV WFPC2 Photometry Check*, Schultz, A., Gonzaga, S., Casertano, S.

- TIR WFPC2 00-02: *Results of the WFPC2 SM3a Lyman-Alpha Throughput Check*, Baggett, S., Heyer, I.
- TIR WFPC2 00-01: *SMOV3a Flat Field Stability Check*, Koekemoer, A., Biretta, J., Wiggs, M.S.
- TIR WFPC2 99-02: *Preliminary Results of the Noiseless Preflash Test*, Schultz, A., Heyer, I., Biretta, J.
- TIR WFPC2 99-01: *WFPC2 Aperture Photometry Corrections as a Function of Chip Position*, Gonzaga, S., O'Dea, C., Whitmore, B.
- TIR WFPC2 98-04A: *Addendum to TIR WFPC2 98-04*, Biretta, J., Baggett, S.
- TIR WFPC2 98-04: *Proposed Modification to the WFPC2 SAA Avoidance Contour*, Biretta, J., Baggett, S.
- TIR WFPC2 98-03: *WFPC2 Dark Current Evolution*, Baggett, S., Casertano, S., Wiggs, M.S.
- TIR WFPC2 98-02: *Analysis of the Excess Charge in WFPC2 Overscans*, Mutchler, M., O'Dea, C., Biretta, J.
- TIR WFPC2 98-01: *Time Dependence of the CTE on the WFPC2*, Whitmore, B.
- TIR WFPC2 97-11: *Long-Term Study of Bias Jumps*, O'Dea, C., McMaster, M., Heyer, I.
- TIR WFPC2 97-10: *WFPC2 Photometry from Subtraction of Observed PSFs*, Surdej, J., Baggett, S., Remy, M., Wiggs, M.S.
- TIR WFPC2 97-09: *The WFPC2 PSF Library*, Wiggs, M.S., Baggett, S., Surdej, J., Tullos, C.
- TIR WFPC2 97-08: *SMOV Flat Field Check*, Biretta, J., Wiggs, M.S.
- TIR WFPC2 97-07: *WFPC2 Internal Monitoring for SM97*, Mutchler, M., Stiavelli, M.
- TIR WFPC2 97-06: *SMOV Check of WFPC2 PSF Stability*, Fruchter, A., McMaster, M.
- TIR WFPC2 97-05: *Results of the WFPC2 SM-2 Lyman-Alpha Throughput Check*, O'Dea, C., Baggett, S., Gonzaga, S.
- TIR WFPC2 97-04: *VISFLAT Channel Monitoring*, Stiavelli, M.
- TIR WFPC2 97-03: *OTA Focus during SMOV*, Casertano, S., Lallo, M., Suchkov, A., Krist, J.
- TIR WFPC2 97-02: *SM-2 UV Monitoring and Cooldown Procedure*, Stiavelli, M., Biretta, J., Baggett, S., Gonzaga, S., Mutchler, M.

- TIR WFPC2 97-01: *Results of the WFPC2 SMOV Relative Photometry Check*, Whitmore, B., Gonzaga, S., Heyer, I.

Other Selected Documents

Available online at:

http://www.stsci.edu/instruments/wfpc2/wfpc2_doc.html.

- *The WFPC2 Instrument Handbook*, Version 8.0
- *The HST Data Handbook*, Version 4.0
- *HST Dither Handbook*, Version 2.0
- *The WFPC2 Tutorial*, a step-by-step guide to reducing WFPC2 data
- *The Space Telescope Analysis Newsletter (*STAN)
- *The WFPC2 History* memo, containing chronological information on decontaminations, darks, focus changes, and miscellaneous items
- How to calibrate WFPC2 Linear Ramp Filter data.
- Time Dependence of the Charge Transfer Efficiency.
- The WFPC2 Reference Files, a complete list of all reference files available for recalibrating WFPC2 data.
- *The STSDAS SYNPHOT User's Guide*.
- *The Guide to WFPC2 SYNPHOT Tables*, which describes the use of the STSDAS task SYNPHOT for WFPC2 photometry.
- WFPC2 Photometry and SYNPHOT.
- Table of up-to-date SYNPHOT photflams and zeropoints.

The WFPC2 Data Analysis Library

The WFPC2 Data Analysis Library (formerly the WFPC2 Clearinghouse) is a web-based tool designed to provide users with a searchable listing of all known journal articles, STScI documentation and reports, as well as user-submitted documents which report on all aspects of the performance, calibration, and scientific use of WFPC2. The Data Analysis Library can be found at:

http://www.stsci.edu/instruments/wfpc2/Wfpc2_clear/wfpc2_clrhs.html

The primary goal of the Data Analysis Library is to make it easier for WFPC2 users to take advantage of the fact that there are hundreds of researchers reducing and analyzing WFPC2 data, and of their results.

We have searched through the astronomical literature and selected all articles that contain any reference or description of the calibration, reduction, and scientific analysis of WFPC2 data. Due to the extremely large volume of material, the on-line database is only complete through 1997. After 1997, we have only continued to update the Data Analysis Library with STScI documentation and reports, including Instrument Science Reports and Technical Instrument Reports. Each article that is included in our database had an estimate of its importance in up to 50 calibration topics. The entry for each article has the following format:

```
Author: Holtzman,Mould, Gallagher, et al.
Title: Stellar Populations in the Large Magellanic Cloud: Evidence
for..
Year: 1997
Reference: AJ 113, 656
Science Keyword: IMF,LMC
Calibration Keyword(3): psf_fitting_photometry(3)
Calibration Keyword(2): bias(2)
Calibration Keyword(1): photometric_zeropoint(1)
Comment: Comparison of aperture and PSF fitting photometry,
```

where the category number following each keyword stands for the following:

- (3)= One of the fundamental references on this topic.
- (2)= Some new information on this topic.
- (1)= General information on the subject.

The user can select from a large list of WFPC2 calibration related topics (see below). The results from a Data Analysis Library search will list, alphabetically by author, all articles containing references to the selected topic. For journal articles, each reference is linked to that article's entry in the ADS Abstract Database, so that users can quickly determine if that particular article is relevant to their individual needs.

The following topics are available:

Aperture Corrections	Object Identification
Aperture Photometry	Observation Planning
Astrometry	Photometric Transformations
Bias Frames	Photometric Zeropoint
Bias Jumps	Pipeline Calibration
Calibration Observations	Polarization
CCD Characteristics	PSF Characterization

Charge Transfer Traps	PSF Fitting Photometry
Chip-to-Chip Normalization	PSF Subtraction
Completeness Corrections	Quad Filters
Cosmic Rays	Recalibration
CTE Losses	Red Leaks
Darks	Residual Images
Data Quality	Saturated Data
Deconvolution	Scattered Light
Dithering	Serial Clocks
Drizzle	Size Measurements
Field Distortion	Software
Flats	Surface Photometry
Focus	SYNPHOT
Hot Pixels	T=77 Observations
Image Anomalies	UV Throughput
Linear Ramp Filters	Vignetting
Long vs. Short Exposures	Woods Filters
Narrow Band Photometry	1997 Servicing Mission

Index

C

D

H

I

J

K

L

M

N

O

P

Q

R

S

T

U

V

W

X

Y

Z